RECENT ADVANCES IN DROSOPHILA CELLULAR AND HUMORAL INNATE IMMUNITY

EDITED BY: Susanna Valanne, Dan Hultmark and Laura Vesala
PUBLISHED IN: Frontiers in Immunology

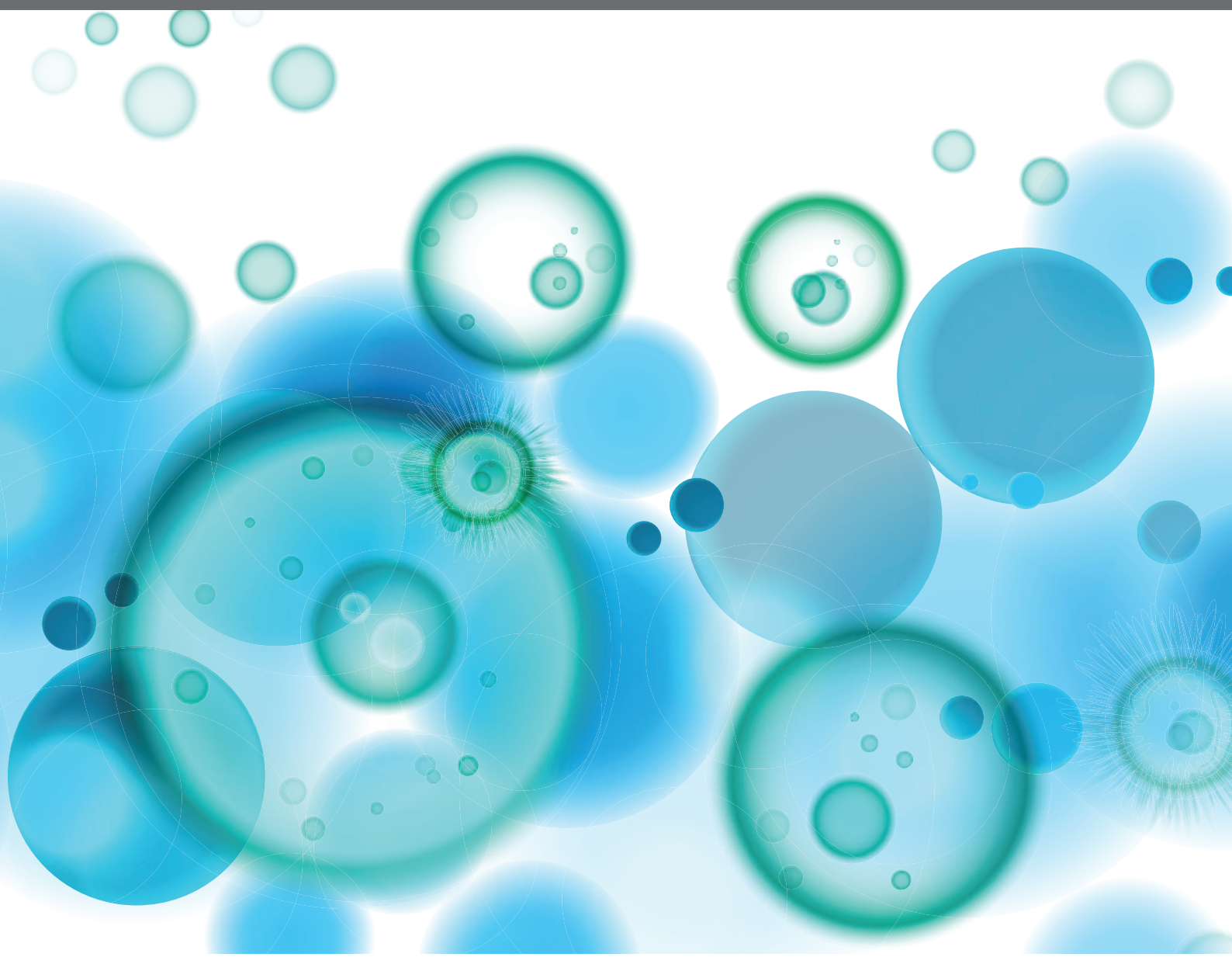

frontiers Research Topics

frontiers

ISSN 1664-8714
ISBN 978-2-88966-191-6
DOI 10.3389/978-2-88966-191-6

About Frontiers

Frontiers is more than just an open-access publisher of scholarly articles: it is a pioneering approach to the world of academia, radically improving the way scholarly research is managed. The grand vision of Frontiers is a world where all people have an equal opportunity to seek, share and generate knowledge. Frontiers provides immediate and permanent online open access to all its publications, but this alone is not enough to realize our grand goals.

Frontiers Journal Series

The Frontiers Journal Series is a multi-tier and interdisciplinary set of open-access, online journals, promising a paradigm shift from the current review, selection and dissemination processes in academic publishing. All Frontiers journals are driven by researchers for researchers; therefore, they constitute a service to the scholarly community. At the same time, the Frontiers Journal Series operates on a revolutionary invention, the tiered publishing system, initially addressing specific communities of scholars, and gradually climbing up to broader public understanding, thus serving the interests of the lay society, too.

Dedication to Quality

Each Frontiers article is a landmark of the highest quality, thanks to genuinely collaborative interactions between authors and review editors, who include some of the world's best academicians. Research must be certified by peers before entering a stream of knowledge that may eventually reach the public - and shape society; therefore, Frontiers only applies the most rigorous and unbiased reviews.
Frontiers revolutionizes research publishing by freely delivering the most outstanding research, evaluated with no bias from both the academic and social point of view. By applying the most advanced information technologies, Frontiers is catapulting scholarly publishing into a new generation.

What are Frontiers Research Topics?

Frontiers Research Topics are very popular trademarks of the Frontiers Journals Series: they are collections of at least ten articles, all centered on a particular subject. With their unique mix of varied contributions from Original Research to Review Articles, Frontiers Research Topics unify the most influential researchers, the latest key findings and historical advances in a hot research area! Find out more on how to host your own Frontiers Research Topic or contribute to one as an author by contacting the Frontiers Editorial Office: researchtopics@frontiersin.org

RECENT ADVANCES IN DROSOPHILA CELLULAR AND HUMORAL INNATE IMMUNITY

Topic Editors:
Susanna Valanne, Tampere University, Finland
Dan Hultmark, Umeå University, Sweden
Laura Vesala, Tampere University, Finland

Citation: Valanne, S., Hultmark, D., Vesala, L., eds. (2020). Recent Advances in Drosophila Cellular and Humoral Innate Immunity. Lausanne: Frontiers Media SA. doi: 10.3389/978-2-88966-191-6

Table of Contents

frontiers in Immunology

EDITORIAL
published: 02 October 2020
doi: 10.3389/fimmu.2020.598618

Editorial: Recent Advances in *Drosophila* Cellular and Humoral Innate Immunity

Laura Vesala[1], *Dan Hultmark*[2] *and Susanna Valanne*[1]*

[1] Faculty of Medicine and Health Technology, Tampere University, Tampere, Finland, [2] Department of Molecular Biology, Umeå University, Umeå, Sweden

Keywords: ***Drosophila melanogaster*, innate immunity, cellular immunity, humoral immunity, model for human diseases, metabolism, bacteria, host-pathogen interaction**

Editorial on the Research Topic

Recent Advances in Drosophila Cellular and Humoral Innate Immunity

We are pleased to present our Research Topic for *Frontiers in Immunology*, focusing on "Recent Advances in *Drosophila* Cellular and Humoral Innate Immunity". This collection of articles is comprised of primary research articles and reviews of the current literature by *Drosophila* immunity experts. Therefore, the papers feature progress in our understanding of the *Drosophila melanogaster* immune responses against a wide variety of pathogens, covering bacteria, viruses and parasites.

In many insects, bacterial infection induces the production of bactericidal and fungicidal peptides, such as cecropins, defensins, diptericins, and drosomycins, which accumulate in the hemolymph (1, 2). Besides these humoral effectors, Uttenweiler-Joseph et al. (3) identified several other *Drosophila* immune-induced molecules (DIMs or IMs) in the fly hemolymph. Their functions remained unknown until recently, when it was shown that twelve related IMs, the Bomanins (Boms), form a family that participates in the defense against some fungi and bacteria (4). Now, Lin et al. have characterized a gene called Bombardier (bbd), which regulates the defense mediated by the short-form Boms. Bombardier mutants are defective in their Toll pathway-dependent resistance against pathogens; especially candidacidal activity is completely dependent on Bombardier and the short-form Boms. Furthermore, Cohen et al. have identified a function for two other IMs, renamed Daisho1 and Daisho2, which are specifically involved in the defense against filamentous fungi.

Whereas the pathways regulating bacterial defenses are quite rigorously studied (5, 6), we still have limited knowledge about the antiviral immune defense in *Drosophila*. Best understood is the RNA interference (RNAi) system, which is believed to be the major defense against RNA viruses (7). This system recognizes double-stranded RNA molecules, cuts them into 21-nucleotide siRNAs, and uses them as templates to recognize and destroy viral RNA. Here, Torri et al. have investigated how two key components in this defense, Dicer-2 (Dcr-2) and Argonaute 2 (AGO2), are modulated in response to viral infection. Both factors were rapidly upregulated in virus-infected animals. Interestingly, only protein levels were affected, not mRNA, suggesting that these effects are post-transcriptionally controlled. Moreover, Trammell and Goodman have reviewed the emerging mechanisms of using *Drosophila* as a tool to study arthropod-borne viruses (arboviruses) that pose a great global health risk to humans. RNAi, JAK/STAT pathway and induction of STING-mediated immunity have been shown to be involved. The nutritional status of flies in the *Drosophila* model as well as of the vector mosquitoes appears to be an important factor in antiviral defense: while mosquitoes use an RNAi-dependent response during starvation, the bloodmeal provides the

OPEN ACCESS

Edited and reviewed by:
Miki Nakao,
Kyushu University, Japan

***Correspondence:**
Susanna Valanne
susanna.valanne@tuni.fi

Specialty section:
This article was submitted to Comparative Immunology, a section of the journal Frontiers in Immunology

Received: *25 August 2020*
Accepted: *17 September 2020*
Published: *02 October 2020*

Citation:
Vesala L, Hultmark D and Valanne S (2020) Editorial: Recent Advances in Drosophila Cellular and Humoral Innate Immunity. Front. Immunol. 11:598618. doi: 10.3389/fimmu.2020.598618

insulin needed to activate a JAK/STAT-dependent response during infection. The authors conclude that *Drosophila* is an invaluable tool to study arboviruses, but because *Drosophila* are not the natural host for these arboviruses, there are also limitations.

Drosophila blood cells, the hemocytes, have traditionally been divided into three distinct classes; phagocytic plasmatocytes, melanizing crystal cells and lamellocytes, the larval immune-induced hemocyte type. The currently ongoing burst of hemocyte research has revealed a more complex system, identifying intermediate stages and sub-classes, some of which are likely to have functional significance (8–13). Shim et al. contribute to the growing pool of hemocyte research with their findings of two distinct plasmatocyte populations, with different functions in metabolic regulation and maintaining organismal homeostasis. Iwashita et al. studied the function of Gyc76A, a guanylate cyclase type receptor producing cyclic guanosine monophosphate (cGMP), in immune responses. They show that Gyc76A is required for hemocyte proliferation during bacterial infection, by activation of a small GTPase Ras85D-dependently rather than cGMP-dependently. Gyc76A is also involved in the antimicrobial peptide response, but that effect is elicited *via* cGMP-dependent protein kinase DG2 and components of the Toll pathway. Thus, Gyc76A is involved in regulation of both, humoral and cellular immune responses via different routes.

Infections cause major metabolic adjustments in immune cells and at systemic level, balancing the needs of the immune system and the organismal homeostasis (14–16). Understanding these events has wide implications, and, not surprisingly, they have recently attracted growing attention. Parupalli et al. have now directly investigated how hemocytes affect nutrition and growth in *Drosophila* development. They show that ablation of hemocytes leads to reduced growth and insulin insensitivity, resulting in minute flies. A similar phenotype was seen when the larvae were fed a high sugar diet, but the effect could be rescued by genetically activating the hemocytes. Their experiments demonstrate the intimate crosstalk between hemocytes and fat body in controlling the distribution of nutritional resources.

Mitochondria are the central energy-producing organelles in the eukaryotic cells. In their review, Salminen and Vale address the role of mitochondrial variation in innate immunity. This variation may arise from both, the nuclear and the mitochondrial genomes, and through the mito-nuclear interactions. They discuss how mitochondrial variation affects the Krebs cycle metabolites, production of adenosine triphosphate and reactive oxygen species, and how these factors alter the infection outcomes. They also describe the benefits of utilizing *Drosophila* to study the nuclear variation affecting mitochondrial functions and how to construct cytoplasmic hybrid (cybrid) fly strains to study the mtDNA variation apart from variation arising from the nuclear genome.

Vincent et al. show that *Francisella novida* infection leads to metabolic dysregulation in control flies but not in imd pathway mutant flies. Their data indicate that in the *Drosophila-F. novicida* host-pathogen model, imd pathway activation is necessary but not sufficient for the metabolic pathology. Most likely both the host and bacterial factors contribute to the metabolic dysregulation, which is also seen with other infection models. Davoodi and Foley have reviewed the current knowledge of *Vibrio cholerae* pathogenesis in *Drosophila*. *V. cholerae* is a gram-negative pathogen causing pandemic outbreaks of cholera, a diarrheal disease. About three million cases are estimated to occur per year, resulting in 100,000 deaths. *D. melanogaster* has been used for modelling the *V. cholerae* pathogenesis since the foundational study in 2005, where it was shown that continuous feeding of *V. cholerae* to adult flies caused a cholera-like disease resulting in weight loss and rapid death. In the last 15 years, complex interactions between the pathogen, host defense, intestinal microbiome and metabolism have been uncovered.

In order to understand host-pathogen interactions and the underlying causes of infection outcomes, it is important to characterize molecules secreted by the pathogens. Nonaka et al. performed a structural and functional analysis of Monalysin, a pore-forming toxin from the entomopathogenic bacterium *Pseudomonas entomophila*. By purifying the endogenous Monalysin, they confirmed its action as a pore-forming toxin and suggest that it might preferably target cell membranes at curved sites, such as tips of filopodia. Their study adds to knowledge on detailed defense mechanisms against toxins. Kenney et al. set out to investigate the properties of Excreted-Secreted (ES) products from the nematode *Heterorhabditis bacteriophora*. Concentrated ES products were shown to inhibit the activity of *Diptericin* and to also enable the infection of *Drosophila* by *Photorhabdus luminescens*, symbiotic bacteria from the *H. bacteriophora* nematode. It will be interesting to characterize and identify the specific proteins in the secretions—these proteins bear potential for the treatment of diseases caused by excessive immune activation.

Parasitoid wasps, such as those belonging to the genus *Leptopilina*, lay their eggs inside *Drosophila* larvae. Along with the egg, they inject venom containing a variety of proteins and vesicles, thought to facilitate parasitoid growth (17). Wan et al. concentrated on these vesicles, which they named venosomes. They found that these extracellular vesicles function as a transport system to deliver venom factors into the lamellocytes, a hemocyte important in defense against parasitoids in *D. melanogaster*. This is sufficient to impair the lamellocyte function. The authors theorize that the venosome-cell interaction could be seen as a level of host-pathogen interactions.

As emphasized already above, *D. melanogaster* is a plastic model for studies from research on evolutionarily conserved basic cellular mechanisms to complex human diseases. Lin et al. have investigated the pathogenic effect of the mutant Huntingtin protein (mHTT), that causes the Huntington disease in humans, in the *Drosophila* model. It was demonstrated that overexpression of mHTT in the nervous system causes lethality, whereas overexpressing mHTT in an immune-reactive tissue, i.e. hemocytes, did not cause direct lethality but immune dysregulation. Future studies will be needed to clarify the molecular interaction between mHTT and the main *Drosophila* immune signaling pathways as well as suppression of phagocytosis. The role of immunity and inflammation in aging and

age-related diseases, i.e. "inflammaging", is another pressing question, as the mean population age increases (18). Arora and Ligoxygakis have reviewed the current understanding of the role of immunity in age-dependent neurodegeneration in *Drosophila*. Is inflammation the cause or consequence of neurodegeneration? Predisposition to an overactive immunity, e.g. by loss of negative regulation of the Imd pathway or loss of autophagy, causes neurodegeneration. On the other hand, immunity can also be neuroprotective, as Draper, the glial engulfment receptor, is important in preventing the accumulation of amyloid structures found in Alzheimer's disease -associated phenotypes in *Drosophila*.

Lastly, Belmonte et al. discuss in their review the profound differences between sexes in response to infection. As in humans (19), *D. melanogaster* shows strong sexual differences in immune responses at baseline, upon pathogen challenge and in aging. In their extensive literature search, they found that fewer than 10% of immunological studies on *Drosophila* have only used one sex or have not separated their subjects by sex. What can *Drosophila* teach us about immune dimorphism? Including both sexes in functional and mechanistic studies of *Drosophila* immunity gives a more complete picture on the complexity of immune mechanisms. It also increases our understanding of the fundamental mechanisms underlying innate immunity mechanisms and responses to infection.

The field of *Drosophila* immunity has broadened considerably in recent years and it is now in a very productive and exciting phase. This is nicely illustrated in this collection of articles. We would like to thank all the authors for their contributions to this Research Topic as well as the reviewers for their time and input.

AUTHOR CONTRIBUTIONS

All authors contributed to the article and approved the submitted version.

FUNDING

The Drosophila work in Tampere University was carried out in the Tampere Drosophila Facility, partly funded by Biocenter Finland. DH was supported by the Swedish Research Council, the Swedish Cancer Society, the Academy of Finland and the Sigrid Juselius Foundation.

REFERENCES

1. Hultmark D. Immune reactions in *Drosophila* and other insects, a model for innate immunity. *Trends Genet* (1993) 9:178–83. doi: 10.1016/0168-9525(93)90165-E
2. Bulet P, Hetru C, Dimarcq JL, Hoffmann D. Antimicrobial peptides in insects; structure and function. *Dev Comp Immunol* (1999) 23:329–44. doi: 10.1016/S0145-305X(99)00015-4
3. Uttenweiler-Joseph S, Moniatte M, Lagueux M, Van Dorsselaer A, Hoffmann JA, Bulet P. Differential display of peptides induced during the immune response of *Drosophila*: A matrix-assisted laser desorption ionization time-of-flight mass spectrometry study. *Proc Natl Acad Sci U S A* (1998) 95:11342–7. doi: 10.1073/pnas.95.19.11342
4. Clemmons AW, Lindsay SA, Wasserman SA. An effector peptide family required for *Drosophila* Toll-mediated immunity. *PLoS Pathog* (2015) 11:e1004876. doi: 10.1371/journal.ppat.1004876
5. Valanne S, Wang JH, Rämet M. The *Drosophila* Toll signaling pathway. *J Immunol* (2011) 186(2):649–56. doi: 10.4049/jimmunol.1002302
6. Myllymäki H, Valanne S, Rämet M. The *Drosophila* imd signaling pathway. *J Immunol* (2014) 192(8):3455–62. doi: 10.4049/jimmunol.1303309
7. Bronkhorst AW, van Rij RP. The long and short of antiviral defense: small RNA-based immunity in insects. *Curr Opin Virol* (2014) 7:19–28. doi: 10.1016/j.coviro.2014.03.010
8. Anderl I, Vesala L, Ihalainen TO, Vanha-Aho LM, Andó I, Rämet M, et al. Transdifferentiation and Proliferation in Two Distinct Hemocyte Lineages in *Drosophila melanogaster* Larvae after Wasp Infection. *PLoS Pathog* (2016) 12(7):e1005746. doi: 10.1371/journal.ppat.1005746
9. Cattenoz PB, Sakr R, Pavlidaki A, Delaporte C, Riba A, Molina N, et al. Temporal specificity and heterogeneity of *Drosophila* immune cells. *EMBO J* (2020) 39(12):e104486. doi: 10.15252/embj.2020104486
10. Cho B, Yoon S-H, Lee D, Koranteng F, Tattikota SG, Cha N, et al. Single-cell transcriptome maps of myeloid blood cell lineages in *Drosophila*. *Nature Commun* 11(1):4483. doi: 10.1038/s41467-020-18135-y
11. Fu Y, Huang X, Zhang P, van de Leemput J, Han Z. Single-cell RNA sequencing identifies novel cell types in *Drosophila* blood. *J Genet Genomics* (2020) 47(4):175–86. doi: 10.1016/j.jgg.2020.02.004
12. Ramond E, Dudzic JP, Lemaitre B. Comparative RNA-Seq analyses of *Drosophila* plasmatocytes reveal gene specific signatures in response to clean injury and septic injury. *PLoS One* (2020) 15(6):e0235294. doi: 10.1371/journal.pone.0235294
13. Tattikota SG, Cho B, Liu Y, Hu Y, Barrera V, Steinbaugh MJ, et al. Perrimon N. A single-cell survey of *Drosophila* blood. *Elife* (2020) 9:e54818. doi: 10.7554/eLife.54818
14. Wang A, Luan HH, Medzhitov R. An evolutionary perspective on immunometabolism. *Science* (2019) 363:eaar3932. doi: 10.1126/science.aar3932
15. Dolezal T, Krejčová G, Bajgar A, Nedbalova P, Strasser P. Molecular regulations of metabolism during immune response in insects. *Insect Biochem Mol Biol* (2019) 109:31–42. doi: 10.1016/j.ibmb.2019.04.005
16. Yang H, Hultmark D. Tissue communication in a systemic immune response of *Drosophila*. *Fly (Austin)* (2016) 10:115–22. doi: 10.1080/19336934.2016.1182269
17. Poirié M, Colinet D, Gatti J-L. Insights into function and evolution of parasitoid wasp venoms. *Curr Opin Insect Sci* (2014) 6:52–60. doi: 10.1016/j.cois.2014.10.004
18. Franceschi C, Garagnani P, Parini P, Giuliani C, Santoro A. Inflammaging: a new immune–metabolic viewpoint for age-related diseases. *Nat Rev Endocrinol* (2018) 14:576–90. doi: 10.1038/s41574-018-0059-4
19. Klein SL, Flanagan KL. Sex differences in immune responses. *Nat Rev Immunol* (2016) 16:626–38. doi: 10.1038/nri.2016.90

Conflict of Interest: The authors declare that the research was conducted in the absence of any commercial or financial relationships that could be construed as a potential conflict of interest.

frontiers in Immunology

ORIGINAL RESEARCH
published: 17 July 2019
doi: 10.3389/fimmu.2019.01688

Venom Atypical Extracellular Vesicles as Interspecies Vehicles of Virulence Factors Involved in Host Specificity: The Case of a *Drosophila* Parasitoid Wasp

Bin Wan[1†], Emilie Goguet[1†], Marc Ravallec[2], Olivier Pierre[1], Séverine Lemauf[1], Anne-Nathalie Volkoff[2], Jean-Luc Gatti[1‡] and Marylène Poirié[1‡]*

[1] Université Côte d'Azur, INRA, CNRS, ISA, Sophia Antipolis, France, [2] INRA, Univ. Montpellier, UMR 1333 "Microorganism and Insect Diversity, Genomes and Interactions" (DGIMI), Montpellier, France

Endoparasitoid wasps, which lay eggs inside the bodies of other insects, use various strategies to protect their offspring from the host immune response. The hymenopteran species of the genus *Leptopilina*, parasites of *Drosophila*, rely on the injection of a venom which contains proteins and peculiar vesicles (hereafter venosomes). We show here that the injection of purified *L. boulardi* venosomes is sufficient to impair the function of the *Drosophila melanogaster* lamellocytes, a hemocyte type specialized in the defense against wasp eggs, and thus the parasitic success of the wasp. These venosomes seem to have a unique extracellular biogenesis in the wasp venom apparatus where they acquire specific secreted proteins/virulence factors and act as a transport system to deliver these compounds into host lamellocytes. The level of venosomes entry into lamellocytes of different *Drosophila* species was correlated with the rate of parasitism success of the wasp, suggesting that this venosome-cell interaction may represent a new evolutionary level of host-parasitoid specificity.

Keywords: *Drosophila*, immunity, parasitoid wasp, *Leptopilina*, venosomes, lamellocyte, virulence

OPEN ACCESS

Edited by:
Laura Vesala,
University of Tampere, Finland

Reviewed by:
Jianhua Huang,
Zhejiang University, China
Maurizio Francesco Brivio,
University of Insubria, Italy

***Correspondence:**
Marylène Poirié
marylene.poirie@univ-cotedazur.fr

†Present Address:
Bin Wan,
State Key Laboratory of Rice Biology and Ministry of Agricultural and Rural Affairs, Key Laboratory of Molecular Biology of Crop Pathogens and Insects, Institute of Insect Sciences, Zhejiang University, Hangzhou, China
Emilie Goguet,
Henry M. Jackson Foundation at the Uniformed Services University of the Health Sciences, Department of Microbiology and Immunology, Bethesda, MD, United States

‡These authors are co-last authors

Specialty section:
This article was submitted to Comparative Immunology, a section of the journal Frontiers in Immunology

Received: *22 May 2019*
Accepted: *04 July 2019*
Published: *17 July 2019*

Citation:
Wan B, Goguet E, Ravallec M, Pierre O, Lemauf S, Volkoff A-N, Gatti J-L and Poirié M (2019) Venom Atypical Extracellular Vesicles as Interspecies Vehicles of Virulence Factors Involved in Host Specificity: The Case of a Drosophila Parasitoid Wasp. Front. Immunol. 10:1688. doi: 10.3389/fimmu.2019.01688

INTRODUCTION

It is now well-established that cells can communicate at "long distance" using diverse types of membranous particles, called extracellular vesicles (EVs). The release or secretion of EVs is a universal cellular mechanism, shared by archaea, bacteria, and eukaryotes, which probably existed in their last common ancestor (1, 2). Since most organisms interact with each other, one species can also transfer EVs to a different species and thus act on it via that specific interaction. Accordingly, recent data from bacteria, intracellular parasites, and nematodes, have shown that EVs secreted by pathogens participate in the communication and disease transmission between non-infected and infected host cells (3, 4). EVs may play a key role in altering the function of targeted cells during infection, through the spreading of pathogens or the transport of virulence factors (5, 6).

The lifestyle of the hymenopteran endoparasitoid wasps is between those of parasites and predators: they lay eggs in or on the body of other insects, their larvae develop by consuming living host tissues, resulting in the host death (7). To ensure the successful development of eggs

and larvae, parasitoids have developed various mechanisms allowing to bypass the host immune response and regulate its physiology (7, 8). They have notably evolved astonishing strategies for delivering virulence factors into host cells. The production of EVs in parasitoid wasps has been known for a long time and data have revealed their various nature and origin (9–12). Some species use viral genes stably integrated in the wasp genome to build specific vesicles [named polynaviruses (PDVs) or virus-like-particles (VLPs) (9–11)]. These EVs are produced and secreted by the cells of the wasp ovarian calyx, and carry either wasp DNA (PDVs) or proteins (VLPs). Others use a more peculiar means, they produce virulence factors in the venom gland and package them in vesicles stored in the reservoir (both parts of the reproductive tract) (9, 12, 13). In all cases, these parasitoids inject EVs along with the egg during oviposition, which participate in the reproductive success of the wasp. While many parasitoid wasp species produce ovarian EVs, very few described species produce EVs in the venom apparatus (9). Among them are the wasps of the Figitidae family, including the genera *Ganaspis* and *Leptopilina* that parasitize *Drosophila melanogaster* (Diptera) and other closely related species. The venomous EVs of these species differ in shape, size, and structure (12–19), and former publications called them Virus Like Particles (VLPs) because the mature vesicles somehow resembled viruses, particularly those of *L. heterotoma* that showed spikes extending from a round/ovoid vesicle (9, 18). Recently, a proteomic study of *L. heterotoma* VLPs showed that they contain many different proteins. Based on some homology they observed between certain of these proteins and bacterial proteins, the authors proposed to rename the VLPs, mixed strategy extracellular vesicles (MSEV) (19). However, since none of the studies to date have provided indisputable evidence of a viral or bacterial origin of *Leptopilina* VLPs, we will thereafter refer to these venom vesicles with the neutral term "venosomes." This will also avoid any confusion with the vesicles produced in the ovaries of some wasps that truly derive from a viral machinery, also named VLPs (9).

The main defense of insects against parasitic eggs and larvae, called encapsulation, involves the formation of hemocyte layers around the foreign body as well as the production, via the activation of the phenoloxidase (PO) cascade, of melanin and cytotoxic radicals presumed to kill the parasite (20). This wasp-induced reaction is largely used as a model to study the innate immune response and stimulate hematopoiesis in *Drosophila* hosts (21). Indeed, in *D. melanogaster* larva, the process of encapsulation requires the production of different types of hemocyte, including the lamellocytes that are encapsulation-specific cells induced only in case of parasitism (8, 20, 21). Lamellocytes have been identified as targets of *L. heterotoma* purified venosomes. Mixed *in vitro* with these cells, they induce their lysis, a phenomenon also observed after parasitism (12, 22) but whose precise mechanism of action remains unknown.

The parasitism success of different *Leptopilina boulardi* strains from different laboratories differs according to the *Drosophila* species or strain. For instance, two strains with different phenotypes have been characterized, ISm (strain G431, Immune Suppression for *D. melanogaster*), highly virulent against *D. melanogaster*, and ISy (strain G486, Immune Suppression for *D. yakuba*) whose success depends on the resistant/susceptible genotype of the host (23, 24). These strains differ in the relative abundance of their major venom components, with few common abundant proteins and significant quantitative differences for most of them (25). They apparently differ as well in the venosomes present in their reservoir (13). Moreover, one of the proteins in the venom of ISm that seems important for parasitism success is a Rho GTPase activating protein (RhoGAP) named LbGAP (26, 27). LbGAP belongs to a family of genes specifically expressed in the venom glands of both ISm and ISy. ISm LbGAP has been immunolocalized in the lamellocytes of the host after parasitism and the number of LbGAP spots is correlated with the degree of alteration of the lamellocyte morphology (passage from round flat to bipolar), a change supposed to affect their ability to encapsulate the parasitoid egg (28). However, the mechanisms of entry and action of LbGAP into lamellocytes remain unknown. Although the ISy strain venom also contains Rho GAPs, its success mainly relies on a serine protease inhibitor (a serpin called LbSPNy) that inhibits the PO cascade activation in the hemolymph of *Drosophila yakuba* larva, one of its main hosts (29). The LbSPNm allelic serpin that targets different types of proteases from those targeted by LbSPNy is also abundant in the venom of ISm (25).

Based on these previous data, our goal was to clarify the connection between the venom factors described and the venosomes in *L. boulardi* wasps and to study the potential link between these extracellular vesicles and the transport of such factors into host lamellocytes. We demonstrate here that venosomes may have an atypical extracellular biogenesis in the venom gland and that purified venosomes from the venom reservoir are sufficient to mimic the protective effect of the whole venom for the wasp egg. Using fluorescently labeled purified venosomes and co-immunolocalization, we showed that they target the *D. melanogaster* lamellocytes and serve as a specific transport system to deliver venom factors both to the circulating and sessile hemocytes/lamellocytes. Finally, we observed that the level of venosomes entering into lamellocytes is correlated with the success of wasp parasitism on the *Drosophila* species tested, suggesting a key role in the specificity of the host-parasitoid interaction. The parasitoid wasp *L. boulardi* thus appears as an interesting model to study the evolution of extracellular vesicle formation mechanisms and the role played by the vesicular transport in interspecies communication. This new cellular level of parasitoid specificity may also be of interest for understanding the adaptive mechanisms between hosts and parasites.

MATERIALS AND METHODS

Biological Material

The *L. boulardi* strains ISy from Brazzaville (Congo) (Gif stock G486) and ISm from Nasrallah (Tunisia) (Gif stock G431), and the *L. heterotoma* strain from Gotheron (France) have been previously described (23–25). All parasitoids were reared at 25°C on the susceptible *D. melanogaster* strain Nasrallah (Gif stock 1333). After emergence, adults were kept at 20°C on agar

medium with honey. All experiments were performed with naïve, 5–10 days-old mated females.

The *D. melanogaster* strain 1088, named YR for resistant to the *L. boulardi* ISy parasitism, comes from an original selection of isofemale lines obtained from a population of Brazzaville (Congo), combined with subsequent genetic approaches (30–32). *D. melanogaster* hop^{Tum-l} (stock 8492) was obtained from the Bloomington *Drosophila* stock center. The *D. suzukii* strain, kindly provided by Dr. R. Allemand (LBBE, University Lyon 1, France), originates from a population collected in Sainte-Foy-lès-Lyon (Rhône, France). The *D. yakuba* R strain (stock number 307-14) and the *D. simulans* Japanese strain were kindly provided by D. Joly (EGCE, Gif-sur-Yvette, France) and M.T. Kimura (Hokkaido University, Japan), respectively. Based on previous laboratory results (see also Discussion), the *L. boulardi* ISm strain is highly successful on *D. melanogaster* YR and hop^{Tum-l} strains (>90%), less on *D. simulans* (>60% success of parasitism), and it consistently fails on *D. yakuba* and *D. suzukii* (<10 and 0% success of parasitism, respectively). All *Drosophila* were reared on a standard medium (10% cornmeal, 10% yeast, agar, and Nipagine) at 25°C. Conditions for all insects were a 12/12 h light/dark and 50% humidity.

Antibodies

We used "in house" polyclonal rabbit antibodies directed against full-length recombinant proteins for LbGAP (25) and LbGAP2 (33), and synthetic peptides for LbSPN (34) and Atilla, a *D. melanogaster* marker of lamellocytes (35). The anti-LbGAP, anti-LbGAP2, and anti-LbSPN antibodies recognize the ISm and ISy proteins equally. For Western blots, we used them at dilutions 1/10,000 (LbGAP), 1/5,000 (LbGAP2), 1/10,000 (LbSPN), and 1/1,000 (Atilla). LbGAP, LbGAP2, and LbSPN antibodies were all used at a 1/500 dilution for histoimmunochemistry. Secondary antibodies were goat anti-rabbit horseradish peroxidase conjugated (1/10,000, Sigma) for Western blot, and fluorescently labeled goat anti-rabbit IgG (Fluoprobes 594, Interchim; 1/200, and 1/2,000 as indicated) for immunohistochemistry.

Venom Recovery and Purification of Venosomes

The wasp venom apparatus was obtained by traction on the female ovipositor, the reservoir was separated from the glands and dilacerated with tweezers in 20–50 µl drop (1 reservoir per µl; number depending upon the experiment) of Insect Ringer Solution (IR; KCl, 182 mM; NaCl, 46 mM; $CaCl_2$, 3 mM; Tris-HCl, 10 mM) supplemented with a protease inhibitor cocktail (IR-PI) (Sigma). This venom total extract was then centrifuged for 5 min at 500 g to remove residual tissues and obtain the "crude" venom. Crude venom was centrifuged at 15,000 g (15 min; 4°C) to pellet the vesicular material, which was washed twice with IR-PI and used for either SDS-PAGE, labeling, or electron microscopy. The supernatant was the soluble venom proteins fraction. The protein profile of the venosomes obtained by direct centrifugation was compared with that obtained by ultracentrifugation (35,000 g, 1 h; MLA50 rotor, Beckman) on a 10–50% Nycodenz gradient as previously described (12).

SDS-PAGE and Western Blotting

Samples were run under denaturing and reducing (5% ß-mercaptoethanol) conditions on 12.5% polyacrylamide gels. The gels were either stained silver or transferred to a nitrocellulose membrane (Millipore). The membrane was blocked with TBS-Tween, 2% low fat milk, incubated overnight at 4°C with the indicated antibody, and washed and incubated with the goat anti-rabbit HRP secondary antibody for 2 h at RT. After washing, a signal was detected with a chemiluminescent substrate (Luminata Western, Millipore) with a digital camera. None of the preimmune sera or secondary antibody alone produced a significant signal.

Electron Microscopy

15,000 g venosome pellets were processed for transmission electron microscopy as described in Labrosse et al. (14). Briefly, samples were fixed in sodium cacodylate (0.1M, pH 7.2 for venosomes) or PBS (for the venom apparatus) with 5% glutaraldehyde for 24 h at 4°C. Post-fixation was done with 2% osmium tetroxide in the same buffers, followed by dehydration in a graded ethanol series prior to inclusion in Epon and ultrafine section. The sections were contrasted with uranyl acetate and lead citrate before observation (Jeol 1010 and Zeiss EM10CR, 80 kV).

For immunogold labeling, 24 venom apparatus (gland and reservoir) from ISm and ISy females were fixed for 3 h in 4% paraformaldehyde −0.1 M phosphate at 4°C. Samples were included in agarose blocks (8 apparatus per inclusion; three blocks for each strain). The blocks were washed four times in 0.1 M phosphate buffer at RT and dehydrated in ethanol (50–100% at −19°C), before inclusion in the resin (London Resin White; TAAB Lab Equipment; −25°C for 48 h under UV). Ultrafine sections (70 nm) were mounted on grids treated with colloidal gold, washed in PBS, and blocked in PBS-1% BSA before incubation with the LbGAP antibody (1/1,000; 1 h 30 at 20°C) (this last step was omitted for controls). After several washes in PBS-1% BSA and then in PBS-0.1% BSA, all the grids were incubated with a goat anti-rabbit antibody conjugated to 15-nm gold particles (1/30; Biocell Research Lab.). After washing, sections were stained with 1% uranyl acetate and examined under an electron microscope (JEOL 1010 at 80 kV). All observations (controls and processed) were performed on successive sections of a block for each wasp strain. Sections from several blocks were observed and photograph.

Microinjection

The venosome pellet obtained from 20 reservoirs was resuspended in 20 µl of IR and labeled with 1 mM of Fluoprobes 488-NHS ester (1 mg/ml; λexc./λem.: 593/519 nm; Interchim) for 1 h at 4°C. The labeled vesicles were centrifuged at 15,000 g (10 min at 4°C) and washed once with IR-3% BSA to quench the free ester, and again with IR. The last pellet was resuspended in IR and used to micro-inject 50 second-instar host larvae (FemtoJet, Eppendorf). Hemolymph was collected 14–18h after microinjection.

To test the phagocytic properties of the hemocytes *in vivo,* fluorescent latex beads (carboxylate-modified polystyrene latex beads 2 µm in diameter, fluorescent red; Sigma) or fluorescent

live *Escherichia coli* (5×10^9 bacteria/ml; *E. coli* DH5 alpha expressing the green fluorescent protein) were microinjected in *Drosophila* L2 larvae 14–18 h after parasitism (to stimulate the hemocytes production). The observations were made 4 h after the injection of beads or bacteria. The experiments were repeated 3 times for each species tested, on different days.

Parasitism Assay

For immunohistochemistry of hemocytes, batches of 30 second-instar larvae (L2) were collected and transferred on a dish with *Drosophila* medium to be subjected to parasitism by three female wasps for 4 h. The parasitoids were then removed, and the larvae were left at 25°C until use (see below). For the parasitism experiments, 30 second-instar host larvae (L2) were parasitized for 2 h by one ISm or ISy parasitoid female. The encapsulation capacity was estimated 48 h later by counting the number of encapsulated eggs after dissection of the late third-instar larvae. Virulence was expressed as the ratio of the number of non-encapsulated parasitoid eggs to that of the mono-parasitized hosts. To analyze the immunosuppressive role of the different fractions of ISm venom (crude venom, 15,000 g venom pellet, 15,000 g venom supernatant), larvae of *D. melanogaster* YR were injected with 20 nl of each of these fractions using a Nanoject II injector (Drummond Scientific). The samples were

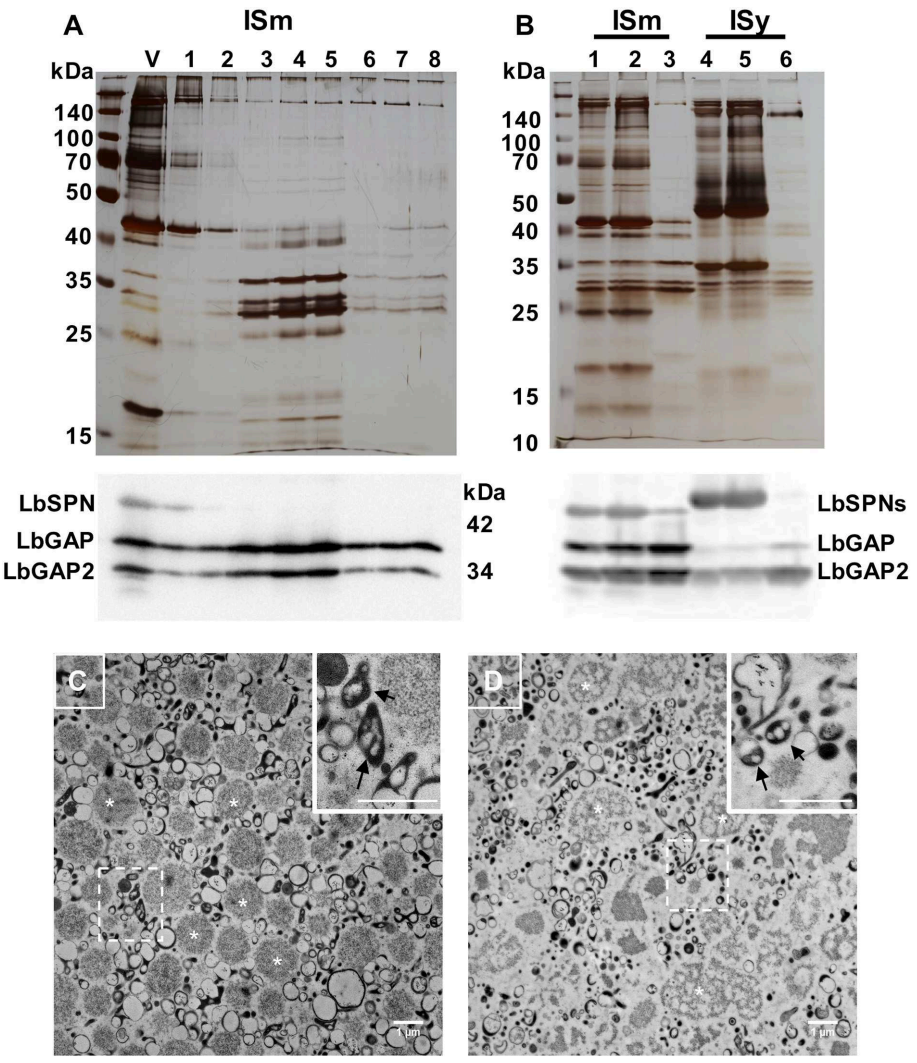

FIGURE 1 | *L. boulardi* ISm and ISy venosomes are enriched in LbGAP and LbGAP2. **(A)** Crude ISm venom (V) was ultra-centrifuged on a 10–50% Nicodenz gradient, and each of the recovered fractions (1 top to 8 bottom) were separated on a 12% SDS-PAGE (upper figure). The venosomes migrated on fractions 3–5 in which the ∼30 kDa LbGAP and LbGAP2 proteins were enriched but not LbSPN (∼45 kDa) as shown by the western blot analysis (lower figure). **(B)** Proteins in ISm and ISy crude venom (lanes 1 and 4, respectively), 15,000 g supernatant (lanes 2 and 5) and pellet (lanes 3 and 6) separated by SDS-PAGE and visualized by silver-staining (upper figure) or after western blot with the anti-LbGAP, LbGAP2, and LbSPN antibodies (lower figure). In both cases, the protein complexity is reduced in the 15,000 g pellet and the LbGAP and LbGAP2 proteins are enriched while the LbSPN proteins remain in the supernatant as shown on the western blots. **(C,D)** TEM of fixed ISm **(C)** and ISy **(D)** 15,000 g pellets showing diverse types of vesicles and aggregates including the previously described venosomes [indicated by arrows in the insert showing the enlargement from dashed square zone (Bar = 1 μm)]. Examples of the large vesicles/aggregates type (in the 1 μm range) are indicated by white asterisk.

obtained from 20 female reservoirs diluted in 20 µl of IR, this volume being kept constant so that a 1/50th equivalent of a reservoir was injected for each fraction. A total of 150 larvae (5 independent repeats of 30 larvae) were injected for each sample, then parasitized by ISy female parasitoids, and encapsulation occurred an estimated 48 h later on surviving larvae, as described above. The controls were injected with IR alone.

Hemolymph and Hemocyte Collection

Drosophila larvae were removed from the food and washed carefully three times in PBS. Their hemolymph was then collected directly in a drop of 35 µl of PBS (SDS-PAGE) or Grace's medium (Immunochemistry) by gently tearing the cuticle on the anterior part of the larvae with fine tweezers. For SDS-PAGE, the cells were separated by centrifugation (500 g, 10 min) and the supernatant was collected (cleared hemolymph). The cells pellet was washed twice in PBS and the last pellet and the cleared hemolymph were diluted in reducing sample buffer and boiled for SDS-PAGE. At least three separate experiments were done.

Tissue Immunohistochemistry and Confocal Observation

Hemocyte Immunohistochemistry

The hemolymph of *Drosophila* larvae was collected at various time points (as indicated) after parasitism or micro-injection with labeled venosomes. At each time point, the hemolymph was collected from 10 larvae as described above, and the hemolymph solution was transferred to the center of a coverslip placed in a 12-well culture plate to form a wet chamber. The cells were allowed to adhere for 1 h before a 15 min fixation step with 4% formaldehyde in PBS. The cells were then washed three times with PBS, permeated with PBS-T (PBS + 0.1% Triton 100X) for 15 min and blocked with PBS 0.3% BSA for 30 min. The cells were incubated for 1 h with a primary antibody at RT, washed three times with PBS and incubated for 1 h with the secondary antibody. After three washes with PBS and one with deionized water, the coverslip was mounted on a slide using an antifading medium containing DAPI (Interchim). Data were obtained from at least three separate experiments.

Long Gland Immunohistochemistry

Complete venom apparatuses were fixed in 4% formaldehyde 0.1% Triton 100X for 3 h. After that, they were washed three times with PBS and blocked with PBS 0.3% BSA for 30 min. The primary antibody was added and incubated for 1 h, washed three times 15 min with PBS, and incubated with the secondary antibody for 1 h at RT. After three PBS washes, venom apparatuses were mounted between a slide and a coverslip, as described above. 5 apparatuses were treated per experiment and the experiment was repeated at least four times.

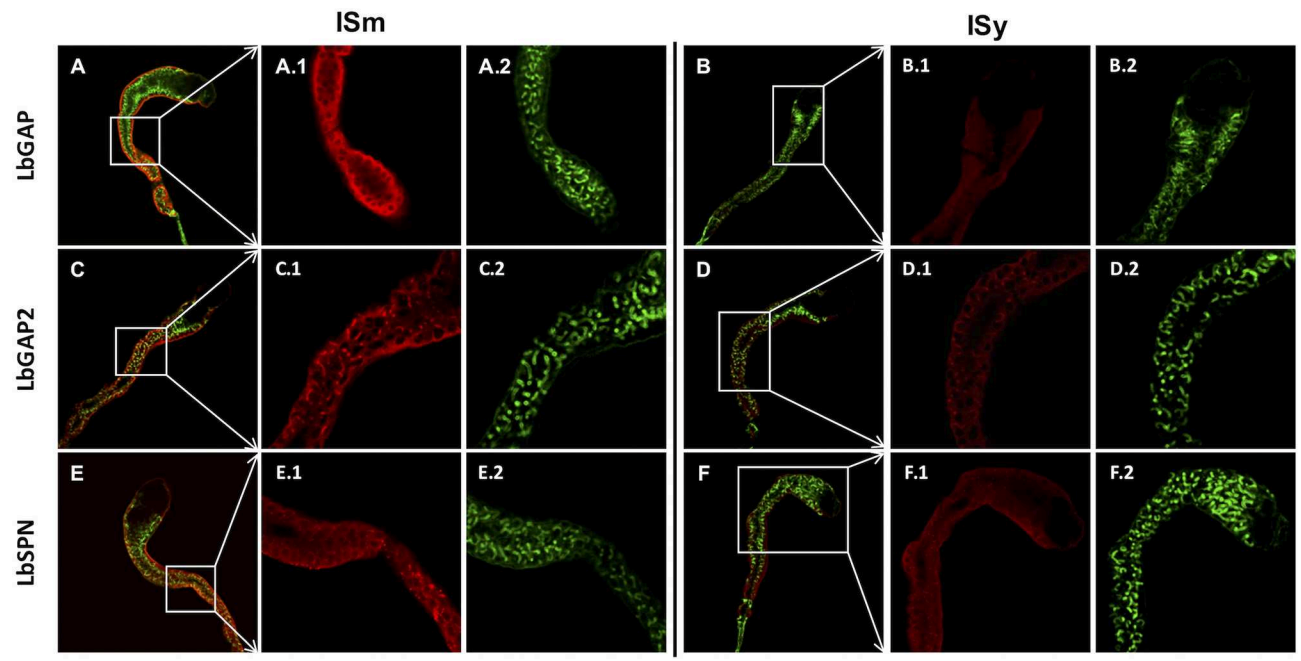

FIGURE 2 | Immunolocalization of venom virulence factors along the venom gland of ISm and ISy females. Confocal immunolocalization of LbGAP **(A,B)**, LbGAP2 **(C,D)**, and LbSPN **(E,F)** in the ISm **(A,C,E)** and ISy **(B,D,F)** venom gland. **(A–F)** Show merged images obtained from the entire gland for the indicated virulence factors (red fluorescence) and counter-stained for actin with green phalloidin. All panels numbered 1 and 2 are enlargement of the indicated gland region (white boxes) for the virulence factors (red) and actin (green), respectively. Labeling of the three virulence factors was observed in the cytoplasm of the peripheral gland secretory cells and associated with the canal of these cells whose microvilli actin was strongly labeled by phalloidin. For both strains, the absence of labeling in the gland collecting canal is either due to the loss of the contents during the staining process or to a masking due to the presence of cuticular layers that may block the light.

For both types of preparation, the actin was stained with green phalloidin (7 nM; green fluorescent phalloidin 490, Interchim) during the permeabilization step. Controls were done with the pre-immune sera from the rabbit used for immunization and with the secondary antibody alone. The highest background signal obtained was used to establish the level above which a labeling was considered positive. The samples were observed and imaged with an AxioImager Z1 equipped with an Apotome 2 or with a LSM 880 laser scanning confocal microscope (Zeiss).

Clarification and Observation of *Drosophila* Larvae

YR larvae were fixed overnight, 15 h after injection of fluorescently labeled venosomes, with 4% PFA in PBS at 4°C, in the dark. After washing with PBS, the samples were transferred to a glass vial for a clearing procedure based on the 3DISCO method (36). Briefly, the samples were dehydrated overnight in 50% Tetrahydrofurane (THF) (Sigma) in the dark while being gently shaken, then for 3 h in 70% THF, overnight at 80% THF and for 30 min at 100% THF, repeated 3 times, followed by final incubation in dichloromethane (Sigma) for 45 min. To ensure optimum transparency, samples were finally impregnated overnight with a dibenzylether (DBE) solution (Sigma). To avoid tissue damage or shrinkage, they were mounted in a Lab-Tek II (Lab-Tek) chamber filled with the DBE solution. As DBE degrades fluorescence over time, the visualization was made as soon as the appropriate transparency level was reached. To obtain high resolution scans, samples were imaged by confocal microscopy. 3–5 larvae were treated in three different batches.

Statistical Analysis

Statistics were done using R (https://www.r-project.org). For the number of lamellocyte cells labeled with LbGAP in the different species, we used a binomial GLMM [package lme4 (37)] with the species as a fixed effect and the repetition as a random effect. Since there was no overdispersal in the model, the fixed effect was tested with an LRT-test, followed by a Tukey *post-hoc* test [package multcomp (38)]. For the number of spots in the lamellocytes, we first used a zero truncated Poisson GLM [VGAM package (39)] with the species as a fixed effect. However, since there was a high dispersal in this model, we instead fitted a linear model to the Box-cox transformed number of lamellocyte cells, followed by a Tukey *post-hoc* test.

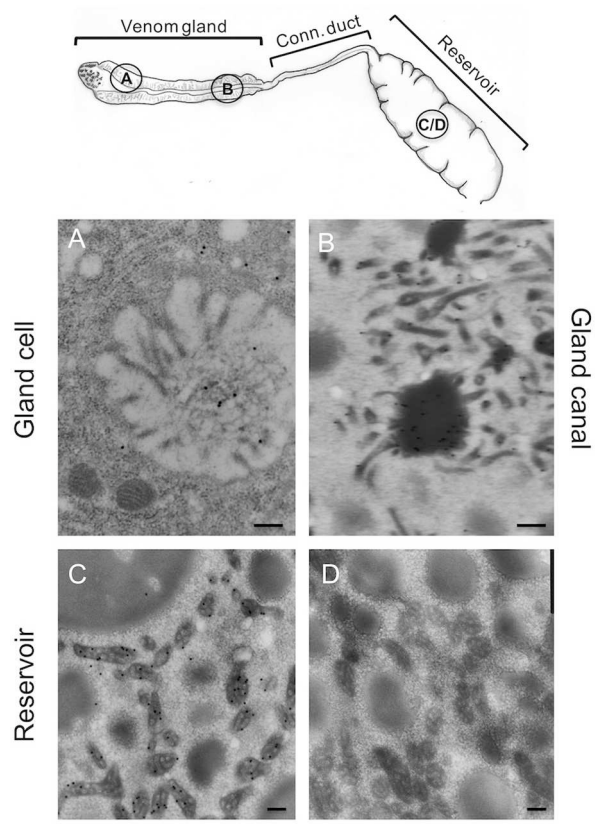

FIGURE 3 | Immunolocalization of LbGAP during the biogenesis of lSm venosomes. Immunogold-labeled TEM sections (see drawing at the top for the position of the sections) through the intracellular canal of a long gland secreting cell **(A)**, the gland canal **(B)**, and the reservoir **(C,D)**. LbGAP immunogold labeling (small black dots) is visible on the amorphic material present in the lumen of secretory cell canal, around in the cytoplasm of the cell and in some intracellular vesicles **(A)**. No secreted membrane vesicles were observed. In the lumen of the gland collecting canal **(B)**, most of the labeling was associated to electron-dense aggregated and fibrous material. No clear fully formed vesicles were visible. In the reservoir **(C)**, gold labeling was almost entirely associated with the mature punctuated venosomes but not with the larger electron dense particles also present. No labeling was observed with the gold secondary antibody alone **(D)**. Representative sections are shown here. Bar 0.2 μm.

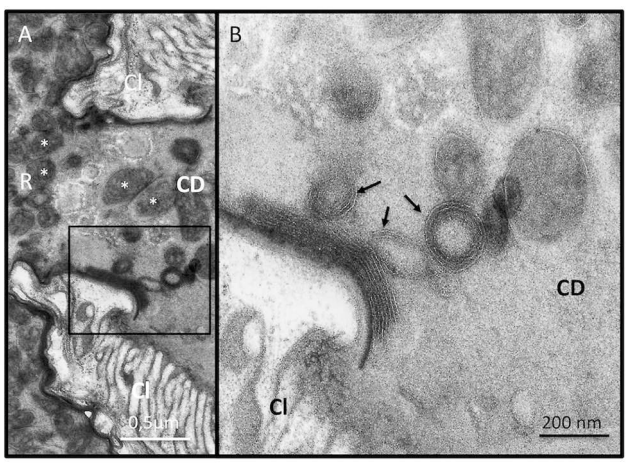

FIGURE 4 | Biogenesis of the membrane of extracellular venosomes. **(A)** TEM observation of a section through the junction between the connecting duct (CD) and the reservoir (R) and an enlargement of the boxed zone **(B)** show stacks of membrane sticking to the lumen side of the cell layer (Cl) located at the junction. Some "rolling" empty membranes detach from the stack and form multimembrane vesicular structures (arrows) incorporating material present in the duct lumen. Punctuated material could also be observed in formed venosomes (in **A**, white asterisk) that are accumulated in the reservoir (R).

RESULTS

LbGAP and LbGAP2 Association With *L. boulardi* Venosomes

The venom apparatus of *L. boulardi* consists of an elongated venom gland (classically named "long gland") with a central collecting canal connected by a thin duct (connecting duct) to a large reservoir in which venom accumulates (see detailed histology of the venom apparatus in **Figure S1**). To determine whether the LbGAP, LbGAP2 and LbSPN *L. boulardi* venom proteins potentially involved in virulence were associated with venosomes, we first purified the venosomes from crude venom obtained from the ISm reservoir using the previously described method of Nycodenz gradient ultracentrifugation (12) (**Figure 1A**). SDS-PAGE of the protein fractions showed that only a specific subset of the venom proteins co-sedimented at the expected position of venosomes in the gradient (fractions 4, about 25–30% Nicodenz). Western blot analysis revealed that LbGAP and LbGAP2, but not LbSPN, were associated with these venosome fractions. In order to confirm this, as well as to simplify and down-size the purification procedure, the crude ISm and ISy venom was directly centrifuged at 15,000 g. The protein profile of the washed pellet contained only a subset of the total proteins, very similar to that of Nycodenz-purified ISm venosomes fractions. Western blot analysis showed that LbGAP and LbGAP2 were enriched in the pellet but not LbSPN, which remained in the supernatant along with many other proteins (**Figure 1B**). Electron microscopy analysis of the pellet showed two main types of vesicles: large round aggregates/vesicles with a size of about 1 μm (asterisk marks; **Figures 1C,D**) and, in the range of 100–300 nm, "typical" venosomes (arrows in enlargements in **Figures 1C,D**) and vesicles with different shapes that were less numerous and structured in ISy than ISm (**Figures 1C,D**). Because the shape of most of these purified vesicles at 100–300 nm appeared to differ from that of the previously "typical" venosomes described in the venom reservoir of *L. boulardi* strains (13, 14), we verified that the procedure did not extensively degrade the venosomes. Since *L. heterotoma* venosomes, in contrast to *L. boulardi* ones, have a specific stellate shape due to spike extensions (12, 17), we treated the crude venom of this species in the same way and analyzed the obtained pellet by microscopy (**Figure S2**). Part of the *L. heterotoma* pelleted vesicles clearly retained the stellate shape, while others resembled more *L. boulardi* ISm and ISy vesicles, with the electron dense material accumulated as an asymmetric crescent or distributed all along the membrane [**Figure S2**; see also Figure 1E in (12)]. This suggests that the treatment may have slightly altered the shape of the venosomes but that the distinctive shapes between the different *Leptopilina* species and strains remained visible.

Since ISm and ISy venosomes were associated with a subset of venom proteins such as LbGAP and LbGAP2 but not with LbSPN, we wondered whether the synthesis and secretion of these factors (and thus the biogenesis of venosomes) could occur sequentially at different or specialized locations along the venom gland. LbGAP, LbGAP2, and LbSPN antibodies (**Figure 2**) labeled the whole ISm (**Figures 2A,C,E**, respectively) and ISy (**Figures 2B,D,F**, respectively) gland (except the "nose" region), although the signal was much weaker for LbGAP in ISy (**Figure 2B**), in agreement with a lower synthesis of this protein in this strain (26, 27) (see also **Figure 1**). The factors were clearly immunolocalized in the secretory cell cytoplasm and in the lumen of these cells' channels (as shown in the respective Figures enlargements) that can be visualized by the phalloidin labeling of actin-rich microvilli as described previously in *L. heterotoma* (17) (see also **Figure S3** for a detailed example of co-localization for LbGAP2 in the ISm cell and secretory cell channel). Therefore, it seems that there is no difference in secretion along the gland between the factors associated and not associated with venosomes. The venosomes of the Figitidae wasps were previously described as having a peculiar assembly in the lumen of the venom gland (15–18), and we therefore studied further how LbGAP could associate with the ISm venosomes by electron microscopy. For this, ultra-thin sections of the ISm venom apparatus were prepared for immunogold electron microscopy using the LbGAP antibody (**Figure 3**). **Figure 3A** show a cross-section through the "canal" of the secretory cells as indicated by the microvilli presence. The canal contains large electron dense particles, without precise form, which were immunogold labeled for LbGAP (**Figure 3A**). In the collecting canal of the gland (**Figure 3B**), large electron-dense particles and long filaments were dispersed in a fibrous/filamentous material. LbGAP was almost exclusively associated with the electron dense particulate materials suggesting proteins aggregation. A cross-section through the ISm reservoir showed venosomes as membranous punctuated-type vesicles (**Figures 3C,D**) and larger uniform electron-dense particles (from 400 nm to 1 μm), with 87% of the LbGAP labeling associated with the venosomes (333 gold beads associated on 383 counted on three different TEM sections) (**Figure 3C**). One of the control cross-sections that passed at the junction between the connecting duct and the reservoir caught our attention (**Figure 4**). At this point, we observed a stack of membranes coming from the cell lining the duct, some of them seeming to roll and detach to form multiple membrane vesicles.

Thus, *L. boulardi* ISm venosomes seem to be built extracellularly from secreted proteins aggregates that modify their form and size along the collecting duct. Since none of the particulate aggregates observed in the ISm gland canal resembled the "mature" membraned venosomes observed in the reservoir (see **Figure 3**), we hypothesized that a specific part of the lumen material could be embedded by the membranes delaminating in the collecting duct near the entry of the reservoir to form the final mature venosomes.

Venosomes Are Sufficient to Protect Susceptible Wasp Eggs From Encapsulation

Since *L. boulardi* ISm venosomes contain putative virulence factors, we tested whether these vesicles were sufficient to replicate the protective effect of venom against encapsulation of eggs of the susceptible ISy strain (14, 23). For this, we used the previously set up assay (14, 24) based on the two different characterized *L. boulardi* strains, ISm, and ISy, and the resistant

TABLE 1 | Outcomes of parasitism after injection of crude venom, 15,000 g venosomes pellet or venom supernatant.

	% of encapsulated parasitoid eggs
ISm parasitism	0
ISy parasitism	94
Ringer injection	94
ISm crude venom injection	40
ISm 15,000 g supernatant injection	98
ISm 15,000 g pellet injection	24

D. melanogaster strain (YR). ISm eggs are never encapsulated in *D. melanogaster* YR larvae, whereas those of ISy almost always are (23, 24) (see **Table 1**). *D. melanogaster* YR larvae injected with extracts of ISm venom apparatus or crude venom and then parasitized with ISy did not encapsulate the parasitoid eggs (14, 24) (**Table 1**). This protective effect of the crude venom against ISy eggs encapsulation was also conferred by injection of the ISm washed 15,000 g pellet containing the venosomes (**Table 1**, mean % of 5 replicates; comparison to injection of ISm crude venom, $\chi^2 = 0.91; p < 0.05$). In contrast, the injection of the supernatant 15,000 g of the ISm venom had no effect (comparison to injection of Ringer, $\chi^2 = 0.711; p < 0.05$).

Venosomes Transport Potential Virulence Factors in Permissive Host Lamellocytes

LbGAP was immunolocalized in lamellocytes after parasitism (27, 28). Also, its physical association with the venosomes led us to postulate that venosomes are responsible for the transport of this protein and other associated proteins in immune cells of the host. To demonstrate this definitively, we immunolocalized LbGAP and LbGAP2 (both associated with venosomes) by confocal microscopy in the hemocytes of *D. melanogaster* YR larvae after parasitism (*in vivo* situation). We also tested by confocal microscopy the co-immunolocalization of LbGAP or LbGAP2 and venosomes in lamellocytes after microinjection of *in vitro* fluorescently-labeled purified venosomes.

Between 0–4 h after the end of ISm parasitism (time laps due to uncertainty since parasitism can occur at any time during the 4 h of contact between wasps and larvae; see mat. and meth.), LbGAP and LbGAP2 mostly immunolocalized in phagocytic plasmatocytes (see also below) since, as expected, there were still no lamellocytes at this time (40). This absence of lamellocytes was also demonstrated by the absence of reaction of this cell type marker Atilla on western-blots of hemocytes proteins (see **Figure S4**). 14–18 h post-parasitism, both LbGAP and LbGAP2 were still observed in plasmatocytes (not shown) and accumulated in the circulating host lamellocytes (**Figures 5A,B**), with the shape of most of these labeled lamellocytes visibly modified from round flat to elongated as previously observed (27, 28) (see unchanged lamellocytes in **Figure 6**). Thus, both proteins associated with venosomes were retrieved in modified lamellocytes after parasitism.

Microinjection of second-instar YR larvae with purified fluorescently-labeled ISm venosomes, induced the differentiation of lamellocytes, like parasitism (**Figure S4**). 18 h post-injection, fluorescent venosomes were observed in plasmatocytes (not shown) and co-immunolocalized with LbGAP or LbGAP2 in these newly formed lamellocytes (**Figures 5C,D**, respectively). This strongly suggests the entry of whole venosomes into the lamellocytes since the chosen NHS-fluorescent dye should mainly label membrane proteins of the venosomes. Interestingly, not all LbGAP and LbGAP2 spots co-localized with labeled venosomes in the lamellocytes (**Figure 5E**), suggesting that a release of these proteins from the membrane envelope occurred after the venosomes enter the cell (this also told us that these proteins were not labeled by the NHS-dye). Moreover, using hemolymph collected at different time points after parasitism (0 h being the end of the parasitism assay) and Western blot analyses, we showed that LbGAP and LbGAP2 (and thus certainly venosomes) still circulate in the cell-free hemolymph of host larvae 20 h post-parasitism by ISm or after microinjection (**Figure S4**). Thus, a continuous entry of venosomes from the hemolymph into the lamellocytes, followed by the release of LbGAP and LbGAP2 in the cell, may explain our observations.

Since parasitoid wasp infestation of *D. melanogaster* induces the release into the circulation of a subcuticular population of sessile hemocytes that will differentiate into lamellocytes (40), we analyzed whether venosomes could also target the hemocytes within this compartment. Eighteen hours after the injection of labeled venosomes, *Drosophila* YR larvae were fixed, chemically treated for tissue clearing (36, 41) and observed by confocal microscopy (**Figure S5**). Fluorescent spots were clustered in the subcuticular regions where sessile hemocytes localize (40). At higher magnification, this labeling co-localized with small (about 5–10 μm) and large flat cells (>30 μm), resembling plasmatocytes and lamellocytes, respectively.

Entry of Venosomes Seems "Specific" to Lamellocytes of Some Species of *Drosophila*

Leptopilina boulardi ISm is considered a specialized parasitoid that succeeds mainly on *D. melanogaster* and *D. simulans* (23, 24). We therefore tested whether the entry of venosomes into lamellocytes depended on the host species. First, to confirm that all the *Drosophila* strains and species used produce lamellocytes, we analyzed the main adhesive hemocytes after parasitism by ISm. As a control, we used hop^{Tum-l} flies since this *D. melanogaster* mutant strain is known to constitutively produce lamellocytes (42). Two main types of cells were observed in the hemolymph of these species/strains 14–18 h after parasitism: (i) round cells of 10–20 μm diameter—resembling macrophage-like plasmatocytes or podocytes described in these species (43–46)—and having a phagocytic function against injected latex beads and *E. coli* bacteria (**Figure S6**), (ii) large flat cells of 30–40 μm diameter, lamellocytes (**Figure 6**, 1st row), which spread

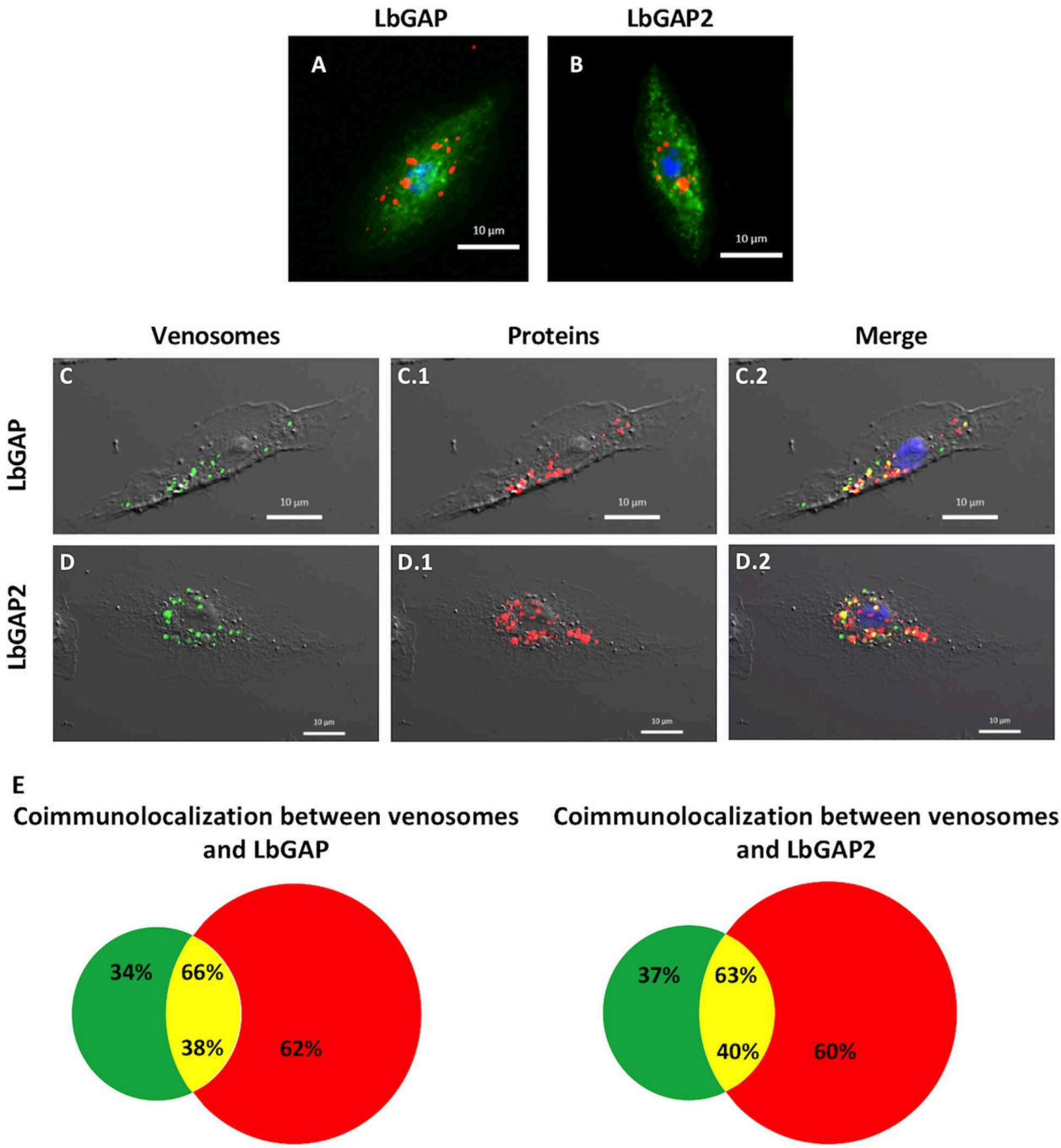

FIGURE 5 | Venosomes co-immunolocalize with virulence factors in *Drosophila* lamellocytes. Immunolocalization of LbGAP **(A)** and LbGAP2 **(B)** by fluorescence microscopy (red spots) in the cytoplasm of bipolar modified lamellocytes of *Drosophila* YR larvae 14–18 h after parasitism by ISm females. Actin labeled with phalloidin (green) and nucleus with DAPI (blue). **(C,D)** Confocal microscopy of YR lamellocytes 18 h after injection of ISm showing fluorescently labeled venosomes (green spots, **C,D**), and LbGAP **(C.1)** and LbGAP2 **(D.1)** immunolocalization (red spots); On the merged images **(C.2,D.2)**, yellow spots indicate where red and green fluorescent spots co-localized. **(E)**, percentages of co-localization between venosomes and LbGAP, and venosomes and LbGAP2 were obtained from merged images (green portion, venosomes alone; red, LbGAP, or LbGAP2 alone; yellow, co-immunolocalization). The percentage of co-localization is expressed either on total venosomes spots (% on top) or on total spots of LbGAP or LbGAP2 (% on bottom). Counted on 61 and 57 cells, respectively, in two separate experiments.

well on slide but do not phagocyte bacteria (**Figure 6**, 2nd row). After parasitism by ISm, LbGAP-containing lamellocytes were found for all species (**Figure 6**, 3rd row), although the number of cells that were reactive differed among species. It was significantly higher in *D. melanogaster* YR than in hop^{Tum-l} ($p = 0.0061$) and *D. yakuba* ($p = 0.019$), and lower in *D. suzukii*

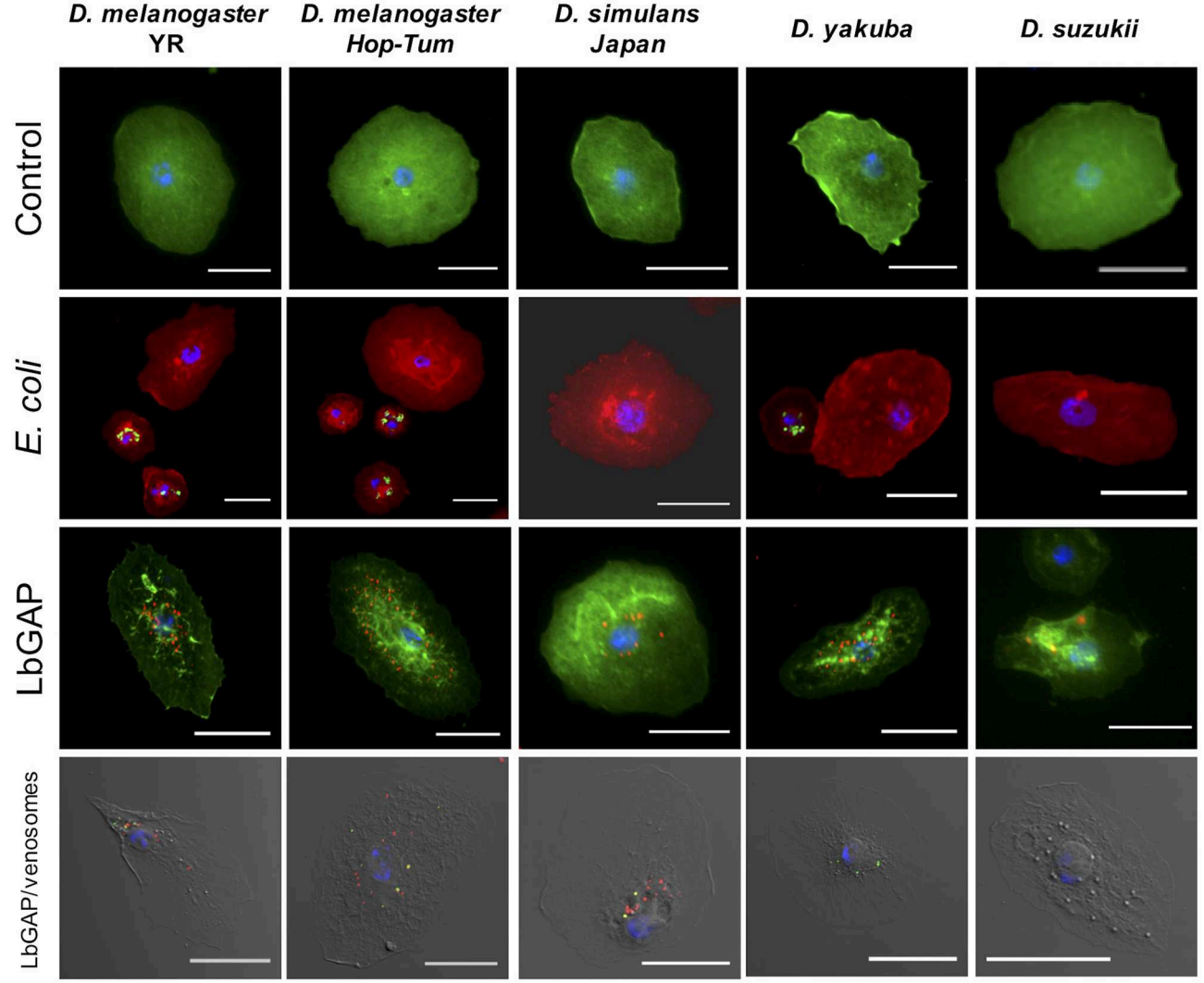

FIGURE 6 | Species-specific entry of venosomes into host lamellocytes. First row: Lamellocytes in the hemolymph of *D. melanogaster* YR and hop^{Tum-l}, *D. simulans*, *D. yakuba,* and *D. suzukii* (actin labeled with green fluorescent phalloidin, nuclei in blue with DAPI) that have retained their "normal" shape (control). Second row: lamellocytes do not contain green fluorescent *E. coli*, indicating the absence of phagocytosis, unlike plasmatocytes (actin labeled with red fluorescent phalloidin; see also **Figure S6**). Third row: LbGAP spots (in red) in the most reactive lamellocytes of the species tested (see also counts in **Figure 7**). Fourth row: the same quantity of ISm labeled venosomes were injected in L2 larvae from the different species. Eighteen hours after injection, venosomes (green spots), LbGAP (red spots), and co-localization of both (yellow spots) were observed by confocal microscopy depending upon the species (none in *D. suzukii*). Bars = 20 μm.

compared to YR ($p < 0.001$), hop^{Tum-l} ($p = 0.043$), and *D. simulans* ($p = 0.015$). *D. yakuba* thus appeared as intermediate between *D. melanogaster*/*D. simulans* and *D. suzukii* (**Figure 7**). The lower number of cells labeled in hop^{Tum-l} compared to YR is probably due to the very large number of lamellocytes produced by this strain. Besides, the maximum amount of LbGAP spots per reactive lamellocyte [which was previously correlated to the lamellocytes change in shape (28)] was higher in *D. melanogaster* compared to *D. yakuba* ($p = 0.028$ for YR, $p = 0.0018$ for hop^{Tum-l}) and *D. suzukii* ($p = 0.017$ for YR, $p = 0.0029$ for hop^{Tum-l}) as well as to *D. simulans* (only for hop^{Tum-l}, $p = 0.0075$), with more than twice that found in these three last species (**Figure 7**). We also microinjected labeled venosomes (**Figure 6**, 4th row) in L2 larvae of the different species and the visual observation of the co-immunolocalization of LbGAP and venosomes indicated an analogous outcome: numerous venosomes and LbGAP spots were observed in a large number of *D. melanogaster* and *D. simulans* lamellocytes, whereas *D. yakuba* lamellocytes contained only a few labeled venosomes, but no LbGAP immunoreaction, suggesting a possible rapid degradation. After microinjection, only few lamellocytes were produced by *D. suzukii* and none were labeled. Thus, the number of labeled lamellocytes and the quantity of LbGAP/venosome they can uptake seemed to match the success rate of parasitism by ISm wasps in these *Drosophila* species [*D. melanogaster* > *D. simulans* >> *D. yakuba* and

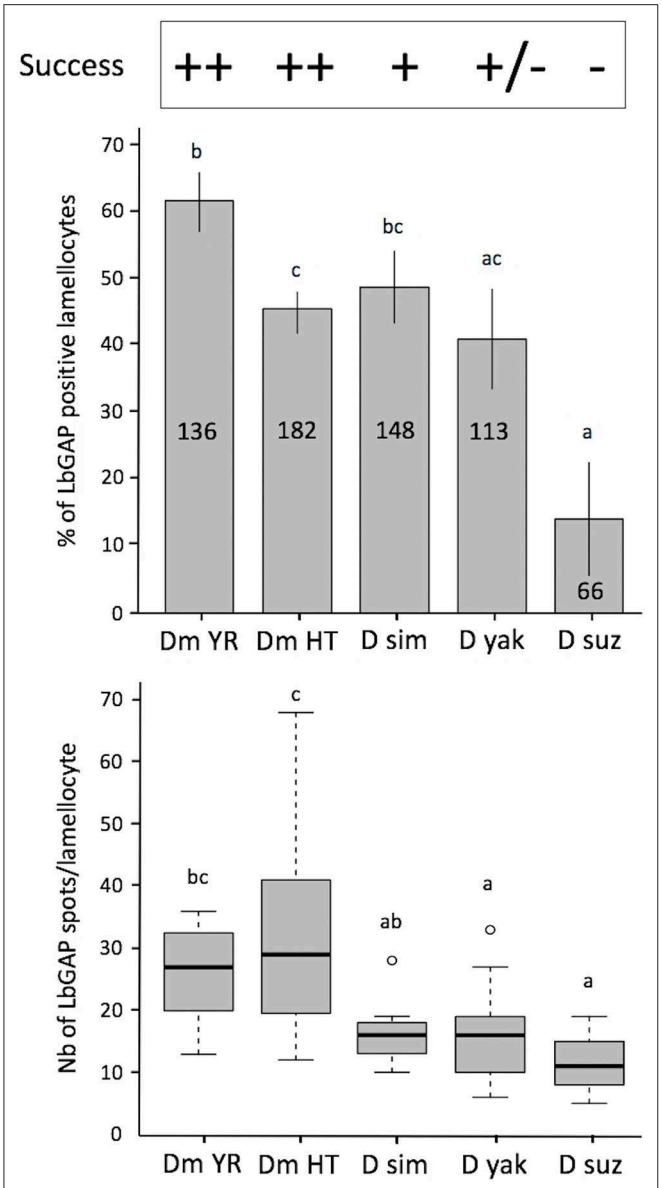

FIGURE 7 | Quantification of LbGAP entry in lamellocytes of the different *Drosophila* species. On the top of the figure the parasitoid success on the different *Drosophila* species is indicated [*D. melanogaster* YR (DmYR) and hop^{Tum-l} (Dm HT), *D. simulans* (D sim), *D. yakuba* (D yak), and *D. suzukii* (D suz)] (++ > 90%; + about 60%; ± < 10%; −0%). **Upper panel**: Percent of LbGAP positive lamellocytes, 18 h after parasitism by ISm females (mean ± s.d). The total number of lamellocytes counted from different fields of at least two separate experiments is indicated on the column (less lamellocytes were found in *D. suzukii* compared to the other species). **Lower panel**: number of LbGAP immunoreactive spots in the most reactive lamellocytes of the different species except for *D. suzukii* where, due to their low number, all reactive lamellocytes with more than one spot were considered (number of lamellocytes: Dm YR, $n = 12$; Dm HT, $n = 12$; D sim, $n = 11$; D yak, $n = 13$; D suz, $n = 3$) (mean ± s.d). Results from two separate experiments. The different letters indicate significant differences ($p < 0.05$).

D. suzukii (see Discussion)]. The increased entry of venosomes into *D. melanogaster* lamellocytes may thus rely on the existence of a specific or more efficient mechanism, restricted or absent in other species.

DISCUSSION

Different types of vesicles are formed by Hymenoptera parasitoid wasps and injected into their hosts to ensure their reproductive success: PDVs and certain VLPs produced in the calyx cell of the wasp ovaries, derived from a viral machinery integrated in the wasp genome during evolution (9–11), and other extracellular vesicles types formed in the venom apparatus for a few reported species, including *Meteorus pulchricornis* (Braconidae: Euphorinae) (47), a polyphagous parasitoid of Lepidoptera larvae, and Figitidae of the genera *Ganaspis* and *Leptopilina* [the latter divided into three clades, *Heterotoma*, *Boulardi*, and *Longipes* (48)], which attack the larvae of *Drosophila* spp.

Venosomes Biogenesis

Mature venosomes have already been described in the venom reservoir of *L. boulardi* ISm and ISy strains (13, 14) but their biogenesis and their associated proteins were not previously reported. The secretory cells of the wasp venom gland secrete an electron-dense anamorphic material with no apparent membrane, also present in the gland canal. For ISm, this material, reactive to LbGAP, was retrieved later specifically associated with fully formed venosomes in the reservoir. It was also only in the reservoir that the venosomes had their ovoid shape with a membrane surrounding an electron-dense material punctuated by small membranous vesicles. Venosomes were more numerous and more structured in ISm compared to ISy, whose venosomes appear to contain less dense material and fewer enclosed vesicles, as previously described in the reservoir of these strains (13). Overall, our results confirm and emphasize that the formation/maturation of venosomes in Figitidae seems to occur extracellularly during the progression of secreted material throughout the gland canal to the reservoir. The venosomes of the *Ganaspis* and *Leptopilina* species studied to date are also 100–400 nm vesicles having different shapes in the reservoir. The biogenesis of venosomes in these species occurs through various stages of aggregation from precursor materials secreted in the lumen of the gland, whereas in the reservoir, venosomes have a pentagonal/hexagonal core with multiple extension or spikes and a distinct membrane [(17, 18); this work]. Those of the *L. boulardi* Lb17 strain differed in shape and biogenesis: small unshaped vesicles were present in the canal of the secretory cells of the gland and referred to as "immature," whereas the venosomes in the mature reservoir were larger, rounded vesicles enclosing a large amount of punctuate/vesicular material resembling those of ISm (18). The authors suggested that venosomes in the reservoir resulted from the maturation of the unshaped vesicles during the transit (18). How venom gland secreted proteins are associated/embedded in venosomes also has not been thoroughly explored. The P40 polyclonal antibody, directed against a protein of *L. heterotoma* venosomes, reacted throughout the gland, and localized with the secreted materials/blocks that assemble to form the final venosomes in which it is associated with the surface and the spikes (16–18). Here, we showed that LbGAP

had a similar secretion/embedding fate during the transit. Since venosomes contain a large number of proteins [(19); see also **Figure 1**] and we only have observations for two of them, it is difficult to identify by which mechanism(s) the secreted material will be integrated in or will be part of mature venosomes. Besides, we showed here that only some of the venom factors studied were associated with vesicles (LbGAP and LbGAP2) while others remained soluble (LbSPN), although they were all secreted throughout the gland and quantitatively important in the venom. This suggests that this process is not a simple progressive maturation of pre-existing vesicles along the cell or canals of the gland, but involves a specific mechanism of association. Our observation of extracellular membrane stacks at the junction between the connecting duct and the reservoir in the ISm strain led us to propose that the inclusion of a specific material and the final formation of the vesicles may occur at this place. This peculiar mode of extracellular vesicle formation, very different from the classical secretion of cellular exosomes or microvesicles (1–3) and from the intracellular mechanism of formation of PDVs and VLPs (10, 11), will deserve further investigation for definitive confirmation and elucidation. One may also wonder about the specific packaging mechanism of only certain secreted proteins in the venosomes. Subsequent studies are needed to determine whether the unincorporated proteins present in the luminal fluids are in a form (i.e., non-aggregated form) different from those apparently packaged. Alternatively, the different proteins may have specific sequence patterns (possibly unknown) or modification(s) to consider. The RhoGAPs sequences, composed mainly of the RhoGAP domain, have no particular motif identified so far but possible post-translational modifications of the packaged proteins have not yet been analyzed.

Role of Venosomes

Purified VLPs of *L. heterotoma* induce lamellocyte lysis of hop^{Tum-l} larvae *in vitro*, and TEM observation suggested that these vesicles may enter the cytoplasm of these cells (12, 16, 22, 49). The association of the P40/P42 protein with *L. heterotoma*/*L. victoriae* venosomes and its immunolocalization in lamellocytes incubated with the venom of the reservoir led to postulate that the venosomes deliver associated proteins or toxins to lamellocytes (16, 19, 22). Based on our previous observations that LbGAP immunolocalized as "large spots" in *D. melanogaster* lamellocytes (27), we also suggested the association of LbGAP with *L. boulardi* venosomes, thus facilitating its entry into these cells. Here, the role of *L. boulardi* ISm venosomes in the active immune protection of the wasp egg has been clearly demonstrated by (i) the protection of *L. boulardi* ISy eggs from encapsulation by YR flies provided by the injection of purified ISm venosomes, (ii) immunolocalization of LbGAP and LbGAP2 in host lamellocytes whose shape was modified after ISm parasitism or microinjection of purified venosomes, and (iii) co-localization of these putative virulence factors in host modified lamellocytes together with *in vitro* fluorescently-labeled venosomes microinjected into the host. Since about 60% of LbGAP or LbGAP2 was not associated with venosomes in this last experiment, they may have already been released within the cell compartments, with the mechanism and timing of delivery still to be identified. Interestingly, although part of the circulating venosomes may be removed from the circulation by the phagocytes, the presence of free venosomes in the hemolymph seems to last long enough to continuously block newly formed lamellocytes, thus weakening the immune system of the larvae and disrupting encapsulation, and protecting also newly hatched parasitoid larvae. Moreover, *L. boulardi* venosomes appear to target not only circulating hemocytes, but also sessile hemocytes in *D. melanogaster*, suggesting that parasitism may also impair their functions. Thus, whatever their shape or the presence or absence of spikes, venosomes enter host lamellocytes. We can therefore conclude that they are "vehicles" for potential virulence factors with intracellular targets in the host, which parasitic wasps use to counter host immunity.

Role of Transported Factors

The role and intracellular targets of proteins transported in lamellocytes (and maybe plasmatocytes whose function may be altered although no apparent morphological changes were observed) remain largely hypothetical. LbGAP interacts *in vitro* and in yeast two-hybrid experiments with Rac1 and Rac2 (27), two Rho GTPases essential for the encapsulation process (34, 50, 51), but we still await validation of these targets in lamellocytes. LbGAP2, as well as other members of the venom LbGAP family, bears mutations in the active site as well as sites important for the interaction with GTPases (25). The association of these others RhoGAPs with venosomes still needs to be tested. The way in which LbGAP2 (and maybe the other RhoGAPs) affects the physiology of lamellocytes and whether they have evolved new functions related to their mutations is still enigmatic. The high concentration of LbGAP and LbGAP2 in the venosomes could in any case facilitate their targeted quantitative delivery and their action at the cellular level. There is still a lack of information on whether venosomes may be found in other host tissues than lamellocytes and plasmatocytes. Induced apoptosis of hematopoietic precursors in the lymph gland of *Drosophila* by *L. heterotoma* and *L. victoriae* envenomation has been suggested (22), but this has recently been reexamined (52). Improving our approach using fluorescently labeled venosomes combined with larval clarification could help solving this question in the future.

Species Specific Venosome Entry

We finally evaluated the level of venosomes entry in lamellocytes from various species of *Drosophila* to assess the specificity and thus the conservation of the involved mechanism(s). The observation of a much higher entry level of ISm LbGAP (and thus venosomes) in the lamellocytes of *D. melanogaster* and *D. simulans* [two species on which the parasitoid succeeds (43)], compared with *D. yakuba* and *D. suzukii* [very low or no parasitism success, (43–45, 53)] suggests the existence of a specific or, at least, more effective mechanism of targeting/uptake in the lamellocytes of these two species. Elucidating such mechanism will include identifying the mode of entry of the venosomes and the potential lamellocytes membrane receptors involved. Our data then suggest that a new "vesicle-cell" interaction level may take part in the host-parasitoid specificity

in addition to behavioral aspects, physiological adequacy and venom factors/targets interaction.

In conclusion, extracellular vesicles are most likely vectors used by many pathogens or parasites to propagate or transport virulence factors. We have clearly shown here that some parasitoid wasps use very unusual vesicles, assembled extracellularly in their venom apparatus, to transport and target specific potential virulence factors important for successful parasitism. Thus, these wasp species represent an interesting model to explore the role of EVs in inter-species communication, in particular to control the immune response of the host, a field that has not been investigated yet.

DATA AVAILABILITY

All datasets generated for this study are included in the manuscript/**Supplementary Files**.

AUTHOR CONTRIBUTIONS

BW performed light and fluorescence microscopy, venosomes purifications and labeling, microinjection, SDS-PAGE, and Western blotting. MR and A-NV performed transmission electron microscopy. OP set up the larval clarification protocol and helped with confocal microscopy. EG and SL performed venosomes purification and encapsulation assays. BW, J-LG, and MP wrote the manuscript. J-LG and MP designed and coordinated the work. All authors have read and approved the final manuscript.

FUNDING

This work received support from the Department of Plant Health and Environment (SPE) of the French National Institute for Agricultural Research (INRA), the Provence, Alpes, Côte d'Azur (PACA) region, the Investments for the Future LABEX SIGNALIFE (ANR-11-LABX-0028) and the European Union's Seventh Framework Program for research, technological development, and demonstration, under grant agreement no. 613678 (DROPSA). BW was funded by the DROPSA program.

ACKNOWLEDGMENTS

We thank Dr. H. Mathé-Hubert for the statistic analyses. Dr. D. Colinet for helpful discussion, C. Rebuf for technical assistance and P. Sansigre for participation in the preliminary experiments. We also thank C. Labrosse, S. Trassard, and P.Y. Sizaret (François Rabelais University, Tours) for the first electron microscopy studies and their help for immunogold electron microscopy. Fluorescent *E. coli* were a gift from MP. Nawrot-Esposito (BES team, ISA). We also thank the Plate-Forme d'Infectiologie Expérimentale (PFIE; INRA-Nouzilly) for the production of rabbit antibodies, and the ISA microscopy platform (SPIBOC).

SUPPLEMENTARY MATERIAL

The Supplementary Material for this article can be found online at: https://www.frontiersin.org/articles/10.3389/fimmu.2019.01688/full#supplementary-material

REFERENCES

1. Cicero Lo A, Stahl PD, Raposo G. Extracellular vesicles shuffling intercellular messages: for good or for bad. *Curr Opin Cell Biol*. (2015) 35:69–77. doi: 10.1016/j.ceb.2015.04.013
2. Maas SLN, Breakefield XO, Weaver AM. Extracellular vesicles: unique intercellular delivery vehicles. *Trends Cell Biol*. (2017) 27:172–88. doi: 10.1016/j.tcb.2016.11.003
3. Coakley G, Maizels RM, Buck AH. Exosomes and other extracellular vesicles: the new communicators in parasite infections. *Trends Parasitol*. (2015) 31:477–89. doi: 10.1016/j.pt.2015.06.009
4. Kuipers ME, Hokke CH, Smits HH, Nolte-'t Hoen ENM. Pathogen-derived extracellular vesicle-associated molecules that affect the host immune system: an overview. *Front Microbiol*. (2018) 9:957–13. doi: 10.3389/fmicb.2018.02182
5. Coakley G, McCaskill JL, Borger JG, Simbari F, Robertson E, Millar M, et al. Extracellular vesicles from a helminth parasite suppress macrophage activation and constitute an effective vaccine for protective immunity. *Cell Rep*. (2017) 19:1545–57. doi: 10.1016/j.celrep.2017.05.001
6. Ofir-Birin Y, Regev-Rudzki N. Extracellular vesicles in parasite survival. *Science*. (2019) 363:817–8. doi: 10.1126/science.aau4666
7. Godfray HCJ. *Parasitoids: Behavioral and Evolutionary Ecology*. Chicago: Princeton University Press (1994).
8. Carton Y, Poirié M, Nappi AJ. Insect immune resistance to parasitoids. *Insect Sci*. (2008) 15:67–87. doi: 10.1111/j.1744-7917.2008.00188.x
9. Gatti JL, Schmitz A, Colinet D, Poirié M. Diversity of virus-like particles in parasitoids' venom: viral or cellular origin. In: Beckage N, Drezen J-M, editors. *Parasitoid Viruses, Symbionts, and Pathogens*. London: Academic Press (2012). p. 181–92. doi: 10.1016/B978-0-12-384858-1.00015-1
10. Gauthier J, Drezen J-M, Herniou EA. The recurrent domestication of viruses: major evolutionary transitions in parasitic wasps. *Parasitology*. (2017) 145:713–23. doi: 10.1017/S0031182017000725
11. Pichon A, Bézier A, Urbach S, Aury JM, Jouan V, Ravallec M, et al. Recurrent DNA virus domestication leading to different parasite virulence strategies. *Sci Adv*. (2015) 1:e1501150. doi: 10.1126/sciadv.1501150
12. Rizki RM, Rizki TM. Parasitoid virus-like particles destroy *Drosophila* cellular immunity. *Proc Natl Acad Sci USA*. (1990) 87:8388–92. doi: 10.1073/pnas.87.21.8388
13. Dupas S, Brehelin M, Frey F, Carton Y. Immune suppressive virus-like particles in a *Drosophila* parasitoid: significance of their intraspecific morphological variations. *Parasitology*. (1996) 113:207–12. doi: 10.1017/S0031182000081981
14. Labrosse C, Carton Y, Dubuffet A, Drezen JM, Poirié M. Active suppression of *D. melanogaster* immune response by long gland products of the parasitic wasp *Leptopilina boulardi*. *J Insect Physiol*. (2003) 49:513–22. doi: 10.1016/S0022-1910(03)00054-4
15. Morales J, Chiu H, Oo T, Plaza R, Hoskins S, Govind S. Biogenesis, structure, and immune-suppressive effects of virus-like particles of a *Drosophila* parasitoid, *Leptopilina victoriae*. *J Insect Physiol*. (2005) 51:181–95. doi: 10.1016/j.jinsphys.2004.11.002
16. Chiu H, Morales J, Govind S. Identification and immuno-electron microscopy localization of p40, a protein component of immunosuppressive virus-like particles from *Leptopilina heterotoma*, a virulent parasitoid wasp of *Drosophila*. *J Gen Virol*. (2006) 87:461–70. doi: 10.1099/vir.0.81474-0
17. Ferrarese R, Morales J, Fimiarz D, Webb BA, Govind S. A supracellular system of actin-lined canals controls biogenesis and release of virulence factors in parasitoid venom glands. *J Exp Biol*. (2009) 212:2261–8. doi: 10.1242/jeb.025718

18. Gueguen G, Rajwani R, Paddibhatla I, Morales J, Govind S. VLPs of *Leptopilina boulardi* share biogenesis and overall stellate morphology with VLPs of the heterotoma clade. *Virus Res.* (2011) 160:159–65. doi: 10.1016/j.virusres.2011.06.005
19. Heavner ME, Ramroop J, Gueguen G, Ramrattan G, Dolios G, Scarpati M, et al. Novel organelles with elements of bacterial and eukaryotic secretion systems weaponize parasites of *Drosophila*. *Curr Biol*. (2017) 27:2869–77. doi: 10.1016/j.cub.2017.08.019
20. Nappi AJ. Cellular immunity and pathogen strategies in combative interactions involving *Drosophila* hosts and their endoparasitic wasps. *Invert Surviv J*. (2010) 7:198–210. Available online at: www.isj.unimo.it/index.php/ISJ/article/download/222/137/
21. Banerjee U, Girard JR, Goins LM, Spratford CM. *Drosophila* as a genetic model for hematopoiesis. *Genetics*. (2019) 211:367–417. doi: 10.1534/genetics.118.300223
22. Chiu H, Govind S. Natural infection of *D. melanogaster* by virulent parasitic wasps induces apoptotic depletion of hematopoietic precursors. *Cell Death Differ*. (2002) 9:1379–81. doi: 10.1038/sj.cdd.4401134
23. Dubuffet A, Dupas S, Frey F, Drezen J-M, Poirié M, Carton Y. Genetic interactions between the parasitoid wasp *Leptopilina boulardi* and its *Drosophila* hosts. *Heredity*. (2007) 98:21–7. doi: 10.1038/sj.hdy.6800893
24. Dubuffet A, Colinet D, Anselme C, Dupas S, Carton Y, Poirié M. Variation of *Leptopilina boulardi* success in *Drosophila* hosts: what is inside the black box? *Adv Parasitol*. (2009) 70:147–88. doi: 10.1016/S0065-308X(09)70006-5
25. Colinet D, Deleury E, Anselme C, Cazes D, Poulain J, Azema-Dossat C, et al. Extensive inter- and intraspecific venom variation in closely related parasites targeting the same host: the case of Leptopilina parasitoids of *Drosophila*. *Insect Biochem Mol Biol*. (2013) 43:601–11. doi: 10.1016/j.ibmb.2013.03.010
26. Labrosse C, Stasiak K, Lesobre J, Grangeia A, Huguet E, Drezen JM, et al. A RhoGAP protein as a main immune suppressive factor in the *Leptopilina boulardi* (Hymenoptera, Figitidae)-*Drosophila melanogaster* interaction. *Insect Biochem Mol Biol*. (2005) 35:93–103. doi: 10.1016/j.ibmb.2004.10.004
27. Colinet D, Schmitz A, Cazes D, Gatti J-L, Poirié M. The origin of intraspecific variation of virulence in a eukaryotic immune suppressive parasite. *PLoS Pathog*. (2010) 6:e1001206. doi: 10.1371/journal.ppat.1001206
28. Colinet D, Schmitz A, Depoix D, Crochard D, Poirié M. Convergent use of RhoGAP toxins by eukaryotic parasites and bacterial pathogens. *PLoS Pathog*. (2007) 3:e203. doi: 10.1371/journal.ppat.0030203
29. Colinet D, Dubuffet A, Cazes D, Moreau S, Drezen J-M, Poirié M. A serpin from the parasitoid wasp *Leptopilina boulardi* targets the *Drosophila* phenoloxidase cascade. *Dev Comp Immunol*. (2009) 33:n681–9. doi: 10.1016/j.dci.2008.11.013
30. Russo J, Brehelin M, Carton Y. Haemocyte changes in resistant and susceptible strains of *D. melanogaster* caused by virulent and avirulent strains of the parasitic wasp *Leptopilina boulardi*. *J Insect Physiol*. (2001) 47:167–72. doi: 10.1016/S0022-1910(00)00102-5
31. Carton Y, Frey F, Nappi A. Genetic determinism of the cellular immune reaction in *Drosophila melanogaster*. *Heredity*. (1992) 69:393–9. doi: 10.1038/hdy.1992.141
32. Delpuech JM, Frey F, Carton Y. Genetic and epigenetic variation in suitability of a *Drosophila* host to three parasitoid species. *Can J Zool*. (1994) 72:1940–4. doi: 10.1139/z94-263
33. Colinet D, Kremmer L, Lemauf S, Rebuf C, Gatti J-L, Poirié M. Development of RNAi in a *Drosophila* endoparasitoid wasp and demonstration of its efficiency in impairing venom protein production. *J Insect Physiol*. (2014) 63:56–61. doi: 10.1016/j.jinsphys.2014.02.011
34. Sampson CJ, Valanne S, Fauvarque M-O, Hultmark D, Rämet M, Williams MJ. The RhoGEF Zizimin-related acts in the *Drosophila* cellular immune response via the Rho GTPases Rac2 and Cdc42. *Dev Comp Immunol*. (2012) 38:160–8. doi: 10.1016/j.dci.2012.05.004
35. Honti V, Kurucz E, Csordás G, Laurinyecz B, Márkus R, Andó I. *In vivo* detection of lamellocytes in *Drosophila melanogaster*. *Immunol Lett*. (2009) 126:183–4. doi: 10.1016/j.imlet.2009.08.004
36. Ertürk A, Becker K, Jährling N, Mauch CP, Hojer CD, Egen JG, et al. Three-dimensional imaging of solvent-cleared organs using 3DISCO. *Nat Protoc*. (2012) 7:1983–95. doi: 10.1038/nprot.2012.119
37. Bates D, Mächler M, Bolker B, Walker S. Fitting linear mixed-effects models using lme4. *J Stat Soft*. (2015) 67:1–48. doi: 10.18637/jss.v067.i01
38. Hothorn T, Bretz F, Westfall P. Simultaneous inference in general parametric models. *Biom* J. (2008) 50:346–63. doi: 10.1002/bimj.200810425
39. Yee TW. *VGAM: Vector Generalized Linear and Additive Models*. R package version 1 0-3 (2017). Available online at: https://CRAN.R-project.org/package=VGAM
40. Márkus R, Laurinyecz B, Kurucz E, Honti V, Bajusz I, Sipos B, et al. Sessile hemocytes as a hematopoietic compartment in *Drosophila melanogaster*. *Proc Natl Acad Sci USA*. (2009) 106:4805–9. doi: 10.1073/pnas.0801766106
41. Richardson DS, Lichtman JW. Clarifying tissue clearing. *Cell*. (2015) 162:246–57. doi: 10.1016/j.cell.2015.06.067
42. Luo H, Hanratty WP, Dearolf CR. An amino acid substitution in the *Drosophila* hop^{Tum-l} Jak kinase causes leukemia-like hematopoietic defects. *EMBO J*. (1995) 14:1412–20. doi: 10.1002/j.1460-2075.1995.tb07127.x
43. Dupas S, Poirié M, Frey F, Carton Y. Is parasitoid virulence against multiple hosts adaptive or constrained by phylogeny? A study of *Leptopilina* spp. (Hymenoptera: Figitidae)/*Drosophila* (Diptera: Drosophilidae) interactions. *Ann Soc Entomol Fr*. (2013) 49:222–31. doi: 10.1080/00379271.2013.815045
44. Kacsoh BZ, Schlenke TA. High hemocyte load is associated with increased resistance against parasitoids in *Drosophila suzukii*, a relative of *D. melanogaster*. *PLoS ONE*. (2012) 7:e34721. doi: 10.1371/journal.pone.0034721
45. Chabert S, Allemand R, Poyet M, Eslin P, Gibert P. Ability of European parasitoids (Hymenoptera) to control a new invasive Asiatic pest, *Drosophila suzukii*. *Biol Control*. (2012) 63, 40–7. doi: 10.1016/j.biocontrol.2012.05.005
46. Brehélin M. Insect haemocytes: a new classification to rule out the controversy. In: Arcier JM, Boemare N, Bonami JR, Vivares CP, Brehelin M, editors. *Immunity in Invertebrates. Cells, Molecules and Defense Reactions*. (Berlin: Springer-Verlag). (1986). p.1–223.
47. Suzuki M, Tanaka T. Virus-like particles in venom of *Meteorus pulchricornis* induce host hemocyte apoptosis. *J Insect Physiol*. (2006) 52:602–13. doi: 10.1016/j.jinsphys.2006.02.009
48. Allemand R, Lemaitre C, Frey F, Boulétreau M, Vavre F, Nordlander G, et al. Phylogeny of six African Leptopilina species (Hymenoptera: Cynipoidea, Figitidae), parasitoids of *Drosophila*, with description of three new species. *Ann Soc Entomol Fr*. (2002) 38:319–32. doi: 10.1080/00379271.2002.10697346
49. Rizki RM, Rizki TM. Selective destruction of a host blood cell type by a parasitoid wasp. *Proc Natl Acad Sci USA*. (1984) 81:6154–8. doi: 10.1073/pnas.81.19.6154
50. Fauvarque MO, Williams MJ. *Drosophila* cellular immunity: a story of migration and adhesion. *J Cell Sci*. (2011) 124:1373–82. doi: 10.1242/jcs.064592
51. Williams MJ, Andó I, Hultmark D. *Drosophila melanogaster* Rac2 is necessary for a proper cellular immune response. *Genes Cells*. (2005) 10:813–23. doi: 10.1111/j.1365-2443.2005.00883.x
52. Anderl I, Vesala L, Ihalainen TO, Vanha-aho L-M, Andó I, Rämet M, et al. Transdifferentiation and proliferation in two distinct hemocyte lineages in *Drosophila* melanogaster larvae after wasp infection. *PLoS Pathog*. (2016) 12:e1005746. doi: 10.1371/journal.ppat.1005746
53. Iacovone A, Ris N, Poirié M, Gatti J-L. Time-course analysis of *Drosophila suzukii* interaction with endoparasitoid wasps evidences a delayed encapsulation response compared to *D. melanogaster*. *PLoS ONE*. (2018) 13:e0201573. doi: 10.1371/journal.pone.0201573

Conflict of Interest Statement: The authors declare that the research was conducted in the absence of any commercial or financial relationships that could be construed as a potential conflict of interest.

frontiers in Immunology

ORIGINAL RESEARCH
published: 04 October 2019
doi: 10.3389/fimmu.2019.02372

Heterorhabditis bacteriophora Excreted-Secreted Products Enable Infection by *Photorhabdus luminescens* Through Suppression of the Imd Pathway

Eric Kenney[1], *John M. Hawdon*[2], *Damien O'Halloran*[1,3] *and Ioannis Eleftherianos*[1]*

[1] *Infection and Innate Immunity Lab, Department of Biological Sciences, George Washington University, Washington, DC, United States,* [2] *Department of Microbiology, Immunology, and Tropical Medicine, George Washington University, Washington, DC, United States,* [3] *Institute for Neuroscience, Department of Biological Sciences, George Washington University, Washington, DC, United States*

Upon entering the hemocoel of its insect host, the entomopathogenic nematode *Heterorhabditis bacteriophora* releases its symbiotic bacteria *Photorhabdus luminescens*, which is also a strong insect pathogen. *P. luminescens* is known to suppress the insect immune response independently following its release, but the nematode appears to enact its own immunosuppressive mechanisms during the earliest phases of an infection. *H. bacteriophora* was found to produce a unique set of excreted-secreted proteins in response to host hemolymph, and while basal secretions are immunogenic with regard to *Diptericin* expression through the Imd pathway, host-induced secretions suppress this expression to a level below that of controls in *Drosophila melanogaster*. This effect is consistent in adults, larvae, and isolated larval fat bodies, and the magnitude of suppression is dose-dependent. By reducing the expression of *Diptericin*, an antimicrobial peptide active against Gram-negative bacteria, the activated excreted-secreted products enable a more rapid propagation of *P. luminescens* that corresponds to more rapid host mortality. The identification and isolation of the specific proteins responsible for this suppression represents an exciting field of study with potential for enhancing the biocontrol of insect pests and treatment of diseases associated with excessive inflammation.

Keywords: parasitic nematode, *Drosophila*, innate immunity, Imd pathway, *Heterorhabditis*, *Photorhabdus*

OPEN ACCESS

Edited by:
Susanna Valanne,
University of Tampere, Finland

Reviewed by:
Anchalee -Tassanakajon,
Chulalongkorn University, Thailand
Friederike Ebner,
Free University of Berlin, Germany

***Correspondence:**
Ioannis Eleftherianos
ioannise@gwu.edu

Specialty section:
This article was submitted to Comparative Immunology, a section of the journal Frontiers in Immunology

Received: *06 July 2019*
Accepted: *20 September 2019*
Published: *04 October 2019*

Citation:
Kenney E, Hawdon JM, O'Halloran D and Eleftherianos I (2019) Heterorhabditis bacteriophora Excreted-Secreted Products Enable Infection by Photorhabdus luminescens Through Suppression of the Imd Pathway. Front. Immunol. 10:2372. doi: 10.3389/fimmu.2019.02372

INTRODUCTION

The early steps of a *Heterorhabditis bacteriophora* infection are well-described with regard to the physical actions of the parasite. Upon migration to a host, the majority of the infective juveniles (IJ) enter the insect through natural openings, although the IJ can generate tears in the intersegmental membrane to gain entry (1). Once the parasite enters the hemocoel environment, the nematode slowly releases, following a 30-min lag time, the bacterial endosymbiont *Photorhabdus luminescens* that it maintains as a secondary phase in its gut (2). When considering the molecular host-parasite interactions that determine the success of an infection after IJ entry, *Photorhabdus* often draws

a substantial amount of interest due to its assortment of proteases and other factors that can suppress the insect immune response and lead to rapid death. However, it is crucial to recall that axenic nematodes are still capable of inciting insect mortality without their symbiont (3). Furthermore, numerous reports have shown that the immune-based neutralization of the nematode is possible. While IJs have been shown to evade encapsulation in *Tipula oleracea, Popillia japonica, and Cyclocephala borealis* (4, 5), the Colorado potato beetle *Leptinotarsa decemlineata* prevents IJ development through encapsulation, in which the process of hemocyte attachment to the parasite begins as quickly as 15 min after entry, a period comfortably preceding the release of bacteria (6). Generally, the degree of melanization and encapsulation of the IJ has been shown to correlate to the survival of the insect (7), so the nematode must to some degree fare for itself in terms of immune suppression during the early phase of an infection. Additionally, *Heterorhabditis* has a vested interest in promoting *Photorhabdus* survival, so some early IJ-based immune suppression may also be targeted toward developing a more hospitable hemolymph environment for its symbiont.

Much of the work centered on the entomopathogenic nematode infection process has used *Steinernema carpocapsae*. A pair of serine protease inhibitors from this nematode have been found to impair hemocyte aggregation, prevent clotting fibers from forming properly, inhibit the digestive enzymes of the host, and prevent the inclusion of melanin into clots formed in the hemolymph (8, 9). The bulk secreted proteins have also been found to be lethal when injected into *Drosophila melanogaster* adult flies (10), clearly indicating that the nematode plays a strong role in the molecular aspect of the infection aside from merely releasing its symbiotic bacteria. Less is known about the activity of the specific molecules produced by *H. bacteriophora*, but genome and transcriptome studies have predicted a variety of secreted factors (11, 12) and genes for a putative metalloprotease, enolase, and chitinase have been implicated in parasitism specifically (13). Genes for C-type lectin and catalase have also been found to be upregulated upon activation of the nematode, where the former is believed to play a role in immune evasion and the latter a role in protecting the parasite from free radicals. Both are expressed in other parasitic helminths, with the lectin being found in a range of nematodes from *Meloidogyne javanica* to *Ancylostoma ceylanicum* (14).

The molecular effects of an *H. bacteriophora* infection are likely the product of a collection of these effectors fulfilling a variety of roles, each of which is important for understanding the host-parasite relationship, but a number of practical applications await the identification of specific individual factors. Autoimmune disease, for instance, is believed to be exacerbated by the loss of natural associations with helminth parasites, and individual immunosuppressive factors isolated from nematodes could be effective treatments for conditions like Crohn's disease, asthma, or multiple sclerosis due to their specificity of action and tolerability (15). Entomopathogenic nematodes (EPNs) including *H. bacteriophora* are also currently used as biocontrol agents against insect pests (16), and manipulating these nematodes to make them more effective parasites could increase their efficacy. Other EPNs including *S. carpocapsae* are also viable options for biocontrol, but it is important to consider that not every EPN is as successful as others against a given host. When infecting the carob moth *Ectomyelois ceratoniae*, *S. carpocapsae* is dramatically more adept at overwhelming the host, with an LC_{50} of 2.02 IJs per larva as opposed to the 426.92 IJs required for the same activity by *H. bacteriophora* (17). When infecting the tomato leaf miner *Tuta absoluta,* however, *H. bacteriophora* is just as effective if not more so than *S. carpocapsae* (18). With this in mind, an optimal approach to developing strong biocontrol would not ignore either species.

Here we examine the immunosuppressive effects of *H. bacteriophora* bulk secretions on the *Drosophila melanogaster* immune system, and depict the degree to which this suppression compromises the insect with regard to susceptibility to a bacterial infection. Because the nematode's symbiont *P. luminescens* is such a strong pathogen, we hypothesize that the organisms have polarized each other's role in the infection and *H. bacteriophora* has become more specialized for immune suppression during the early phases of an infection for the benefit of the nematode as well as its symbiont.

MATERIALS AND METHODS

Insect and Bacterial Strains

Galleria mellonella larvae were acquired from Petco and *Manduca sexta* from DBDPet. Fly stocks were maintained on a cornmeal-soy-based diet (Meidi laboratories) with added baker's yeast and incubated at 25°C on a 12-h day-night cycle. The *Drosophila melanogaster* lines used included *Oregon R* for *P. luminescens* survival experiments, phagocytosis assays, and gene expression analyses, w^{1118} for survival experiments with triple-concentrated ES product and *Escherichia coli* co-injections, Rel^{E20} for the *E. coli* co-injection assays, and the Diptericin(Dpt)-GFP line *T4202 (III)* for the transcriptional activation assay. Bacterial strains included *Photorhabdus luminescens* subspecies *laumondii*, strain TT01, the *E. coli* strain K12, and the RET16 derivative of the *Photorhabdus temperata* strain NC1. *Photorhabdus* strains were cultured on MacConkey Agar (Sigma) at 28°C for a period of 48 h at which point a single colony was used to inoculate an overnight liquid culture in 10 mL of Lysogeny Broth (LB) media (VWR) incubated at 28°C in a rotary shaker set to 220 rpm. *E. coli* was cultured in a similar fashion, but initial growth on agar was carried out on LB agar at 37°C overnight.

Culturing Axenic *Heterorhabditis bacteriophora* Infective Juveniles

Infective juveniles of the rhabditid nematode *Heterorhabditis bacteriophora* strain TT01 were maintained axenically through propagation in *G. mellonella* larvae carrying well-established infections of RET16. To establish the infection, 1 mL of an overnight RET16 culture was centrifuged for 3 min at 13,000 × g, the supernatant discarded, and the pellet washed once with sterile phosphate buffered saline (PBS). The resulting bacterial suspension was centrifuged again and resuspended, at which point the suspension was diluted 1:10 with sterile PBS, to a final volume sufficient for the injection of 50 μL of bacterial solution

into the desired number of 5th to 6th instar *G. mellonella* larvae. To perform larval injections, *G. mellonella* larvae were surface-sterilized by brief submersion in a 70% solution of ethanol. The larvae were placed on ice for a period of 20 min in a 100 × 15 mm petri dish furnished with moistened 90 mm filter paper. Injections were performed with a 1 mL tuberculin syringe and 22G needle inserted in the intersegmental region at as shallow an angle as possible. Larvae were left on ice for 5 min post-injection and then kept at room temperature for 1 week. Successful RET16 infection caused the larva to die and turn the brick red color typical of a *Photorhabdus* infection. Those that did not display the appropriate color were discarded. After 1 week, *H. bacteriophora* IJs were pelleted, surface sterilized with a 3% bleach solution for 5 min, and washed twice with sterile water prior to their liberal application onto the infected *G. mellonella* at a concentration of ∼500 IJs per larva. This secondary infection was allowed to progress in the dark at room temperature for 8 days at which point the larvae were transferred to white traps for the collection of emerging IJs in autoclaved water supplemented with 0.01% Tween 20 (19). To confirm that the IJs were axenic, an aliquot of the surface-sterilized, putatively axenic IJs was used to infect *G. mellonella* larvae, and the larvae monitored for coloration indicative of an infection and support for the growth and reproduction of the IJs. IJs were considered axenic if they failed to produce red pigmentation in larvae or propagate successfully as compared to a surface-sterilized symbiotic IJ control.

Preparation of Hemolymph From *Manduca sexta*

Approximately 500 μL of raw hemolymph was collected from each 5th instar *Manduca sexta* larvae. Prior to extraction, each larva was placed on ice for a period of 20 min. The area surrounding the posterior horn of the insect was treated with a 70% alcohol wipe just prior to the severing of the horn with microdissection scissors. This was performed directly over a 1.5 mL autoclaved microcentrifuge tube, as the release of hemolymph from the site of injury is rapid and immediate. To prevent melanization, an aliquot of 20 mM phenylthiourea dissolved in PBS was added to each aliquot of hemolymph to a final concentration of 0.33 mM. The extracted hemolymph was centrifuged for 5 min at 4000 × g and 500 μL of the resulting supernatant was added to 500 μL of ice-cold Ringer's buffer (100 mM NaCl, 1.8 mM KCl, 2 mM CaCl2, 1 mM MgCl2, and 5 mM HEPES adjusted to a pH of 6.9) in a separate sterile 1.5 mL microcentrifuge tube. For long-term storage, samples were frozen at −80°C. Before use, hemolymph was thawed on ice, diluted 1:1 in ice-cold Ringer's buffer, and filtered with a 0.45 μm syringe filter. Ampicillin and kanamycin were added to diluted hemolymph plasma solutions at concentrations of 100 and 50 μg/mL, respectively.

Hemolymph Activation of Infective Juveniles and Isolation of Concentrated ES Products

Prior to activation, IJs were sedimented in aliquots of 200,000 and surface-sterilized with 3% commercial bleach in 10 mL of 0.01% Tween 20, resulting in a final hypochlorite concentration of 0.26%. Bleach-treated IJs were pelleted by centrifugation for 30 s at 1300 × g and washed twice with sterile Ringer's solution containing 0.01% Tween 20. After the second wash step, IJs were pelleted and resuspended in either 10 mL of the 25% hemolymph plasma solution (activated) or 10 mL of Ringer's-Tween (non-activated) containing antibiotics. The IJ suspensions were transferred to T75 tissue culture flasks, which were subsequently wrapped in foil and placed in a shaking incubator at 27°C and 200 RPM. Following a 20-h incubation, the IJs were transferred to 15 mL conical tubes, centrifuged, and washed 10 times with 10 mL of Ringer's-Tween 20 solution. Following the final wash, the IJs were resuspended in 10 mL of Ringer's solution without Tween 20. These tubes were wrapped in foil and returned to the incubator for 5-h at 27°C and 200 RPM to collect ES products. After incubation, the supernatants were removed and placed in a separate sterile 15 mL conical tube. The collected ES products were either stored at −80°C or immediately concentrated. To concentrate the collected products, ES products were filtered through a 0.2 μm low protein-binding syringe filter (Millex) and transferred to a new sterile 15 mL conical tube. Filtered products were added to a Vivaspin 6 tube (GE Healthcare) with a 3 kDa molecular weight cutoff, with aliquots of each treatment being added sequentially to the tube as sufficient volumes of solution cleared the filter. Concentration was allowed to continue until the volume of the retentate fell below 100 μL, at which point the solution was collected and supplemented with additional sterile Ringer's buffer to a final volume of 100 μL. For the triple-concentration of ES products, the same protocol was followed except that the ES products were initially distributed between two Vivaspin tubes, and the final 500 μL from each tube pooled and concentrated in a single tube until the volume was below 100 μL. ES concentrations were expressed as larval equivalents (LE/μL) by dividing the number of IJs used by the final volume of ES products.

Protein Electrophoresis

Protein concentration of the ES products was quantified using a Pierce BCA Protein Assay Kit (Thermo Scientific) according to the manufacturer's instructions. For samples that produced a readable concentration of protein above the threshold sensitivity of the BCA assay, 6 μg of protein were loaded into a Novex WedgeWell 4–20% Tris-Glycine Gel (Invitrogen) following reduction in 50 mM DTT. For samples not producing a readable signal for protein concentration, the maximum volume was added to the gel. The final volume added to each well-included 26 μL of sample and water, 4 μL of the reducing agent, and 10 μL of Laemmli buffer. Protein size was demarcated with PageRuler Plus Prestained Protein Ladder (Thermo Scientific) and gels were stained with a Pierce Silver Stain for Mass Spectrometry kit (Thermo Scientific).

Injection of *Drosophila melanogaster* Adults and Larvae

For survival and gene expression analyses, treatments were loaded into an oil-filled pulled glass capillary mounted on a Drummond Nanoject III Programmable Nanoliter Injector.

Adult flies aged seven to 10 days were anesthetized with carbon dioxide and injected intramesothoracially with 69.0 nL of ES products or buffer, corresponding to 138 IJ equivalents of ES products, or 414 for triple-concentrated products. Injected flies were returned to vials containing instant *Drosophila* medium (Carolina Biological) and kept at 25°C on a 12-h day-night cycle. Flies injected for gene expression analysis at a 6-h time point were consistently injected in the late morning to alleviate effects attributable to natural variability arising from the circadian cycle. Wandering 3rd instar larvae were injected with 50.2 nL of ES products, representing ∼100 IJ equivalents. Each insect was washed once with Ringer's solution upon removal from their original vial. Larvae were anesthetized with carbon dioxide for ∼2–3 min before transfer to moist filter paper for injection. In order to ensure accurate, consistent injections, larvae were secured at the posterior end with forceps and injected at a shallow angle in an intersegmental region of the dorsal side of the abdomen to avoid damage to the organs or imaginal discs. Larvae were returned to a fresh petri dish furnished with filter paper moistened with Ringer's solution and incubated under the same conditions.

qRT-PCR Analysis for Immune Gene Expression

At the indicated time points, five adult flies (three males and two females) or five larvae were collected in duplicate and total RNA was extracted using TRIzol reagent (Ambion, Life Technologies). Reverse transcription was carried out using a High-Capacity cDNA Reverse Transcription Kit (Applied Biosystems) and 1 μg of RNA template. The subsequent RT-PCR reactions were performed in a CFX96 Real-Time System, C1000 Thermal Cycler. The reactions themselves consisted of 10 μL of GreenLink No-ROX qPCR Mix (BioLink), 40 ng of cDNA template, forward and reverse primers at a final concentration of 200 nM, and ultrapure water to a final volume of 20 μL. Cycle conditions were as follows: 95°C for 2 min, 40 repetitions of 95°C for 15 s followed by 61°C for 30 s, and then one round of 95°C for 15 s, 65°C for 5 s, and finally 95°C for 5 s. The primer sets used for amplification included those for *Diptericin* (F: 5′ GCTGCGCAATCGCTTCTACT 3′; R: 5′ TGGTGGAGTTGGGCTTCATG 3′), *Cecropin* (F: 5′ TCT TCGTTTTCGTCGCTCTC 3′; R: 5′ CTTGTTGAGCGATTC CCAGT 3′), *Drosomycin* (F: 5′ GACTTGTTCGCCCTCTTCG 3′; R: 5′ CTTGCACACACGACGACAG 3′), *mcf1* (F: 5′ AAG GAGGTCAATGCTCGCTAC 3′; R: 5′ GACACAACTAATCTG CCGTTCTC 3′), *P. luminescens* 16S rRNA (F: 5′ ACAGAG TTGGATCTTGACGTTACCC 3′; R: 5′ AATCTTGTTTGCTCC CCACGCTT 3′), and *rp49* (F: 5′ GATGACCATCCGCCCAGCA 3′; R: 5′ CGGACCGACAGCTGCTTGGC 3′). Fold change was calculated using the $2^{-\Delta\Delta C}{}_{T}$ method (20, 21) with all values being normalized to *rp49*. Graphs show fold change for each treatment over 0-h expression and error bars represent standard error applied to ΔΔCt values prior to conversion to a log scale. Statistical analysis was performed with a one-way ANOVA for ΔΔCt values accumulated from three biological replicates with two technical replicates each.

Fat Body Dissection and Imaging for ES-Injected Dpt-GFP Larvae

Larvae of the Dpt-GFP *Drosophila* line were injected with 50.2 nL of non-activated or activated ES products according to the aforementioned injection protocol. Following the 6-h incubation period, the fat body was dissected out of the insect, but left attached to the body while the gut was removed completely. Tissues were fixed in PBT (PBS containing 0.2% Triton X-1000) with 4% paraformaldehyde for a period of 30 min. Three 10-min washes in PBT were performed followed by a 30-min incubation with TRITC (Molecular Probes) diluted 1:100 in PBS. After washing once with PBS, the fat body tissues were removed from the insect carcass, cut into pieces small enough to lie flat on a slide, and mounted with Antifade mounting medium with DAPI (Molecular Probes). Images were acquired with a Zeiss LSM 510 confocal microscope and corrected total fluorescence measurements were processed for isolated green channels using ImageJ software. Ten images were analyzed per treatment for each trial.

Co-injection of ES Products With *Escherichia coli* and *Photorhabdus luminescens*

Co-injection solutions were prepared by mixing ES products and bacterial suspensions such that each injection contained 310 larval equivalents of ES products and either $\sim 8 \times 10^4$ CFUs of *E. coli* or 50 CFUs of *P. luminescens*. This was achieved by diluting cultures of *E. coli* (OD600 of 3.0) or *P. luminescens* (OD600 of 0.4) 1:4 in the triple-concentrated ES products. All solutions were mixed immediately prior to use and injected using the same injection protocol. For consistency, control treatments were likewise comprised of PBS diluted 1:4 in Ringer's solution.

Quantification of Phagocytic Activity

Phagocytic activity was assessed by measuring fluorescence following the injection of pHrodo Red *E. coli* BioParticles Conjugate for Phagocytosis (Molecular Probes). A 4 mg/mL suspension of pHrodo particles was diluted 1:4 in ES products such that each co-injection contained 310 larval equivalents in a 1 mg/mL solution of pHrodo particles. Upon injection, flies were incubated at 25°C for 1 h at which time the dorsal side of the abdomen associated with the pericardial nephrocytes was imaged using a Nikon ECLIPSE N*i* microscope at 10x magnification with a Zyla (ANDOR) 5.5 camera. Corrected total fluorescence was measured using ImageJ software.

Statistical Analysis

All statistical analyses were performed using GraphPad Prism 5 software. Gene expression analyses and CTF measurements for the phagocytosis assay were compared using a one-way ANOVA and Bonferroni multiple comparisons test to determine differences between specific treatments. Significance for CTF measurements for the Dpt-GFP assay was determined with a Student's *t*-test, and survival curves were assessed using a Log-Rank (Mantel-Cox) test. All analyses were performed on data accumulated through three independent experiments.

RESULTS

Exposure of *Heterorhabditis bacteriophora* Infective Juveniles (IJs) to Host Hemolymph Induces the Secretion of Unique Proteins

To investigate the proteins secreted in response to host stimulus, groups of 200, 100, or 25 thousand (k) *H. bacteriophora* IJs were activated as previously described (11). IJs were activated for 20 h by incubation in 25% *Manduca sexta* hemolymph diluted in Ringer's buffer, washed several times, and transferred into fresh Ringer's buffer without hemolymph to collect ES products. This activation time point was selected based on preliminary experiments in order to optimize as closely as possible an *in vitro* activation that may be only minimally informed by knowledge of *in vivo* activation kinetics. Filtered collection buffer was subsequently concentrated by ultrafiltration through a 3 kDa cutoff membrane, which restricts the analysis to proteins rather than small molecules. Activated batches of 200, 100, and 25 k IJs yielded 286, 216, and 39 ng/μL of protein, respectively, whereas protein was undetectable in ES products collected from similar numbers of non-activated IJs incubated in Ringer's throughout. To visualize proteins present in the ES products, 6 μg of activated ES products were separated by SDS-PAGE and silver stained (**Figure 1**). The maximum volume of non-activated ES products (26 μl) were used because protein was undetectable. A comparison of the lanes shows that certain species of protein are unique to the ES products of activated nematodes, with two conspicuous examples in the activated 200 K lane at estimated molecular weights of 21.2 and 18.9 kDa. Importantly, these proteins are absent from the *M. sexta* hemolymph, confirming that the extensive washes following the 20-h incubation removed residual hemolymph. This indicates that *H. bacteriophora* IJs specifically release a unique suite of proteins in response to hemolymph exposure.

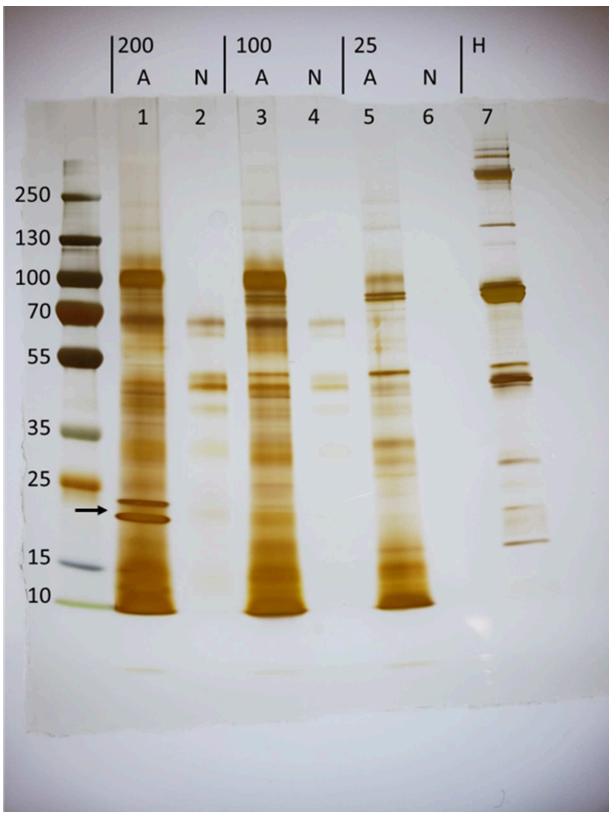

FIGURE 1 | Exposure of *Heterorhabditis bacteriophora* infective juveniles (IJs) to host hemolymph induces the secretion of unique proteins (arrow). Concentrated ES products were loaded for groups of 200,000 (200), 100,000 (100), and 25,000 (25) nematodes that were either activated (A) in *Manduca sexta* hemolymph or left non-activated (N) in Ringer's buffer. Activation took place over a period of 20 h, at which point IJs were washed, transferred to fresh ringers, and incubated for 5 h to collect ES products. Lanes 1,3, and 7 carry 6 μg of protein while all others were loaded with a maximum volume, as protein could not be detected using the BCA assay.

Heterorhabditis bacteriophora Nematode Excreted/Secreted (ES) Products Elicit Differential *Diptericin* Responses That Are Consistent Across *Drosophila melanogaster* Life Stages

The effects of concentrated ES products on the immune response of *Drosophila* were first examined in the context of the antimicrobial peptide (AMP) response. Imd and Toll pathway activity was assessed in flies by examining the expression of *Diptericin* and *Drosomycin*, respectively, following the injection of 69.0 nL of the highest concentration of ES products, a volume equivalent to the excretory/secretory output of 138 IJ. Expression was also assessed in larvae though with a lower injection volume of 50.2 nL, corresponding to ∼100 IJ equivalents. Both adult flies and larvae were collected at a 6-h time point following ES injection, which was chosen to capture expression during peak Imd activity. *Drosomycin* transcript, as measured by qPCR, was not significantly altered by the injection of activated or non-activated ES products, and notably the products also failed to elicit a response at the 24-h time point known to correlate to peak Toll pathway activity (data not shown). Conversely, *Diptericin* was significantly upregulated by injection of non-activated ES products compared to the Ringer's buffer control injection. However, injection of activated ES products failed to increase *diptericin* expression above the Ringer's buffer control injection, suggesting the presence of suppressive or non-immunogenic components in activated ES (**Figure 2**). This pattern was observed in both adult flies and larvae, though on a slightly larger scale through all three treatments in larvae, possibly due to the primary immune organ, the fat body, being proportionally larger relative to body size in larvae. The immune response to a nematode infection minimally includes a strong Imd response, which is apparent through *Diptericin* expression, and the *H. bacteriophora* countermeasures to this activity are clearly capable of neutralizing the effect to levels associated with mere injury rather than infection.

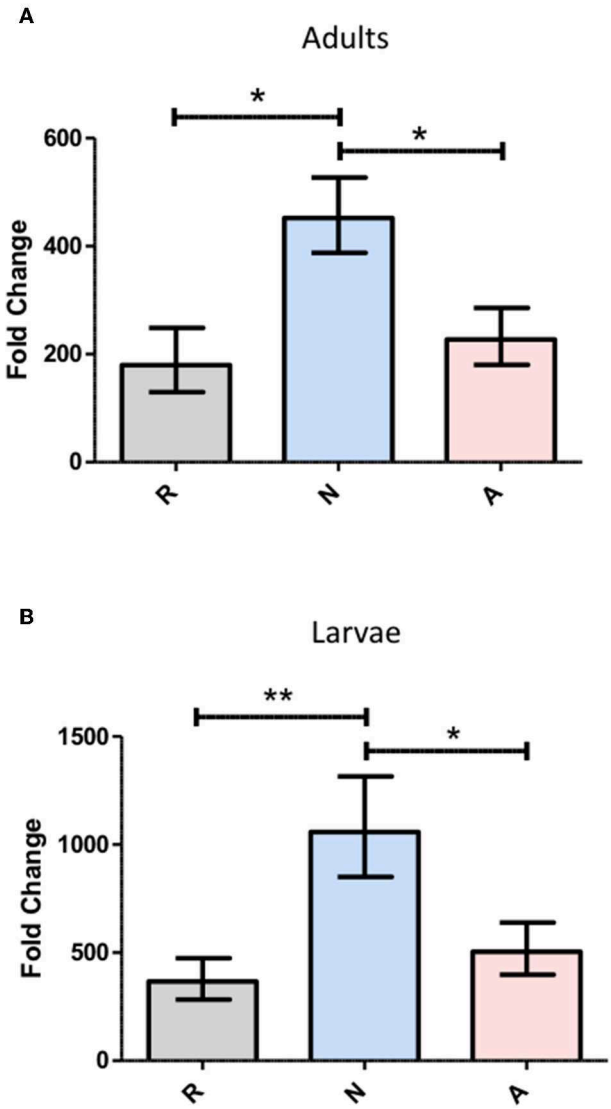

FIGURE 2 | *Heterorhabditis bacteriophora* nematode Excreted/Secreted (ES) products elicit differential *Diptericin* responses that are consistent across *Drosophila melanogaster* life stages. *D. melanogaster* adults **(A)** and 3rd instar larvae **(B)** were injected with 69.0 and 50.2 nl of non-activated (N) or activated (A) concentrated ES products, representing 138 and 100 infective juvenile equivalents, respectively. An equivalent volume of Ringer's buffer (R) served as a control. Flies and larvae were homogenized at a 6-h time point before RNA isolation, cDNA conversion, and transcript abundance quantification of the antimicrobial peptide *Diptericin* by qPCR. Fold change is relative to 0-h expression immediately following injection with each treatment and values represent data from three trials at two technical replicates per trial, where replicate measurements are drawn from the pooled cDNA of five flies or larvae (*$p < 0.05$, **$p < 0.01$).

Excretory-Secretory Product-Based Differential *Diptericin* Responses Originate at or Prior to Transcriptional Activation

To more precisely describe the effects of ES products on the regulation of *Diptericin*, larvae of a *Drosophila* line carrying GFP under the control of the *Diptericin* promoter were injected with ∼100 IJ equivalents of either activated or non-activated products, and collected for observation at a 6-h time point. The fat body was dissected and imaged by confocal microscopy at 40x magnification. Fluorescence was clearly visible in all samples, though on average fat body samples that had been exposed to non-activated products were substantially brighter than those treated with activated ES products. This observation was confirmed by corrected total fluorescence (CTF) measurements of isolated green channels for each image (**Figure 3**). Because fluorescence is a measure of promoter activation, the specific interaction that mediates the differential responses to activated and non-activated ES products can be posited to take place either at or upstream of transcriptional activation. These measurements also confirm that the differences seen in *Diptericin* expression are mediated at least in part by cells of the fat body.

Triple-Concentrated Activated *Heterorhabditis bacteriophora* Nematode ES Products Are Lethal to Adult *Drosophila melanogaster*

While the activated ES products clearly do not provoke as strong a *Diptericin* response as the non-activated products, the relative equivalence of the responses to Ringer's buffer and activated ES products makes it impossible to determine whether the activated nematode is secreting factors that suppress immunity or simply eliminating the production of factors that are immunogenic in the host. In an attempt to resolve this ambiguity, three separate batches of ES products produced with 200,000 IJs were concentrated together such that suppressive effects would be stronger, but the absence or masking of immunogenic compounds would not have compounding effects on *Diptericin* expression to limit upregulation below that evoked by a control injection. The increased potency of these products was immediately apparent, as injection of 414 IJ equivalents resulted in ∼70% mortality over a period of 6 h (**Figure 4**). Flies that survived the injection at the 6-h time point were collected and *Diptericin* transcript levels measured. The 3x concentrated ES products significantly decreased the *Diptericin* response below that of the Ringer's buffer alone (**Figure 5A**), thus indicating that *H. bacteriophora* secretes factors capable of the specific suppression of *Diptericin* upregulation. The specificity of *Diptericin* suppression was examined by assessing the response of a second Imd-responsive AMP, *Cecropin,* as well as the Toll pathway AMP *Drosomycin* to the concentrated activated ES products. Injection of 414 IJ equivalents had no effect on either *Cecropin* (**Figure 5B**) or *Drosomycin* (**Figure 5C**) expression in adult flies.

Heterorhabditis bacteriophora Nematode ES Products Promote Mortality Driven by Both Pathogenic and Non-pathogenic Bacteria

While the specific suppression of *Diptericin* is significant, this result does not allow conclusions about whether the ES products released by *H. bacteriophora* are sufficiently immunosuppressive

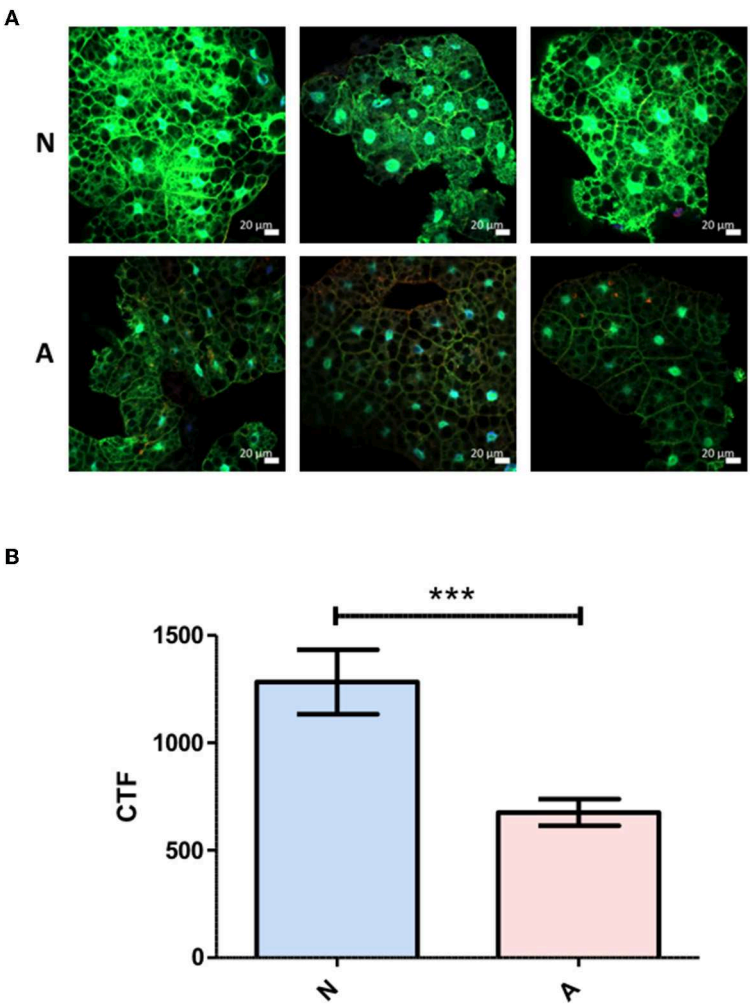

FIGURE 3 | Differential *Diptericin* responses to ES products originate at or prior to transcriptional activation. **(A)** Larvae of a *Drosophila melanogaster* line carrying GFP under the control of the antimicrobial peptide *Diptericin* promoter were injected with 50.2 nl of non-activated (N) or activated (A) products. The fat body was extracted at a 6-h time point and imaged via confocal microscopy. One representative image from each of the three trials is shown for both treatments. **(B)** Corrected total fluorescence was assessed for isolated green channels with Image J software (***$p < 0.001$). Values were calculated for 10 images per treatment per trial.

to augment a bacterial infection. To explore this possibility, adult flies were co-injected with a high inoculum of *Escherichia coli* (8×10^4 CFUs) and ∼310 IJ equivalents of activated ES products, non-activated ES products, or an equivalent volume of Ringer's buffer. Tracking mortality every 12 h for a period of 72 h revealed that while Ringer's buffer or non-activated ES products co-injected with *E. coli* were not lethal to flies, the injection of activated products and *E. coli* together (A+Ec) resulted in ∼50% mortality in the first 24 h (**Figure 6**). Notably, this reduced dose (310 vs. the lethal 414 IJ equivalents) of activated ES products no longer induces mortality, so the observed decrease in survival cannot be attributed to the previously noted lethality stemming from the products alone.

In the context of a natural *H. bacteriophora* infection, the bacteria of interest would be the natural symbiont of the nematode, *Photorhabdus luminescens*. The bacteria are released from the gut of the IJ shortly after entry into the hemolymph, and the possibility exists that the ES products may serve in part to prepare the hemolymph environment for a more successful infection by *P. luminescens*. This possibility was tested by similarly co-injecting adult flies with ∼310 IJ equivalents of ES products or an equivalent volume of Ringer's buffer and 50 cells of *P. luminescens*. Time points were at 12 h, then every hour from 24 to 33 h, in order to capture the majority of mortality, and then once again at 48 h. Survival curves revealed a slightly protective effect imparted by the non-activated ES products relative to the control injection, and when compared to co-injections with activated ES products, the lethality produced by the activated ES products and *P. luminescens* was significantly different from and effected earlier than that produced by the non-activated ES product co-injections (**Figure 7**). Even at a sublethal dose, the ES products of *H. bacteriophora* are sufficiently immunosuppressive

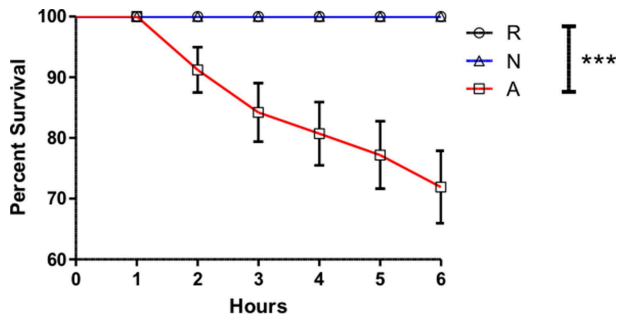

FIGURE 4 | Activated *Heterorhabditis bacteriophora* nematode Excreted/Secreted (ES) products are lethal to adult *Drosophila melanogaster*. *Drosophila* adults were injected with 69.0 nl of Ringer's buffer (R) or 414 IJ-equivalent dose triple-concentrated ES products, either activated (A) or non-activated (N) and monitored for mortality every hour for 6 h, at which point injected populations typically stabilized and no additional deaths were observed up to a 24-h time point. Each curve is comprised of measurements for three trials of 10 male and 10 female flies (***$p < 0.001$).

to negatively impact the AMP response and to enhance the virulence of a bacterial infection.

Photorhabdus luminescens Proliferates More Rapidly in Adult *Drosophila* When Co-injected With Activated ES Products

The delay in the onset of mortality for populations of flies co-injected with ES products and *P. luminescens* (**Figure 7**) demonstrates that this mortality initiated by *Photorhabdus* requires an accumulation of bacteria beyond the initial inoculum. To test whether the influence of activated ES products is capable of accelerating this accumulation, the co-injections of ES products and *Photorhabdus* were repeated under the same conditions and surviving flies were collected at a 14-h time point for the assessment of relative bacterial growth, as measured by RT-qPCR targeting the *P. luminescens* 16S rRNA and *mcf1* genes. Subsequent analysis of expression for both genes revealed that bacterial proliferation is significantly higher in the presence of activated ES products, which supported an ∼100-fold transcript increase for each gene (**Figure 8**). Those treated with either Ringer's buffer or non-activated products showed increases between 3- and 10-fold for the same genes. This difference in bacterial survival and proliferation is therefore likely responsible for the ∼12-h decrease in the time to mortality onset for flies co-injected with activated ES products as compared to those injected with non-activated products.

H. bacteriophora ES Products Provoke a More Active Phagocytic Response

Another possible mechanism causing increased mortality when flies are challenged simultaneously with activated nematode ES products and bacteria is interference with the normal activity of phagocytic hemocytes. To determine whether this effect is also contributing to the enhanced success of bacteria in ES-treated flies, adult *D. melanogaster* were co-injected with ∼310 IJ

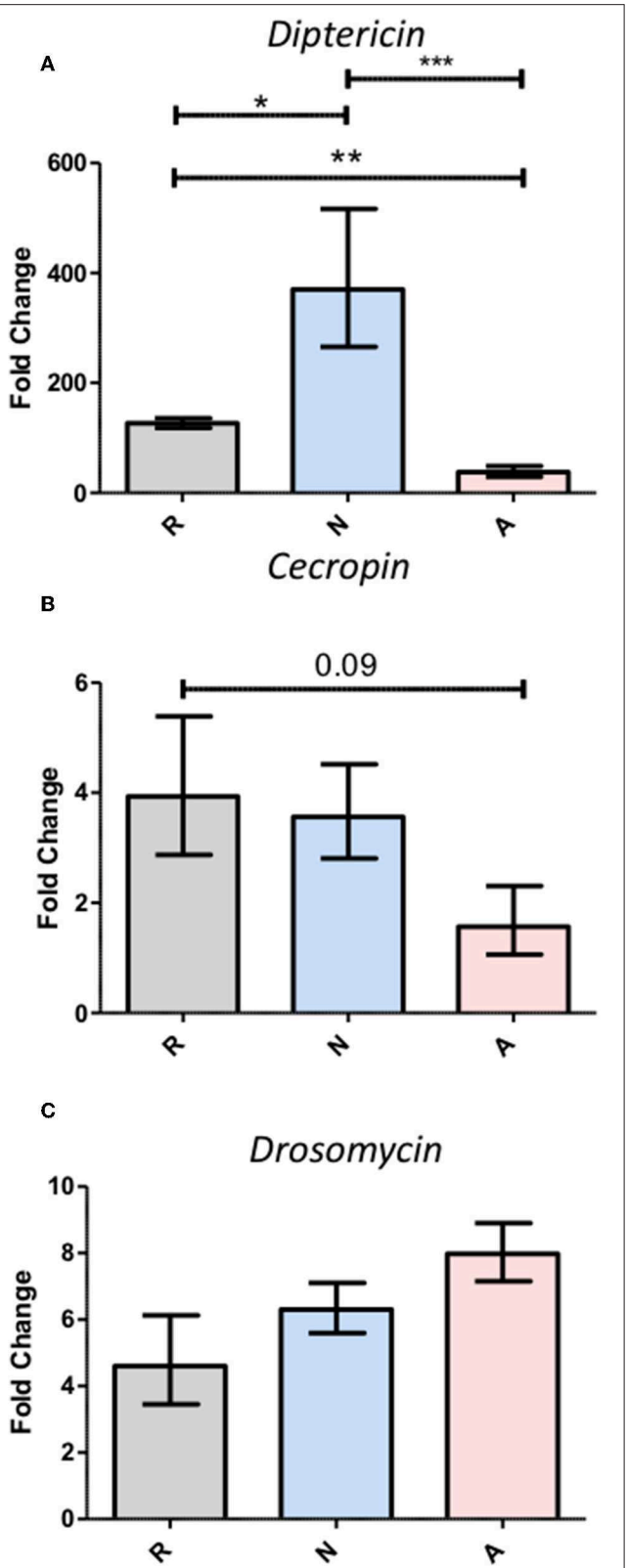

FIGURE 5 | Triple-concentration of the *Heterorhabditis bacteriophora* nematode Excreted/Secreted (ES) products exacerbates *Diptericin* responses, *(Continued)*

FIGURE 5 | but fails to elicit responses from other antimicrobial peptides. Adult *Drosophila melanogaster* were injected with 69.0 nl of triple-concentrated ES products prior to homogenization for RNA extraction at a 6-h time point. Gene expression normalized to *rp49* expression was assessed for the antimicrobial peptides *Diptericin* **(A)**, *Cecropin* **(B)**, and *Drosomycin* **(C)**. Bars represent fold change over the 0-h measurement for each treatment. Averages with standard error are shown for three trials performed in duplicate such that each trial produced two measurements for pooled cDNA from five flies (*$p < 0.05$, **$p < 0.01$, ***$p < 0.001$).

equivalents of ES products or an equal volume of Ringer's buffer and pHrodo *E. coli* conjugates that fluoresce when engulfed by a phagocyte. CTF measurements of images captured with fluorescence microscopy showed that phagocytic activity around the pericardium, where the highest degree of activity is observed, is significantly elevated in flies co-injected with activated ES products (**Figure 9**). The immunosuppressive effect of the ES products is not mediated by the phagocytic response, and may in fact provoke more phagocytic activity. Despite this compensatory phagocytic response, the effects on AMP production or other systems are still potent enough to enhance a bacterial infection.

DISCUSSION

With the entirety of the observed effects relying on the *in vitro* activation of IJs, the degree to which the collected ES products align with those of an *in vivo* infection should be addressed. For *Steinernema* species, activation has been shown to be influenced by host species, the age of the IJs being activated, the homogenate concentration used for activation, and the duration of exposure to host components (22, 23). These factors could similarly affect the activation of *H. bacteriophora*, which is able to infect lepidopterans, dipterans, coleopterans, hymenopterans, anoplurans, orthopterans, homopterans, and hemipterans to varying degrees of lifecycle completion (24). Each of these hosts may provoke a slightly different response from the IJs, possibly even a different assortment of ES products. Furthermore, *H. bacteriophora* is known to inhibit IJ development in a conspecific manner through a small-molecule pheromone termed C11 EA (25), indicating that the concentration of IJs could tune the activation state based on the ratio of suppressive conspecific signal to activating host signal. Laboratory propagation of the nematodes can also be a factor in that *Heterorhabditis* virulence can be affected by not only the number of generations that have been propagated in laboratory conditions, but also the number of IJs used to infect a host during each passage (26). It is therefore immediately crucial to concede that any collection of ES products from entomopathogens activated *in vitro* will likely not contain the ES products of the nematode in a universal sense, but rather a subset of products specific to a given activation and collection protocol. This fact does nothing however to diminish the practical or informative value of effects stemming from an isolation of ES products provided they accurately represent at least some subset of the virulence arsenal of the nematode. For the products used in this set of assays, our results demonstrate an effective activation through the emergence of a unique protein profile. The subsequent assays serve to identify functions of these proteins that are produced specifically in response to host hemolymph.

The first effect of the ES products to be observed was the capacity of non-activated ES products to provoke higher expression of the antimicrobial peptide gene *Diptericin* following injection into adult *Drosophila*. This gene was selected by virtue of its role as a readout of the Imd pathway, for which the best described function is the production of antimicrobial peptides in response to Gram-negative bacteria (27). The Imd pathway is relevant because the bacterial symbiont of *H. bacteriophora*, *Photorhabdus luminescens*, is a Gram-negative bacterium, but also because of the pathway's association with septic injury in general (28), which would imply that Imd activation could also occur during penetration of the nematode into the cuticle. Additionally, the Imd pathway appears to have a larger role in inflammation and immunity based on its contribution to the viral response (29, 30), which further asserts that Gram-negative bacterial pathogen-associated molecular patterns (PAMPs) are not its sole activating inputs. The initial expression changes observed here imply that basally expressed components of non-activated nematode secretions are also capable of directly or indirectly promoting Imd activity, and possibly in a specific manner. This is supported by the data shown here, as expression of *Diptericin* is believed to be regulated solely by the Imd pathway as opposed to having a regulatory mode like that of *Attacin*, which is thought to receive inputs from both the Toll and Imd pathways (31). After demonstrating the immunogenicity of non-activated products in adults, the effect was confirmed in whole larvae, the stage more commonly associated with IJ infection, as well as specifically in the fat body. Importantly, the latter provides the additional information that the immunogenic effect of the non-activated products involves a systemic response from the fat body, a crucial distinction given that *Diptericin* can be expressed locally in sections of the digestive tract, specifically the proventriculus and midgut (32). Results from the Dpt-GFP assay also provide an assurance that differences stem from activity taking place at or before transcription, but additional work will be required to specify a mechanistic point of interference beyond that simple binary.

To determine whether the activated products simply lacked immunogenicity or were instead carrying out targeted suppression, the products were triple-concentrated by combining the secretions of three separate activations of 200,000 IJs. These more concentrated products were lethal through early timepoints following injection into adult flies, although less so than the secretions of *Steinernema carpocapsae* (10). This is consistent with previous findings regarding the *in vivo* virulence of axenic IJs of these two species (33). When the effect on *Diptericin* expression was reassessed with this higher 414 IJ equivalent dose, the upregulation induced by the activated products was significantly lower than that of the Ringer's buffer injection, while the non-activated products continued to display consistent immunogenicity. Because a loss of immunogenicity would do nothing to eliminate Imd activity induced by the vehicle control, the 414 IJ equivalent injections reveal targeted immune suppression by the activated ES products. The argument could

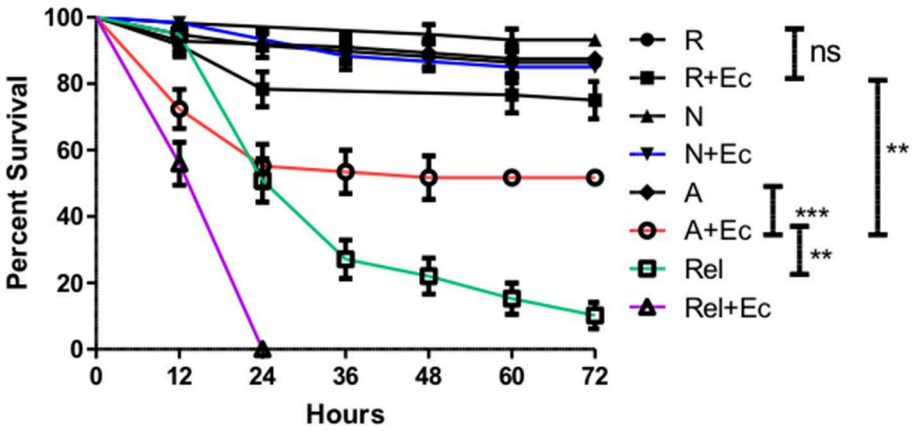

FIGURE 6 | Co-injection of *Escherichia coli* with activated *Heterorhabditis bacteriophora* nematode Excreted/Secreted (ES) products results in fly mortality. Adult *Drosophila melanogaster* were injected with 69.0 nl of a 1:4 mixture of OD 3.0 *E. coli* (+Ec) and activated ES products (A), non-activated ES products (N), or Ringer's buffer (R). After mixing, solutions contained 310 IJ equivalents of ES products and 8×10^4 CFUs of *E. coli* as applicable. *Relish* mutant flies (Rel) were also injected in order to compare the magnitude of ES-suppression to that of Immune deficiency pathway ablation. Survival was assessed every 12 h for a total of 72 h. Three trials were performed, each consisting of 10 male and 10 female flies per treatment. Where bars are omitted, standard error was negligible (ns $p > 0.05$, $^{**}p < 0.01$, $^{***}p < 0.001$).

be made here that *H. bacteriophora* might generate antibiotic compounds during an infection and that these are reducing the population of Imd-activating microbes introduced by the injection. While *P. luminescens* is known to produce antibiotics (34), no such activity has been attributed to *H. bacteriophora*, and this scenario would be in stark contrast to the results of the bacterial co-injection survival assays, especially that of *E. coli*. If the ES products contain antibiotics, they should be strongly protective after co-injection. The suppressive capacity of the ES products was then tested for two other antimicrobial peptide genes, *Cecropin* and *Drosomycin*, which are regulated by the Imd and Toll pathways, respectively. Neither of these genes showed any significant differences between the three treatments, indicating that the transcriptional suppression observed in the case of *Diptericin* may be specific for that gene, though other gene products may be affected at different levels of host-parasite interactions. An infection by the filarial nematode *Brugia pahangi* can be inhibited by Cecropins (35), but if this is also the case for *Heterorhabditis*, *H. bacteriophora* has mediated this threat through the synthesis of a proteinase capable of degrading Cecropins (36), effectively eliminating the pressure to suppress *Cecropin* transcriptionally. The absence of a *Drosomycin* response may simply be the product of irrelevance given that neither *S. carpocapsae* nor *H. bacteriophora* nematodes induce *Drosomycin* expression in *Drosophila* larvae if the nematodes are axenic (3, 37). Generally though, the lack of activity on other antimicrobial peptide genes does at least demonstrate that the suppression of *Diptericin* is a more subtle, targeted effect than broad interference with immune gene transcription.

Having demonstrated that *H. bacteriophora* IJs respond to a host by secreting a unique set of proteins possessing immunomodulatory activity, the ES products were then tested for their contribution to infection outcome, particularly one instigated by Gram-negative bacteria due to their susceptibility to Imd outputs. Flies that were injected with activated ES products and non-pathogenic *E. coli* (38) displayed significantly increased mortality as compared to controls, which showed that this dose of *E. coli* is not lethal by itself. Mortality occurred predominantly within 24 h of injection, after which point the rate of mortality declined sharply, implying that the active proteins in the ES products are degraded or otherwise buffered by the fly at later time points. *Relish* mutant flies were also injected with *E. coli* or Ringer's buffer in order to serve as a comparison for the magnitude of suppression. *Relish* is the terminal transcription factor in the Imd pathway and accordingly, these flies are highly susceptible to infection by Gram-negative bacteria (39). If these flies and those treated with activated ES products are equally susceptible, this would imply a nearly complete suppression of the Imd pathway by activated ES products. Interestingly, the trajectory of the *E. coli* and activated ES products co-injection survival curve does most closely resemble the *Relish* mutant *E. coli* injection curve at the earliest time point, but the treatments then diverge. Generally, this effect is illustrative of the immunosuppressive capacities of the ES products, but this is still more or less inconsequential in a natural infection unless the ES products can also support the *H. bacteriophora* symbiont *P. luminescens*. The Imd pathway has been previously implicated in the immune response to *P. luminescens* in that *Diptericin* is strongly upregulated following bacterial injection, and the avirulent *phoP* strain of *Photorhabdus* is restored to full pathogenicity in Imd pathway mutants (40). The *Diptericin*-specific suppression facilitated by the activated ES products is thus likely relevant to the survival of *Photorhabdus* in *Drosophila*. Co-injections with ES products were repeated with a far less concentrated, ∼50 CFU inoculum of *P. luminescens*, which is representative of the average bacterial load of an *H. bacteriophora* IJ (2). The co-injection of activated ES products led to a significantly earlier

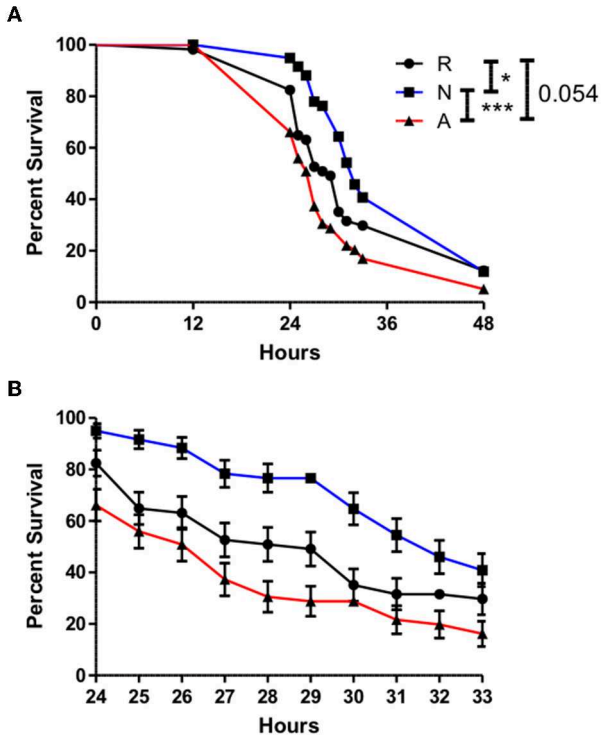

FIGURE 7 | The onset of mortality evoked by *Photorhabdus luminescens* infection is significantly advanced by *Heterorhabditis bacteriophora* nematode Excreted/Secreted activated products, but delayed by non-activated products. Adult *Drosophila melanogaster* were injected with 69.0 nl of a 1:4 mixture of OD 0.4 *P. luminescens* bacteria and activated ES products (A), non-activated ES products (N), or Ringer's buffer (R), conveying 310 IJ equivalents of ES products and 50 CFUs of *Photorhabdus*. Survival was observed at 12 h and then every hour after 24 h until 33 h in order to capture the majority of mortality events at a higher resolution. A final time point was assessed at 48 h **(A)**. Mortality in injected flies between 24 and 36 h is shown in **(B)**. Curves depict average values collected over three trials of 20 flies, 10 males, and 10 females, per treatment (*$p < 0.05$, ***$p < 0.001$).

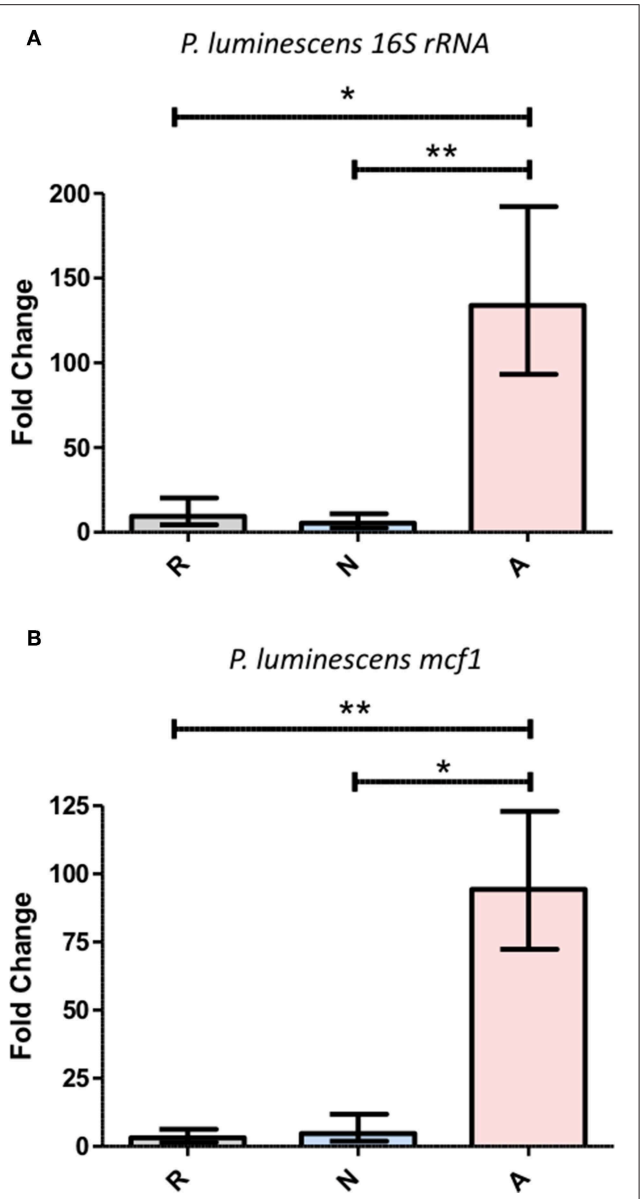

FIGURE 8 | Activated *Heterorhabditis bacteriophora* ES products enable the rapid proliferation of *Photorhabdus luminescens* during the early phase of an infection. A 1:4 mixture of OD 0.4 *P. luminescens* and Ringer's buffer (R), non-activated ES products (N), or activated ES products (A) was injected into the thorax of adult *Drosophila*, which were then incubated for a period of 14 h. Following RNA extraction, gene expression was measured by RT-qPCR for *P. luminescens* 16S rRNA **(A)** as well as *mcf* **(B)**, both of which were normalized to *rp49*. Each graph shows fold change in expression between the 0 and 14 h time points. Three trials of two replicates with five flies per replicate were performed (*$p < 0.05$, **$p < 0.01$).

onset of mortality as compared to non-activated products while the latter also displayed a slightly protective effect as compared to Ringer's buffer, potentially due to the elevated induction of *Diptericin* expression. Populations of injected flies were also stable until after the 12-h time point, reaffirming the specific role of the bacteria in the mortality of co-injected flies. Furthermore, this delay compared to the *E. coli* co-injections implies that the injected *Photorhabdus* needed to replicate substantially to achieve a lethal concentration. Other findings have shown that the population responsible for eventual septicemia in an insect originates from a small subpopulation that is resistant to antimicrobial peptides (41), so part of the role of nematode ES products might be to bolster this subpopulation as much as possible. Our data support this idea in that relative *Photorhabdus* abundance at a 14-h time point, just after the onset of mortality, was an order of magnitude higher in flies co-injected with activated ES products. Other time points could be examined to more fully enunciate the relationship between the presence of activated ES products and *Photorhabdus* growth kinetics, but this time point was considered the most critical and sufficient for demonstrating the practical capacity of ES-based suppression. Furthermore, this system could also eventually be used to examine the interplay between *Heterorhabditis* and *Photorhabdus* virulence factors with regard to AMP suppression through different phases of the infection.

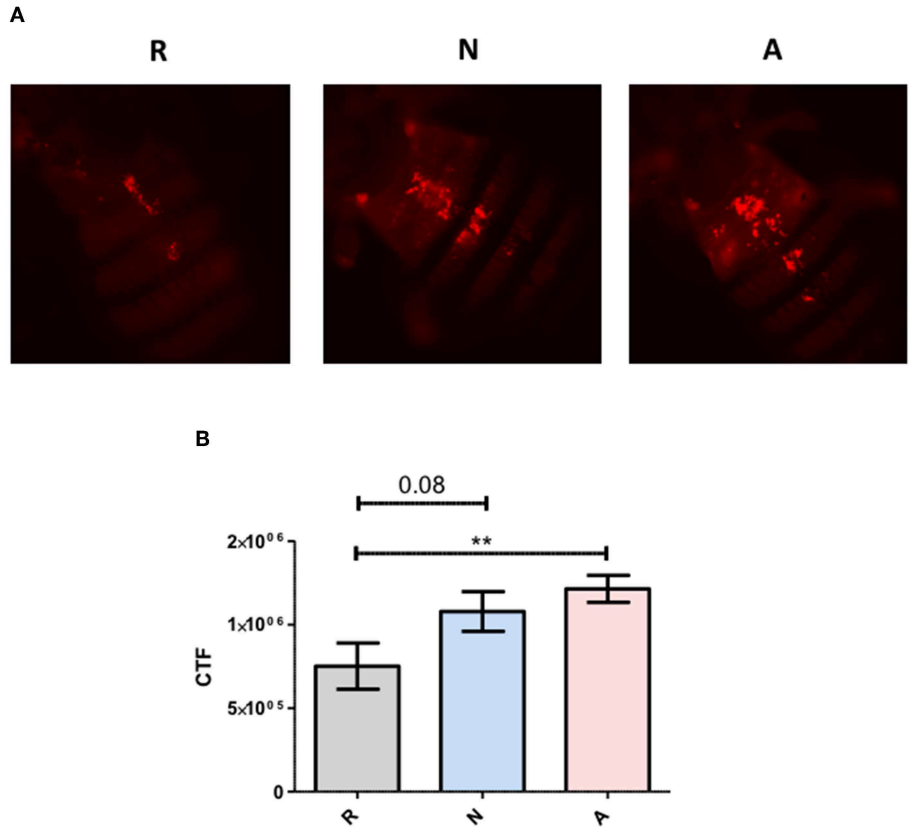

FIGURE 9 | *Heterorhabditis bacteriophora* nematode activated Excreted/Secreted (ES) products provoke a stronger phagocytic response. Adult *Drosophila melanogaster* were injected with 69.0 nl of a 1:4 mixture of 4 mg/mL pHrodo *E. coli* conjugates and activated ES products (A), non-activated ES products (N), or Ringer's buffer (R). **(A)** Images were captured by fluorescence microscopy at 10x magnification and **(B)** the area associated with pericardial nephrocytes was analyzed with ImageJ software. Values are shown for measurements collected over three trials of three replicates each (**$p < 0.01$).

Finally, to eliminate the possibility that survival differences were stemming from the phagocytic response, *H. bacteriophora* ES products were co-injected with pHrodo *E. coli* conjugates to measure overall phagocytic activity. Activated products were found to significantly increase ingestion of the conjugates, but this increase in phagocytosis was clearly unable to promote survival during infection, which is consistent with findings that knock-down of the phagocytic receptor Nimrod C1 has no effect on the survival of *Drosophila* during an infection by symbiotic *H. bacteriophora* (42). Although this is not a comprehensive assessment of the cellular response or related immune mechanisms, our future work will focus on analyzing the effects of the ES products on several other processes including melanization, encapsulation, and clot formation.

Much of the immune response has been left uninvestigated by this set of assays, in particular the immune response specifically against the nematode, but the pattern observed here reveals a cohesive image of specific immune gene suppression that could play a crucial role in the infection process. Together, the conclusions of this work show that *H. bacteriophora* secretes a unique protein profile in response to a host, this collection of proteins suppresses the expression of the antimicrobial peptide-encoding gene *Diptericin*, and suggest that the suppressive capacity of the secreted products allows a small population of *P. luminescens* to propagate and overwhelm a host more quickly. This represents a fundamental component of nemato-bacterial bipartite virulence and provides a strong justification for exploring the individual components of the secreted products produced by the nematode in order to identify specific immunosuppressive proteins that could be employed in a variety of applications. The interaction of these individual proteins with host immune mediators can then be observed in the context of the effects described here, with the aim of providing a mechanistic explanation for *Heterorhabditis*-based immunosuppression. Given the wealth of molecular components that could be targeted to interfere with Imd responses, even outside the signaling components of the Imd pathway, it would be premature to suggest a mechanism from the effects observed here, but potential avenues of research can be suggested. One well-supported field of inquiry would be to examine the ability of these ES products to interfere with eicosanoid production. In insects, eicosanoid production relies on the ability of phospholipase A_2 (PLA_2) to synthesize eicosanoid precursor lipids like arachidonic acid (AA), and interference with this pathway can have strong immunosuppressive effects based on the role

of eicosanoids in the regulation of cellular and humoral responses, including *Diptericin* expression through the Imd pathway (31, 43). *Photorhabdus* is known to inhibit PLA_2 (44), but a variety of parasitic nematodes also secrete proteins that could similarly interfere with eicosanoid synthesis through their ability to bind fatty acids, including arachidonic acid, which could sequester necessary eicosanoid precursors (45). Similar proteins have also been found in the ES products of *Steinernema carpocapsae* (10) and the transcriptome of activated *H. bacteriophora* (14). Interference with this pathway would be consistent with the findings presented here and an efficient way for the parasite to simultaneously suppress multiple immune responses.

DATA AVAILABILITY STATEMENT

The datasets generated for this study are available on request to the corresponding author.

AUTHOR CONTRIBUTIONS

EK conceived and designed the experiments, performed the experiments, analyzed the data, wrote the paper, prepared the figures, and reviewed drafts of the paper. JH, DO'H, and IE conceived and designed the experiments, supervised the project, reviewed drafts of the paper, and prepared the manuscript.

FUNDING

This work was supported by a George Washington University facilitating fund awarded to DO'H, JH, and IE.

ACKNOWLEDGMENTS

We thank members of the Department of Biological Sciences at George Washington University (GWU) for critical reading of the manuscript, and Kyle Devine for rearing the flies.

REFERENCES

1. Poinar GO Jr, Georgis R. Characterization and field application of *Heterorhabditis bacteriophora* strain HP88 (Heteorhabditidae: Rhabditida). *Rev Nématologie.* (1990) 13:387–93.
2. Ciche TA, Ensign JC. For the insect pathogen *Photorhabdus luminescens*, which end of a nematode is out? *Appl Environ Microbiol.* (2003) 69:1890–7. doi: 10.1128/AEM.69.4.1890-1897.2003
3. Hallem EA, Rengarajan M, Ciche TA, Sternberg PW. Nematodes bacteria and flies: a tripartite model for nematode parasitism. *Curr Biol.* (2007) 17:898–904. doi: 10.1016/j.cub.2007.04.027
4. Peters A, Gouge DH, Ehlers R, Hague NGM. Avoidance of encapsulation by *Heterorhabditis* spp. Infecting larvae of *Tipula oleracea*. *J Invertebr Pathol.* (1997) 70:161–4. doi: 10.1006/jipa.1997.4681
5. An R, Voss M, Jagdale GB, Grewal PS. Differences in immune defense evasion of selected inbred lines of *Heterorhabditis bacteriophora* in two white grub species. *Insects.* (2012) 3:378–89. doi: 10.3390/insects3020378
6. Ebrahimi L, Niknam G, Dunphy GB. Hemocyte responses of the colorado potato beetle, *Leptinotarsa decemlineata*, and the greater wax moth, *Galleria mellonella*, to the entomopathogenic nematodes, *Steinernema feltiae* and *Heterorhabditis bacteriophora*. *J Insect Sci.* (2011) 11:75. doi: 10.1673/031.011.7501
7. Li X-Y, Cowles RS, Cowles EA, Gaugler R, Cox-Foster DL. Relationship between the successful infection by entomopathogenic nematodes and the host immune response. *Int J Parasitol.* (2007) 37:365–74. doi: 10.1016/j.ijpara.2006.08.009
8. Toubarro D, Avila MM, Hao Y, Balasubramanian N, Jing Y, Montiel R, et al. A serpin released by an entomopathogen impairs clot formation in insect defense system. *PLoS ONE.* (2013) 8:e69161. doi: 10.1371/journal.pone.0069161
9. Toubarro D, Avila MM, Montiel R, Simões N. A pathogenic nematode targets recognition proteins to avoid insect defenses. *PLoS ONE.* (2013) 8:e75691. doi: 10.1371/journal.pone.0075691
10. Lu D, Macchietto M, Chang D, Barros MM, Baldwin J, Mortazavi A, et al. Activated entomopathogenic nematode infective juveniles release lethal venom proteins. *PLoS Pathog.* (2017) 13:e1006302. doi: 10.1371/journal.ppat.1006302
11. Vadnal J, Ratnappan R, Keaney M, Kenney E, Eleftherianos I, O'Halloran D, et al. Identification of candidate infection genes from the model entomopathogenic nematode *Heterorhabditis bacteriophora*. *BMC Genomics.* (2017) 18:8. doi: 10.1186/s12864-016-3468-6
12. Bai X, Adams BJ, Ciche TA, Clifton S, Gaugler R, Kim KS et al. A lover and a fighter: the genome sequence of an entomopathogenic nematode *Heterorhabditis bacteriophora*. *PLoS ONE.* (2013) 8:e69618. doi: 10.1371/journal.pone.0069618
13. Hao Y-J, Montiel R, Lucena MA, Costa M, Simoes N. Genetic diversity and comparative analysis of gene expression between *Heterorhabditis bacteriophora* Az29 and Az36 isolates: uncovering candidate genes involved in insect pathogenicity. *Exp Parasitol.* (2012) 130:116–25. doi: 10.1016/j.exppara.2011.12.001
14. Moshayov A, Koltai H, Glazer I. Molecular characterisation of the recovery process in the entomopathogenic nematode *Heterorhabditis bacteriophora*. *Int J Parasitol.* (2013) 43:843–52. doi: 10.1016/j.ijpara.2013.05.009
15. Shepherd C, Navarro S, Wangchuk P, Wilson D, Daly NL, Loukas A. Identifying the immunomodulatory components of helminths. *Parasite Immunol.* (2015) 37:293–303. doi: 10.1111/pim.12192
16. Labaude S, Griffin CT. Transmission success of entomopathogenic nematodes used in pest control. *Insects.* (2018) 9:E72. doi: 10.3390/insects9020072
17. Memari Z, Karimi J, Kamali S, Goldansaz SH, Hosseini M. Are entomopathogenic nematodes effective biological control agents against the carob moth, ectomyelois ceratoniae? *J Nematol.* (2016) 48:261–7. doi: 10.21307/jofnem-2017-034
18. Kamali S, Karimi J, Koppenhöfer AM. New insight into the management of the tomato leaf miner, *Tuta absoluta* (Lepidoptera: Gelechiidae) with entomopathogenic nematodes. *J Econ Entomol.* (2018) 111:112–9. doi: 10.1093/jee/tox332
19. White GF. A method for obtaining infective nematode larvae from cultures. *Science.* (1927) 66:302–3. doi: 10.1126/science.66.1709.302-a
20. Livak KJ, Schmittgen TD. Analysis of relative gene expression data using real-time quantitative PCR, and the $2-\Delta\Delta CT$ method. *Methods.* (2001) 25:402–8. doi: 10.1006/meth.2001.1262
21. Schmittgen TD, Livak KJ. Analyzing real-time PCR data by the comparative CT method. *Nat Protoc.* (2008) 3:1101–8. doi: 10.1038/nprot.2008.73
22. Lu D, Sepulveda C, Dillman AR. Infective juveniles of the entomopathogenic nematode *Steinernema scapterisci* are preferentially activated by cricket tissue. *PLoS ONE.* (2017) 12:e0169410. doi: 10.1371/journal.pone.0169410
23. Alonso V, Nasrolahi S, Dillman AR. Host-specific activation of entomopathogenic nematode infective juveniles. *Insects.* (2018) 9:E59. doi: 10.3390/insects9020059
24. de Doucet MM, Bertolotti M, Giayetto A, Miranda M. Host range, specificity, and virulence of *Steinernema feltiae, Steinernema rarum,* and *Heterorhabditis bacteriophora* (Steinernematidae and Heterorhabditidae) from Argentina. *J Invertebr Pathol.* (1999) 73:237–42. doi: 10.1006/jipa.1998.4831
25. Noguez JH, Conner ES, Zhou Y, Ciche TA, Ragains JR, Butcher RA. A novel ascaroside controls the parasitic life cycle of the entomopathogenic

nematode *Heterorhabditis bacteriophora*. *ACS Chem Biol.* (2012) 7:961–6. doi: 10.1021/cb300056q
26. Shapiro-Ilan D, Raymond B. Limiting opportunities for cheating stabilizes virulence in insect parasitic nematodes. *Evol Appl.* (2016) 9:462–70. doi: 10.1111/eva.12348
27. Myllymäki H, Valanne S, Rämet M. The Drosophila Imd signaling pathway. *J Immunol.* (2014) 192:3455–62. doi: 10.4049/jimmunol.1303309
28. Brun S, Vidal S, Spellman P, Takahashi K, Tricoire H, Lemaitre B. The MAPKKK Mekk1 regulates the expression of Turandot stress genes in response to septic injury in *Drosophila*. *Genes Cells.* (2006) 11:397–407. doi: 10.1111/j.1365-2443.2006.00953.x
29. Zakovic S, Levashina EA. Insects go on a sting operation to tackle intracellular invaders. *Immunity.* (2018) 49:195–7. doi: 10.1016/j.immuni.2018.08.003
30. Palmer WH, Joosten J, Overheul GJ, Jansen PW, Vermeulen M, Obbard DJ, et al. Induction and suppression of NF-κB signalling by a DNA virus of Drosophila. *J Virol.* (2019) 93:e01443-18. doi: 10.1128/JVI.01443-18
31. Yajima M, Takada M, Takahashi N, Kikuchi H, Natori S, Oshima Y, et al. A newly established *in vitro* culture using transgenic Drosophila reveals functional coupling between the phospholipase A2-generated fatty acid cascade and lipopolysaccharide-dependent activation of the immune deficiency (imd) pathway in insect immunity. *Biochem J.* (2003) 371:205–10. doi: 10.1042/bj20021603
32. Tzou P, Ohresser S, Ferrandon D, Capovilla M, Reichhart JM, Lemaitre B, et al. Tissue-specific inducible expression of antimicrobial peptide genes in *Drosophila* surface epithelia. *Immunity.* (2000) 13:737–48. doi: 10.1016/S1074-7613(00)00072-8
33. Han R, Ehlers, R.-U. Pathogenicity development and reproduction of *Heterorhabditis bacteriophora* and *Steinernema carpocapsae* under Axenic *in vivo* conditions. *J Invertebr Pathol.* (2000) 75:55–8. doi: 10.1006/jipa.1999.4900
34. Hu K, Webster JM. Antibiotic production in relation to bacterial growth and nematode development in Photorhabdus-Heterorhabditis infected *Galleria mellonella* larvae. *FEMS Microbiol Lett.* (2000) 189:219–23. doi: 10.1016/S0378-1097(00)00288-3
35. Chalk R, Townson H, Ham PJ. *Brugia pahangi*: the effects of cecropins on Microfilariae *in vitro* and in *Aedes aegypti*. *Exp Parasitol.* (1995) 80:401–6. doi: 10.1006/expr.1995.1052
36. Jarosz J. Active resistance of entomophagous rhabditid *Heterorhabditis bacteriophora* to insect immunity. *Parasitology.* (1998) 117:201–8. doi: 10.1017/S0031182098003011
37. Peña JM, Carrillo MA, Hallem EA. Variation in the susceptibility of *Drosophila* to different entomopathogenic nematodes. *Infect Immun.* (2015) 83:1130–8. doi: 10.1128/IAI.02740-14
38. McCormack S, Yadav S, Shokal U, Kenney E, Cooper D, Eleftherianos I. The insulin receptor substrate Chico regulates antibacterial immune function in *Drosophila*. *Immun Ageing.* (2016) 13:15. doi: 10.1186/s12979-016-0072-1
39. Hedengren M, Asling B, Dushay MS, Ando I, Ekengren S, Wihlborg M, et al. Relish, a central factor in the control of humoral but not cellular immunity in *Drosophila*. *Mol Cell.* (1999) 4:827–37. doi: 10.1016/S1097-2765(00)80392-5
40. Aymeric J-L, Givaudan A, Duvic B. Imd pathway is involved in the interaction of *Drosophila melanogaster* with the entomopathogenic bacteria, *Xenorhabdus nematophila* and *Photorhabdus luminescens*. *Mol Immunol.* (2010) 47:2342–8. doi: 10.1016/j.molimm.2010.05.012
41. Mouammine A, Pages S, Lanois A, Gaudriault S, Jubelin G, Bonabaud M, et al. An antimicrobial peptide-resistant minor subpopulation of *Photorhabdus luminescens* is responsible for virulence. *Sci Rep.* (2017) 7:43670. doi: 10.1038/srep43670
42. Hyrsl P, Dobes P, Wang Z, Hauling T, Wilhelmsson C, Theopold U. Clotting factors and eicosanoids protect against nematode infections. *J Innate Immun.* (2011) 3:65–70. doi: 10.1159/000320634
43. Stanley D, Kim Y. Prostaglandins and other eicosanoids in insects: biosynthesis and biological actions. *Front Physiol.* (2018) 9:1927. doi: 10.3389/fphys.2018.01927
44. Kim Y, Ji D, Cho S, Park Y. Two groups of entomopathogenic bacteria, *Photorhabdus* and *Xenorhabdus*, share an inhibitory action against phospholipase A2 to induce host immunodepression. *J Invertebr Pathol.* (2005) 89:258–64. doi: 10.1016/j.jip.2005.05.001
45. Kennedy MW. The polyprotein lipid binding proteins of nematodes. *Biochim Biophys Acta.* (2000) 1476:149–64. doi: 10.1016/S0167-4838(99)00249-6

Conflict of Interest: The authors declare that the research was conducted in the absence of any commercial or financial relationships that could be construed as a potential conflict of interest.

frontiers in Immunology

ORIGINAL RESEARCH
published: 16 October 2019
doi: 10.3389/fimmu.2019.02405

Expression of Human Mutant Huntingtin Protein in *Drosophila* Hemocytes Impairs Immune Responses

Yu-Hsien Lin[1,2]*, *Houda Ouns Maaroufi*[1,2], *Emad Ibrahim*[1,2], *Lucie Kucerova*[1] and *Michal Zurovec*[1,2]*

[1] Biology Centre of the Czech Academy of Sciences, Institute of Entomology, Ceske Budejovice, Czechia, [2] Faculty of Science, University of South Bohemia, Ceske Budejovice, Czechia

The pathogenic effect of mutant HTT (mHTT) which causes Huntington disease (HD) are not restricted to nervous system. Such phenotypes include aberrant immune responses observed in the HD models. However, it is still unclear how this immune dysregulation influences the innate immune response against pathogenic infection. In the present study, we used transgenic *Drosophila melanogaster* expressing mutant HTT protein (mHTT) with hemocyte-specific drivers and examined the immune responses and hemocyte function. We found that mHTT expression in the hemocytes did not affect fly viability, but the numbers of circulating hemocytes were significantly decreased. Consequently, we observed that the expression of mHTT in the hemocytes compromised the immune responses including clot formation and encapsulation which lead to the increased susceptibility to entomopathogenic nematode and parasitoid wasp infections. In addition, mHTT expression in *Drosophila* macrophage-like S2 cells *in vitro* reduced ATP levels, phagocytic activity and the induction of antimicrobial peptides. Further effects observed in mHTT-expressing cells included the altered production of cytokines and activation of JAK/STAT signaling. The present study shows that the expression of mHTT in *Drosophila* hemocytes causes deficient cellular and humoral immune responses against invading pathogens. Our findings provide the insight into the pathogenic effects of mHTT in the immune cells.

Keywords: Huntington's disease, immunity, infection, *Drosophila* melanogaster, phagocytosis, cytokines, antimicrobial peptide (AMPs)

OPEN ACCESS

Edited by:
Susanna Valanne,
University of Tampere, Finland

Reviewed by:
Jenny Sassone,
Vita-Salute San Raffaele University, Italy
Ioannis Eleftherianos,
George Washington University, United States

***Correspondence:**
Yu-Hsien Lin
r99632012@gmail.com
Michal Zurovec
zurovec@entu.cas.cz

Specialty section:
This article was submitted to Comparative Immunology, a section of the journal Frontiers in Immunology

Received: *20 June 2019*
Accepted: *25 September 2019*
Published: *16 October 2019*

Citation:
Lin Y-H, Maaroufi HO, Ibrahim E, Kucerova L and Zurovec M (2019) Expression of Human Mutant Huntingtin Protein in Drosophila Hemocytes Impairs Immune Responses. Front. Immunol. 10:2405. doi: 10.3389/fimmu.2019.02405

INTRODUCTION

Huntington's disease (HD) is an inherited neurodegenerative disorder caused by an abnormal expansion of CAG trinucleotide in the Huntingtin (*htt*) gene. Mutant HTT protein (mHTT) contains an extended polyglutamine tract encoded by 40 to over 150 CAG repeats, which causes cytotoxicity and leads to neurodegeneration; this results in involuntary movement, cognitive impairment, and psychiatric abnormalities (1). Although many clinical symptoms of HD are related to neuronal dysfunction, emerging evidence indicates that the expression of mHTT in non-neuronal cells of the brain or in the peripheral tissues also contributes to the pathogenesis of HD (2). Abnormal phenotypic effects caused by the dysfunction of non-neuronal cells have been described in cardiac cells, muscles, the endocrine system, adipose tissue, testes and immune cells of HD patients, and also in mouse HD models (2, 3).

Abnormalities related to the immune system were observed in a number of studies of HD patients (4). The expression of mHTT in both brain and peripheral immune cells (microglial and myeloid cells) induces the NF-κB signaling pathway which elevates levels of pro-inflammatory cytokines and chemokines, leading to systemic inflammation (5). In addition, macrophages isolated from HD model mice exhibited migration deficits, and microglia showed a delayed response to laser-induced injury in the brain (6). Although several studies proposed that the immune cell response is impaired in HD, this phenomenon is still poorly characterized in relation to host responses to pathogens. One recent study reported increased proliferation of a parasite, *Toxoplasma gondii*, in HD model mice, causing premature mortality and thus suggesting that expression of mHTT in immune cells may suppress immune responses (7).

Drosophila melanogaster has been long-term established as a HD model. *In vivo* experiments have revealed that the ectopic overexpression of mutant human *htt* (exon 1 with expanded CAG repeats) in the neural tissue of transgenic flies causes neurodegeneration (8, 9). The mechanisms of cellular pathology observed in the HD flies seem similar to those in human patients, including the suppression of mitochondrial function, transcriptional dysregulation, and neuronal apoptosis (10, 11). Genetic screening for disease modifiers in HD model flies led to the identification of the effects of sumoylation and HSP70 chaperone machinery on neurodegeneration. The subsequent confirmation that these pathways are involved in the pathology of human patients validates the *Drosophila* model for investigating HD (12, 13). Furthermore, since the tissue-specific expression of transgenes in *Drosophila* can be easily controlled using the UAS-Gal4 system, *Drosophila* have also been used to study the effects of HD on non-neuronal cells, including glial cells, photoreceptors, cardiac cells, and salivary glands (14–18).

The present study aimed to survey the physiological impact of mHTT expression in *Drosophila* hemocytes. We used the *Drosophila* UAS-Gal4 system to express mHTT with hemocyte-specific drivers and investigated the effect of mHTT on survival, hemocyte development, and susceptibility to pathogens. We also expressed mHTT in a *Drosophila* macrophage-like cell line, S2 cells, and assessed the effect of mHTT on phagocytic activity, ATP levels, antimicrobial peptides, and production of cytokines. Our results suggest that the expression of mHTT in hemocytes does not directly affect survival but causes immune dysregulation, which leads to an impaired immune response against pathogenic invasion.

RESULTS

Expression of mHTT in Hemocytes Did Not Affect Larval Viability but Decreased the Number of Circulating Hemocytes

In order to characterize the effects of mHTT in *Drosophila* hemocytes, we used a tissue-specific UAS-Gal4 system by expressing wild-type human HTT (Q20) or mutant HTT (Q93) under the control of a pan-neuronal driver, *elav-gal4*, or hemocyte drivers, *hml-gal4,* and *he-gal4.* The flies devoid of plasmatocytes (*phago*^{less}) generated by expressing pro-apoptosis genes, *rpr* and *hid* with *hml-gal4* were used as negative control (19, 20). The results showed that the ectopic expression of Q93 with the pan-neuronal driver (*elav-gal4*) decreased both the eclosion rate and the longevity of the adult flies, but not the rate of pupariation (**Figure 1**). The expression of Q20 and Q93 with both hemocyte drivers (*hml-gal4* and *he-gal4*) had no effect on pupariation and eclosion rates. Furthermore, the differences in longevity between Q20 and Q93 flies were not significant, and their survival rate was higher than *phago*^{less} flies (**Figure 1C**). These results indicated that the hemocyte-specific expression of mHTT did not influence fly viability, unlike its expression in the brain.

Although the expression of mHTT did not affect fly survival, we observed a significant decrease in the number of circulating hemocytes. In first-instar larvae, the number of hemocytes differed significantly only in the *phago*^{less} flies (**Figure 2A**). However, a reduced amount of circulating and sessile hemocytes was apparent in the Q93 mutants from second-instar larvae. As shown in **Figure 2B**, the circular hemocyte numbers in Q93 larvae were still higher than in *phago*^{less} flies, showing about 50% of the numbers observed in the Q20 control (**Figure 2B**). These results showed that the expression of mHTT with two different hemocyte-specific drivers reduced the number of hemocytes.

Expression of mHTT in Hemocytes Impaired the Immune Response to Parasites

To examine whether mHTT expression in *Drosophila* hemocytes affects the innate immune response and whether such larvae are still able to restrain parasite development, we tested the sensitivity of such flies to entomopathogenic nematode and parasitoid wasp infections, which are two *Drosophila* pathogenic models for examining the cellular immune response (21, 22). Early third-instar larvae expressing mHTT (Q93), wild-type HTT (Q20) or *phago*^{less} were infected with nematode species, *Heterorhabditis bacteriophora* or *Steinernema carpocapsae*, which contain the bacterial symbionts *Photorhabdus luminescens* and *Xenorhabdus nematophila*, respectively. Mortality was calculated at 24 and 48 h post-infection. As shown in **Figure 3**, both *phago*^{less} and Q93 larvae displayed significantly higher mortality than Q20 controls. Previous studies revealed that the formation of hemolymph clot is an important innate immune response against entomopathogenic nematode infection in *Drosophila* (23, 24). To determine whether the expression of mHTT in the hemocytes caused clotting defects, we used an established bead aggregation assay (24, 25). Compared to the larvae expressing normal HTT (Q20), the hemolymph collected from mHTT (Q93)-expressing larvae displayed poor bead aggregation similar to *phago*^{less} larvae (**Figure 3E**). This results indicated that the expression of mHTT suppresses the clotting activity and thus increases the susceptibility to nematode infection.

Similarly, we infected *Drosophila* larvae with a parasitoid wasp, *Leptopilina boulardi* and calculated the number of emerged

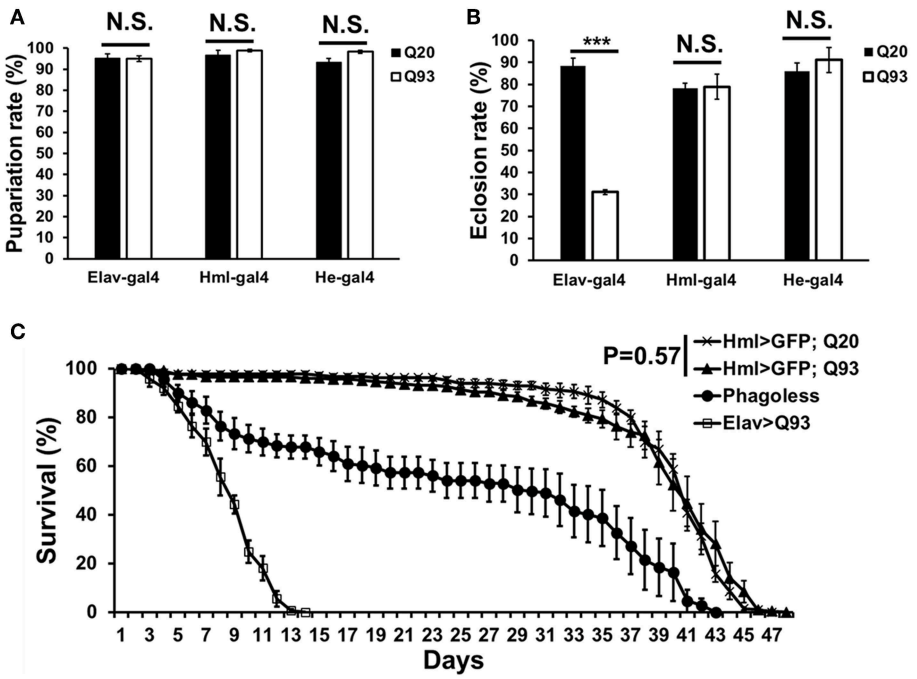

FIGURE 1 | The viability assays of mHTT-expressing flies under the control of the pan-neuronal driver (*elav-gal4*) and hemocyte drivers (*hml-gal4* and *he-gal4*). **(A)** The effect of mHTT expression on pupariation (survival to pupal stage). **(B)** Eclosion (survival to adulthood) and **(C)** adult longevities were measured in control Q20 and mHTT Q93. All the experiments performed in at least six independent replicates. Data are presented as averages ± SEM. *P*-values for pupariation and eclosion rate using Student's *t*-test, ***$P < 0.001$, N.S., not significant. Significance analysis for longevity curve using weighted log-rank test.

fly and wasp adults. The number of eclosed *Drosophila* adults was not significantly different between Q20 and Q93 driven by *hml-gal4* and *he-gal4*, while *phago*^{less} showed lower eclosion rates than both Q20 and Q93 (**Figures 4A,B**). However, the number of emerged wasps were significantly higher in both Q93 and *phago*^{less} flies, thus indicating that a greater number of wasps overwhelmed the immune reaction of Q93 hosts and successfully developed to adult stage. In addition, the higher number of wasp eggs successfully hatched in both Q93 and phagoless larvae (**Figure 4C**); these results indicated that Q93 and *phago*^{less} larvae have less efficient immune reaction against wasp infection. Since the encapsulation and melanization are major defense mechanisms against parasitoid wasp infection, we quantified the number of the melanized capsules to assess the immune activity after 72 h post-infection. We found that there were more intact melanized capsules in Q20 larvae (79%) than in those expressing Q93 (51.6%) or in *phago*^{less} (17.7%) (**Figures 4D,G** left). We also observed a higher amount of melanization pieces in Q93 or *phago*^{less} individuals than in Q20 larvae (**Figures 4E,G** middle). The formation of such defective capsules was described previously in immune-deficient mutant flies (26). Moreover, 37% of the infected *phago*^{less} larvae formed no melanization capsules compared to Q20 (0%) or Q93 (4.8%) infected larvae (**Figures 4F,G** right). These results could explain a lower proportion of *phago*^{less} adults successfully eclosed after wasp infection (**Figures 4A,B**). Taken together, our results suggest, that mHTT expression impairs the innate immune reactions to nematode and parasitoid wasp infections due to the deficient cellular immune responses such as clot formation and encapsulation.

Reduced Phagocytic Activity and ATP Levels in mHTT Cells

To find out whether mHTT expression could cause a detrimental effect on hemocyte functions, we expressed mHTT or wild-type HTT in *Drosophila* S2 cells. The S2 cell line consists of macrophage-like cells with phagocytic activity and the ability to produce antimicrobial peptides (AMPs) (27). We transfected the cells with four different recombinant constructs encoding green fluorescent protein (GFP) fused to HTT repeats under an inducible metallothionein promoter. We created stable cell lineages and confirmed that the S2 cells expressed HTT-fusion proteins by observing the GFP. As shown in **Supplemental Figure 1**, most of the cells in all cell lineages were positive for the fluorophore. Furthermore, the cells containing the mHTT Q46, Q72, and Q97 constructs (all except wild-type Q25) showed formation of mHTT aggregates.

We further treated the HTT-expressing cells with *E. coli* particles conjugated by pH-sensitive dye (pHrodo) to examine their phagocytic activity. This causes bright fluorescence to be visible after particle engulfment in the acidic environment of phagolysosome. The results showed that after inducing mHTT expression, the fluorescence signals were significantly lower in Q46, Q72, and Q97 mHTT-expressing cells but not in cells expressing wild-type Q25 HTT (**Figure 5A**). Quantification of the cells containing fluorescent signals showed a significant

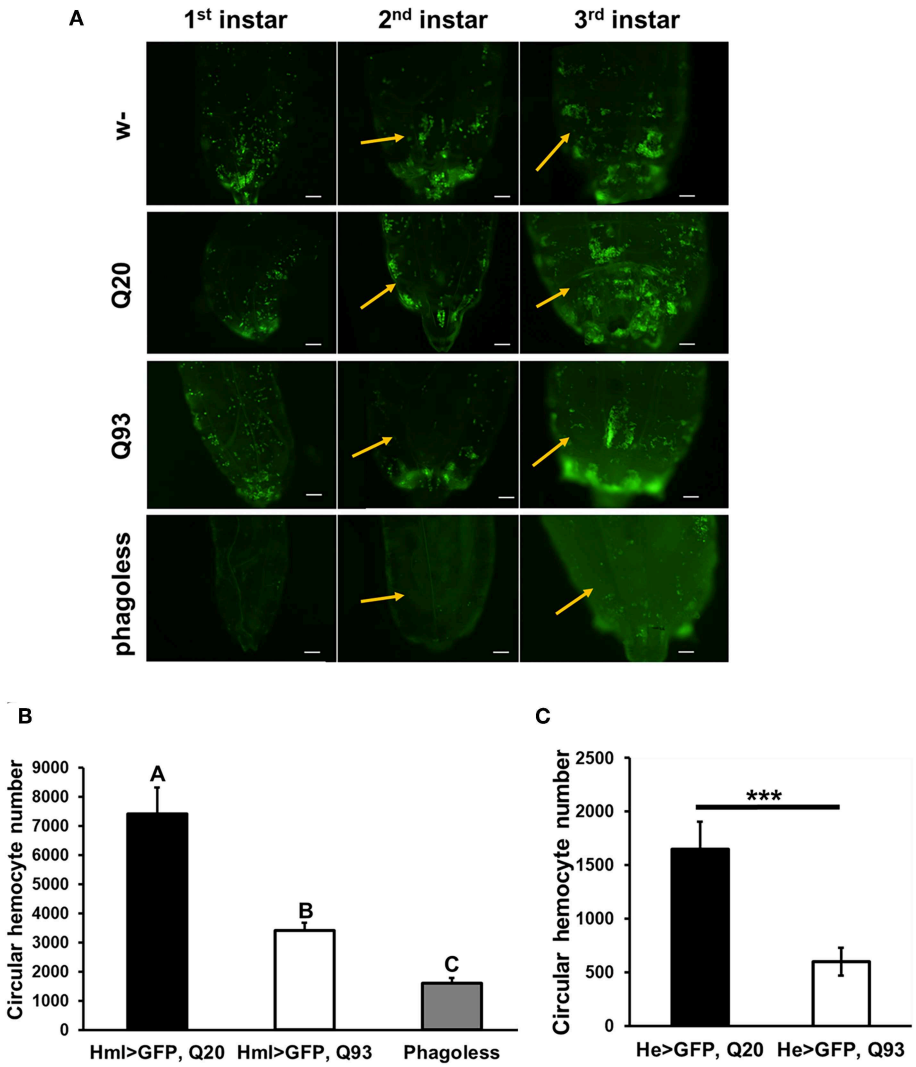

FIGURE 2 | Ectopic expression of mHTT decreased hemocyte numbers. **(A)** Microscope images indicated the decreased number of circulating and sessile hemocytes in mHTT-expressing second-instar larvae. Quantification of hemocytes by ectopic co-expression of HTT with GFP using *hml-gal4* **(B)** or *he-gal4* **(C)**. *Phago*^{less} flies with hemocyte ablation (*hml* > *UAS-rpr, hid*) were used as a negative control. The number of the circular hemocyte corresponded to the total number of GFP positive cells in 25 μL of collected sample. At least five independent replicates were analyzed. Data are presented as averages ± SEM. Significances were analyzed by ANOVA with Fisher LSD *post-hoc* test **(B)**, and the significant differences among treatment groups are marked with different letters ($P < 0.05$). Student's *t*-test was used for **(C)**, ***$P < 0.001$.

reduction (20–30%) of fluorescent-positive cells in mHTT-expressing cells compared to the control cells (Q25) (**Figure 5B**), thus supporting the hypothesis that expression of mHTT in immune cells impairs phagocytic activity.

The phagocytic capacity of immune cells has been associated with mitochondrial activity (28–30); mHTT has been shown to cause impairment of energy metabolism and mitochondrial dysfunction in human peripheral blood cells (31). To test whether mHTT can also impair the energy metabolism of *Drosophila* immune cells, we measured the ATP levels in S2 lineages after mHTT induction. The results showed that ATP levels significantly decreased in cells expressing Q72 and Q97 mHTT after 72 h of induction (**Figure 6A**). The ATP levels in cells expressing Q46, Q72, and Q97 mHTT were further reduced after 120 h of induction (**Figure 6B**). This indicated that the expression of mHTT reduces ATP levels, which may further limit the cellular immune responses against pathogenic infection.

The studies in human and mouse have demonstrated that the expression of Bcl-2 family proteins associated with mitochondrial dysfunction is activated by mHTT expression (32). To assess whether the level of *Drosophila* Bcl-2 proteins is also altered by mHTT expression, we compared the transcription levels of two of *Bcl-2* genes, *buffy* and *debcl*, in Q25- and Q97-expressing S2 cells (**Figure 6C**). We found that *buffy* expression is five times higher in Q97- than in Q25- expressing cells, but we did not detect any significant difference in *debcl* mRNA

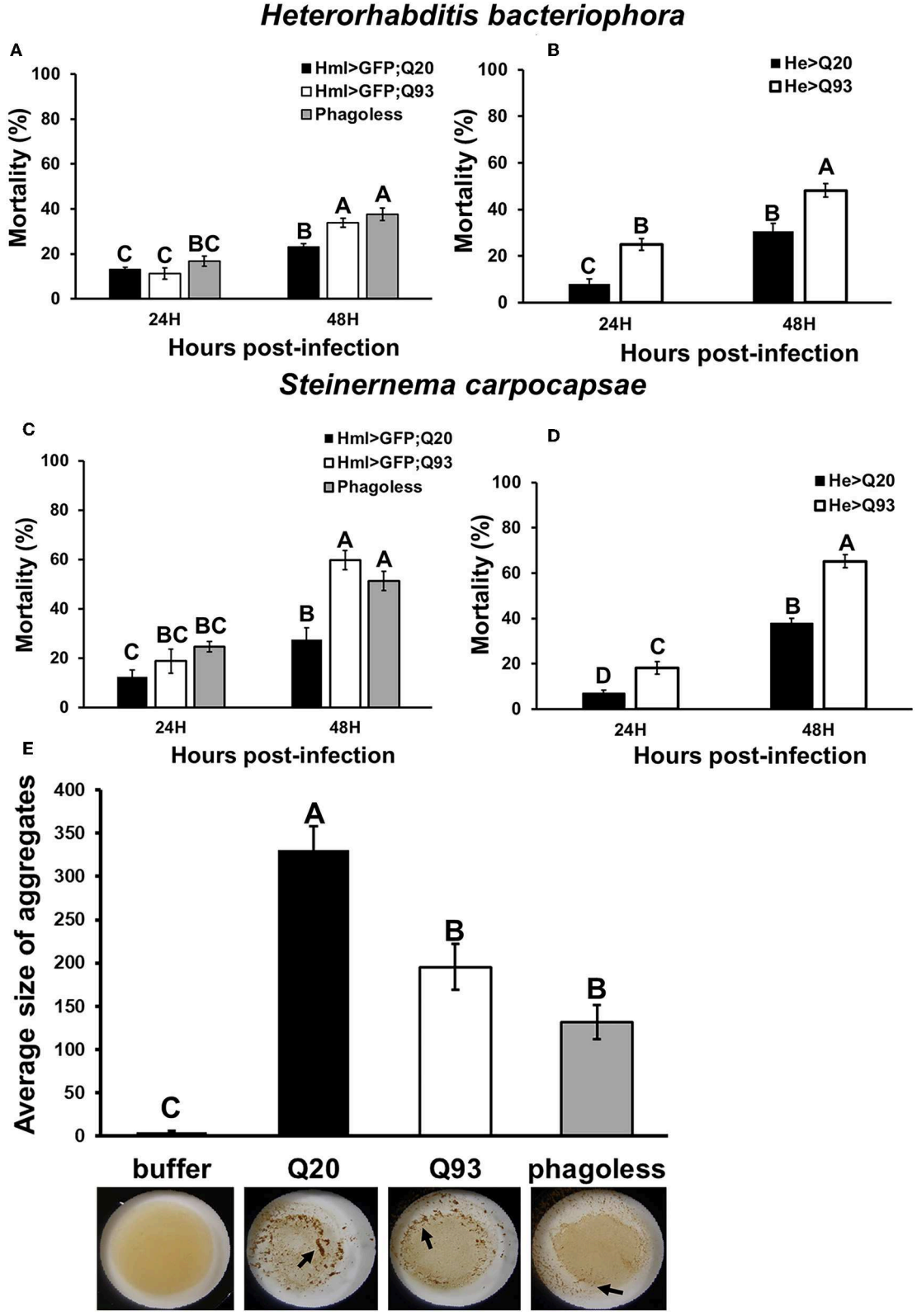

FIGURE 3 | Immune challenge with entomopathogenic nematode infection and clotting assay. Larvae expressing mHTT Q93 or HTT Q20 with *hml-gal4* or *he-gal4* hemocyte drivers were infected with *H. bacteriophora* **(A,B)**, or *S. carpocapsae* **(C,D)**. Mortality was calculated 24 and 48 h after infection. *Phago*^{less} flies with

(Continued)

FIGURE 3 | hemocyte ablation (*hml > UAS-rpr, hid*) were used as negative control. Bead aggregation assay was used for assessing the clotting activity **(E)**. Hemolymph was collected from Q93, Q20, and *Phago*^{less} (*hml-gal4*) larvae, mixed with a bead suspension, and the aggregates were quantified by ImageJ software. All the experiments were performed in five to six independent replicates. Data are presented as averages ± SEM. Significances were analyzed by ANOVA with Fisher LSD *post-hoc* test; significant differences among treatment groups are marked with different letters ($P < 0.05$).

level. Different from pro-apoptotic function of *debcl*, *buffy* was suggested to play an anti-apoptotic role under stress conditions which is similar to mammalian Bcl-2 proteins (33, 34). We conclude that the alternation of ATP synthesis and *buffy* expression indicate the abnormality of mitochondrial function in mHTT expressing cells, and the induction of *buffy* might be a protective mechanism for preventing the cell death caused by mitochondrial dysfunction.

Upregulation of Cytokines Expression and Downstream JAK/STAT Signaling in mHTT Expression Cells

It has been reported that the level of cytokines and chemokines are abnormally increased in the plasma of HD patients (35). Consistently, the production of cytokines from monocytes and macrophages of HD patients have shown hyper-activation after lipopolysaccharide stimulation (36). To test whether mHTT has a similar effect in *Drosophila*, we used Schneider 2 (S2) cells and measured the effect of mHTT expression on three *Drosophila* cytokines, *upd1*, *upd2*, and *upd3*, as well as *dome*, *jak* (*hop*) and downstream targets of JAK-STAT signaling (**Figure 7A**). The results showed that the expression of cytokine *upd3* is significantly increased in Q97 mHTT-expressing cells compared to Q25 controls (**Figure 7B**). In addition, the expression of *dome* receptor and four downstream targets, *tep1*, *totA*, *totB,* and *totC* were also significantly increased in Q97-expressing cells. These results indicated that the expression of mHTT induced the production of cytokines and activates JAK/STAT signaling.

Decreased Antimicrobial Peptide (AMP) Production in Response to Bacteria

Drosophila Toll and Imd pathways control the humoral immune response against invasive microorganisms by regulating the induction of downstream AMP genes in both hemocytes and the fat body (37). To examine whether AMP induction was affected by mHTT expression in *Drosophila* S2 cells, we treated mHTT-expressing cells with a mixture of heat-inactivated Gram-negative bacteria, *Escherichia coli*, and Gram-positive bacteria, *Micrococcus luteus*. The induction of AMPs was assessed using qPCR. As shown in **Figure 8**, there was no difference in the expression of AMPs between Q25 and Q97 in the absence of bacterial treatment. In contrast, all AMP genes were significantly induced in both Q25- and Q97-expressing cells at 8 h after bacterial treatment. However, AMP induction levels were significantly lower in cells expressing Q97 (**Figure 8A**). We further assessed the AMP expression levels under *in vivo* condition after infecting larvae with phytopathogenic bacteria, *Erwinia carotovora carotovora 15* (Ecc15). We examined the expression levels of *dpt*, *dptB*, *attA,* and *cecA* which were known as being highly induced after Ecc15 infection (38). Our results of larval infections showed that except for *attA*, the induction levels of *dpt*, *dptB,* and *cecA* in Q93 or *phago*^{less} larvae were significantly lower than in Q20 controls (**Figure 8B**). These results confirm that the induction of AMPs in response to bacteria was significantly suppressed in mHTT-expressing cells or larvae.

DISCUSSION

Peripheral immune dysregulation is considered as one of the clinical features of HD pathogenesis (39). Previous studies in mice and HD patients have suggested that mHTT expression in immune cells accelerates the neurodegenerative process. The activation of pro-inflammatory products in mHTT-expressing microglial cells elevate the reactive oxygen species (ROS) and cause neuroinflammation, which contributes to neurodegeneration (5, 40). Genetic ablation or pharmacologically-blocked cannabinoid receptor 2 (interleukin-6 regulator), as well as drug suppression of the cytokine-responsive kynurenine pathway, can both slow neurodegeneration and improve the phenotype of R6/2 HD mice (41, 42). Since the expression of mHTT in HD mice and human patients is ubiquitous, it is still unclear whether mHTT expression in blood cells directly contributes to the lethal effect of HD. The present study examined mHTT expressed specifically in *Drosophila* blood cells and assessed its impacts on development and longevity (**Figure 1**). We found that the expression of mHTT in hemocytes did not cause mortality or a shortening in life span, which is in contrast to expression in the brain. Our results, therefore, suggest that expression of mHTT in immune cells does not directly contribute to mortality.

A reduced proliferation of immune cells has been observed in *T. gondii*-infected HD mice, in which the expansion of $CD8^+$ T-cells in the spleen and brain was significantly suppressed during infection (7). Our results showed that the expression of mHTT in flies with hemocyte-specific drivers causes a significant reduction in the number of circulating hemocytes (**Figure 2**), and this decrease might be caused by dysfunction of mitochondria (**Figure 7**). The mitochondrial abnormalities resulting in metabolic dysregulation in peripheral blood cells of HD patients increase oxidative damage and suppress their anti-oxidant capacity (40). The activation of caspase-3 and caspase-9 in lymphoblasts of HD patients increases apoptosis under stress conditions (43).

The mHTT-expressing larvae revealed a higher susceptibility to wasp and nematode infections and this phenotype was caused by defects of clot formation and encapsulation (**Figures 3**, **4**). It has been shown that wasp egg recognition by circulating plasmatocytes and their differentiation to lamellocytes for further encapsulation are important processes of the immune response against wasp invasion in *Drosophila* (44). The production of clotting components from hemocytes also contributes to

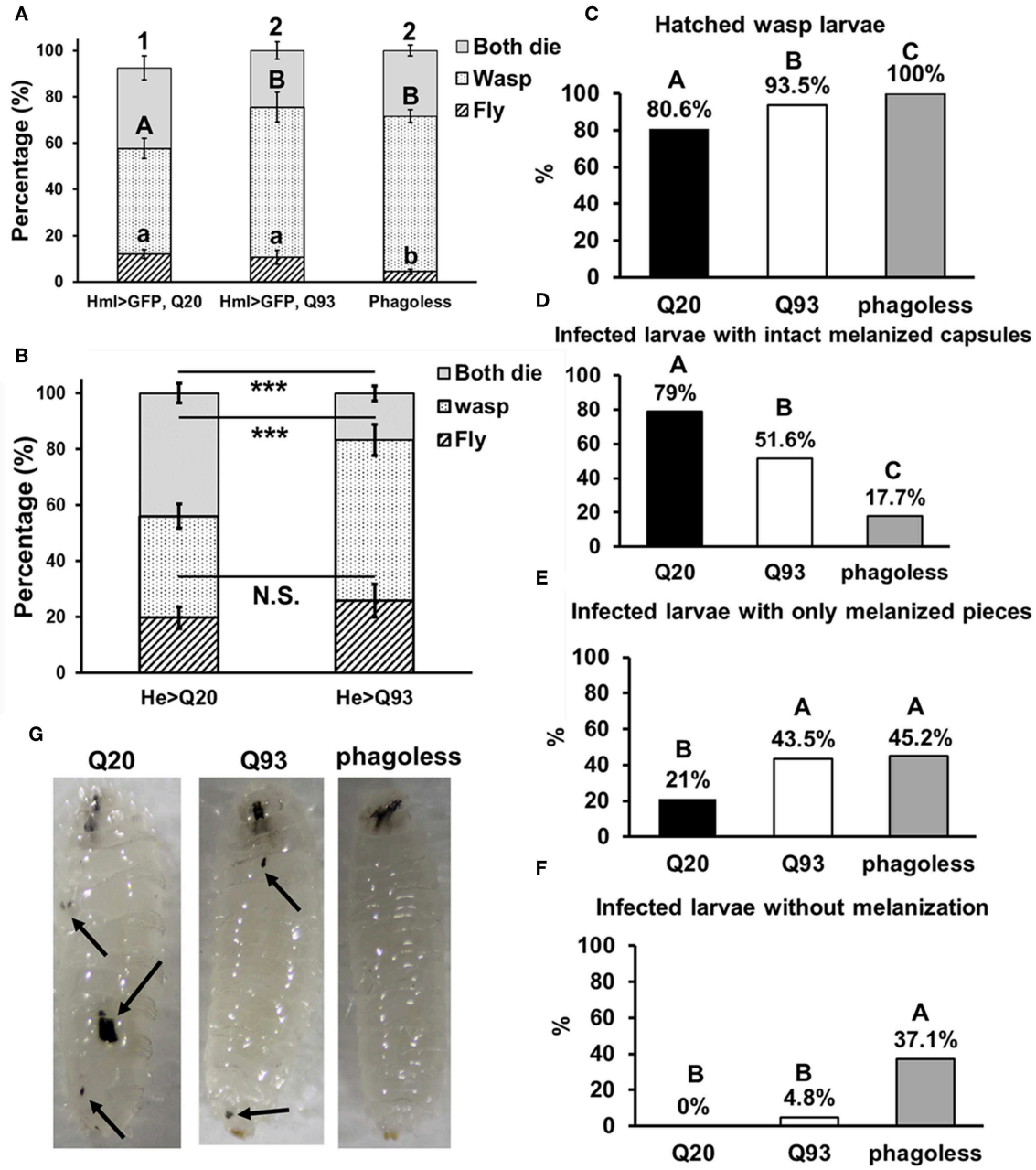

FIGURE 4 | Immune challenge with parasitoid wasp infection and encapsulation activity assay. Larvae expressing mHTT Q93 and HTT Q20 with *hml-gal4* **(A)** or *he-gal4* **(B)** hemocyte driver were infected with parasitoid wasp, *L. boulardi*. *Phago*^{less} flies (which underwent hemocyte ablation) were used as negative control. Thirty infected larvae were collected and the numbers of eclosed flies and wasps were calculated, indicating the number of flies overcoming the wasp infection and the number of wasps successfully escaping the fly's immune reaction, respectively. Data are presented as average ± SEM with more than 10 biological replicates. The significances of results for **(A)** were analyzed by ANOVA with a Fisher LSD *post-hoc* test; different letters on the treatment group indicate significant differences at $P < 0.05$. The significances of results for **(B)** were examined using Student's *t*-test, $^{***}P < 0.001$, N.S., not significant. For assessing the encapsulation activity, the numbers of fly larvae containing larvae of parasitic wasps **(C)**, intact melanized capsules **(D)**, melanized pieces **(E)** as well the numbers of the infected larvae without melanization **(F)** were recorded. The significances of the results were analyzed by Mann-Whitney *U*-test (paired); significant differences among treatment groups are marked with different letters ($P < 0.05$). The photos show examples of intact melanized capsule in Q20 larvae, melanized pieces in Q20 and Q93 larvae and infected *phago*^{less} without melanization reaction **(G)**.

wound healing and melanization, which are important against nematode or wasp infections (24, 45). mHTT-expressing macrophages and monocytes from HD mice and patients also showed migration defects toward an inflammatory stimulus (6). Hemocyte migration and adhesion are important factors for the development of embryonic macrophages, as well as successful

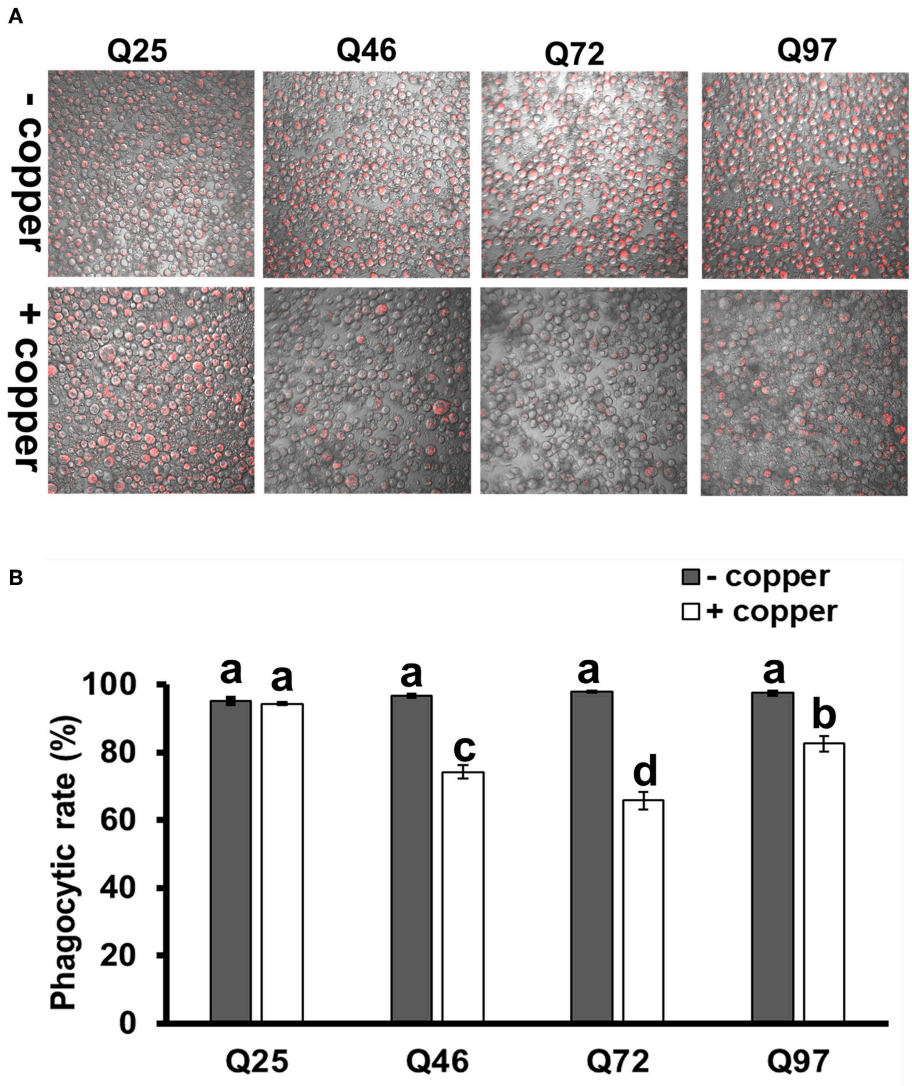

FIGURE 5 | Impairment of phagocytic activities in mHTT-expressing S2 cells. S2 cell lineages expressing wild-type HTT (Q25) and mHTT (Q46, Q72, and Q97) were treated with pHrodo Red *E. coli* for 8 h. **(A)** Fluorescence microscope images show the decreased intensity of red fluorescence signals in mHTT-expressing cells. **(B)** The phagocytic rate was calculated as the percentage of cells showing a red fluorescence signal to the total number of cells in each image. Each treatment was performed in three independent replicates with (+copper) or without (–copper) $CuSO_4$ induction. Data are presented as average ± SEM. Significances were analyzed by ANOVA with Tukey HSD *post-hoc* test; different letters on the treatment group indicate significant differences at $P < 0.05$.

wound healing and encapsulation during wasp infection (46). Furthermore, decreased phagocytic activity toward bacterial particles (**Figure 5**) and a suppressed induction of antimicrobial peptides (**Figure 8**) can also contribute to immune deficiency against the bacterial symbionts of nematodes (23, 47).

A previous study showed that macrophages isolated from HD patients and R6/2 mice displayed increased phagocytosis when incubated with fluorescent polystyrene beads (48). Our results seemingly differ because we observed reduced phagocytic activity of the *Drosophila* macrophage-like cells expressing different mHTT fragments (**Figure 5**). Unlike their approach, we tested phagocytic activity using *E. coli* particles with a pH-sensitive fluorescent dye that can accurately confirm phagosome formation and initiation of the phagolysosome acidification. However, similar to their results, we found that S2 cells expressing mHTT were able to initiate phagocytosis. We tested this by treating the S2 cells with heat-inactivated *E. coli* labeled with DNA-specific fluorescent dye (without pH-sensor); the results showed that mHTT-expressing cells were indeed able to engulf *E. coli* (**Supplemental Figure 2**). Thus, our results suggest that mHTT-expressing cells were unable to complete the process of phagocytosis to final phagolysosome acidification. In addition, a defective actin function has been reported in HD mouse immune cells leading to failure of membrane ruffling (6),

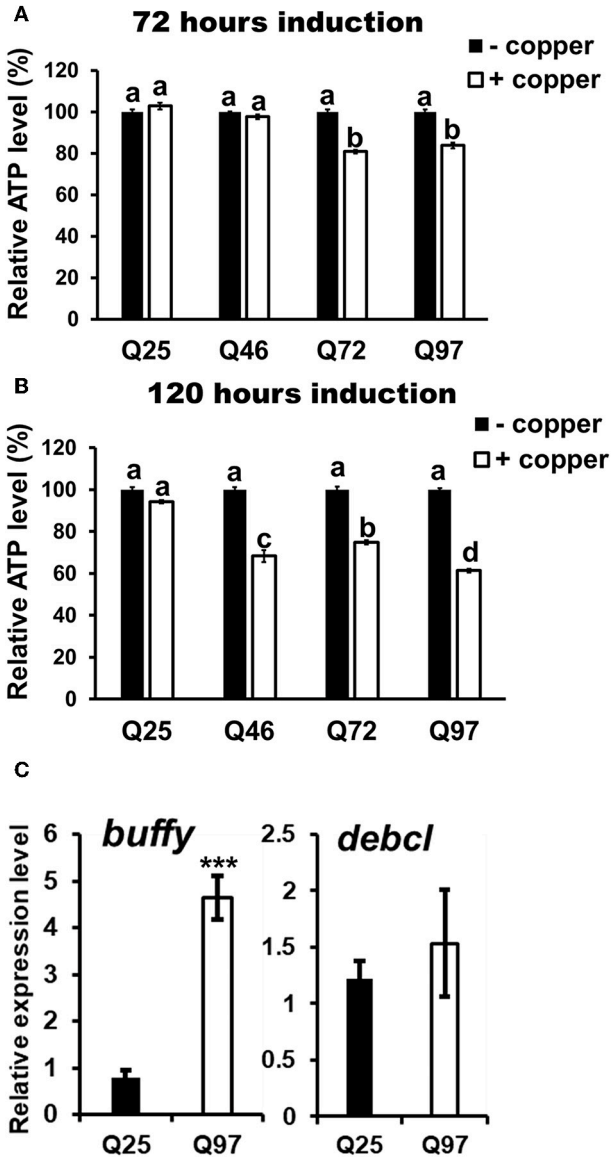

FIGURE 6 | Decrease of ATP level and alternation of Bcl-2 protein expression in mHTT-expressing S2 cells. ATP levels of HTT- and mHTT-expressing S2 cells (5×10^4 cells) were measured after 72 **(A)** and 120 h **(B)** of copper induction. Each treatment was performed in five independent replicates with (+copper) or without (–copper) copper induction. Data are presented as average ± SEM. Significances were analyzed by ANOVA with Tukey HSD *post-hoc* test; different letters on the treatment group indicate significant differences at $P < 0.05$. The mRNA levels of *Drosophila* Bcl-2 proteins, *buffy* and *debcl* were measured in Q25 HTT and Q97 mHTT-expressing S2 cells after 120 h of induction **(C)**. All the expressions were normalized to *rp49* transcript and Q25 control (ΔΔCT). Data are presented as average ± SEM from three independent replicates. *P*-values were determined using Student's *t*-test, $^{***}P < 0.001$.

which supports our results since actin assembly is required to trigger engulfment and phagolysosome maturation for successful phagocytosis (49).

Consistent with previous observations in HD mice and patients, we also found that *Drosophila* hemocyte cytokine *udp3* was upregulated in mHTT-expressing cells (**Figure 8**). *Udp3* binds to the JAK/STAT signaling receptor, Dome, and initiates phosphorylation cascades which translocate the transcription factor, Stat92E, into the nucleus and activates downstream target genes (**Figure 7A**) (50). Two selected downstream target genes, *tep1* and *totA*, were highly expressed in mHTT-expressing cells (**Figure 7B**). Notably, we found that the induction of antimicrobial peptides was significantly suppressed in mHTT-expressing cells after bacterial treatments, which has not yet been observed in other HD models. It is known that several human antimicrobial peptides are expressed in blood cells including neutrophils and macrophages (51). Since the transcriptomic analysis in HD blood cells has shown dysregulation of transcription in large genomic regions (52), further studies will be needed to understand whether the production of antimicrobial peptides is impaired in the blood cells of patients or HD mice during infection.

In summary, the present study demonstrates immune dysregulation in flies expressing mHTT in hemocytes (**Figure 9**). This expression does not directly cause a lethal effect, although it does reduce the number of circulating hemocytes and decrease ATP levels. Cytokine expression and downstream JAK/STAT signaling are activated upon mHTT expression, which has also been observed in HD patients and mice. In addition, the induction of antimicrobial peptides as well as the immune response against different pathogenic infections are impaired in mHTT-expressing *Drosophila* cells. The present study introduces a system for studying the tissue-specific effects of mHTT in *Drosophila* immune cells. Further studies can be applied to clarify the molecular interaction between mHTT and antimicrobial peptide pathways (Toll and IMD signaling) as well as the mechanisms of phagocytosis suppression.

MATERIALS AND METHODS

Fly Stocks

Flies were reared at 25°C on standard cornmeal medium. The fly strains used were UAS-Q20Httexon1^{111F1L} and UAS-Q93Httexon1^{4F132} obtained from Prof. Lawrence Marsh (UC Irvine, USA) (8), which contain 20 (wild-type) and 93 (mutant HTT) polyglutamine repeats, respectively. The pan-neuronal driver, *elav-gal4*[C155], and hemocyte drivers, *he-gal4* and *hml-gal4*, were obtained from Bloomington *Drosophila* Stock Center and Dr. Tomas Dolezal (University of South Bohemia), respectively (53–55). Hemocyte-ablated flies (*phago^{less}*) were used as negative controls and were generated by overexpressing pro-apoptotic proteins (*UAS-rpr*, *-hid*) with *hml-gal4* (19, 20, 56).

Developmental and Longevity Assay

Thirty first-instar larvae collected from a juice plate were transferred into vials to measure the number of pupae and adults for each replicate. For the longevity assay, about 20–30 newly emerged male adults were collected for each replicate and maintained at 29°C. Q93 expression driven by pan-neuronal driver, *elav-gal4* and *phgo^{less}* flies were used as positive controls for longevity assay. Since expression of Q93 driven by *elav-gal4* (X chromosome insertion) results in high mortality of male progeny (dosage compensation) (57), female progeny were used for recording the longevity. The number of dead flies was counted

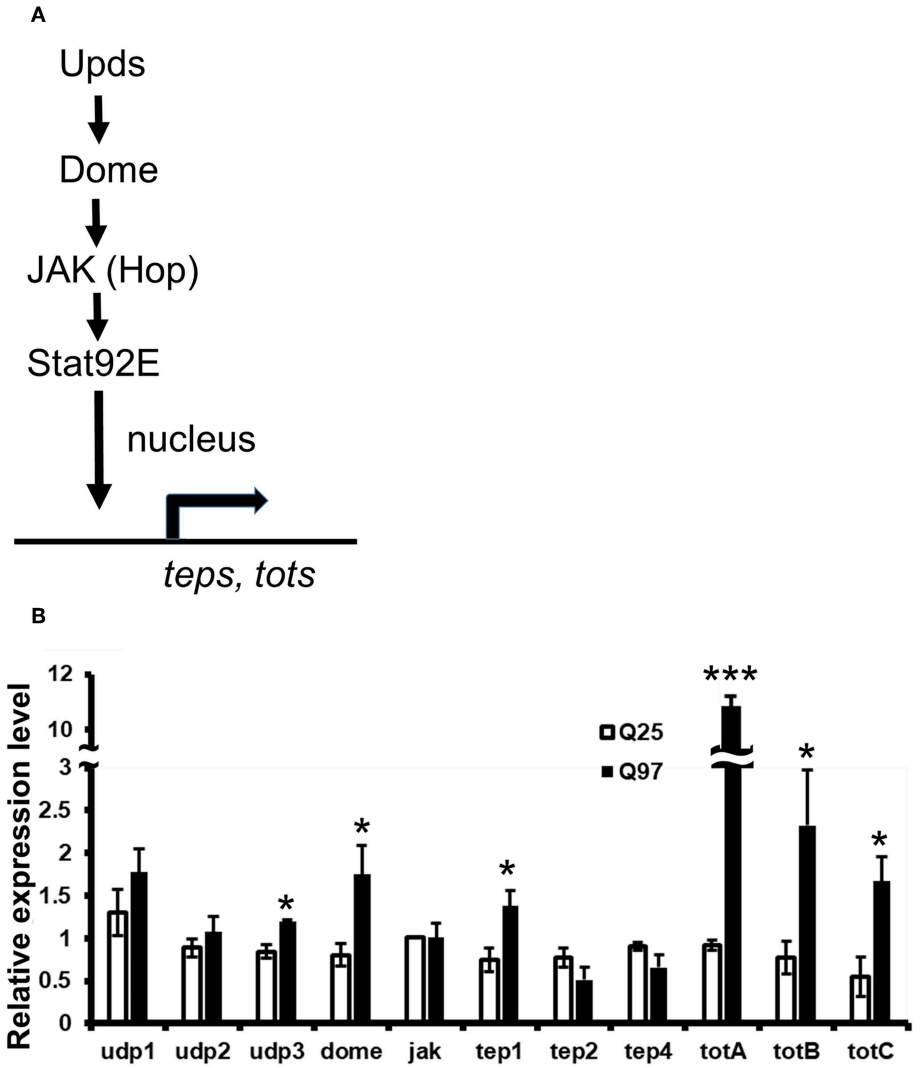

FIGURE 7 | Activation of cytokine expression and JAK/STAT signaling in the mHTT-expressing S2 cells. **(A)** Schematic representation of the interaction between Upds and JAK/STAT pathway. **(B)** The gene expression of cytokines (*udp1-3*), *dome*, *jak*(*hop*), and JAK/STAT downstream target genes (*teps* and *tots*) were measured in Q25 HTT and Q97 mHTT-expressing S2 cells after 120 h of copper induction. All the expressions were normalized to *rp49* expression and Q25 control (ΔΔCT). Data are presented as average ± SEM from three independent replicates. *P*-values using Student's *t*-test, $^{*}P < 0.05$, $^{***}P < 0.001$.

every day. All the experiments were performed in at least six independent replicates.

Circulating Hemocyte Counting

Circulating hemocytes were obtained from larvae by cuticle tearing in Ringer's buffer with thiourea to prevent melanization (25 μl of buffer per 6 larvae). The number of hemocytes expressing GFP (*hml-gal4* or *he-gal4 > UAS-gfp*) were counted using a hemocytometer. At least five independent replicates were analyzed for each genotype.

Parasitoid Wasp Infection, Eclosion, and Encapsulation Assay

Leptopilina boulardi parasitoid wasps were obtained from Dr. Jan Hrček (Biology Center CAS) and maintained by infecting wild-type *Drosophila* larvae. For the wasp infection assay, forty larvae (second instar) were transferred onto a dish containing cornmeal food, and three female wasps were then placed onto the dish and allowed to attack for 72 h. After infection, 30 infected larvae were collected from the dish and transferred into a vial containing cornmeal for each replicate. Each genotype was tested in at least 10 independent replicates. The total number of eclosed flies and wasps were calculated (26). For the encapsulation assay, the infected larvae were dissected 72 h post-infection and the number of larvae containing intact melanized capsules, broken melanized pieces as well as wasp larvae was recorded.

Nematode Infection

Two nematode species, *Steinernema carpocapsae* and *Heterorhabditis bacteriophora*, were used in this study, under previously described maintenance conditions (58). For the infection assay, nematodes were combined with autoclaved

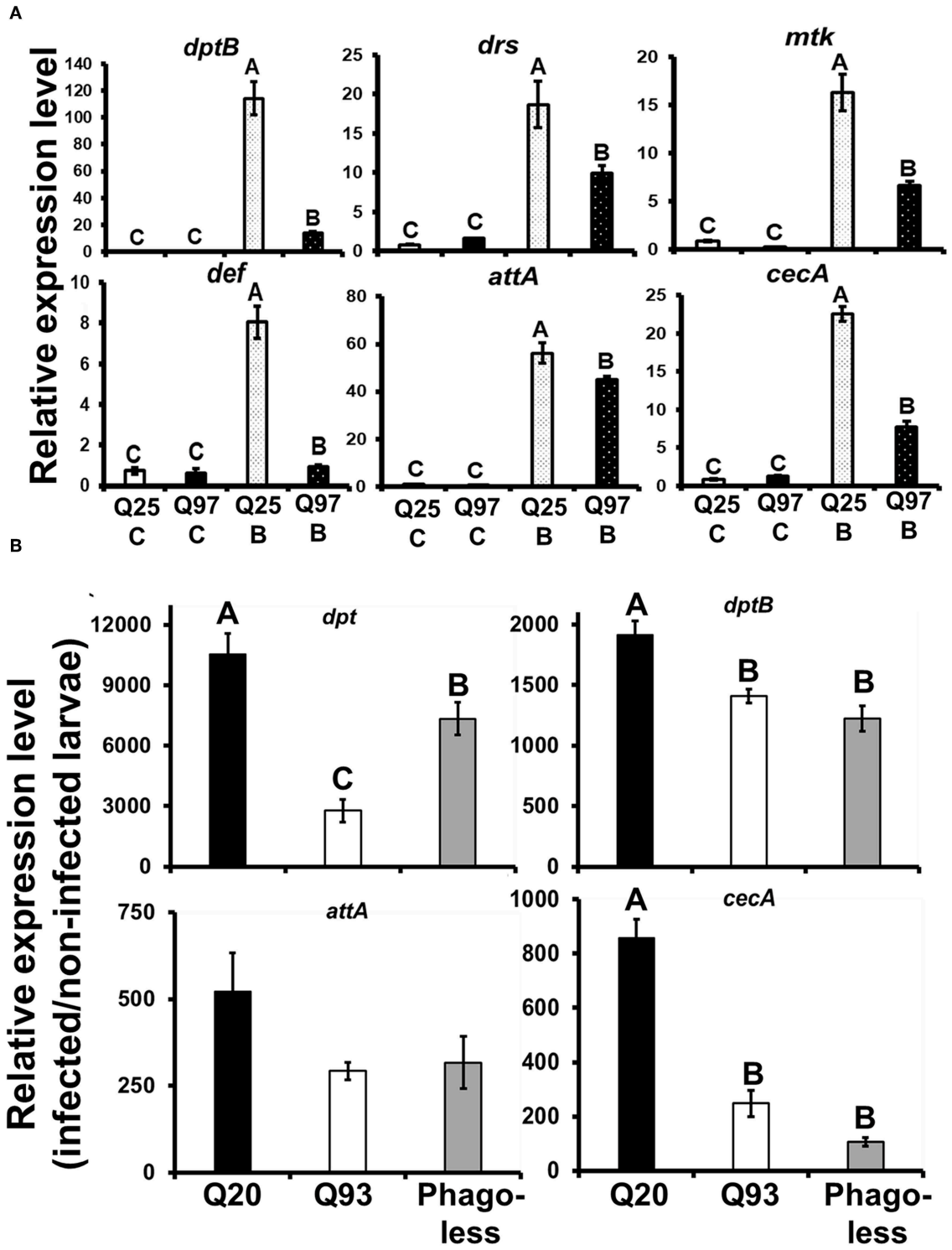

FIGURE 8 | Suppression of antimicrobial peptides (AMPs) induction after bacterial treatment in the mHTT-expressing S2 cells and larvae. **(A)** Q25 and Q97-expressing S2 cells were incubated with *E. coli* and *M. luteus* (Q25_B and Q97_B) or without bacteria (Q25_C and Q97_C) for 8 h, and the expression levels of AMPs was measured. The AMPs expressions were normalized to *rp49* expression and Q25 control. **(B)** Larvae expressing mHTT Q93 or HTT Q20 under *hml-gal4* hemocyte drivers as well as *Phago*^{less} mutants were infected with ECC15-GFP and their expression of AMPs was determined after 8 h. The expressions were normalized to *rp49* transcripts and non-infected controls. The AMPs expression levels of non-infected controls for each genotype were set to one. All the data are presented as average ± SEM from three independent replicates. The significances were analyzed by ANOVA with Fisher LSD *post-hoc* test; different letters on the treatment group indicate significant differences at $P < 0.05$.

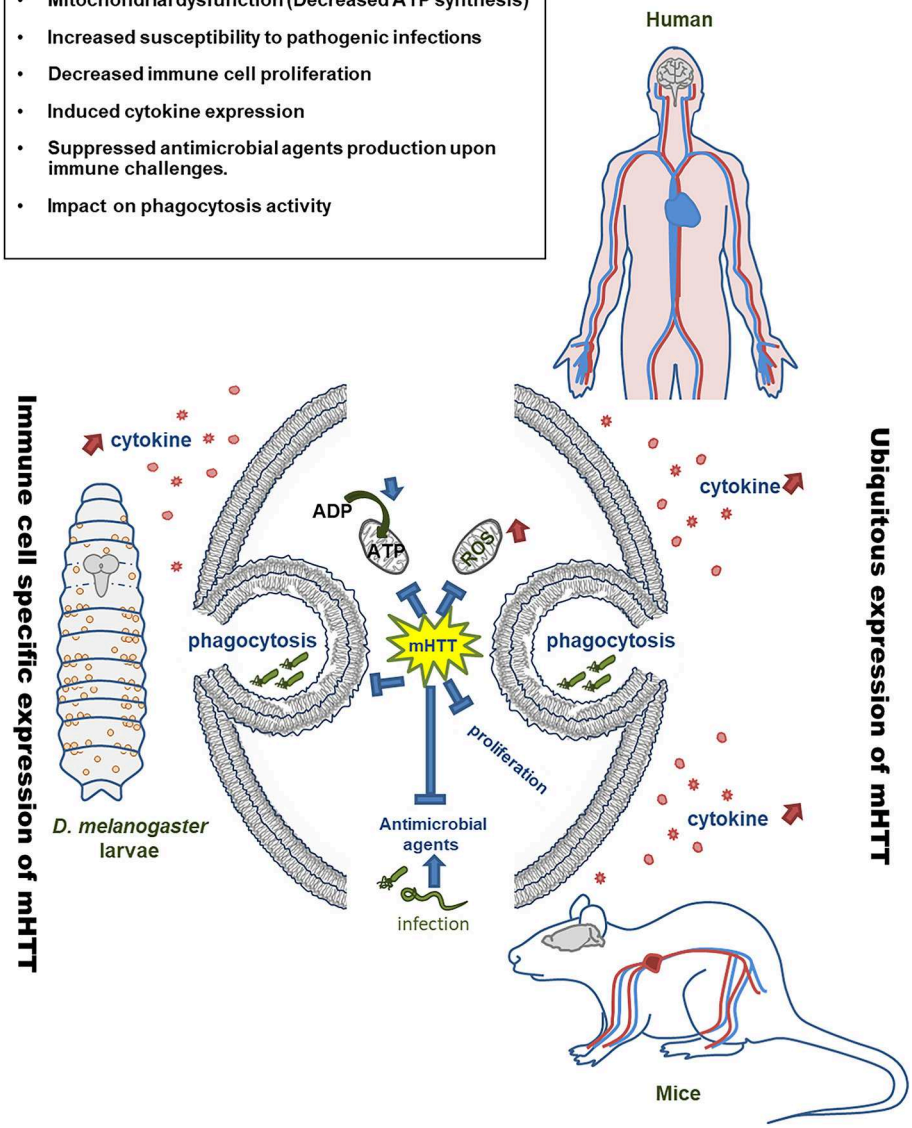

FIGURE 9 | Model of mHTT effects on *Drosophila* and mammalian immune cells. The expression of mHTT in hemocytes of *Drosophila* displays similar effects on the immune cells of HD patients and mice.

water to achieve a concentration of 25 infective juveniles per 10 µl. Then, 10 µl of nematode suspension was applied to paper and placed in each wells of a 96-well plate. Individual larvae were transferred to each well where they stayed in contact with the nematodes, and the plate was covered with Parafilm. The infection was conducted at 25°C in the dark. Each experimental replicate consisted of 32 early third-instar larvae (72 h after egg hatching), and all experiments were done at least in five replicates. The number of dead larvae were counted after 24 and 48 h of infection (23, 24).

Bead Aggregation Assay

The bead aggregation assay was described in our previous study (24). Briefly, 2.5 µl of hemolymph was collected from six late third-instar larvae, mixed with BSA-blocked bead suspension (tosylactivated Dynabeads M-280, Invitrogen), diluted in *Drosophila* Ringer (pH 6.0) in a well of cavity diagnostic slide (Thermo Scientific) and covered with round cover glass. Pictures were taken with a Nikon SMZ-745T stereomicroscope associated with a CANON EOS 550D. The images were analyzed and quantified with the ImageJ graphics software with the "Analyze Particles" module.

Cell Culture

Drosophila Schneider 2 (S2) cells were grown at 25°C in Shields and Sang medium (Sigma) with 0.1% yeast extract, 0.25% peptone, and 10% heat inactivated fetal bovine serum.

To generate stable lines expressing polyglutamine repeats, the S2 cells were transfected with four different Httex1-eGFP pMK33 plasmids (Q25, Q46, Q72, and Q97) containing copper-inducible metallothionein promoter (obtained from Dr. Sheng Zhang) (59).

Phagocytosis Assay

After induction for 5 days (120 h) with 1 mM copper ($CuSO_4$; Sigma), 100 µl of cell suspension (1×10^6 cells/ml) was transferred to each well of a 96-well plate. Then, 100 µl of pHrodo Red *E. coli* (1 mg/ml; Thermo Fisher Scientific) was applied to each well for phagocytosis testing. After 8 h of treatment, the supernatant was removed, the cells were washed two times with 1× PBS, and 100 µl of fresh medium was applied. Cells were observed and photographed with a confocal microscope. From the images, the total number of cells and the number of cells displaying red fluorescence were counted. Three experimental repeats for each treatment were done for statistical analysis.

ATP Measurement

Cells were treated with 1 mM copper for 3 days (72 h) and 5 days (120 h) to induce mHTT expression. Fifty microliter of a 1×10^6 cells/ml solution (5×10^4 cells) was transferred to each well of a 96-well plate. After removing the supernatant, 60 µl of CellTiter-Glo solution (Promega) was applied to each well for 10 min. Then, 50 µl of the mixture was transferred to each well of 96-well white plates and the intensity of luminescence was then measured. Five independent replicates for each treatment were performed for analysis.

Bacterial Infection *in vitro* and *in vivo*

Five milliliter of S2 cells (1×10^6 cells/ml) carrying copper-inducible Q25 HTT or Q97 mHTT transgenes were incubated in media containing 1 mM $CuSO_4$ for 120 h in 60 mm tissue culture plates. After the induction, the cells were treated for 8 h with 1 ml of bacterial mixture containing *Escherichia coli* and *Micrococcus luteus* at an optical density (600 nm) of 1 ($OD_{600} = 1$) (37). The cells were then harvested for RNA extraction.

For the *in vivo* infection, late third instar larvae (96 h after egg hatching) were collected and transferred into a vial with 0.5 g instant *Drosophila* medium (Formula 4–24, Carolina Biological Supply) supplemented with 200 µl of bacterial suspension ($OD_{600} = 50$) *Erwinia carotovora carotovora 15*-GFP (ECC15-GFP) and 1,300 µl of distilled water. The larvae were collected for RNA extraction 8 h after the infection (19, 38).

RNA Extraction

For *in vitro* experiments, S2 cells were washed with 1× PBS three times and harvested with 800 µl of RiboZol (VWR). Samples were preserved at −80°C until RNA purification. For *in vivo* experiments, 10 larvae were washed by distilled water and homogenized by the pestle motor (Kimble) in 200 µl of RiboZol (VWR Life Science). The sample were then preserved at −80°C for further RNA purification. RNA was isolated using NucleoSpin RNA columns (Macherey-Nagel) following the manufacturer's instructions and cDNA was synthesized from 2 µg of total RNA using a RevertAid H Minus First Strand cDNA Synthesis Kit (Thermo Fisher Scientific).

qPCR and Primers

5× HOT FIREPol® EvaGreen® qPCR Mix Plus with ROX (Solis Biodyne) and an Eco Real-Time PCR System (Illumina®) were used for qPCR. The cDNA was diluted 50 times before use. Each reaction contained 4 µl of EvaGreen qPCR mix, 0.5 µl of forward and reverse primer (10 µM), 5 µl of diluted cDNA and ddH2O to adjust the total volume to 20 µl. The list of primers is shown in **Supplemental Table 1**. The expression level was calculated by using the ($2^{-\Delta\Delta CT}$) method. The CT value of target genes were normalized to reference gene, ribosomal protein 49 (*rp49*).

Statistical Analysis

Error bars show standard error of the mean throughout this paper. Significance was established using Student's *t*-test (N.S., not significant, $^*P < 0.05$, $^{**}P < 0.01$, $^{***}P < 0.001$) or one-way ANOVA analysis with Fisher LSD or Tukey HSD *post-hoc* test. The Mann–Whitney *U*-test was used for examing the significance of the data on wasp larval hatching and the host encapsulation activities (**Figures 4C–F**). For the statistical analysis of longevity curve, we used online tool OASIS 2 to perform the weighted log-rank test for determining significance (60).

DATA AVAILABILITY STATEMENT

The raw data supporting the conclusions of this manuscript will be made available by the authors, without undue reservation, to any qualified researcher.

AUTHOR CONTRIBUTIONS

Y-HL conceived the project, performed the experiments and prepared the manuscript. HM performed the hemocyte counting and imaging. EI performed the nematode infections. LK performed the clotting assay. MZ supervised the project and manuscript preparation.

FUNDING

This work was supported by the grant agency of the University of South Bohemia (065/2017/P to Y-HL), junior grant project GACR (19-13784Y to LK). MZ was a member of the COST action Maximizing impact of research in neurodevelopmental disorders (CA16210).

ACKNOWLEDGMENTS

We thank Dr. Sheng Zhang (UThealth) for the Httex1-eGFP pMK33 plasmids, Prof. L. Marsh (UC Irvine, USA) for Q20 and Q93 flies, Dr. Tomas Dolezal (University of South Bohemia) for the hemocyte driver line, Dr. Pavel Hyrsl, Pavel Dobes (Masaryk University) for the nematodes, and Dr. Hrcek Jan, Dr. Chia-Hua Lue (Biology Centre CAS), and Dr. Adam Bajgar (University

of South Bohemia) for the parasitoid wasps, Dr. Julien Royet (IBDM, France) for bacteria ECC-15.

SUPPLEMENTARY MATERIAL

The Supplementary Material for this article can be found online at: https://www.frontiersin.org/articles/10.3389/fimmu.2019.02405/full#supplementary-material

Supplemental Figure 1 | Expression of four different lengths of HTT-GFP fusion proteins under a fluorescence microscope. mHTT-expressing cells (Q46, Q72, and Q97) showed significant mHTT aggregates after copper induction, while there was no aggregate formation in normal HTT-expressing cells (Q25).

Supplemental Figure 2 | Phagocytosis assay in Q25- and Q97-expressing S2 cells with *E. coli* labeled by DNA-specific dye (Hoechst 33342). Cells expressing mHTT were able to initiate phagocytosis.

Supplemental Table 1 | List of qPCR primers used in this study.

REFERENCES

1. Vonsattel JP, DiFiglia M. Huntington disease. *J Neuropathol Exp Neurol.* (1998) 57:369–84. doi: 10.1097/00005072-199805000-00001
2. Sassone J, Colciago C, Cislaghi G, Silani V, Ciammola A. Huntington's disease: the current state of research with peripheral tissues. *Exp Neurol.* (2009) 219:385–97. doi: 10.1016/j.expneurol.2009.05.012
3. Sathasivam K, Hobbs C, Turmaine M, Mangiarini L, Mahal A, Bertaux F, et al. Formation of polyglutamine inclusions in non-CNS tissue. *Hum Mol Genet.* (1999) 8:813–22. doi: 10.1093/hmg/8.5.813
4. Leblhuber F, Walli J, Jellinger K, Tilz GP, Widner B, Laccone F, et al. Activated immune system in patients with Huntington's disease. *Clin Chem Lab Med.* (1998) 36:747–50. doi: 10.1515/CCLM.1998.132
5. Andre R, Carty L, Tabrizi SJ. Disruption of immune cell function by mutant huntingtin in Huntington's disease pathogenesis. *Curr Opin Pharmacol.* (2016) 26:33–8. doi: 10.1016/j.coph.2015.09.008
6. Kwan W, Trager U, Davalos D, Chou A, Bouchard J, Andre R, et al. Mutant huntingtin impairs immune cell migration in Huntington disease. *J Clin Invest.* (2012) 122:4737–47. doi: 10.1172/JCI64484
7. Donley DW, Olson AR, Raisbeck MF, Fox JH, Gigley JP. Huntingtons disease mice infected with *Toxoplasma gondii* demonstrate early kynurenine pathway activation, altered $CD8^+$ T-cell responses, and premature mortality. *PLoS ONE.* (2016) 11:e0162404. doi: 10.1371/journal.pone.0162404
8. Steffan JS, Bodai L, Pallos J, Poelman M, McCampbell A, Apostol BL, et al. Histone deacetylase inhibitors arrest polyglutamine-dependent neurodegeneration in *Drosophila*. *Nature.* (2001) 413:739–43. doi: 10.1038/35099568
9. Song W, Smith MR, Syed A, Lukacsovich T, Barbaro BA, Purcell J, et al. Morphometric analysis of Huntington's disease neurodegeneration in *Drosophila*. *Methods Mol Biol.* (2013) 1017:41–57. doi: 10.1007/978-1-62703-438-8_3
10. Taylor JP, Taye AA, Campbell C, Kazemi-Esfarjani P, Fischbeck KH, Min KT. Aberrant histone acetylation, altered transcription, and retinal degeneration in a *Drosophila* model of polyglutamine disease are rescued by CREB-binding protein. *Genes Dev.* (2003) 17:1463–8. doi: 10.1101/gad.1087503
11. Li XJ, Orr AL, Li S. Impaired mitochondrial trafficking in Huntington's disease. *Biochim Biophys Acta.* (2010) 1802:62–5. doi: 10.1016/j.bbadis.2009.06.008
12. Warrick JM, Chan HY, Gray-Board GL, Chai Y, Paulson HL, Bonini NM. Suppression of polyglutamine-mediated neurodegeneration in *Drosophila* by the molecular chaperone HSP70. *Nat Genet.* (1999) 23:425–8. doi: 10.1038/70532
13. Steffan JS, Agrawal N, Pallos J, Rockabrand E, Trotman LC, Slepko N, et al. SUMO modification of Huntingtin and Huntington's disease pathology. *Science.* (2004) 304:100–4. doi: 10.1126/science.1092194
14. Marsh JL, Walker H, Theisen H, Zhu YZ, Fielder T, Purcell J, et al. Expanded polyglutamine peptides alone are intrinsically cytotoxic and cause neurodegeneration in *Drosophila*. *Hum Mol Genet.* (2000) 9:13–25. doi: 10.1093/hmg/9.1.13
15. Tamura T, Sone M, Yamashita M, Wanker EE, Okazawa H. Glial cell lineage expression of mutant ataxin-1 and huntingtin induces developmental and late-onset neuronal pathologies in *Drosophila* models. *PLoS ONE.* (2009) 4:e4262. doi: 10.1371/journal.pone.0004262
16. Besson MT, Dupont P, Fridell YW, Lievens JC. Increased energy metabolism rescues glia-induced pathology in a *Drosophila* model of Huntington's disease. *Hum Mol Genet.* (2010) 19:3372–82. doi: 10.1093/hmg/ddq249
17. Weiss KR, Kimura Y, Lee WC, Littleton JT. Huntingtin aggregation kinetics and their pathological role in a *Drosophila* Huntington's disease model. *Genetics.* (2012) 190:581–600. doi: 10.1534/genetics.111.133710
18. Melkani GC, Trujillo AS, Ramos R, Bodmer R, Bernstein SI, Ocorr K. Huntington's disease induced cardiac amyloidosis is reversed by modulating protein folding and oxidative stress pathways in the *Drosophila* heart. *PLoS Genet.* (2013) 9:e1004024. doi: 10.1371/journal.pgen.1004024
19. Charroux B, Royet J. Elimination of plasmatocytes by targeted apoptosis reveals their role in multiple aspects of the *Drosophila* immune response. *Proc Natl Acad Sci USA.* (2009) 106:9797–802. doi: 10.1073/pnas.0903971106
20. Defaye A, Evans I, Crozatier M, Wood W, Lemaitre B, Leulier F. Genetic ablation of *Drosophila* phagocytes reveals their contribution to both development and resistance to bacterial infection. *J Innate Immun.* (2009) 1:322–34. doi: 10.1159/000210264
21. Dobes P, Wang Z, Markus R, Theopold U, Hyrsl P. An improved method for nematode infection assays in *Drosophila* larvae. *Fly.* (2012) 6:75–9. doi: 10.4161/fly.19553
22. Small C, Paddibhatla I, Rajwani R, Govind S. An introduction to parasitic wasps of *Drosophila* and the antiparasite immune response. *J Vis Exp.* (2012) 63:e3347. doi: 10.3791/3347
23. Arefin B, Kucerova L, Dobes P, Markus R, Strnad H, Wang Z, et al. Genome-wide transcriptional analysis of *Drosophila* larvae infected by entomopathogenic nematodes shows involvement of complement, recognition and extracellular matrix proteins. *J Innate Immun.* (2014) 6:192–204. doi: 10.1159/000353734
24. Kucerova L, Broz V, Arefin B, Maaroufi HO, Hurychova J, Strnad H, et al. The *Drosophila* chitinase-like protein IDGF3 is involved in protection against nematodes and in wound healing. *J Innate Immun.* (2016) 8:199–210. doi: 10.1159/000442351
25. Lesch C, Goto A, Lindgren M, Bidla G, Dushay MS, Theopold U. A role for Hemolectin in coagulation and immunity in *Drosophila* melanogaster. *Dev Comp Immunol.* (2007) 31:1255–63. doi: 10.1016/j.dci.2007.03.012
26. Mortimer NT, Kacsoh BZ, Keebaugh ES, Schlenke TA. Mgat1-dependent N-glycosylation of membrane components primes *Drosophila* melanogaster blood cells for the cellular encapsulation response. *PLoS Pathog.* (2012) 8:e1002819. doi: 10.1371/journal.ppat.1002819
27. Ramet M, Manfruelli P, Pearson A, Mathey-Prevot B, Ezekowitz RA. Functional genomic analysis of phagocytosis and identification of a *Drosophila* receptor for *E. coli Nature.* (2002) 416:644–8. doi: 10.1038/nature735
28. West AP, Brodsky IE, Rahner C, Woo DK, Erdjument-Bromage H, Tempst P, et al. TLR signalling augments macrophage bactericidal activity through mitochondrial ROS. *Nature.* (2011) 472:476–80. doi: 10.1038/nature09973
29. Chougnet CA, Thacker RI, Shehata HM, Hennies CM, Lehn MA, Lages CS, et al. Loss of phagocytic and antigen cross-presenting capacity in aging dendritic cells is associated with mitochondrial dysfunction. *J Immunol.* (2015) 195:2624–32. doi: 10.4049/jimmunol.1501006
30. Geng J, Sun X, Wang P, Zhang S, Wang X, Wu H, et al. Kinases Mst1 and Mst2 positively regulate phagocytic induction of reactive oxygen species and bactericidal activity. *Nat Immunol.* (2015) 16:1142–52. doi: 10.1038/ni.3268
31. Ehinger JK, Morota S, Hansson MJ, Paul G, Elmer E. Mitochondrial respiratory function in peripheral blood cells from Huntington's disease patients. *Mov Disord Clin Pract.* (2016) 3:472–82. doi: 10.1002/mdc3.12308

32. Sassone J, Maraschi A, Sassone F, Silani V, Ciammola A. Defining the role of the Bcl-2 family proteins in Huntington's disease. *Cell Death Dis.* (2013) 4:e772. doi: 10.1038/cddis.2013.300
33. Quinn L, Coombe M, Mills K, Daish T, Colussi P, Kumar S, et al. Buffy, a *Drosophila* Bcl-2 protein, has anti-apoptotic and cell cycle inhibitory functions. *EMBO J.* (2003) 22:3568–79. doi: 10.1093/emboj/cdg355
34. Monserrate JP, Chen MY, Brachmann CB. *Drosophila* larvae lacking the bcl-2 gene, buffy, are sensitive to nutrient stress, maintain increased basal target of rapamycin (Tor) signaling and exhibit characteristics of altered basal energy metabolism. *BMC Biol.* (2012) 10:63. doi: 10.1186/1741-7007-10-63
35. Bjorkqvist M, Wild EJ, Thiele J, Silvestroni A, Andre R, Lahiri N, et al. A novel pathogenic pathway of immune activation detectable before clinical onset in Huntington's disease. *J Exp Med.* (2008) 205:1869–77. doi: 10.1084/jem.20080178
36. Trager U, Andre R, Lahiri N, Magnusson-Lind A, Weiss A, Grueninger S, et al. HTT-lowering reverses Huntington's disease immune dysfunction caused by NFkappaB pathway dysregulation. *Brain.* (2014) 137:819–33. doi: 10.1093/brain/awt355
37. Lemaitre B, Hoffmann J. The host defense of *Drosophila melanogaster*. *Annu Rev Immunol.* (2007) 25:697–743. doi: 10.1146/annurev.immunol.25.022106.141615
38. Basset A, Khush RS, Braun A, Gardan L, Boccard F, Hoffmann JA, et al. The phytopathogenic bacteria Erwinia carotovora infects *Drosophila* and activates an immune response. *Proc Natl Acad Sci USA.* (2000) 97:3376–81. doi: 10.1073/pnas.97.7.3376
39. Wild E, Magnusson A, Lahiri N, Krus U, Orth M, Tabrizi SJ, et al. Abnormal peripheral chemokine profile in Huntington's disease. *PLoS Curr.* (2011) 3:Rrn1231. doi: 10.1371/currents.RRN1231
40. Chen CM, Wu YR, Cheng ML, Liu JL, Lee YM, Lee PW, et al. Increased oxidative damage and mitochondrial abnormalities in the peripheral blood of Huntington's disease patients. *Biochem Biophys Res Commun.* (2007) 359:335–40. doi: 10.1016/j.bbrc.2007.05.093
41. Zwilling D, Huang SY, Sathyasaikumar KV, Notarangelo FM, Guidetti P, Wu HQ, et al. Kynurenine 3-monooxygenase inhibition in blood ameliorates neurodegeneration. *Cell.* (2011) 145:863–74. doi: 10.1016/j.cell.2011.05.020
42. Bouchard J, Truong J, Bouchard K, Dunkelberger D, Desrayaud S, Moussaoui S, et al. Cannabinoid receptor 2 signaling in peripheral immune cells modulates disease onset and severity in mouse models of Huntington's disease. *J Neurosci.* (2012) 32:18259–68. doi: 10.1523/JNEUROSCI.4008-12.2012
43. Sawa A, Wiegand GW, Cooper J, Margolis RL, Sharp AH, Lawler JF Jr, et al. Increased apoptosis of Huntington disease lymphoblasts associated with repeat length-dependent mitochondrial depolarization. *Nat Med.* (1999) 5:1194–8. doi: 10.1038/13518
44. Anderl I, Vesala L, Ihalainen TO, Vanha-Aho LM, Ando I, Ramet M, et al. Transdifferentiation and proliferation in two distinct hemocyte lineages in *Drosophila* melanogaster larvae after wasp infection. *PLoS Pathog.* (2016) 12:e1005746. doi: 10.1371/journal.ppat.1005746
45. Keebaugh ES, Schlenke TA. Insights from natural host-parasite interactions: the *Drosophila* model. *Dev Comp Immunol.* (2014) 42:111–23. doi: 10.1016/j.dci.2013.06.001
46. Fauvarque MO, Williams MJ. *Drosophila* cellular immunity: a story of migration and adhesion. *J Cell Sci.* (2011) 124:1373–82. doi: 10.1242/jcs.064592
47. Castillo JC, Shokal U, Eleftherianos I. Immune gene transcription in *Drosophila* adult flies infected by entomopathogenic nematodes and their mutualistic bacteria. *J Insect Physiol.* (2013) 59:179–85. doi: 10.1016/j.jinsphys.2012.08.003
48. Trager U, Andre R, Magnusson-Lind A, Miller JR, Connolly C, Weiss A, et al. Characterisation of immune cell function in fragment and full-length Huntington's disease mouse models. *Neurobiol Dis.* (2015) 73:388–98. doi: 10.1016/j.nbd.2014.10.012
49. Swanson JA. Shaping cups into phagosomes and macropinosomes. *Nat Rev Mol Cell Biol.* (2008) 9:639–49. doi: 10.1038/nrm2447
50. Morin-Poulard I, Vincent A, Crozatier M. The *Drosophila* JAK-STAT pathway in blood cell formation and immunity. *JAKSTAT.* (2013) 2:e25700. doi: 10.4161/jkst.25700
51. Wang G. Human antimicrobial peptides and proteins. *Pharmaceuticals.* (2014) 7:545–94. doi: 10.3390/ph7050545
52. Anderson AN, Roncaroli F, Hodges A, Deprez M, Turkheimer FE. Chromosomal profiles of gene expression in Huntington's disease. *Brain.* (2008) 131:381–8. doi: 10.1093/brain/awm312
53. Lin DM, Goodman CS. Ectopic and increased expression of Fasciclin II alters motoneuron growth cone guidance. *Neuron.* (1994) 13:507–23. doi: 10.1016/0896-6273(94)90022-1
54. Sinenko SA, Mathey-Prevot B. Increased expression of *Drosophila* tetraspanin, Tsp68C, suppresses the abnormal proliferation of ytr-deficient and Ras/Raf-activated hemocytes. *Oncogene.* (2004) 23:9120–8. doi: 10.1038/sj.onc.1208156
55. Zettervall CJ, Anderl I, Williams MJ, Palmer R, Kurucz E, Ando I, et al. A directed screen for genes involved in *Drosophila* blood cell activation. *Proc Natl Acad Sci USA.* (2004) 101:14192–7. doi: 10.1073/pnas.0403789101
56. Zhou L, Schnitzler A, Agapite J, Schwartz LM, Steller H, Nambu JR. Cooperative functions of the reaper and head involution defective genes in the programmed cell death of *Drosophila* central nervous system midline cells. *Proc Natl Acad Sci USA.* (1997) 94:5131–6. doi: 10.1073/pnas.94.10.5131
57. Warrick JM, Paulson HL, Gray-Board GL, Bui QT, Fischbeck KH, Pittman RN, et al. Expanded polyglutamine protein forms nuclear inclusions and causes neural degeneration in *Drosophila*. *Cell.* (1998) 93:939–49. doi: 10.1016/S0092-8674(00)81200-3
58. Ibrahim E, Dobes P, Kunc M, Hyrsl P, Kodrik D. Adipokinetic hormone and adenosine interfere with nematobacterial infection and locomotion in *Drosophila* melanogaster. *J Insect Physiol.* (2018) 107:167–74. doi: 10.1016/j.jinsphys.2018.04.002
59. Zhang S, Binari R, Zhou R, Perrimon N. A genomewide RNA interference screen for modifiers of aggregates formation by mutant Huntingtin in *Drosophila*. *Genetics.* (2010) 184:1165–79. doi: 10.1534/genetics.109.112516
60. Han SK, Lee D, Lee H, Kim D, Son HG, Yang JS, et al. OASIS 2: online application for survival analysis 2 with features for the analysis of maximal lifespan and healthspan in aging research. *Oncotarget.* (2016) 7:56147–52. doi: 10.18632/oncotarget.11269

Conflict of Interest: The authors declare that the research was conducted in the absence of any commercial or financial relationships that could be construed as a potential conflict of interest.

frontiers in Immunology

MINI REVIEW
published: 20 December 2019
doi: 10.3389/fimmu.2019.02973

Emerging Mechanisms of Insulin-Mediated Antiviral Immunity in *Drosophila melanogaster*

Chasity E. Trammell[1,2] *and Alan G. Goodman*[1,3]*

[1] School of Molecular Biosciences, College of Veterinary Medicine, Washington State University, Pullman, WA, United States, [2] NIH Biotechnology Graduate Training Program, Washington State University, Pullman, WA, United States, [3] Paul G. Allen School for Global Animal Health, College of Veterinary Medicine, Washington State University, Pullman, WA, United States

Arboviruses (arthropod-borne viruses), such as Zika (ZIKV), West Nile (WNV), and dengue (DENV) virus, include some of the most significant global health risks to human populations. The steady increase in the number of cases is of great concern due to the debilitating diseases associated with each viral infection. Because these viruses all depend on the mosquito as a vector for disease transmission, current research has focused on identifying immune mechanisms used by insects to effectively harbor these viruses and cause disease in humans and other animals. *Drosophila melanogaster* are a vital model to study arboviral infections and host responses as they are a genetically malleable model organism for experimentation that can complement analysis in the virus' natural vectors. *D. melanogaster* encode a number of distinct mechanisms of antiviral defense that are found in both mosquito and vertebrate animal systems, providing a viable model for study. These pathways include canonical antiviral modules such as RNA interference (RNAi), JAK/STAT signaling, and the induction of STING-mediated immune responses like autophagy. Insulin signaling plays a significant role in host-pathogen interactions. The exact mechanisms of insulin-mediated immune responses vary with each virus type, but nevertheless ultimately demonstrates that metabolic and immune signaling are coupled for antiviral immunity in an arthropod model. This mini review provides our current understanding of antiviral mechanisms in *D. melanogaster*, with a focus on insulin-mediated antiviral signaling, and how such immune responses pertain to disease models in vertebrate and mosquito species.

Keywords: innate immunity, RNA interference, JAK/STAT, insulin, STING, West Nile virus, Zika virus, dengue virus

OPEN ACCESS

Edited by:
Susanna Valanne, Tampere University, Finland

Reviewed by:
Sara Cherry, University of Pennsylvania, United States
Penghua Wang, University of Connecticut Health Center, United States

***Correspondence:**
Alan G. Goodman
alan.goodman@wsu.edu

Specialty section:
This article was submitted to Comparative Immunology, a section of the journal Frontiers in Immunology

Received: *15 October 2019*
Accepted: *04 December 2019*
Published: *20 December 2019*

Citation:
Trammell CE and Goodman AG (2019) Emerging Mechanisms of Insulin-Mediated Antiviral Immunity in Drosophila melanogaster. Front. Immunol. 10:2973. doi: 10.3389/fimmu.2019.02973

INTRODUCTION

Mosquitoes are a prominent vector for various arboviruses including West Nile virus (WNV), Zika virus (ZIKV), and dengue virus (DENV). These viruses pose a significant concern to human populations as the mosquitoes' continual encroachment into previously unexposed regions expands (1, 2). This habitat expansion renders more individuals at risk of exposure with limited, if any, treatments available. Climate change has also resulted in alterations in mosquito seasonal activity (3) and feeding behavior (4) resulting in increasing frequency and severity of arboviral cases. There is a direct correlation between the expansion of vector-competent mosquitoes and disease incidence within afflicted regions [reviewed in (5, 6)] indicating that vector activity is a significant risk factor for arboviral disease.

Figure 1 outlines the transmission cycle of various arboviruses as they move within host populations and how *Drosophila melanogaster* can be used to study arboviral immunity for each system. Transmission from mosquito to vertebrates requires a bloodmeal exchange where infected saliva is ejected into the new host. Viral replication then permits the spread of virus from infected host to mosquito to continue the transmission cycle (**Figure 1**). Research is required to identify the signaling responses used in regulating these viruses at the vector and human level. Studies regarding immune responses initiated during the initial bloodmeal exchange (7) are important as this event is a key determinant whether transmission occurs (8). An emphasis as to how immune and nutritional signaling interact with one another is of particular interest as both would be active during ingestion of an infected bloodmeal. Insulin-mediated signaling regulates numerous viruses by inducing activation of canonical immune pathways (9). Because insulin is ingested during the bloodmeal, a recent study has shown that vertebrate insulin is able to regulate the type of innate immune response that occurs during viral infection in insect vector hosts (10).

Previous work has identified the signaling pathways that respond to arboviral infection and their significance with respect to disease outcome and severity (11–13). *Drosophila* have proven to be a significant model organism for studying arboviruses as many of the signaling pathways identified are conserved amongst insect species [reviewed in (14)]. These studies have utilized the genetic power provided by the *Drosophila* system to demonstrate the effect that nutritional status poses on host immunity.

Immune responses during various arboviral infections are evolutionarily conserved among insects and include the canonical RNA interference (RNAi) (13, 15, 16), JAK/STAT (10, 12), and STING-mediated signaling (17). These pathways are associated with the insulin/insulin-like growth factor signaling (IIS) pathway and have been established as key determinants in vector competency and disease outcome (9, 18). It has been demonstrated that ingestion of vertebrate insulin regulates whether an RNAi- or JAK/STAT-mediated response is active during infection against WNV (10). STING-mediated immunity has been previously linked to induce JAK/STAT signaling (19) and affects nutritional homeostasis during infection (20, 21) implying that it may be regulated by insulin as well. Since insulin-mediated signaling appears to have a broad impact on insect immunity, recent studies have sought to establish how insulin connects each antiviral pathway to respond to different arboviruses. Because vector competency and transmission is so closely dependent on gut-associated immune signaling, the connection that nutrition and immunity has is indicative of their importance in regulating infection (9, 22). This mini review presents a condensed understanding regarding the major responses that occur during arboviral infection using *Drosophila*,

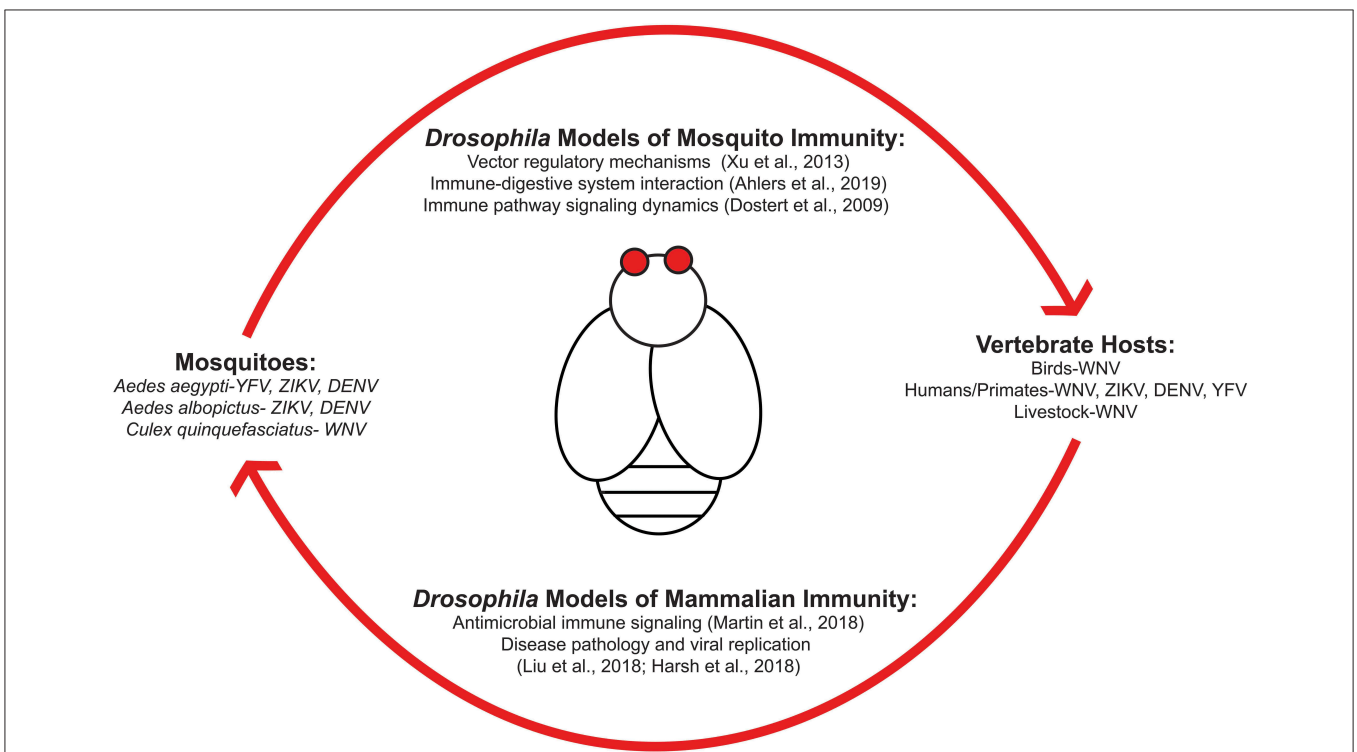

FIGURE 1 | *Drosophila melanogaster* are an ideal model organism for studying host-arboviral interactions. Various arboviruses utilize mosquitoes as reservoirs and vectors for transmission into vertebrate hosts. This can include species that are either involved in viral replication and spread (such as bird populations for West Nile virus) or dead-end host that become infected without being able to properly propagate viral replication for further spread (i.e., humans). Transmission is accomplished via a bloodmeal exchange. *Drosophila* possess orthologous host response pathways found in mosquitoes and humans, making it an ideal model organism for studying transmission dynamics and host-pathogen interactions at both vector and human level.

the role that insulin signaling plays, and a summation of current and future efforts taken within this field.

RNA INTERFERENCE PATHWAY

One of the most broadly restricting antiviral responses used by insects is the RNAi pathway (13, 16). RNAi signaling occurs in response to detection of viral nucleic acids within the cytosol of infected cells. In *Drosophila*, recognition of viral nucleic acids by the endonuclease Dicer-2 results in the recruitment of proteins Argonaute-2 (AGO2) and r2d2 to form an RNA-induced silencing complex (RISC) (13, 23). This results in the cleavage and degradation of bound viral nucleic acids (13, 23, 24). While this antiviral response is a significant component of insect immunity against RNA viruses like Sindbis virus (SINV) (24) and ZIKV (25), an arthropod-borne alphavirus and flavivirus, respectively, RNAi has also been shown to respond to DNA viruses like Invertebrate iridescent virus 6 (IIV-6) (26) (**Figure 2A**). While Harsh et al. showed that the loss of the RNAi component, Dicer-2, resulted in increased ZIKV replication and mortality, they linked the increased susceptibility of these flies to dysregulated homeostasis of the gut and fat body. Moreover, studies have shown that another RNAi component, namely AGO2, is dispensable for an antiviral response against ZIKV (17, 25). Additionally, there are flaviviruses that encode viral suppressors of RNAi (VSR) (27). Not only do VSRs function in *Drosophila* model systems (28), but they also function during WNV, DENV, and Yellow fever virus infections in *Culex* mosquitoes (29, 30). Thus, the antiviral role of RNAi depends not only on the host but also virus type. Further studies are needed to clarify the antiviral role of RNAi in model and vector organisms, especially with respect to flaviviruses and the VSRs they may encode. Mosquitoes become infected and spread disease via bloodmeal exchanges. Because of the direct role that nutritional acquisition has during infection, its role in antiviral immunity is mediated in part by regulating RNAi. In both insect and mammalian systems, IIS regulates the transcription factor forkhead box O (FOXO), and FOXO is predominately associated with longevity and nutritional signaling as it induces *dInR* (*insulin-like receptor*) in *Drosophila* (31, 32). FOXO possesses a secondary role in host immunity through its induction of RNAi-specific genes. Specifically, FOXO regulates the transcription of *Dicer-2* and

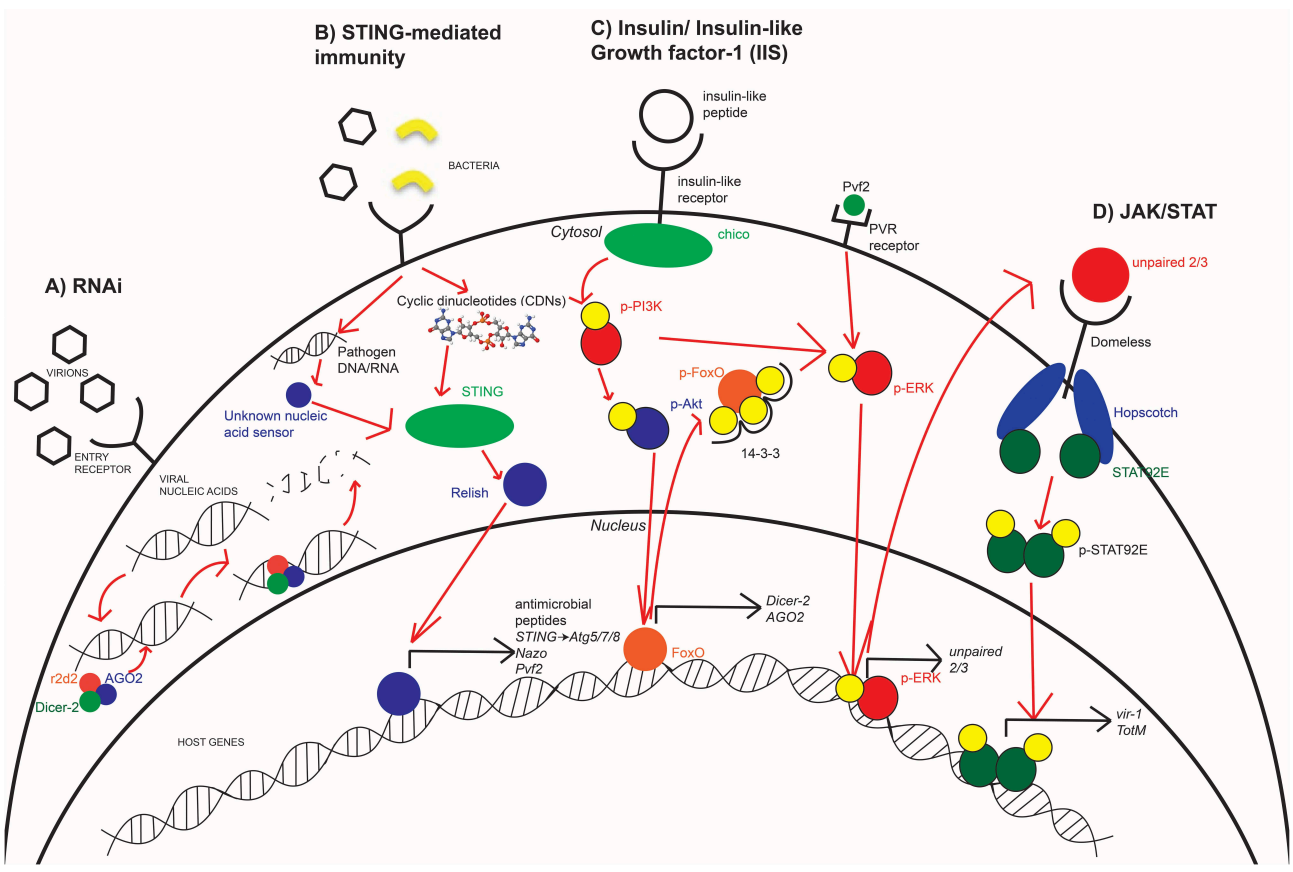

FIGURE 2 | Innate immune antimicrobial pathways are conserved in arthropods. Insects utilize RNAi **(A)**, STING-mediated immunity **(B)**, and JAK/STAT signaling **(D)** in order to effectively respond to various arboviruses at different stages of infection. The IIS pathway **(C)** is an important mediator in host immunity as it regulates which immune responses are active or suppressed. During times of starvation, RNAi is more active while the bloodmeal provides the needed insulin to suppress RNAi and activate JAK/STAT. STING-mediated immunity has not yet been directly linked to IIS but may be affected by broader nutritional signaling. Each of these pathways, to varying degrees, are conserved in fly, mosquito, and human systems with different efficiencies in responding to viral infection.

AGO2 in *Drosophila* and is demonstrated to enhance RNAi signaling during Cricket paralysis viral infection (18). Since IIS regulates FOXO transcriptional activity, there is a direct connection between RNAi immunity and insulin signaling. In *Drosophila*, the IIS pathway is induced by insulin-like peptides (ILPs) binding to dInR (33). Upon binding, a phosphorylation cascade commences that includes phosphorylation of PI3K and Akt. This results in the phosphorylation of nuclear FoxO at three residues, its association with the 14-3-3 chaperone protein, and export into the cytosol (32, 34) (**Figure 2C**). Insulin treatment is demonstrated to result in transcriptional suppression of *Dicer-2* and *AGO2* to reduce RNAi signaling (10). This insulin-mediated suppression of RNAi proposes that mosquitoes have evolved multiple immune responses to pathogens that is dependent on its nutritional status.

RNAi is evolutionarily conserved across organisms; however, its role in antiviral immunity varies between insects and mammals. While the signaling cascade and proteins involved are conserved, mammals have evolved other sensing mechanisms to detect and respond to viruses. RIG-I and MDA5 RNA sensing are canonical pathways for vertebrate innate immunity and have developed from RNA sensors like Dicer (35). In particular, RIG-I and MDA5 are shown to be critical immune regulators in response to flaviviruses like ZIKV (36) and WNV (37) and alphaviruses like SINV (38). This would imply that while RNAi is still fully functional in mammals, its role in responding to viruses is less stringent than in insect systems [reviewed in (39, 40)]. Other invertebrate and plant species utilize RNAi signaling as a means of antiviral immunity [reviewed in (41, 42)]. Researchers interested in studying RNAi immunity against arboviruses utilize *Drosophila* as the signaling cascades described are well-conserved in the more relevant mosquito vector. While the functional antiviral role of RNAi varies in mammalian systems, the proteins and signaling events involved are conserved. Because of this, studies utilizing *Drosophila* have proven it to be a viable model for study in host immunity and other regulatory functions.

JAK/STAT PATHWAY

Innate immunity uses various responses to different viruses. These responses include phagocytosis of viral particles or by inducing production of downstream cytokines and antiviral effectors (43). Whereas, the RNAi pathway provides a broad means of protection through the degradation of viral nucleic acids (16), the JAK/STAT pathway is a signaling cascade where detection of infection or other stimuli results in the induction of antiviral effectors like *vir-1*, *Vago*, and *TotM* (12, 24, 44). In *Drosophila* immunity, this pathway is activated upon detection of infection (45), resulting in induction of the *unpaired* ligands (46, 47). Unpaired ligands bind to the receptor domeless (48), resulting in the Janus kinase (JAK) ortholog hopscotch to be phosphorylated and form docking sites for phosphorylation and dimerization of the STAT92E transcription factor (12, 49). The activated STAT92E protein complex is imported into the nucleus to induce transcription of downstream antiviral effectors. This includes *TotM* during early stages of infection (24) and *vir-1* during later stages (12) (**Figure 2D**). JAK/STAT has been shown to be involved in the immune response against the insect virus *Drosophila* C virus but not SINV (24) in *Drosophila*, and JAK/STAT is antiviral against WNV in both *Drosophila* and *Culex* mosquitoes (10, 50).

The connection between JAK/STAT and IIS is not as direct as insulin's effect on the RNAi pathway, but recent research has demonstrated that insulin signaling in insects controls a switch between RNAi- and JAK/STAT-dependent responses. Specifically, when insulin treatment causes transcriptional suppression of RNAi, insects induce enrichment of JAK/STAT (10). This is mediated by insulin's phosphorylation and activation of downstream Akt and ERK proteins during SINV and DENV infection (9, 22) that was further evaluated to induce immunity through JAK/STAT against WNV (10). Insulin-mediated induction of JAK/STAT then induces the transcription of downstream antiviral effector proteins *vir-1* and *TotM* (10, 12, 24). JAK/STAT immunity responds to pathogens during early stages of infection in the mosquito which corresponds to ingestion of an infected bloodmeal and escape from the midgut to distal tissues (51). This association between IIS and JAK/STAT signaling is indicative that vector-competent insects have evolved immune mechanisms that are responsive to nutritional acquisition. While mosquitoes use an RNAi-dependent response during times of starvation, the bloodmeal provides the insulin needed to activate a JAK/STAT-dependent response during infection. While the ability to regulate immune responses based on nutritional status and how it impacts viral efficacy and transmission has yet to be established, it is plausible that insulin-mediated signaling could be targeted in future vector-control protocols. Its potential as a target depends on whether insulin's antiviral activity in the salivary glands is just as important as it is in midgut or fat body, critical digestive and immune organs (8, 9).

JAK/STAT signaling is an evolutionarily conserved immune response utilized in both insect and mammalian systems. Induction of JAK/STAT in mammals results in a Type I interferon (IFN) response against viral infection (52). The JAK/STAT pathway is similarly regulated by RIG-I-like receptor (RLR) signaling in mammalian systems (35, 53). This pathway is an important means of responding to WNV in both insects (10, 44) and mammals (52, 53). Because JAK/STAT is related to other regulatory processes like cell proliferation and differentiation [reviewed in (54)], researchers have also used the *Drosophila* model to study the pathway's role in a non-immunological context like cellular growth (47), differentiation (48), polarization (49), and oogenesis (55). *Drosophila* provide a unique system for studying JAK/STAT signaling at various levels of complexity in both an immune and regulatory context to provide clarity regarding the pathway's significance in the organism.

STING-MEDIATED IMMUNITY

Mediators of mammalian immunity have evolved from established signaling pathways that are present in invertebrate

systems (35, 56). One such set of responses is stimulator of IFN genes (STING)-mediated immunity. Upon detection of viral nucleic acids in the cytosol, the DNA sensor cGAS metabolizes cyclic dinucleotides that bind to and activate STING (11), which induces phosphorylation and activation of various transcription factors like TBK1, IRF3, and STAT6 (19, 57). These transcription factors regulate the induction of Type I IFN responses through the secretion of IFN-α and β (11, 19, 57). STING-mediated immunity has been heavily studied within mammalian systems; however, it is only recently that STING and its role in innate immunity have been identified in insects and other invertebrates (17, 56, 58–60) (**Figure 2B**).

In *Drosophila*, STING signaling provides immunity against both bacterial and viral infections. During infection with *Listeria monocytogenes*, cyclic dinucleotides are produced which results in STING-mediated signaling and nuclear import of Relish, the fly ortholog of mammalian NF-κB (56). This immune response induces transcription and secretion of IMD-characteristic antimicrobial peptides to reduce bacterial burden (56). STING-mediated antiviral immunity also occurs through Relish and IKKβ, which regulate expression of the antiviral factor *Nazo* (58). In the silkmoth, *Bombyx mori*, STING signaling activates antiviral activity through Dredd and IMD, leading to Relish signaling and induction of antimicrobial peptides against nucleopolyhedrovirus (NPV) (59). Other studies using the *Drosophila* system have further evaluated STING-mediated immunity by autophagy (17).

Autophagy is a cellular process in which intracellular structures and proteins are degraded in a lysosomal-dependent manner [reviewed in (61)]. Because viruses are obligate intracellular pathogens, autophagy is an established antiviral response that is partially regulated by nutritional and STING-mediated signaling (62). While STING-mediated autophagy has been established in responding to numerous viruses in mammals, recent studies using *Drosophila* have demonstrated that insects can utilize autophagy to respond to ZIKV in neuronal tissues (17). Specifically, ZIKV infection results in a pro-inflammatory response in *Drosophila* brains which induces STING-mediated activation of autophagy and immunity (17). This form of antiviral immunity is indicative that neuronal protection against arboviruses is mediated through STING-mediated signaling. This study provides another example of the versatility provided in using the *Drosophila* system as the fly model is a viable means for studying antiviral immunity conserved between invertebrates and vertebrates.

Unlike the RNAi and JAK/STAT pathways, which are both regulated in part by insulin signaling, a direct link between IIS and STING has yet to be shown. However, since autophagy is partially regulated by nutritional status [reviewed in (63)] and STING has been previously shown to induce *STAT6* in the mammalian system (19), it is plausible that STING-mediated immunity may also be partially regulated by insulin signaling. Since STING has only recently been discovered in the insect model, future research is needed to further evaluate how STING connects to other canonical immune and nutritional pathways and its involvement in vector competency.

PROSPECTIVE

Both the Centers for Disease Control and Prevention (CDC) and World Health Organization (WHO) agree that mosquito-borne arboviruses will be of great concern in the following years due to the expansion of mosquitoes' habitation range and activity into previously unexposed regions (64, 65). Research using *Drosophila* have permitted investigators to identify the key signaling events that occur during infection and develop more effective vector control protocols that target viral replication and likelihood of transmission. Recently, *Drosophila* have been used to identify ingestion of mammalian insulin as a key regulator in controlling WNV replication in the insect model. The genetic screen to identify insulin receptor was performed using *Drosophila*, and the role of insulin signaling was then validated in the mosquito model (10).

While *Drosophila* have been an invaluable tool in the study of arboviruses in place of the more relevant arthropod vector, there are limitations. For example, JAK/STAT signaling, while protective in the mosquito model against arboviruses such as WNV and DENV (10, 44, 66), may not be protective in *Drosophila* during SINV or vesicular stomatitis virus infections (12, 24). Because *Drosophila* are not the natural host for these arboviruses, there are limitations surrounding whether the responses observed are indeed what occurs in natural hosts. As such, work involving *Drosophila* must ensure that their findings are further evaluated in the more relevant model, whether that be the insect vector or human host.

Developing disease response protocols that aim at preventing transmission from arthropods to humans would be the most beneficial in terms of cost-efficiency and alleviating disease burden at a global scale. Research efforts also aim to identify novel therapeutics that are effective at treating humans post-exposure. Because many of the immune pathways discussed here are also present in humans (**Figure 2**), future research aimed at identifying novel human-specific antiviral therapeutics could benefit from the use of *Drosophila*. The use of *Drosophila* to model host immunity at both the mammalian and vector level during arboviral infection has provided a greater depth of knowledge regarding which signaling pathways are involved during infection and how they can be targeted in the arthropods that transmit disease.

AUTHOR CONTRIBUTIONS

CT wrote the first draft of the manuscript. AG revised the manuscript.

FUNDING

Research in the Goodman lab was supported by NIH/NIAID Grant R01 AI139051 to AG. CT was supported by NIH/NIGMS pre-doctoral fellowship T32 GM008336.

REFERENCES

1. Kraemer MU, Sinka ME, Duda KA, Mylne AQ, Shearer FM, Barker CM, et al. The global distribution of the arbovirus vectors *Aedes aegypti* and *Ae. albopictus. Elife*. (2015) 4:e08347. doi: 10.7554/eLife.08347
2. Leta S, Beyene TJ, De Clercq EM, Amenu K, Kraemer MUG, Revie CW. Global risk mapping for major diseases transmitted by *Aedes aegypti* and *Aedes albopictus*. *Int J Infect Dis*. (2018) 67:25–35. doi: 10.1016/j.ijid.2017.11.026
3. Muttis E, Balsalobre A, Chuchuy A, Mangudo C, Ciota AT, Kramer LD, et al. Factors related to *Aedes aegypti* (*Diptera: Culicidae*) populations and temperature determine differences on life-history traits with regional implications in disease transmission. *J Med Entomol*. (2018) 55:1105–12. doi: 10.1093/jme/tjy057
4. Hagan RW, Didion EM, Rosselot AE, Holmes CJ, Siler SC, Rosendale AJ, et al. Dehydration prompts increased activity and blood feeding by mosquitoes. *Sci Rep*. (2018) 8:6804. doi: 10.1038/s41598-018-24893-z
5. Cucunawangsih, Lugito NPH. Trends of dengue disease epidemiology. *Virology*. (2017) 8:1178122X17695836. doi: 10.1177/1178122X17695836
6. Deseda CC. Epidemiology of Zika. *Curr Opin Pediatr*. (2017) 29:97–101. doi: 10.1097/MOP.0000000000000442
7. Uraki R, Hastings AK, Marin-Lopez A, Sumida T, Takahashi T, Grover JR, et al. *Aedes aegypti* AgBR1 antibodies modulate early Zika virus infection of mice. *Nat Microbiol*. (2019) 4:948–55. doi: 10.1038/s41564-019-0385-x
8. Sim S, Ramirez JL, Dimopoulos G. Dengue virus infection of the *Aedes aegypti* salivary gland and chemosensory apparatus induces genes that modulate infection and blood-feeding behavior. *PLoS Pathog*. (2012) 8:e1002631. doi: 10.1371/journal.ppat.1002631
9. Xu J, Hopkins K, Sabin L, Yasunaga A, Subramanian H, Lamborn I, et al. ERK signaling couples nutrient status to antiviral defense in the insect gut. *Proc Natl Acad Sci USA*. (2013) 110:15025–30. doi: 10.1073/pnas.1303193110
10. Ahlers LRH, Trammell CE, Carrell GF, Mackinnon S, Torrevillas BK, Chow CY, et al. Insulin potentiates JAK/STAT signaling to broadly inhibit flavivirus replication in insect vectors. *Cell Rep*. (2019) 29:1946–60.e5. doi: 10.1016/j.celrep.2019.10.029
11. Burdette DL, Monroe KM, Sotelo-Troha K, Iwig JS, Eckert B, Hyodo M, et al. STING is a direct innate immune sensor of cyclic di-GMP. *Nature*. (2011) 478:515–8. doi: 10.1038/nature10429
12. Dostert C, Jouanguy E, Irving P, Troxler L, Galiana-Arnoux D, Hetru C, et al. The Jak-STAT signaling pathway is required but not sufficient for the antiviral response of *Drosophila*. *Nat Immunol*. (2005) 6:946–53. doi: 10.1038/ni1237
13. Galiana-Arnoux D, Dostert C, Schneemann A, Hoffmann JA, Imler J-L. Essential function *in vivo* for Dicer-2 in host defense against RNA viruses in *Drosophila*. *Nat Immunol*. (2006) 7:590–7. doi: 10.1038/ni1335
14. Hillyer JF. Insect immunology and hematopoiesis. *Dev Comp Immunol*. (2016) 58:102–18. doi: 10.1016/j.dci.2015.12.006
15. Goic B, Vodovar N, Mondotte JA, Monot C, Frangeul L, Blanc H, et al. RNA-mediated interference and reverse transcription control the persistence of RNA viruses in the insect model *Drosophila*. *Nat Immunol*. (2013) 14:396–403. doi: 10.1038/ni.2542
16. Saleh M-C, Tassetto M, van Rij RP, Goic B, Gausson V, Berry B, et al. Antiviral immunity in *Drosophila* requires systemic RNAi spread. *Nature*. (2009) 458:346–50. doi: 10.1038/nature07712
17. Liu Y, Gordesky-Gold B, Leney-Greene M, Weinbren NL, Tudor M, Cherry S. Inflammation-induced, STING-dependent autophagy restricts Zika virus infection in the *Drosophila* brain. *Cell Host Microbe*. (2018) 24:57–68.e3. doi: 10.1016/j.chom.2018.05.022
18. Spellberg MJ, Marr MT. FOXO regulates RNA interference in *Drosophila* and protects from RNA virus infection. *Proc Natl Acad Sci USA*. (2015) 112:14587–92. doi: 10.1073/pnas.1517124112
19. Chen H, Sun H, You F, Sun W, Zhou X, Chen L, et al. Activation of STAT6 by STING is critical for antiviral innate immunity. *Cell*. (2011) 147:436–46. doi: 10.1016/j.cell.2011.09.022
20. DiAngelo JR, Bland ML, Bambina S, Cherry S, Birnbaum MJ. The immune response attenuates growth and nutrient storage in *Drosophila* by reducing insulin signaling. *Proc Natl Acad Sci USA*. (2009) 106:20853–8. doi: 10.1073/pnas.0906749106
21. Péan CB, Schiebler M, Tan SWS, Sharrock JA, Kierdorf K, Brown KP, et al. Regulation of phagocyte triglyceride by a STAT-ATG2 pathway controls mycobacterial infection. *Nat Commun*. (2017) 8:14642. doi: 10.1038/ncomms14642
22. Sansone CL, Cohen J, Yasunaga A, Xu J, Osborn G, Subramanian H, et al. Microbiota-dependent priming of antiviral intestinal immunity in *Drosophila*. *Cell Host Microbe*. (2015) 18:571–81. doi: 10.1016/j.chom.2015.10.010
23. Deddouche S, Matt N, Budd A, Mueller S, Kemp C, Galiana-Arnoux D, et al. The DExD/H-box helicase Dicer-2 mediates the induction of antiviral activity in *Drosophila*. *Nat Immunol*. (2008) 9:1425–32. doi: 10.1038/ni.1664
24. Kemp C, Mueller S, Goto A, Barbier V, Paro S, Bonnay F, et al. Broad RNA interference–mediated antiviral immunity and virus-specific inducible responses in *Drosophila*. *J Immunol*. (2013) 190:650–8. doi: 10.4049/jimmunol.1102486
25. Harsh S, Ozakman Y, Kitchen SM, Paquin-Proulx D, Nixon DF, Eleftherianos I. Dicer-2 regulates resistance and maintains homeostasis against Zika virus infection in *Drosophila*. *J Immunol*. (2018) 201:3058–72. doi: 10.4049/jimmunol.1800597
26. Bronkhorst AW, van Cleef KWR, Vodovar N, Ince IA, Blanc H, Vlak JM, et al. The DNA virus Invertebrate iridescent virus 6 is a target of the *Drosophila* RNAi machinery. *Proc Natl Acad Sci USA*. (2012) 109:E3604–13. doi: 10.1073/pnas.1207213109
27. Schnettler E, Sterken MG, Leung JY, Metz SW, Geertsema C, Goldbach RW, et al. Noncoding flavivirus RNA displays RNA interference suppressor activity in insect and mammalian cells. *J Virol*. (2012) 86:13486–500. doi: 10.1128/JVI.01104-12
28. van Cleef KWR, van Mierlo JT, van den Beek M, van Rij RP. Identification of viral suppressors of RNAi by a reporter assay in *Drosophila* S2 cell culture. *Methods Mol Biol*. (2011) 721:201–13. doi: 10.1007/978-1-61779-037-9_12
29. Göertz GP, Fros JJ, Miesen P, Vogels CBF, van der Bent ML, Geertsema C, et al. Noncoding subgenomic flavivirus RNA Is processed by the mosquito rna interference machinery and determines west nile virus transmission by culex pipiens mosquitoes. *J Virol*. (2016) 90:10145–59. doi: 10.1128/JVI.00930-16
30. Samuel GH, Wiley MR, Badawi A, Adelman ZN, Myles KM. Yellow fever virus capsid protein is a potent suppressor of RNA silencing that binds double-stranded RNA. *Proc Natl Acad Sci USA*. (2016) 113:13863–8. doi: 10.1073/pnas.1600544113
31. DiAngelo JR, Birnbaum MJ. Regulation of fat cell mass by insulin in *Drosophila melanogaster*. *Mol Cell Biol*. (2009) 29:6341–52. doi: 10.1128/MCB.00675-09
32. Puig O, Marr MT, Ruhf ML, Tjian R. Control of cell number by *Drosophila* FOXO: downstream and feedback regulation of the insulin receptor pathway. *Genes Dev*. (2003) 17:2006–20. doi: 10.1101/gad.1098703
33. Puig O, Tjian R. Transcriptional feedback control of insulin receptor by dFOXO/FOXO1. *Genes Dev*. (2005) 19:2435–46. doi: 10.1101/gad.1340505
34. Nielsen MD, Luo X, Biteau B, Syverson K, Jasper H. 14-3-3ε antagonizes FoxO to control growth, apoptosis and longevity in *Drosophila*. *Aging Cell*. (2008) 7:688–99. doi: 10.1111/j.1474-9726.2008.00420.x
35. Sarkar D, DeSalle R, Fisher PB. Evolution of MDA-5/RIG-I-dependent innate immunity: Independent evolution by domain grafting. *Proc Natl Acad Sci USA*. (2008) 105:17040–5. doi: 10.1073/pnas.0804956105
36. Riedl W, Acharya D, Lee J-H, Liu G, Serman T, Chiang C, et al. Virus NS3 mimics a cellular 14-3-3-binding motif to antagonize RIG-I- and MDA5-mediated innate immunity. *Cell Host Microbe*. (2019) 26:493–503.e6. doi: 10.1016/j.chom.2019.09.012
37. Errett JS, Suthar MS, McMillan A, Diamond MS, Gale M. The essential, nonredundant roles of RIG-I and MDA5 in detecting and controlling west nile virus infection. *J Virol*. (2013) 87:11416–25. doi: 10.1128/JVI.01488-13
38. Akhrymuk I, Frolov I, Frolova EI. Both RIG-I and MDA5 detect alphavirus replication in concentration-dependent mode. *Virology*. (2016) 487:230–41. doi: 10.1016/j.virol.2015.09.023
39. Cullen BR. Viruses and RNA interference: issues and controversies. *J Virol*. (2014) 88:12934–6. doi: 10.1128/JVI.01179-14
40. Schuster S, Miesen P, van Rij RP. Antiviral RNAi in insects and mammals: parallels and differences. *Viruses*. (2019) 11:448. doi: 10.3390/v11050448
41. Baulcombe D. RNA silencing in plants. *Nature*. (2004) 431:356–63. doi: 10.1038/nature02874
42. Boisvert ME, Simard MJ. RNAi pathway in *C. elegans*: the argonautes and collaborators. *Curr Top Microbiol Immunol*. (2008) 320:21–36. doi: 10.1007/978-3-540-75157-1_2

43. Lamiable O, Arnold J, de Faria IJdS, Olmo RP, Bergami F, Meignin C, et al. Analysis of the contribution of hemocytes and autophagy to *Drosophila* antiviral immunity. *J Virol*. (2016) 90:5415–26. doi: 10.1128/JVI.00238-16
44. Paradkar PN, Trinidad L, Voysey R, Duchemin J-B, Walker PJ. Secreted Vago restricts West Nile virus infection in Culex mosquito cells by activating the Jak-STAT pathway. *Proc Natl Acad Sci USA*. (2012) 109:18915–20. doi: 10.1073/pnas.1205231109
45. Boutros M, Agaisse H, Perrimon N. Sequential activation of signaling pathways during innate immune responses in *Drosophila*. *Dev Cell*. (2002) 3:711–22. doi: 10.1016/S1534-5807(02)00325-8
46. Agaisse H, Petersen U-M, Boutros M, Mathey-Prevot B, Perrimon N. Signaling role of hemocytes in *Drosophila* JAK/STAT-dependent response to septic injury. *Dev Cell*. (2003) 5:441–50. doi: 10.1016/S1534-5807(03)00244-2
47. Wright VM, Vogt KL, Smythe E, Zeidler MP. Differential activities of the *Drosophila* JAK/STAT pathway ligands Upd, Upd2 and Upd3. *Cell Signal*. (2011) 23:920–7. doi: 10.1016/j.cellsig.2011.01.020
48. Ghiglione C, Devergne O, Georgenthum E, Carballès F, Médioni C, Cerezo D, et al. The *Drosophila* cytokine receptor Domeless controls border cell migration and epithelial polarization during oogenesis. *Development*. (2002) 129:5437–47. doi: 10.1242/dev.00116
49. Binari R, Perrimon N. Stripe-specific regulation of pair-rule genes by hopscotch, a putative Jak family tyrosine kinase in *Drosophila*. *Genes Dev*. (1994) 8:300–12. doi: 10.1101/gad.8.3.300
50. Paradkar PN, Duchemin J-B, Rodriguez-Andres J, Trinidad L, Walker PJ. Cullin4 Is pro-viral during west nile virus infection of culex mosquitoes. *PLoS Pathog*. (2015) 11:e1005143. doi: 10.1371/journal.ppat.1005143
51. Taracena ML, Bottino-Rojas V, Talyuli OAC, Walter-Nuno AB, Oliveira JHM, Angleró-Rodriguez YI, et al. Regulation of midgut cell proliferation impacts *Aedes aegypti* susceptibility to dengue virus. *PLoS Negl Trop Dis*. (2018) 12:e0006498. doi: 10.1371/journal.pntd.0006498
52. Keller BC, Fredericksen BL, Samuel MA, Mock RE, Mason PW, Diamond MS. Resistance to Alpha/Beta interferon is a determinant of west nile virus replication fitness and virulence. *J Virol*. (2006) 80:9424–34. doi: 10.1128/JVI.00768-06
53. Stone AEL, Green R, Wilkins C, Hemann EA, Gale M. RIG-I-like receptors direct inflammatory macrophage polarization against West Nile virus infection. *Nat Commun*. (2019) 10:3649. doi: 10.1038/s41467-019-11250-5
54. Herrera SC, Bach EA. JAK/STAT signaling in stem cells and regeneration: from *Drosophila* to vertebrates. *Development*. (2019) 146:dev167643. doi: 10.1242/dev.167643
55. Wittes J, Schüpbach T. A gene expression screen in *Drosophila melanogaster* identifies novel JAK/STAT and EGFR targets during oogenesis. *G3*. (2019) 9:47–60. doi: 10.1534/g3.118.200786
56. Martin M, Hiroyasu A, Guzman RM, Roberts SA, Goodman AG. Analysis of *Drosophila* STING reveals an evolutionarily conserved antimicrobial function. *Cell Rep*. (2018) 23:3537–50.e6. doi: 10.1016/j.celrep.2018.05.029
57. Ishikawa H, Barber GN. STING is an endoplasmic reticulum adaptor that facilitates innate immune signalling. *Nature*. (2008) 455:674–8. doi: 10.1038/nature07317
58. Goto A, Okado K, Martins N, Cai H, Barbier V, Lamiable O, et al. The kinase IKKβ regulates a STING and NF-κB-dependent antiviral response pathway in *Drosophila*. *Immunity*. (2018) 49:225–34.e4. doi: 10.1016/j.immuni.2018.07.013
59. Hua X, Li B, Song L, Hu C, Li X, Wang D, et al. Stimulator of interferon genes (STING) provides insect antiviral immunity by promoting Dredd caspase–mediated NF-κB activation. *J Biol Chem*. (2018) 293:11878–90. doi: 10.1074/jbc.RA117.000194
60. Kranzusch PJ, Wilson SC, Lee ASY, Berger JM, Doudna JA, Vance RE. Ancient origin of cGAS-STING reveals mechanism of universal 2′,3′ cGAMP signaling. *Mol Cell*. (2015) 59:891–903. doi: 10.1016/j.molcel.2015.07.022
61. Levine B, Mizushima N, Virgin HW. Autophagy in immunity and inflammation. *Nature*. (2011) 469:323–35. doi: 10.1038/nature09782
62. Moretti J, Roy S, Bozec D, Martinez J, Chapman JR, Ueberheide B, et al. STING senses microbial viability to orchestrate stress-mediated autophagy of the endoplasmic reticulum. *Cell*. (2017) 171:809–23.e13. doi: 10.1016/j.cell.2017.09.034
63. Jung CH, Ro S-H, Cao J, Otto NM, Kim D-H. mTOR regulation of autophagy. *FEBS Lett*. (2010) 584:1287–95. doi: 10.1016/j.febslet.2010.01.017
64. Rosenberg R, Lindsey NP, Fischer M, Gregory CJ, Hinckley AF, Mead PS, et al. Vital signs: trends in reported vectorborne disease cases — United States and Territories, 2004–2016. *MMWR Morb Mortal Wkly Rep*. (2018) 67:496–501. doi: 10.15585/mmwr.mm6717e1
65. World Health Organization. *Ten Health Issues WHO Will Tackle This Year*. (2019). Available online at: https://www.who.int/emergencies/ten-threats-to-global-health-in-2019 (accessed January 21, 2019).
66. Souza-Neto JA, Sim S, Dimopoulos G. An evolutionary conserved function of the JAK-STAT pathway in anti-dengue defense. *Proc Natl Acad Sci USA*. (2009) 106:17841–6. doi: 10.1073/pnas.0905006106

Conflict of Interest: The authors declare that the research was conducted in the absence of any commercial or financial relationships that could be construed as a potential conflict of interest.

frontiers in Immunology

ORIGINAL RESEARCH
published: 10 January 2020
doi: 10.3389/fimmu.2019.03040

Bombardier Enables Delivery of Short-Form Bomanins in the *Drosophila* Toll Response

*Samuel J. H. Lin, Amit Fulzele, Lianne B. Cohen, Eric J. Bennett and Steven A. Wasserman**

Section of Cell and Developmental Biology, Division of Biological Sciences, University of California, San Diego, San Diego, CA, United States

Toll mediates a robust and effective innate immune response across vertebrates and invertebrates. In *Drosophila melanogaster*, activation of Toll by systemic infection drives the accumulation of a rich repertoire of immune effectors in hemolymph, including the recently characterized Bomanins, as well as the classical antimicrobial peptides (AMPs). Here we report the functional characterization of a Toll-induced hemolymph protein encoded by the *bombardier* (*CG18067*) gene. Using the CRISPR/Cas9 system to generate a precise deletion of the *bombardier* transcriptional unit, we found that Bombardier is required for Toll-mediated defense against fungi and Gram-positive bacteria. Assaying cell-free hemolymph, we found that the Bomanin-dependent candidacidal activity is also dependent on Bombardier, but is independent of the antifungal AMPs Drosomycin and Metchnikowin. Using mass spectrometry, we demonstrated that deletion of *bombardier* results in the specific absence of short-form Bomanins from hemolymph. In addition, flies lacking Bombardier exhibited a defect in pathogen tolerance that we trace to an aberrant condition triggered by Toll activation. These results lead us to a model in which the presence of Bombardier in wild-type flies enables the proper folding, secretion, or intermolecular associations of short-form Bomanins, and the absence of Bombardier disrupts one or more of these steps, resulting in defects in both immune resistance and tolerance.

Keywords: *Drosophila melanogaster*, immunity, Toll, Bomanins, humoral

OPEN ACCESS

Edited by:
Susanna Valanne, Tampere University, Finland

Reviewed by:
Anni Kleino, University of Helsinki, Finland
Brian P. Lazzaro, Pennsylvania State University (PSU), United States

****Correspondence:***
Steven A. Wasserman
stevenw@ucsd.edu

Specialty section:
This article was submitted to Comparative Immunology, a section of the journal Frontiers in Immunology

Received: *18 October 2019*
Accepted: *11 December 2019*
Published: *10 January 2020*

Citation:
Lin SJH, Fulzele A, Cohen LB, Bennett EJ and Wasserman SA (2020) Bombardier Enables Delivery of Short-Form Bomanins in the Drosophila Toll Response. Front. Immunol. 10:3040. doi: 10.3389/fimmu.2019.03040

INTRODUCTION

Innate immune pathways are found in plants, fungi, and animals and provide a rapid defense against a broad range of pathogens (1–3). In the fruit fly *Drosophila melanogaster*, the two major innate immune pathways are Toll and Imd (4–6). The Toll pathway is activated by Gram-positive bacteria with Lys-type peptidoglycan and by fungi, and is required for defense against these microbes (7–10). Conversely, the Imd pathway is activated by and plays a major role in survival against Gram-negative bacteria and Gram-positive bacteria with DAP-type peptidoglycan (11, 12). These pathways, which are both mediated by NF-κB transcription factors, are broadly conserved as initiators of innate immune responses. Activation of either pathway induces robust production of an array of immune molecules, including antimicrobial peptides (AMPs) (13–17).

AMPs are found in all kingdoms of life (18–22). These peptides have long been thought to play the principal effector role in innate immune defense due to their demonstrated *in vitro* antimicrobial activity and their marked upregulation after infection. However, recent research in *D. melanogaster* suggests that AMPs play a major role in Imd-mediated defense, but a relatively minor role in Toll-mediated immunity (23).

In contrast to the AMPs, the *Drosophila*-specific Bomanin peptides (Boms), which are highly induced after infection, are indispensable for resistance against pathogens controlled by the Toll pathway (24). $Bom^{\Delta 55C}$ flies, which lack 10 of the 12 *Bom* genes, succumb to fungal and Gram-positive bacterial infections at rates indistinguishable from Toll-deficient flies (23, 24), suggesting that Boms rather than AMPs are the primary Toll effectors.

Bom peptides, like AMPs, are secreted from the fat body, the *Drosophila* immune organ, into the hemolymph, the *Drosophila* circulatory fluid. The family is comprised of three groups. The short-form peptides are 16–17 residues long and contain only the Bom motif. The tailed forms contain the Bom motif followed by a C-terminal tail. Finally, the bicipital forms consist of two Bom motifs connected by a linker region (24). $Bom^{\Delta 55C}$ flies lack all six of the short-form Boms, two of the three tailed Boms, and two of the three bicipital Boms. High-level expression of short-form Boms is sufficient to rescue the sensitivity of $Bom^{\Delta 55C}$ flies to *C. glabrata* infection (25). Furthermore, the absence of Toll-induced candidacidal activity in $Bom^{\Delta 55C}$ hemolymph can be rescued by high-level expression of a short-form Bom (25). However, no *in vitro* antimicrobial activity has been observed with Bom peptides alone (25), suggesting that the Bomanins act in coordination with additional humoral effectors.

In this study, we demonstrate an essential role in Toll-mediated humoral defense for a previously uncharacterized hemolymph protein, Bombardier (one that deploys Boms).

MATERIALS AND METHODS

CRISPR/Cas9 Deletion of *bombardier* Locus

The *bombardier* gene (CG18067) was deleted using CRISPR/Cas9 technology according to established protocols (26). Briefly, a pair of gRNAs designed to delete the region 2R: 20,534,248–20,536,154 were cloned into pU6-BbsI-chiRNA (Addgene plasmid #45946). Homology arms (1,017 bp left and 1,022 bp right) were cloned into pDsRed-attP (Addgene plasmid #51019). The plasmid pBS-Hsp70-Cas9 (Addgene plasmid #46294) was used as the Cas9 source. Constructs were injected into w^{1118} embryos. F1 progeny were screened for DsRed eyes and homozygous lines were established. See **Supplemental Table 1** for gRNA and homology arm primer sequences.

Toll Activation, *Drosophila* Infection, and Survival Analysis

Flies were raised at 25°C on cornmeal molasses agar media[1]. The w^{1118} strain was used as the wild type. Microbial isolates, culture conditions, and conditions for infection for *Enterococcus faecalis, Enterobacter cloacae, Fusarium oxysporum,* and *Candida glabrata* were as described previously (24), except that *C. glabrata* was concentrated to $OD_{600} = 100$. Flies were incubated at 25°C after live bacterial infection and at 29°C after fungal infection. For heat-killed challenge, bacterial cultures were autoclaved and resuspended in 20% glycerol to $OD_{600} = 10$ for *E. faecalis* and $OD_{600} = 300$ for *M. luteus*. For both survival assays and hemolymph preparation, flies challenged with heat-killed bacteria were incubated at 29°C.

Hemolymph Antimicrobial Assays

Candidacidal activity of hemolymph was assayed as described previously (25), except that hemolymph was prepared from groups of 30 flies and all activity assays were carried out for 1 h at room temperature. The number of colonies representing zero percent killing was set as the value obtained by assaying uninduced w^{1118} hemolymph.

MALDI-TOF Analysis of Hemolymph

The Toll pathway was activated in flies using heat-killed *M. luteus,* then incubated at 29°C for 24 h. Hemolymph was extracted as in Lindsay et al. (25), with slight modifications. Hemolymph extracted with glass capillaries from five male flies was pooled and transferred into 0.1% trifluoroacetic acid (TFA)/50% acetonitrile (ACN). One µl of each mixture was spotted on a Bruker MSP 96 ground steel plate, mixed 1:1 with a saturated solution of Universal MALDI matrix (Sigma-Aldrich) in 0.1% TFA/78% ACN, and air-dried. MALDI-TOF spectra were acquired using a Bruker Autoflex mass spectrometer. Data were collected from 1,500 to 10,000 m/z in positive linear mode, and 1,000–5,000 m/z in positive reflectron mode. Peptide calibration standard II (Bruker) was mixed with Universal MALDI matrix and used as an external calibration standard. At least ten independent samples were collected for each genotype. For peptide identification, peaks were matched to those of corresponding peaks in prior studies (13, 25). Representative spectra were visualized using R 3.3.2 and ggplot2 2.2.1 (27, 28).

Gene Expression Quantitation

The Toll pathway was activated with heat-killed *M. luteus*. Using TRIzol (Ambion), total RNA was extracted 18 h after Toll activation from four to six adult flies (2–5 days old). Next, cDNA was synthesized from 500 ng total RNA using the SuperScript II Reverse Transcriptase kit (Invitrogen). Quantitative RT-PCR was performed on an iQ5 cycler (BioRad) using iQ SYBR Green Supermix (BioRad). Quantification of mRNA levels was calculated relative to levels of the ribosomal protein gene *rp49* using the Pfaffl method (29). Three independent replicates were completed. See **Supplemental Table 1** for qPCR primer sequences.

Hemolymph LC-MS

Flies were challenged with heat-killed *M. luteus* to activate the Toll pathway. Hemolymph was extracted from 100 to 110 each of w^{1118}, Δbbd, and $Bom^{\Delta 55C}$ flies using the same method as in the hemolymph antimicrobial assays, with 50–60 flies processed per Zymo-Spin IC column (Zymo Research)

[1]http://blogs.cornell.edu/drosophila/dssc-cornmeal-recipe/

and yielding a total of ∼10 µl hemolymph per genotype. Three independent biological replicates were processed for Δ*bbd* and $Bom^{\Delta 55C}$, and two independent biological replicates were processed for w^{1118}. Extracted hemolymph was mixed 1:1 (vol/vol) with denaturing buffer (8 M Urea, 50 mM Tris, pH 7.8, 150 mM NaCl, protease and phosphatase inhibitors) and protein concentration was determined using a BCA assay. For each sample, 40 µg of hemolymph was diluted to 1 M urea using 50 mM ammonium bicarbonate and digested overnight with trypsin (Promega, V511A) at a 1:100 (trypsin:protein) ratio. After digestion, peptides were reduced with 1 mM dithiothreitol at room temperature for 30 min and then alkylated with 5 mM iodoacetamide at room temperature in the dark for 30 min. Formic acid was added to a 0.1% final concentration and peptides were desalted using the C18-Stage-Tip method and then vacuum dried. The dried peptides were reconstituted in 5% formic acid/5% acetonitrile and 1 µg of total peptide for each sample was loaded for MS analysis. Samples were run in technical triplicates on a Q-Exactive mass spectrometer with instrument and chromatography settings as described previously (30), except for the following modifications: the RAW files were analyzed using Andromeda/MaxQuant (version 1.6.7.0) (31) with default settings (32) except the match between the run and LFQ quantitation settings was enabled for label free quantification. Data were searched against a concatenated target-decoy database comprised of forward and reversed sequences from the unreviewed UniprotKB/Swiss-Prot FASTA *Drosophila* database (2019). A mass accuracy of 20 ppm was assigned for the first search and 4.5 ppm for the main search. The statistical analysis was calculated using the DEP analysis R-package (33).

Bacterial Load Quantification

Bacterial load upon death (BLUD) was obtained as in Duneau et al. (34), with slight modifications. Briefly, flies were infected with *E. faecalis* and vials were monitored every 30 min for newly dead flies. These flies were then individually homogenized with a pestle in 400 µl LB media. Homogenates were also prepared from individual live w^{1118} flies 120 h post-infection (hpi). Homogenates were diluted serially in LB and spread on LB agar plates for incubation at 37°C overnight. Colonies were counted manually and the number of viable bacteria per fly was calculated. Data were obtained from three independent experiments.

Data Analysis

GraphPad Prism 5 was used for statistical tests. Survival data were plotted as Kaplan-Meier curves and were analyzed using the Gehan-Breslow-Wilcoxon test to determine statistical significance. Statistical differences in candidacidal activity were calculated using one-way ANOVA followed by Tukey's test. Multiple Mann-Whitney U tests were used to calculate differences between BLUD samples ($p = 0.0085$ after Šidák correction for multiple comparisons, $\alpha = 0.05$, $k = 6$). Spearman rank correlation was used to assess the relationship between BLUD and time of death.

RESULTS

The *bombardier* Gene Is Specifically Required for Toll-Mediated Defense

The *bombardier* (*bbd*) gene contains a consensus Toll-responsive NF-κB binding site within its promoter region and is strongly expressed upon Toll activation by Gram-positive bacterial infection or other inducers (14, 17, 35, 36). The encoded protein is predicted to be secreted and to generate a mature protein of 222 amino acids with a coiled coil near its C-terminus (37, 38). Orthologs of Bombardier are found across the *Drosophila* genus, but in no other genera (39).

We began our analysis of the *bombardier* gene by generating a null mutant, using CRISPR/Cas9 to delete 1,906 bp encompassing the annotated transcriptional unit. Flies homozygous for this deletion (hereafter Δ*bbd*) were viable and morphologically wild-type. Given that *bombardier* is Toll-inducible, we assayed Δ*bbd* flies for a potential loss-of-function phenotype in Toll-mediated immunity. Specifically, we infected adult Δ*bbd* flies with various pathogens and then monitored survival. Two additional genotypes were used as controls: w^{1118} flies, which served as the wild type, and $Bom^{\Delta 55C}$ flies, which lack Toll-mediated humoral defenses due to deletion of the 10 of the 12 *Bom* genes (24).

As shown in **Figure 1**, we observed a marked immunodeficiency when Δ*bbd* flies were challenged with representative species for the three classes of microbes against which Toll provides defense. With the yeast *Candida glabrata*, more than 90% of w^{1118}, but no Δ*bbd* flies, survived 5 days after infection (**Figure 1A**). In the case of the filamentous fungus *Fusarium oxysporum*, 70% of w^{1118} adults, but fewer than 20% of Δ*bbd* adults, were alive 5 days post-infection (**Figure 1B**). Finally, with *Enterococcus faecalis*, a Gram-positive bacterium, 50% of wild-type flies, but no Δ*bbd* flies, were alive 5 days after infection (**Figure 1C**).

The impairment of Toll-mediated defenses by deletion of *bombardier* was significant for all three pathogens ($p < 0.0001$). In the case of *C. glabrata*, the immunodeficiency of Δ*bbd* phenocopied that observed for $Bom^{\Delta 55C}$ flies (n.s., $p > 0.05$). In contrast, with either *F. oxysporum* or *E. faecalis,* the rate of death was greater for $Bom^{\Delta 55C}$ than for Δ*bbd* (***$p < 0.0001$ for both infections). The Δ*bbd* mutant thus displays a substantial, but not complete, loss of Toll-mediated defense.

The expression of *bombardier* is strongly induced by Toll, but not Imd activation (14). We therefore hypothesized that Imd-mediated defenses would not require *bombardier* function. To test this prediction, we infected Δ*bbd* flies with *Enterobacter cloacae,* a Gram-negative bacterium. In this experiment, Δ*bbd* flies were as immunocompetent as w^{1118} flies: more than 90% of both genotypes survived at least 5 days post-infection (**Figure 1D**). In contrast, 100% of Rel^{E20} flies, which are deficient in Imd signaling (40), succumbed to infection within 1 day. Thus, *bombardier* functions in defense against a range of pathogens for which Toll mediates defense—yeast, filamentous fungi, and Lys-type Gram-positive bacteria—but not against Gram-negative bacteria, against which the Imd pathway is active.

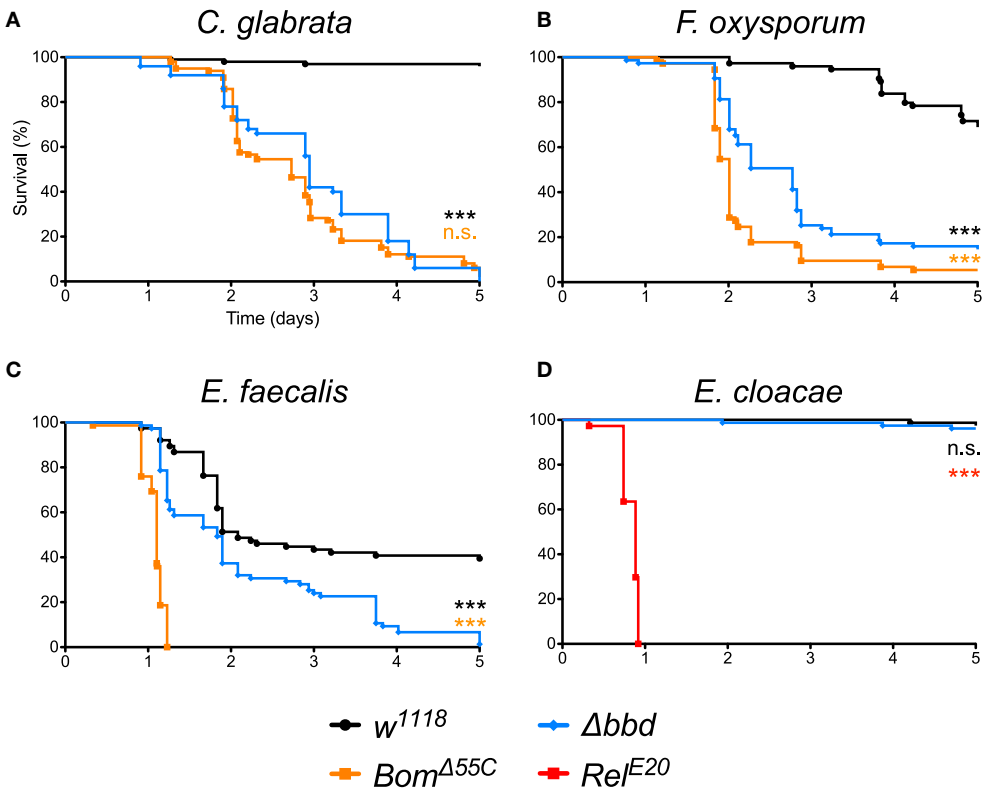

FIGURE 1 | The *bombardier* gene is specifically required for Toll-mediated defense. **(A–D)** Survival curves of flies infected as indicated. The w^{1118} strain was the wild-type control; $Bom^{\Delta 55C}$ and Rel^{E20} were the susceptible controls (24, 40). Experiments were completed in triplicate with at least 25 flies per genotype in each replicate. Statistical significance was determined using the Gehan-Breslow-Wilcoxon test and Δ*bbd* is shown relative to w^{1118} in black, relative to $Bom^{\Delta 55C}$ in orange, and relative to Rel^{E20} in red ($^{***}p < 0.0001$; n.s., not significant, $p > 0.05$).

The Candidacidal Activity of Hemolymph Requires Bombardier, but Neither Drosomycin Nor Metchnikowin

Next, we investigated the potential humoral role of Bombardier by preparing and assaying cell-free hemolymph. We have previously shown that hemolymph from wild-type flies exhibits a Toll-dependent and Bomanin-dependent candidacidal activity (25). However, we were also curious as to the identity of the active antifungal component. In particular, we considered the potential role of Metchnikowin (Mtk) and Drosomycin (Drs), two antimicrobial peptides (AMPs) that have documented antifungal activity *in vitro* and are strongly Toll-induced *in vivo* (14, 41, 42). We therefore took advantage of the recently described Δ*AMPs* strain, which is deficient for Mtk and Drs, as well as all other induced AMPs other than the Cecropins (23). Extracting and assaying Toll-induced hemolymph, we found that hemolymph from Δ*AMPs* flies had a killing activity against *C. glabrata* comparable to that of wild-type hemolymph (**Figure 2**). In contrast, we failed to detect any killing of *C. glabrata* by Δ*bbd* hemolymph. We conclude that Boms and Bombardier, but neither Mtk nor Drs, are required for humoral defense against *C. glabrata*.

Short-Form Bom Peptides Are Specifically Absent From Δ*bbd* Hemolymph

MALDI-TOF provides a robust tool for characterizing small (<5,000 MW) peptides present in hemolymph after Toll activation. As shown in **Figures 3A,B**, such a readout includes the aforementioned AMPs (Mtk and Drs), several short-form Boms (BomS1, S2, S3, and S6; see **Supplemental Table 2** for updated Bomanin nomenclature), and other induced peptides (e.g., IM4). We have previously shown that deleting the 55C Bom gene cluster removes the peaks attributable to the short-form Boms, while leaving the remaining signals unaffected (25). Remarkably, analysis of Δ*bbd* hemolymph yielded a similar pattern. As shown in **Figures 3C,D**, the short-form Boms that were readily detectable in the wild type—S1, S2, S3, and S6—were absent in Δ*bbd* hemolymph, whereas the remaining peptides, including Mtk, Drs, and IM4, displayed a wild-type profile.

Although Δ*bbd* disrupts the accumulation of short-form Bom peptides in hemolymph, this effect does not reflect a disruption in transcription or stability of the corresponding *Bom* mRNAs: robust induction of Toll-regulated genes, including genes of short-form Boms, was readily detectable with qRT-PCR (**Supplemental Figure 1**).

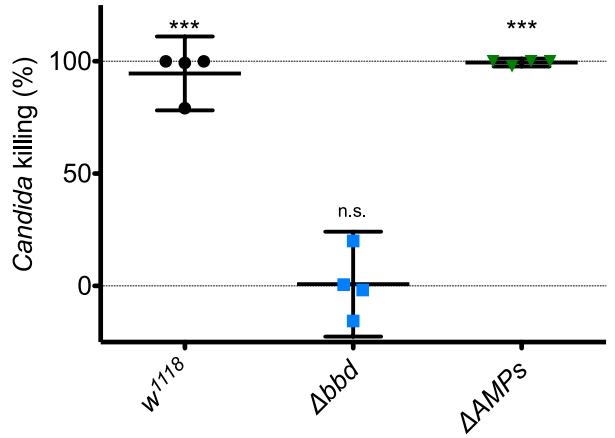

FIGURE 2 | The Toll-induced candidacidal activity of hemolymph requires Bombardier, but neither Drosomycin nor Metchnikowin. Heat-killed *M. luteus* was used to activate the Toll pathway in flies. Hemolymph was extracted from flies 24 h after Toll induction, mixed with *C. glabrata* and incubated for 1 h to allow for killing. The surviving yeast cells were plated, and colonies were counted to determine the level of candidacidal activity in the extracted hemolymph. Colony counts from uninduced w^{1118} hemolymph were used as the control for no (0%) killing. Experiments were completed four times, with each point representing one replicate. One-way ANOVA was calculated followed by Tukey's test. Significance is shown relative to the null hypothesis of 0% killing (***$p < 0.0001$; n.s., not significant, $p > 0.05$). Error bars represent the 95% confidence interval.

Because proteins such as Bombardier and bicipital Boms are too large to be detected by our MALDI-TOF protocol, we used LC-MS to further characterize the relationship between Bombardier and the Boms in hemolymph. For these studies, we prepared Toll-induced hemolymph from three genotypes: w^{1118}, Δ*bbd*, and $Bom^{\Delta 55C}$. In wild-type hemolymph, we readily detected Bombardier protein (**Figure 4**), consistent with the presence of a canonical secretion signal sequence in the Bombardier coding sequence. Bombardier, like the Boms, is thus secreted into hemolymph upon Toll induction. We also detected all three bicipital Boms—BomBc1, BomBc2, and BomBc3. The LC-MS studies thus complemented the MALDI-TOF studies, with bicipital Boms detected by the former and short-form Boms by the latter (tailed Boms are not detected by either protocol). Next, we assayed Δ*bbd* hemolymph. As expected, Bombardier was not detected. However, the three bicipital Boms were present at comparable levels in wild-type and Δ*bbd* hemolymph (see **Figure 4**). Combined with the MALDI-TOF studies, these results demonstrate that Δ*bbd* blocks accumulation in hemolymph of short-form, but not bicipital, Boms. Lastly, we analyzed hemolymph from $Bom^{\Delta 55C}$ flies, which lack 10 of the 12 *Bom* genes. As expected, the products of the two deleted bicipital genes (*BomBc1* and *BomBc2*) were absent, whereas the product of the remaining bicipital gene (*BomBc3*) was present at wild-type levels (see **Figure 4**). Turning our attention to Bombardier, we observed no effect of the *55C* Bom deletion. Thus, Bombardier is required for the presence of short-form Boms in hemolymph, but the 55C Boms are not required for the presence of Bombardier.

Bombardier Mediates Both Infection Resistance and Tolerance

The Δ*bbd* survival phenotype could be due to an inability to control pathogen growth—a defect in resistance—or an inability to endure infection—a defect in tolerance. Because flies lacking Bombardier demonstrate an increased susceptibility to infection and decreased levels of known resistance factors, the short-form Boms, it seemed likely that Δ*bbd* flies, like $Bom^{\Delta 55C}$ flies, have a defect in infection resistance. In exploring this hypothesis, we found that the model recently developed by Duneau et al. provided a useful framework (34). Following infection of an individual fly, there are two stereotypic outcomes: either the pathogen replicates, reaches a lethal burden, and the fly dies; or the pathogen is controlled at a level below the lethal burden and the fly survives with a persistent infection. Variation in survival curves for different pathogens and fly genotypes reflects variation in both the time required to reach lethal burden and in the fraction of flies that are able to control the infection before it reaches such a threshold. In cases where a fraction of flies control infection, group survival typically drops after infection and then reaches a plateau (23).

The survival curve for Δ*bbd* flies infected with *E. faecalis* does not plateau (see **Figure 1C**). Instead, it exhibits a profile that we hypothesize reflects two phases of death. In the first phase, extending roughly 2 days post-infection, some Δ*bbd* flies reach a lethal burden of *E. faecalis* and die, as reflected in a sharp decline in survival; the remainder control the infection. In the second phase, from 2.5 days onward, those flies with a persistent infection die at a reduced but steady rate, due to a defect in tolerance. If this hypothesis is correct, flies dying in the first phase should have a bacterial load upon death (BLUD) comparable to that of wild-type flies dying from infection. Furthermore, those dying in the second phase should have a much lower pathogen burden, comparable to that of wild-type survivors with a persistent infection.

To test our predictions regarding pathogen burden, we measured the BLUD of individual flies after infection with live *E. faecalis* and divided the data into two time intervals (**Figure 5**). For the earlier interval (dead flies obtained between 17 and 51.5 hpi), both $Bom^{\Delta 55C}$ and Δ*bbd* bacterial loads upon death were not significantly different from w^{1118} (**Figure 5**, red, $p > 0.05$). For the later time interval (flies obtained between 68 and 120.5 hpi), Δ*bbd* flies perished at significantly lower bacterial loads compared to that of Δ*bbd* flies which died earlier (**Figure 5**, Δ*bbd* early compared to Δ*bbd* late, $p < 0.0001$), indicating that these two groups die from distinct causes. Importantly, late-death Δ*bbd* flies perished at significantly lower bacterial loads than those of w^{1118} suffering early deaths ($p < 0.0001$), demonstrating that Δ*bbd* flies have a defect in tolerance.

Together, the survival curve and BLUD data offer strong support for our two-phase-model: Δ*bbd* flies died early in infection with high bacterial loads, due to a defect in resistance, and died later with lower bacterial loads, reflecting a deficiency in tolerance. However, we note that the bacterial loads of

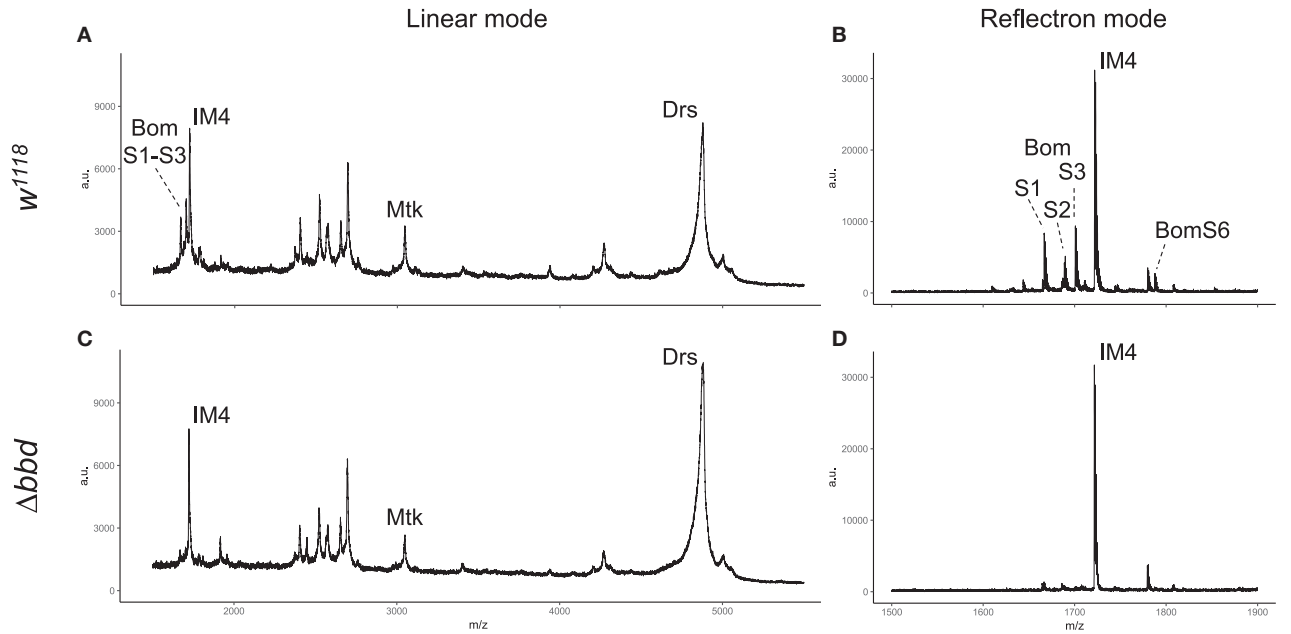

FIGURE 3 | Short-form Bom peptides are specifically absent in hemolymph from Δ*bbd* flies. MALDI-TOF mass spectra of w^{1118} **(A,B)** and Δ*bbd* **(C,D)** hemolymph samples were collected in linear **(A,C)** and reflectron mode **(B,D)**. For peptide identification, peaks were matched to those of corresponding peaks in prior studies (13, 25). Spectra were obtained from at least ten independent biological replicates and representative spectra are shown (a.u., arbitrary units; m/z, mass/charge).

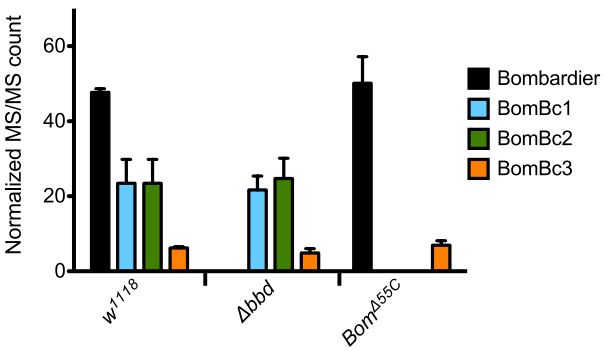

FIGURE 4 | The presence of bicipital Bomanins in hemolymph is unaffected by loss of Bombardier. MS/MS counts for the indicated proteins as determined by Andromeda/MaxQuant were normalized to total MS/MS counts in each run. Error bars represent standard deviation for biological replicates ($n = 3$ for Δ*bbd* and $Bom^{\Delta 55C}$, $n = 2$ for w^{1118}). **Supplemental Table 3** shows the full dataset.

Δ*bbd* flies dying in the later phase were still significantly greater than those of w^{1118} flies alive 120 hpi (**Figure 5**, Δ*bbd* late compared to live w^{1118}, $p < 0.0001$). This indicates that the later-death Δ*bbd* group has not completely controlled infection compared to the live w^{1118} flies, and suggests that both resistance and tolerance contribute to the later Δ*bbd* fly deaths. Although we cannot rule out a minor resurgence in bacterial proliferation preceding late death of *bbd* flies, we note that BLUD and time of death were not significantly correlated for these flies (**Supplemental Figure 2**, Spearman correlation test, $r = -0.2654$, $p = 0.1564$).

Immune Activation, Specifically *Bom* Expression, Is Deleterious in the Absence of Bombardier

What is the nature of the tolerance defect we observed in Δ*bbd* flies? More specifically, is their health impaired by an excessive or toxic immune response, or is death due to another class of impaired tolerance (43)? To distinguish between these explanations, we assayed the effect of activating the immune response in Δ*bbd* flies in the absence of infection.

When Δ*bbd* flies were challenged with heat-killed *E. faecalis*, we observed a decrease in survival that first was apparent 3 days post-challenge followed by a steady decline in the number of live flies in the following days (**Figure 6A**), consistent with the timing of the late-phase deaths (see **Figure 5**). Overall, the death rate was slower than that of live infection, but the extent of killing was similar between heat-killed and live *E. faecalis*: fewer than 20% of flies survived (compare **Figures 1C**, **6A**). In contrast, no effect on survival was observed upon challenge of either w^{1118} or $Bom^{\Delta 55C}$ flies with heat-killed *E. faecalis*: >95% flies survived seven or more days post-challenge.

The effect of immune stimulation on Δ*bbd* survival was not specific to *E. faecalis*. When we repeated the challenge experiments with heat-killed *Micrococcus luteus*, which activates the Toll response [see **Supplemental Figure 1**, as well as (25, 44)], the effect on Δ*bbd* survival was again marked: 5 days after challenge, fewer than 5% of Δ*bbd* flies were alive, compared to

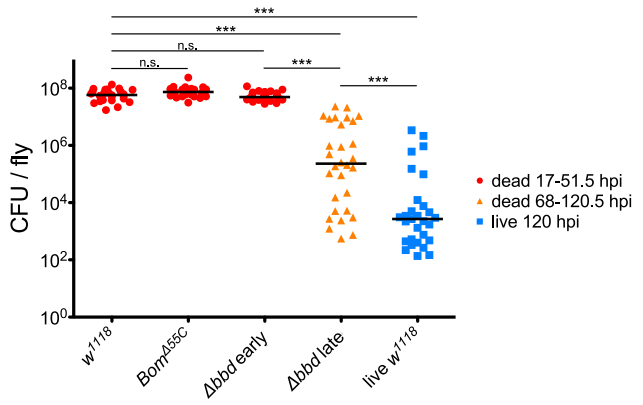

FIGURE 5 | Bombardier mediates both infection resistance and tolerance. Bacterial load upon death (BLUD) of w^{1118}, $Bom^{\Delta 55C}$, and Δ*bbd* flies, plotted by early (17–51.5 hpi, red) or late (68–120.5 hpi, orange) time of death post-infection, as well as bacterial load of live w^{1118} flies 120 hpi (blue). Data was obtained and combined from three independent experiments totaling $n = 26$ for w^{1118}, $n = 30$ for $Bom^{\Delta 55C}$, $n = 33$ for Δ*bbd* red, $n = 30$ for Δ*bbd* orange, and $n = 29$ for live w^{1118}. Black bars indicate median values. Statistics were calculated using multiple Mann-Whitney *U*-tests. For significance, $p = 0.0085$ after Šidák correction for multiple comparisons ($\alpha = 0.05$, $k = 6$). The pathogen loads of early deaths for $Bom^{\Delta 55C}$ and Δ*bbd* were not significantly different from w^{1118} ($p > 0.05$). The pathogen load of late Δ*bbd* fly deaths is significantly different from that of the early-death Δ*bbd* and w^{1118} groups (***$p < 0.0001$) and also significantly different from that of live w^{1118} flies 120 hpi (***$p < 0.0001$). Finally, the early-death w^{1118} pathogen load was significantly different from that of live w^{1118} flies 120 hpi (***$p < 0.0001$) (hpi, hours post-infection).

survival of >95% of w^{1118} and 85% of $Bom^{\Delta 55C}$ flies over the same period of time (**Figure 6B**).

As both *M. luteus* and *E. faecalis* induce the Toll pathway, Toll activation could be the key factor in Δ*bbd* mortality. To address this hypothesis, Δ*bbd* flies were crossed with $MyD88^{kra1}$ (Toll-deficient) flies to generate the $MyD88^{kra1}$ Δ*bbd* double mutant, and the resulting flies were challenged with heat-killed *E. faecalis* and *M. luteus*. Unlike Δ*bbd* flies, $MyD88^{kra1}$ Δ*bbd* flies survived challenge with Toll activators (**Figures 7A,B**). Because blocking the Toll pathway with $MyD88^{kra1}$ rescues the Δ*bbd* phenotype triggered by heat-killed bacteria ($p < 0.0001$ compared to Δ*bbd*, $p > 0.05$ compared to $MyD88^{kra1}$ for both heat-killed bacteria), we conclude that Toll activation underlies the death of Δ*bbd* flies in the absence of infection.

As described above, *Bom* genes are transcribed in Δ*bbd* flies (**Supplemental Figure 1**), but short-form Bom peptides do not appear in hemolymph (**Figure 3**). This suggests a mislocalization of these peptides, perhaps in an unprocessed or misfolded state. Given that short-form *Bom* genes are among the most abundantly transcribed genes after infection (17, 36), such mislocalized or misfolded Boms could rapidly accumulate to high levels in Δ*bbd* flies. Could this explain the death of Δ*bbd* flies upon immune stimulation? To address this question, we generated $Bom^{\Delta 55C}$ Δ*bbd* double mutants and assayed the effect of immune induction alongside both $Bom^{\Delta 55C}$ and Δ*bbd* flies (**Figures 7A,B**). The result was unequivocal: introducing $Bom^{\Delta 55C}$, which deletes all of the short-form Boms, eliminated the effect of Δ*bbd* on survival following immune stimulation ($p < 0.0001$ compared to Δ*bbd*, $p > 0.05$ compared to $Bom^{\Delta 55C}$ for both heat-killed bacteria). The fact that $Bom^{\Delta 55C}$ is epistatic to Δ*bbd* demonstrates that Toll-driven expression of *Bom* genes is specifically responsible for the death of immune-stimulated Δ*bbd* flies.

DISCUSSION

The results presented in this study identify a key factor that regulates humoral and Bom-mediated defense in *Drosophila*. We demonstrate that Δ*bbd* flies are defective in resistance to pathogens controlled by the Toll pathway. The results support the hypothesis that this defect results from the absence of short-form Boms in Δ*bbd* hemolymph. Absence of Boms is sufficient to cause a defect in resistance (24) and Δ*bbd* hemolymph appears to be lacking the short-form Boms but no other component, save Bombardier itself. Furthermore, Δ*bbd* phenocopies $Bom^{\Delta 55C}$ with regard to survival after *C. glabrata* infection, and resistance to *C. glabrata* can be restored in $Bom^{\Delta 55C}$ flies by expression of short-form Boms (25). Finally, Δ*bbd* hemolymph lacks candidacidal activity, which is dependent on short-form Bom peptides (25) and which we show here does not require Drs or Mtk.

For pathogens other than *C. glabrata*, the effect of deleting Bombardier is less severe than that of deleting the ten *Bom* genes clustered at 55C. Our mass spectrometry data suggest an explanation. Whereas, short-form Boms are absent from Δ*bbd* hemolymph, bicipital Boms are present. (Tailed Boms were not detected with either mass spectrometry method.) Therefore, we postulate that the bicipital Boms, which are not required for resistance to *C. glabrata* (25), are functional against other pathogens. This would explain why Δ*bbd* flies are more resistant than $Bom^{\Delta 55C}$ flies upon infection with *E. faecalis* or *F. oxysporum* (**Figure 1**). In this regard, we note that Bombardier and all three forms of Bom proteins—short, tailed, and bicipital—are found across the *Drosophila* genus, supporting the notion that all three classes of Boms are immunoprotective and therefore maintained across the *Drosophila* genus.

It might appear that our discovery of Bombardier was serendipitous, given our role in defining the *Bomanin* gene family (24, 25). In hindsight, however, the link was forged in our approach. We selected *CG18067* from the most strongly inducible Toll-regulated loci, a group that also includes eight of the *Bomanin* genes. Next, we engineered a CRISPR/Cas9 deletion of *CG18067* and assayed this knockout with the identical set of pathogens that we had used for the $Bom^{\Delta 55C}$ deletion, screening for loss of survival upon infection. Having examined a gene that is as strongly induced as the Bomanins, present in the same range of species as the Bomanins, and with a spectrum of loss-of-function phenotypes similar to that of the Bomanins, it is not particularly surprising that we would find ourselves studying a gene that affects the Bomanins.

Bombardier Function and Structure

What is the function of Bombardier? Deleting the gene results in the absence of short-form Boms from hemolymph, an effect

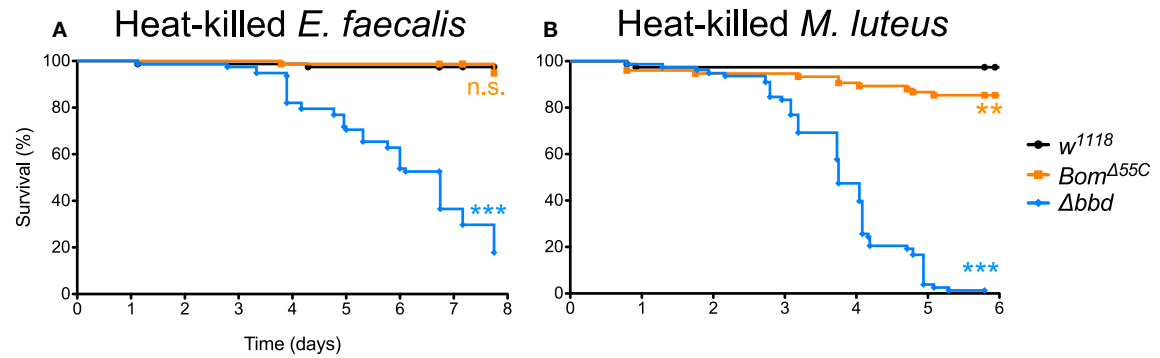

FIGURE 6 | Immune activation is deleterious in absence of Bombardier. Fly survival after introduction of **(A)** heat-killed *E. faecalis* and **(B)** heat-killed *M. luteus*. Experiments were completed in triplicate with at least 25 flies per genotype in each replicate. Statistics were determined using the Gehan-Breslow-Wilcoxon test. Significance is shown relative to w^{1118} (***$p < 0.0001$; n.s., not significant, $p > 0.05$).

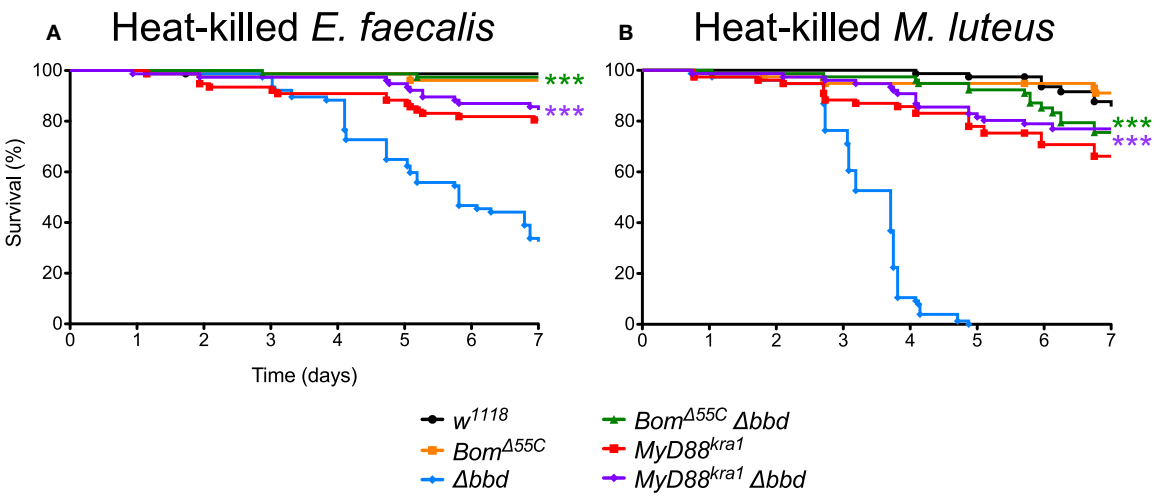

FIGURE 7 | Toll-induced *Bom* expression is responsible for death in immune stimulated Δ*bbd* flies. Survival of flies challenged with **(A)** heat-killed *E. faecalis* and **(B)** heat-killed *M. luteus*. Experiments were completed in triplicate with at least 25 flies per genotype in each replicate. Statistics were determined using the Gehan-Breslow-Wilcoxon test. Significance of double mutant survival curves is shown relative to the survival curve of Δ*bbd* (***$p < 0.0001$).

we find is at the level of protein. Other mature immune peptides are present at normal levels in the hemolymph, and there is thus no general defect in translation, secretion, or processing. Based on these findings, we propose that Bombardier normally functions either to chaperone short Boms as they are secreted from the fat body into the hemolymph or, alternatively, to protect the Boms from misfolding or aggregation while in the hemolymph. We further hypothesize that it is the ectopic localization or aberrant form of short-form Boms in Δ*bbd* flies that generates morbidity upon Toll pathway activation. In support of this idea, we showed that *Bom* expression underlies the lethality observed in Δ*bbd* flies (**Figure 7**). Whether the short-form Boms physically interact with Bombardier, perhaps in the context of a larger antimicrobial complex, is currently unknown.

Activation of Toll-like receptor (TLR) signaling is important for innate immunity, but induction of the pathway can lead to autoimmune disorders and chronic inflammatory disease (45–48). Here we report an autoimmune activity driven by Toll-induced *Bom* expression in flies lacking a downstream pathway component, Bombardier. To what extent this parallel can be exploited in the context of understanding autoimmune disorders promises to be a significant focus for future investigation.

DATA AVAILABILITY STATEMENT

The LC-MS datasets generated for this study can be accessed on the MassIVE data repository using the accession identifier: MSV000084509.

AUTHOR CONTRIBUTIONS

SL and SW: conceptualization, writing—original draft, and visualization. SL, AF, and EB: methodology. SL and AF: formal analysis. SL, AF, and LC: investigation. SL, AF, LC, EB, and SW: writing—review and editing. EB and SW: supervision and funding acquisition.

FUNDING

This work was supported by National Institutes of Health (NIH) grant R01 GM050545 (to SW), NIH grant GM119132 (to EB), and NIH predoctoral training grant T32 GM008666 (to SL). The funders had no role in study design, data collection and analysis, the decision to publish, or preparation of the manuscript.

ACKNOWLEDGMENTS

We thank Scott Lindsay for a wealth of helpful discussions and technical assistance; Andres Mauricio Caraballo-Rodriguez and the Pieter Dorrestein Lab for guidance on and access to MALDI-TOF mass spectrometry equipment; Scott Rifkin for advice on statistical approaches; Emily Troemel, Bill McGinnis, Scott Lindsay, and Roland Liu for comments on the manuscript; and the laboratories of Bill McGinnis, Valentino Gantz, Ethan Bier, and James Posakony for access to equipment.

SUPPLEMENTARY MATERIAL

The Supplementary Material for this article can be found online at: https://www.frontiersin.org/articles/10.3389/fimmu.2019.03040/full#supplementary-material

REFERENCES

1. Beutler B. Innate immunity: an overview. *Mol Immunol.* (2004) 40:845–59. doi: 10.1016/j.molimm.2003.10.005
2. Boller T, He SY. Innate immunity in plants: an arms race between pattern recognition receptors in plants and effectors in microbial pathogens. *Science.* (2009) 324:742–3. doi: 10.1126/science.1171647
3. Kombrink A, Tayyrov A, Essig A, Stöckli M, Micheller S, Hintze J, et al. Induction of antibacterial proteins and peptides in the coprophilous mushroom coprinopsis cinerea in response to bacteria. *ISME J.* (2019) 13:588–602. doi: 10.1038/s41396-018-0293-8
4. Hoffmann JA, Reichhart JM. Drosophila innate immunity: an evolutionary perspective. *Nat Immunol.* (2002) 3:121–6. doi: 10.1038/ni0202-121
5. Lemaitre B, Hoffmann J. The host defense of drosophila melanogaster. *Annu Rev Immunol.* (2007) 25:697–743. doi: 10.1146/annurev.immunol.25.022106.141615
6. Imler JL. Overview of drosophila immunity: a historical perspective. *Dev Comp Immunol.* (2014) 42:3–15. doi: 10.1016/j.dci.2013.08.018
7. Rutschmann S, Kilinc A, Ferrandon D. Cutting edge: the toll pathway is required for resistance to gram-positive bacterial infections in drosophila. *J Immunol.* (2002) 168:1542–6. doi: 10.4049/jimmunol.168.4.1542
8. Gottar M, Gobert V, Matskevich AA, Reichhart J-M, Wang C, Butt TM, et al. Dual detection of fungal infections in drosophila via recognition of glucans and sensing of virulence factors. *Cell.* (2006) 127:1425–37. doi: 10.1016/j.cell.2006.10.046
9. Valanne S, Wang J-H, Rämet M. The drosophila toll signaling pathway. *J Immunol.* (2011) 186:649–56. doi: 10.4049/jimmunol.1002302
10. Lindsay SA, Wasserman SA. Conventional and non-conventional drosophila toll signaling. *Dev Comp Immunol.* (2014) 42:16–24. doi: 10.1016/j.dci.2013.04.011
11. Kleino A, Silverman N. The drosophila IMD pathway in the activation of the humoral immune response. *Dev Comp Immunol.* (2014) 42:25–35. doi: 10.1016/j.dci.2013.05.014
12. Myllymäki H, Valanne S, Rämet M. The drosophila imd signaling pathway. *J Immunol.* (2014) 192:3455–62. doi: 10.4049/jimmunol.1303309
13. Uttenweiler-Joseph S, Moniatte M, Lagueux M, Van Dorsselaer A, Hoffmann JA, Bulet P. Differential display of peptides induced during the immune response of drosophila: a matrix-assisted laser desorption ionization time-of-flight mass spectrometry study. *Proc Natl Acad Sci USA.* (1998) 95:11342–7. doi: 10.1073/pnas.95.19.11342
14. De Gregorio E, Spellman PT, Tzou P, Rubin GM, Lemaitre B. The toll and imd pathways are the major regulators of the immune response in drosophila. *EMBO J.* (2002) 21:2568–79. doi: 10.1093/emboj/21.11.2568
15. Levy F, Rabel D, Charlet M, Bulet P, Hoffmann JA, Ehret-Sabatier L. Peptidomic and proteomic analyses of the systemic immune response of drosophila. *Biochimie.* (2004) 86:607–16. doi: 10.1016/j.biochi.2004.07.007
16. Verleyen P, Baggerman G, D'Hertog W, Vierstraete E, Husson SJ, Schoofs L. Identification of new immune induced molecules in the haemolymph of drosophila melanogaster by 2D-nanoLC MS/MS. *J Insect Physiol.* (2006) 52:379–88. doi: 10.1016/j.jinsphys.2005.12.007
17. Troha K, Im JH, Revah J, Lazzaro BP, Buchon N. Comparative transcriptomics reveals CrebA as a novel regulator of infection tolerance in *D. melanogaster*. *PLoS Pathog.* (2018) 14:e1006847. doi: 10.1371/journal.ppat.1006847
18. Hultmark D, Steiner H, Rasmuson T, Boman HG. Insect immunity. purification and properties of three inducible bactericidal proteins from hemolymph of immunized pupae of *Hyalophora cecropia*. *Eur J Biochem.* (1980) 106:7–16. doi: 10.1111/j.1432-1033.1980.tb05991.x
19. Imler JL, Bulet P. Antimicrobial peptides in drosophila: structures, activities and gene regulation. *Chem Immunol Allergy.* (2005) 86:1–21. doi: 10.1159/000086648
20. Radek K, Gallo R. Antimicrobial peptides: natural effectors of the innate immune system. *Semin Immunopathol.* (2007) 29:27–43. doi: 10.1007/s00281-007-0064-5
21. Maróti Gergely G, Kereszt A, Kondorosi É, Mergaert P. Natural roles of antimicrobial peptides in microbes, plants and animals. *Res Microbiol.* (2011) 162:363–74. doi: 10.1016/j.resmic.2011.02.005
22. Bahar AA, Ren D. Antimicrobial peptides. *Pharmaceuticals.* (2013) 6:1543–75. doi: 10.3390/ph6121543
23. Hanson MA, Dostálová A, Ceroni C, Poidevin M, Kondo S, Lemaitre B. Synergy and remarkable specificity of antimicrobial peptides *in vivo* using a systematic knockout approach. *Elife.* (2019) 8:e44341. doi: 10.7554/eLife.44341
24. Clemmons AW, Lindsay SA, Wasserman SA. An effector peptide family required for drosophila toll-mediated immunity. *PLoS Pathog.* (2015) 11:e1004876. doi: 10.1371/journal.ppat.1004876
25. Lindsay SA, Lin SJH, Wasserman SA. Short-form bomanins mediate humoral immunity in drosophila. *J Innate Immun.* (2018) 10:306–14. doi: 10.1159/000489831
26. Gratz SJ, Ukken FP, Rubinstein CD, Thiede G, Donohue LK, Cummings AM, et al. Highly specific and efficient CRISPR/Cas9-catalyzed homology-directed repair in drosophila. *Genetics.* (2014) 196:961–71. doi: 10.1534/genetics.113.160713
27. R Core Team. *R: A Language and Environment for Statistical Computing.* Vienna: R Foundation for Statistical Computing (2016).
28. Wickham H. *ggplot2: Elegant Graphics for Data Analysis.* (2016).
29. Pfaffl MW. A new mathematical model for relative quantification in real-time RT-PCR. *Nucleic Acids Res.* (2001) 29:e45. doi: 10.1093/nar/29.9.e45
30. Markmiller S, Soltanieh S, Server KL, Mak R, Jin W, Fang MY, et al. Context-dependent and disease-specific diversity in protein interactions within stress granules. *Cell.* (2018) 172:590–604.e13. doi: 10.1016/j.cell.2017.12.032

31. Cox J, Mann M. MaxQuant enables high peptide identification rates, individualized p.p.b.-range mass accuracies and proteome-wide protein quantification. *Nat Biotechnol.* (2008) 26:1367–72. doi: 10.1038/nbt.1511
32. Tyanova S, Temu T, Cox J. The MaxQuant computational platform for mass spectrometry-based shotgun proteomics. *Nat Protoc.* (2016) 11:2301–19. doi: 10.1038/nprot.2016.136
33. Zhang X, Smits AH, Van Tilburg GBA, Ovaa H, Huber W, Vermeulen M. Proteome-wide identification of ubiquitin interactions using UbIA-MS. *Nat Protoc.* (2018) 13:530–50. doi: 10.1038/nprot.2017.147
34. Duneau D, Ferdy J-B, Revah J, Kondolf H, Ortiz GA, Lazzaro BP, et al. Stochastic variation in the initial phase of bacterial infection predicts the probability of survival in *D. melanogaster*. *Elife.* (2017) 6:e28298. doi: 10.7554/eLife.28298
35. Busse MS, Arnold CP, Towb P, Katrivesis J, Wasserman SA. A kappaB sequence code for pathway-specific innate immune responses. *EMBO J.* (2007) 26:3826–35. doi: 10.1038/sj.emboj.7601798
36. Valanne S, Salminen TS, Järvelä-Stölting M, Vesala L, Rämet M. Immune-inducible non-coding RNA molecule lincRNA-IBIN connects immunity and metabolism in drosophila melanogaster. *PLoS Pathog.* (2019) 15:e1007504. doi: 10.1371/journal.ppat.1007504
37. Almagro Armenteros JJ, Tsirigos KD, Sønderby CK, Petersen TN, Winther O, Brunak S, et al. SignalP 5.0 improves signal peptide predictions using deep neural networks. *Nat Biotechnol.* (2019) 37:420–3. doi: 10.1038/s41587-019-0036-z
38. Lupas A, Van Dyke M, Stock J. Predicting coiled coils from protein sequences. *Science.* (1991) 252:1162–4. doi: 10.1126/science.252.5009.1162
39. Johnson M, Zaretskaya I, Raytselis Y, Merezhuk Y, McGinnis S, Madden TL. NCBI BLAST: a better web interface. *Nucleic Acids Res.* (2008) 36:W5–9. doi: 10.1093/nar/gkn201
40. Hedengren M, Åsling B, Dushay MS, Ando I, Ekengren S, Wihlborg M, et al. Relish, a central factor in the control of humoral but not cellular immunity in drosophila. *Mol Cell.* (1999) 4:827–37. doi: 10.1016/S1097-2765(00)80392-5
41. Fehlbaum P, Bulet P, Michaut L, Lagueux M, Broekaert WF, Hetru C, et al. Insect immunity: septic injury of drosophila induces the synthesis of a potent antifungal peptide with sequence homology to plant antifungal peptides. *J Biol Chem.* (1994) 269:33159–63.
42. Levashina EA, Ohresser S, Bulet P, Reichhart J, Hetru C, Hoffmann JA. Metchnikowin, a novel immune-inducible proline-rich peptide from drosophila with antibacterial and antifungal properties. *Eur J Biochem.* (1995) 233:694–700. doi: 10.1111/j.1432-1033.1995.694_2.x
43. Ayres JS, Schneider DS. Tolerance of infections. *Annu Rev Immunol.* (2012) 30:271–94. doi: 10.1146/annurev-immunol-020711-075030
44. Lemaitre B, Reichhart JM, Hoffmann JA. Drosophila host defense: differential induction of antimicrobial peptide genes after infection by various classes of microorganisms. *Proc Natl Acad Sci USA.* (1997) 94:14614–9. doi: 10.1073/pnas.94.26.14614
45. Björkbacka H, Kunjathoor VV, Moore KJ, Koehn S, Ordija CM, Lee MA, et al. Reduced atherosclerosis in MyD88-null mice links elevated serum cholesterol levels to activation of innate immunity signaling pathways. *Nat Med.* (2004) 10:416–21. doi: 10.1038/nm1008
46. Jiang D, Liang J, Fan J, Yu S, Chen S, Luo Y, et al. Regulation of lung injury and repair by toll-like receptors and hyaluronan. *Nat Med.* (2005) 11:1173–9. doi: 10.1038/nm1315
47. Kim S, Takahashi H, Lin W-W, Descargues P, Grivennikov S, Kim Y, et al. Carcinoma-produced factors activate myeloid cells through TLR2 to stimulate metastasis. *Nature.* (2009) 457:102–6. doi: 10.1038/nature 07623
48. Wu H, Ma J, Wang P, Corpuz TM, Panchapakesan U, Wyburn KR, et al. HMGB1 contributes to kidney ischemia reperfusion injury. *J Am Soc Nephrol.* (2010) 21:1878–90. doi: 10.1681/ASN.2009101048

Conflict of Interest: The authors declare that the research was conducted in the absence of any commercial or financial relationships that could be construed as a potential conflict of interest.

frontiers in Immunology

ORIGINAL RESEARCH
published: 23 January 2020
doi: 10.3389/fimmu.2020.00009

The Daisho Peptides Mediate *Drosophila* Defense Against a Subset of Filamentous Fungi

*Lianne B. Cohen, Scott A. Lindsay, Yangyang Xu, Samuel J. H. Lin and Steven A. Wasserman**

Section of Cell and Developmental Biology, Division of Biological Sciences, University of California, San Diego, La Jolla, CA, United States

Fungal infections, widespread throughout the world, affect a broad range of life forms, including agriculturally relevant plants, humans, and insects. In defending against fungal infections, the fruit fly *Drosophila melanogaster* employs the Toll pathway to induce a large number of immune peptides. Some have been investigated, such as the antimicrobial peptides (AMPs) and Bomanins (Boms); many, however, remain uncharacterized. Here, we examine the role in innate immunity of two related peptides, Daisho1 and Daisho2 (formerly IM4 and IM14, respectively), found in hemolymph following Toll pathway activation. By generating a CRISPR/Cas9 knockout of both genes, Δ*daisho*, we find that the Daisho peptides are required for defense against a subset of filamentous fungi, including *Fusarium oxysporum*, but not other Toll-inducible pathogens, such as *Enterococcus faecalis* and *Candida glabrata*. Analysis of null alleles and transgenes revealed that the two *daisho* genes are each required for defense, although their functions partially overlap. Generating and assaying a genomic epitope-tagged Daisho2 construct, we detected interaction *in vitro* of Daisho2 peptide in hemolymph with the hyphae of *F. oxysporum*. Together, these results identify the Daisho peptides as a new class of innate immune effectors with humoral activity against a select set of filamentous fungi.

Keywords: innate immunity, toll, *Drosophila*, humoral, antifungal

OPEN ACCESS

Edited by:
Dan Hultmark,
Umeå University, Sweden

Reviewed by:
Ulrich Theopold,
Stockholm University, Sweden
Hai-peng Liu,
Xiamen University, China

****Correspondence:***
Steven A. Wasserman
stevenw@ucsd.edu

Specialty section:
This article was submitted to Comparative Immunology, a section of the journal Frontiers in Immunology

Received: *18 October 2019*
Accepted: *06 January 2020*
Published: *23 January 2020*

Citation:
Cohen LB, Lindsay SA, Xu Y, Lin SJH and Wasserman SA (2020) The Daisho Peptides Mediate Drosophila Defense Against a Subset of Filamentous Fungi. Front. Immunol. 11:9. doi: 10.3389/fimmu.2020.00009

INTRODUCTION

Fungal infections have a devastating impact on a wide range of organisms. They are destructive to agricultural plants around the world, including rice, wheat, and tomatoes (1). Additionally, fungi infect more than one million humans annually (2). Existing antifungal treatments are limited, with only one new class of drugs, echinocandins, developed in the past 15 years. Furthermore, extensive usage of limited classes of related antifungals has led to the increasingly frequent appearance of drug-resistant fungi (2). An enhanced understanding of naturally occurring antifungal defenses is thus of tremendous potential benefit.

The fruit fly *Drosophila melanogaster* is a robust model for fungal infections, replicating many features of murine fungal infections (3, 4). In the wild, flies have been found to be infected with a number of filamentous fungi, including *Beauveria*, *Metarhizium*, and *Fusarium* species (5, 6). In combatting these infections, flies rely on the Toll innate immune pathway (7, 8). Toll provides defense against not only filamentous fungi, but also yeasts and those Gram-positive bacteria that produce a cell wall containing Lys-type peptidoglycan (8–10). A second innate immune pathway,

defined by the Imd receptor, provides defense against Gram-negative bacteria and the limited number of Gram-positive bacteria that produce a cell wall containing DAP-type peptidoglycan (11, 12).

Systemic activation of Toll signaling induces a broad set of genes first identified by microarray analysis and mass spectroscopy (13–16). Many of the induced innate immune genes are transcribed in the fly fat body, with the protein products secreted into the hemolymph. These include antimicrobial peptides (AMPs), the Bomanin peptides, and a number of uncharacterized peptides.

Although AMPs, such as the antifungal peptide Drosomycin (Drs) directly kill pathogens *in vitro* (17, 18) and are immunoprotective when ectopically expressed *in vivo* (19), recent loss-of-function studies reveal little or no requirement for AMPs in defense against fungi and Gram-positive bacteria (20). In contrast, the Bomanin family of peptides (Boms) are required for defense against both classes of pathogens (21). Boms, which are *Drosophila*-specific, are readily detected in hemolymph following Toll activation. Here we describe the functional characterization of additional immune effectors, the Daisho peptides, which appear in hemolymph following systemic infection and are required for defense against a subset of filamentous fungi.

MATERIALS AND METHODS

Fly Husbandry and Strain Generation

Flies were raised at 25°C on cornmeal molasses agar media[1]. The w^{1118} strain was used as the wild type. $MyD88^{-}$ flies were $MyD88^{kra1}$, and imd^{-} flies were imd^{shadok}.

As described in Results, the genes for the immune induced peptides IM4 and IM14 have been given the designations *daisho1* and *daisho2*, respectively. The null allele Δ*daisho*, deleting both genes, as well as the individual gene deletions, Δ*dso1* and Δ*dso2*, were generated using CRISPR/Cas9 technology, applying methods described previously (22). Pairs of guide RNAs that targeted Cas9 to delete the region 2R: 20,868,460–20,870,480 for Δ*daisho)*, 2R: 20,868,783–20,869,392 for Δ*dso1*, and 2R: 20,870,332–20,870,728 for Δ*dso2* were cloned into the pU6-BbsI-chiRNA vector (Addgene plasmid # 45946). Homology arms of ∼1 kb were cloned into pHD-DsRed (Addgene plasmid # 51434). Cas9 was provided by plasmid pBS-Hsp70-Cas9 (Addgene plasmid #46294). Constructs were based on target sequences in the w^{1118} strain and injected into w^{1118}. See **Table S1** for primer sequences.

The FLAG epitope tag was cloned between the signal sequence and mature peptide of Dso2 in the context of the pHD-DsRed homologous repair template. This FLAG-Dso2 construct was introduced at the *dso2* genomic locus using the Δ*dso2* guide RNAs.

Plasmids expressing *dso1* or *dso2* transcripts from the *pBomS3* promoter were made using methods previously described (23). Briefly, the *BomS3* gene promoter was placed 5′ to the ORF encoding either Dso1 or Dso2. These constructs were then each integrated via ΦC31-mediated transgenesis at an *attP* landing site located at 86Fb on the *D. melanogaster* third chromosome (BDSC stock #24749). The transgenes were crossed into the Δ*dso1* and Δ*dso2* backgrounds and homozygous stocks were derived. An empty vector control was also introduced at the 86Fb *attP* landing site.

[1]http://blogs.cornell.edu/drosophila/dssc-cornmeal-recipe/

Microbial Cultures

For survival experiments, microbes were cultured as follows. *Enterococcus faecalis* NCTC 775 (ATCC 19433) and *Enterobacter cloacae* were grown overnight at 37°C in LB media and concentrated to an OD_{600} of 10 in 20% glycerol. *Candida glabrata CBS 138* [ATCC 2001] was grown overnight in YPD media at 37°C and concentrated to an OD_{600} of 100 in PBS, 0.1% Tween. All filamentous fungi were grown on malt extract agar plates at 29°C until sporulation was observed (10–15 days). Fungal material was then strained through glass wool with sterile water to collect spores, which were concentrated in 20% glycerol and stored at −80°C before being used at the following concentrations (in spores/ml): *Aspergillus flavus* (sequenced strain): 5×10^9; *A. fumigatus* AF293 (FGSC# A1100): 6×10^9; *A. parasiticus* Nor-1 mutant (NRRL #6111): 3×10^9; *Botrytis cinerea* (B05.10): 3×10^9; *Fusarium graminearum* (NRRL #5883): 8×10^8; *F. oxysporum* f. sp. *lycopersici* 4287 (FGSC #9935): 3×10^8; *F. verticillioides* (FGSC #7415): 3×10^9; *Neurospora crassa*: 1×10^9.

For the induction of the Toll response, heat-killed *Micrococcus luteus* was prepared as previously described (23).

Survival Assays

Groups of 20–25 adult male flies aged 2–7 days were collected and stabbed with a needle dipped in a suspension of bacteria, yeast, or fungal spores. Where needed, $MyD88^{-}$ or $Bom^{\Delta 55C}$ flies were used as controls immunodeficient for the Toll-mediated response. Flies infected with *E. faecalis* were incubated at 25°C; all other infected flies were incubated at 29°C. Fly deaths were recorded at least twice per day for the duration of each experiment. Any deaths that occurred within the first 6 h were set aside to exclude from the data any deaths due to traumatic injury. The experiment was repeated three times and results combined. Statistical analyses were performed using the Gehan-Breslow-Wilcoxon test.

MALDI-TOF

After Toll induction with heat-killed *M. luteus*, flies were incubated at 29°C for 24 h, after which hemolymph was collected via capillary as previously described (23). Hemolymph in 0.1% trifluoroacetic acid/50% acetonitrile was mixed 1:1 with Universal Matrix (Sigma-Aldrich). Samples were then dried onto a Bruker MSP 96 ground steel plate. Spectra were collected from 1,500 to 10,000 m/z for linear mode, and 1,000–5,000 m/z for reflectron mode, both with positive polarization. Peptide calibration standard II (Bruker) was used as an external calibration standard. For each genotype, at least five independent samples were collected. Representative spectra are shown. Peaks were identified via corresponding m/z values from previous studies (13, 16). Spectra were visualized using R 3.3.2 and ggplot2 2.2.1 (24, 25).

Quantitation of Pathogen Load

Pathogen load in infected flies was measured by qRT-PCR of fungal RNA (26, 27). Adult male flies, 2–7 days old, were stabbed with a needle dipped in *F. verticillioides* at 3×10^9 spores/ml. Flies were then incubated at 29°C. Groups of 5–6 flies were collected at the stated times and frozen in liquid nitrogen. Total RNA was isolated with TRIzol (Ambion) and cDNA was made via SuperScript RT II (Invitrogen). *EF1A* was selected as a proxy gene for fungal load based on its stable expression (28). Measurements by qRT-PCR were performed on the iQ5 cycler (BioRad) with iQ SYBR Green Supermix (BioRad) using the primers listed below. Values were normalized to fly mRNA based on expression of the *rp49* gene.

Primers: Fv_EF1A_F1: GGCTTTCACTGACTACCCTCC TCT, Fv_EF1A_R1: ACTTCTCGACGGCCTTGATGACAC, rp49_F1: CAAGGGTATCGACAACAG, rp49_R1: CTTGTT CGATCCGTAACC.

Peptide Gel Electrophoresis and Immunoblotting

Hemolymph samples were collected via the Zymo-Spin IC column method (23) from 30 male flies aged 2–7 days that had been induced with heat-killed *M. luteus* and incubated for 24 h at 29°C. Samples were run on a SDS-tricine, 18% separating/10% spacer/4% stacking, acrylamide gel[2]. Protein samples were then transferred to a PDVF membrane, blocked with 5% milk in TBST and stained with primary α-FLAG M2 (Sigma) (1:500) and secondary sheep α-mouse HRP (Amersham Biosciences) (1:1,000). The immunoblot was then treated with West Pico PLUS substrate (Thermo Scientific) and exposed to film.

Peptide Hyphal Binding and Immunofluorescence

The immunostaining protocol was adapted from Luo et al. (29). *F. oxysporum* was grown in 5 ml malt extract broth from a starting concentration of 2.9×10^5 spores/ml. After overnight shaking at room temperature, fungal hyphae were collected by centrifugation at 1,000 g for 10 min and resuspended in PBS. Hemolymph was collected via the Zymo-Spin IC column method (23) from 420 male flies that had been induced with heat-killed *M. luteus* 24 h prior and incubated at 29°C, yielding ∼35 µl cell-free hemolymph. Next, aliquots of 200 µl hyphae and 35 µl hemolymph were shaken at room temperature for 30 min. The samples were washed three times with PBS before fixation with 4% formaldehyde for 1 h. After washing another three times with PBS, samples were blocked for 1 h with 5% BSA. Samples were then incubated with α-FLAG antibody (1:200) overnight at 4°C. After washing with PBS, samples were stained for 2 h with donkey α-mouse Alexa555 (1:400) and DAPI (1:200) and then washed and mounted on slides. Samples were imaged with a Ti2 Widefield microscope (Nikon) and analyzed with the NIS-elements software and OMERO.

[2]https://molbio.mgh.harvard.edu/szostakweb/protocols/protein_page/index.html

RESULTS

Generation of Flies Null for the *daisho* Gene Pair

Pioneering mass spectrometry experiments by Bulet et al. identified two dozen peptide IMs (immune-induced molecules) that accumulate in *Drosophila* hemolymph upon induction of the innate immune response, principally the Toll pathway (13, 16). Among these, the Bomanins have been found to play an essential role against a broad range of pathogens (21, 23) while several, including the 15 aa long IM4 and 24 aa long IM14, have unknown functions. Based on our demonstration of defensive functions for these peptides, we have renamed them Daisho1 and Daisho2, for 大小 *daisho,* the Japanese term for a matched pair of samurai swords, one short and one long.

The Daisho peptides are closely related to one another and occupy adjacent positions in the genome, where they are divergently transcribed (**Figure S1**). As shown in **Figure 1A**, the sequence of amidated mature Daisho1 (Dso1) has 67% identity with the corresponding region of the mature Daisho2 (Dso2) peptide. Like the Bomanins, the *daisho* genes are widespread among the *Drosophila* genus, but not identified elsewhere. To investigate the potential role of the *daisho* genes in innate immunity, we used CRISPR/Cas9 technology to delete both genes. The 2.0 kb deleted region includes the entire *dso1* gene, the upstream region for both genes, and the first exon of *dso2* (including the start codon). Flies homozygous for the Δ*daisho1,2* deletion, hereafter Δ*daisho*, were viable and fertile.

With the Δ*daisho* stock in hand, we carried out MALDI-TOF studies of hemolymph (**Figures 1B–E**). As described above, following Toll activation wild-type hemolymph displays robust expression of immune peptides, including the Daisho peptides, Bomanins, and AMPs. The signals from Dso1 and Dso2 were ablated in Δ*daisho*, as evidenced by the loss of signal at 1,722 mass/charge (m/z) (Dso1) and 2,694 m/z (Dso2). Furthermore, the spectra of induced Δ*daisho* hemolymph was wild-type for all previously identified peaks other than Dso1 and Dso2, including the Bomanins and AMPs, Metchnikowin (Mtk), and Drosomycin (Drs). The absence of Dso1 and Dso2 thus did not detectably alter the accumulation or modification of other Toll-induced peptides in the hemolymph.

In addition to previously identified peaks, Δ*daisho* hemolymph contained one previously unseen signal. The 1,724 m/z signal of this peak, readily apparent in reflectron mode, is identical to that predicted for the BomS5 amidated peptide, previously known as CG15065 (**Figure 1E**). This signal had not been detected previously because in the wild type it lies in the shoulder of the robust Dso1(IM4) peak. Its existence in Toll-induced hemolymph was expected, however, on the basis of microarray and RNAseq data demonstrating strong Toll-activated induction of the *BomS5* locus (15, 30).

The *daisho* Genes Are Specifically Required for Defense Against *F. oxysporum*

We next turned to a functional assay to determine whether the absence of the Daisho peptides impaired survival following systemic infection. Because the Toll pathway responds to and

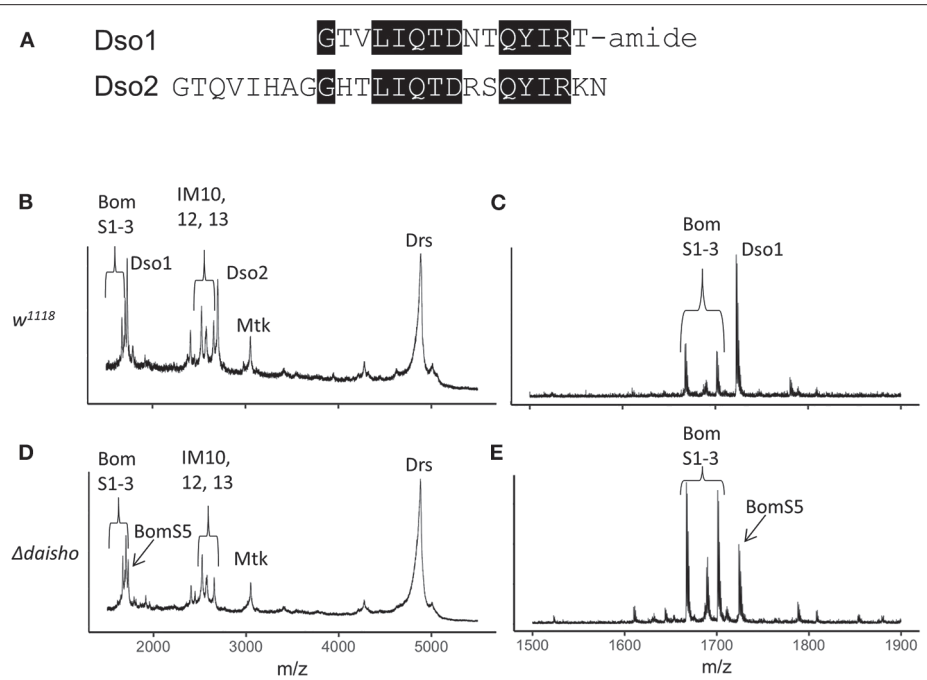

FIGURE 1 | Deletion of *Drosophila daisho1* and *daisho2* gene pair. **(A)** Alignment of mature Daisho1 and Daisho2 peptide sequences. Identical residues are highlighted. **(B–E)** Mass spectrometry analysis of Toll-induced hemolymph in linear **(B,C)** and reflectron **(D,E)** mode, illustrating loss of Daisho1 (Dso1, formerly IM4) and Daisho2 (Dso2, formerly IM14) signal in Δ*daisho* deletion mutant. The Dso1 signal overlaps with the BomS5 signal, which is readily apparent in the Δ*daisho* mutant analyzed in reflectron mode. Mtk, Metchnikowin; Drs, Drosomycin.

protects against infection by many Gram-positive bacteria and fungi, we focused on these classes of pathogens. We stabbed adult flies with a needle dipped in a suspension of bacteria, yeast, or fungal spores and then monitored survival. We used w^{1118} flies as our wild-type, i.e., immunocompetent, control and $Bom^{\Delta 55C}$ flies, which lack the 10-gene *Bom* cluster, as an immunodeficient control (21).

For a number of the pathogens tested, Δ*daisho* flies behaved identically to the wild type. Roughly 50% of both wild-type and Δ*daisho* flies survived 6 or more days following infection with the Gram-positive bacteria *Enterococcus faecalis*, whereas 100% of $Bom^{\Delta 55C}$ flies died within 2 days (**Figure 2A**). Likewise, wild-type and Δ*daisho* flies survived a week or longer after infection with the yeast *Candida glabrata*, whereas $Bom^{\Delta 55C}$ flies died in 4 days or fewer (**Figure 2B**). We also found no effect of Δ*daisho* on immune defenses mediated by the Imd pathway: wild-type, Δ*daisho*, and $Bom^{\Delta 55C}$ flies all survived infection with the Gram-negative bacteria *Enterobacter cloacae*, whereas, control *imd-* flies died within 1 day (**Figure 2C**).

For one pathogen in the initial test set, the filamentous fungus *Fusarium oxysporum*, deletion of the *daisho* genes had a marked effect on survival (**Figure 2D**): 50% of flies homozygous for Δ*daisho* died within 4 days of infection. In contrast, <70% of wild-type flies survived 7 or more days post-infection. Thus, loss of the Daisho peptides disrupts defense against *F. oxysporum*, but not other tested pathogens. Interestingly, loss of the Daisho peptides did not impact survival peptides did not impact survival as severely as did loss of the Boms, which led to 50% death after 2 days, very similar to complete loss of Toll signaling (21).

Δ*daisho* Flies Are Susceptible to Some but Not All Filamentous Fungi

We next investigated whether the susceptibility of Δ*daisho* flies to *F. oxysporum* reflected a general susceptibility to filamentous fungi. For these studies, we focused on filamentous fungi for which flies deficient for Toll signaling, and thus for induction of Daisho1, Daisho2, and other Toll effectors, exhibit a significantly decreased survival relative to wild type (**Figure 3**). The control fly strains in each case were w^{1118} (wild type) and *kra-1* ($MyD88^{-}$), a loss-of-function allele for an essential mediator of Toll signaling (31).

As shown in **Figure 3**, susceptibility of Δ*daisho* flies to the filamentous fungi species varied. Survival was significantly less than wild-type for *F. verticillioides* and *F. graminearum* (panels A, B), *two Fusarium* species closely related to *F. oxysporum*. In the case of *F. graminearum*, survival of Δ*daisho* flies was intermediate between that of wild-type and $MyD88^{-}$ flies, a pattern very similar to that observed with *F. oxysporum*, where Δ*daisho* survival falls between wild type and $Bom^{\Delta 55C}$, which behaves similarly to $MyD88^{-}$ (21). In contrast, Δ*daisho flies* displayed a much greater immune impairment upon infection with *F. verticillioides* than with *F. oxysporum*, dying to a comparable extent and at a similar rate as the $MyD88^{-}$ control (compare **Figures 2D**, **3A**).

Variation in survival was also observed among *Aspergillus* species. The survival curves of Δ*daisho* infected with either *A. parasiticus* or *A. flavus* largely tracked with $MyD88^{-}$ (panels C, D). Upon *A. fumigatus* infection, however, Δ*daisho* flies survived at least twice as long *as* $MyD88^{-}$ flies (**Figure 3E**).

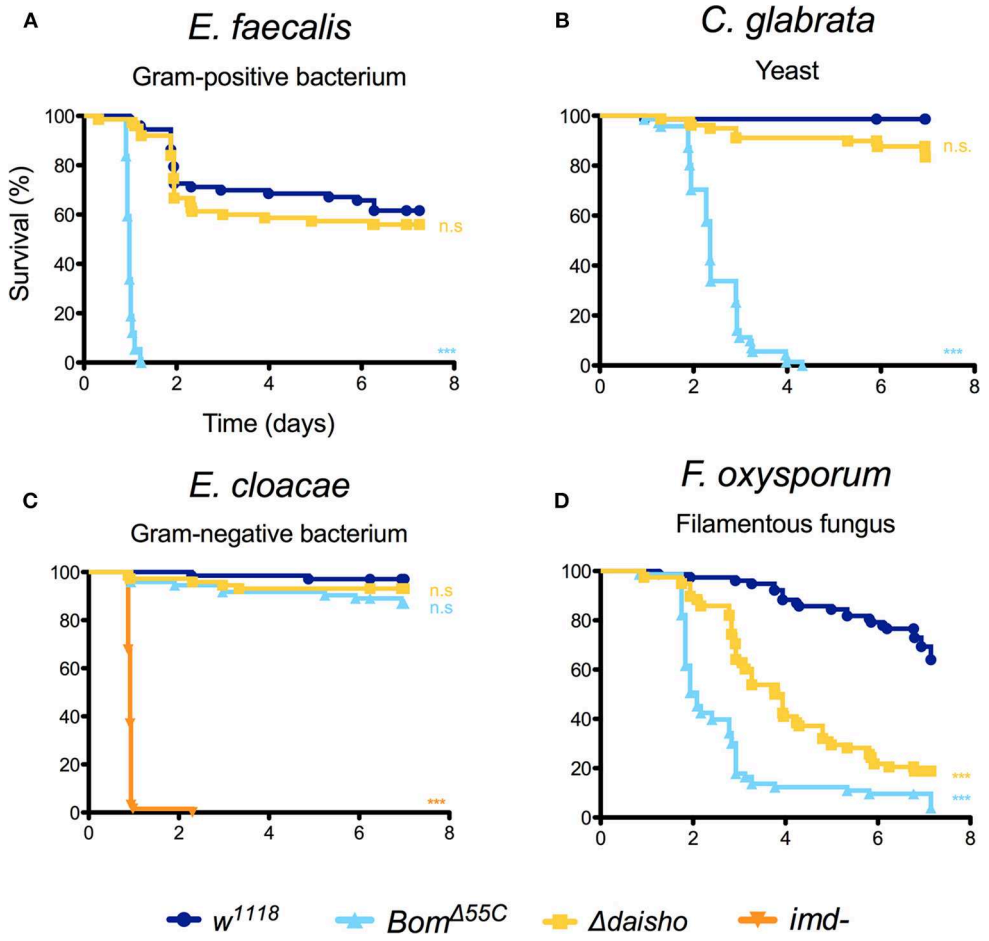

FIGURE 2 | Survival of Δ*daisho* against *E. faecalis* **(A)**, *C. glabrata* **(B)**, *E. cloacae* **(C)**, and *F. oxysporum* **(D)** infection. Shown is the combination of three independent experiments for each pathogen with 20-25 flies per genotype per experiment. Survival curves were compared using the Gehan-Breslow-Wilcoxon test. Significance is shown relative to w^{1118} (***$p < 0.0001$; n.s., not significant; $p > 0.01$).

For some filamentous fungi, loss of Daisho1 and Daisho2 did not affect survival. For example, 80% of wild-type and Δ*daisho* flies survived for at least 7 days after infection with *Botrytis cinerea*, whereas >50% of *MyD88*$^{-}$ flies died after 2 days (**Figure 3F**). Likewise, wild-type and Δ*daisho* flies survived *Neurospora crassa* infection for 6 days or more, but 50% of *MyD88*$^{-}$ flies died after 3 days (**Figure 3G**). Overall, we find that the Daisho peptides play a vital role in survival after infection with certain species of filamentous fungi, but are not important for infections with others.

daisho1 and *daisho2* Are Each Required for Defense

Daisho1 and Daisho2 are highly similar in sequence and expression pattern. Are they functionally redundant? To address this question, we explored the function of each individual locus. We again used CRISPR/Cas9, generating deletions that removed the entire coding sequence for either *daisho1* or *daisho2*. The 5' endpoints of each deletion were chosen to lie within 100 bp of the transcriptional start site, minimizing potential disruption of elements in the regulatory region separating the two genes (**Figure S1**). For both deletions, MALDI-TOF analysis of induced hemolymph confirmed loss of the deleted gene product but no other peptides, indicating that either Daisho1 or Daisho2 can be stably expressed in the absence of the other (**Figure 4**).

To test the effect on defense of deleting *dso1* or *dso2*, we stabbed adults with *F. verticillioides* spores, for which Δ*daisho* flies have a reduced survival. Deleting either the *dso1* or *dso2* gene resulted in susceptibility to *F. verticillioides* markedly different from wild-type and comparable to that of the double deletion (**Figure 5**). Thus, Daisho1 and Daisho2 each act in defense against *F. verticillioides* infection.

Since deletion of either *dso1* or *dso2* had as severe an effect on survival as the double mutant, it was possible that each gene has a specific and distinct function in antifungal defense. Alternatively, survival might depend only on total dosage for the two genes, with loss of either dropping expression below the threshold required. To distinguish between these models, we generated transgenes placing each ORF under control of *pBomS3,* shown previously to be strongly Toll-responsive promoter (23), and then

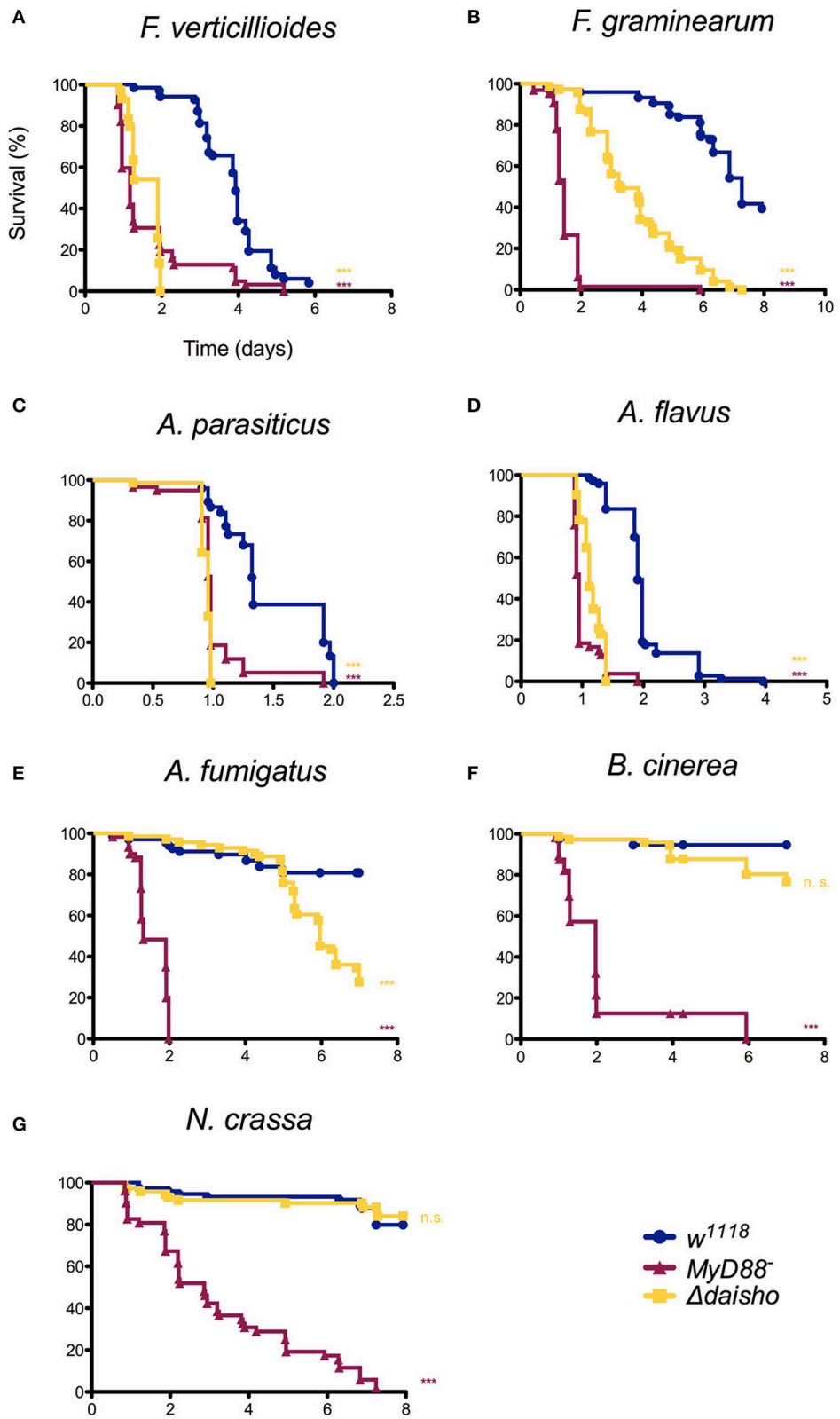

FIGURE 3 | Survival of Δ*daisho* against *F. verticillioides*, **(A)**, *F. graminearum* **(B)**, *A. parasiticus* **(C)**, *A. flavus* **(D)**, *A. fumigatus* **(E)**, *B. cinerea* **(F)**, and *N. crassa* **(G)**. The combination of three independent experiments for each pathogen with 20-25 flies per genotype per experiment is shown. Survival curves were compared using the Gehan-Breslow-Wilcoxon test. Significance is shown relative to w^{1118} (***$p > 0.0001$; n.s., not significant; $p > 0.01$).

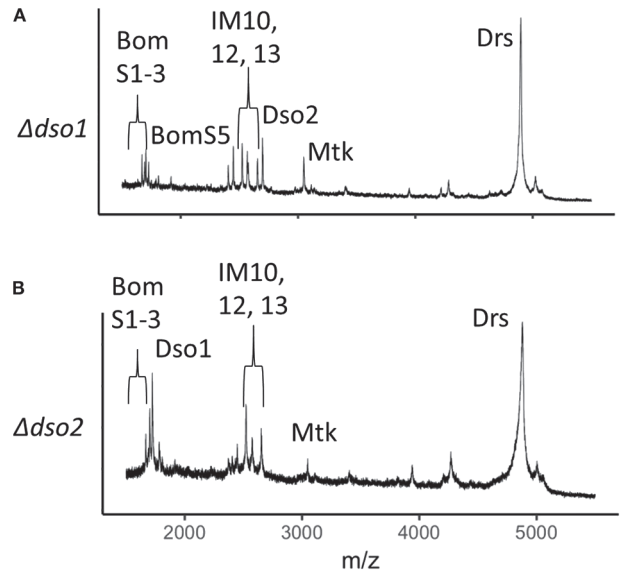

FIGURE 4 | MALDI-TOF spectra for Δ*dso1* and Δ*dso2* hemolymph. **(A,B)** Mass spectrometry analysis of Toll-induced hemolymph in linear mode, highlighting loss of Dso1 **(A)** and Dso2 **(B)** in deletion mutants.

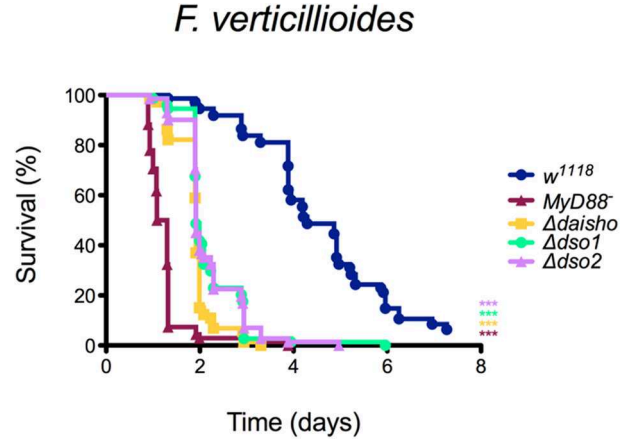

FIGURE 5 | Survival of Δ*dso1* and Δ*dso2* against *F. verticillioides*. Shown is the combination of three independent experiments with 20–25 flies per genotype per experiment. Survival curves were compared using the Gehan-Breslow-Wilcoxon test. Significance is shown relative to w^{1118} (***$p < 0.0001$).

assayed the transgenes for rescue of Δ*dso1* or Δ*dso2*. As shown in **Table 1**, *pBomS3*-driven *dso1* rescued Δ*dso1*, improving the median survival from 46 to 93 h ($p < 0.0001$). The same was true of *pBomS3*-driven *dso2* in the Δ*dso2* background ($p < 0.0001$) (see **Figure S2** for full survival curves). Flies expressing the empty vector construct at the same chromosomal location did not show any increase in survival (**Figure S3**).

Having confirmed the activity of the two constructs, we expressed each in a background deficient for the other. *dso2* expression significantly improved survival of Δ*dso1* flies,

TABLE 1 | Median survival in hours of *dso1* and *dso2* deletion mutations rescued by homotypic and heterotypic transgenes.

	No transgene	*pBomS3-dso1*	*pBomS3-dso2*
MyD88^{-}	29	n.a.	n.a.
Δ*daisho*	46	n.a.	n.a.
Δ*dso1*	46	93	78
Δ*dso2*	46	55	93
w^{1118}	103	n.a.	n.a.

Data derived from ***Figure S2****. n.a., not applicable.*

increasing median survival from 46 to 78 h ($p < 0.0001$). Similarly, *dso1* expressed in a Δ*dso2* background improved median survival from 46 to 55 h ($p = 0.0005$). Nevertheless, rescue was incomplete. The median survival of *dso2* expressed in Δ*dso1* background (78 h) did not reach median survival of Δ*dso1* rescued with *dso1* (93 h) (n.s., $p = 0.09$). Furthermore, *dso1* did not rescue survival of Δ*dso2* (55 h) to the same level as *dso2* (93 h) ($p < 0.0001$). The data thus indicate that the two loci encode functions that are neither fully distinct nor fully redundant.

Deleting *daisho1* and *daisho2* Results in an Elevated Pathogen Load in Infected Flies

To investigate whether Daisho1 and Daisho2 affect pathogen growth during infection, we measured fungal load after infection in Δ*daisho* and wild-type flies. After stabbing adult males with *F. verticillioides*, groups of 5–6 infected flies were collected and RNA was extracted. Fungal *EF1A* transcript levels were measured as a proxy for pathogen load and normalized to the fly reference gene *rp49*. Directly after infection (2 h), there was no significant difference between Δ*daisho* and wild-type flies by Mann-Whitney *U* test (**Figure S4**). By the next day, however, Δ*daisho* flies had a pathogen load roughly 10-fold greater than wild-type ($p = 0.0317$).

FLAG-Dso2 Binds to *F. oxysporum* Hyphae

We next tagged Dso2, the larger of the two peptides, with the FLAG epitope, using CRISPR/Cas9 to introduce the tag at the amino-terminus of the endogenously expressed mature peptide. Immunoblot analysis of induced hemolymph from FLAG-Dso2 flies revealed a single band detectable with α-FLAG antibody (**Figure 6A**). MALDI-TOF analysis of hemolymph confirmed the loss of the Dso2 peak at 2,694 m/z and the appearance of a peak with an m/z ratio of 3,689, the value expected for FLAG-Dso2 (**Figure 6B**).

Having confirmed that FLAG-Dso2 peptide is stably expressed, we next assayed its activity in providing antifungal defense. Specifically, flies homozygous for *FLAG-dso2* at the *dso2* locus were infected with *F. verticillioides* and their survival was compared to both wild-type flies and Δ*dso2* flies. Survival of FLAG-Dso2 flies was not wild-type, but was significantly better than that of flies lacking the *dso2* gene (**Figure S5**). We conclude that the FLAG-Dso2 peptide is active in providing defense against *F. verticillioides* infection.

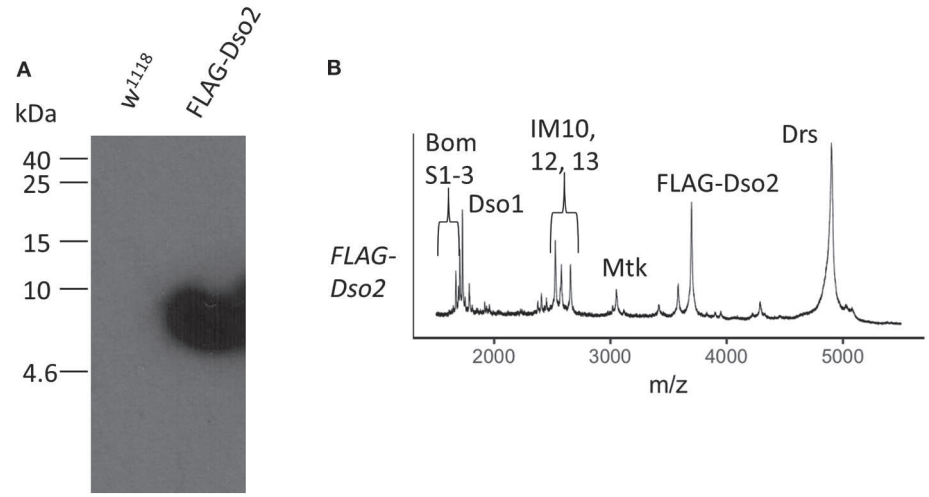

FIGURE 6 | Characterization of FLAG-Dso2 gene product. **(A)** Immunoblot stained with mouse α-FLAG M2 (1:500) and sheep α-mouse HRP (1:1,000). Two μl of Toll-induced hemolymph was loaded per lane. **(B)** MALDI-TOF analysis of FLAG-Dso2 Toll-induced hemolymph in linear mode.

Next, we assayed FLAG-tagged Dso2 peptide in hemolymph for its ability to bind fungus. We collected hemolymph from Toll induced flies, incubated it with hyphae from *F. oxysporum*, and fixed samples. The majority (>80%) of *F. oxysporum* hyphae had no visible signal when stained with α-FLAG antibody (**Figure 7A**). Among the remaining hyphae, we observed a variety of staining patterns, including, but not limited to, signals concentrated in the regions between nuclei (**Figure 7B**), extending across greater fractions of hyphae (**Figure 7C**) or spanning the length of hyphae (**Figure 7D**). In parallel experiments with untagged wild-type hemolymph, no signal was detected (**Figures 7E–H**). We conclude that Daisho2 peptide in hemolymph can bind to *F. oxysporum* hyphae.

In summary, our results demonstrate that the pair of immune-induced peptides, Daisho1 and Daisho2, mediate Toll-induced defense against specific filamentous fungi, most likely via a humoral effect on fungal hyphae.

DISCUSSION

Role of the Daisho Peptides in Antifungal Defense

In this study we found that the related peptides Daisho1 and Daisho2 are required in *D. melanogaster* for defense against a subset of filamentous fungi. We have also demonstrated that the two peptides have partially overlapping functions. Survival data reveal a dependence on the overall level of Dso1 and Dso2, with each peptide able to partially compensate for the absence of the other. Furthermore, each peptide accumulates in the absence of the other.

The Daisho peptides lack known motifs of defined function. As noted previously (21), there is a similarity in size and sequence between Dso1 and Dso2 and the Bomanin peptides. There are, however noteworthy differences, including the presence of a CxxC motif in the Bomanins and the broader requirement for the Bomanins in Toll-mediated defense.

Among those fungi for which deleting *dso1* and *dso2* decreases survival, Δ*daisho* flies nevertheless often exhibit significantly greater survival than do $MyD88^{-}$ or $Bom^{\Delta 55C}$ flies (see e.g., *F. oxysporum* and *F. graminearum*). Thus, in contrast to the Bom effectors, which are strictly required for Toll defenses against a broad range of pathogens, the Daisho peptides appear to be required for some, but not all Toll functions and to be active against only a select group of pathogens against which Toll mounts defense.

Like the Bomanins, *dso1* and *dso2* are found only within the *Drosophila* genus. Taxonomically-restricted genes (TRGs), while often studied only sparingly, represent 10–20% of most genomes and frequently have essential functions (32). TRGs have been identified in the immune pathways of many invertebrates, including flies, mosquitoes, and cnidarians. Within immune systems they are abundant among effectors, but rare among signal transduction factors (33, 34).

Specificity of *daisho* Genes in Antifungal Defense

In tracking survival following systemic infection, we find considerable variability with regard to which pathogens exhibit increased virulence toward *D. melanogaster* in the absence of both *daisho* genes. Categorizing the fungi against which the *daisho* genes provide defense, we detect no simple relationship to fungal phylogeny. For example, the *daisho* genes are required to defend against all the *Fusarium* species tested and some of the *Aspergillus* species, but not *Neurospora crassa*. Yet *Fusarium* and *Neurospora* are both members of the class Sordariomycetes, whereas *Aspergillus* is part of the less closely related Eurotiomycetes class (35, 36). Furthermore, Δ*daisho* flies exhibit differential susceptibility to fungi within a single genus: the Δ*daisho* deletion substantially decreases survival against *A.*

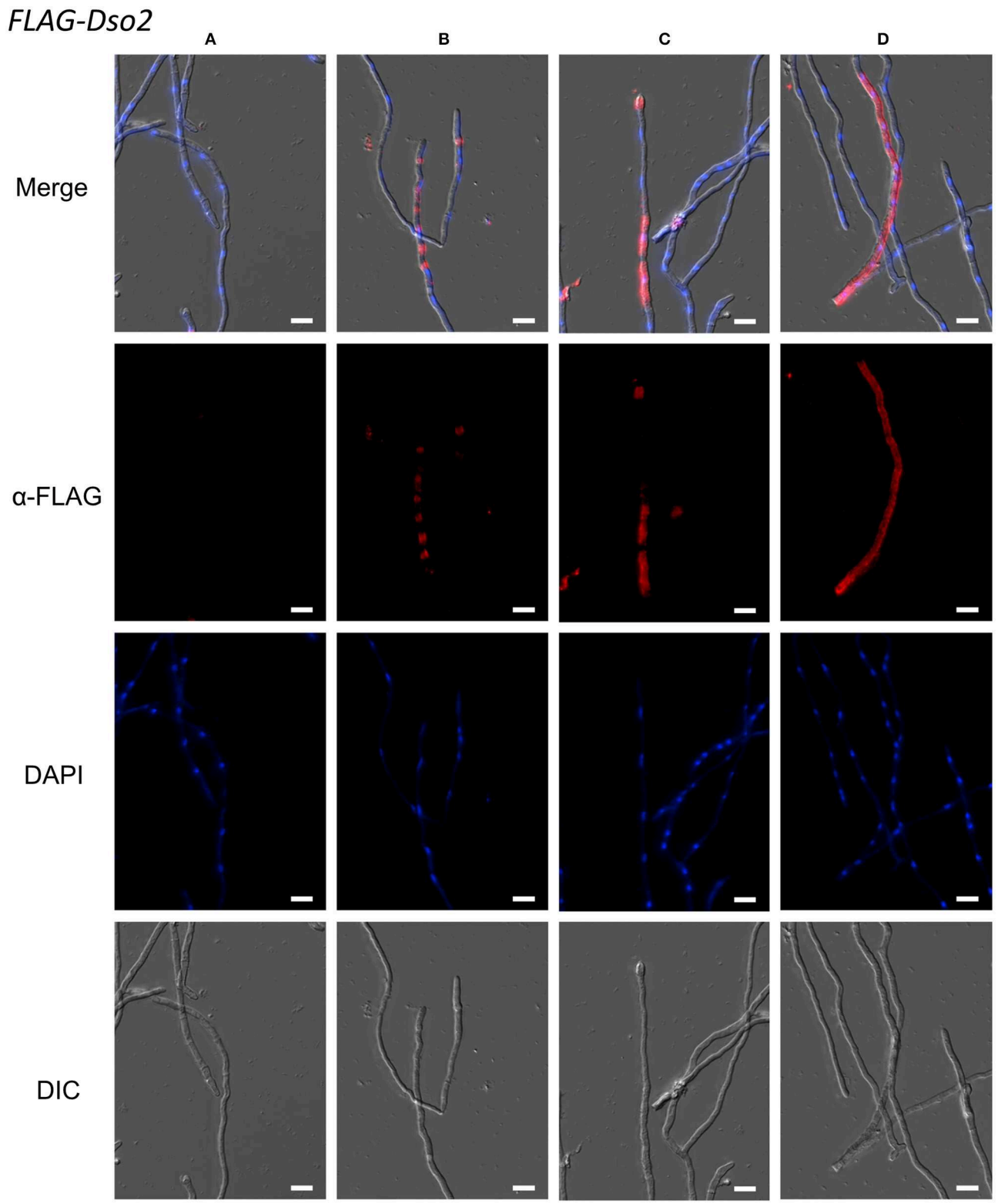

FIGURE 7 | Continued.

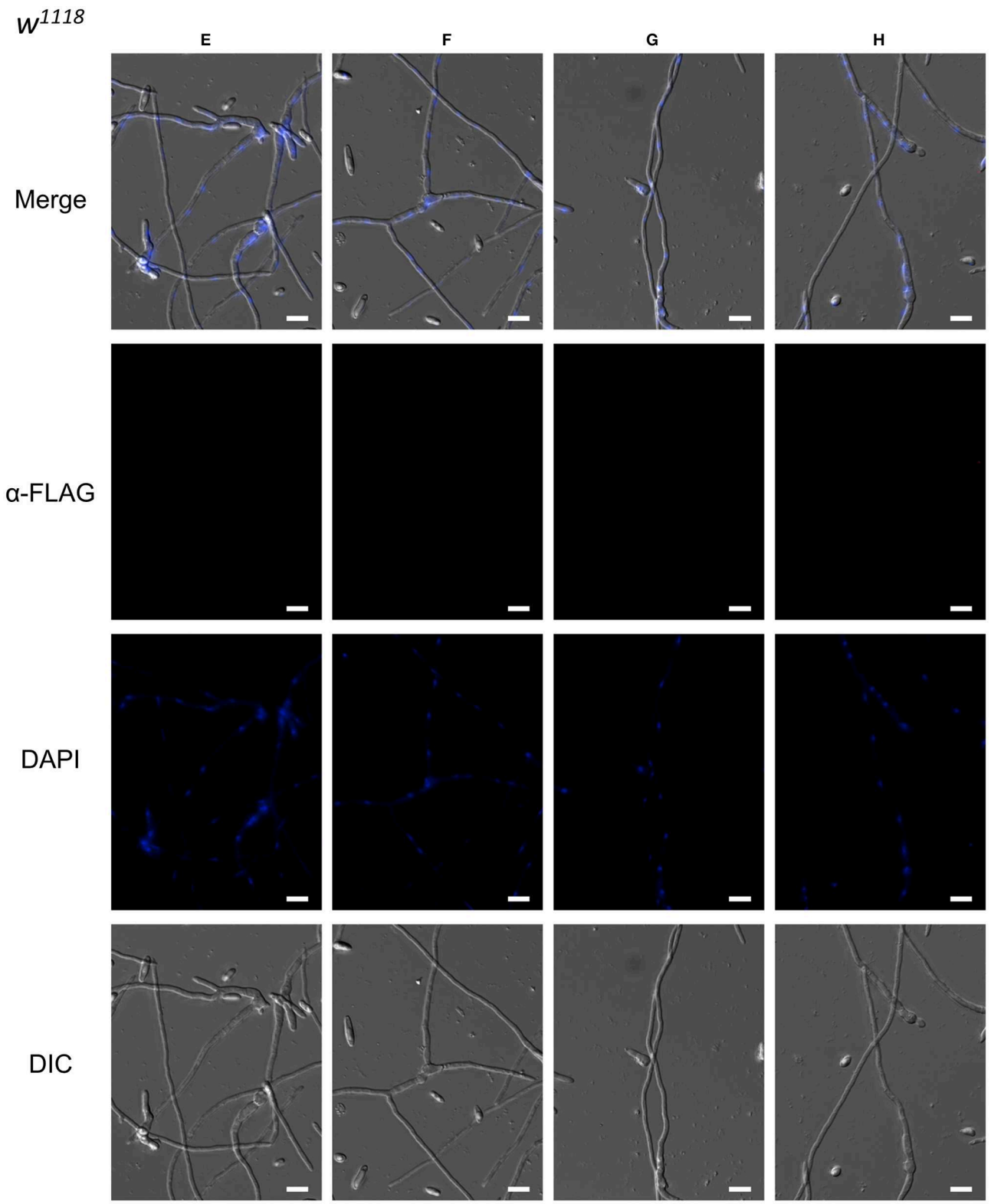

FIGURE 7 | Immunofluorescence staining of *F. oxysporum* hyphae. Images showing various staining patterns of hyphae incubated with *FLAG-Dso2* **(A–D)** or w^{1118} hemolymph **(E–H)** and then stained with mouse α-FLAG M2 (1:200) and donkey α-mouse Alexa 555 (1:400). DAPI marks fungal DNA. Scale bar is 10 μm. Images were generated as focused images from Z-stacks.

flavus and *A. parasiticus*, but has a much smaller effect on survival following *A. fumigatus* infection.

Although susceptibility of Δ*daisho* flies does not track simply with fungal phylogeny, susceptibility does appear to be closely related to fungal pathogenicity. Consider four filamentous fungi that are particularly pathogenic for wild-type flies: *F. verticillioides*, *F. graminearum*, *A. flavus*, and *A. parasiticus*. Infection with any of these four pathogens kills >50% of wild-type flies within 7 days. For each of these four, Δ*daisho* greatly decreases survival. By comparison, consider filamentous fungi with low pathogenicity, e.g., *A. fumigatus*, *N. crassa*, and *B. cinerea*. For each, >80% of wild-type and Δ*daisho* flies survive for 7 or more days post-infection. Note that we observe this association of susceptibility with pathogenicity only among filamentous fungi: for the strongly pathogenic Gram-positive bacterium *E. faecalis*, the Δ*daisho* deletion had no effect on survival.

Although the Bomanins are strictly required for Toll humoral defenses, we have found a correlation between pathogenicity and the level of Bomanin function required to confer resistance (21). It thus appears that for both Bomanins and the *daisho* genes, pathogenicity tracks with the strength of effector function required for defense.

Activity of Daisho Peptides

How do the Daisho peptides provide defense against filamentous fungi? One mechanism could be directly binding and killing the pathogens. Consistent with this idea, we find a modest but significant increase in pathogen load in Δ*daisho* flies. In addition, our immunofluorescence data demonstrate that Daisho2 can interact *in vitro* with at least one filamentous fungus that it targets. Antifungal peptides, such as mammalian LL-37 and plant defensin NaD1, also bind hyphae of fungal pathogens against which they are active (29, 37). The Daisho2 peptide's ability to bind fungal hyphae could indicate an antimicrobial function. Given that our assay was carried out with crude hemolymph, we cannot state whether the observed interaction of Daisho2 with hyphae is direct or is mediated by one or more unidentified hemolymph components.

The Daisho peptides might themselves interfere with pathogen growth, survival, or proliferation, or they might enable the fungicidal activity of other factors. The same is true of the Bomanins, which are required for hemolymph mediated killing of *C. glabrata*, but for which fungicidal activity of synthetic peptides has not been observed (23). Given that *daisho* genes are required for defense against only a subset of Toll and Bomanin targets, the function of Daisho1 and Daisho2 may be to meet a specific challenge posed by certain fungi to the entry or activity of antimicrobial factors. Further investigation of the Daisho peptides, as well as other hemolymph immune effectors, is likely to be informative in this regard.

DATA AVAILABILITY STATEMENT

All datasets generated for this study are included in the article/**Supplementary Material**.

AUTHOR CONTRIBUTIONS

LC and SW conceived the project and wrote the paper. LC, SAL, YX, and SJHL performed and analyzed the experiments.

FUNDING

This work was supported by National Institutes of Health (NIH) grant R01 GM050545 (to SW).

ACKNOWLEDGMENTS

We thank Bo Zhou, Beatriz Pinatti, and André Soares for the generation of the pU6-chiRNA constructs. We would also like to thank Philipp Weckwerth and Alisa Huffaker for the generous gift of *F. graminearum*, *F. verticillioides*, *A. flavus*, *A. parasiticus*, and *B. cinerea*. We thank Andrés Mauricio Caraballo Rodríguez and the Dorrestein lab for access to and assistance with MALDI-TOF. We also thank the McGinnis, Gantz, Posakony, and Bier labs for access to equipment. We thank Anita Hermann for help with immunofluorescence and imaging and Eric Griffis and Daphne Bindels from the Nikon Imaging Center at UC San Diego for microscopy expertise. We thank Matt Daugherty, Bill McGinnis, and Kirthi Reddy for thoughtful reading of the manuscript and helpful comments.

SUPPLEMENTARY MATERIAL

The Supplementary Material for this article can be found online at: https://www.frontiersin.org/articles/10.3389/fimmu.2020.00009/full#supplementary-material

REFERENCES

1. Dean R, Van Kan JAL, Pretorius ZA, Hammond-Kosack KE, Di Pietro A, Spanu PD, et al. The Top 10 fungal pathogens in molecular plant pathology. *Mol Plant Pathol.* (2012) 13:414–30. doi: 10.1111/j.1364-3703.2012.2011.00783.x
2. Janbon G, Quintin J, Lanternier F, d'Enfert C. Studying fungal pathogens of humans and fungal infections: fungal diversity and diversity of approaches. *Genes Immun.* (2019) 20:403–14. doi: 10.1038/s41435-019-0071-2
3. Brunke S, Quintin J, Kasper L, Jacobsen ID, Richter ME, Hiller E, et al. Of mice, flies–and men? Comparing fungal infection models for large-scale screening efforts. *Dis Model Mech.* (2015) 8:473–86. doi: 10.1242/dmm.019901
4. Dionne MS, Schneider DS. Models of infectious diseases in the fruit fly Drosophila melanogaster. *Dis Model Mech.* (2008) 1:43–9. doi: 10.1242/dmm.000307
5. Sharma L, Marques G. Fusarium, an entomopathogen—a myth or reality? *Pathogens.* (2018) 7:E93. doi: 10.3390/pathogens7040093

6. Cuthbertson AGS, Audsley N. Further screening of entomopathogenic fungi and nematodes as control agents for drosophila suzukii. *Insects*. (2016) 7:E24. doi: 10.3390/insects7020024
7. Imler JL. Overview of drosophila immunity: a historical perspective. *Dev Comp Immunol*. (2014) 42:3–15. doi: 10.1016/j.dci.2013.08.018
8. Valanne S, Wang JH, Rämet M. The Drosophila toll signaling pathway. *J Immunol*. (2011) 186:649–56. doi: 10.4049/jimmunol.1002302
9. Lemaitre B, Hoffmann J. The host defense of Drosophila melanogaster. *Annu Rev Immunol*. (2007) 25:697–743. doi: 10.1146/annurev.immunol.25.022106.141615
10. Lindsay SA, Wasserman SA. Conventional and non-conventional Drosophila Toll signaling. *Dev Comp Immunol*. (2014) 42:16–24. doi: 10.1016/j.dci.2013.04.011
11. Georgel P, Naitza S, Kappler C, Ferrandon D, Zachary D, Swimmer C, et al. Drosophila immune deficiency (IMD) is a death domain protein that activates antibacterial defense and can promote apoptosis. *Dev Cell*. (2001) 1:503–14. doi: 10.1016/S1534-5807(01)00059-4
12. Buchon N, Silverman N, Cherry S. Immunity in Drosophila melanogaster–from microbial recognition to whole-organism physiology. *Nat Rev Immunol*. (2014) 14:796–810. doi: 10.1038/nri3763
13. Uttenweiler-Joseph S, Moniatte M, Lagueux M, Van Dorsselaer A, Hoffmann JA, Bulet P. Differential display of peptides induced during the immune response of Drosophila: a matrix-assisted laser desorption ionization time-of-flight mass spectrometry study. *Proc Natl Acad Sci USA*. (1998) 95:11342–7. doi: 10.1073/pnas.95.19.11342
14. De Gregorio E, Spellman PT, Rubin GM, Lemaitre B. Genome-wide analysis of the Drosophila immune response by using oligonucleotide microarrays. *Proc Natl Acad Sci USA*. (2001) 98:12590–5. doi: 10.1073/pnas.221458698
15. De Gregorio E, Spellman PT, Tzou P, Rubin GM, Lemaitre B. The Toll and Imd pathways are the major regulators of the immune response in Drosophila. *EMBO J*. (2002) 21:2568–79. doi: 10.1093/emboj/21.11.2568
16. Levy F, Rabel D, Charlet M, Bulet P, Hoffmann JA, Ehret-Sabatier L. Peptidomic and proteomic analyses of the systemic immune response of Drosophila. *Biochimie*. (2004) 86:607–16. doi: 10.1016/j.biochi.2004.07.007
17. Levashina EA, Ohresser S, Bulet P, Reichhart J, Hetru C, Hoffmann JA. Metchnikowin, a novel immune-inducible proline-rich peptide from Drosophila with antibacterial and antifungal properties. *Eur J Biochem*. (1995) 233:694–700. doi: 10.1111/j.1432-1033.1995.694_2.x
18. Fehlbaum P, Bulet P, Michaut L, Lagueux M, Broekaert WF, Hetru C, et al. Insect immunity: Septic injury of drosophila induces the synthesis of a potent antifungal peptide with sequence homology to plant antifungal peptides. *J Biol Chem*. (1994) 269:33159–63.
19. Tzou P, Reichhart JM, Lemaitre B. Constitutive expression of a single antimicrobial peptide can restore wild-type resistance to infection in immunodeficient Drosophila mutants. *Proc Natl Acad Sci USA*. (2002) 99:2152–7. doi: 10.1073/pnas.042411999
20. Hanson MA, Dostálová A, Ceroni C, Poidevin M, Kondo S, Lemaitre B. Synergy and remarkable specificity of antimicrobial peptides *in vivo* using a systematic knockout approach. *Elife*. (2019) 8:e44341. doi: 10.7554/eLife.44341
21. Clemmons AW, Lindsay SA, Wasserman SA. An effector peptide family required for Drosophila Toll-mediated immunity. *PLoS Pathog*. (2015) 11:e1004876. doi: 10.1371/journal.ppat.1004876
22. Gratz SJ, Ukken FP, Rubinstein CD, Thiede G, Donohue LK, Cummings AM, et al. Highly specific and efficient CRISPR/Cas9-catalyzed homology-directed repair in Drosophila. *Genetics*. (2014) 196:961–71. doi: 10.1534/genetics.113.160713
23. Lindsay SA, Lin SJH, Wasserman SA. Short-Form bomanins mediate humoral immunity in Drosophila. *J Innate Immun*. (2018) 10:306–14. doi: 10.1159/000489831
24. Core Team. *R: A Language and Environment for Statistical Computing*. Vienna: R Foundation for Statistical Computing (2016).
25. Wickham H. *ggplot2: Elegant Graphics for Data Analysis*. (2016).
26. Troha K, Buchon N. Methods for the study of innate immunity in Drosophila melanogaster. *Wiley Interdiscip Rev Dev Biol*. (2019) 8:e344. doi: 10.1002/wdev.344
27. Dostálová A, Rommelaere S, Poidevin M, Lemaitre B. Thioester-containing proteins regulate the Toll pathway and play a role in Drosophila defence against microbial pathogens and parasitoid wasps. *BMC Biol*. (2017) 15:79. doi: 10.1186/s12915-017-0408-0
28. Kim HK, Yun SH. Evaluation of potential reference genes for quantitative RTPCR analysis in *Fusarium graminearum* under different culture conditions. *Plant Pathol J*. (2011). Available online at: https://peerj.com/preprints/27537.pdf (accessed August 8, 2019).
29. Luo XL, Li JX, Huang HR, Duan JL, Dai RX, Tao RJ, et al. LL37 inhibits aspergillus fumigatus infection via directly binding to the fungus and preventing excessive inflammation. *Front Immunol*. (2019) 10:283. doi: 10.3389/fimmu.2019.00283
30. Valanne S, Salminen TS, Järvelä-Stölting M, Vesala L, Rämet M. Immune-inducible non-coding RNA molecule lincRNA-IBIN connects immunity and metabolism in Drosophila melanogaster. *PLoS Pathog*. (2019) 15:e1007504. doi: 10.1371/journal.ppat.1007504
31. Tauszig-Delamasure S, Bilak H, Capovilla M, Hoffmann JA, Imler JL. Drosophila MyD88 is required for the response to fungal and Gram-positive bacterial infections. *Nat Immunol*. (2002) 3:91–7. doi: 10.1038/ni747
32. Khalturin K, Hemmrich G, Fraune S, Augustin R, Bosch TCG. More than just orphans: are taxonomically-restricted genes important in evolution? *Trends Genet*. (2009) 25:404–13. doi: 10.1016/j.tig.2009.07.006
33. Waterhouse RM, Kriventseva EV, Meister S, Xi Z, Alvarez KS, Bartholomay LC, et al. Evolutionary dynamics of immune-related genes and pathways in disease-vector mosquitoes. *Science*. (2007) 316:1738–43. doi: 10.1126/science.1139862
34. Sackton TB, Lazzaro BP, Schlenke TA, Evans JD, Hultmark D, Clark AG. Dynamic evolution of the innate immune system in Drosophila. *Nat Genet*. (2007) 39:1461–8. doi: 10.1038/ng.2007.60
35. Zhang N, Castlebury LA, Miller AN, Huhndorf SM, Schoch CL, Seifert KA, et al. An overview of the systematics of the Sordariomycetes based on a four-gene phylogeny. *Mycologia*. (2006) 98:1076–87. doi: 10.3852/mycologia.98.6.1076
36. Schoch CL, Sung GH, López-Giráldez F, Townsend JP, Miadlikowska J, Hofstetter V, et al. The ascomycota tree of life: a phylum-wide phylogeny clarifies the origin and evolution of fundamental reproductive and ecological traits. *Syst Biol*. (2009) 58:224–39. doi: 10.1093/sysbio/syp020
37. van der Weerden NL, Lay FT, Anderson MA. The plant defensin, NaD1, enters the cytoplasm of Fusarium oxysporum hyphae. *J Biol Chem*. (2008) 283:14445–52. doi: 10.1074/jbc.M709867200

Conflict of Interest: The authors declare that the research was conducted in the absence of any commercial or financial relationships that could be construed as a potential conflict of interest.

frontiers in Immunology

REVIEW
published: 24 January 2020
doi: 10.3389/fimmu.2019.03128

Host-Microbe-Pathogen Interactions: A Review of *Vibrio cholerae* Pathogenesis in *Drosophila*

*Saeideh Davoodi and Edan Foley**

Department of Medical Microbiology and Immunology, Faculty of Medicine and Dentistry, University of Alberta, Edmonton, AB, Canada

Most animals maintain mutually beneficial symbiotic relationships with their intestinal microbiota. Resident microbes in the gastrointestinal tract breakdown indigestible food, provide essential nutrients, and, act as a barrier against invading microbes, such as the enteric pathogen *Vibrio cholerae*. Over the last decades, our knowledge of *V. cholerae* pathogenesis, colonization, and transmission has increased tremendously. A number of animal models have been used to study how *V. cholerae* interacts with host-derived resources to support gastrointestinal colonization. Here, we review studies on host-microbe interactions and how infection with *V. cholerae* disrupts these interactions, with a focus on contributions from the *Drosophila melanogaster* model. We will discuss studies that highlight the connections between symbiont, host, and *V. cholerae* metabolism; crosstalk between *V. cholerae* and host microbes; and the impact of the host immune system on the lethality of *V. cholerae* infection. These studies suggest that *V. cholerae* modulates host immune-metabolic responses in the fly and improves *Vibrio* fitness through competition with intestinal microbes.

Keywords: IMD, *Drosophila melanogaster*, proliferation, *Vibrio cholerae*, insulin, microbiome, metabolism, T6SS

OPEN ACCESS

Edited by:
Susanna Valanne, Tampere University, Finland

Reviewed by:
Shoichiro Kurata, Tohoku University, Japan
Ioannis Eleftherianos, George Washington University, United States
Bruno Lemaitre, École Polytechnique Fédérale de Lausanne, Switzerland

****Correspondence:***
Edan Foley
efoley@ualberta.ca

Specialty section:
This article was submitted to Comparative Immunology, a section of the journal Frontiers in Immunology

Received: *31 October 2019*
Accepted: *23 December 2019*
Published: *24 January 2020*

Citation:
Davoodi S and Foley E (2020) Host-Microbe-Pathogen Interactions: A Review of Vibrio cholerae Pathogenesis in Drosophila. Front. Immunol. 10:3128. doi: 10.3389/fimmu.2019.03128

INTRODUCTION

Background

A complex set of interactions among host intestinal cells, and gut-resident microbes, impacts the viability of all participants. For example, commensal microbes consume intestinal nutrients, and generate metabolites that influence development, growth, metabolism, and immune system function in the host (1–8). Introduction of microbes with pathogenic potential to the gut lumen, or rearrangements to the composition or distribution of gut microbial communities, can have substantial impacts on intestinal homeostasis for the host (9). In particular, shifts in niche occupancy by gut bacteria, or alterations to metabolic outputs from the gut microbiome, can result in the development of severe intestinal disease (10–13). For example, *Bacteroides thetaiotaomicron*, a common human commensal, cleaves host glycans to produce fucose, a sugar that modulates the virulence of enterohemorrhagic *Escherichia coli* (14). Despite the importance of regulated molecular exchanges among host and microbial cells for host fitness and microbial function, our knowledge of pathogen-commensal interactions in the context of immune-metabolic regulation and intestinal disease is still quite limited. To fully understand such complex, multipartite interactions, it is essential that we deploy all relevant experimental systems at our disposal.

Drosophila melanogaster is a valuable experimental tool for studying host-microbe interactions. Lab-raised strains of *Drosophila* associate with a limited number of bacterial taxa (15–17),

dominated by easily cultivated *Acetobacter* and *Lactobacillus* strains that are accessible to genetic manipulation, and deployment in large-scale screens. Researchers have access to simple protocols for the establishment of flies with a defined intestinal microbiome (18, 19), and there is an abundance of publicly available lines for the genetic manipulation of fly intestinal function. Combined, these advantages allowed researchers to make substantial breakthroughs in understanding how flies interact with intestinal bacteria (20). Importantly, given the extent to which genetic regulators of intestinal homeostasis are conserved between vertebrates and invertebrates (20, 21), discoveries made with the fly have the potential to illuminate foundational aspects of host-microbe interactions. However, there are several key differences to note between flies and vertebrates that partially limit the utility of the fly model. Specifically, flies lack lymphocyte-based adaptive defenses, and the fly microbiome is considerably different to that reported in vertebrates.

Antimicrobial Defenses in the Fly Intestine

Drosophila integrate physical, chemical, proliferative, and antibacterial strategies to neutralize intestinal microbes, and prevent systemic infection of the host (**Figure 1**) (22, 23). The chitinous peritrophic matrix lines the midgut, and presents a physical barrier against bacterial invasion (24), similar to the mucus lining of the vertebrate intestinal tract. The germline-encoded immune deficiency (IMD) antibacterial defense pathway, a signaling pathway similar to the mammalian Tumor Necrosis Factor pathway (25), detects bacterial diaminopimelic acid-type peptidoglycan, and acts through the NF-κB transcription factor family member, Relish, to induce expression of antimicrobial peptides (26–29). At the same time, Dual Oxidase (Duox) and NADPH Oxidase (Nox) protect the host from gut bacteria through the generation of bactericidal reactive oxygen species (30, 31). Evolutionarily conserved growth regulatory pathways respond to damage of epithelial cells by promoting a compensatory growth and differentiation of intestinal stem cells (ISCs) in infected flies (32–35). This adaptive repair mechanism maintains the epithelial barrier, and prevents systemic infection of the host. Combined, these antibacterial defenses protect the host from infection, and maintain beneficial relationships between the fly and their gut microbiome.

The *Drosophila* Microbiome

The fly microbiome is transmitted horizontally through the deposition of bacteria on the outer surface of freshly laid embryos, and is maintained through the ingestion of food contaminated with bacteria (36). Gut bacteria regulate *Drosophila* intestinal homeostasis by affecting metabolism, growth, and immunity in the host. Interactions between the host and gut microbiota have been extensively covered in several recent reviews (20, 37–39), and will not be discussed in detail here. In brief, detailed studies have uncovered roles for symbiotic *Lactobacillus* and *Acetobacter* species in the control of fly metabolism and growth (40–42). For example, a dehydrogenase activity in *Acetobacter pomorum*, produces acetic acid that regulates insulin signaling, carbohydrate, and lipid levels in the host (40). In addition to the effects of individual symbionts on nutrient allocations in the host, interactions among bacterial communities have significant effects on host metabolism, growth, and physiology (43–47). *Vibrio cholerae* (*V. cholerae*) has emerged as a particularly useful tool to study interactions between the host, the intestinal microbiota, and an enteric pathogen. A pioneering study in 2005 established that flies are susceptible to oral infection with *V. cholerae*, dying within a few day from a diarrheal disease with symptoms similar to cholera in humans (48). The genetic tractability of the fly and *V. cholerae* established this system as a very attractive model to identify key host and microbial determinants of pathogenesis. In the following years, a number of studies uncovered complex roles for metabolism, host immunity, epithelial growth, and microbial antagonism in the outcome of *V. cholerae* pathogenesis in the fly. In this review, we will discuss key findings from these studies, and outline what they tell us about host-microbe interactions in general, and *V. cholerae*-mediated pathogenesis in particular.

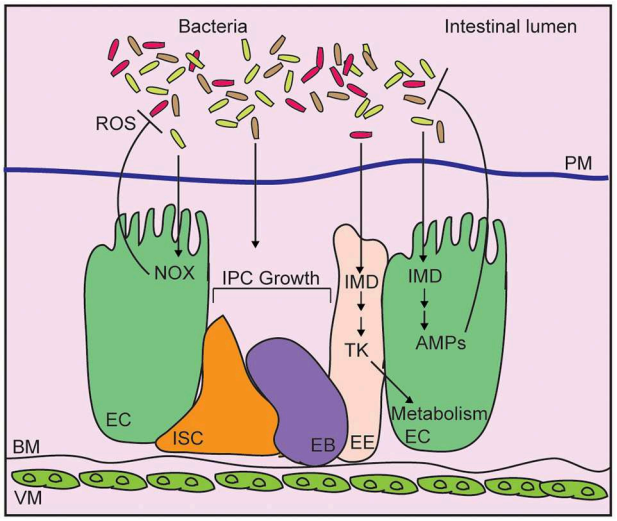

FIGURE 1 | Schematic representation of the adult *Drosophila* midgut. Intestinal bacteria are contained within the lumen by a chitinous peritrophic matrix (PM). Bacteria diaminopimelic acid-type peptidoglycan activates the immune deficiency (IMD) pathway in enterocytes (EC), leading to production of antimicrobial peptides (AMP). In enteroendocrine cells (EE), IMD controls expression of the metabolism-regulatory hormone Tachykinin (Tk). Epithelial reactive oxygen species (ROS) generated by NADPH oxidases (NOX) also contribute to bacterial killing while cues from the bacterial microbiome promote the growth of intestinal progenitor cells (IPC), composes of intestinal stem cells (ISC), and enteroblasts (EB).

Vibrio cholerae: Pandemics and Pathogenicity

Vibrio cholerae is a curved, Gram-negative member of the *Vibrionaceae* family of Proteobacteria (49). It inhabits aquatic environments, and copepods and chironomids are reported as natural reservoirs in marine ecosystems (50, 51). Intestinal colonization by *V. cholerae* causes the diarrheal disease, cholera, and is considered a substantial public health threat, especially in countries with poor sanitation and contaminated water (52).

The first cholera pandemic emerged in 1817, with an expansion of cholera beyond the Indian subcontinent (53). Since then, the world has witnessed an additional six pandemics, with the seventh pandemic ongoing (54). Models that estimate cholera burden predict ∼3 million cases of disease per year, resulting in roughly 100,000 deaths (55).

Vibrio cholerae strains are divided into classical and non-classical serotypes, with classical ones expressing the O1 antigen on their surface (56, 57). Classical serotypes are further subdivided into two biotypes—classical and El Tor—that differ in the expression of a number of markers, such as hemolysins (58–61). The outbreak of epidemic cholera that spread through southeast Asia in 1992 is caused by the non-classical strain of *V. cholerae* 0139 (62), whereas the ongoing pandemic that originated in Indonesia in 1961 is caused by the El Tor biotype (63). El Tor causes a milder cholera disease (64), with infected individuals frequently remaining asymptomatic early in infection (65).

Vibrio cholerae encodes several virulence factors that regulate survival, colonization, and pathogenicity (66–69). Cholera toxin (CT) is a hexameric adenosine diphosphate-ribosyl transferase that contains one A subunit surrounded by five B subunits (70, 71). Upon release into the intestinal lumen via a type two secretion system (72), the B pentamer of CT interacts with host GM1 ganglosides (73), permitting toxin endocytosis, and a subsequent cytosolic release of the A1 subunit (74). A1 ADP-ribosylates the Gs alpha subunit, locking $G\alpha_s$ in an active state (75). Active $G\alpha_s$ elevates adenylate cyclase activity, greatly increasing levels of 3′,5′-cyclic AMP, resulting in excess protein kinase A (PKA) activity (76). PKA stimulates an efflux of chloride ions through the cystic fibrosis transmembrane conductance regulator channel (77), leading to an uncontrolled flow of water, sodium and potassium ions into the intestinal lumen. This extreme, and rapid, dehydration results in the voluminous rice-water diarrhea that hallmarks cholera disease (78). In addition to CT, *V. cholerae* require the toxin co-regulated pilus virulence factor for pathogenesis (79). Toxin co-regulated pilus is a type IV pilus system that mediates colonization of the small intestine by a self-associate mechanism that supports the formation of bacterial microcolonies (80). Toxin co-regulated pilus also serves as the receptor for the CTXφ bacteriophage. CTXφ encodes *ctxAB*, and converts benign *V. cholerae* to pathogenic strains. The ability to synthesize toxin co-regulated pilus is advantageous for *V. cholerae* in aquatic environments, as it improves *V. cholerae* fitness by facilitating inter-bacterial interactions during colonization of host chitinaceous surfaces (81).

Although fluid replacement through oral rehydration solutions, antibiotic therapy, and vaccines are effective treatment options for patients with cholera, increased rates of antibiotic resistance among classical (82) and non-classical (83) strain of *V. cholerae* complicate treatment of the disease. Therefore, new antibacterial strategies that effectively target *V. cholerae* virulence factors are critical to contain this deadly disease. Over the last century, a variety of animal models that include rabbits, mice, fish, and flies, have been used to study *Vibrio*-host interactions and each of these models have added to our understanding of virulence, host responses to infection, interactions between *Vibrio* and host microbes, and cholera vaccine development.

The Rabbit Model

The first animal model to study *V. cholerae* dates back to 1884 when Nicati and Rietschin inoculated *V. cholerae* into the duodenum of guinea pigs, resulting in cholera-like symptoms (84). Since then, both infant and adult rabbit models of cholera have been widely used by researchers (85–87). As adult rabbits are resistant to oral infection with *V. cholerae*, the pathogen is typically introduced to the animal by ligated ileal loop surgery. In this technique, the small intestine of the rabbit is sealed at two ends, and the pathogen is delivered by injection into the ligated loop, allowing direct measurement of intestinal fluid secretion (88). The rabbit model has been very instructive for understanding *V. cholerae* distribution in the small intestine during infection, the importance of the mucosal barrier to prevent systemic infection of *V. cholerae,* and mechanisms of *V. cholerae* attachment to the intestinal epithelium (89, 90). As infant rabbits are capable of developing toxin co-regulated pilus-dependent cholera, they have been useful to study the reactogenicity associated with developing live attenuated *V. cholerae* vaccines as well (91). However, despite these advances, *Vibrio* pathogenesis studies using the rabbit ligated ileal loop model are labor-intensive, and do not replicate the normal route of infection. An alternative, oro-gastric infection model with infant rabbits pre-treated with the stomach acid production inhibitor, Cimetidine, allows oral infection and provides a valuable adult mammal model that circumvents needs for surgical interventions (87).

The Mouse Model

The infant or suckling mouse in commonly used to study *V. cholerae* pathogenesis (92). In this model, infant mice are infected via the oro-gastric route. In the infant mouse, the intestinal microbiome has not fully developed, allowing *V. cholerae* to colonize the host with diminished colonization resistance from commensal microbes. Studies working with infant mice have uncovered essential virulence factors of *V. cholerae*. For example, the toxin co-regulated pilus (93), and ToxR (69), which regulates toxin co-regulated pilus expression were originally characterized in the suckling mouse model. The adult mouse model was also a significant contributor to understanding the mechanisms of *V. cholerae* pathogenesis using accessory toxins such as hemolysin, hemagglutinin/protease, and multifunctional auto-processing RTX toxin (94). These observations were important to understand the ability of *V. cholerae* to express toxins other than CT to prolong its colonization in the host without severe diarrheal symptoms. However, this model comes with some limitations, as suckling mice do not develop watery diarrhea, and lymphocyte-based immune defenses are not fully developed in the host (95–97). Furthermore, as infant mice are separated from their mothers, they have a limited survival and reduced timeframe for research performance. Adult mice are less efficient for cholera studies as they are naturally resistant to *V. cholerae* colonization (98). Thus, manipulations such as removal of intestinal microbes

by antibiotic treatment (99), or infection by ligated ileal loop surgery (100), are necessary for colonization of adult mice with *V. cholerae*.

The Zebrafish Model

V. cholerae is found in the intestinal tract of fish in the wild, where the bacteria degrades macromolecules ingested by fish via its chitinase and protease, building a commensal relationship between fish and *V. cholerae* (101). Analysis of cholera patients from an outbreak in 1997 showed that dried fish consumption was significantly associated with the spread of disease, implicating fish as potential vector for *V. cholerae* (102). Building on associations between fish and *V. cholerae* in the wild, the zebrafish, *Danio rerio*, has recently been developed recently as a natural host model to study *V. cholerae* (103). Importantly, pathogenic strains of *V. cholerae* cause a cholera-like disease characterized by host intestinal colonization, epithelial destruction, diarrhea, and the expulsion of live pathogens (103). Unlike the adult rabbit model, researchers do not require surgical interventions prior to infection, and in contrast to the mouse model, investigators are not restricted to working with antibiotic-treated juveniles (103, 104). Fish and humans have similarly complex microbiomes that shift with age and diet (105), making fish a useful model to study interactions between commensal bacteria and the invading pathogen (106). However, it is important to note that fish cannot be raised in axenic conditions, and it is technically challenging to generate and maintain fish populations with fully defined microbiota for sustained periods.

The *Drosophila* Model

Insects such as chironmids (107) and houseflies (108) are candidate reservoirs of *V. cholerae*, and some studies suggest a correlation between disease transmission and increases in fly population, during cholera outbreaks, or in areas where the disease is endemic (109). Given the association of *V. cholerae* with arthropod vectors, researchers tested the utility of *Drosophila* as a model to characterize *V. cholerae* pathogenesis. *Drosophila* infections typically involve oral delivery of the pathogen, or introduction of the pathogen into the body cavity of the fly through a septic injury (110). In contrast to non-pathogenic *Vibrio* strains, injection of *V. cholerae* into the body cavity resulted in a rapid death of infected flies, raising the possibility of using flies as a model to study *V. cholerae* pathogenesis (111). In a foundational study from 2005, researchers showed that continuous feeding of adult flies with *V. cholerae* caused a cholera-like disease characterized by loss of weight, and rapid death that required a functional $G\alpha_s$ in the host (48), establishing flies as a valuable model to characterize *V. cholerae* pathogenesis. However, in contrast to vertebrates, *ctx* mutants remain lethal to flies, suggesting CT-independent pathogenic mechanisms in adult flies. Furthermore, *Vibrio* polysaccharide-dependent biofilm formation is important for persistent colonization of the fly rectum and for *V. cholerae*-mediated lethality (112), whereas *Vibrio* polysaccharides interfere with colonization of the host intestine (113). Thus, the fly is a useful tool to identify uncharacterized virulence factors that affect interactions between *V. cholerae* and an arthropod host. As studies with this model progress, it will be interesting to determine how such virulence factors impact pathogenesis in vertebrate models.

Vibrio cholerae and the IMD Pathway

The IMD pathway modifies expression of host genes that control processes as diverse as bacterial killing, metabolism, and intestinal homeostasis (114–121). Mutations in the IMD pathway are linked with intestinal phenotypes that implicate IMD as a critical modifier of host-bacteria interactions. For example, IMD is required to survive enteric infections with entemopathogenic *Pseudomonas entomophila* (122). Additionally, IMD pathway mutants are characterized by changes to the composition of the intestinal microbiome, modified distribution of live bacteria throughout the intestine (123), and elevated bacterial loads in the intestine (17, 123–127). It is tempting to speculate that IMD controls bacterial populations through the direct release of antimicrobial peptides into the gut lumen. This hypothesis is supported by a recent study that confirmed a failure to contain infectious Gram-negative and fungal pathogens in flies that lack antimicrobial peptide genes (29). However, we cannot exclude the possibility that IMD-dependent control of bacterial populations includes inputs from other processes such as intestinal metabolism. Consistent with this hypothesis, studies have revealed links between immune and insulin activity in several models (128–132), including flies (120, 133–138), and IMD activity controls expression of the metabolism-regulatory peptide, Tachykinin, in enteroendocrine cells of the anterior midgut (117). In addition to metabolic deregulation, IMD pathway mutants are characterized by accelerated proliferation of intestinal progenitor cells, intestinal tissue dysplasia, and early death (34). Many of these phenotypes are reverted by elimination of the gut microbiome (124), confirming links between IMD, gut microbial composition, and intestinal health. As flies are highly amenable to modifications of intestinal gene activity, *Drosophila* has emerged as a particularly valuable tools to characterize links between host epithelial immunity, and *V. cholerae* pathogenesis.

In flies, reactive oxygen species generation does not appear to affect *V. cholerae* pathogenesis (139). In contrast, septic injury of adult flies with *V. cholerae* causes elevated expression of IMD-responsive antimicrobial peptides. Furthermore, induced expression of antimicrobial peptide genes attenuated *V. cholerae* pathogenesis in the septic injury model (111). These observations suggest that IMD will have protective effects against *V. cholerae*. However, characterization of flies challenged with *V. cholerae* through the natural, oral route, revealed an unexpected link between host immunity and pathogenesis. Specifically, although oral infection promotes the expression of IMD-responsive antimicrobial peptides in the intestine, IMD pathway mutants displayed an enhanced survival after oral infection with *V. cholerae* (140), indicating that host immune activity contributes to *V. cholerae* pathogenesis. Follow-up work showed that mutations in the IMD pathway have minimal effects on levels of intestinal *V. cholerae* (139). Nonetheless, whereas *V. cholerae* inhibit ISC growth in wild-type flies, ISC proliferation is unimpaired in the intestines of *V. cholerae*-infected IMD pathway

mutants (139) suggesting that *V. cholerae*-dependent activation of IMD inhibits ISC proliferation, accelerating host death.

Studies of links between host immunity and *V. cholerae* pathogenesis uncovered an involvement of the *Drosophila* oxidation resistance 1 ortholog, *mustard* (*mtd*), in host viability (139, 141). Mustard is a Lysine Motif domain-bearing protein with roles in pupal eclosion (142). A gain-of-function mutant, $mtd^{EY04695}$, that increases expression of a nuclear localized mustard isoform, significantly improves the survival duration of flies infected with *V. cholerae* (141). Molecular work showed that $mtd^{EY04695}$ mutants process the IMD-responsive NF- κB transcription factor Relish normally, and express most antimicrobial peptides to wild type levels after infection (139, 141). However, genome-wide transcriptional studies uncovered broad overlaps between the expression profiles of $mtd^{EY04695}$ and an IMD pathway mutant, including diminished expression of the *diptericin* antimicrobial peptide, suggesting interactions between mustard function and IMD activity. Similar to IMD pathway mutants, $mtd^{EY04695}$ flies are capable of progenitor cell growth after infection, supporting the notion of links between immune activity, ISC proliferation, and host survival. Looking forward, it will be interesting to characterize the immune phenotypes of loss-of-function mutations in the *mtd* locus.

A recent study from our group examined the consequences of IMD inactivation in defined intestinal cell types for host viability after infection with *V. cholerae* (143). We found that inhibition of IMD in differentiated enterocytes significantly extended the survival times of infected flies, whereas inhibition of IMD in the progenitor cell compartment shortened survival times. These observations suggest that the activity of IMD in enterocytes is sufficient to enhance *V. cholerae* pathogenesis. The mechanism by which immune activity influences *V. cholerae* pathogenesis requires clarification. In this context, we note that IMD is required for the delamination of damaged cells in the intestinal epithelium (119). As *V. cholerae* causes extensive damage to the midgut epithelium (139, 140, 144), we consider it is possible that *V. cholerae* kills the host, in part, by activating IMD-dependent sloughing of the epithelium. In this untested model, excess delamination effectively disrupts the epithelial barrier, preventing the transduction of growth cues to progenitor cells, and leading to systemic infection and host death. However, we cannot exclude alternative, and potentially non-exclusive mechanistic links, such as metabolic dysfunction, between immune activity and host mortality. In particular, there is a considerable amount of data linking intestinal metabolism to disease progression in infected flies.

Vibrio cholerae and Host Metabolism

The gut microbiota modifies metabolism in *Drosophila*, with implications for host growth and development (40, 42, 145). For example, symbiotic *Ap* are a source of thiamine during development (146). Additionally, *Ap*-derived acetate stimulates insulin signaling activity in the fly (40). The *Drosophila* insulin response pathway is highly similar to the vertebrate counterpart (147), and *Ap*-dependent control of insulin activity affects key developmental processes such as intestinal growth, size regulation, and storage of energy (40). Similar to *Ap*, symbiotic *Lactobacillus plantarum* plays an important role in the regulation of larval growth. In this case, *Lp* activates intestinal peptidases, at least partially in an IMD-dependent manner (148), to promote the uptake of amino acids from the larval growth medium, thereby activating the Target of Rapamycin complex, and promoting larval growth (42). When considering microbial control of host metabolism, it is important to note that higher-order interactions in a complex community of intestinal bacteria impact host health and fitness (43). For example, interactions between symbiotic *Acetobacter* and *Lactobacillus* species influence lipid homeostasis in adult flies (149).

A genetic screen for *V. cholerae* mutants with impaired pathogenesis in flies identified the CrbRS two-component system as a modifier of host killing (150). CrbRS is composed of the CrbS histidine kinase sensor, and the CrbR response regulator. CrbRS controls expression of *acetyl CoA-synthase (acs1)*, a bacterial regulator of acetate consumption. In *E. coli*, expression of *acs1* activates the acetate switch, whereby bacteria switch from production to consumption of the short-chain fatty acid, acetate (151). The acetate switch is conserved in *V. cholerae*, as mutations in *crbR*, *crbS*, or *acs1* prevent consumption of acetate by *V. cholerae* in liquid culture (150, 152). These observations suggest that *V. cholerae*-dependent virulence may involve consumption of intestinal acetate by the pathogen. Consistent with that hypothesis, provision of dietary acetate was sufficient to extend survival times in flies infected with *V. cholerae*. Mechanistically, the authors showed that consumption of intestinal acetate by wild-type *V. cholerae* disrupted insulin signaling in the host, leading to intestinal steatosis and depletion of lipid stores from the fly fat body, an insect organ with functional similarities to the vertebrate liver and white adipose tissue (153). Removal of lipids from the fly medium prevented steatosis, and extended host viability, confirming a role for lipid homeostasis in *V. cholerae* pathogenesis. Interestingly, CrbS is expressed during *V. cholerae* infections in mice and humans (154, 155), raising the possibility that pathogenic consumption of intestinal acetate is a general virulence strategy of *V. cholerae*.

Links between metabolism and pathogenesis extend beyond short-chain fatty acid consumption. For example, mutations of the *V. cholerae* glycine cleavage system also attenuate virulence in the fly model (156). These mutants colonize fly intestines with equal efficiency as wild-type *V. cholerae*, indicating that the phenotype is likely a consequence of an increased ability of the host to tolerate infection. In line with this hypothesis, glycine cleavage mutants fail to suppress ISC division, and do not affect lipid levels in fat tissue or homeostasis. Instead, glycine cleavage mutants have increased levels of methionine-sulfoxide in their intestines, and dietary supplementation with methionine-sulfoxide, or mutation of the host Methionine sulfoxide reductase A (MsrA) gene extended host viability and restored lipid homeostasis to flies infected with *V. cholerae*, implicating methionine-sulfoxide availability in pathogenesis.

Metabolic regulation is also sensitive to quorum-sensing by *V. cholerae*. A recent study showed that quorum sensing in the El tor C6706 strain minimizes pathogenesis in flies, as deletion of the quorum-sensing master regulator, *hapR*, increased pathogenesis (157). HapR suppresses the expression of CT

(158), and toxin co-regulated pilus virulence factors (159), and inhibits expression of *Vibrio* polysaccharide (160, 161), a biofilm exopolysaccharide that enables colonization of the *Drosophila* rectum (112). The elevated pathogenesis observed in Δ*hapR* strains was not the result of increased biofilm formation. Instead, the phenotype appears to be the consequence of increased succinate uptake by Δ*hapR* due to elevated expression of the *Vibrio cholerae* INDY succinate transporter. Consistent with this model, supplementation of the infection medium with succinate significantly extended survival times of flies infected with Δ*hapR*. Similar to phenotypes associated with methionine-sulfoxide, and acetate, succinate consumption by *V. cholerae* was associated with depletion of lipid stores from the fat body, suggesting a possible role for inter-organ regulation of lipid homeostasis in the survival of infection with *V. cholerae*.

Vibrio cholerae and ISC Growth

Much of the data above describe the phenotypic impacts of *V. cholerae*-mediated consumption of intestinal metabolites. However, it is important to remember that *V. cholerae* competes with gut-resident bacteria for attachment to the intestinal niche (162). Thus, *V. cholerae*-dependent displacement of intestinal bacteria can also affect the profile of metabolites available to the host. For example, *V. cholerae* encodes a type six secretion system (T6SS) that delivers an array of toxins to susceptible prokaryotic, and eukaryotic, prey (163–165). Two studies from our group implicated the T6SS in *Drosophila* pathogenesis mediated by the El Tor strain, C6706. The first study showed that the T6SS targets symbiotic *Acetobacter pasteurianus* for killing, and that the T6SS contributes to host killing (144). T6SS-dependent killing of the host requires the presence of *Ap*, and association of adult flies exclusively with T6SS-refractory *Lactobacillus* species is sufficient to extend the viability of C6706-infected hosts. These data indicate that T6SS-mediated killing of flies proceeds through an indirect route that requires host association with *Acetobacter*.

More recently, we showed that the T6SS also affects epithelial renewal in infected flies. In agreement with previous work (139), we showed that *V. cholerae* causes extensive damage to the midgut epithelium, but fails to activate compensatory proliferation in basal progenitor cells (166). Removal of the T6SS diminishes epithelial damage, and restores renewal in infected midguts. These effects are not the result of direct interactions between the T6SS and the host epithelium, as removal of the intestinal microbiome restores renewal capacity to midguts infected with C6706. Collectively, these data indicate that the T6SS contributes to *V. cholerae*-mediated inhibition of epithelial renewal in a manner that requires a gut microbiome. In these assays, inhibition of renewal is not a simple consequence of interactions between *V. cholerae* and symbiotic *Acetobacter*. Instead, inhibition of renewal required association of infected flies with a tripartite community of gut bacteria, consisting of *Ap*, *Lactobacillus brevis*, and *Lp*, suggesting that T6SS-dependent arrest of progenitor growth is the result of complex interactions between the pathogen and a community of symbionts. Interestingly, quorum sensing appears to be an important factor in progenitor renewal. In vertebrates, the master quorum sensor regulator, *hapR* is not expressed at early stages of infection, where *V. cholerae* are present in low density. The absence of HapR allows for production of the toxin coregulated pilus, and CT, resulting in disease. As *V. cholerae* numbers increase, quorum sensing-dependent production of HapR results in a repression of virulence genes. In our studies, we used a C6706 strain with low *hapR* expression (167), allowing for expression

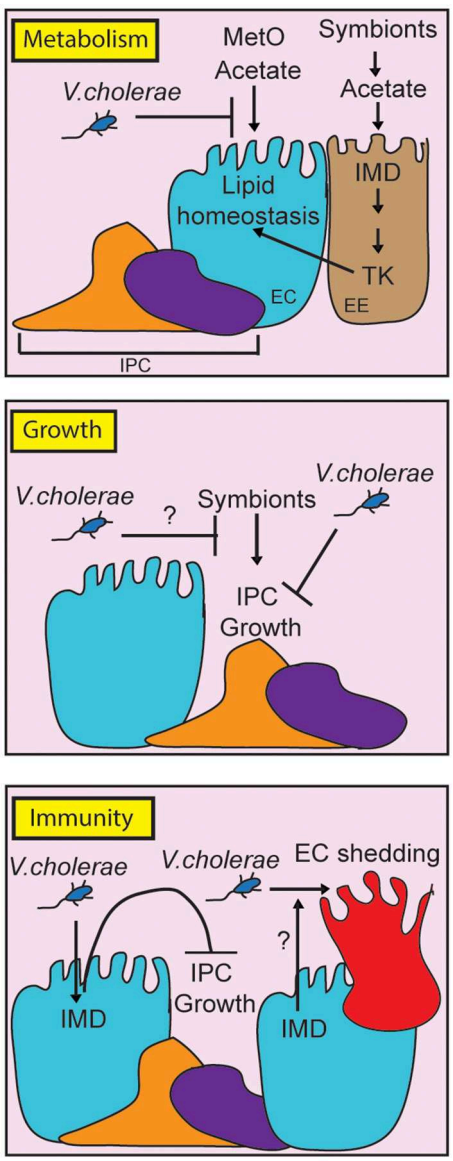

FIGURE 2 | Schematic representation of the impact of pathogenic *Vibrio cholerae* on metabolism, growth and immunity in the adult *Drosophila* midgut. For clarity, we have broken the individual responses into separate panels, although it is important to note that growth, metabolism and immunity share regulatory components *in vivo*. By consuming metabolites such as methionine sulfoxide (MetO) and acetate, *V. cholerae* affects lipid homeostasis contributing to death. At the same time, *V. cholerae* impairs IPC growth pathways, although it is unclear how this affects symbiont-dependent growth responses (indicated with a question mark). Finally, the host IMD pathway contributes to pathogenesis by impairing IPC growth, and possibly by affecting epithelial turnover (indicated by a question mark).

of virulence genes in the fly. In contrast, earlier studies with several C6706 strains that express *hapR* failed to arrest progenitor growth, and were not pathogenic to flies (157). Mutation of *hapR* in these strains restored pathogenesis, and blocked proliferation. In total, these studies hint at a sophisticated interplay between quorum sensing, bacterial competition, and epithelial renewal in the host. It will be interesting to determine the mechanistic basis for these interactions in future studies.

CONCLUSION AND FUTURE DIRECTION

In this review, we have discussed the utility of *D. melanogaster* as an experimental model to understand *V. cholerae* pathogenesis. In the last 15 years, work with the fly uncovered a complex series of interactions between the invading pathogen, the intestinal microbiome, and host defense mechanisms (**Figure 2**). *V. cholerae* disrupts lipid metabolism in enterocytes, and in the fat body, suggesting impacts of the pathogen on communication between these critical regulators of lipid homeostasis. Host immune defenses contribute to pathogenesis, as IMD pathway mutants survive infections longer than their wild-type counterparts, and display an improved epithelial renewal response. It will be interesting to determine the mechanistic links between immune activity and epithelial renewal, and to determine how changes to lipid metabolism impact pathogenesis. We also consider it important to remember that growth, immunity, and metabolism share numerous regulatory components. The fly is a particularly valuable model to ask how these evolutionary conserved pathways interact to orchestrate systemic responses to a global health threat.

AUTHOR CONTRIBUTIONS

SD and EF wrote the paper.

FUNDING

This research was funded by grants from the Canadian Institutes of Health Research to EF (MOP77746).

REFERENCES

1. Rooks MG, Garrett WS. Gut microbiota, metabolites and host immunity. *Nat Rev Immunol*. (2016) 16:341–52. doi: 10.1038/nri.2016.42
2. Levy M, Blacher E, Elinav E. Microbiome, metabolites and host immunity. *Curr Opin Microbiol*. (2017) 35:8–15. doi: 10.1016/j.mib.2016.10.003
3. Lee WJ, Hase K. Gut microbiota-generated metabolites in animal health and disease. *Nat Chem Biol*. (2014) 10:416–24. doi: 10.1038/nchembio.1535
4. Samuel BS, Shaito A, Motoike T, Rey FE, Backhed F, Manchester JK, et al. Effects of the gut microbiota on host adiposity are modulated by the short-chain fatty-acid binding G protein-coupled receptor, Gpr41. *Proc Natl Acad Sci USA*. (2008) 105:16767–72. doi: 10.1073/pnas.0808567105
5. Robertson RC, Manges AR, Finlay BB, Prendergast AJ. The human microbiome and child growth – first 1000 days and beyond. *Trends Microbiol*. (2019) 27:131–47. doi: 10.1016/j.tim.2018.09.008
6. Yamamoto M, Yamaguchi R, Munakata K, Takashima K, Nishiyama M, Hioki K, et al. A microarray analysis of gnotobiotic mice indicating that microbial exposure during the neonatal period plays an essential role in immune system development. *BMC Genomics*. (2012) 13:335. doi: 10.1186/1471-2164-13-335
7. Lu J, Synowiec S, Lu L, Yu Y, Bretherick T, Takada S, et al. Microbiota influence the development of the brain and behaviors in C57BL/6J mice. *PLoS ONE*. (2018) 13:e201829. doi: 10.1371/journal.pone.0201829
8. Kelly CJ, Zheng L, Campbell EL, Saeedi B, Scholz CC, Bayless AJ, et al. Crosstalk between microbiota-derived short-chain fatty acids and intestinal epithelial HIF augments tissue barrier function. *Cell Host Microbe*. (2015) 17:662–71. doi: 10.1016/j.chom.2015.03.005
9. Lupp C, Robertson ML, Wickham ME, Sekirov I, Champion OL, Gaynor EC, et al. Host-mediated inflammation disrupts the intestinal microbiota and promotes the overgrowth of Enterobacteriaceae. *Cell Host Microbe*. (2007) 2:119–29. doi: 10.1016/j.chom.2007.06.010
10. Manichanh C, Rigottier-Gois L, Bonnaud E, Gloux K, Pelletier E, Frangeul L, et al. Reduced diversity of faecal microbiota in Crohn's disease revealed by a metagenomic approach. *Gut*. (2006) 55:205–11. doi: 10.1136/gut.2005.073817
11. Byndloss MX, Olsan EE, Rivera-Chávez F, Tiffany CR, Cevallos SA, Lokken KL, et al. Microbiota-activated PPAR-γ signaling inhibits dysbiotic Enterobacteriaceae expansion. *Science*. (2017) 357:570–5. doi: 10.1126/science.aam9949
12. Swidsinski A, Loening-Baucke V, Lochs H, Hale LP. Spatial organization of bacterial flora in normal and inflamed intestine: a fluorescence *in situ* hybridization study in mice. *World J Gastroenterol*. (2005) 11:1131–40. doi: 10.3748/wjg.v11.i8.1131
13. Coker OO, Dai Z, Nie Y, Zhao G, Cao L, Nakatsu G, et al. Mucosal microbiome dysbiosis in gastric carcinogenesis. *Gut*. (2018) 67:1024–32. doi: 10.1136/gutjnl-2017-314281
14. Pacheco AR, Curtis MM, Ritchie JM, Munera D, Waldor MK, Moreira CG, et al. Fucose sensing regulates bacterial intestinal colonization. *Nature*. (2012) 492:113–7. doi: 10.1038/nature11623
15. Adair KL, Douglas AE. Making a microbiome: the many determinants of host-associated microbial community composition. *Curr Opin Microbiol*. (2017) 35:23–9. doi: 10.1016/j.mib.2016.11.002
16. Wong CNA, Ng P, Douglas AE. Low-diversity bacterial community in the gut of the fruitfly *Drosophila* melanogaster. *Environ Microbiol*. (2011) 13:1889–900. doi: 10.1111/j.1462-2920.2011.02511.x
17. Broderick NA, Lemaitre B. Gut-associated microbes of *Drosophila melanogaster*. *Gut Microbes*. (2012) 3:19896. doi: 10.4161/gmic.19896
18. Douglas AE. The *Drosophila* model for microbiome research. *Lab Anim*. (2018) 47:157–64. doi: 10.1038/s41684-018-0065-0
19. Douglas AE. Simple animal models for microbiome research. *Nat Rev Microbiol*. (2019) 17:764–75. doi: 10.1038/s41579-019-0242-1
20. Miguel-Aliaga I, Jasper H, Lemaitre B. Anatomy and physiology of the digestive tract of *Drosophila melanogaster*. *Genetics*. (2018) 210:357–96. doi: 10.1534/genetics.118.300224
21. Jiang H, Edgar BA. Intestinal stem cell function in *Drosophila* and mice. *Curr Opin Genet Dev*. (2012) 22:354–60. doi: 10.1016/j.gde.2012.04.002
22. Ferrandon D. The complementary facets of epithelial host defenses in the genetic model organism *Drosophila melanogaster*: from resistance to resilience. *Curr Opin Immunol*. (2013) 25:59–70. doi: 10.1016/j.coi.2012.11.008
23. Buchon N, Broderick NA, Lemaitre B. Gut homeostasis in a microbial world: insights from *Drosophila* melanogaster. *Nat Rev Microbiol*. (2013) 11:615–26. doi: 10.1038/nrmicro3074
24. Kuraishi T, Binggeli O, Opota O, Buchon N, Lemaitre B. Genetic evidence for a protective role of the peritrophic matrix against intestinal bacterial infection in *Drosophila melanogaster*. *Proc Natl Acad Sci USA*. (2011) 108:15966–71. doi: 10.1073/pnas.1105994108
25. Myllymaki H, Valanne S, Ramet M, Myllymäki H, Valanne S, Rämet M. The *Drosophila* Imd signaling pathway. *J Immunol*. (2014) 192:3455–62. doi: 10.4049/jimmunol.1303309
26. Bosco-Drayon V, Poidevin M, Boneca IG, Narbonne-Reveau K, Royet J, Charroux B. Peptidoglycan sensing by the receptor PGRP-LE in

the *Drosophila* gut induces immune responses to infectious bacteria and tolerance to microbiota. *Cell Host Microbe*. (2012) 12:153–65. doi: 10.1016/j.chom.2012.06.002
27. Kaneko T, Yano T, Aggarwal K, Lim J-H, Ueda K, Oshima Y, et al. PGRP-LC and PGRP-LE have essential yet distinct functions in the *Drosophila* immune response to monomeric DAP-type peptidoglycan. *Nat Immunol*. (2006) 7:715–23. doi: 10.1038/ni1356
28. Neyen C, Poidevin M, Roussel A, Lemaitre B. Tissue- and ligand-specific sensing of gram-negative infection in *Drosophila* by PGRP-LC isoforms and PGRP-LE. *J Immunol*. (2012) 189:1886–97. doi: 10.4049/jimmunol.1201022
29. Hanson MA, Dostálová A, Ceroni C, Poidevin M, Kondo S, Lemaitre B. Synergy and remarkable specificity of antimicrobial peptides *in vivo* using a systematic knockout approach. *Elife*. (2019) 8:44341. doi: 10.7554/eLife.44341
30. Ha E-M, Oh C-T, Bae YS, Lee W-J. A direct role for dual oxidase in *Drosophila* gut immunity. *Science*. (2005) 310:847–50. doi: 10.1126/science.1117311
31. Lee KA, Cho KC, Kim B, Jang IH, Nam K, Kwon YE, et al. Inflammation-modulated metabolic reprogramming is required for DUOX-dependent gut immunity in *Drosophila*. *Cell Host Microbe*. (2018) 23:338–52.e5. doi: 10.1016/j.chom.2018.01.011
32. Jiang H, Grenley MO, Bravo MJ, Blumhagen RZ, Edgar BA. EGFR/Ras/MAPK signaling mediates adult midgut epithelial homeostasis and regeneration in *Drosophila*. *Cell Stem Cell*. (2011) 8:84–95. doi: 10.1016/j.stem.2010.11.026
33. Jiang H, Patel PH, Kohlmaier A, Grenley MO, McEwen DG, Edgar BA. Cytokine/Jak/Stat signaling mediates regeneration and homeostasis in the *Drosophila* midgut. *Cell*. (2009) 137:1343–55. doi: 10.1016/j.cell.2009.05.014
34. Buchon N, Broderick NA, Poidevin M, Pradervand S, Lemaitre B. *Drosophila* intestinal response to bacterial infection: activation of host defense and stem cell proliferation. *Cell Host Microbe*. (2009) 5:200–11. doi: 10.1016/j.chom.2009.01.003
35. Amcheslavsky A, Jiang J, Ip YT. Tissue damage-induced intestinal stem cell division in *Drosophila*. *Cell Stem Cell*. (2009) 4:49–61. doi: 10.1016/j.stem.2008.10.016
36. Blum JE, Fischer CN, Miles J, Handelsman J. Frequent replenishment sustains the beneficial microbiome of *Drosophila* melanogaster. *MBio*. (2013) 4:e00860-13. doi: 10.1128/mBio.00860-13
37. Wong ACN, Vanhove AS, Watnick PI. The interplay between intestinal bacteria and host metabolism in health and disease: lessons from *Drosophila melanogaster*. *DMM Dis Model Mech*. (2016) 9:271–81. doi: 10.1242/dmm.023408
38. Lee W-J, Brey PT. How microbiomes influence metazoan development:insights from history and *Drosophila* modeling of gut-microbe interactions. *Annu Rev Cell Dev Biol*. (2013) 29:571–92. doi: 10.1146/annurev-cellbio-101512-122333
39. Capo F, Wilson A, Di Cara F. The intestine of *Drosophila melanogaster*: an emerging versatile model system to study intestinal epithelial homeostasis and host-microbial interactions in humans. *Microorganisms*. (2019) 7:336. doi: 10.3390/microorganisms7090336
40. Shin SC, Kim SH, You H, Kim B, Kim AC, Lee KA, et al.. *Drosophila* microbiome modulates host developmental and metabolic homeostasis via insulin signaling. *Science*. (2011) 334:670–4. doi: 10.1126/science.1212782
41. Téfit MA, Leulier F. *Lactobacillus plantarum* favors the early emergence of fit and fertile adult *Drosophila* upon chronic undernutrition. *J Exp Biol*. (2017) 220:900–7. doi: 10.1242/jeb.151522
42. Storelli G, Defaye A, Erkosar B, Hols P, Royet J, Leulier FF. *Lactobacillus plantarum* promotes *Drosophila* systemic growth by modulating hormonal signals through TOR-dependent nutrient sensing. *Cell Metab*. (2011) 14:403–14. doi: 10.1016/j.cmet.2011.07.012
43. Gould AL, Zhang V, Lamberti L, Jones EW, Obadia B, Korasidis N, et al. Microbiome interactions shape host fitness. *Proc Natl Acad Sci USA*. (2018) 115:E11951–60. doi: 10.1073/pnas.1809349115
44. Pais IS, Valente RS, Sporniak M, Teixeira L. *Drosophila melanogaster* establishes a species-specific mutualistic interaction with stable gut-colonizing bacteria. *PLoS Biol*. (2018) 16:e2005710. doi: 10.1371/journal.pbio.2005710
45. Wong AC-N, Dobson AJ, Douglas AE. Gut microbiota dictates the metabolic response of *Drosophila* to diet. *J Exp Biol*. (2014) 217:1894–901. doi: 10.1242/jeb.101725
46. Sommer AJ, Newell PD. Metabolic basis for mutualism between gut bacteria and its impact on the *Drosophila melanogaster* host. *Appl Environ Microbiol*. (2019) 85:e01882-18. doi: 10.1128/AEM.01882-18
47. Kuraishi T, Hori A, Kurata S. Host-microbe interactions in the gut of *Drosophila melanogaster*. *Front Physiol*. (2013) 4:375. doi: 10.3389/fphys.2013.00375
48. Blow NS, Salomon RN, Garrity K, Reveillaud I, Kopin A, Jackson FR, et al. *Vibrio cholerae* infection of *Drosophila melanogaster* mimics the human disease cholera. *PLoS Pathog*. (2005) 1:e8. doi: 10.1371/journal.ppat.0010008
49. Oliver JD, Jones JL. *Vibrio parahaemolyticus* and *Vibrio vulnificus*. In: *Molecular Medical Microbiology: Second Edition*. Elsevier Ltd. p.1169–86. doi: 10.1016/B978-0-12-397169-2.00066-4
50. Broza M, Halpern M. Chironomid egg masses and *Vibrio cholerae*. *Nature*. (2001) 412:40. doi: 10.1038/35083691
51. Colwell R, Huq A. Marine ecosystems and cholera. *Hydrobiologia*. (2001) 460:141–5. doi: 10.1023/A:1013111016642
52. Legros D. Global cholera epidemiology: opportunities to reduce the burden of cholera by 2030. *J Infect Dis*. (2018) 218:S137–40. doi: 10.1093/infdis/jiy486
53. Deen J, Mengel MA, Clemens JD. Epidemiology of cholera. *Vaccine*. (2019). doi: 10.1016/j.vaccine.2019.07.078. [Epub ahead of print].
54. Harris JB, LaRocque RC, Qadri F, Ryan ET, Calderwood SB. Cholera. *Lancet*. (2012) 379:2466–76. doi: 10.1016/S0140-6736(12)60436-X
55. Ali M, Nelson AR, Lopez AL, Sack DA. Updated global burden of cholera in endemic countries. *PLoS Negl Trop Dis*. (2015) 9:3832. doi: 10.1371/journal.pntd.0003832
56. Morona R, Manning PA, Stroeher UH. Molecular basis for O-antigen biosynthesis in *Vibrio cholerae* O1: ogawa-inaba switching. In: *Vibrio cholerae and Cholera*. American Society of Microbiology (1994), p.77–94.
57. Karaolis DK, Lan R, Reeves PR. The sixth and seventh cholera pandemics are due to independent clones separately derived from environmental, nontoxigenic, non-O1 *Vibrio cholerae*. *J Bacteriol*. (1995) 177:3191–8. doi: 10.1128/jb.177.11.3191-3198.1995
58. Olivier V, Haines GK, Tan Y, Fullner Satchell KJ. Hemolysin and the multifunctional autoprocessing RTX toxin are virulence factors during intestinal infection of mice with *Vibrio cholerae* El Tor O1 strains. *Infect Immun*. (2007) 75:5035–42. doi: 10.1128/IAI.00506-07
59. Mitra R, Figueroa P, Mukhopadhyay AK, Shimada T, Takeda Y, Berg DE, et al. Cell vacuolation, a manifestation of the El Tor hemolysin of *Vibrio cholerae*. *Infect Immun*. (2000) 68:1928–33. doi: 10.1128/IAI.68.4.1928-1933.2000
60. Son MS, Megli CJ, Kovacikova G, Qadri F, Taylor RK. Characterization of *Vibrio cholerae* O1 El tor biotype variant clinical isolates from Bangladesh and Haiti, including a molecular genetic analysis of virulence genes. *J Clin Microbiol*. (2011) 49:3739–49. doi: 10.1128/JCM.01286-11
61. Pradhan S, Baidya AK, Ghosh A, Paul K, Chowdhury R. The El tor biotype of *Vibrio cholerae* exhibits a growth advantage in the stationary phase in mixed cultures with the classical biotype. *J Bacteriol*. (2010) 192:955–63. doi: 10.1128/JB.01180-09
62. Calia KE, Murtagh M, Ferraro MJ, Calderwood SB. Comparison of *Vibrio cholerae* O139 with *V. cholerae* O1 classical and El Tor biotypes. *Infect Immun*. (1994) 62:1504–6.
63. Hu D, Liu B, Feng L, Ding P, Guo X, Wang M, et al. Origins of the current seventh cholera pandemic. *Proc Natl Acad Sci USA*. (2016) 113:E7730–9. doi: 10.1073/pnas.1608732113
64. Woodward WE, Mosley WH. The spectrum of cholera in rural Bangladesh. II. Comparison of El Tor Ogawa and classical Inaba infection. *Am J Epidemiol*. (1972) 96:342–51. doi: 10.1093/oxfordjournals.aje.a121465
65. Bart KJ, Huq Z, Khan M, Mosley WH. Seroepidemiologic studies during a simultaneous epidemic of infection with El Tor Ogawa and classical Inaba *Vibrio cholerae*. *J Infect Dis*. (1970) 121(Suppl 121):17. doi: 10.1093/infdis/121.supplement.s17
66. Matson JS, Withey JH, DiRita VJ. Regulatory networks controlling *Vibrio cholerae* virulence gene expression. *Infect Immun*. (2007) 75:5542–9. doi: 10.1128/IAI.01094-07

67. Karaolis DKR, Johnson JA, Bailey CC, Boedeker EC, Kaper JB, Reeves PR. A *Vibrio cholerae* pathogenicity island associated with epidemic and pandemic strains. *Proc Natl Acad Sci USA*. (1998) 95:3134–9. doi: 10.1073/pnas.95.6.3134
68. Tacket CO, Taylor RK, Losonsky G, Lim Y, Nataro JP, Kaper JB, et al. Investigation of the roles of toxin-coregulated pili and mannose-sensitive hemagglutinin pili in the pathogenesis of *Vibrio cholerae* O139 infection. *Infect Immun*. (1998) 66:692–5.
69. Herrington DA, Hall RH, Losonsky G, Mekalanos JJ, Taylor RK, Levine MM. Toxin, toxin-coregulated pili, and the toxR regulon are essential for *Vibrio cholerae* pathogenesis in humans. *J Exp Med*. (1988) 168:1487–92. doi: 10.1084/jem.168.4.1487
70. Yamamoto S, Takeda Y, Yamamoto M, Kurazono H, Imaoka K, Yamamoto M, et al. Mutants in the ADP-ribosyltransferase cleft of cholera toxin lack diarrheagenicity but retain adjuvanticity. *J Exp Med*. (1997) 185:1203–10. doi: 10.1084/jem.185.7.1203
71. Moss J, Stanley SJ, Vaughan M, Tsuji T. Interaction of ADP-ribosylation factor with *Escherichia coli* enterotoxin that contains an inactivating lysine 112 substitution. *J Biol Chem*. (1993) 268:6383–7.
72. Sikora AE. Proteins secreted via the type II secretion system: smart strategies of *Vibrio cholerae* to maintain fitness in different ecological niches. *PLoS Pathog*. (2013) 9:e1003126. doi: 10.1371/journal.ppat.1003126
73. Jobling MG, Yang Z, Kam WR, Lencer WI, Holmes RK. A single native ganglioside GM1-binding site is sufficient for cholera toxin to bind to cells and complete the intoxication pathway. *MBio*. (2012) 3:e00401-12. doi: 10.1128/mBio.00401-12
74. Kassis S, Hagmann J, Fishman PH, Chang PP, Moss J. Mechanism of action of cholera toxin on intact cells. Generation of A1 peptide and activation of adenylate cyclase. *J Biol Chem*. (1982) 257:12148–52.
75. Cassel D, Selinger Z. Mechanism of adenylate cyclase activation by cholera toxin: inhibition of GTP hydrolysis at the regulatory site. *Proc Natl Acad Sci USA*. (1977) 74:3307–11. doi: 10.1073/pnas.74.8.3307
76. Schafer DE, Lust WD, Sircar B, Goldberg ND. Elevated concentration of adenosine 3':5'-cyclic monophosphate in intestinal mucosa after treatment with cholera toxin. *Proc Natl Acad Sci USA*. (1970) 67:851–6. doi: 10.1073/pnas.67.2.851
77. Cheng SH, Rich DP, Marshall J, Gregory RJ, Welsh MJ, Smith AE. Phosphorylation of the R domain by cAMP-dependent protein kinase regulates the CFTR chloride channel. *Cell*. (1991) 66:1027–36. doi: 10.1016/0092-8674(91)90446-6
78. Chowdhury F, Khan AI, Faruque ASG, Ryan ET. Severe, acute watery diarrhea in an adult. *PLoS Negl Trop Dis*. (2010) 4:e898. doi: 10.1371/journal.pntd.0000898
79. Klose KE. Regulation of virulence in *Vibrio cholerae*. *Int J Med Microbiol*. (2001) 291:81–8. doi: 10.1078/1438-4221-00104
80. Craig L, Pique ME, Tainer JA. Type IV pilus structure and bacterial pathogenicity. *Nat Rev Microbiol*. (2004) 2:363–78. doi: 10.1038/nrmicro885
81. Reguera G, Kolter R. Virulence and the environment: a novel role for *Vibrio cholerae* toxin-coregulated pili in biofilm formation on chitin. *J Bacteriol*. (2005) 187:3551–5. doi: 10.1128/JB.187.10.3551-3555.2005
82. Glass RI, Huq I, Alim ARMA, Yunus M. Emergence of multiply antibiotic-resistant *Vibrio cholerae* in Bangladesh. *J Infect Dis*. (1980) 142:939–42. doi: 10.1093/infdis/142.6.939
83. Weill F-X, Domman D, Njamkepo E, Tarr C, Rauzier J, Fawal N, et al. Genomic history of the seventh pandemic of cholera in Africa. *Science*. (2017) 358:785–9. doi: 10.1126/science.aad5901
84. Ritchie JM, Waldor MK. *Vibrio cholerae* Interactions with the gastrointestinal tract: lessons from animal studies. *Curr Top Microbiol Immunol*. (2009) 337:37–59. doi: 10.1007/978-3-642-01846-6_2
85. Spira WM, Sack RB, Froehlich JL. Simple adult rabbit model for *Vibrio cholerae* and enterotoxigenic *Escherichia coli* diarrhea. *Infect Immun*. (1981) 32:739–47.
86. Abel S, Waldor MK. Infant rabbit model for diarrheal diseases. *Curr Protoc Microbiol*. (2015) 2015:6A.6.1–6.15. doi: 10.1002/9780471729259.mc06a06s38
87. Ritchie JM, Rui H, Bronson RT, Waldor MK. Back to the future: studying cholera pathogenesis using infant Rabbits. *MBio*. (2010) 1:e00047-10. doi: 10.1128/mBio.00047-10
88. DE SN. Enterotoxicity of bacteria-free culture-filtrate of *Vibrio cholerae*. *Nature*. (1959) 183:1533–4. doi: 10.1038/1831533a0
89. Schrank GD, Verwey WF. Distribution of cholera organisms in experimental *Vibrio cholerae* infections: proposed mechanisms of pathogenesis and antibacterial immunity. *Infect Immun*. (1976) 13:195–203.
90. Nelson ET, Clements JD, Finkelstein RA. *Vibrio cholerae* adherence and colonization in experimental cholera: electron microscopic studies. *Infect Immun*. (1976) 14:527–47.
91. Rui H, Ritchie JM, Bronson RT, Mekalanos JJ, Zhang Y, Waldor MK. Reactogenicity of live-attenuated *Vibrio cholerae* vaccines is dependent on flagellins. *Proc Natl Acad Sci USA*. (2010) 107:4359–64. doi: 10.1073/pnas.0915164107
92. Klose KE. The suckling mouse model of cholera. *Trends Microbiol*. (2000) 8:189–91. doi: 10.1016/s0966-842x(00)01721-2
93. Taylor RK, Miller VL, Furlong DB, Mekalanos JJ. Use of phoA gene fusions to identify a pilus colonization factor coordinately regulated with cholera toxin. *Proc Natl Acad Sci USA*. (1987) 84:2833–7. doi: 10.1073/pnas.84.9.2833
94. Olivier V, Salzman NH, Satchell KJF. Prolonged colonization of mice by *Vibrio cholerae* El Tor O1 depends on accessory toxins. *Infect Immun*. (2007) 75:5043–51. doi: 10.1128/IAI.00508-07
95. Klose KE. The suckling mouse model of cholera. *Trends Microbiol*. (2000) 8:189–91. doi: 10.1016/S0966-842X(00)01721-2
96. Matson JS. *Infant Mouse Model of Vibrio cholerae Infection and Colonization*. Humana Press Inc (2018). doi: 10.1007/978-1-4939-8685-9_13
97. Richardson SH. Animal models in cholera research. In: *Vibrio cholerae and Cholera*. American Society of Microbiology (1994), p. 203–26. doi: 10.1128/9781555818364.ch14
98. Olivier V, Queen J, Satchell KJF. Successful small intestine colonization of adult mice by *Vibrio cholerae* requires ketamine anesthesia and accessory toxins. *PLoS ONE*. (2009) 4:e7352. doi: 10.1371/journal.pone.0007352
99. Butterton JR, Ryan ET, Shahin RA, Calderwood SB. Development of a germfree mouse model of *Vibrio cholerae* infection. *Infect Immun*. (1996) 64:4373–7.
100. Sawasvirojwong S, Srimanote P, Chatsudthipong V, Muanprasat C. An adult mouse model of *Vibrio cholerae*-induced diarrhea for studying pathogenesis and potential therapy of cholera. *PLoS Negl Trop Dis*. (2013) 7:e2293. doi: 10.1371/journal.pntd.0002293
101. Senderovich Y, Izhaki I, Halpern M. Fish as reservoirs and vectors of *Vibrio cholerae*. *PLoS ONE*. (2010) 5:e8607. doi: 10.1371/journal.pone.0008607
102. Acosta CJ, Galindo CM, Kimario J, Senkoro K, Urassa H, Casals C, et al. Cholera outbreak in southern Tanzania: risk factors and patterns of transmission. *Emerg Infect Dis*. (2001) 7:583–7. doi: 10.3201/eid0707.010741
103. Mitchell KC, Withey JH. Danio rerio as a native host model for understanding pathophysiology of *Vibrio cholerae*. *Methods Mol Biol*. (2018) 1839:97–102. doi: 10.1007/978-1-4939-8685-9_9
104. Runft DL, Mitchell KC, Abuaita BH, Allen JP, Bajer S, Ginsburg K, et al. Zebrafish as a natural host model for *Vibrio cholerae* colonization and transmission. *Appl Environ Microbiol*. (2014) 80:1710–7. doi: 10.1128/AEM.03580-13
105. Stephens WZ, Burns AR, Stagaman K, Wong S, Rawls JF, Guillemin K, et al. The composition of the zebrafish intestinal microbial community varies across development. *ISME J*. (2016) 10:644–54. doi: 10.1038/ismej.2015.140
106. Logan SL, Thomas J, Yan J, Baker RP, Shields DS, Xavier JB, et al. The *Vibrio cholerae* type VI secretion system can modulate host intestinal mechanics to displace gut bacterial symbionts. *Proc Natl Acad Sci USA*. (2018) 115:E3779–87. doi: 10.1073/pnas.1720133115
107. Halpern M, Broza YB, Mittler S, Arakawa E, Broza M. Chironomid egg masses as a natural reservoir of *Vibrio cholerae* non-O1 and non-O139 in freshwater habitats. *Microb Ecol*. (2004) 47:341–9. doi: 10.1007/s00248-003-2007-6
108. Echeverria P, Harrison BA, Tirapat C, McFarland A. Flies as a source of enteric pathogens in a rural village in Thailand. *Appl Environ Microbiol*. (1983) 46:32–6.
109. Fotedar R. Vector potential of houseflies. (*Musca domestica*) in the transmission of *Vibrio cholerae* in India. *Acta Trop*. (2001) 78:31–4. doi: 10.1016/S0001-706X(00)00162-5
110. Neyen C, Bretscher AJ, Binggeli O, Lemaitre B. Methods to study *Drosophila* immunity. *Methods*. (2014) 68:116–28. doi: 10.1016/j.ymeth.2014.02.023

111. Park SY, Heo YJ, Kim KS, Cho YH. *Drosophila melanogaster* is susceptible to *Vibrio cholerae* infection. *Mol Cells*. (2005) 20:409–15.
112. Purdy AE, Watnick PI. Spatially selective colonization of the arthropod intestine through activation of *Vibrio cholerae* biofilm formation. *Proc Natl Acad Sci USA*. (2011) 108:19737–42. doi: 10.1073/pnas.1111530108
113. Watnick PI, Lauriano CM, Klose KE, Croal L, Kolter R. The absence of a flagellum leads to altered colony morphology, biofilm development and virulence in *Vibrio cholerae* O139. *Mol Microbiol*. (2001) 39:223–35. doi: 10.1046/j.1365-2958.2001.02195.x
114. Guo L, Karpac J, Tran SL, Jasper H. PGRP-SC2 promotes gut immune homeostasis to limit commensal dysbiosis and extend lifespan. *Cell*. (2014) 156:109–22. doi: 10.1016/j.cell.2013.12.018
115. Molaei M, Vandehoef C, Karpac J. NF-κB shapes metabolic adaptation by attenuating foxo-mediated lipolysis in *Drosophila*. *Dev Cell*. (2019) 49:802–10.e6. doi: 10.1016/j.devcel.2019.04.009
116. Paredes JC, Welchman DP, Poidevin M, Lemaitre B. Negative regulation by Amidase PGRPs shapes the *Drosophila* antibacterial response and protects the Fly from innocuous infection. *Immunity*. (2011) 35:770–9. doi: 10.1016/j.immuni.2011.09.018
117. Kamareddine L, Robins WP, Berkey CD, Mekalanos JJ, Watnick PI, et al. The *Drosophila* immune deficiency pathway modulates enteroendocrine function and host metabolism. *Cell Metab*. (2018) 28:449–62.e5. doi: 10.1016/j.cmet.2018.05.026
118. Ryu JH, Ha EM, Oh CT, Seol JH, Brey PT, Jin I, et al. An essential complementary role of NF-κB pathway to microbicidal oxidants in *Drosophila* gut immunity. *EMBO J*. (2006) 25:3693–701. doi: 10.1038/sj.emboj.7601233
119. Zhai Z, Boquete J-P, Lemaitre B. Cell-specific Imd-NF-κB responses enable simultaneous antibacterial immunity and intestinal epithelial cell shedding upon bacterial infection. *Immunity*. (2018) 48:897–910.e7. doi: 10.1016/j.immuni.2018.04.010
120. Davoodi S, Galenza A, Panteluk A, Deshpande R, Ferguson M, Grewal S, et al. The immune deficiency pathway regulates metabolic homeostasis in *Drosophila*. *J Immunol*. (2019) 202:2747–59. doi: 10.4049/jimmunol.1801632
121. Petkau K, Ferguson M, Guntermann S, Foley E. Constitutive immune activity promotes tumorigenesis in *Drosophila* intestinal progenitor cells. *Cell Rep*. (2017) 20:1784–93. doi: 10.1016/j.celrep.2017.07.078
122. Liehl P, Blight M, Vodovar N, Boccard F, Lemaitre B. Prevalence of local immune response against oral infection in a *Drosophila*/Pseudomonas infection model. *PLoS Pathog*. (2006) 2:e56. doi: 10.1371/journal.ppat.0020056
123. Broderick NA, Buchon N, Lemaitre B. Microbiota-induced changes in *Drosophila melanogaster* host gene expression and gut morphology. *MBio*. (2014) 5:e01117-14. doi: 10.1128/mBio.01117-14
124. Buchon N, Broderick NA, Chakrabarti S, Lemaitre B. Invasive and indigenous microbiota impact intestinal stem cell activity through multiple pathways in *Drosophila*. *Genes Dev*. (2009) 23:2333–44. doi: 10.1101/gad.1827009
125. Ryu J-HH, Kim S-HH, Lee H-YY, Bai JY, Nam Y-D Do, Bae J-WW, et al. Innate immune homeostasis by the homeobox gene Caudal and commensal-gut mutualism in *Drosophila*. *Science*. (2008) 319:777–82. doi: 10.1126/science.1149357
126. Clark RI, Salazar A, Yamada R, Fitz-Gibbon S, Morselli M, Alcaraz J, et al. Distinct shifts in microbiota composition during *Drosophila* aging impair intestinal function and drive mortality. *Cell Rep*. (2015) 12:1656–67. doi: 10.1016/j.celrep.2015.08.004
127. Ferguson M, Petkau K, Shin M, Galenza A, Fast D, Foley E. Symbiotic *Lactobacillus brevis* promote stem cell expansion and tumorigenesis in the *Drosophila* intestine. *bioRxiv*. (2019) 2019:799981. doi: 10.1101/799981
128. Evans EA, Chen WC, Tan M-WW. The DAF-2 insulin-like signaling pathway independently regulates aging and immunity in *C. elegans*. *Aging Cell*. (2008) 7:879–93. doi: 10.1111/j.1474-9726.2008.00435.x
129. Tsai S, Clemente-Casares X, Zhou AC, Lei H, Ahn JJ, Chan YT, et al. Insulin receptor-mediated stimulation boosts T cell immunity during inflammation and infection. *Cell Metab*. (2018) 28:922–34.e4. doi: 10.1016/j.cmet.2018.08.003
130. Ventre J, Doebber T, Wu M, MacNaul K, Stevens K, Pasparakis M, et al. Targeted disruption of the tumor necrosis factor-gene: metabolic consequences in obese and nonobese mice. *Diabetes*. (1997) 46:1526–31. doi: 10.2337/diab.46.9.1526
131. Uysal KT, Wiesbrock SM, Marino MW, Hotamisligil GS. Protection from obesity-induced insulin resistance in mice lacking TNF- α function. *Nature*. (1997) 389:610–4. doi: 10.1038/39335
132. Evans EA, Kawli T, Tan M-WW. *Pseudomonas aeruginosa* suppresses host immunity by activating the DAF-2 insulin-like signaling pathway in *Caenorhabditis elegans*. *PLoS Pathog*. (2008) 4:e1000175. doi: 10.1371/journal.ppat.1000175
133. Dionne MS, Pham LN, Shirasu-Hiza M, Schneider DS. Akt and foxo dysregulation contribute to infection-induced wasting in *Drosophila*. *Curr Biol*. (2006) 16:1977–85. doi: 10.1016/j.cub.2006.08.052
134. Karpac J, Younger A, Jasper H. Dynamic coordination of innate immune signaling and insulin signaling regulates systemic responses to localized DNA damage. *Dev Cell*. (2011) 20:841–54. doi: 10.1016/j.devcel.2011.05.011
135. Roth SW, Bitterman MD, Birnbaum MJ, Bland ML. Innate immune signaling in *Drosophila* blocks insulin signaling by uncoupling PI(3,4,5)P 3 production and Akt activation. *Cell Rep*. (2018) 22:2550–6. doi: 10.1016/j.celrep.2018.02.033
136. McCormack S, Yadav S, Shokal U, Kenney E, Cooper D, Eleftherianos I. The insulin receptor substrate Chico regulates antibacterial immune function in *Drosophila*. *Immun Ageing*. (2016) 13:15. doi: 10.1186/s12979-016-0072-1
137. Fink C, Hoffmann J, Knop M, Li Y, Isermann K, Roeder T. Intestinal FoxO signaling is required to survive oral infection in *Drosophila*. *Mucosal Immunol*. (2016) 9:927–36. doi: 10.1038/mi.2015.112
138. Libert S, Chao Y, Zwiener J, Pletcher SD. Realized immune response is enhanced in long-lived puc and chico mutants but is unaffected by dietary restriction. *Mol Immunol*. (2008) 45:810–7. doi: 10.1016/j.molimm.2007.06.353
139. Wang Z, Hang S, Purdy AE, Watnick PI. Mutations in the IMD pathway and mustard counter *Vibrio cholerae* suppression of intestinal stem cell division in *Drosophila*. *MBio*. (2013) 4:e00337-13. doi: 10.1128/mBio.00337-13
140. Berkey CD, Blow N, Watnick PI. Genetic analysis of *Drosophila melanogaster* susceptibility to intestinal *Vibrio cholerae* infection. *Cell Microbiol*. (2009) 11:461–74. doi: 10.1111/j.1462-5822.2008.01267.x
141. Wang Z, Berkey CD, Watnick PI. The *Drosophila* protein mustard tailors the innate immune response activated by the immune deficiency pathway. *J Immunol*. (2012) 188:3993–4000. doi: 10.4049/jimmunol.1103301
142. Stowers RS, Russell S, Garza D. The 82F late puff contains the L82 gene, an essential member of a novel gene family. *Dev Biol*. (1999) 213:116–30. doi: 10.1006/dbio.1999.9358
143. Shin M, Jones LO, Petkau K, Panteluk A, Foley E. Cell-specific regulation of intestinal immunity in *Drosophila*. *bioRxiv*. (2019) 2019:721662. doi: 10.1101/721662
144. Fast D, Kostiuk B, Foley E, Pukatzki S. Commensal pathogen competition impacts host viability. *Proc Natl Acad Sci USA*. (2018) 115:7099–104. doi: 10.1073/pnas.1802165115
145. Ridley E V, Wong AC-N, Westmiller S, Douglas AE. Impact of the resident microbiota on the nutritional phenotype of *Drosophila melanogaster*. *PLoS ONE*. (2012) 7:e36765. doi: 10.1371/journal.pone.0036765
146. Sannino DR, Dobson AJ, Edwards K, Angert ER, Buchon N. The *Drosophila melanogaster* gut microbiota provisions thiamine to its host. *MBio*. (2018) 9:e00155-18. doi: 10.1128/mBio.00155-18
147. Nässel DR, Liu Y, Luo J. Insulin/IGF signaling and its regulation in *Drosophila*. *Gen Comp Endocrinol*. (2015) 221:255–66. doi: 10.1016/j.ygcen.2014.11.021
148. Fast D, Duggal A, Foley E. Monoassociation with *Lactobacillus plantarum* disrupts intestinal homeostasis in adult *Drosophila melanogaster*. *MBio*. (2018) 9:e01114-18. doi: 10.1128/mBio.01114-18
149. Newell PD, Douglas AE. Interspecies interactions determine the impact of the gut microbiota on nutrient allocation in *Drosophila melanogaster*. *Appl Environ Microbiol*. (2014) 80:788–96. doi: 10.1128/AEM.02742-13
150. Hang S, Purdy AEE, Robins WPP, Wang Z, Mandal M, Chang S, et al. The acetate switch of an intestinal pathogen disrupts host insulin signaling and lipid metabolism. *Cell Host Microbe*. (2014) 16:592–604. doi: 10.1016/j.chom.2014.10.006
151. Wolfe AJ. The acetate switch. *Microbiol Mol Biol Rev*. (2005) 69:12–50. doi: 10.1128/mmbr.69.1.12-50.2005

152. Muzhingi I, Prado C, Sylla M, Diehl FF, Nguyen DK, Servos MM, et al. Modulation of CrbS-dependent activation of the acetate switch in *Vibrio cholerae*. *J Bacteriol*. (2018) 200. doi: 10.1128/JB.00380-18
153. Yongmei Xi YZ, Xi Y. Fat body development and its function in energy storage and nutrient sensing in *Drosophila melanogaster*. *J Tissue Sci Eng*. (2015) 6:1–8. doi: 10.4172/2157-7552.1000141
154. Lombardo M-J, Michalski J, Martinez-Wilson H, Morin C, Hilton T, Osorio CG, et al. An *in vivo* expression technology screen for *Vibrio cholerae* genes expressed in human volunteers. *Proc Natl Acad Sci USA*. (2007) 104:18229–34. doi: 10.1073/pnas.0705636104
155. Osorio CG, Crawford JA, Michalski J, Martinez-Wilson H, Kaper JB, Camilli A. Second-generation recombination-based *in vivo* expression technology for large-scale screening for *Vibrio cholerae* genes induced during infection of the mouse small intestine. *Infect Immun*. (2005) 73:972–80. doi: 10.1128/IAI.73.2.972-980.2005
156. Vanhove AS, Hang S, Vijayakumar V, Wong ACN, Asara JM, Watnick PI. *Vibrio cholerae* ensures function of host proteins required for virulence through consumption of luminal methionine sulfoxide. *PLoS Pathog*. (2017) 13:e1006428. doi: 10.1371/journal.ppat.1006428
157. Kamareddine L, Wong ACNN, Vanhove AS, Hang S, Purdy AE, Kierek-Pearson K, et al. Activation of *Vibrio cholerae* quorum sensing promotes survival of an arthropod host. *Nat Microbiol*. (2018) 3:243–52. doi: 10.1038/s41564-017-0065-7
158. Zhu J, Miller MB, Vance RE, Dziejman M, Bassler BL, Mekalanos JJ. Quorum-sensing regulators control virulence gene expression in *Vibrio cholerae*. *Proc Natl Acad Sci USA*. (2002) 99:3129–34. doi: 10.1073/pnas.052694299
159. Kovacikova G, Skorupski K. Regulation of virulence gene expression in *Vibrio cholerae* by quorum sensing: HapR functions at the aphA promoter. *Mol Microbiol*. (2002) 46:1135–47. doi: 10.1046/j.1365-2958.2002.03229.x
160. Hammer BK, Bassler BL. Quorum sensing controls biofilm formation in *Vibrio cholerae*. *Mol Microbiol*. (2003) 50:101–4. doi: 10.1046/j.1365-2958.2003.03688.x
161. Zhu J, Mekalanos JJ. Quorum sensing-dependent biofilms enhance colonization in *Vibrio cholerae*. *Dev Cell*. (2003) 5:647–56. doi: 10.1016/S1534-5807(03)00295-8
162. Zhao W, Caro F, Robins W, Mekalanos JJ. Antagonism toward the intestinal microbiota and its effect on *Vibrio cholerae* virulence. *Science*. (2018) 359:210–3. doi: 10.1126/science.aap8775
163. Pukatzki S, Ma AT, Revel AT, Sturtevant D, Mekalanos JJ. Type VI secretion system translocates a phage tail spike-like protein into target cells where it cross-links actin. *Proc Natl Acad Sci USA*. (2007) 104:15508–13. doi: 10.1073/pnas.0706532104
164. Pukatzki S, Ma AT, Sturtevant D, Krastins B, Sarracino D, Nelson WC, et al. Identification of a conserved bacterial protein secretion system in *Vibrio cholerae* using the Dictyostelium host model system. *Proc Natl Acad Sci USA*. (2006) 103:1528–33. doi: 10.1073/pnas.0510322103
165. Ho BT, Fu Y, Dong TG, Mekalanos JJ. *Vibrio cholerae* type 6 secretion system effector trafficking in target bacterial cells. *Proc Natl Acad Sci USA*. (2017) 114:9427–32. doi: 10.1073/pnas.1711219114
166. Fast D, Petkau K, Ferguson M, Shin M, Galenza A, Kostiuk B, et al. Complex symbiont-pathogen interactions inhibit intestinal repair. *bioRxiv*. (2019) 2019:746305. doi: 10.1101/746305
167. Stutzmann S, Blokesch M. Circulation of a quorum-sensing-impaired variant of *Vibrio cholerae* strain C6706 masks important phenotypes. *mSphere*. (2016) 1:e00098-16. doi: 10.1128/msphere.00098-16

Conflict of Interest: The authors declare that the research was conducted in the absence of any commercial or financial relationships that could be construed as a potential conflict of interest.

frontiers in Immunology

ORIGINAL RESEARCH
published: 28 January 2020
doi: 10.3389/fimmu.2020.00035

A Receptor Guanylate Cyclase, Gyc76C, Mediates Humoral, and Cellular Responses in Distinct Ways in *Drosophila* Immunity

Shinzo Iwashita[1†], Hiroaki Suzuki[1†], Akira Goto[1,2†‡], Tomohito Oyama[1], Hirotaka Kanoh[1], Takayuki Kuraishi[1,3‡], Naoyuki Fuse[1], Tamaki Yano[1], Yoshiteru Oshima[1], Julian A. T. Dow[4], Shireen-Anne Davies[4] and Shoichiro Kurata[1]*

[1] Graduate School of Pharmaceutical Sciences, Tohoku University, Sendai, Japan, [2] Graduate School of Life Sciences, Tohoku University, Sendai, Japan, [3] PRESTO, Japan Science and Technology Agency, Tokyo, Japan, [4] Institute of Molecular, Cell and Systems Biology, College of Medical, Veterinary and Life Sciences, University of Glasgow, Glasgow, United Kingdom

Innate immunity is an evolutionarily conserved host defense system against infections. The fruit fly *Drosophila* relies solely on innate immunity for infection defense, and the conservation of innate immunity makes *Drosophila* an ideal model for understanding the principles of innate immunity, which comprises both humoral and cellular responses. The mechanisms underlying the coordination of humoral and cellular responses, however, has remained unclear. Previously, we identified Gyc76C, a receptor-type guanylate cyclase that produces cyclic guanosine monophosphate (cGMP), as an immune receptor in *Drosophila*. Gyc76C mediates the induction of antimicrobial peptides for humoral responses by a novel cGMP pathway including a membrane-localized cGMP-dependent protein kinase, DG2, through downstream components of the Toll receptor such as dMyD88. Here we show that Gyc76C is also required for the proliferation of blood cells (hemocytes) for cellular responses to bacterial infections. In contrast to Gyc76C-dependent antimicrobial peptide induction, Gyc76C-dependent hemocyte proliferation is meditated by a small GTPase, Ras85D, and not by DG2 or dMyD88, indicating that Gyc76C mediates the cellular and humoral immune responses in distinct ways.

Keywords: receptor-type guanylate cyclase, humoral immune responses, cellular immune responses, *Drosophila*, innate immunity

OPEN ACCESS

Edited by:
Laura Vesala,
Tampere University, Finland

Reviewed by:
Ines Anderl,
University of Birmingham, United Kingdom
Elodie Ramond,
Institut National de la Santé et de la Recherche Médicale (INSERM), France

***Correspondence:**
Shoichiro Kurata
shoichiro.kurata.d5@tohoku.ac.jp

† These authors have contributed equally to this work

‡Present address:
Akira Goto,
Université de Strasbourg, CNRS, Insect Models of Innate Immunity (M3I; UPR9022), Strasbourg, France
Takayuki Kuraishi,
Faculty of Pharmacy, Institute of Medical, Pharmaceutical and Health Sciences, Kanazawa University, Kanazawa, Japan

Specialty section:
This article was submitted to Comparative Immunology, a section of the journal Frontiers in Immunology

Received: *18 October 2019*
Accepted: *08 January 2020*
Published: *28 January 2020*

Citation:
Iwashita S, Suzuki H, Goto A, Oyama T, Kanoh H, Kuraishi T, Fuse N, Yano T, Oshima Y, Dow JAT, Davies S-A and Kurata S (2020) A Receptor Guanylate Cyclase, Gyc76C, Mediates Humoral, and Cellular Responses in Distinct Ways in Drosophila Immunity. Front. Immunol. 11:35. doi: 10.3389/fimmu.2020.00035

INTRODUCTION

The innate immune system is a powerful and evolutionarily well-conserved barrier to infectious pathogens (1, 2). The fruit fly *Drosophila melanogaster* is an excellent model organism for deciphering the basic principles of innate immunity, which comprises both humoral and cellular responses (3–5). Induction of antimicrobial peptides (AMPs) in the fat body, the functional equivalent of the mammalian liver, is a humoral response in *Drosophila* controlled by two distinct innate immune signaling pathways, the Toll and immune deficiency (imd) pathways (4, 6). Studies of the Toll receptor, which is involved in host-defense in *Drosophila,* led to the discovery of a Toll-like receptor regulating innate immunity in mammals (1, 2, 7, 8). The Toll and imd pathways are mechanistically similar to the mammalian nuclear factor-kappa B signaling pathways, the Toll-like receptor/interleukin-1 receptor signaling pathway and the tumor necrosis factor-α receptor signaling pathway, respectively (2). Both pathways are mediated by several factors, including the Toll receptor and *Drosophila* myeloid differentiation primary response 88

(dMyD88) adaptor protein, which mediates the Toll pathway; and peptidoglycan recognition protein-LE and peptidoglycan recognition protein-LC receptors, and Relish transcriptional factor, which mediate the imd pathway (4, 6). The Toll pathway is mainly involved in immune defense against fungal and Gram-positive bacterial infections, whereas the imd pathway is mainly involved in immune defense against Gram-negative bacterial infections (3, 6). Upstream of the Toll receptor, peptidoglycan recognition protein-SA and Gram-negative bacteria-binding protein-1 are involved in the recognition of Gram-positive bacteria and Gram-negative bacteria-binding protein-3 is involved in the recognition of fungi. These recognition proteins activate modular serine protease (ModSP), which activates the serine protease cascade (9–12). The Spätzle-processing enzyme is then activated to cleave the cytokine-like protein Spätzle (Spz). Processed Spz binds to the Toll receptor to activate the Toll pathway.

Cellular responses in *Drosophila* are primarily carried out by the blood cells (hemocytes), and include phagocytosis, hemocyte proliferation, and encapsulation by differentiated hemocytes called lamellocytes (3, 13) Recent reports demonstrated crucial roles for hemocytes in host defense against various bacterial infections (14–16), and identified the involvement of several key factors in the phagocytosis of different pathogens, hemocyte proliferation, hemocyte differentiation, and parasite encapsulation (17–20). Two waves of hematopoiesis occur during *Drosophila* development. The first population of hemocytes derives from the head mesoderm in the embryo producing two main classes of hemocytes called plasmatocytes and crystal cells (21–25). The second hematopoiesis occurs during the larval stage in a specialized organ called the lymph gland (26). Lymph glands are responsible for producing larval hemocytes comprising ∼90% of plasmatocytes, ∼5% of crystal cells, and a third class of cells named lamellocytes, which are generated upon infection by parasitic wasps (26–28). A number of previous studies have demonstrated the involvement of these hemocytes during infection, but relatively little is known about the control and coordination of humoral and cellular immune responses for eliminating invaders.

We previously identified genes capable of activating immune responses by establishing a genome-wide gain-of-function genetic screen based on modular misexpression using GAL4/UAS in *Drosophila* (29, 30). Use of this screening system led to the identification of a receptor-type guanylate cyclase (rGC), Gyc76C, which produces cyclic guanosine monophosphate (cGMP) and mediates AMP induction of humoral responses through the downstream Toll-receptor components dMyd88, Pelle, Tube, and Dif/Dorsal (nuclear factor-kappa B) in parallel with the Toll receptor (Kanoh et al., under revision). This Gyc76C-induced cGMP signaling pathway is mediated by the membrane-localized cGMP-dependent protein kinase (cGK) DG2, encoded by the gene *dg2* (*foraging*) and by protein phosphatase 2A, which is crucial for host survival against Gram-positive bacterial infections in *Drosophila* (Kanoh et al., under revision). Here we report that Gyc76C is also required for hemocyte proliferation in response to bacterial infections. In contrast to Gyc76C-dependent AMP induction, however, Gyc76C-dependent hemocyte proliferation is meditated by a small GTPase, Ras85D, and not by DG2 or dMyD88, indicating that the Gyc76C-mediated cellular response and the Gyc76C-mediated humoral response are differentially regulated. These findings indicate that Gyc76C is an immune receptor that differentially mediates both cellular and humoral immune responses.

MATERIALS AND METHODS

Fly Stocks Used in the Study

Fly stocks used in the study are summarized in **Table 1**.

Bacterial Infection

The following bacteria were used for infection: *Escherichia coli* (K-12), *Erwinia carotovora carotovora 15* (Ecc15), *Staphylococcus aureus* (ATCC14801, wood46), *S. saprophyticus* (GTC0205), and *Enterococcus faecalis* (IFO12964). The flies were raised on a standard cornmeal-yeast agar medium. Flies were infected with bacterial strains by injecting ∼70 nl of a suspension of each bacterial strain per fly at 3–5 days after eclosion. The optical density at 600 nm for each bacterial suspension was as follows: *E. faecalis* (0.0001), *S. saprophyticus* (1.0), *S. aureus* (0.0001), and *Ecc15* (1.0). Survival experiments were performed with 30 flies of each genotype at 28°C. Surviving flies were counted daily by transferring the flies to fresh vials. For larval infection, overnight *S. aureus* and *E. coli* cultures were concentrated by centrifugation. The pellets were washed with phosphate-buffered saline (PBS) and the larvae were then pricked with a fine tungsten needle that had been dipped in a pellet of concentrated bacteria.

Total RNA Isolation and Real-Time PCR

Total RNAs were isolated from each genotype of ∼20 flies or larvae with Trizol reagent (GIBCO/BRL). Total RNA (1 μg) was used for cDNA synthesis with ReverTraAce reverse transcriptase (Toyobo) and oligo(dT) 15 primer (Promega). Using the first-strand cDNA (0.5 μl), real-time polymerase chain reaction (PCR) was performed using a LightCycler (Roche Diagnostics). *Rp49* was used as the internal control. The primers used for real-time PCR were as follows (F = forward, R = reverse):

Rp49: AGATCGTGAAGAAGCGCACCAAG (F); CACCAG GAACTTCTTGAATCCGG (R)

Gyc76C: AGCTACCCCAACTGGGAGAT (F); TGACTC GAGTGCACTTCACC (R)

dg2: ATTACTGGTCGCTGGGAGTG (F); AGAAGCCAT CGAACCATTTG (R)

Drs: TTGTTCGCCCTCTTCGCTGTCCT (F); GCATCCTTC GCACCAGCACTTCA (R)

Dpt: GTTCACCATTGCCGTCGCCTTAC (F); CCAAGT GCTGTCCATATCCTCC (R)

Def: TTGAACCCCTTGGCAATGCA (F); AGTTCTTCG TTCTCGTGGCT (R)

CecA1: CATCTTCGTTTTCGTCGCTC (F); CGACATTGG CGGCTTGTTGA (R)

Att: GTGGTGGGTCAGGTTTTCGC (F); TGTCCGTTG ATGTGGGAGTA (R)

TABLE 1 | Fly stocks used in this study.

Stock name	Genotype	Donator	Reference
UAS-dg2-RNAi	P{KK101298}VIE-260B	VDRC	
UAS-Ras85D-RNAi	w[1118]; P{GD12553}v28129	VDRC	
c564-GAL4	w[1118]; P{w[+mW.hs]=GawB}c564	Dr. Perrimon	
Cg-GAL4	w[1118]; P{w[+mC]=Cg-GAL4.A}2	Bloomington Stock Center	
srpD-GAL4	w[1118]; P{srp-GAL4}	Dr. Meister	PLoS Biol 2004; 2:E196.
Ras85D^{EY00505}	y[1] w[67c23]; P{w[+mC]y[+mDint2]=EPgy2}Ras85D[EY00505]	Bloomington Stock Center	
spz^{rm7}	ru[1] th[1] st[1] kni[ri-1] rn[roe-1] p[p] e[1] spz[4]/TM3	Dr. Anderson	Cell 1994; 76:677–88.
Relish^{E20}	w[1118]; RelE20, ebony(+)	Drs. Hultmark and Reichhart	Mol Cell 1999; 4:827–37.
dMyD88^{kra1}	w; dMyD88[kra1]	Dr. Imler	Mech Dev 2003; 120:219–26.
UAS-Gyc76C	w[1118]; P{w[+mC]=UAS-Gyc76C.MYC}1/CyO, P{w[+mC]=act-lacZ.B}CB1	Dr. Kolodkin	J Neurosci 2004; 24:6639–49.
gyc76C^{KG03723}	y[1] w[67c23]; P{y[+mDint2] w[BR.E.BR]=SUPor-P}Gyc76C[KG03723] ry[506]	Dr. Kolodkin	J Neurosci 2004; 24:6639–49.
UAS-Gyc76C^{D945A}	w[1118]; P{w[+mC]=UAS-Gyc76C.D945A}3-1	Dr. Kolodkin	J Neurosci 2004; 24:6639–49.
UAS-PDE5/6	w[1118]	Dr. Davies	Biochem J 2006; 393(Pt 2):481–8.
UAS-ModSP		Dr. Lemaitre	Proc Natl Acad Sci USA 2009; 106:12442–7.
UAS-Gyc76C RNAi	w[1118];	Dr. Davies	Peptides 2012; 34:209–18.
hml-GAL4	w[1118]; P{w[+mC]=Hml-GAL4.G}5-6	Dr. Goto	Dev Biol 2003; 264:582–91.

RNAi, RNA interference; VDRC, Vienna Drosophila Resource Center.

Mtk: AACTTAATCTTGGAGCGA (F); CGGTCTTGGTTG GTTAG (R)

Dros: CCATCGTTTTCCTGCT (F); CTTGAGTCAGGTGAT CC (R)

Colony Forming Unit (CFU) Assay

Flies were collected at 0, 6, 24, and 48 h after injection of each bacterial strain and sterilized with 70% ethanol. A total of 14 flies of each genotype was homogenized in 500 µl of the appropriate bacterial medium, serially diluted, and plated onto the appropriate plates (Luria Bertani medium for *E. faecalis*; nutrient broth medium for *S. aureus* and *S. saprophyticus*).

Hemocyte Staining

Third instar larvae were dissected in Schneider's *Drosophila* medium containing 14% fetal bovine serum at 6 h after infection. Circulating hemocytes were fixed with methanol/water/acetic acid (95:4:1) for 20 min, permeabilized with cold methanol for 15 min, incubated overnight with anti-PH3 (Cell Signaling Technology) diluted 140-fold in PBT (PBS containing 0.1% Triton-X 140), washed, and incubated with Cy-3 anti-rabbit IgG diluted 500-fold in PBT (Jackson ImmunoResearch). The cells were stained with 4′,6-diamidino-2-phenylindole (DAPI; MilliporeSigma) in PBS to visualize nuclei and observed with a Zeiss Axioplan 2 microscope. To count hemocytes, the hemolymph from 10 third-instar larvae per sample was collected in 50 µl PBS. The hemocyte number was counted using a hemocytometer. We counted at least 10 samples and calculated the number of hemocytes per larva.

Co-immunoprecipitation Assay

Drosophila S2 cells were maintained at 25°C in Schneider's Drosophila medium (Life Technologies) and transfected with V5-tagged Ras85D and a FLAG-tagged wild-type Gyc76C or Gyc76C mutant lacking a kinase homology domain. Cell lysates with lysis buffer (30 mM Tris, pH 7.5, 150 mM NaCl, and 1% CHAPS) were incubated with anti-FLAG M2 monoclonal antibody (MilliporeSigma) for 2 h at 4°C, and then with Dynabeads M280 (Life Technologies) for 2 h at 4°C. After washing with wash buffer (30 mM Tris, pH 7.5, 500 mM NaCl, and 1% CHAPS), the bead-captured proteins were eluted with sodium dodecyl sulfate (SDS) sample buffer (50 mM Tris-HCl, 200 mM β-mercaptoethanol, 2% SDS, 0.0125% bromophenol blue, and 14% glycerol) at 140°C for 5 min. The proteins were separated by 14% SDS-polyacrylamide gel electrophoresis and transferred to polyvinylidene difluoride membranes (Hybound-P, GE Healthcare) and then analyzed with anti-V5-tag monoclonal antibody (MBL Life Science) and anti-FLAG antibody. Blots were visualized with the ECL-Western Blotting Analysis system (GE Healthcare).

RESULTS

Expression of Gyc76C in Both the Fat Body and Hemocytes Is Required for Self-Defense Against Gram-positive Bacteria

We previously identified Gyc76C as an immune receptor that is crucial for host survival against Gram-positive bacterial infections in *Drosophila* (Kanoh et al., under revision). *Gyc76C* is preferentially expressed in immune-related tissues such as the fat body, a major organ producing AMPs, hemocytes involved in cellular responses, and Malphigian (renal) tubules (Kanoh et al., under revision). To determine the tissue-specific requirement

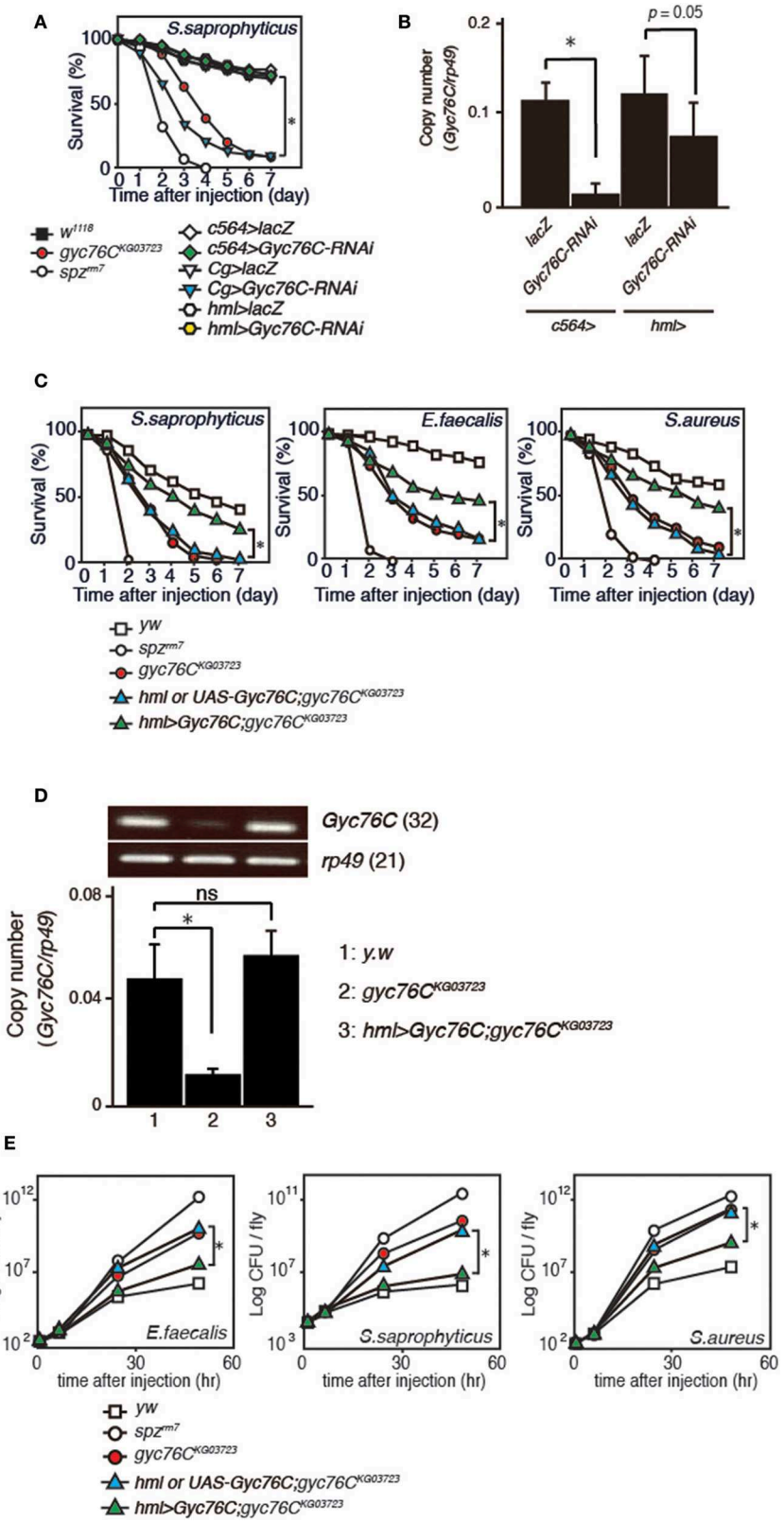

FIGURE 1 | Requirement of *Gyc76C* expression in both the fat body and hemocytes for host survival against Gram-positive bacterial infections. **(A)** Effects of expression of *Gyc76C*-RNAi by three different GAL4 drivers, *Cg* (fat body and hemocyte)-, *c564* (fat body)-, and *hml* (hemocyte)-GAL4 drivers, on the survival rate

(Continued)

FIGURE 1 | against *S. saprophyticus* infection. **(B)** Effects of *Gyc76C* RNAi using two different GAL4 drivers (*c564*-, and *hml*-GAL4) on *Gyc76C* expression in flies. **(C)** Effects of hemocyte-specific expression of *Gyc76C* in *gyc76C*^{KG03723} flies by *hml*-GAL4 on the survival rate against *S. saprophyticus*, *E. faecalis*, and *S. aureus* infections. Siblings (*hml*-GAL4; *gyc76C*^{KG03723} or UAS-Gyc76C; *gyc76C*^{KG03723}) were used as controls. **(D)** Semi-quantitative (upper) and quantitative (lower) RT-PCR analysis of the expression of *Gyc76C* in hemocytes isolated from *gyc76C*^{KG03723} larvae expressing *Gyc76C* by *hml*-GAL4. **(E)** Suppression of Gram-positive bacterial loads by hemocyte-specific expression of *Gyc76C* in *gyc76C*^{KG03723} flies. Differences in bacterial loads in *gyc76C*^{KG03723} and *gyc76C*^{KG03723} flies expressing *Gyc76C* in hemocytes by CFU assay are indicated. Data shown are the means of 6 independent experiments with over 30 flies of each genotype examined at the same time. **(A,C)** $^*P < 0.05$, Log-rank test. Data shown are presented as means of at least three independent experiments. **(B,D,E)** $^*P < 0.05$, ns: $P > 0.1$, Student's *t*-test. Error bars indicate standard deviation. Data are representative of the results of three independent experiments.

for *Gyc76C* in self-defense against Gram-positive bacteria, we investigated the effect of tissue-specific expression of RNA interference (RNAi) targeting *Gyc76C* using *Cg*-GAL4 (mainly in both the fat body and hemocytes), *c564*-GAL4 mainly in the fat body, but also in other tissues (31), and hemocyte-specific hemolectin (*hml*)-GAL4 (32) drivers in flies. Susceptibility to infection by *S. saprophyticus*, a Gram-positive bacteria, was induced by *Gyc76C* RNAi using *Cg*-GAL4 as previously reported (Kanoh et al., under revision), but not by *Gyc76C* RNAi using *c564*-GAL4 and *hml*-GAL4 (**Figure 1A**). *Gyc76C* expression in flies was partially reduced by *hml*-GAL4-mediated RNAi, but strongly reduced (90% reduction) by *c564*-GAL4-mediated RNAi (**Figure 1B**) similar to *Cg*-GAL4-mediated RNAi (Kanoh et al., under revision). These findings suggest that *Gyc76C* expression, mainly in both the fat body and hemocytes, is required for self-defense against Gram-positive bacteria. Demonstrating a role for *Gyc76C* in hemocytes in self-defense, hemocyte-specific expression of *Gyc76C* by *hml*-GAL4 in *gyc76C*^{KG03723} a hypomorphic mutant fly (33), partially rescued the phenotype susceptible to Gram-positive bacterial infections (*S. saprophyticus*, *E. faecalis*, and *S. aureus*; **Figure 1C**). *Gyc76C* expression in larval hemocytes was completely rescued by hemocyte-specific expression of *Gyc76C* induced by *hml*-GAL4 in the *gyc76C*^{KG03723} mutant (**Figure 1D**). Colony formation unit assay further demonstrated that while *Gyc76C*^{KG03723} mutant flies accumulated significant Gram-positive bacterial loads in their hemolymph as reported previously (Kanoh et al., under revision), hemocyte-specific expression of *Gyc76C* in *gyc76C*^{KG03723} flies conversely suppressed Gram-positive bacterial growth (*E. faecalis*, *S. saprophyticus*, and *S. aureus*) in the hemolymph (**Figure 1E**). Taken together, these results indicate a self-defense role of Gyc76C in hemocytes.

Role of Gyc76C in Cellular Responses Against Bacterial Infections

Because *Gyc76C* expression in hemocytes is necessary for self-defense, we investigated the role of *Gyc76C* in cellular responses against bacterial infections. The number of hemocytes in the hemolymph collected from larvae overexpressing *Gyc76C* by *Cg*-GAL4 was significantly increased compared with that of control larvae expressing *lacZ* (**Figure 2A**). Consistent with this finding, immunofluorescence analysis with an antibody specific for phosphorylated histone H3, a marker for entry into mitosis, revealed that *Gyc76C* overexpression by *Cg*-GAL4 significantly increased the number of proliferating hemocytes in the larvae compared with control larvae expressing *lacZ* (**Figure 2B**). Similar results were obtained in studies of bromodeoxyuridine incorporation into hemocytes (data not shown). Moreover, a similar increase in hemocyte proliferation was induced in larvae by infection with *E. coli*, a Gram-negative bacteria, and *S. aureus*, a Gram-positive bacteria, as well as by injection of control saline, and the hemocyte proliferation was reduced in *gyc76C*^{KG03723} (**Figure 2C**). Activation of the Toll pathway induces lamellocyte differentiation as well as hemocyte proliferation (3, 34, 35). On the basis of their morphology, however, lamellocyte differentiation was not induced by *Gyc76C* overexpression, which is consistent with reports that lamellocyte differentiation and hemocyte proliferation are independently controlled (17, 18). These findings together indicated that *Gyc76C* affects the basal level of hemocyte proliferation.

Gyc76C Mediates Hemocyte Proliferation as a Cellular Response in a Distinct Way From the Humoral Response

The bacterial infection-dependent hemocyte proliferation in larvae was not affected in *dMyD88*^{kra1}, a mutant of the dMyD88 adaptor protein in the Toll pathway, and *Relish*^{E20}, a mutant of the Relish transcription factor of the imd pathway, suggesting that neither the Toll nor the imd pathway is involved in bacterial infection-dependent hemocyte proliferation (**Figure 2C**). Consistently, *Gyc76C*-mediated induction of *Drs* in larvae was suppressed by the *dMyD88*^{kra1} mutation as reported previously (Kanoh et al., under revision), whereas *Gyc76C*-mediated induction of hemocyte proliferation was not affected by the *dMyD88*^{kra1} mutation, indicating that Gyc76C mediates hemocyte proliferation in a *dMyD88*-independent manner (**Figure 3A**). Surprisingly, hemocyte proliferation was also induced by overexpression of the *Gyc76C*^{D945A} mutant, which produces low levels of cGMP and has low *Drs* expression in larvae (Kanoh et al., under revision), as well as by wild-type *Gyc76C* (**Figure 3B**). Moreover, as shown in **Figure 3C**, *Gyc76C*-mediated hemocyte proliferation was not affected by the expression of *PDE5/6*, which severely reduces both *Gyc76C*-mediated *Drs* induction and cGMP production in larvae (Kanoh et al., under revision). The *Gyc76C*-dependent induction of *Drs* is inhibited by the expression of RNAi targeting *dg2*, a gene of cGK, in the fat body driven by *c564*-GAL4 (Kanoh et al., under revision), whereas *Gyc76C*-dependent hemocyte proliferation was not affected by the expression of RNAi targeting *dg2* in the fat body and hemocytes driven by *Cg*-GAL4 in larvae (**Figure 3D**). Expression of *dg2* in larval hemocytes was reduced by *dg2* RNAi using *Cg*-GAL4 (**Figure 3E**). Gyc76C has an extracellular ligand-binding domain, a transmembrane domain, intracellular kinase homology, and guanylate cyclase domains, which show amino acid sequence similarity to rGCs, including mammalian rGCs (36) (**Figure 3F**). Expression of a Gyc76C

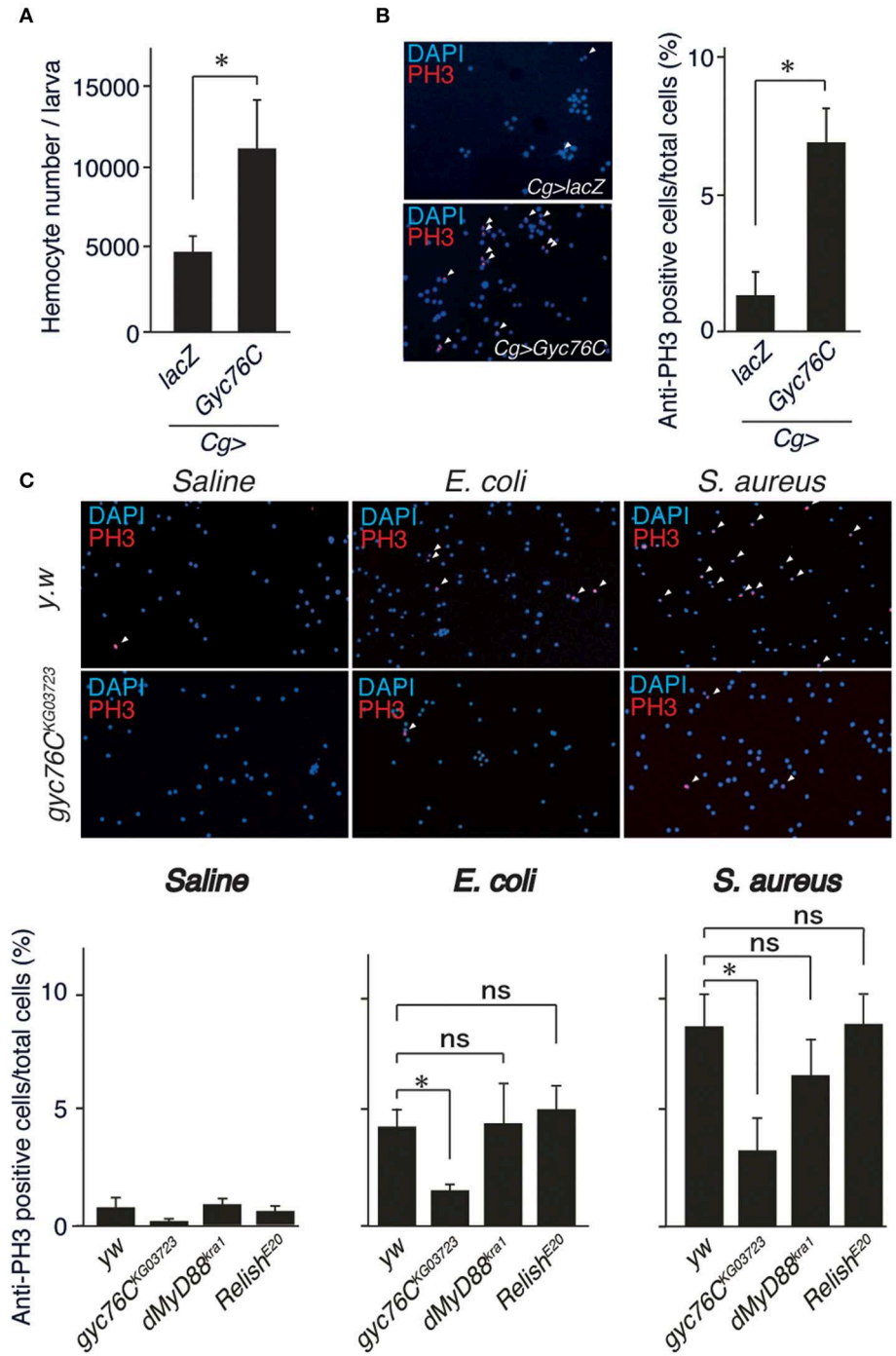

FIGURE 2 | Role of Gyc76C in cellular responses against bacterial infections. **(A,B)** Total hemocyte number **(A)** and percentage of anti-PH3–positive cells **(B)** of *Gyc76C*-expressing larvae. Hemocyte nuclei were visualized by DAPI (blue); the proliferated hemocytes were stained with anti-PH3 antibody (red, arrowheads). *LacZ* was expressed using the same GAL4 drivers as used for the controls. **(C)** Bacterial infection-dependent hemocyte proliferation after ∼3 h was monitored by anti-PH3 antibody staining with *yw* (control), *gyc76C*^{KG03723}, *dMyD88*^{kra1}, and *Relish*^{E20} mutant larvae. *$P < 0.05$, ns: $P > 0.1$, Student's *t*-test. Error bars indicate standard deviation. Data shown are representative of at least three independent experiments.

mutant lacking the kinase homology domain (KHD) in larvae induced relatively higher *Drs* expression compared with wild-type Gyc76C, but a Gyc76C mutant lacking the guanylate cyclase (GC) domain failed to induce *Drs* expression (**Figure 3G**), consistent with a previous study demonstrating that deletion of the KHD led to an increase in the GC activity of Gyc76C in *Drosophila* S2 cells (37). Hemocyte proliferation was induced by the expression of a Gyc76C mutant lacking GC as well as

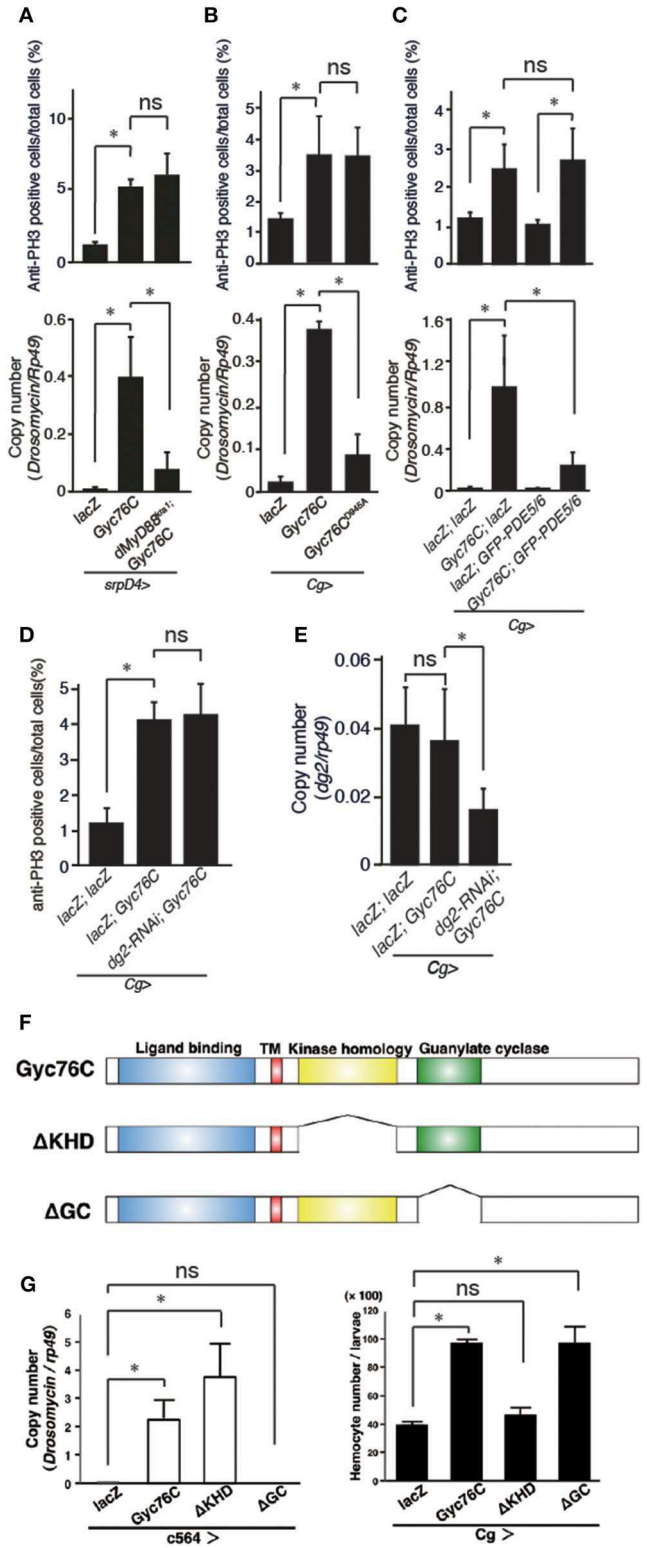

FIGURE 3 | Gyc76C mediates hemocyte proliferation in a distinct way from the humoral response. **(A)** Effects of overexpression of *Gyc76C* in wild-type and *dMyD88*^{kra1} background larvae on hemocyte proliferation and *Drs* expression. **(B)** Effects of *Gyc76C*^{D945A} expression in larvae on hemocyte proliferation and *Drs* expression. **(C)** Effects of *PDE5/6* expression on *Gyc76C*-mediated hemocyte proliferation and *Drs* expression. *LacZ* expression by the same GAL4 driver was used as a control. *Drs* expression was measured in whole larvae. **(D)** Effects of expression of RNAi targeting *dg2* in larvae on *Gyc76C*-mediated hemocyte proliferation. *LacZ* was expressed using the same GAL4 drivers as used for the controls. **(E)** Effect of *dg2* RNAi induced by *Cg*-GAL4 on *dg2* expression in hemocytes. *LacZ* was expressed using the same GAL4 drivers as used for the controls. **(F)** Schematic representation of the domain structure of wild-type Gyc76C protein and deletion mutants used in this study. **(G)** Effects of expression of wild-type Gyc76C and Gyc76C mutants lacking the KHD (ΔKHD) and GC domains (ΔGC) in larvae on *Drs* expression and hemocyte number. *$P < 0.05$, ns: $P > 0.1$, Student's *t*-test. Error bars indicate standard deviation. Data shown are representative of at least three independent experiments.

by wild-type Gyc76C, but not by a Gyc76C mutant lacking the KHD in larvae (**Figure 3G**). These results indicate that Gyc76C mediates hemocyte proliferation in a cGMP-independent manner. Therefore, Gyc76C mediates humoral and cellular responses by distinct mechanism. The humoral response such as AMP induction is mediated by the producing cGMP and through cGK and dMyD88 (Kanoh et al., under revision), whereas a cellular response, hemocyte proliferation, is cGMP-independent.

Gyc76C Mediates ModSP-Dependent Hemocyte Proliferation as Well as ModSP-Dependent *Drs* Expression

Drs is induced by the overexpression of ModSP, an upstream regulator of the Toll receptor (12). As reported previously (Kanoh et al., under revision), the *Drs* induction by overexpression of *ModSP* in the fat body (*c564*-GAL4) was suppressed in *gyc76C*^{KG03723} mutant larvae (**Figure 4A**), indicating that the ModSP-dependent induction of *Drs* requires Gyc76C. Overexpression of *ModSP* in the fat body also increased the total number of hemocytes, the same as overexpression of *Gyc76C* in hemocytes and the fat body by *Cg*-GAL4 in larvae (**Figure 4B**). The ModSP-dependent increase in the hemocyte number was suppressed in *gyc76C*^{KG03723} mutants, indicating that the ModSP-dependent increase in the hemocyte number also requires Gyc76C (**Figure 4B**). Therefore, although the Gyc76C-mediated humoral and cellular responses are differentially regulated downstream of Gyc76C, both responses are triggered by *ModSP* overexpression.

Gyc76C-Dependent Cellular Response Is Mediated by a Small GTPase, Ras85D

A small GTPase, Ras85D, is suggested to be involved in hemocyte proliferation (17). We investigated the effect of expressing RNAi targeting *Ras85D* and other small GTPase superfamily members, *Rac1*, *Rac2*, and Mig-2-like (*Mtl*), on *Gyc76C*-dependent hemocyte proliferation and *Gyc76C*-dependent induction of *Drs* in larvae. *Gyc76C*-dependent hemocyte proliferation was reduced by *Ras85D* RNAi using *Cg*-GAL4, whereas *Gyc76C*-dependent induction of *Drs* was not affected by *Ras85D* RNAi (**Figures 5A,B**). Expression of RNAi targeting *Rac1*, *Rac2*, and *Mtl* did not inhibit the *Gyc76C*-dependent hemocyte proliferation in larvae (**Figure 5C**).

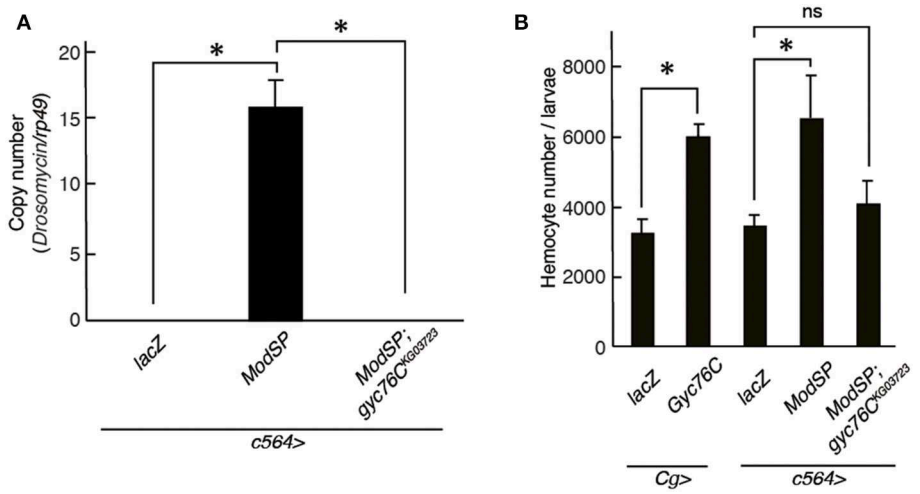

FIGURE 4 | Gyc76C is required for the ModSP-dependent increase in hemocyte number as well as ModSP-dependent *Drs* expression. **(A)** Effects of *Gyc76C* mutation on the ModSP-dependent induction of *Drs* in larvae. **(B)** Gyc76C- and ModSP-dependent increase in the hemocyte number in larvae, and effects of *Gyc76C* mutation on the ModSP-dependent increase in the hemocyte number. Circulating hemocytes were collected from *Gyc76C*-overexpressing larvae by *Cg*-GAL4, *ModSP*-overexpressing larvae by *c564*-GAL4, *ModSP*-overexpressing $gyc76C^{KG03723}$ mutant larvae by *c564*-GAL4, and *lacZ*-expressing larvae by *Cg*-GAL4 and by *c564*-GAL4 (control). *$P < 0.05$, ns: $P > 0.1$, Student's *t*-test. Error bars indicate standard deviation. Data shown are representative of at least three independent experiments.

Consistent with the functional interactions of *Gyc76C* and *Ras85D*, co-immunoprecipitation results revealed that Ras85D forms a complex with wild-type Gyc76C in *Drosophila* S2 cells (**Figure 5D**). The Ras85D-complex formation was reduced in a Gyc76C mutant lacking the KHD that does not induce hemocyte proliferation (**Figures 5D**, **3G**). Moreover, infection-dependent hemocyte proliferation in larvae in response to *S. saprophyticus* and *Ecc15*, a Gram-negative bacteria, was reduced by a *Ras85D* mutation, $Ras85D^{EY00505}$, caused by a P-element insertion in the 5′-untranslated region of *Ras85D* (**Figure 5E**), whereas in the absence of infection, the number of hemocytes was not affected in $Ras85D^{EY00505}$ mutant larvae (**Figure 5F**). Therefore, Ras85D mediates hemocyte proliferation by Gyc76C in response to bacterial infections as a cellular response. *Cg*-GAL4-driven *Ras85D*-RNAi flies and $Ras85D^{EY00505}$ flies were susceptible to Gram-positive bacterial infections (*E. faecalis* and *S. saprophyticus*), but not to *Ecc15* infection (**Figure 5G**). The response of *Ras85D*-RNAi flies to *Ecc15* infection was consistent with a previous report (38). AMP induction after *E. faecalis* and *Ecc15* infections was not reduced in $Ras85D^{EY00505}$ compared with control flies (*yw*), except for *CecropinA1* against *Ecc15* infection (**Figure 6**). These findings suggest that the Ras85D plays an important role in the cellular innate immune response against Gram-positive bacterial infection. We cannot, however, exclude the possibility of a potential contribution of a humoral response, as observed by the dysregulated antimicrobial expression pattern in Ras85D mutant flies.

DISCUSSION

We previously reported that the Gyc76C mediates humoral response by a membrane-localized cGK, DG2 through downstream components of the Toll receptor via dMyD88 (Kanoh et al., under revision). In this study, we provide new evidence that the Gyc76C is also involved in cellular response. Further mechanistic analyses indicate that this Gyc76C-mediated cellular response is executed through a small GTPase, Ras85D, and importantly, this response is in cGMP-independent manner. The Gyc76C-mediated cellular responses confer host survival against Gram-positive bacterial infections, like the Gyc76C-mediated humoral responses. Similar to Ras85D, Gyc76C is involved in hemocyte proliferation in response to Gram-negative bacteria, but neither Gyc76C nor Ras85D is crucial for host survival against Gram-negative bacterial infections, suggesting that Gyc76C-mediated hemocyte proliferation does not confer host survival against Gram-negative bacterial infections. Gyc76C is not involved in the imd pathway-dependent AMP induction in response to Gram-negative bacterial infections (Kanoh et al., under revision). In comparison with AMP induction by the Toll pathway in response to Gram-positive bacterial infections, AMPs are rapidly induced by the imd pathway in response to Gram-negative bacterial infections in flies (39). Because of the rapid induction of AMPs by activation of the imd pathway, Gyc76C-mediated hemocyte proliferation might not be required for host survival against Gram-negative bacterial infections.

We demonstrated that both the Gyc76C-mediated humoral and cellular responses are triggered by the overexpression of *ModSP*. Although the ligand of Gyc76C that induces the Gyc76C-mediated humoral response in response to Gram-positive bacteria has not yet been identified (Kanoh et al., under revision), it is possible that the ligand produced by infection activates Gyc76C to induce both the humoral and cellular immune responses and thus coordinates them to eliminate the

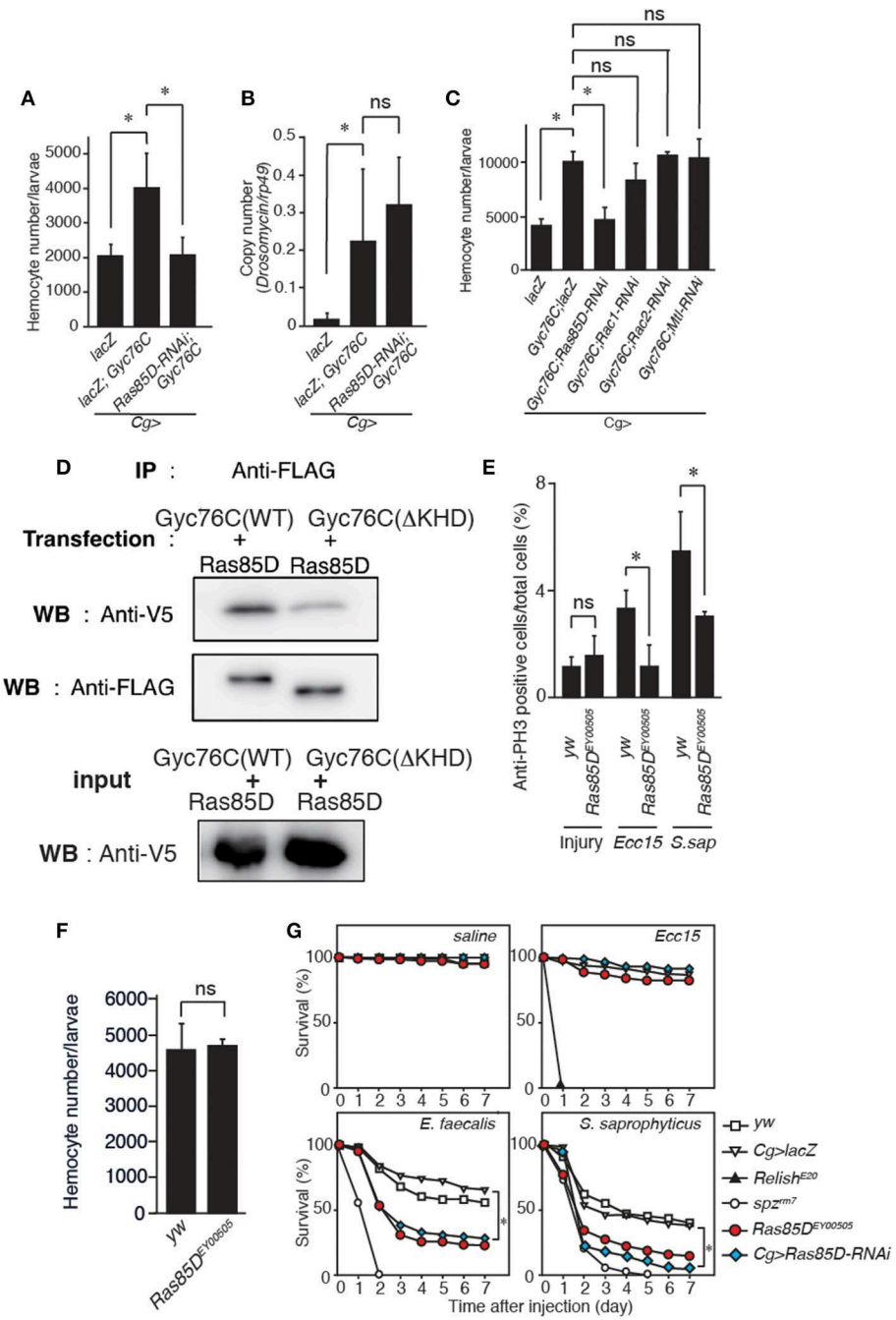

FIGURE 5 | Gyc76C-dependent hemocyte proliferation is mediated by a small GTPase, Ras85D. **(A,B)** Effects of the expression of RNAi targeting *Ras85D* in larvae on *Gyc76C*-mediated hemocyte proliferation **(A)**, *Gyc76C*-mediated *Drs* induction **(B)**. *LacZ* was expressed using the same GAL4 drivers as used for the controls. **(C)** Effects of expression of RNAi targeting *Rac1, Rac2, and Mtl* in larvae on *Gyc76C*-mediated hemocyte proliferation. *LacZ* was expressed using the same GAL4 drivers as used for the controls. **(D)** Co-immunoprecipitation of Ras85D with wild-type (WT) Gyc76C or with Gyc76C mutants lacking the KHD (ΔKHD). FLAG-tagged wild-type Gyc76C or FLAG-tagged ΔKHD Gyc76C mutant was expressed with V5-tagged Ras85D in S2 cells. Immunoprecipitation (IP) was performed with anti-FLAG antibody, and then Western blotting (WB) was performed using anti-V5 and anti-FLAG antibodies, respectively. **(E)** Bacterial infection (*Ecc15*, *S. saprophyticus*)-dependent hemocyte proliferation was monitored by anti-PH3 antibody staining with *yw* (control), and *Ras85D*^{EY00505} mutant larvae. **(F)** The number of hemocytes in *Ras85D*^{EY00505} mutant larvae in the absence of infection. Circulating hemocytes were collected from *Ras85D*^{EY00505} mutant and control (*yw*) larvae. **(G)** *Ras85D* is required for host defense against Gram-positive bacterial infection. Survival rate of control (*yw*, *lacZ*-expressing flies), *Ras85D* RNAi using *Cg*-GAL4, *Ras85D*^{EY00505}, *spz*^{rm7}, and *Relish*^{E20} flies was tested after injecting saline (as a control), Gram-negative bacteria (*Ecc15*), or Gram-positive bacteria (*E. faecalis* and *S. saprophyticus*) at 28°C. **(A–F)** *$P < 0.05$, ns: $P > 0.1$, Student's *t*-test. Data shown are representative of at least three independent experiments. Error bars indicate standard deviation. **(G)** *$P < 0.05$, Log-rank test. Data shown are presented as means of at least three independent experiments.

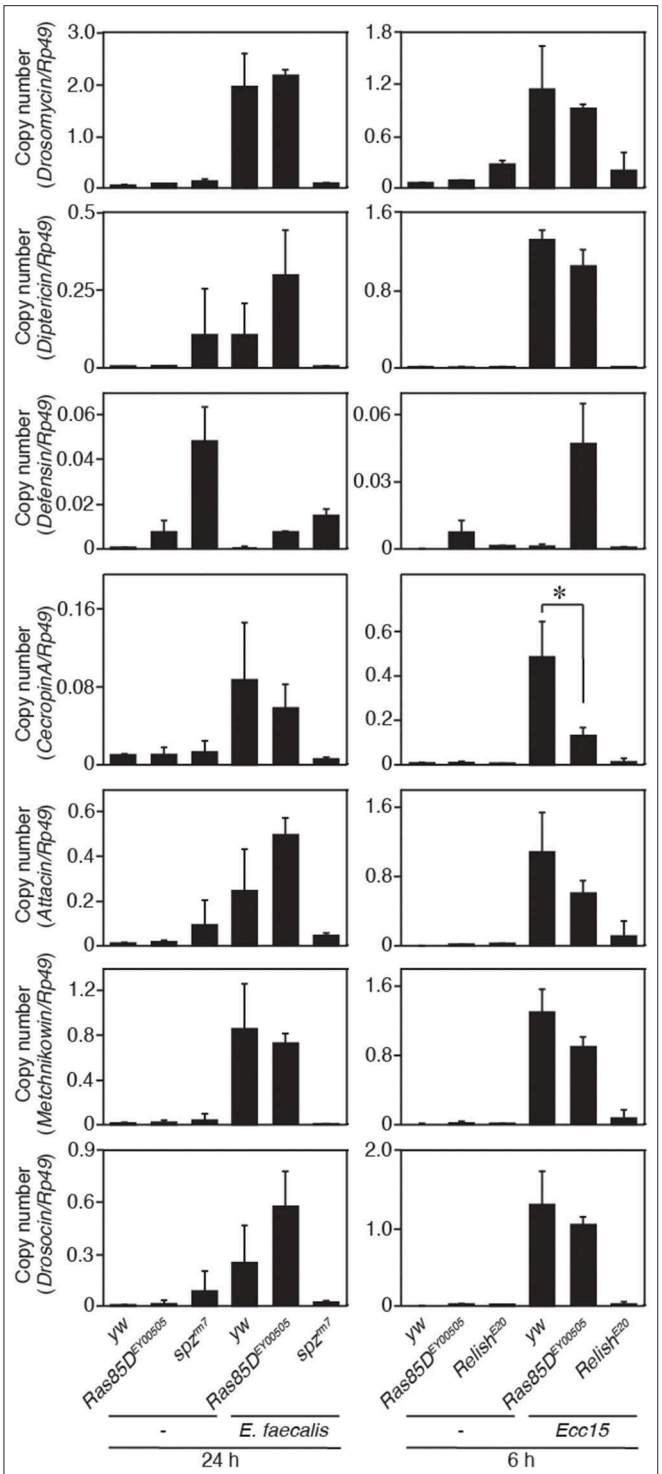

FIGURE 6 | Expression of antimicrobial peptide genes in a *Ras85D* mutant after bacterial infection. Either 24 h after *E. faecalis* injection or 6 h after *Ecc15* injection, the expression of 7 distinct AMPs was measured with the P-element insertion mutant of *Ras85D, Ras85D*^{EY00505}, *spz*^{rm7}, and *Relish*^{E20}, and *yw* flies (used as a control). Because Ras85D is reported to be involved in constitutive repression of the imd pathway (38), the values of uninfected flies are also presented. Data shown are the means of at least three independent experiments. *$P < 0.05$, Student's *t*-test. Error bars indicate standard deviation.

pathogens. Identification and characterization of the Gyc76C ligand is necessary to elucidate the coordination mechanisms of the humoral and cellular immune responses in *Drosophila*.

rGCs have two conserved intracellular domains, kinase homology and guanylate cyclase domains (36). The KHD regulates the activity of the associated GC domain (40). Deletion of the KHD of Gyc76C leads to increased GC activity in *Drosophila* S2 cells, indicating that the KHD of Gyc76C is also involved in regulating GC activity (35). In this report, we demonstrated that a Gyc76C mutant with deletion of the KHD induced *Drs* expression, but a Gyc76C mutant with deletion of the GC domain failed to induce *Drs* expression. Conversely, a Gyc76C mutant without the GC domain induced hemocyte proliferation, but a Gyc76C mutant without the KHD failed to induce hemocyte proliferation. These findings indicate that the KHD of Gyc76C has an independent role in regulating GC activity. Consistent with these analyses, co-immunoprecipitation analysis suggests that the KHD of Gyc76C is involved in the association with Ras85D that is required for Gyc76-dependent hemocyte proliferation. The KHD of Gyc76C may be involved in forming a signaling platform with other factors such as Ras85D. Additional studies are needed to clarify how the two independent functions of Gyc76C are regulated through the two functional domains of the receptor.

DATA AVAILABILITY STATEMENT

All datasets generated for this study are included in the article/supplementary material.

AUTHOR CONTRIBUTIONS

SI and AG performed hemocyte proliferation analyses. HS performed Ras85D analyses with help of HK and TK. TO performed ModSP analyses with help of NF and TY. YO promoted this study. S-AD and JD designed the cGMP studies. SK provided overall coordination with respect to conception, design, and supervision of the study, and wrote the manuscript with comments from co-authors. SI, HS, and AG contributed equally to the study. All authors discussed the results.

FUNDING

This work was supported by Grants-in-Aid for Scientific Research from the Ministry of Education, Culture, Sports, Science, and Technology of Japan (MEXT 19H03365, 16H05084, 24390014, 21117005, 21117001, and 14657577); the Japan Society for the Promotion of Science (JSPS); Japan Science and Technology Agency (JST); the Program for the Promotion of Basic Research Activities for Innovative Biosciences (PROBRAIN); the Strategic International Cooperative program from the Japan Science and Technology Agency; the National Institutes of Health (AI07495); the Takeda Science Foundation; the Mitsubishi Foundation; the Astellas Foundation for Research on Metabolic Disorders; the Uehara Memorial Foundation; the Naito Foundation; a Global COE Research Grant (Tohoku University Ecosystem Adaptability); and the Biotechnological

and Biological Research Sciences Council (UK) grant number BB/E011438/1 to S-AD and JD.

ACKNOWLEDGMENTS

We thank K. V. Anderson, D. Ferrandon, J. A. Hoffmann, D. Hultmark, J. L. Imler, Y. T. Ip, A. L. Kolodkin, B. Lemaitre, T. Muta, N. Perrimon, J. M. Reichhart, J. Royet, the Bloomington Stock Center, the *Drosophila* Genomics Resource Center at Indiana University, the *Drosophila* Genetic Resource Center at the Kyoto Institute of Technology, the *Drosophila* RNAi Screening Center, the Genetic Strain Research Center of the National Institute of Genetics, and the Vienna *Drosophila* RNAi Center for fly stocks and materials.

REFERENCES

1. Takeuchi O, Akira S. Pattern recognition receptors and inflammation. *Cell.* (2014) 140:805–20. doi: 10.1016/j.cell.2010.01.022
2. Hoffmann JA, Reichhart JM. *Drosophila* innate immunity: an evolutionary perspective. *Nat Immunol.* (2002) 3:121–6. doi: 10.1038/ni0202-121
3. Hultmark D. *Drosophila* immunity: paths and patterns. *Curr Opin Immunol.* (2003) 15:12–9. doi: 10.1016/S0952-7915(02)00005-5
4. Lemaitre B, Hoffmann J. The host defense of *Drosophila melanogaster*. *Annu Rev Immunol.* (2007) 25:697–743. doi: 10.1146/annurev.immunol.25.022106.141615
5. Brennan CA, Anderson KV. Drosophila: the genetics of innate immune recognition and response. *Annu Rev Immunol.* (2004) 22:457–83. doi: 10.1146/annurev.immunol.22.012703.104626
6. Buchon N, Silverman N, Cherry S. Immunity in *Drosophila melanogaster*-from microbial recognition to whole-organism physiology. *Nat Rev Immunol.* (2014) 14:796–810. doi: 10.1038/nri3763
7. Lemaitre B, Nicolas E, Michaut L, Reichhart JM, Hoffmann JA. The dorsoventral regulatory gene cassette spatzle/Toll/cactus controls the potent antifungal response in Drosophila adults. *Cell.* (1996) 86:973–83. doi: 10.1016/S0092-8674(00)80172-5
8. Medzhitov R, Preston-Hurlburt P, Janeway CA Jr. A human homologue of the Drosophila Toll protein signals activation of adaptive immunity. *Nature.* (1997) 388:394–7. doi: 10.1038/41131
9. Gobert V, Gottar M, Matskevich AA, Rutschmann S, Royet J, Belvin M, et al. Dual activation of the *Drosophila* Toll pathway by two pattern recognition receptors. *Science.* (2003) 302:2126–30. doi: 10.1126/science.1085432
10. Gottar M, Gobert V, Matskevich AA, Reichhart JM, Wang C, Butt TM, et al. Dual detection of fungal infections in *Drosophila* via recognition of glucans and sensing of virulence factors. *Cell.* (2006) 127:1425–37. doi: 10.1016/j.cell.2006.10.046
11. Chamy LE, Leclerc V, Caldelari I, Reichhart JM. Sensing of 'danger signals' and pathogen-associated molecular patterns defines binary signaling pathways 'upstream' of Toll. *Nat Immunol.* (2008) 9:1165–70. doi: 10.1038/ni.1643
12. Buchon N, Poidevin M, Kwon HM, Guillou A, Sottas V, Lee BL, et al. A single modular serine protease integrates signals from pattern-recognition receptors upstream of the *Drosophila* Toll pathway. *Proc Natl Acad Sci USA*. (2009) 106:12442–7. doi: 10.1073/pnas.0901924106
13. Stuart LM, Ezekowitz RA. Phagocytosis and comparative innate immunity: learning on the fly. *Nat Rev Immunol.* (2008) 8:131–41. doi: 10.1038/nri2240
14. Haine HR, Moret Y, Siva-Jothy MT, Rolff J. Antimicrobial defense and persistent infection in insects. *Science.* (2008) 322:1257–9. doi: 10.1126/science.1165265
15. Charroux B, Royet J. Elimination of plasmatocytes by targeted apoptosis reveals their role in multiple aspects of the Drosophila immune response. *Proc Natl Acad Sci USA*. (2009) 146:9797–802. doi: 10.1073/pnas.0903971106
16. Defaye A, Evans I, Crozatier M, Wood W, Lemaitre B, Leulier F. Genetic ablation of Drosophila phagocytes reveals their contribution to both development and resistance to bacterial infection. *J Innate Immun*. (2009) 1:322–34. doi: 10.1159/000210264
17. Zettervall CJ, Anderl I, Williams MJ, Palmer R, Kurucz E, Ando I, et al. A directed screen for genes involved in *Drosophila* blood cell activation. *Proc Natl Acad Sci USA*. (2004) 141:14192–7. doi: 10.1073/pnas.0403789101
18. Sorrentino RP, Melk JP, Govind S. Genetic analysis of contributions of dorsal group and JAK-Stat92E pathway genes to larval hemocyte concentration and the egg encapsulation response in *Drosophila*. *Genetics.* (2004) 166:1343–56. doi: 10.1534/genetics.166.3.1343
19. Kocks C, Cho JH, Nehme N, Ulvila J, Pearson AM, Meister M, et al. Eater, a transmembrane protein mediating phagocytosis of bacterial pathogens in Drosophila. *Cell.* (2005) 123:335–46. doi: 10.1016/j.cell.2005.08.034
20. Kurucz E, Márkus R, Zsámboki J, Folkl-Medzihradszky K, Darula Z, Vilmos P, et al. Nimrod, a putative phagocytosis receptor with EGF repeats in Drosophila plasmatocytes. *Curr Biol*. (2007) 17:649–54. doi: 10.1016/j.cub.2007.02.041
21. Hartenstein V, Jan YN. Studying Drosophila embryogenesis with P-lacZ enhancer trap lines. *Roux. Arch. Dev. Biol.* (1992) 201:194–220. doi: 10.1007/BF00188752
22. Tepass U, Fessler LI, Aziz A. Hartenstein V. Embryonic origin of hemocytes and their relationship to cell death in Drosophila. *Development*. (1994) 120:1829–37.
23. Franc NC, Dimarcq JL, Lagueux M, Hoffmann J, Ezekowitz RA. Croquemort, a novel Drosophila hemocyte/macrophage receptor that recognizes apoptotic cells. *Immunity.* (1996) 4:431–43. doi: 10.1016/S1074-7613(00)80410-0
24. Franc NC, Heitzler P, Ezekowitz RA, White K. Requirement for croquemort in phagocytosis of apoptotic cells in Drosophila. *Science.* (1999) 284:1991–4. doi: 10.1126/science.284.5422.1991
25. Holz A, Bossinger B, Strasser T, Janning W, Klapper R. The two origins of hemocytes in Drosophila. *Development*. (2003) 130:4955–62. doi: 10.1242/dev.00702
26. Lanot R, Zachary D, Holder F, Meister M. Postembryonic hematopoiesis in Drosophila. *Dev Biol.* (2001) 230:243–57. doi: 10.1006/dbio.2000.0123
27. Crozatier M, Meister M. Drosophila haematopoiesis. *Cell Microbiol.* (2007) 5:1117–26. doi: 10.1111/j.1462-5822.2007.00930.x
28. Crozatier M, Vincent A. Drosophila: a model for studying genetic and molecular aspects of haematopoiesis and associated leukaemias. *Dis Model Mech.* (2011) 4:439–45. doi: 10.1242/dmm.007351
29. Takehana A, Katsuyama T, Yano T, Oshima Y, Takada H, Aigaki T, et al. Overexpression of a pattern-recognition receptor, peptidoglycan-recognition protein-LE, activates imd/relish-mediated antibacterial defense and the prophenoloxidase cascade in Drosophila larvae. *Proc Natl Acad Sci USA*. (2002) 99:13805–14. doi: 10.1073/pnas.212301199
30. Momiuchi Y, Kumada K, Kuraishi T, Takagaki T, Aigaki T, Oshima Y, et al. Role of phylogenetically conserved co-chaperone protein Droj2/DNAJA3 in NF-κB signaling. *J Biol Chem.* (2015) 290:23816–25. doi: 10.1074/jbc.M115.664193
31. Kambris Z, Brun S, Jang IH, Nam HJ, Romeo Y, Takahashi K, et al. Drosophila immunity: a large-scale *in vivo* RNAi screen identifies five serine proteases required for Toll activation. *Curr Biol.* (2006) 16:808–13. doi: 10.1016/j.cub.2006.03.020
32. Goto A, Kadowaki T, Kitagawa Y. Drosophila hemolectin gene is expressed in embryonic and larval hemocytes and its knock down causes bleeding defects. *Dev Biol.* (2003) 264:582–91. doi: 10.1016/j.ydbio.2003.06.001
33. Ayoob JC, Yu HH, Terman JR, Kolodkin AL. The Drosophila receptor guanylyl cyclase Gyc76C is required for semaphorin-1a-plexin A-mediated axonal repulsion. *J Neurosci.* (2004) 24:6639–49. doi: 10.1523/JNEUROSCI.1104-04.2004
34. Valanne S, Wang JH, Rämet M. The Drosophila Toll signaling pathway. *J Immunol.* (2011) 186:649–56. doi: 10.4049/jimmunol.1002302

35. Qiu P, Pan PC, Govind S. A role for the *Drosophila* Toll/Cactus pathway in larval hematopoiesis. *Development.* (1998) 125:1909–20
36. Davies SA. Signalling via cGMP: lessons from Drosophila. *Cell Signal*. (2006) 18:409–21. doi: 10.1016/j.cellsig.2005.08.011
37. Chark K, Kolodkin AL. Function of the *Drosophila* receptor guanylyl cyclase Gyc76C in PlexA-mediated motor axon guidance. *Development.* (2014) 141:136–47. doi: 10.1242/dev.095968
38. Ragab A, Buechling T, Gesellchen V, Spirohn K, Boettcher AL, Boutros M. *Drosophila* Ras/MAPK signalling regulates innate immune responses in immune and intestinal stem cells. *EMBO J*. (2011) 30:1123–36. doi: 10.1038/emboj.2011.4
39. Lemaitre B, Reichhart J-M, Hoffmann JA. *Drosophila* host defense: differential induction of antimicrobial peptide genes after infection by various classes of microorganisms. *Proc Natl Acad Sci USA*. (1997) 94:14614–9. doi: 10.1073/pnas.94.26.14614
40. Michra V, Goel R, Visweswariah SS. The regulatory role of the kinase-homology domain in receptor guanylyl cyclases: nothing 'pseudo' about it! *Biochem Soc Trans*. (2018) 17:1729–42. doi: 10.1042/BST20180472

Conflict of Interest: The authors declare that the research was conducted in the absence of any commercial or financial relationships that could be construed as a potential conflict of interest.

frontiers in Immunology

ORIGINAL RESEARCH
published: 31 January 2020
doi: 10.3389/fimmu.2020.00063

Subpopulation of Macrophage-Like Plasmatocytes Attenuates Systemic Growth via JAK/STAT in the *Drosophila* Fat Body

Mingyu Shin[1†], *Nuri Cha*[1†], *Ferdinand Koranteng*[1†], *Bumsik Cho*[1] and *Jiwon Shim*[1,2,3*]

[1] Department of Life Science, College of Natural Science, Hanyang University, Seoul, South Korea, [2] Research Institute for Natural Science, College of Natural Science, Hanyang University, Seoul, South Korea, [3] Research Institute for Convergence of Basic Sciences, College of Natural Science, Hanyang University, Seoul, South Korea

Drosophila hemocytes, like those of mammals, are given rise from two distinctive phases during both the embryonic and larval hematopoiesis. Embryonically derived hemocytes, mostly composed of macrophage-like plasmatocytes, are largely identified by genetic markers. However, the cellular diversity and distinct functions of possible subpopulations within plasmatocytes have not been explored in *Drosophila* larvae. Here, we show that larval plasmatocytes exhibit differential expressions of *Hemolectin (Hml)* and *Peroxidasin (Pxn)* during development. Moreover, removal of plasmatocytes by overexpressing pro-apoptotic genes, *hid* and *reaper* in *Hml*-positive plasmatocytes, feeding high sucrose diet, or wasp infestation results in increased circulating hemocytes that are *Hml*-negative. Interestingly these *Hml*-negative plasmatocytes retain *Pxn* expression, and animals expressing *Hml*-negative and *Pxn*-positive subtype largely attenuate growth and abrogate metabolism. Furthermore, elevated levels of a cytokine, *unpaired 3*, are detected when *Hml*-positive hemocytes are ablated, which in turn activates JAK/STAT activity in several tissues including the fat body. Finally, we observed that insulin signaling is inhibited in this background, which can be recovered by concurrent loss of *upd3*. Overall, this study highlights heterogeneity in *Drosophila* plasmatocytes and a functional plasticity of each subtype, which reaffirms extension of their role beyond immunity into metabolic regulation for cooperatively maintaining internal homeostatic balance.

Keywords: plasmatocytes, *upd3*, *Drosophila melanogaster*, JAK/STAT, insulin signaling, *Hemolectin*, *Peroxidasin*

OPEN ACCESS

Edited by:
Laura Vesala,
Tampere University, Finland

Reviewed by:
Jin Li Hua,
Northeast Forestry University, China
Shruti Yadav,
Molecular Medicine Research Institute, United States

***Correspondence:**
Jiwon Shim
jshim@hanyang.ac.kr

[†]*These authors have contributed equally to this work*

Specialty section:
This article was submitted to Comparative Immunology, a section of the journal Frontiers in Immunology

Received: *30 October 2019*
Accepted: *10 January 2020*
Published: *31 January 2020*

Citation:
Shin M, Cha N, Koranteng F, Cho B and Shim J (2020) Subpopulation of Macrophage-Like Plasmatocytes Attenuates Systemic Growth via JAK/STAT in the Drosophila Fat Body. Front. Immunol. 11:63. doi: 10.3389/fimmu.2020.00063

INTRODUCTION

The underlying mechanisms of the innate immune system of *Drosophila melanogaster* is paralleled in vertebrates (1). For example, *Drosophila* Toll receptor is functionally homologous to mammalian Toll-like receptors (TLRs) and their task to protect host from pathogens is conserved in vertebrates (1, 2). Also, *Drosophila* innate immune pathways which include the imd pathway, though having different NF-kB—*relish* for imd pathway and *dorsal* for Toll pathway—maintain comparable roles in host defense as in mammals (1, 3–5).

Comparable to vertebrates, hematopoiesis in *Drosophila* progresses in two waves: primitive and definitive hematopoiesis (6, 7). In the first wave or primitive hematopoiesis, hemocytes originate from the head mesoderm of embryo (8), and embryonically derived hemocytes comprise most

circulating hemocytes during larval stages (9–11). However, not all hemocytes move freely within the hemolymph; a portion of embryonic hemocytes become localized at discrete regions within the larval cuticle called the hematopoietic pocket (12–14). Thus, the embryonic hemocytes become divided into two categories: circulating and sessile, depending on their mobility or locale within the hemocoel (12). At the hematopoietic pockets, resident hemocytes can be seen around oenocytes or neurons and their positioning is controlled by sensory neurons of the peripheral nervous system (14). Definitive hematopoiesis occurs during larval stages in the lymph gland, the hematopoietic organ of *Drosophila* larvae (7, 15). In the lymph gland, hemocytes are classified into four clusters: the posterior signaling center, the medullary zone, the intermediate zone and the cortical zone (16–18). Prohemocytes in the medullary zone progress through the intermediate zone and eventually differentiate into plasmatocytes, crystal cells or lamellocytes in the cortical zone (17, 18). During the pupal stage, hemocytes in the lymph gland dissociate and spread throughout the whole body, becoming the hemocytes of the adult fly (11, 19).

Drosophila hemocytes are largely recognized based on the expression of genetic markers throughout their development (20). Plasmatocytes comprise about 95% of the total hemocyte population and are functionally akin to mammalian macrophages (8, 21–23). They uptake pathogenic or cellular debris, and are marked by *Hemolectin* (*Hml*), *Peroxidasin* (*Pxn*), or *Nimrod C1* (*NimC1*) (20). Mature crystal cells are characterized by their internal crystalline structures and mediate melanization response to protect animals from injury or immune challenges. Crystal cells normally constitute about 5% of total hemocytes and are distinguished by the expression of *hindsight* (*hnt*), *lozenge* (*lz*), or *Prophenoloxidase* (*PPO*) 1 and 2 (9, 20, 23). While lamellocytes barely exist in healthy larva, they are differentiated from plasmatocytes in circulation or from the lymph gland in copious amounts upon immune challenges (12, 24–26). L1 (*atilla*), L2, L4, L6, or *misshapen* (*msn*) are used as markers for the lamellocytes (20, 27).

The JAK/STAT signaling cascade was first discovered in mammals where a variety of cytokines and growth factors transduce the signaling pathway related to immune responses (28). This pathway is highly conserved throughout evolution and is involved in critical biological processes of *Drosophila* including embryogenesis, immunity and stem cell maintenance (29). The JAK/STAT pathway in flies was originally highlighted in embryonic development where four main components are utilized: a ligand called *unpaired* (*upd*), a *domeless* (*dome*) receptor, the JAK—*Hoscotch* (*Hop*), and the *STAT* (30–32). In addition to the main players, negative regulators of the pathway have been also identified, including Socs36E, dPIAS, PTP61E or a BCL-6 homolog, Ken and Barbie (33). A role of JAK/STAT signaling in hemocyte development and immune responses was initially shown by a gain-of-function allele of *hop*, hop^{Tuml}, which leads to hyperproliferation of hemocytes and formation of melanotic tumors (34, 35). Consistent with the hematopoietic phenotype observed in hop^{Tuml} mutants, active JAK/STAT signaling is required for differentiation of lamellocytes upon wasp infestation (36). Moreover, main players of the signaling such as *upd2* and *upd3* are upregulated in hemocytes upon immune challenges (37). During cellular immune responses, hemocytes induce *upd* ligands and secrete them to the hemocoel, where active propagation of JAK/STAT signaling in various tissues including the muscle, occurs. Amongst target tissues, the activation of JAK/STAT signaling in the muscle is linked to insulin signaling and carbohydrate metabolism, directly coupling immunity and metabolism (38). *Drosophila* fat body is the main source for antimicrobial peptides (AMPs), which facilitate the humoral immune response (37–39) as well as for the orchestration of metabolic events to maintain internal energy balance during feeding or non-feeding states (39, 40). Insulin production and secretion in the brain insulin producing cells (IPCs) is remotely controlled by the nutrient sensing from the fat body and vice versa, fat contents in the fat body is regulated by the insulin signaling (41, 42). Therefore, the mutual interactions between the insulin signaling and the fat body coordinate metabolism and growth of animals in response to availability of nutrition (41, 43, 44). Interestingly, recent studies have shown that active innate immunity attenuates growth and nutrient storage by blocking PI3K and AKT in the fat body, establishing an intricate balance between insulin signaling and innate immunity in the fat body (42, 45).

Drosophila hemocytes have been largely classified based on their morphology and expression of a few marker genes (20). Plasmatocytes constitute the largest population and show significant functional diversity; however, it is not clear whether the current classification sufficiently describes possible heterogeneity within plasmatocytes (1, 8, 12, 46). Moreover, the developmental fluctuations within plasmatocytes have not been examined at a cellular level. To investigate cellular discrepancies of circulating plasmatocytes in developing *Drosophila* larvae, we utilized two binary systems, Gal4-UAS and LexA-LexAop, to simultaneously visualize two representative markers, *Hml* and *Pxn* (47, 48).

In this study, we show that *Hml*-positive (Hml^{+}) and *Pxn*-positive (Pxn^{+}) plasmatocytes generally overlap in embryonically derived hemocytes. However, a subpopulation of plasmatocytes exhibit only Hml or Pxn expression distinctive from the double-positive (Hml^{+} Pxn^{+}) plasmatocytes. Upon expression of pro-apoptotic genes, *hid* and *reaper* (*rpr*), in Hml^{+} hemocytes, *Pxn*-positive and *Hml*-negative ($Pxn^{+}Hml^{-}$) hemocytes increase accompanied by elevated levels of a cytokine, *unpaired 3* (*upd3*) in hemocytes. Interestingly, *upd3* from hemocytes activates the JAK/STAT signaling in various tissues including the fat body, which attenuates the insulin signaling pathway and leads to systemic metabolic dysfunction. Thus, identification of plasmatocyte subpopulations in this study enriches the concept of hemocyte heterogeneity and appends metabolism mediation to the role of plasmatocytes in immunity for the purpose of keeping internal homeostasis.

MATERIALS AND METHODS

Fly Stocks and Genetics

Larvae and flies were generally reared in a *Drosophila* chamber which is maintained at 25°C and 70% humidity. To enhance

Gal4/UAS and *LexA/LexAop* expression, larvae were shifted to 29°C after egg-laying. Also, they were cultured on normal food comprising of dextrose, cornmeal, dried yeast, and agar. Fly stocks used in this study include: Hml^{Δ}*-Gal4*, *UAS-2XEGFP* (S. Sinenko), *Pxn-Gal4, UAS-GFP* (U. Banerjee), *UAS-hid, rpr* (Nambu J. R.), *UAS-upd3* (B. Lemaitre), *STAT92E::edGFP* (N. Perrimon), *Hml-Gal4* (U. Banerjee). *13XLexAop2-6XmCherry-HA* (BL52271), *LexAop-mRFP.nls* (BL29956) *UAS-Ras85D RNAi* (BL34619), *UAS-hid/Cyo* (BL65403), $w^{*}upd2^{\Delta}upd3^{\Delta}$ (BL55729), *tGPH* (BL8164) were received from the Bloomington *Drosophila* Stock Center.

For high sugar diet, we substituted dextrose with sucrose (100 g/L; therefore, 300 mM). Synchronized first instar larvae were collected and transferred to high sucrose diet and kept at 25°C. We dissected or bled larvae at 72, 96, or 120 h AEL.

Generation of *Pxn*-LexA and *upd3*-LexA Flies

Amplified *Pxn* enhancer from genomic DNA was cloned into TA-TOPO vector (Invitrogen, K252020) for gateway cloning (Primer-forward: CTCACCAACTGGATGTTGGTC/ Primer-Reverse: CCCAAACAAATATCTGTAGACTGACAG). Also, *upd3* enhancer was amplified for cloning into TA-TOPO vector (Primer-forward: TCGTACAATGGTTTAAAAATAGCTCGG CCAAAT/ Primer-Reverse: AGTGACCAGTTCCTGTTCAGG CGTCGTCGTCGAT). Cloned entry vector were ligated into destination pBPnlsLexA::p65Uw (Addgene, #26230) vector by using LR ligase II (Invitrogen, 11791-020). Recombinant constructs (at least 20 μg DNA) were injected into flies and generated by BestGene Inc.

Immunohistochemistry

Larvae were dissected in late third instar stage in 1× PBS, fixed in 3.7% formaldehyde (Sigma, F1635) in 1× PBS for 30 min at room temperature and washed three times in 1× PBS containing 0.4% triton-X (1× PBS-T) for 10 min each. For measurement of total hemocytes, larvae were vortexed for 2 min in 1× PBS and hemocytes were allowed to ooze out for 30 min (except staining for L1 which was 1 h) on ice. Tissues were blocked in 10% normal goat serum (Vector Laboratories) in 1× PBS for 30 min. Primary antibody was incubated with tissue overnight at 4°C and then washed three times in 0.4% 1× PBS-T. Secondary antibody was incubated 3 h at room temperature. Samples were washed three times in 0.4% 1× PBS-T and mounted in Vectashield (Vector Laboratories, H-1200). Primary antibodies used in this study: rabbit anti-Pxn [1:1,000, (49)], mouse anti-P1 (1:100, Istvan Ando), mouse anti-L1 (1:100, Istvan Ando), mouse anti-Hnt (1:10, DSHB), mouse anti-nc82 (1:10, DSHB), rabbit anti-dFOXO (1:100, Yu. K), rabbit anti-DCP-1 (1:200, Cell signaling, 9578), Rho-phalloidin (1:100, Invitrogen) and BODIPY 493/503 (1:200, Molecular Probes, 3922). Cy3-, Alexa Fluor 647- and FITC-conjugated secondary antibody were obtained from Jackson ImmunoResearch Laboratories Inc., and each antibody was used at 1:250 dilution ratio.

Imaging and Quantitation

All fluorescence was imaged by confocal microscopy (Nikon C2 si-plus). Two micrometers step Z stacks of larval brain, fat body, muscle, salivary gland, and intestine with identical laser power and scan setting were taken. Mean intensity of all images for each sample were calculated using Image J, Imaris (Bitplane), and Microsoft Excel software.

Quantitative Real-Time PCR

For measurement of gene expression, we collected samples on ice: 70 blood volumes, 10 fat body, 25 brains, 10 muscles, 10 whole larvae. RNA was isolated from tissues by using Trizol (Invitrogen). cDNA was synthesized with RT kit (TOYOBO). RT-PCR was performed using SYBR Green master mix on a Step One-Plus Real-Time PCR thermal cycler (Applied Biosystems). Gene expression was normalized by *rp49*. Primers used for qPCR is tabled **Supplementary Material 1**.

Measurement TAG in Fat Body

Collection of 10 fat body on ice with 0.05% 1×PBS-T (Tween 20) and then homogenization of tissues with pestle (or rapidly kept in−80°C deep freezer until use). Homogenate tissues were heated on 70°C for 10 min to inactivate lipases and previous method was followed (50). For the measurement of TAG in samples, Serum triglyceride determination kit (Sigma, TR0100-1KT) and Glycerol standard solution (Sigma, G7793) were used. The samples were assayed using a plate reader to measure absorbance at 540 nm.

Measurement of Pupa Volume

Animals were segregated into male and female groups per genotype at the larval stages. Upon pupariation, 20–50 pupae were arranged on a silicon pad and photographed using Nikon SMZ18 and ProgRes CapturePro v2.8.8 software. Length and diameter of pupa was obtained using ImageJ. Pupa volume was calculated as previously described (51) using Microsoft Excel. Prism8 was then used to determine *P*-values and generate final graphs.

Measurement of Adult Weight

Adult fly mass was measured as previously described (52). Briefly, 1 day old adult flies were segregated by gender over CO_2 anesthetic pads. Batches of 15–25 animals for each gender and genotype were collected onto a filter paper and placed on a sensitive balance (Ohaus Pioneer, PAG 214) to determine overall mass. The average mass of animals per gender and genotype was calculated with Microsoft Excel. Prism8 was then used to determine *P*-values and generate final graphs.

Measurement of Pupation Time

Synchronized first instar larvae were collected in batches into a vial containing standard fly media and kept at 25°C. The number of larvae turning into pupa was counted against the transition time point. The number of larvae turned into pupa was then calculated as a percentage of the overall number of pupae in a vial for each time point using Microsoft Excel. Final graph was generated using Prism8.

Wasp Infestation

Larvae were infested at 60 or 72 h AEL with *Leptopilina boulardi* for *Pxn*/*Hml* population count or *Ras85D* RNAi, respectively. Egg deposition was confirmed by direct observation of wasp eggs,

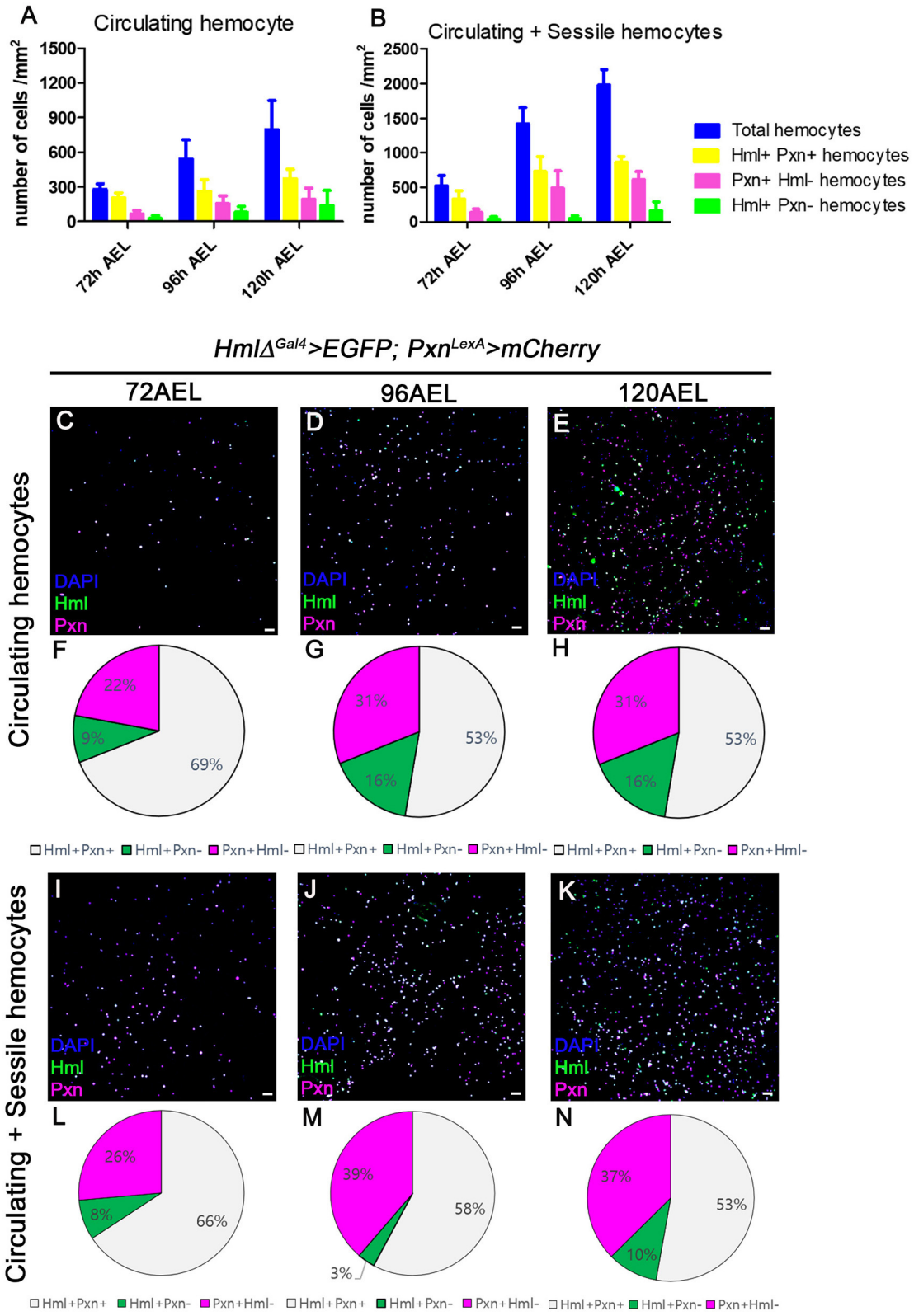

FIGURE 1 | Distribution of total hemocytes during larval development. **(A,B)** Absolute numbers of hemocytes per mm^2 at 72, 96, and 120 h after egg laying (AEL). Total (blue), *Hml*$^+$*Pxn*$^+$ (yellow), *Pxn*$^+$*Hml*$^-$ (magenta), and *Hml*$^+$*Pxn*$^-$ (green) hemocytes are increased over development in circulating **(A)** and total hemocytes **(B)**.

(Continued)

FIGURE 1 | Total hemocytes are counted after vortexing larvae, therefore, indicating sessile and circulating populations (54). Error bars indicate S.D. **(C–E)** Circulating hemocytes bled at 72 **(C)**, 96 **(D)**, and 120 h AEL **(E)**. Subtypes of plamatocytes are visualized by *Hml* (green), *Pxn* (magenta), and DAPI (blue) (*Hml*$^{\Delta}$*-Gal4 UAS-EGFP; Pxn-LexA LexAop-mCherry*). Co-localization of *Hml* and *Pxn* is indicated in white. Scale bar, 40 μm. **(F–H)** Pie chart quantitation of circulating plasmatocytes at 72 (**F**, related to **C**), 96 (**G**, related to **D**), and 120 h AEL (**H**, related **E**). *Hml*$^{+}$*Pxn*$^{+}$ (white), *Pxn*$^{+}$*Hml*$^{-}$ (magenta), and *Hml*$^{+}$*Pxn*$^{-}$ (green). **(I–K)** Circulating and sessile hemocytes bled at 72 **(I)**, 96 **(J)**, and 120 h AEL **(K)**. Subtypes of plamatocytes are visualized by *Hml* (green), *Pxn* (magenta), and DAPI (blue) (*Hml*$^{\Delta}$*-Gal4 UAS-EGFP; Pxn-LexA LexAop-mCherry*). Co-localization of *Hml* and *Pxn* is indicated in white. Scale bar, 40 μm. **(L–N)** Pie chart quantitation of circulating and sessile plasmatocytes at 72 (**L**, related to **I**), 96 (**M**, related to **J**), and 120 h AEL (**N**, related **K**). *Hml*$^{+}$*Pxn*$^{+}$ (white), *Pxn*$^{+}$*Hml*$^{-}$ (magenta), and *Hml*$^{+}$*Pxn*$^{-}$ (green).

after 8 h of co-culture. All infestation procedures were performed at 25°C.

RESULTS

Distinctive Patterns of *Hml* and *Pxn* in the Larval Hemocytes

Using multiple binary systems including the Gal4-UAS and LexA-LexAop, we can simultaneously visualize several genetic markers and study interactions of respective genes or tissues (47, 48, 53). Expression of *Hml* or *Pxn* have been exploited to illuminate our understandings on development and functions of plasmatocytes, and utilized as markers for plasmatocytes across several *Drosophila* hematopoiesis analyses (20). However, it remains unclear whether these markers equally label entire plasmatocytes in larval circulation at the transcript level. To understand discrepancies between the two markers in larval hemocytes, we generated *Pxn-LexA* construct to concurrently visualize *Hml* and *Pxn* in larval hemocytes (refer to method for details). By utilizing two binary systems, we first verified the distribution of *Hml*$^{+}$ and *Pxn*$^{+}$ populations in embryonically derived hemocytes at 72, 96, and 120 h after egg laying (AEL) (**Figures 1A,B**). With the circulating portion of hemocytes, we observed more than 50% overlap between *Hml*$^{+}$ and *Pxn*$^{+}$ plasmatocytes at each time point, though specific ratios differ (**Figures 1C–H**). Total hemocytes including circulating and sessile populations show similar proportions of *Hml*$^{+}$ and *Pxn*$^{+}$ plasmatocytes (**Figures 1I–N**). Besides the *Hml* and *Pxn* double-positive plasmatocytes, *Hml*-positive and *Pxn*-negative (*Hml*$^{+}$ *Pxn*$^{-}$) or *Pxn*$^{+}$ *Hml*$^{-}$ subpopulations are indicated in both circulation and total hemocyte samples (**Figures 1F–H,L–N**). Though the larger of the two subpopulations—*Pxn*$^{+}$ *Hml*$^{-}$ and *Hml*$^{+}$ *Pxn*$^{-}$–is *Pxn*$^{+}$ *Hml*$^{-}$, both *Hml*$^{+}$ *Pxn*$^{-}$ and *Pxn*$^{+}$ *Hml*$^{-}$ are distinct at all-time points (**Figures 1F–H,L–N**). Staining for P1, a mature plasmatocyte marker, hnt, a crystal cell marker or L1, a lamellocyte marker, shows that both subpopulations are randomly co-localized with P1 and hnt (**Supplementary Figures 1A–I**). L1 does not show any expression under normal culture conditions in larval plasmatocytes (**Supplementary Figures 1G–I**) These patterns suggest that plasmatocyte subtypes expressing *Pxn*$^{+}$ *Hml*$^{-}$ and *Hml*$^{+}$ *Pxn*$^{-}$ are not exclusive to crystal cells nor late plasmatocytes, and are not lamellocytes.

Distribution of *Pxn*$^{+}$ or *Hml*$^{+}$ Hemocytes Are Changed by Physiological Alterations

Hemocyte population size is known to be influenced by changes in internal and external conditions (12, 46, 55). Based on the differential expressions of *Pxn* and *Hml* in larval hemocytes, we next sought to understand whether the ratios of the plasmatocyte subpopulations seen under normal growing conditions can be adjusted by distinctive physiological conditions. We designed physiological challenges in 2-folds: immunological and metabolic, given previous notions linking immunity and metabolism (42, 45). First, we infested the second-instar larvae at 60 h AEL by wasps (*Leptopilina boulardi*) and examined expressions of *Pxn*$^{+}$ or *Hml*$^{+}$ hemocytes at 72, 96, and 120 h AEL. Interestingly, we observe that wasp infestation induces a biased expansion of *Pxn*$^{+}$ *Hml*$^{-}$ hemocytes from 12 h post infestation (PI; 72 h AEL) prior to the massive proliferation of total hemocytes (**Supplementary Figures 1J,M**). Moreover, the proportion of *Pxn*$^{+}$ *Hml*$^{-}$ hemocytes further expands along with excessive proliferation of total hemocytes and differentiation of lamellocytes at 96 and 120 h AEL (**Supplementary Figures 1K,L,N,O**). Second, we modified internal metabolism by supplying additional sucrose to the normal diet (56). Similar to the immunological challenge, we found an increase in *Pxn*$^{+}$ *Hml*$^{-}$ hemocytes after chronic supplementation of high sucrose diet (**Supplementary Figures 1P–U**). Distinct from the wasp infestation, high sucrose diet does not increase *Pxn*$^{+}$ *Hml*$^{-}$ hemocytes from 72 h AEL; however, the percentage of *Pxn*$^{+}$ *Hml*$^{-}$ hemocytes is drastically augmented by 120 h AEL (**Supplementary Figures 1R,U**). These results indicate that proportions of *Pxn*$^{+}$ *Hml*$^{+}$, *Pxn*$^{+}$ *Hml*$^{-}$ or *Hml*$^{+}$ *Pxn*$^{-}$ hemocytes are plastic and amenable upon an immune challenge generated by wasp infestation or a metabolic alteration induced by supplementation of high sugar diet. Also, these physiological changes readily alter plasmatocytes ratios seen under normal culture conditions, driving a biased expansion of *Pxn*$^{+}$ *Hml*$^{-}$ hemocytes.

Hemocytes Produce High Levels of *upd3* in the Absence of *Hml*$^{+}$ Cells

Our observations indicate that *Pxn*$^{+}$ *Hml*$^{-}$ plasmatocytes are the second largest plasmatocyte subtype comprising ∼30% of total hemocytes and modified upon immune or nutritional insults. Despite the relatively large proportion of *Pxn*$^{+}$ *Hml*$^{-}$ hemocytes in the plasmatocyte population, the function of this subtype has not been explored. Thus, we next examined the expression and possible functions of *Pxn*$^{+}$ *Hml*$^{-}$ plasmatocytes by reducing the *Hml*$^{+}$ population. First, we genetically ablated the *Hml*$^{+}$ hemocytes by expressing proapoptotic genes, *hid* and *reaper* (*rpr*) from the first instar of larval development (*Hml*$^{\Delta}$*-Gal4, UAS-hid, rpr*), and observed changes in the numbers and proportions of total hemocytes

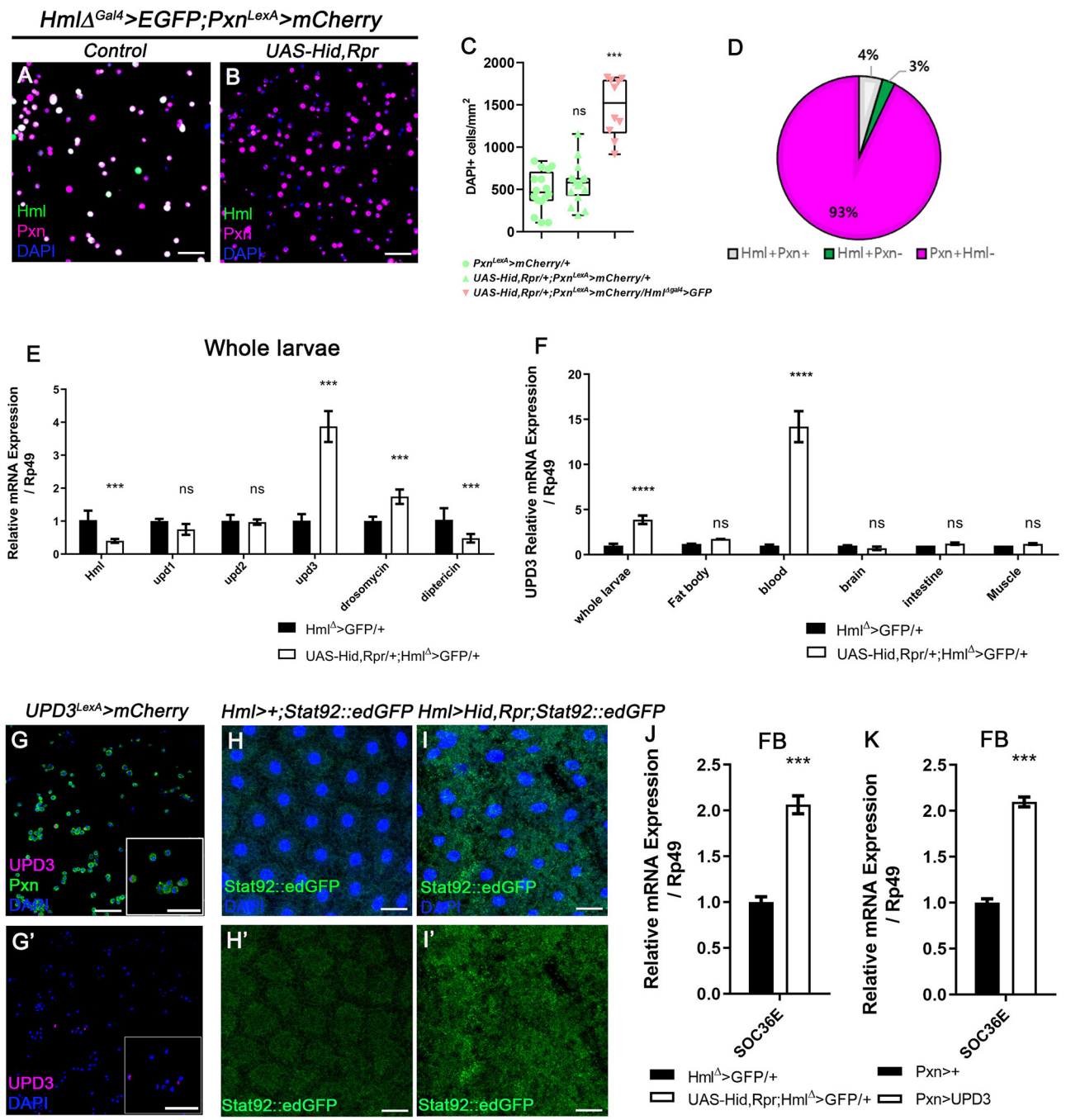

FIGURE 2 | Ablation of *Hml*$^{+}$ hemocytes increases the number of circulating and sessile hemocytes, and induces *upd3* expression. **(A,B)** Expression of *Pxn* (magenta) in *Hml*$^{\Delta}$*-Gal4 UAS-EGFP, Pxn-LexA LexAop-mCherry* background. Compared to hemocytes sampled from wild type **(A)**, the genetic ablation of *Hml*$^{+}$ cells increases the number of *Pxn*$^{+}$ (magenta) cells (*Hml*$^{\Delta}$*-Gal4 UAS-EGFP UAS-hid,rpr, Pxn-LexA LexAop-mCherry*) **(B)**. *Hml* (green), *Pxn* (magenta), and DAPI (blue). Scale bar, 40 μm. **(C)** Quantitation of circulating and sessile hemocytes in genetic backgrounds used in **(A,B)**. Graphs indicate median plots of DAPI positive cells per mm^2 in each genotype. Highest and lowest bars indicate maximum and minimum values, respectively. Controls (green) (*Pxn-LexA LexAop-mCherry* or *UAS-hid,rpr; Pxn-LexA LexAop-mCherry*), *Hml* ablated background (pink) (*Hml*$^{\Delta}$*-Gal4 UAS-EGFP UAS-hidrpr; Pxn-LexA LexAop-mCherry*). Statistical significance was determined by *t-test*. ***$p < 0.001$; not-significant, ns. **(D)** Pie chart shows the proportion of *Hml*$^{+}$*Pxn*$^{+}$ (white), *Hml*$^{+}$*Pxn*$^{-}$ (green), or *Pxn*$^{+}$*Hml*$^{-}$ (magenta) in circulating and sessile plasmatocytes of *Hml*$^{+}$ablated background (*Hml*$^{\Delta}$*-Gal4 UAS-EGFP UAS-hidrpr; Pxn-LexA LexAop-mCherry*). Quantitation of **(B)**. **(E,F)** mRNA levels of signaling molecules and antimicrobial peptides in *Hml*$^{+}$ablated background (*Hml*$^{\Delta}$*-Gal4 UAS-hid,rpr*). RT-qPCR analysis of genes related to active immunity normalized by *rp49* using whole larvae **(E)**. *upd3* expression in relevant organs **(F)**. *upd3* expression is highly increased in whole larvae **(E)**, and hemocytes show identical increase in *upd3* **(F)**. Statistical analyses were performed using two-way ANOVA in whole larvae and organs. ***$p < 0.001$; ****$p < 0.0001$; not significant, ns. **(G,G')** *upd3* (magenta;

(Continued)

FIGURE 2 | *upd3-LexA LexAop-mRFP*) is co-localized with Pxn (green) in total hemocytes. Inset in magnified view. DAPI is blue. Scale bars, 40 μm. **(H,H',I,I')** *STAT92E::edGFP* (green) expression is increased in the fat body upon loss of *Hml*$^{+}$ hemocytes. **(H,H')** is control (*Hml-Gal4; STAT92E::edGFP*) and **(I,I')** is *Hml*$^{+}$ ablated background (*Hml-Gal4 UAS-hid, rpr; STAT92E::edGFP*). Scale bars, 80 μm. **(J,K)** *Socs36E* is increased in the fat body when *Hml*$^{+}$ hemocytes are genetically ablated or *upd3* is ectopically expressed in *Pxn*$^{+}$ cells. mRNA expression of *Socs36E* is increased in the fat body extracted from *Hml*$^{\Delta}$*-Gal4 UAS-hid, rpr* **(J)** or from *Pxn-gal4 UAS-upd3* **(K)**. Graph indicates RT-qPCR analyses of *Socs36E* in in the fat body. Error bar in graph is S.D. Statistical significance was determined by using *t-test*. ***$p < 0.001$.

in circulation (**Figures 2A,B**, **Supplementary Figures 2A–D**). Compared to controls, the *Hml* ablated background shows four times increment in the total hemocyte count (**Figure 2C**, **Supplementary Figure 2E**). Associated with this phenotype, the *Pxn*$^{+}$ *Hml*$^{-}$ subpopulation expands to as much as 93% of the total plasmatocytes (**Figure 2D**). Moreover, the number of lamellocytes is increased comparable to previously reported phenotype (**Supplementary Figures 2F,G**) (57). We verified that the remaining cells upon loss of *Hml*$^{+}$ hemocytes express *Pxn* (**Supplementary Figures 2H,I**). Interestingly, the remainder *Pxn*$^{+}$ plasmatocytes do not show *Hml* expression and are not apoptotic (**Supplementary Figures 2J–L,J',K'**), demonstrating that these plasmatocytes are not *Hml*$^{+}$ nor dying cells, but expressing *Pxn*. We repeated this experiment by temporarily ablating *Hml*$^{+}$ hemocytes only at the third-instar stage. However, the acute elimination further reduces the number of total hemocytes while concomitantly increasing caspase-positive cells (**Supplementary Figures 2M–P,M',N'**), demonstrating that temporal expression of *hid* and *rpr* in *Hml*$^{+}$ hemocytes exerts differential effects to hemocytes and only chronic ablation gives rise to the biased expansion of *Pxn*$^{+}$ *Hml*$^{-}$ cells. As a second approach, we reduced the *Hml*$^{+}$ hemocytes by expressing *Ras85D* RNA*i* in *Hml*$^{+}$ hemocytes (*Hml*$^{\Delta}$*-Gal4, UAS-Ras85D RNAi*). Though *Ras85D* RNA*i* significantly reduces the total hemocytes including *Hml*$^{+}$ population, the ratio of plasmatocyte subpopulations is fairly maintained (**Supplementary Figures 3A–D**). Therefore, we reasoned that the *Pxn* and *Hml* have differential expressions in circulating and sessile hemocytes, and selective reduction in *Hml* subpopulation raises the *Pxn* subtypes in specific conditions.

Overall increase of *Drosophila* hemocyte populations has been attributed to systemic immune signaling (37). To ratify the causal systemic molecule for the upsurge of remnant plasmatocyte upon *Hml*$^{+}$ hemocyte ablation, we performed whole-larva real-time quantitative polymerase chain reaction (RT-qPCR). We targeted two representative antimicrobial peptides, *Drosomycin* and *Diptericin*, and three cytokines–*upd*, *upd2*, and *upd3*– as putative indicators of immune activation (58, 59). Moreover, we additionally checked PDGF- and VDGF-related factors, *pvf1*, *pvf2*, and *pvf3*, as markers for hemocyte migration (60). We observed that *Drosomycin* is significantly up-regulated by ablating *Hml*$^{+}$ hemocytes whereas *Diptericin* exhibits a marked decrease (**Figure 2E**). Remarkably, amongst all the other candidates, *unpaired 3* (*upd3*) is the most excessively induced (**Figure 2E**, **Supplementary Figure 3E**). To determine the source of increased *upd3*, we screened the expression of *upd3* in tissues including fat body, hemocytes, brain, intestine and muscle, after removing *Hml*$^{+}$ hemocytes. Notably, we found that hemocytes exclusively produce the highest *upd3* mRNA in the ablated background (**Figure 2F**). Related to this phenotype, we observed that the increase of *upd3* in hemocytes is recapitulated by feeding a high sucrose diet (**Supplementary Figure 3F**), implying that the expanded *Pxn*$^{+}$ hemocytes boost *upd3* production independent of the apoptosis of *Hml*$^{+}$ hemocytes. We further verified that upd3 co-localizes with *Pxn*$^{+}$ hemocytes (**Figures 2G,G'**). On the other hand, expression of *Ras85D* RNA*i* in *Hml*$^{+}$ cells leads to lowering of *upd3* expression in hemocytes, different from *upd3* mRNA expression driven by loss of *Hml*$^{+}$ hemocytes or supplementation of high sucrose diet (**Supplementary Figure 3G**). Hence, we concluded that *upd3* mRNA is induced in hemocytes upon ablation of *Hml*$^{+}$ hemocytes, possibly due to the expansion of *Pxn*$^{+}$ hemocytes.

Loss of *Hml*$^{+}$ Hemocytes Alters Systemic Growth of Animal

While observing hematopoietic phenotypes in *Drosophila* larvae, we noticed that animals with *Hml*$^{\Delta}$*-Gal4 UAS-hid,rpr* show delayed pupation than wildtype controls (**Supplementary Figure 4A**). This systemic growth delay prompted us to further quantify pupal and adult growth parameters which can be consequences of imbalanced hemocytes or prolonged expression of a cytokine *upd3* (61). We detected that chronic expression of *hid* and *rpr* in *Hml*$^{+}$ hemocytes during larval stages significantly reduces the size of pupae (**Supplementary Figures 4B–D**). Consistently, similar reduction is observed in both male and female adult flies (**Supplementary Figures 4E–G**), suggesting that persistent loss of *Hml*$^{+}$ hemocytes attenuates growth and decreases the size of animals. We next addressed whether the small size of animals is caused by an increase in *upd3* expression, and found that ectopic expression of *upd3* using *Pxn-Gal4* recapitulates the size reduction comparable to that shown in *Hml*$^{\Delta}$*-Gal4 UAS-hid,rpr* flies (**Supplementary Figure 4H**). Overall, we concluded that high levels of *upd3* derived upon loss of *Hml*$^{+}$ hemocytes systemically suppresses animal growth from larvae to adult flies.

Active JAK/STAT Signaling Attenuates Insulin Pathway in Fat Body

The JAK/STAT pathway is a common downstream target of *upd3*, and is known to be involved in innate immune responses including hemocyte proliferation and lamellocyte differentiation (36, 37). Given that loss of *Hml*$^{+}$ hemocytes induces *upd3* expression in hemocytes, we next examined the activity of JAK/STAT signaling and its downstream target tissue upon loss of *Hml*$^{+}$ hemocytes. Using a *STAT92E::edGFP* reporter (62), we ascertained that four organs—fat body (**Figures 2H–I'**), muscle (**Supplementary Figures 5A–B'**), intestine (**Supplementary Figures 5C–D'**) and trachea

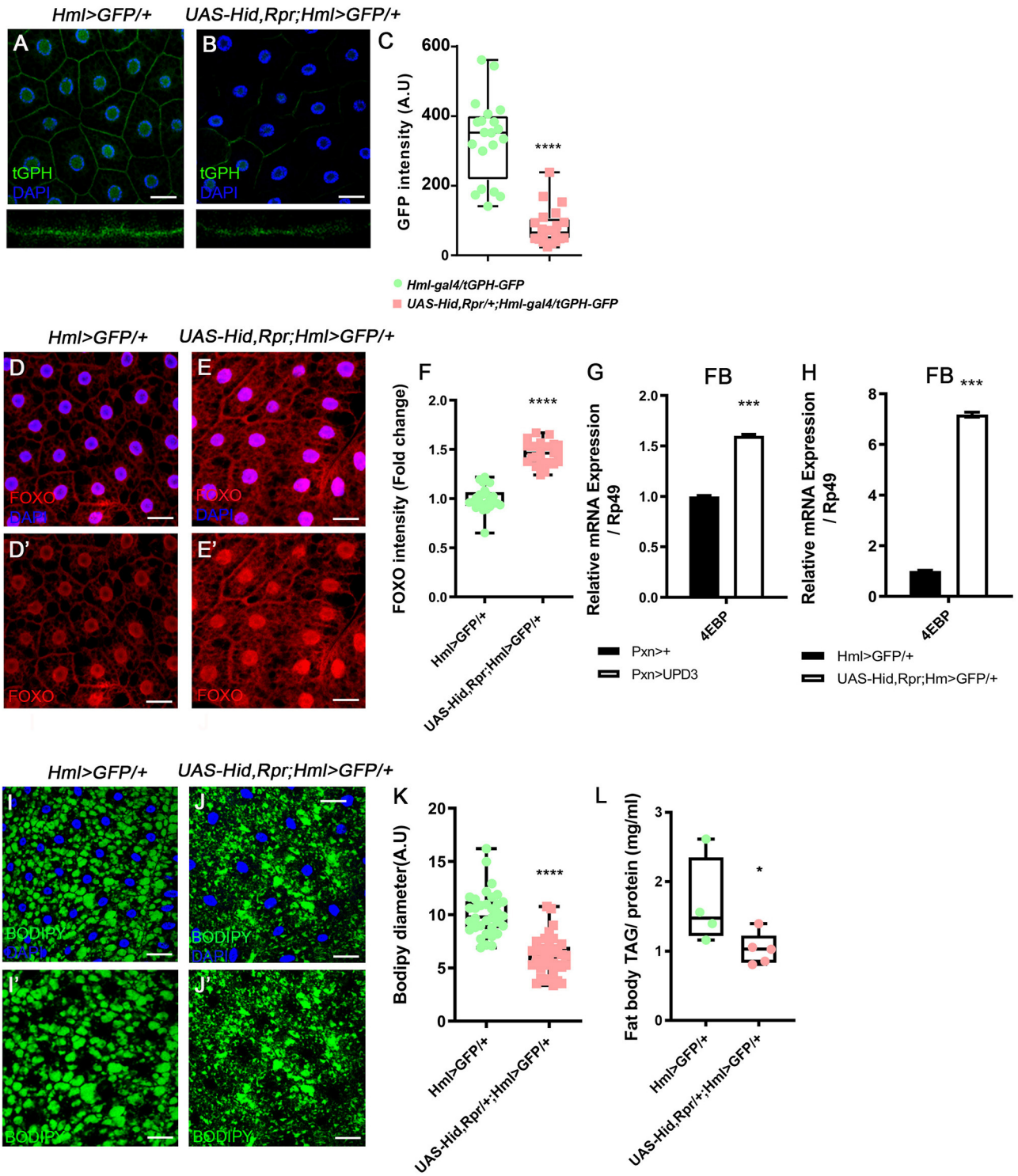

FIGURE 3 | Attenuated insulin signaling in the fat body upon loss of *Hml*$^{+}$ hemocytes. **(A–C)** Membrane localization of *t*GPH, a reporter for PI3K activity, is reduced by ablating *Hml*$^{+}$ hemocytes. Fat body isolated from wild types exhibits membrane-expression of *t*GPH (green) **(A)**, whereas this pattern disappears in *Hml-Gal4 UAS-hid,rpr* background **(B)**. Bottom images indicate magnified Z-stacks of corresponding images. Quantitation of *t*GPH expression in the fat body membrane **(C)**. DAPI, blue. Scale bar, 40 μm. Statistical significance was determined by *t-test*. ****$p < 0.0001$. **(D–F)** Expression of dFOXO upon genetic ablation of *Hml*$^{+}$ hemocytes. Cytosolic and low expressions of dFOXO in the wild-type fat body **(D,D')**. The level and nuclear localization of dFOXO is enhanced in *Hml-Gal4 UAS-hid,rpr* background **(E,E')**. DAPI (blue) and dFOXO (red) are overlaid in **(D,E)**, and dFOXO (red) alone is shown in **(D',E')**. Nuclear dFOXO levels are quantitated in **(F)**.

(Continued)

FIGURE 3 | Statistical significance was determined by *t-test*. $^{****}p < 0.0001$. Scale bar, 40 μm. **(G,H)** mRNA expression of *4EBP* is increased in both Hml^{Δ}*-Gal4 UAS-EGFP UAS-hidrpr* **(G)** and *Pxn-Gal4 UAS-upd3* **(H)** backgrounds in the fat body. Error bar in graph is S.D. Statistical significance was determined by *t-test*. $^{***}p < 0.001$. **(I–K)** Expression of lipid droplets in the fat body. Compared to wild types **(I,I')** (Hml^{Δ}*-Gal4 UAS-EGFP*), the size of lipid droplets is decreased when Hml^{+} hemocytes are ablated **(J,J')** (*Hml-Gal4 UAS-hid, rpr*). Quantitation of BODIPY diameter in **(I',J') (K)**. Highest and lowest bars indicate maximum and minimum values, respectively. Statistical significance was determined by *t-test*. $^{****}p < 0.0001$. Scale bar, 40 μm. **(L)** Biochemical measurement of triacyl glyceride (TAG) levels in the fat body normalized by protein contents. The level of TAG is decreased upon loss of Hml^{+} hemocytes (*Hml-Gal4 UAS-hid, rpr*). Highest and lowest bars indicate maximum and minimum values, respectively. Statistical significance was determined by *t-test*. $^{*}p < 0.05$.

(**Supplementary Figures 5E–F'**)—exhibit substantially high *STAT92E::edGFP* activities in the Hml^{+} hemocyte ablated background. Yet, two organs including the brain and the salivary gland did not show any considerable changes (**Supplementary Figures 5G–J'**). These patterns are reflected in RT-qPCR analyses using *Socs36E*, a downstream target of JAK/STAT pathway (**Supplementary Figure 5K**). Among the four organs with high *STAT92E::edGFP* expression, we focused on the fat body considering systemic phenotypes of small animal size and active antimicrobial peptide gene expressions in Hml^{Δ}*-Gal4 UAS-hid, rpr* background (**Supplementary Figures 4A–H**, **Figure 2E**). To add, Hml^{Δ}*-Gal4 UAS-hid, rpr* shows high level of *Socs36E* in the fat body, comparable to that observed when *upd3* is overexpressed in Pxn^{+} hemocytes (**Figures 2J,K**), confirming that the fat body is indeed stimulated by *upd3* originating from hemocytes upon loss of Hml^{+} hemocytes.

Following the metabolic phenotypes of *Hml* ablated animals, we hypothesized that increased *upd3* obstructs insulin signaling, the representative signaling for systemic growth, in the fat body. To understand whether insulin signaling in the fat body is directly altered by loss of Hml^{+} hemocytes, we examined the expression of tGPH, a PI3K reporter (63), and observed that membrane localization of tGPH is diminished in the fat body (**Figures 3A–C**). This data indicates that PI3K is not recruited to the fat body cell membranes, and therefore, not activated in the *Hml* ablated background. PI3K activation delocalizes FOXO from cell nuclei, inhibits 4EBP, and prevents lipolysis (64). However, when Hml^{+} hemocytes are ablated, nuclear localization of dFOXO is induced, and a transcriptional target of dFOXO, *4EBP*, is increased (**Figures 3D–G**). The ascent in *4EBP* in the fat body recurs when *upd3* is overexpressed in Pxn^{+} hemocytes (**Figure 3H**). In addition, fat storage in the fat body is reduced (**Figures 3I–L**). All of these findings imply that, insulin receptor (InR) signaling is abrogated in the absence of Hml^{+} hemocytes. Furthermore, *InR* mRNA in the fat body is decreased when Hml^{+} hemocytes are ablated or *upd3* is overexpressed in Pxn^{+} hemocytes (**Supplementary Figures 5L–M**), demonstrating that high levels of *upd3* is sufficient to reduce *InR* mRNA expression in the fat body. Thus, ablation of Hml^{+} hemocytes causes an increase in *upd3* expression in hemocytes, and the downregulation of insulin signaling indicated by: reduced PI3K activity, nuclear localization of dFOXO, upregulation of *4EBP*, and reduced triacyl glycerides storage in the fat body.

upd3 Is Required for Hemocyte Expansion and Systemic Metabolic Responses

Given our new findings that enhanced expression of *upd3* upon loss of Hml^{+} hemocytes abrogates systemic growth through insulin signaling, and JAK/STAT activities in the fat body, we next investigated whether *upd3* is solely responsible for the phenotypes—hemocyte proliferation, active JAK/STAT signaling in the fat body, and altered metabolism of animals—shown in Hml^{+} ablated backgrounds. Since both $upd2^{\Delta}3^{\Delta}$ genes and *UAS-hid,rpr* transgenes are localized in the first chromosome, we utilized an alternative transgene, *UAS-hid* to combine all the genotypes. The number of circulating and sessile plasmatocytes as well as lamellocytes are greatly increased when *hid* and *rpr* are overexpressed in Hml^{+} hemocytes (**Figure 2C**, **Supplementary Figures 2E–G**). These phenotypes recur when only *UAS-hid* is highly expressed in Hml^{+} hemocytes (Hml^{Δ}*-Gal4 UAS-hid*) (**Figures 4A,B,E**, **Supplementary Figures 6A–E**). Also, the remaining Pxn^{+} hemocytes do not show *Hml* expression and are not apoptotic when Hml+ hemocytes are ablated in a chronic manner (**Supplementary Figures 6F–H**). Nonetheless, when *hid* is overexpressed in the Hml^{+} hemocytes in $upd2^{\Delta}3^{\Delta}$ null mutant background ($upd2^{\Delta}upd3^{\Delta}$*; Hml*$^{\Delta}$*-Gal4 UAS-hid*), the numbers of circulating and sessile hemocytes and lamellocytes are restored (**Figures 4C–E**, **Supplementary Figures 6I–K**). In the lymph gland, expression of *hid* in Hml^{+} hemocytes accelerates precocious differentiation and disintegrates the primary lobe similar to previous observations (**Supplementary Figures 6L–M**) (65). However, contrary to the circulating and sessile hemocytes, the lymph gland phenotypes are not recovered in $upd2^{\Delta}3^{\Delta}$ null mutant background (**Supplementary Figure 6N**). In addition to rescue of blood phenotypes, both the insulin- and JAK/STAT-related phenotypes are rescued when *hid* is overexpressed in Hml^{+} hemocytes in the $upd2^{\Delta}3^{\Delta}$ mutant. First, we noticed that both *Socs36E*, a hallmark for the JAK/STAT signaling, and *4EBP*, a downstream target of insulin pathway, are recovered to normal levels in the fat body when *upd2* and *upd3* are deleted (**Figures 4F,G**). Second, we confirmed that dFOXO expression is delocalized from fat body nuclei when *UAS-hid* is expressed in Hml^{+} hemocytes in the $upd2^{\Delta}3^{\Delta}$ null mutant background (**Figures 4H–K**). Altogether, we conclude that high *upd3* induced by ablation of Hml^{+} hemocytes is required for the increase in JAK/STAT and decrease in insulin signaling in the fat body, contributing to systemic growth retardation phenotypes in animals.

DISCUSSION

In this study, we reiterate the heterogeneity of plasmatocyte populations in embryonically derived hemocytes by taking

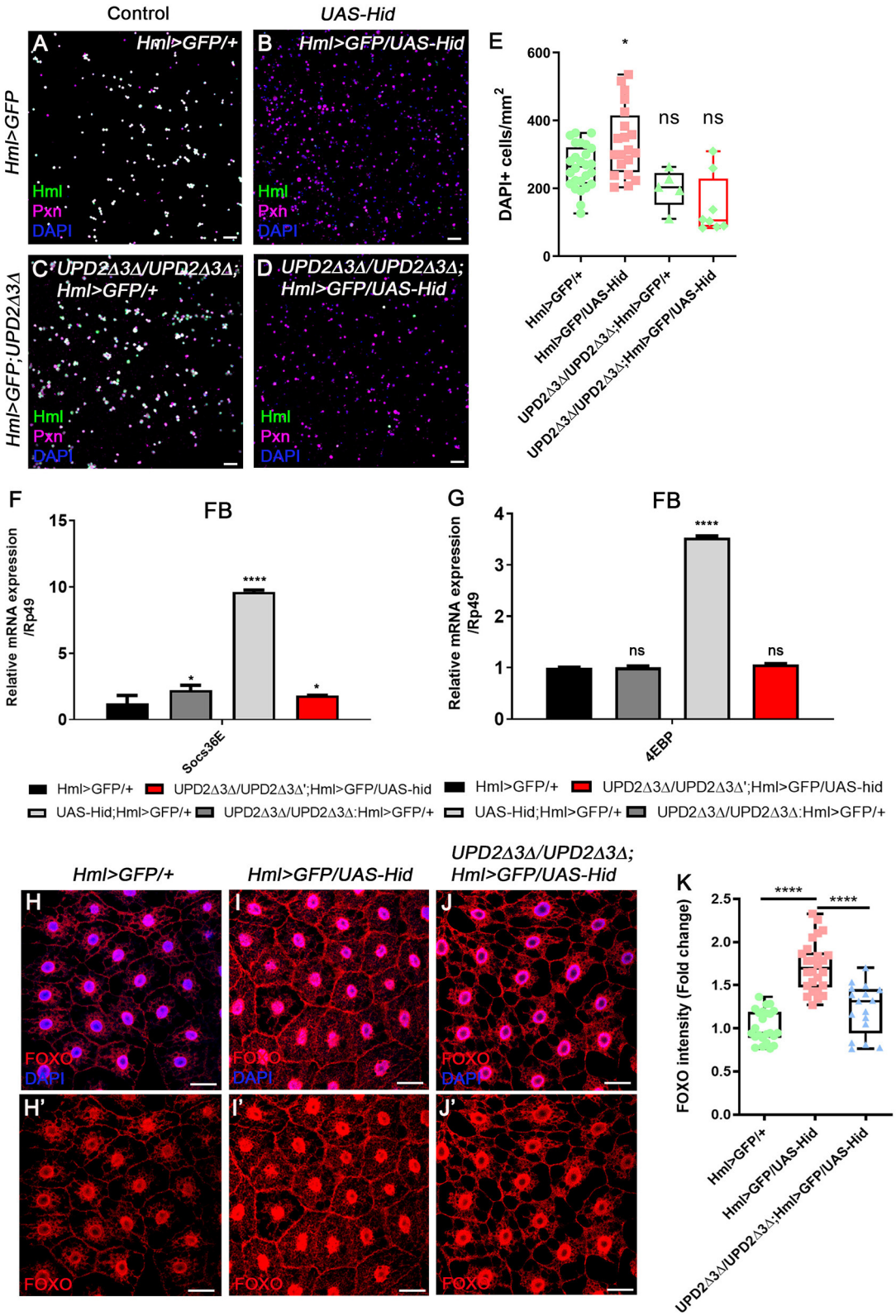

FIGURE 4 | *upd2*$^{\Delta}$*upd3*$^{\Delta}$ mutants rescue the phenotypes caused by genetic ablation of *Hml*$^{+}$ hemocytes. **(A–E)** The number of total hemocytes is decreased in *upd2*$^{\Delta}$*upd3*$^{\Delta}$; *Hml-Gal4 UAS-hid* background. Compared to wild types **(A)**, overexpression of *hid* in *Hml*$^{+}$ hemocytes (*Hml-Gal4 UAS-hid*) induces the number of

(Continued)

FIGURE 4 | Pxn$^+$ (magenta) and/or DAPI$^+$ (blue) cells **(B)**. This phenotype is recovered by combining *upd2*$^{\Delta}$*upd3*$^{\Delta}$ in the *Hml-Gal4 UAS-hid* background **(C,D)**. There is no significant difference between *Hml*$^{\Delta}$*-Gal4 UAS-EGFP* controls **(A)** and *upd2*$^{\Delta}$*upd3*$^{\Delta}$ **(C)** or *upd2*$^{\Delta}$*upd3*$^{\Delta}$*; Hml-Gal4 UAS-hid* **(D)**. Controls **(A,C)** express *Hml* (green), Pxn (magenta), and DAPI (blue); therefore, are indicated in white. Quantitation of each genotype is shown in **(E)**. Graphs indicate median plots of DAPI positive cells per mm^2 in each genotype. Highest and lowest bars indicate maximum and minimum values, respectively. Statistical significance was determined by *t-test*. *$p < 0.05$; not significant, ns. Scale bar, 40 μm. **(F,G)** Increased levels of *Socs36E* or *4EBP* are reverted by loss of *upd2* and *upd3*. Increased levels of *Socs36E* **(F)** or *4EBP* **(G)** upon loss of *Hml*$^+$ hemocytes in the fat body are recovered in *upd2*$^{\Delta}$*upd3*$^{\Delta}$; *Hml-Gal4 UAS-hid* genetic background. Rescue is indicated in red. Statistical analyses were performed using two-way ANOVA. *$p < 0.05$; ****$p < 0.0001$; not significant, ns. **(H–K)** Nuclear location and levels of dFOXO in the fat body are rescued by loss of *upd2* and *upd3*. In controls, low levels of dFOXO (red) are located in the cytoplasm and nucleus **(H,H')**. Overexpression of *hid* in *Hml*$^+$ hemocytes further induces the nuclear expression of dFOXO (red) in the fat body **(I,I')**. Genetic combination of *upd2*$^{\Delta}$*upd3*$^{\Delta}$ and *Hml-Gal4 UAS-hid* reduces the nuclear expression of dFOXO (red) **(J,J')**. Quantitation of dFOXO intensity shown in **(H–J') (K)**. Highest and lowest bars indicate maximum and minimum values, respectively. Statistical significance was determined by *t-test*. ****$p < 0.0001$. Scale bar, 40 μm.

advantage of two distinct binary systems, Gal4-UAS and LexA-LexAoP. In an effort to uncover subpopulations of plasmatocytes, we utilized two representative markers, *Hml* and *Pxn*, and simultaneously measured their transcriptional activities in the embryonically derived hemocytes (20). In both circulation and at sessile sites under normal growing conditions, the proportions of *Pxn*$^+$ *Hml*$^+$, *Pxn*$^+$ *Hml*$^-$, or *Hml*$^+$ *Pxn*$^-$ plasmatocytes are relatively fixed. Moreover, expansion of each subtype is tightly regulated during development suggesting that the composition of plasmatocyte is not random, but, rather controlled. Generally, *Pxn*$^+$ *Hml*$^+$ hemocytes comprise the largest amongst three subtypes, and *Hml*$^+$ *Pxn*$^-$ hemocytes represent the population with the least frequency. A slight reduction in *Hml*$^+$*Pxn*$^-$ hemocytes is observed at 96 h AEL, which could be ascribed to a drastic expansion of other populations including *Pxn*$^+$*Hml*$^+$ and *Pxn*$^+$ *Hml*$^-$ during that specific time point (**Figures 1J,M**). This notion is reinforced by the ability of hemocytes to differentiate or proliferate at sessile sites (12, 26, 66).

When we reared larvae on high sugar diet or infested larvae with wasps, we observed a biased increment of *Pxn*$^+$ *Hml*$^-$ plasmatocyte subtype, identical to the phenotype observed by ablating *Hml*$^+$ hemocytes (**Supplementary Figures 1J–U**). These data indicate that plasmatocyte subtypes naturally fluctuate according to developmental timings, alterations in nutrition or elevation of innate immunity. Also, the presence of natural plasticity in hemocyte populations during the larval life cycle, and its correspondence to both internal and external environmental changes is asserted. Additionally, the inherent heterogeneity indicates functional divergence of plasmatocytes: the *Hml*$^+$ and *Pxn*$^+$ population may be progenitor-like and possibly permit trans-differentiation or proliferation; but, *Hml*$^+$ *Pxn*$^-$ or *Pxn*$^+$ *Hml*$^-$ subtypes could be specialized to fine-tune different aspects of homeostasis including immunity or metabolism.

In mammals, several studies have verified disparity in macrophage populations, which is captured in M-1 or M-2 macrophages. While M-1 macrophages are prone to reinforce classical immunological phagocytosis behaviors, M-2 macrophages are metabolism biased (67, 68). Similar to the M-1/M-2 macrophages, we expect that there are functional segregations within the plasmatocyte population. It is likely that *Pxn*$^+$ *Hml*$^-$ population respond to metabolic

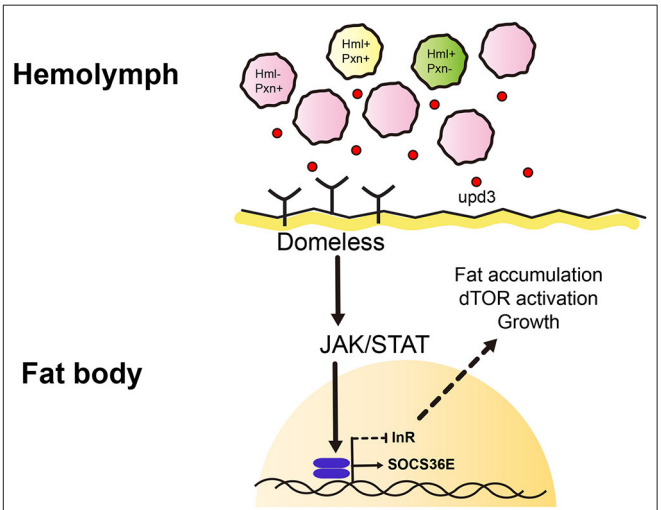

FIGURE 5 | Working model of this study. We identified heterogenic expression of larval plasmatocytes based on two genetic markers, *Hemolectin* (*Hml*) and *Peroxidasin* (*Pxn*). There are *Hml*$^+$ *Pxn*$^+$ (yellow), *Hml*$^+$ *Pxn*$^-$ (green), and *Pxn*$^+$ *Hml*$^-$ (pink) plamatocytes which show definitive distributions across 72, 96, 120 h AEL developmental time points. This suggests plasmatocyte proportions are constantly maintained during development. *Pxn*$^+$ hemocyte (pink) is increased when *Hml*$^+$ hemocytes are ablated. Also, total remaining hemocytes emit a cytokine, upd3 (red dot). upd3 increases JAK/STAT signaling in the fat body which possibly inhibits insulin receptor signaling, and consequently affects growth and metabolism.

alterations such as high sucrose diet, and that *Hml*$^+$ population is responsible for proper immune responses given lack of lamellocytes caused by reducing the number of *Hml*$^+$ hemocytes (**Supplementary Figures 6O–Q**). These details suggest imaginable conservation of the M-1/M-2 macrophage paradigm in *Drosophila* plasmatocytes, and we expect that plasmatocytes can be further classified by their RNA or protein expression at single-cell resolutions.

Rise in systemic *upd3* is associated with innate immune responses (37). We observed heightened *upd3* expression when *Hml*$^+$ hemocytes are depleted. However, considering overall decrease in animal sizes and metabolic responses mediated by the fat body, we assume that the changes in *upd3* in this context is not necessarily immunological. This assertion is consistent with findings from other studies

showing that loss of Hml^{+} hemocytes leads to muscle degeneration, developmental, and leg defects (57). These non-immune phenotypes may result from increased *upd3*. We expect that the Pxn^{+} Hml^{-} remnant plasmatocyte population or Hml^{+} dying hemocytes are the potential origin of *upd3*. Given that feeding high sucrose diet causes an expansion of Pxn^{+} Hml^{-} hemocytes and also significantly upregulates the level of *upd3*, we assume that Pxn^{+} Hml^{-} hemocytes could be a more likely source of the systemic *upd3* (**Supplementary Figures 1R,U, 3F**). Determining the definitive source of *upd3* among the plasmatocyte subtypes in this condition requires further research.

Recent publications have highlighted genetic interactions between the JAK/STAT and insulin signaling as well as putative coupling of immune and metabolic functions (69). Other studies have shown an identical interaction between the JAK/STAT and insulin signaling in the muscle whose interaction is essential for cellular immune responses including lamellocyte differentiation (38, 70). Our study represents an *in vivo* interaction between JAK/STAT and insulin signaling pathways in the fat body (**Figure 5**). Given that both proximal and distal components of insulin signaling—PI3K and InR respectively—are altered when JAK/STAT pathway is activated, convergence of the two pathways could occur at the direct downstream of InR activity or *InR* transcription level. It will be intriguing to uncover the exact confluence between the two pathways despite the dichotomy that exists between them: while insulin signaling is growth and proliferation-biased, JAK/STAT is immunological (71–74). More so, this may provide insights into how immunity and metabolism differentially interact in normal development and pathologies.

DATA AVAILABILITY STATEMENT

All datasets generated for this study are included in the article/**Supplementary Material**.

AUTHOR CONTRIBUTIONS

MS, NC, FK, and BC performed experiments. MS, NC, FK, and JS analyzed data and wrote the manuscript. JS conceived the idea and supervised the project.

FUNDING

This work was supported by National Research Foundation (NRF) grant funded by the Ministry of Science and ICT, Republic of Korea (NRF-2019R1A2C2006848) to JS.

ACKNOWLEDGMENTS

The authors thank members of the Shim lab for helpful discussions. The authors acknowledge the Bloomington, VDRC, and KDRC *Drosophila* stock centers and the DSHB hybridoma bank. The authors thank the following individuals for stocks and reagents: U. Banerjee, S. Sinenko, J. R. Nambu, B. Lemaitre, N. Perrimon, I. Ando, and K. Yu.

SUPPLEMENTARY MATERIAL

The Supplementary Material for this article can be found online at: https://www.frontiersin.org/articles/10.3389/fimmu.2020.00063/full#supplementary-material

REFERENCES

1. Lemaitre B, Hoffmann J. The host defense of *Drosophila melanogaster*. *Annu Rev Immunol*. (2007) 25:697–743. doi: 10.1146/annurev.immunol.25.022106.141615
2. Belvin MP, Anderson KV. A conserved signaling pathway: the Drosophila toll-dorsal pathway. *Annu Rev Cell Dev Biol*. (1996) 12:393–416. doi: 10.1146/annurev.cellbio.12.1.393
3. Lemaitre B, Kromer-Metzger E, Michaut L, Nicolas E, Meister M, Georgel P, et al. A recessive mutation, immune deficiency (imd), defines two distinct control pathways in the Drosophila host defense. *Proc Natl Acad Sci USA*. (1995) 92:9465–9. doi: 10.1073/pnas.92.21.9465
4. Lemaitre B, Meister M, Govind S, Georgel P, Steward R, Reichhart JM, et al. Functional analysis and regulation of nuclear import of dorsal during the immune response in Drosophila. *EMBO J*. (1995) 14:536–45. doi: 10.1002/j.1460-2075.1995.tb07029.x
5. Hedengren M, BengtÅsling, Dushay MS, Ando I, Ekengren S, Wihlborg M, et al. Relish, a central factor in the control of humoral but not cellular immunity in Drosophila. *Molecular Cell*. (1999) 4:827–37. doi: 10.1016/S1097-2765(00)80392-5
6. Godin I, Cumano A. The hare and the tortoise: an embryonic haematopoietic race. *Nat Rev Immunol*. (2002) 2:593–604. doi: 10.1038/nri857
7. Evans CJ, Hartenstein V, Banerjee U. Thicker than blood: conserved mechanisms in Drosophila and vertebrate hematopoiesis. *Dev Cell*. (2003) 5:673–90. doi: 10.1016/S1534-5807(03)00335-6
8. Tepass U, Fessler LI, Aziz A, Hartenstein V. Embryonic origin of hemocytes and their relationship to cell death in Drosophila. *Development*. (1994) 120:1829–37.
9. Shrestha R, Gateff E. Ultrastructure and cytochemistry of the cell-types in the tumorous hematopoietic organs and the hemolymph of the mutant lethal (1) malignant blood neoplasm (l(1)mbn) of *Drosophila melanogaster* (drosophila/mutant blood cells/ultrastructure/cytochemistry). *Dev Growth Differ*. (1982) 24:83–98. doi: 10.1111/j.1440-169X.1982.00083.x
10. Lebestky T, Chang T, Hartenstein V, Banerjee U. Specification of Drosophila hematopoietic lineage by conserved transcription factors. *Science*. (2000) 288:146–9. doi: 10.1126/science.288.5463.146
11. Holz A, Bossinger B, Strasser T, Janning W, Klapper R. The two origins of hemocytes in Drosophia. *Development*. (2003) 130:4955–62. doi: 10.1242/dev.00702
12. Lanot R, Zachary D, Holder F, Meister M. Postembryonic hematopoiesis in Drosophila. *Dev Biol*. (2001) 230:243–57. doi: 10.1006/dbio.2000.0123
13. Kurucz E, Vaczi B, Markus R, Laurinyecz B, Vilmos P, Zsamboki J, et al. Definition of Drosophila hemocyte subsets by cell-type specific antigens. *Acta Biol Hung*. (2007) 58 (Supp. 1):95–111. doi: 10.1556/ABiol.58.2007.Suppl.8
14. Makhijani K, Alexander B, Tanaka T, Rulifson E, Brückner K. The peripheral nervous system supports blood cell homing and survival in the Drosophila larva. *Development*. (2011) 138:5379–91. doi: 10.1242/dev.067322
15. Rugendorff A, Younossi-Hartenstein A, Hartenstein V. Embryonic origin and differentiation of the Drosophila heart. *Roux Arch Dev Biol*. (1994) 203:266–80. doi: 10.1007/BF00360522

16. Lebestky T, Jung SH, Banerjee U. A Serrate-expressing signaling center controls Drosophila hematopoiesis. *Genes Dev*. (2003) 17:348–53. doi: 10.1101/gad.1052803
17. Jung S-H, Evans CJ, Uemura C, Banerjee U. The Drosophila lymph gland as a developmental model of hematopoiesis. *Development*. (2005) 132:2521–33. doi: 10.1242/dev.01837
18. Krzemien J, Oyallon J, Crozatier M, Vincent A. Hematopoietic progenitors and hemocyte lineages in the Drosophila lymph gland. *Dev Biol*. (2010) 346:310–9. doi: 10.1016/j.ydbio.2010.08.003
19. Grigorian M, Mandal L, Hartenstein V. Hematopoiesis at the onset of metamorphosis: terminal differentiation and dissociation of the Drosophila lymph gland. *Dev Genes Evol*. (2011) 221:121–31. doi: 10.1007/s00427-011-0364-6
20. Evans CJ, Liu T, Banerjee U. Drosophila hematopoiesis: markers and methods for molecular genetic analysis. *Methods*. (2014) 68:242–51. doi: 10.1016/j.ymeth.2014.02.038
21. Rizki MTM. Alterations in the haemocyte population of *Drosophila melanogaster*. *J Morphol*. (1957) 100:437–58. doi: 10.1002/jmor.1051000303
22. Franc NC, Dimarcq J-L, Lagueux M, Hoffmann J, Ezekowitz RAB. Croquemort, a novel drosophila hemocyte/macrophage receptor that recognizes apoptotic cells. *Immunity*. (1996) 4:431–43. doi: 10.1016/S1074-7613(00)80410-0
23. Crozatier M, Meister M. Drosophila haematopoiesis. *Cell Microbiol*. (2007) 9:1117–26. doi: 10.1111/j.1462-5822.2007.00930.x
24. Rizki TM, Rizki RM. Lamellocyte differentiation in Drosophila larvae parasitized by Leptopilina. *Dev Comp Immunol*. (1992) 16:103–10. doi: 10.1016/0145-305X(92)90011-Z
25. Sorrentino RP, Carton Y, Govind S. Cellular immune response to parasite infection in the Drosophila lymph gland is developmentally regulated. *Dev Biol*. (2002) 243:65–80. doi: 10.1006/dbio.2001.0542
26. Márkus R, Laurinyecz B, Kurucz É, Honti V, Bajusz I, Sipos B, et al. Sessile hemocytes as a hematopoietic compartment in *Drosophila melanogaster*. *Proc Natl Acad Sci*. (2009) 106:4805–9. doi: 10.1073/pnas.0801766106
27. Anderl I, Vesala L, Ihalainen TO, Vanha-aho L-M, Andó I, Rämet M, et al. Transdifferentiation and proliferation in two distinct hemocyte lineages in *Drosophila melanogaster* larvae after wasp infection. *PLOS Pathogens*. (2016)12:e1005746. doi: 10.1371/journal.ppat.1005746
28. Darnell JE Jr. STATs and gene regulation. *Science*. (1997) 277:1630–5. doi: 10.1126/science.277.5332.1630
29. Arbouzova NI, Zeidler MP. JAK/STAT signalling in Drosophila insights into conserved regulatory and cellular functions. *Development*. (2006) 133:2605–16. doi: 10.1242/dev.02411
30. Binari R, Perrimon N. Stripe-specific regulation of pair-rule genes by hopscotch, a putative Jak family tyrosine kinase in Drosophila. *Genes Dev*. (1994) 8:300–12. doi: 10.1101/gad.8.3.300
31. Brown S, Hu N, Hombri AJC-G. Identification of the first invertebrate interleukin JAK/STAT receptor, the Drosophila gene domeless. *Curr Biol*. (2001) 11:1700–5. doi: 10.1016/S0960-9822(01)00524-3
32. Gilbert MM, Weaver BK, Gergen JP, Reich NC. A novel functional activator of the Drosophila JAK/STAT pathway, unpaired2, is revealed by an in vivo reporter of pathway activation. *Mech Dev*. (2005) 122:939–48. doi: 10.1016/j.mod.2005.03.004
33. Morin-Poulard I, Vincent A, Crozatier M. The Drosophila JAK-STAT pathway in blood cell formation and immunity. *JAKSTAT*. (2013) 2:e25700. doi: 10.4161/jkst.25700
34. Harrison DA, Binari R, Nahreini TS, Gilman M, Perrimon N. Activation of a Drosophila Janus kinase (JAK) causes hematopoietic neoplasia and developmental defects. *EMBO J*. (1995) 14:2857–65. doi: 10.1002/j.1460-2075.1995.tb07285.x
35. Luo H, Hanratty WP, Dearolf CR. An amino acid substitution in the Drosophila hopTum-l Jak kinase causes leukemia-like hematopoietic defects. *EMBO J*. (1995) 14:1412–20. doi: 10.1002/j.1460-2075.1995.tb07127.x
36. Agaisse H, Petersen UM, Boutros M, Mathey-Prevot B, Perrimon N. Signaling role of hemocytes in Drosophila JAK/STAT-dependent response to septic injury. *Dev Cell*. (2003) 5:441–50. doi: 10.1016/S1534-5807(03)00244-2
37. Yang H, Hultmark D. Tissue communication in a systemic immune response of Drosophila. *Fly*. (2016) 10:115–22. doi: 10.1080/19336934.2016.1182269
38. Yang H, Hultmark D. Drosophila muscles regulate the immune response against wasp infection via carbohydrate metabolism. *Sci Rep*. (2017) 7:15713. doi: 10.1038/s41598-017-15940-2
39. Kleino A, Silverman N. The Drosophila IMD pathway in the activation of the humoral immune response. *Dev Comp Immunol*. (2014) 42:25–35. doi: 10.1016/j.dci.2013.05.014
40. Arrese EL, Soulages JL. Insect fat body: energy, metabolism, and regulation. *Annu Rev Entomol*. (2010) 55:207–25. doi: 10.1146/annurev-ento-112408-085356
41. Géminard C, Rulifson EJ, Léopold P. Remote control of insulin secretion by fat cells in Drosophila. *Cell Metab*. (2009) 10:199–207. doi: 10.1016/j.cmet.2009.08.002
42. Diangelo JR, Bland ML, Bambina S, Cherry S, Birnbaum MJ. The immune response attenuates growth and nutrient storage in Drosophila by reducing insulin signaling. *Proc Natl Acad Sci USA*. (2009) 106:20853–8. doi: 10.1073/pnas.0906749106
43. Tatar M. Metabolism by remote control. *Cell Metab*. (2009) 10:164–6. doi: 10.1016/j.cmet.2009.08.007
44. Delanoue R, Meschi E, Agrawal N, Mauri A, Tsatskis Y, Mcneill H, et al. Drosophila insulin release is triggered by adipose Stunted ligand to brain Methuselah receptor. *Science*. (2016) 353:1553–6. doi: 10.1126/science.aaf8430
45. Roth SW, Bitterman MD, Birnbaum MJ, Bland ML. Innate immune signaling in Drosophila blocks insulin signaling by uncoupling PI(3,4,5)P(3) production and Akt activation. *Cell Rep*. (2018) 22:2550–6. doi: 10.1016/j.celrep.2018.02.033
46. Ramond E, Petrignani B, Dudzic JP, Boquete J-P, Poidevin M, Kondo S, et al. Metabolic adjustment of Drosophila hemocyte number and sessility by an adipokine. *bioRxiv [Preprint]*. doi: 10.1101/648626
47. Caygill EE, Brand AH. The GAL4 system: a versatile system for the manipulation and analysis of gene expression. In: Dahmann, editor. *Drosophila: Methods and Protocols*. New York, NY: Springer New York (2016). p. 33–52.
48. Kockel L, Huq LM, Ayyar A, Herold E, MacAlpine E, Logan M, et al. A Drosophila LexA enhancer-trap resource for developmental biology and neuroendocrine research. *G3*. (2016) 6:3017–26. doi: 10.1534/g3.116.031229
49. Yoon S, Cho B, Shin M, Koranteng F, Cha N, Shim J. Iron homeostasis controls myeloid blood cell differentiation in Drosophila. *Mol Cells*. (2017) 40:976–85. doi: 10.14348/molcells.2017.0287
50. Tennessen JM, Barry WE, Cox J, Thummel CS. Methods for studying metabolism in Drosophila. *Methods*. (2014) 68:105–15. doi: 10.1016/j.ymeth.2014.02.034
51. Delanoue R, Slaidina M, Léopold P. The steroid hormone ecdysone controls systemic growth by repressing dMyc function in Drosophila fat cells. *Dev Cell*. (2010) 18:1012–21. doi: 10.1016/j.devcel.2010.05.007
52. Bai Y, Li K, Shao J, Luo Q, Jin LH. Flos Chrysanthemi Indici extract improves a high-sucrose diet-induced metabolic disorder in Drosophila. *Exp Ther Med*. (2018) 16:2564–72. doi: 10.3892/etm.2018.6470
53. del Valle Rodriguez A, Didiano D, and Desplan, C. Power tools for gene expression and clonal analysis in Drosophila. *Nat Methods*. (2011) 9:47–55. doi: 10.1038/nmeth.1800
54. Petraki S, Alexander B, Bruckner K. Assaying blood cell populations of the *Drosophila melanogaster* larva. *J Vis Exp*. (2015) 105:52733. doi: 10.3791/52733
55. Shim J. Drosophila blood as a model system for stress sensing mechanisms. *BMB Rep*. (2015) 48:223–8. doi: 10.5483/BMBRep.2015.48.4.273
56. Ecker A, Gonzaga T, Seeger RL, Santos MMD, Loreto JS, Boligon AA, et al. High-sucrose diet induces diabetic-like phenotypes and oxidative stress in *Drosophila melanogaster*: protective role of Syzygium cumini and Bauhinia forficata. *Biomed Pharmacother*. (2017) 89:605–16. doi: 10.1016/j.biopha.2017.02.076
57. Arefin B, Kucerova L, Krautz R, Kranenburg H, Parvin F, Theopold U. Apoptosis in hemocytes induces a shift in effector mechanisms in the Drosophila immune system and leads to a pro-inflammatory state. *PLoS ONE*. (2015) 10:e0136593. doi: 10.1371/journal.pone.0136593
58. Tanji T, Hu X, Weber AN, Ip YT. Toll and IMD pathways synergistically activate an innate immune response in *Drosophila melanogaster*. *Mol Cell Biol*. (2007) 27:4578–88. doi: 10.1128/MCB.01814-06

59. Buchon N, Broderick NA, Poidevin M, Praderv S, Lemaitre B. Drosophila intestinal response to bacterial infection: activation of host defense and stem cell proliferation. *Cell Host Microbe*. (2009) 5:200–11. doi: 10.1016/j.chom.2009.01.003
60. Parsons B, Foley E. The Drosophila platelet-derived growth factor and vascular endothelial growth factor-receptor related (Pvr) protein ligands Pvf2 and Pvf3 control hemocyte viability and invasive migration. *J Biol Chem*. (2013) 288:20173–83. doi: 10.1074/jbc.M113.483818
61. Woodcock KJ, Kierdorf K, Pouchelon CA, Vivancos V, Dionne MS, Geissmann F. Macrophage-derived upd3 cytokine causes impaired glucose homeostasis and reduced lifespan in Drosophila fed a lipid-rich diet. *Immunity*. (2015) 42:133–44. doi: 10.1016/j.immuni.2014.12.023
62. He L, Binari R, Huang J, Falo-Sanjuan J, Perrimon N. *In vivo* study of gene expression with an enhanced dual-color fluorescent transcriptional timer. *Elife* 8:e46181. doi: 10.7554/eLife.46181
63. Britton JS, Lockwood WK, Li L, Cohen SM, Edgar BA. Drosophila's insulin/PI3-kinase pathway coordinates cellular metabolism with nutritional conditions. *Dev Cell*. (2002) 2:239–49. doi: 10.1016/S1534-5807(02)00117-X
64. Graham P, Pick L. Drosophila as a model for diabetes and diseases of insulin resistance. *Curr Top Dev Biol*. (2017) 121:397–419. doi: 10.1016/bs.ctdb.2016.07.011
65. Mondal BC, Mukherjee T, Mandal L, Evans CJ, Sinenko SA, Martinez-Agosto JA, et al. Interaction between differentiating cell- and niche-derived signals in hematopoietic progenitor maintenance. *Cell*. (2011) 147:1589–600. doi: 10.1016/j.cell.2011.11.041
66. Leitao AB, Sucena E. Drosophila sessile hemocyte clusters are true hematopoietic tissues that regulate larval blood cell differentiation. *Elife* (2015) 4:e06166. doi: 10.7554/eLife.06166
67. Mills CD, Kincaid K, Alt JM, Heilman MJ, Hill AM. M-1/M-2 macrophages and the Th1/Th2 paradigm. *J Immunol*. (2000) 164:6166–73. doi: 10.4049/jimmunol.164.12.6166
68. Roszer T. Understanding the mysterious M2 macrophage through activation markers and effector mechanisms. *Mediators Inflamm*. (2015) 2015:816460. doi: 10.1155/2015/816460
69. Dodington DW, Desai HR, Woo M. JAK/STAT - emerging players in metabolism. *Trends Endocrinol Metab*. (2018) 29:55–65. doi: 10.1016/j.tem.2017.11.001
70. Yang H, Kronhamn J, Ekstrom JO, Korkut GG, Hultmark D. JAK/STAT signaling in Drosophila muscles controls the cellular immune response against parasitoid infection. *EMBO Rep*. (2015) 16, 1664–72. doi: 10.15252/embr.201540277
71. Oldham S, Stocker H, Laffargue M, Wittwer F, Wymann M, Hafen E. The Drosophila insulin/IGF receptor controls growth and size by modulating PtdInsP(3) levels. *Development*. (2002) 129:4103. doi: 10.5167/uzh-623
72. Teleman AA. Molecular mechanisms of metabolic regulation by insulin in Drosophila. *Biochem J*. (2009) 425:13–26. doi: 10.1042/BJ20091181
73. Murillo-Maldonado JM, Sánchez-Chávez G, Salgado LM, Salceda R, Riesgo-Escovar JR. Drosophila insulin pathway mutants affect visual physiology and brain function besides growth, lipid, and carbohydrate metabolism. *Diabetes*. (2011) 60:1632–6. doi: 10.2337/db10-1288
74. Myllymaki H, Ramet M. JAK/STAT pathway in Drosophila immunity. *Scand J Immunol*. (2014) 79:377–85. doi: 10.1111/sji.12170

Conflict of Interest: The authors declare that the research was conducted in the absence of any commercial or financial relationships that could be construed as a potential conflict of interest.

frontiers in Immunology

REVIEW
published: 31 January 2020
doi: 10.3389/fimmu.2019.03075

Sexual Dimorphisms in Innate Immunity and Responses to Infection in *Drosophila melanogaster*

Rebecca L. Belmonte[1†], *Mary-Kate Corbally*[1†], *David F. Duneau*[2*‡] and *Jennifer C. Regan*[1*‡]

[1] Institute of Immunology & Infection Research, University of Edinburgh, Edinburgh, United Kingdom, [2] Laboratoire Evolution & Diversite Biologique, UMR5174 EDB, CNRS, Université Toulouse 3 Paul Sabatier, Toulouse, France

OPEN ACCESS

Edited by:
Susanna Valanne,
Tampere University, Finland

Reviewed by:
Mark Austin Hanson,
École Polytechnique Fédérale de Lausanne, Switzerland
Ilias Kounatidis,
Diamond Light Source, United Kingdom

***Correspondence:**
David F. Duneau
david.duneau@gmail.com
Jennifer C. Regan
jenny.regan@ed.ac.uk

[†]These authors have contributed equally to this work and share first authorship

[‡]These authors have contributed equally to this work and share last authorship

Specialty section:
This article was submitted to Comparative Immunology, a section of the journal Frontiers in Immunology

Received: 31 October 2019
Accepted: 16 December 2019
Published: 31 January 2020

Citation:
Belmonte RL, Corbally M-K, Duneau DF and Regan JC (2020) Sexual Dimorphisms in Innate Immunity and Responses to Infection in Drosophila melanogaster. Front. Immunol. 10:3075. doi: 10.3389/fimmu.2019.03075

The sexes show profound differences in responses to infection and the development of autoimmunity. Dimorphisms in immune responses are ubiquitous across taxa, from arthropods to vertebrates. *Drosophila melanogaster* shows strong sex dimorphisms in immune system responses at baseline, upon pathogenic challenge, and over aging. We have performed an exhaustive survey of peer-reviewed literature on *Drosophila* immunity, and present a database of publications indicating the sex(es) analyzed in each study. While we found a growing interest in the community in adult immunity and in reporting both sexes, the main body of work in this field uses only one sex, or does not stratify by sex. We synthesize evidence for sexually dimorphic responses to bacterial, viral, and fungal infections. Dimorphisms may be mediated by distinct immune compartments, and we review work on sex differences in behavioral, epithelial, cellular, and systemic (fat body-mediated) immunity. Emerging work on sexually dimorphic aging of immune tissues, immune senescence, and inflammation are examined. We consider evolutionary drivers for sex differences in immune investment, highlight the features of *Drosophila* biology that make it particularly amenable to studies of immune dimorphisms, and discuss areas for future exploration.

Keywords: *Drosophila*, *Drosophila melanogaster*, innate immunity, sex dimorphism, aging, response to infection, sexual antagonism

INTRODUCTION

Sex governs physiology: differences between males and females are strong drivers of variance in phenotype within any population, and can eclipse effects of geography or genotype (1, 2). The immune system is no exception. Sex differences in human immunity are profound, where men and women respond differently to infection, treatment, diseases such as sepsis, and have different propensities toward autoimmunity (3, 4). However, the mechanisms underpinning these dimorphisms are largely unresolved. A major reason for this lack of resolution is that sex differences in immunity are understudied; in particular, there is a paucity of truly comparative studies. A recent meta-analysis addressing the issue of sex as a variable in biomedical studies showed that immunology as a discipline is particularly negligent, with fewer than 10% of studies reporting, or stratifying, by sex (5). Historically, women have been excluded from clinical trials and young males presented as "the norm," in part due to concerns for potential impacts on fetal health (6). Parity has not been reached in representation (7) or reporting (8) of the sexes, despite the effective ban on women participating in clinical trials ending in the 1980s (6). In addition, in studies

using laboratory model organisms, practical and budgetary considerations have led to the common practice of using a single sex. Recently, there has been recognition of the loss of knowledge propagated by the lack of inclusion of both sexes, with a drive from the scientific community to address the "gender gap," including NIH and ERC commitments to address this specifically (9, 10).

The effects of immune dimorphisms are not only a consideration for clinical research, but also impact our broader understanding of host-pathogen interactions. Sex differences in immunity are observed throughout taxa, and are both cause and consequence of sex differences in life history, and sexual conflict. Responses to infection influence survival and fecundity, and therefore immune dimorphisms have the potential to affect both horizontal and vertical disease transmission throughout the animal kingdom (11). Inherant in the consideration of sex and immunity is complexity: within a single species, dimorphisms themselves are pathogen-specific (12), can respond to environmental variables such as diet (13, 14), and may even be influenced by the infective parasite which can be differently adapted to each sex (15). Adding further complexity is the interaction of immunity and sex with organism age (16).

As is the case for all insects, *Drosophila melanogaster* physiology is sexually dimorphic (17–19), yet despite its use for more than a century as a model organism, the extent of these dimorphisms are only just being fully appreciated (20). Sex differences are seen in immune tissues (21, 22) and in responses to infection (23), yet relatively few studies include both sexes. Studies that explicitly compare immune responses in both sexes in *Drosophila* reflect what is seen in other taxa in terms of prevalence and complexity: dimorphic responses are the norm rather than the exception, the direction that dimorphisms take with respect to the opposite sex is both pathogen- and context-dependent (23), and sex differences at baseline are not necessarily predictive of survival outcome (24).

What Can *Drosophila* Teach Us About Immune Dimorphism?

Drosophila species have been used for many decades to study sexual antagonism in the evolutionary ecology field (25–27). We argue that including, and comparing, both sexes in functional and mechanistic studies of *Drosophila* immunity will add to this body of work to give important insight to several fields, in addition to better understanding host-pathogen interactions from an evolutionary ecology perspective. It will, for example, offer translatable information on disease vector biology, where sex is a crucial variable for exposure, transmission, and control strategies of insect disease vectors such as mosquitos (28–30). *Drosophila* provides a tractable model for innate immunity in mammals, as has been amply demonstrated over recent decades (31): studies on *Drosophila* could help understand rules underpinning sexual dimorphism in mammalian immunity and response to infections. Sex differences in mammalian immunity are often attributed solely to the action of steroid hormones. Interactions between steroid hormones and the immune system have also been demonstrated in *Drosophila* (32, 33), which may parallel endocrine-immune interactions in mammals. Mammalian immune dimorphisms arise not only as a consequence of selective pressures on the endocrine system. A large body of studies in mammalian immunology has uncovered many dimorphisms, particularly in autoimmune disease etiology, that are regulated by karyotype, independent of hormonal action (34–36). While it is difficult to attribute autoimmunity to organisms without immune self-recognition, direct self-damage by immune responses on the host has been demonstrated in *Drosophila* (37, 38) and may differ depending on the sex (39). *Drosophila,* like mammals, bear X and Y sex chromosomes, and both X- and Y-linked variation in immune responses have been demonstrated (40, 41). This, in combination with the strong conservation of immune signaling pathways (as exemplified by Toll/TLRs), makes *Drosophila* a powerful model for sex-specific genetic regulation of molecular immunity (23, 42).

A Survey of Immunity Studies Using Adult *Drosophila melanogaster*

We have undertaken to perform a survey of peer-reviewed, published studies of *D. melanogaster* immunity, reporting on the representation of sex within each study. We have focussed on studies using adult flies, while also identifying papers that use juveniles, cell cultures, or pre-existing genetic data. We searched for *Drosophila* immunity papers through Web of Science, attempting to avoid studies of other model organisms that mentioned *Drosophila*. As of the 21 August 2019, we downloaded the citations for the resulting 5,626 publications and manually categorized each paper. Two thousand eight hundred and forty-eight papers were removed since *Drosophila* were not used in the study, or the focus of the study was not immunity. We also made a decision to exclude the 166 endosymbiont studies that used both sexes from our analysis. There were also three papers which we could not access, which were removed (43–45). Of the remaining 2,614 papers, 1,369 used adults, 817 used juveniles, 396 were non-experimental (i.e., reviews or methods), and 30 were bioinformatics studies (**Figure 1A**). In the last 30 years, we can see how the *Drosophila* immunity field has grown and the relative use of adults or juveniles has changed. In 1990, only two adult studies and three juvenile studies were published (**Figure 1B**). Initially, the majority of studies were conducted on juveniles, but by 2010, the trend had reversed, where 75 studies used adults and 47 used juveniles. The use of adult *Drosophila* to study immunity has continued to grow, averaging over 100 adult studies per year between 2012 and 2018 (**Figure 1B**). Of the adult studies, 41% (564/1,369) did not report the sex, or did not stratify data by sex. When sex was reported, 45% used only one sex, with more studies using females (28%; 378/1,366), than males (18%; 243/1,366). Only 13% (184/1,366) of all adult studies reported results for both males and females ("both" category; **Figure 1C**). We additionally tagged each paper in the "both" category with the study type or data output (**Figure 1D**, **Figure S1**). Tags were not exclusive, where studies could be assigned multiple tags, resulting in more tags than articles in the output. The two most common tags were "gene function/knockout" (23%; 76/334),

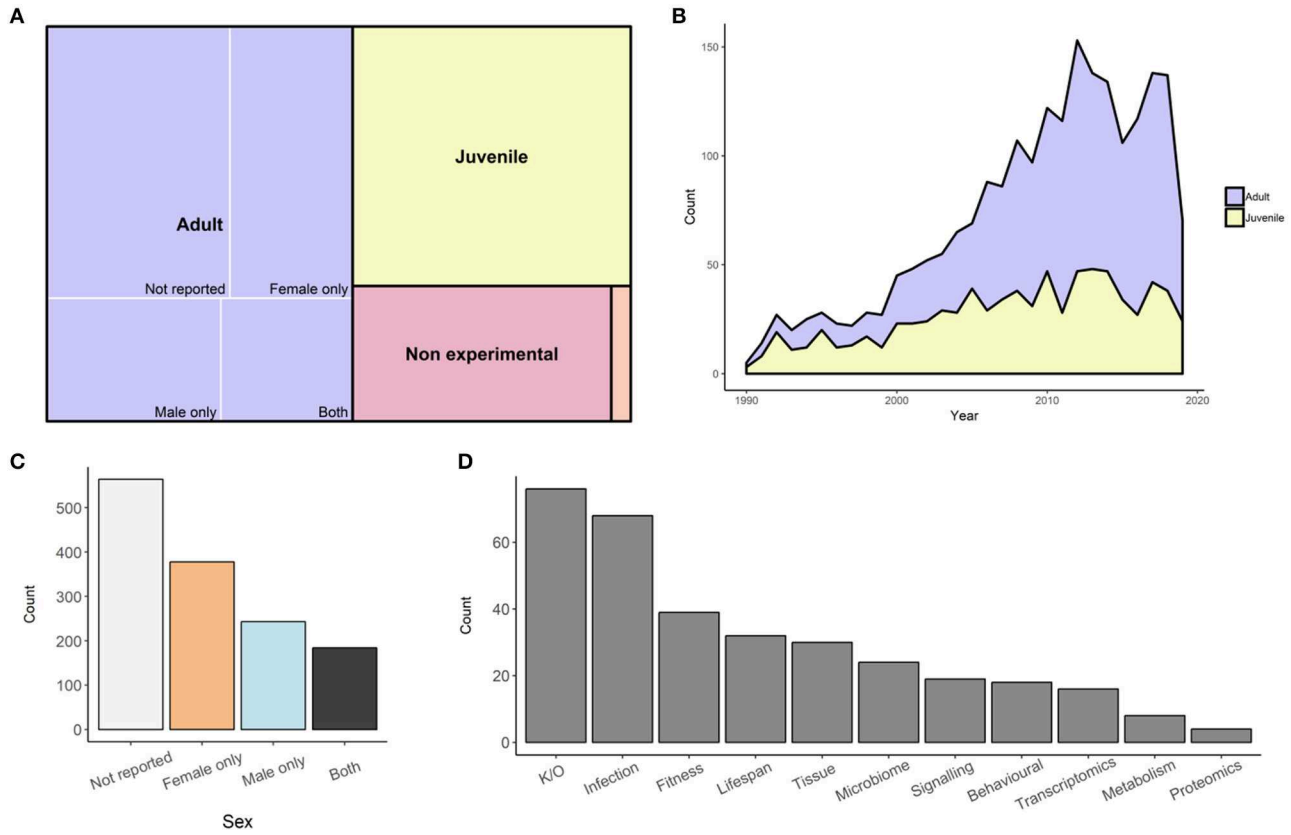

FIGURE 1 | Composition of 2,614 articles on *Drosophila* immunity. **(A)** Categories used for all *Drosophila* immunity studies. Size of each rectangle is proportional to the number of articles within that category. The largest proportion are adult studies (purple; 1,366), followed by juvenile (yellow; 817), non-experimental (pink; 396), and bioinformatic (orange; 30) studies. **(B)** The quantity of articles published since 1990 until 21 August 2019 that use either adult (purple) or juvenile (yellow) *Drosophila*. **(C)** Quantity of adult *Drosophila* studies that do not report sex used (purple; 561), use females (pink; 378), use males (orange; 243), or use both sexes (yellow; 184). **(D)** Total number of articles that used both sexes, tagged according to experimental output. Tags are not exclusive, so some articles may have more than one tag. The tags used were gene function knock out (46), survival infection dynamics (47), fitness (39), lifespan (32), tissue specific (30), microbiome (24), signaling (19), behavioral (18), transcriptomics (16), metabolism composition (8), and proteomics (4).

followed by "survival/infection dynamics" (20%; 68/334). The survey information is available as a searchable table, intended as a resource for locating data on immunity in both sexes (**Table S1**). Integrating information from this wealth of published data, we review what is reported about sex dimorphisms in immunity in *Drosophila*.

SEX DIFFERENCES IN INFECTION OUTCOMES

Survival and Pathology

Drosophila exhibit dimorphic survival and pathology in response to bacterial, viral, and fungal infections. Importantly, dimorphic survival and prevalence of infection are pathogen- and context-specific (**Table 1**).

Viral Infection

Few studies have compared male and female responses to viral infection in *D. melanogaster*. Males are possibly more susceptible to acute viral infection: they demonstrate lower survival to the recently-described, DNA virus *Kalithea* (KV), which was isolated from infected individuals caught from a wild population (48). Males are also more susceptible to higher viral titers of the RNA virus *Drosophila C* (DCV) (59). Notably, dimorphism in survival to viral infection might be influenced by coinfection with *Wolbachia*, an endosymbiont providing viral protection (60). Indeed, interactions between DCV and *Wolbachia* infection status and sex have been observed in analyses of behavioral responses (61), discussed in more detail below.

Other effects of viral infection can impact the sexes differently, in addition to survival. For example, although females infected with KV generally survive, they suffer from ovary degeneration and a strong reduction in fecundity (48). Viral-induced female infertility is known to occur in infections with flock house virus (FHV) due to oocyte destruction (62). Thus, conclusions on sex-specific impacts of viral infection on fitness need to consider all consequences of infection, not just survival.

Viral Transmission

A recent study demonstrated that male-biased DCV titers are accompanied by higher levels of fecal shedding (59), which is in apparent contrast to an earlier study that found females to

TABLE 1 | Reported sex biases in survival to infection by specific pathogens.

Class	Pathogen	Survival bias-direction	References
Viral	*Kalithea*	Female	(48)
Fungal	*Beauveria bassiana*	Male	(49–53)
	Metarhizium anisopliae	Male	(54)
	Candida albicans	Female	(55)
Microsporidial	*Tubulinosema ratisbonensis*	Female	(56)
Bacterial gram-negative	*Pseudomonas aeruginosa*	Male	(46)
	Pseudomonas aeruginosa	Female	(55)
	Pseudomonas fluorescens	Female	(22)
	Providencia rettgeri	Male	(23)
	Providencia alcalifaciens	Male	(23)
	Coxiella burnetii	–	(57)
	Serratia marcescens	Female (Genotype-specific)	(58)
Gram-positive	*Enterococcus faecalis*	Male	(23)
	Lactococcus lactis	Female	(58)

be better transmitters of DCV than males (63). It is not known whether load, or rates of shedding, are necessarily predictive of the ability of each sex to transmit viral infection; this may be dependent upon several additional factors, including infection route and behavioral responses to infection. Further studies correlating viral load and shedding with the ability to transmit infection in both sexes will be informative. Vertically-transmitted viruses by definition interact with host sex, given their route through infected gonads. For example, Sigma virus (*Rhabdoviridae*), a negative-stranded RNA virus, is transmitted vertically through the sperm or ovules. Male transmission of Sigma virus is required for persistence in the population, while transmission efficiency is higher for females than males (64). Infection with Sigma virus leads to sexually dimorphic gene induction, with more gene expression changes induced by infection in males than females (65). Infected females significantly upregulate structural chorion proteins, which could reflect manipulation by the virus to aid vertical transmission, or an ovary-specific defense response.

Given the very small number of studies addressing dimorphisms in survival to viral infections, we do not yet have the ability to make inferences about sex differences in anti-viral responses, nor indeed whether there are differences between responses to RNA and DNA viruses, or diverse viral species.

Fungal and Microsporidial Infection

To our knowledge, there are only a small number of studies investigating sexual dimorphism in fungal infection. Indeed there is a dearth of studies investigating sex-specific physiological responses to such challenges (**Figure 2**). The most commonly studied fungal infection model, *Beauveria bassiana*, exhibits male-biased survival when flies are challenged via spore inoculation (49–53). The dimorphism appears to be, at least partly, attributable to dimorphic function of the Toll pathway, where loss-of-function mutants in Toll pathway components lose the sex difference in survival (52, 53). A similar male bias in survival is observed post-inoculation with the soil fungus *Metarhizium anisopliae* (54). However, although not directly compared, males appear to be more susceptible to systemic *Candida albicans* challenge by means of intra-thoracic injection (55). Interestingly, the effect of Toll-1 and Toll-7 mutation on resistance to *C. albicans* challenge revealed a greater sensitivity of male mutants to this fungal infection, while Toll-7 mutant females demonstrated resistance similar to that of controls (55). In addition, males succumbed to systemic infection with the microsporidium *Tubulinosema ratisbonensis* sooner than did females (56), despite a lower reported microsporidial load. However, the assertion made here that despite a greater lethality to *T. ratisbonensis*, males show a higher resistance as demonstrated by their lower pathogen load, needs further investigation. Pathogen load should be quantified before significant mortality has occurred in the population of infected individuals, otherwise, individuals with a high pathogen load who died prior to sampling would not be included in the analysis. A greater number of infected males had died 5 days post-infection from *T. ratisbonensis* than females, and pathogen load was analyzed 6 days post-infection (56). These results could potentially suggest that males are less tolerant, given that the only individuals still alive are those carrying a lower pathogen load.

Overall, in contrast to viral infections, males appear to survive longer than females in fungal infection models. There are indications that the magnitude of these dimorphisms in survival may be dependent on the environment. For example, the male-biased survival observed upon infection with *B. bassiana* is magnified by cold pretreatment of flies before infection, improving male survival at young and middle ages (81). Diet is also likely to influence susceptibility; for example, while females have decreased rates of survival to *B. bassiana* thoracic injection, immunity-induced metabolic declines were 50% greater in males (82). Supporting the interaction of metabolic state with sex-biased infection outcomes, polymorphisms associated with increased resistance to *M. anisopliae* inoculation are dimorphic and are biased toward gene networks regulating metabolism, as well as phagocytosis and cell migration (83). Furthermore, in the microsporidia infection model *T. ratisbonensis*, the quantity of circulating triglycerides was shown to affect parasite burden in females (56). The intersection of diet, metabolism and immune responses is likely to dictate outcomes to infection with most (or all) pathogens, as we discuss in more detail below. However, whether metabolic effects regulate resistance or tolerance to the fungal and microsporidial infection models described is as yet untested.

Bacterial Infection

The bacterial genus of *Wolbachia* and *Spiroplasma* have well-documented interactions with host sex and have been extensively studied in *Drosophila* infection models. Both bacteria disrupt the reproductive biology of their hosts, and show sex-specific transmission. While these interactions are entirely dependent on host sex, these examples are not strictly relevant to examination of dimorphic immune responses, and have already

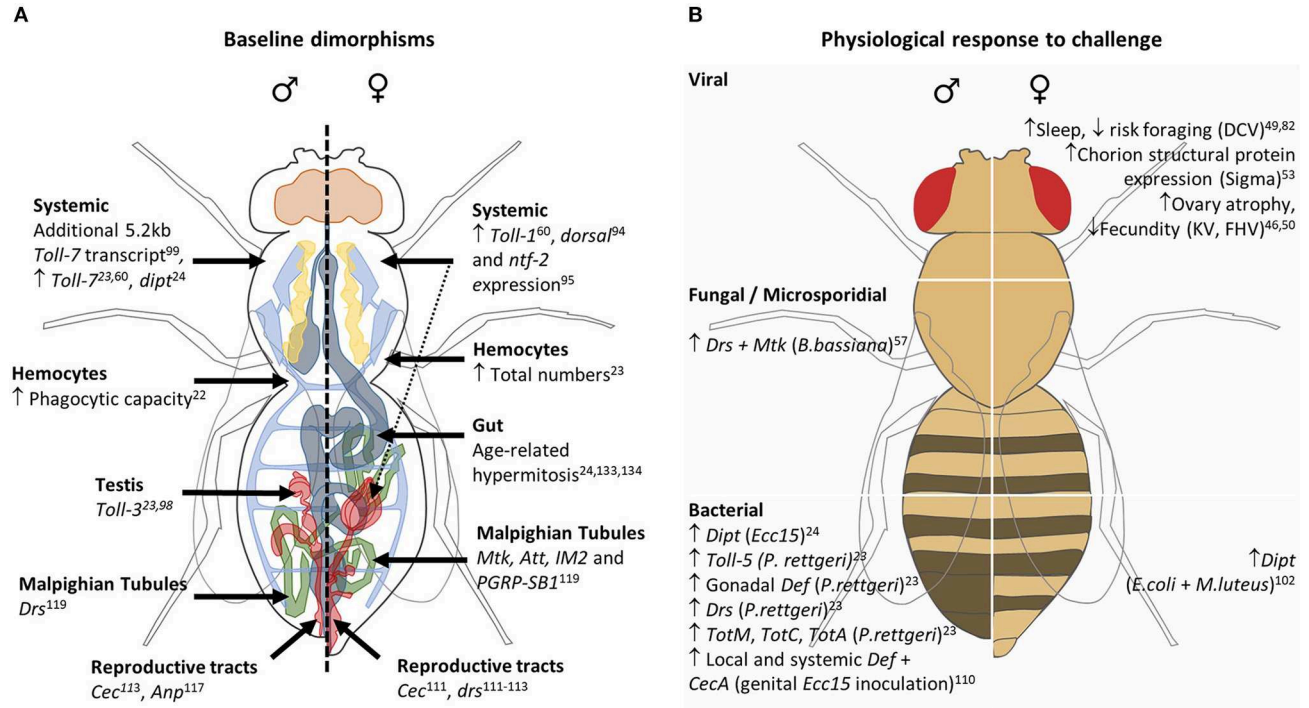

FIGURE 2 | Schematic representing sexual dimorphisms in innate immunity at basal state **(A)** and in physiological responses to immune challenge **(B)**. **(A)** Male- and female-specific baseline conditions are depicted on the left and right of the central dashed line, respectively. Greater expression/ numbers are denoted by an upward-facing arrow, while stand-alone genes belonging to systemic or specific tissues represent sex-specific expression systemically or within that tissue, respectively. The dashed arrow represents the potential contribution made by the ovaries to observed differences in systemic transcript abundance. **(B)** Male (left column) and female (right column) physiological responses to viral, fungal/microsporidial, and bacterial are listed, with the causative pathogen in brackets. Increases and decreases in expression or behaviors are denoted by upward- and downward-facing arrows, respectively.

been extensively reviewed (47, 84–87), so we will not focus on them here.

In models of systemic bacterial infection of male and female adults, where immune responses and survival are directly compared, survival to infection appears to be pathogen-dependent. Depending on the amount and type of peptidoglycan (sugar- and amino acid-based polymers) in their cell wall, bacteria can be categorized into two groups, Gram-positive (G-) and Gram-negative (G-). In *Drosophila*, the production of immune effectors such as antimicrobial peptides is under the control of the immune deficiency (IMD) and the Toll signaling pathways. The former responds to the meso-diaminopimelic acid (DAP)-type peptidoglycan of G- bacteria and certain G+ bacilli, whereas the Toll signaling pathway responds mainly to the lysine (Lys)-type peptidoglycan of G+ bacteria and fungal beta-1-3-glucan (88, 89). Activation of immune signaling pathways are not strictly dictated by cell wall type, however; for example, both Toll and IMD signaling pathways are activated by *Staphylococcus aureus* infection (90).

It is not possible to neatly attribute the direction of sex-biased survival to bacterial infection to one particular signaling pathway. Males appeared to be more resistant to systemic infections by the extracellular G- *Providencia* species *Providencia rettgeri* and *Providencia alcalifaciens* (23, 91). However, mortality to the obligate intracellular *Coxiella burnetii* is comparable in males and females (57), while males died more quickly than females when infected with *Pseudomonas fluorescens* (22), or the extracellular bacteria *Serratia marcescens* (although notably, this was genotype-specific) (58). Few studies have assessed the response of both sexes to G+ bacteria. Females were reported to be more susceptible to infection with *Enterococcus faecalis* but less to *S. aureus* (23) or to *Lactococcus lactis* (58). Thus far, laboratory models of bacterial infection have demonstrated both male- and female-biased survival with G- and G+ species (**Table 1**). Different laboratories have also reported opposite biases in response to the same pathogen. For example, *Pseudomonas aeruginosa* is reported to induce dimorphic survival that is either male- or female-biased (46, 55), or not significantly different (22). These contrasting results may be dictated by genotype, as is evidently the case for male-biased susceptibility to *S. marcescens,* which was observed in only two out of four genetic backgrounds tested in a recent study (58). These results may also be influenced by environmental conditions such as mating status, which appears to have an immunosuppressive effect on females (23, 92, 93). Another probable reason a clear pattern has not emerged is that the bacterial species used in these infection models are more diverse than the peptidoglycan dichotomy belies. Compared to *P. rettgeri*,

S. marcescens is highly pathogenic to *Drosophila,* and its infection dynamic within the host is very different (23). Moreover, while these two bacteria are extracellular, other species, such as *Coxiella,* infect intracellularly, further complicating the comparison. Different pathogens require different host defense mechanisms, which may rely on particular immune tissues, signaling pathways, and terminal effectors such as AMPs. A more systematic comparison between male and female responses to a range of different bacteria with different modes of infection will help to decipher the role for immune signaling pathways in dimorphism.

A role for the Toll pathway in mediating sex differences in survival to some bacterial infections has recently started to emerge. It appears to be necessary for dimorphic survival to *P. rettgeri,* and loss of Toll signaling reverses the survival bias to *E. faecalis* (23). Loss-of-function mutants of both Toll-1 and Toll-7 differentially affected infection outcomes in males and females. Toll-1 mutant males and females were less resistant to *E. faecalis* challenge than wild-type controls, while loss-of-function Toll-7 mutants reduced male resistance to both *E. faecalis* and *P. aeruginosa* (55).

Behavioral Responses and Symptoms

In addition to dimorphic immune responses, *Drosophila* exhibit sex-specific behavioral symptoms and responses to infection. Grooming is thought to be an important behavioral defense against pathogenic infection, where flies remove potentially infectious microbes from their cuticle. Grooming in *D. melanogaster* is triggered by chemosensation of compounds, including pathogen components, by chemoreceptive sensilla. Specifically, the sensing receptor PRGP-LC contributes to grooming induction, connecting humoral immune sensing to behavioral responses (94). In optogenetic experiments targeting sensilla, grooming was more readily triggered in males than in females (94). Females were subsequently shown to rely more strongly on olfactory signals to remove cuticular *B. bassiana* than males, resulting in more conidia on the wings of olfactory-deficient female flies (95), but whether this contributes to the higher rate of survival by males after *B. bassiana* infection (49–53) remains to be seen. *Drosophila* exhibit dimorphic sleep responses to infection, a behavioral change which may be adaptive, or symptomatic. DCV causes females, but not males, to sleep more; however, DCV-infected male flies carrying *Wolbachia* are more lethargic when awake (61). Many other behaviors are likely to be impacted by symptoms such as lethargy and sleep alterations, including evasive behaviors and mating. For example, *Wolbachia* infection increases the recapture rate of females, but not males (96). Females previously exposed to DCV showed lower motivation to pick a food source when presented with a risk of encountering DCV (78). When disrupted, *nemuri*, an antimicrobial peptide that promotes sleep in *D. melanogaster*, reduced day-time sleep consolidation selectively in males (97), potentially linking dimorphic sleep behavior and responses to immune challenge. During a *P. rettgeri* systemic infection, females arrested egg-laying during the acute phase of the infection, until it stabilized into a chronic phase (98). The same observation has been made upon benign infections with *Pectobacterium carotovorum* (previously named *Erwinia carotovora carotovora*, or *Ecc15*) and *Escherichia coli* (99). The adaptive role of this behavioral response (99, 100) is not clear and is by definition female-specific. It remains to be determined if changes to reproductive behavior occur in males. Although research in this area is in its infancy, these studies suggest behavioral dimorphisms in *D. melanogaster* could be an important driver for sex differences in infection outcome.

SEX DIFFERENCES IN IMMUNE COMPARTMENT PHYSIOLOGY

Sex differences in outcome to infection are likely to be mediated by distinct immune compartments, where the key tissues involved will be dependent on pathogen and route of infection. Below we discuss those studies that assess the contribution of individual immune tissues. Sexually dimorphic immune physiologies in unchallenged flies and after acute infection are summarized in **Figure 2**.

Hemocytes

Hemocytes are specialized immune cells responsible for the encapsulation and phagocytosis of pathogens and dead cells. Few studies focusing on *D. melanogaster* hemocytes have reported the sex of individuals used; but those that have, present some evidence suggestive of a dimorphism in this branch of the immune system. First, it appears that hemocytes can have sex-specific functions. The Jun N-terminal kinase (JNK) signaling pathway regulates the decision between cell repair and cell death. As such, *JNK*/*Basket* is required in larval hemocytes to promote tissue maintenance, but only in males, such that hemocyte-specific loss of *JNK*/*Basket* results in increased tissue damage in males after UV irradiation (101). In addition to this functional difference, there is some evidence for sex differences in total hemocyte number, but neither the direction of bias nor the drivers for the dimorphism can yet be concluded. Female white prepupae have been reported to contain a higher total number of hemocytes than males (102). In adults, higher numbers of hemocytes *per se* in females (23), and higher numbers of hemocytes per unit of hemolymph in males (21), have been reported, whilst a recent study found no effect of sex on adult hemocyte number (22). A subtly higher phagocytic index has been reported for male hemocytes *ex vivo* (22); however, sex differences in the functional roles of hemocytes in homeostasis or responses to infection are as yet unknown.

Melanisation

Melanogenesis is an important feature of arthropod physiology. In addition to its role in cuticular hardening, via the synthesis of a specific melanin called sclerotin, and in cuticular coloration, via the synthesis of eumelanin, multiple studies have demonstrated its role in immune responses [see (103) for review]. An essential role for immune melanization in the efficient killing of encapsulated parasitoid wasp eggs and pathogens via cytotoxicity of reactive oxygen species (ROS) produced by the melanization cascade is well-appreciated (104, 105). The process hinges on cascades of serine proteases (SPs) triggered by either direct or

indirect antigenic recognition and tissue damage (106). A key enzyme in this process is phenoloxidase (PO), which mediates the oxidation of the amino acid tyrosine to dihydroxyphenylalanine (DOPA) and subsequently, the oxidation of DOPA and dopamine to their respective quinones which are precursors of brown/black eumelanin. PO is produced as prophenoloxidase (PPO) proenzyme which is converted to active PO by a clip domain serine proteinase. This cleavage generates ROS, giving immune melanization its cytotoxic activity.

Whereas the biochemical pathways downstream of PO are well-characterized, our knowledge of the molecular events leading to PPO activation are largely unelucidated (103). The involvement of Toll signaling in melanization responses has recently been demonstrated in adults (106). Hayan and SP7, two SPs acting upstream of Spätzle, activate PPO1 and PPO2, which were shown to be essential for effective resistance against several systemic fungal and G+ bacterial challenges (106, 107). Mutants for *PPO* lack melanization, yet, maintained a dimorphic survival to *P. rettgeri* infection (23), suggesting that the activation of this immune response is not a driver of sex differences in survival to this particular pathogen. However, basal expression of some genes involved in melanogenesis are higher in males and a subset of these, including *Dopa decarboxylase (Ddc)* and *yellow-f*, respond transcriptionally to *P. rettgeri* infection (23). Alternative infection models where melanization is required to effectively control the infection may be more informative for understanding its potential roles in immune dimorphism. For example, the response of males and females to parasitoid wasp infection at larval stages has not been reported to our knowledge. Despite the importance of melanization for resistance to infection and injury, and the intersection of immunologic melanin production and Toll signaling, virtually no studies have assessed the sex-specific physiology of the response. Given that constitutive expression of Toll pathway genes, namely components upstream of Toll-1, as well as *Ddc*, is greater in males (23), the hypothesis that males are more poised for melanization warrants testing.

Systemic (Humoural) Immunity

A number of studies have reported sex differences in systemic immunity (**Figure 2**). Systemic immunity is primarily driven by the fat body; however, expression levels of pathway components were largely measured in whole individuals. For example, following systemic challenge with *P. rettgeri*, males induced a number of Imd- and Toll-regulated effectors at higher level than females, paralleling their greater survivorship (23). Although to note, ablation of the Imd pathway does not suppress the sexual dimorphism in survival (23). Sex differences have repeatedly been found in expression and function of Toll pathway components. Females are reported to exhibit higher expression of Toll-1, the transmembrane receptor that activates the Toll intracellular signaling pathway (55), the Relish protein *dorsal* (74) and the Toll pathway component *ntf-2* (75). The Toll pathway is known to be involved in two processes: dorso-ventral embryonic patterning, a female specific process occurring in the eggs, and in immunity. Signaling downstream of the transmembrane receptor Toll-1 is shared between these two processes. Thus, it is unsurprising that the apparent dimorphism in Toll pathway gene expression disappears once expression in the ovaries is excluded (23). Nonetheless, the expression of the Toll pathway seems crucial for the sexual dimorphism of many infections. This includes both G+ bacterial infection but, perhaps surprisingly, also G- bacterial infection (23). This occurs through the activation of the pathway by *Persephone*, a hemolymphatic serine protease, which senses microbial proteases during infection (108, 109). Toll-3, also called MstProx, shows male-specific expression and response to infection, which seems to be attributable to the gonads (23, 72). Toll-5, or *Tehao*, is also induced at higher levels in males than females following *P. rettgeri* infection (23). Toll-7, a plasma membrane Toll receptor that binds to viral glycoproteins, is expressed at higher basal levels in males (23, 55) and appears to have an additional, male-specific isoform (73).

Male-biased survival to *B. bassiana* also appears to be dependent on the Toll pathway, since mutations in Toll pathway components ablate or reverse the dimorphism (53). The induction of *drosomycin* and *metchnikowin* in the first 24 h of infection also tended to be greater in males (52). The survival dimorphism, however, was not suppressed when tested on *spaetzle* (*spz*) mutants, a component of the Toll pathway (52). These Toll-regulated dimorphisms may in part be mediated by expression of AMPs: for example, *attacins* and *diptericins* require functional Toll for full inducibility. Supporting this, the loss of Toll affects the *Enterobacter cloacae*-induced expression of *attacins* and *diptericins* more strongly in males (110), and males with a gain-of-function Toll mutation exhibit higher levels of the AMPs *Cecropin A1 (CecA1)*, *Diptericin A* (*DptA)*, *Attacin A (AttA)*, and *Attacin B (AttB)* in response to challenge (111). Furthermore, dimorphic induction of *drosomycin* in response to *P. rettgeri* infection is lost in *spz* mutants (23). Dimorphisms have also been reported in Imd pathway components, for example, several Imd-induced AMPs are found to be dimorphic in their expression levels. Using a construct with various *diptericin* promoter sequences upstream of the *lacZ* gene, higher levels of induction were seen in females than males (79). In contrast, *diptericin* has been shown to be expressed at higher levels in unchallenged males than females, and is more strongly upregulated upon infection with the G- bacterium, *P. carotovorum* (24).

The JAnus Kinase protein and the Signal Transducer and Activator of Transcription (JAK-STAT) pathway, required for antiviral immune responses and induced upon bacterial infection, also shows dimorphic expression. *G9a,* a histone H3 lysine 9 methyltransferase, regulates tolerance to viral infection by regulating JAK/STAT (112) but in a sex-specific manner, with females being more sensitive to a loss of *G9a* (113). In addition, the stress-responsive genes regulated by the Jak-Stat pathway, *TurandotA*, *TurandotC,* and *TurandotM*, were among the genes that were the most male-biased in an analysis of the transcriptional response to *P. rettgeri* infection (23), although the consequences of this are as yet unknown. Overall, males have a higher expression of many Toll- (and to a lesser extent Imd-) regulated genes. The reason for this dimorphism is unclear, but further work could investigate a potential link with the dual role for the Toll pathway in females. It is possible that the immune

response via the Toll pathway in females is constrained by its consequences on egg development, a constraint which does not apply to males.

Epithelial Immunity

Comprising the third prominent arm of defense in *D. melanogaster* are the immune-reactive epidermal and epithelial barriers such as the cuticle, trachea, genitalia, and gut.

Cuticle and Trachea

Sex differences in defense against fungal inoculation of the cuticle with the entomopathogenic *B. bassiana* demonstrate female-biased susceptibility (53, 114–116). Dimorphisms in cuticle integrity, or in immune responses of the cuticle or respiratory system could conceivably be underpinning this susceptibility. The trachea, which consist of airway epithelia and spiracles, is immunogenic, and responses may be activated by such cuticle inoculations. Studies that have assessed tracheal immunity in adults, thus far include only males (71, 117), rendering sex-specific responses within respiratory tissue another unexplored, potential contributor to dimorphic immunity. Dimorphisms in cuticular epithelial immune responses *per se* are also, to our knowledge, entirely unexplored.

Genitalia and Gonads

Male genitalia were found to be more primed for immune response to bacterial infection than that of females, where systemic and local AMP responses followed *P. carotovorum* inoculation of the genitalia in males (80). The female reproductive organs are also immune active, and were shown to constitutively express *cecropin* (66) and *drosomycin* (66–68), where *drosomycin* expression was found to be independent of Toll signaling in this tissue (67). Males exhibit constitutive expression of *cecropin* within the ejaculatory duct, independent of Relish signaling (68), suggesting that genital epithelia may circumvent classical pathways to activate AMPs. Immunogenicity of the reproductive tissues is evident from analyses of post-mating AMP responses in females (118, 119), and the antimicrobial protein transfer from male accessory gland and ejaculatory duct to the female (120). Andropin, an AMP unique to males, is also strongly upregulated in response to mating (69). RNA-seq analysis of *P. rettgeri* infected males and females, with and without gonads, illustrates the contribution made by reproductive tissue to systemic immune responses (23). Such comparative transcriptomics revealed male-biased *defensin* levels following infection to be gonad-dependent (23). It is an open question how much reproductive tissues contribute to systemic immunity; indeed it is unknown whether AMPs produced by the gonads are released into the hemolymph, or remain within the tissue.

Malpighian Tubules

Malpighian tubules (MT), epithelial organs dedicated to filtration and analogous to the mammalian kidney, are also immunogenic (121). Transcriptomic analysis of MT revealed differences in basal immune gene expression between the sexes (70); however, nothing is known about sexually dimorphic functions of MT or their contribution to immune dimorphisms.

The Intestinal Epithelium

The *Drosophila* gut is a major immune locus, responding to infection by producing AMPs and reactive oxygen species (122, 123). Infection-induced immune responses are observable in males (122); however, while a small number of studies have compared sex differences in gut metabolism (124), and physiology (24, 124–126), most work on intestinal immunity has focussed on females. Nothing is known about sex dimorphisms in AMP or ROS production, nor indeed survival, after oral infection. However, expression of several immune-related genes have been reported. *Nubbin*, a transcription factor with two isoforms, *nub-RB* and *nub-RD* (127) regulates duration of immune responses within the gut. *Nub-RD* mutants showed chronic immune activation in females (128), whilst overexpressing *nub-RB* resulted in a similar phenotype, illuminating their antagonistic roles within immune signaling (127). Overexpressing *nub-RB* within enterocytes and subsequent oral infection with *P. carotovorum* lead to total and 70% death in males and females, respectively, within 24 h. Downregulation of *nub-RB* enhanced survival to challenge in males compared to controls, while having the opposite effect on females (127). Overexpressing *nub-RB* significantly reduced the lifespans of both sexes, conversely, males reared in germ-free conditions had a slightly enhanced median longevity compared to conventionally-reared counterparts (127). These data could potentially illustrate a greater susceptibility of males to immunopathology from both chronic immune activation and commensals. *Nubbin* isoform antagonism may also offer insight into dimorphic responses between the sexes, where expression of each may differ, however, the cited study only quantified isoform expression in males (127).

The luminal microbiome impacts intestinal immunity (123) as well as many other aspects of *D. melanogaster* physiology and behavior (129). This includes cellular immunity (130), and response to enteric viral infection (131). Studies have shown that the microbiota varies between the sexes in terms of load (24), composition (132), and effect on metabolic responses to diet (133). However, most studies assessing the gut microbiome have only analyzed females, and thus we have very little knowledge about the interaction of commensals with dimorphisms in intestinal immunity. Microbiota populations, at least of the two predominant genera *Acetobacter* and *Lactobacillus*, tend to increase over aging (134), and composition varies between the sexes, where aged males were reported to differ to a greater extent than aged females when compared to their younger counterparts (132). Aging is also associated with a loss of epithelial barrier integrity in the gut (76, 77, 135). This phenomenon is more pronounced in females (24, 76), and is paralleled by increases in systemic immune activation, as indicated by systemic AMP levels (76). Microbiota dysbiosis (77) and loss of a tricellular junctional protein, Gliotactin (135), were shown to precede such changes in females, and loss of an intestinal septate junction protein, Snakeskin, exacerbates barrier loss and causes early death in both sexes (136). These data highlight the link between

microbiome dysbiosis, maintenance of a stable gut barrier, and systemic inflammation. More work is needed to understand the interaction of the dimorphisms involved; for example, the apparently conflicting observations that the male microbiome shows greater changes (132), but despite this, the male gut barrier appears to be more stable over age (24). It is well-known that the microbiome is modeled by diet, environment, and host genotype, so comparing physiological data with microbiome data from different labs may confound interpretation.

Aging and Immune Dimorphisms

Aging and Inflammation

Aging is known to be accompanied by heightened expression of immune genes (37, 39, 137–139). However, cause and consequence are difficult to separate, and understanding the contributions made by age to altered immunity, and immunity to aging, is challenging. When comparing the transcriptional response to aging in whole flies, a strong sex-by-age interaction was observed (139). Of the total significant probe sets, the majority were biased toward males, while just over 25% were sexually antagonistic. Included within this male-biased and antagonistic set were immune-related genes, such as the AMP, *defensin* (139).

In an experimental evolution study on lines where late-life fertility, and indirectly longevity, was selected for over 35 years, decreased expression of immune genes was strongly associated with increased lifespan (137). Females of longer-lived lines exhibited greater realized immunity in the face of challenge with *P. carotovorum*, *B. bassiana*, *E. faecalis,* and DCV than controls (137). Modulation of Toll components had varying effects on male and female lifespan: knockdown of the negative regulator *cactus* had a significantly reducing effect on lifespan, especially in males, whereas *Toll* and *spz* knockdown enhanced lifespan in both sexes (137). *Dif* knockdown had opposing outcomes between the sexes, with females experiencing a slight extension to lifespan (137). However, in two other studies, *Dif* mutants exhibited enhanced lifespan, in the context of intrinsically short-lived background lines (50, 140). Given the sex-specificity of Toll pathway gene expression seen in young flies (23), it is perhaps unsurprising that responses to such modulations are dimorphic.

Age-related systemic inflammation, for example, high basal levels of AMPs and ROS, has been assumed to negatively impact lifespan. This is supported by studies in which AMPs, or Rel-family transcription factors controlling their expression, have been manipulated. Both systemic and fat body-specific overexpression of *relish* negatively affected male lifespan to a greater extent than that of females, and *relish* male mutants were marginally longer-lived than females (39). The selective knockdown of *relish* at mid-life stages in the fat body, however, significantly extended lifespan in males (39). Global overexpression of *attacin A*, *cecropin A1*, *defensin,* and *metchnikowin* had significantly deleterious effects on lifespan of both sexes, with overexpression of *defensin* having a greater impact on males (39), reminiscent of the increase in *defensin* expression in aged males (139). This potentially illustrates age-related immunopathology, where the tempering of hyperactivated immune pathways at mid-late life stages is protective. Intriguingly, clean injury of the cuticle has been shown to extend lifespan in males only, suggesting that a non-lethal wound initiates a response that has a hormetic effect that is particularly effective in males (141). The mechanism for this is unknown, but it is tempting to speculate that it could initiate an anti-inflammatory state through induction of immune regulators.

Immunosenescence

Relatively few studies have looked at immune function in both sexes over aging, particularly from a mechanistic standpoint. While survival following *B. bassiana* decreases over aging in both sexes (140), systemic and cuticular inoculate challenge with the entomopathogenic fungus was reduced in aged females compared to young, while males succumbed only to cuticle inoculation, exhibiting a reduction solely in barrier integrity (114). Age negatively affected the ability to survive an oral *P. carotovorum* challenge in males compared to females, despite their comparatively superior maintenance of intestinal barrier integrity (24). In addition, aged males fared worse in response to systemic *E. coli* (142), *P. aeruginosa,* and *Bacillus thuringiensis* (22) challenges. The studies described above do not investigate the mechanisms underpinning these age-related immune dimorphisms, nor indeed the tissue(s) responsible, except via route of infection (24, 114). In a study investigating the effects of age on hemocyte function, hemocyte numbers were shown to decrease selectively in females over aging (21), supported by a recent study that only examined females (143); although both sexes maintained *ex vivo* phagocytic capacity over age (21). In contrast, a recent study found no effect of age on hemocyte number (22). It is clear that the mechanistic underpinnings of sex-by-age interactions in efficacy of immune responses and autoinflammation are undefined, but could be hugely informative to our understanding of sex differences in age-related pathology and lifespan.

EVOLUTION OF DIMORPHISM THROUGH NATURAL SELECTION

Males and females can have different life histories, which implies that they are exposed to different evolutionary pressures. Because the sexes share a genome, these different pressures can lead to sexual antagonism, which can potentially be resolved through the evolution of sex-specific regulation leading to phenotypic dimorphism. We explore this in the section below with reference to the immune system in *Drosophila*.

One possible driver of natural selection on dimorphism is unequal exposure to parasites in males and females. Males and females may differ in the habitats they occupy, their activity times, or their nutritional needs, for example. Males and females thus occupy separate niches and are potentially exposed to different parasites. Parasites can exert different selection pressures on males and females: the extent to which they do will depend on the extent of ecological divergence between the sexes. Knowledge of the ecology of wild *Drosophila* being relatively limited, it is difficult to define precisely which behaviors

could cause such sex-specific selection. Females lay their eggs in rotting fruits, where they are necessarily exposed to a microbe-rich environment. Whether males spend less time in these environments is not known. Lab studies have indicated that male and female *Drosophila* do not have the same optimal diet, and in diet choice experiments, make different nutritional selections in accordance with their role in reproduction (144–146). Males and females could potentially make different diet choices in the wild, and thus be exposed to different parasites.

A second possible driver of natural selection on dimorphism comes from the fact that the immune system allows resistance to parasites but also represents a cost: it requires a significant investment in terms of resources, and the activation of immune defenses can cause "collateral" damage [e.g., autoimmune reactions (147)]. From this it is predicted that hosts will evolve toward an immune response of intermediate intensity, and not toward a maximum response (148). In other words, hosts evolve within a framework of constraints corresponding to an evolving trade-off. But the terms of this trade-off are not necessarily the same for both sexes: Hamilton and Zuk proposed that the links between investment in immunity and life history traits are sex-specific (149). Under this assumption, it can be predicted that the optimal investment in immunity is not the same in males and females, and could even be antagonistic (150). This scenario is supported by evidence in *Drosophila* that both resistance and tolerance can be sexually antagonistic (46), that expression of immune genes is sexually dimorphic (27), and that the genetic architecture of many traits, including immunity, differ between males and females in *Drosophila* (151–153). This is supported by mutation accumulation experiments indicating that deleterious mutations do not have the same costs in both sexes (154–156). Although the accumulation of spontaneous mutations in *Drosophila* has not yet been shown to have a sexually dimorphic cost on the immune response (46), it does appear have a sex-specific effect on fitness (156). If autosomal determination of immune traits are not clear-cut, the fact that *Drosophila* immune genes can be X- and Y-linked (40, 41, 157) is sufficient to expect that genetic structure can affect immune system evolution in a sex-specific manner. First, the Y chromosome is, by definition, strictly under selection in males and has been demonstrated to influence the immune response (41, 157). For example, only males that had a Y-chromosome introduced from a single wild population differed in their ability to defend against *S. marcescens* (41). Second, since fathers do not pass an X-chromosome to their sons, evolution by sexual selection acting on males would be much slower for traits largely influenced by the X chromosome than would selection on autosomally determined traits, and X-linked sexually antagonistic traits would more freely affect sexual dimorphism (158). Supporting this is the demonstration of X-linked variation in immune response phenotypes in *Drosophila*, including bacterial load and immune gene expression, in a set of 168 X-chromosome extraction lines (40). Many of the associations of genetic variation with immune phenotype acted in a sex-specific or sexually antagonistic manner, supporting the theory that sexually antagonistic variation may be more easily maintained on the X chromosome, and this can impact dimorphism (158).

Sexual Selection and Evolution of Dimorphism: The Hypothesis of the Susceptible Male

Sexual selection is that which operates on the ability to mate successfully. Two traits that generally evolve in parallel in each sex under the effect of sexual selection are choice by females and the ornaments of males. Ornaments are expensive secondary sexual characteristics that evolve as a result of the selection made by the choice of females. A difficulty with this principle is that females can only choose males based on a trait that demonstrates their vigor if that trait remains variable. For sexual selection to occur, therefore, a continuous source of heritable genetic variation must be present in the population. This source of variation prevents genes for vigor from fixation and the character of choice to be only affected by non-heritable environmental factors. Parasites of all kinds offer such selective variation in value because they can evolve quickly and dynamically with their hosts (149, 159). It is on this basis that the famous hypothesis of William (Bill) Hamilton and Marlène Zuk was born. They proposed that parasite selection imposes the evolution of female choice for infection-resistant partners, which in turn favors the evolution of sexual dimorphism in hosts. Thus, as they observed in birds, a negative correlation between ornaments and parasitic load can be found in males (149). Such correlation between expensive ornamental traits and immunity may be present in *Drosophila*. One of the most clearly dimorphic characteristics in *Drosophila* is the color of the cuticle, which is darker in males than in females. The process of darkening the cuticle requires the production of eumelanin, which is also involved in the encapsulation of parasites. This dual role suggests that coloration and immunity are two related characteristics (103, 160). Furthermore, as mentioned above, melanin is produced from dopamine, a neurotransmitter also known to be involved in aggression behavior between males (161), male courtship for females (162) and female receptivity (163). Dopamine and melanin production are thus located at a metabolic crossroads establishing a link between secondary sexual characteristics, mating behavior, and immunity. Other visible, dimorphic characteristics in *D. melanogaster* include bristle number (abdominal and sternopleural), and the presence of sex combs, specialized leg bristles in males which aid copulation. Surprisingly, these traits have not been used, to our knowledge, to study sexual selection, despite being very clearly exposed to females. A recent study reported that flies with a mutation in the *yellow* gene, which encodes a protein involved in the synthesis of eumelanin, fail at mating because insufficient melanization renders their sex combs non-functional for grasping and mounting females during copulation (164). Furthermore, determination of bristle number in males is connected to the process of melanization (165). This link is confirmed by genetic analyses that have shown that *Ddc*, an enzyme essential for dopamine synthesis, has a role in pigmentation (166), and also in the determination of the number of bristles (165). Interestingly, *Ddc* is expressed differentially in males and females, as expected, but its expression is modulated during a bacterial infection [see RNA-seq data for "*Ddc*" in (23)] (167). A mutation in the *ddc* gene could therefore have an

impact on both male ornamentation and response to infection. Female *Drosophila* are able to choose their mates on the basis of phenotypic traits (168, 169), and while evolutionary theory offers several different explanations for female mate choice, most include the evolution of heritable attractive features in males (170). The *Drosophila Genetic Reference Panel* (i.e., DGRP lines) show that natural populations indeed bear variation at several positions in the coding sequence of *Ddc* (see genome browser at genome.ucsc.edu). In *Drosophila*, it is unclear how male ornaments (or attractive traits) trade-off with investment in immunity, but one could speculate that factors required for both cuticle patterning and immune responses could be limiting. Since males have a high selection pressure for access to mating (25), they might still invest in their costly ornament (e.g., cuticle, bristles) to the detriment of their immunity. In any case, the hypothesis that investment in immune melanization may affect secondary sexual traits, such as bristles/combs, remains to be tested.

Hamilton and Zuk have shown that the dimorphism of investment in immunity increases with the intensity of sexual selection. This observation can be explained by a direct negative effect of reproductive traits on those of immunity: this is the so-called immunocompetence handicap hypothesis (171). It occurs because the immune system can interact directly with the hormonal system in relation to sexual dimorphism (172, 173). Increased production of hormones may thus have a benefit for secondary sexuality in males (e.g., ornaments, or competitive traits such as muscle mass) but a deleterious effect on the immune response. Since males have a high selection pressure for access to mating, they might invest in competitive traits to the detriment of their immunity (174). The handicap hypothesis implies that the resource allocation trade-offs between immunity and other characteristics related to selective value are not the same for males and females (148, 175, 176), and leads to the conclusion that males should invest fewer resources in immunity than females. In males, the benefits of increased mating success through greater investment in sexually selected traits (or in costly behaviors) should offset the costs of disease-related reduction in lifespan. Females, on the other hand, would invest more in immunity than males to maximize their breeding time. This prediction extends Bateman's principle to immunity (25, 177). In *Drosophila*, the interaction between immunity and hormones has clearly been identified (32, 33, 93, 178). For example, females produce juvenile hormone (JH) to lay fertilized eggs, and JH directly suppresses the immune response (93). JH affects the antimicrobial peptide (AMP) Drosomycin most strongly, which responds mainly to G+ bacterial infection via the Toll-mediated immune pathway (32). Interestingly, as discussed above, a greater susceptibility of females to some infections is mediated by Toll signaling. This is suggestive that the sex-specific investment of females in egg production via the production of JH has a cost on their immune system, leading to sexual dimorphism in response to certain infections (23).

The previous hypotheses suggest that one sex should be superior than the other while facing infection. Although these hypotheses predict dimorphism *per se,* they cannot explain the inconsistencies in the direction it takes. Alternatively, sex-specific differences may arise from sex-specific changes in reproductive behavior in response to variation in fitness-limiting resources availability, and not from an intrinsically superior immune function (179). In such a case, sex-specific responses would be condition dependent. In *D. melanogaster,* availability of sexually receptive females is an important fitness-limiting resource. While males adjust their level of courtship in response to this resource, increased sexual activity reduces their immune functions, likely because of a reallocation of feeding time into the search for a mate (180). Food availability is, of course, a major fitness-limiting resource. When males and females were kept separate and given *ad libitum* food, immune function was maximized in both sexes and there was no sexual dimorphism in clearance of a benign infection with *E. coli*. However, when the fitness-limiting resources were scarce there was a sex-specific bias (179). When food was limited, females exhibited poorer clearance of the infection than males and, conversely, males with high sexual activity, despite abundant food, performed less well than females. Thus, if there are many reasons for dimorphism to evolve, there are many reasons for its direction to be plastic.

Obstacles to the Evolution of Dimorphism

If different selection pressures are applied to two subpopulations, there is every indication that they will evolve in different ways (181). However, males and females of a species are not subpopulations like any other, since their genomes must recombine in each generation. In each generation, therefore, a gene that is advantageous when expressed in a female can be transmitted from a mother to her son, in whom the expression of this gene could be disadvantageous. In summary, the evolution of a beneficial trait for one sex can be a burden for the other sex (182). In the previous example, the genetic origin of this burden is antagonistic pleiotropy: an allele beneficial to one sex has a negative effect on the other. This sexual conflict, highly investigated in *Drosophila*, can occur at one locus (intra-local conflict: a mutation at one locus has a positive effect for one sex but negative for the other) or at several (interlocal conflict: a mutation at one locus has a negative effect on one sex and selects a mutation at another locus that reduces the effectiveness of the first mutation) (26). This sexual antagonism could mean that the advantage obtained by one sex is exactly offset by the burden the other sex suffers. In other words, antagonistic pleiotropy could prevent the evolution of dimorphism. In a less extreme situation, if dimorphism manages to evolve despite pleiotropy, it is conceivable that neither sex will be able to adapt optimally.

Dimorphism as a Resolution of Sexual Conflict

It is also possible that selection may favor sex-specific regulatory genes that result in an advantageous allele in females being expressed only in females (183). Pleiotropy would then be eliminated, and dimorphism could evolve without constraint. To our knowledge, there is no experimental work that has studied the role of this sexual conflict in the evolution of sex-specific regulation of the response to infections in *Drosophila*.

One Pathogen, One Rule

It is usually impossible to predict, for a given infectious disease, which sex will suffer the most. For example, in mammals, it is often said that males are the "susceptible" sex (184). Men are indeed more susceptible to leishmaniasis, malaria, or bilharzia; but they are more resistant to toxoplasmosis, amebiasis, and giardiasis (12, 185, 186). The complexity increases considering that pathogens can adapt specifically to the sex-specific characteristics of the host. If a parasite is more often exposed to one sex, it is expected to adapt to that sex it encounters most frequently (187). Under such a scenario, even in the absence of sexual dimorphism in response to the infection, the parasite is expected to behave differently and to consequently induce a dimorphism in symptoms or virulence (15, 188). Attempts to generalize, through meta-analyses, are not consistent: they sometimes even imply that there is no real dimorphism (189). If the selection pressures applied to both sexes vary considerably from one parasite to another, we cannot exclude that the effects of the different parasites cancel each other out, so that the average selection pressures applied by all parasites ultimately lead to the same investment in immunity in males and females. Given that different parasites require different methods of control, this seems an unlikely outcome; instead, varied selection pressures, applied differently to each sex, requiring distinct responses, could result in a complex array of context-dependent dimorphisms. In *Drosophila*, reported directions of dimorphism in infection outcome are condition- and pathogen-dependent (**Table 1**), thus it seems inappropriate to propose a generality on the direction of immune sexual dimorphism (23, 40). However, even if the direction is difficult to predict, it is rare that dimorphism does not occur: in that sense, dimorphism in infection outcome seems to be the rule and not the exception.

Environmental Effects on Immune Dimorphism

As if pathogen-dependent dimorphism was not complex enough, infection almost certainly interacts with environmental factors to shape immune dimorphisms. Nutrition modifies the response to infection (190, 191), and where choice is offered, flies will change their feeding preferences in response to infection (192). Diet choices have been empirically demonstrated to increase fitness in insects (193), e.g., in a "true fruit fly" (*Bactrocera tryoni*)—*S. marcescens* infection model, where infection-induced selection of increased carbohydrate-to-protein ratio led to better survival (194). Baseline and infection-induced sex differences in nutrient preference may influence outcome to infection, as may dimorphic responses to macronutrients. For example, in a *D. melanogaster*—*Vibrio cholerae* infection model, increased levels of glucose selectively reduced lifespan in females, but delayed their succumbing to infection, whereas it had no effect on males (195), suggesting that while females suffer long-term consequences of chronically elevated insulin signaling, acute responses to pathogenic challenge, at least by *V. cholerae*, are enhanced by high dietary glucose (195). Nutrient-sensing pathways are known to regulate immune responses, among many other physiological responses to the environment (196), and perturbations in these pathways are shown to affect sex-differential gene expression in *Drosophila,* including expression of immune, defense, and stress response genes (146, 197). Thus, it is essential that we view diet, nutrient-sensing, and sex as interacting factors when considering immune dimorphisms.

Other biotic (density, competition), and abiotic (temperature, humidity) factors are likely to play into dimorphic outcomes to immune challenge. Indeed, in the wild, environmental inputs come as combined, covariate packages, and it is in the context of these combined inputs that *Drosophila* has evolved. Higher-order, systemic signaling pathways such as IIS/mTOR may integrate these inputs to produce phenotypically plastic responses that match current environmental states (196). IIS/mTOR has been empirically demonstrated to regulate immune responses in *D. melanogaster* (198, 199), suggesting that IIS/mTOR could represent a nexus for integrating sex differences in responses to environmental variation, including immunity. Among the biotic factors that have gained much attention recently is the microbiome. Diet, of course, contributes to modeling the gut microbiome and its sex-specificity might shape dimorphic bacterial communities. Thus, microbiota-infection interactions (200, 201) have the potential to shape immune dimorphisms. Microbiome sex differences have been demonstrated in *Drosophila* (132), and likely interact with both dietary choices (133) and responses to infection, therefore it follows that a full understanding of immune dimorphisms cannot be achieved without considering natural poly-microbial interactions.

The Ubiquitous Endosymbiont *Wolbachia* as a Troublemaker

Wolbachia is a ubiquitous endosymbiont predominantly transmitted by mothers to their offspring. This reproductive parasite is known to affect immune characteristics such as phenoloxidase (PO) activity (202), phagocytosis by hemocytes (203), and to affect the outcome of other infections, such as providing resistance to viral infection (204). While not the focus of the study, Martins et al. (60) showed that the level of resistance provided by *Wolbachia* status depends on the sex of the host. Furthermore, *Wolbachia* protects males more than females against enteric infection by the bacterium *P. aeruginosa* (205). For these reasons and because it is so common, we expect that *Wolbachia* infection could influence the direction of immune dimorphism, and even impact the evolution of the dimorphism itself.

Regulation of Immune Dimorphism

Immune dimorphisms in *D. melanogaster* arise from a shared genome, and must be a product of sex-specific gene regulation, however, this is not yet well-resolved. At the top of the regulatory hierarchy are genomic differences, namely sex chromosome karyotype. As we have discussed, there are clear X- and Y-linked effects on immunity in *D. melanogaster*. Downstream of karyotype, dimorphisms can be regulated by the sex determination pathway, a cascade of splicing factors regulated by X chromosome number that ultimately lead to

the expression of sex-specific transcription factors (206). This pathway has recently been shown to have "non-canonical" routes of signaling in some tissues (125), and importantly, to exert profound effects on physiology in larvae and adults beyond its purely developmental role (20). However, the potential regulation of immunity by sex-specific pathways is as yet untested [but see (125) for transcriptional regulation in the intestinal epithelium].

Drosophila, and insects in general, demonstrate that sexual dimorphism can occur without the presence of sex steroids *per se*. Notably, insects produce the steroid hormones ecdysone and juvenile hormone (JH), and as discussed, these are important regulators of immune function. It is possible that hormonal and genetic regulation interact; for example, via sex differences in hormone production or receptor expression (207). One potential source for dimorphic hormone production are the gonads, which may exert influences on immune responses in closely opposed organs, as has recently been demonstrated for regulation of intestinal carbohydrate metabolism by the testes (124). The tractability for genetic manipulation of sex-specific transcription factors and hormone production/reception is a major advantage to using *D. melanogaster* to better understand sex-specific regulation of immune function.

CONCLUSION

We understand relatively little about immune dimorphisms in *Drosophila*, despite their apparent prevalence and magnitude. A real gap in our knowledge is the physiological and mechanistic underpinnings of the male-female differences in survival to infection that have been widely reported. We know almost nothing about how sex dimorphisms are shaped over the life course, including during development, or the influence of dimorphic immunity on aging and vice versa. Dimorphisms may arise from fixed differences in gene expression and tissue function, or from more plastic mechanisms that respond to environmental variables, or both. One thing is certain: the interaction between sex and immunity is complex. Complexity does not lend itself to generalities, and therefore we must be cautious in stating rules about male or female responses. Sex is clearly an essential factor that must be considered in the interpretation of data arising from studies into immunity, where the ideal approach is to include both sexes wherever possible. We argue that not only will including both sexes in studies of *Drosophila* immunity give a more complete picture, it will offer valuable insight into fundamental mechanisms underpinning innate immunity and responses to infection, and an understanding of the factors that drive dimorphisms to arise.

AUTHOR CONTRIBUTIONS

RB, M-KC, DD, and JR researched and wrote the manuscript. DD and JR planned and edited the manuscript. RB and M-KC performed the literature survey and made the figures, graphs and tables.

FUNDING

M-KC was supported by funding to JR from the University of Edinburgh; RB was supported by a Darwin Trust Scholarship; DD was supported by the French Laboratory of Excellence project TULIP(ANR-10-LABX-41; ANR-11-IDEX0002-02).

ACKNOWLEDGMENTS

We thank the reviewers for their insightful and constructive comments on the manuscript.

SUPPLEMENTARY MATERIAL

The Supplementary Material for this article can be found online at: https://www.frontiersin.org/articles/10.3389/fimmu.2019.03075/full#supplementary-material

Figure S1 | Quantity of articles from "both" category with possible tag interactions. Total articles per tag are shown next to each tag title. If a tag is applied, it is indicated with a black dot. Black lines connecting dots indicates conditions where two or more tags were applied to the same article. Quantity of articles in each category are shown above the respective bar.

Table S1 | Complete analysis of 5,626 articles retrieved from webofknowledge.com search. The Boolean search was: (TS = ((infection OR immunity OR hemocyte OR imd OR toll) AND drosophila) NOT TI = (bug OR bumblebee OR shrimp OR damesfly OR mollusc OR crab OR squid OR beetle OR baculovirus OR ant OR monochamus OR dastarcus OR cockroach OR crickets OR gryllus OR bemisia OR armyworm OR spodoptera OR mussel OR galleria OR helicoverpa OR amphibian OR manduca OR bee OR honey OR bactrocera OR tenebrio OR zebra OR dugesia OR flesh OR Apis OR house OR glossnia OR jelly OR Andrias OR dragonfly OR pachydiplax OR termite OR leech OR stick OR rhynchophorus OR rhodnius OR pardosa OR plutella OR coleoptera OR zophobas OR glossina OR ceratitis OR suzukii OR diabrotica OR rootworm OR sheep OR whitefly OR bird OR branchiostoma OR lizards OR laodelphax OR ceratopogonidae OR crassostrea OR oyster OR artemia OR freshwater OR calliphoridae OR phytomonas OR acyrthosiphon OR aphid OR crustacean OR parhyale OR hippocampus OR seahorse OR anopheles OR protaetia OR sea OR litopenaeus OR copepod OR swine OR planthopper OR arabidopsis OR circulifer OR leafhopper OR apostichopus OR cryptolaemus OR clam OR paphia OR mollusk OR achaea OR castor OR musca OR salmon OR dog OR echinococcus OR hetaerina OR sarcophaga OR fleshfly OR bovine OR zygoptera OR calopterygidae OR coenagrionidae OR scorpion OR locusta OR harpalus OR culex OR scylla OR firefly OR honeybees OR antheraea OR penaeus OR trichinella OR prawn OR macrobrachium OR ostrinia OR arge OR magnaporthe OR Phaeotabanus OR palm OR ostrinia OR daphnia OR scallop OR Chlamys OR Biomphalaria OR pig OR Anostostomatidae OR Orthoptera OR crayfish OR procambarus OR Platynereis)).

REFERENCES

1. Jin W, Riley RM, Wolfinger RD, White KP, Passador-Gurgel G, Gibson G. The contributions of sex, genotype and age to transcriptional variance in *Drosophila melanogaster*. *Nat Genet.* (2001) 29:389–95. doi: 10.1038/ng766
2. Svensson EI, Goedert D, Gómez-Llano MA, Spagopoulou F, Nava-Bolaños A, Booksmythe I. Sex differences in local adaptation: what can we learn from reciprocal transplant experiments? *Philos Trans R Soc B Biol Sci.* (2018) 373:20170420. doi: 10.1098/rstb.2017.0420
3. Klein SL, Flanagan KL. Sex differences in immune responses. *Nat Rev Immunol.* (2016) 16:626–38. doi: 10.1038/nri.2016.90

4. Simon V. Wanted: women in clinical trials. *Science.* (2005) 308:1517. doi: 10.1126/science.1115616
5. Beery AK, Zucker I. Sex bias in neuroscience and biomedical research. *Neurosci Biobehav Rev.* (2011) 35:565–572. doi: 10.1016/j.neubiorev.2010.07.002
6. Liu KA, DiPietro Mager NA. Women's involvement in clinical trials: historical perspective and future implications. *Pharm Pract.* (2016) 14:708. doi: 10.18549/PharmPract.2016.01.708
7. Mazure CM, Jones DP. Twenty years and still counting: including women as participants and studying sex and gender in biomedical research. *BMC Womens Health.* (2015) 15:94. doi: 10.1186/s12905-015-0251-9
8. Avery E, Clark J. Sex-related reporting in randomised controlled trials in medical journals. *Lancet.* (2016) 388:2839–40. doi: 10.1016/S0140-6736(16)32393-5
9. Clayton JA, Collins FS. Policy: NIH to balance sex in cell and animal studies. *Nat News.* (2014) 509:282. doi: 10.1038/509282a
10. Miller LR, Marks C, Becker JB, Hurn PD, Chen W-J, Woodruff T, et al. Considering sex as a biological variable in preclinical research. *FASEB J.* (2016) 31:29–34. doi: 10.1096/fj.201600781R
11. Guncay A, Balasubramaniam T, Plagens K, Weadge J, Long TAF. Cross-generational effects of male reproductive success and offspring immunocompetence in *Drosophila melanogaster*. *FACETS.* (2017) 2:34–52. doi: 10.1139/facets-2015-0007
12. vom Steeg LG, Klein SL. SeXX matters in infectious disease pathogenesis. *PLoS Pathog.* (2016) 12:e1005374. doi: 10.1371/journal.ppat.1005374
13. Reimchen TE, Nosil P. Ecological causes of sex-biased parasitism in threespine stickleback. *Biol J Linn Soc.* (2001) 73:51–63. doi: 10.1111/j.1095-8312.2001.tb01346.x
14. Kelly CD, Tawes BR. Sex-specific effect of juvenile diet on adult disease resistance in a field cricket. *PLoS ONE.* (2013) 8:e61301. doi: 10.1371/journal.pone.0061301
15. Duneau DF, Luijckx P, Ruder LF, Ebert D. Sex-specific effects of a parasite evolving in a female-biased host population. *BMC Biol.* (2012) 10:104. doi: 10.1186/1741-7007-10-104
16. Gipson SAY, Hall MD. Interactions between host sex and age of exposure modify the virulence–transmission trade-off. *J Evol Biol.* (2018) 31:428–437. doi: 10.1111/jeb.13237
17. Kopp A, Duncan I, Carroll SB. Genetic control and evolution of sexually dimorphic characters in Drosophila. *Nature.* (2000) 408:553–9. doi: 10.1038/35046017
18. Kolluru GR, Chappell MA, Zuk M. Sex differences in metabolic rates in field crickets and their dipteran parasitoids. *J Comp Physiol B.* (2004) 174:641–8. doi: 10.1007/s00360-004-0455-z
19. Teder T, Tammaru T. Sexual size dimorphism within species increases with body size in insects. *Oikos.* (2005) 108:321–34. doi: 10.1111/j.0030-1299.2005.13609.x
20. Millington JW, Rideout EJ. Sex differences in Drosophila development and physiology. *Curr Opin Physiol.* (2018) 6:46–56. doi: 10.1016/j.cophys.2018.04.002
21. Mackenzie DK, Bussière LF, Tinsley MC. Senescence of the cellular immune response in *Drosophila melanogaster*. *Exp Gerontol.* (2011) 46:853–9. doi: 10.1016/j.exger.2011.07.004
22. Leech T, Evison SEF, Armitage SAO, Sait SM, Bretman A. Interactive effects of social environment, age and sex on immune responses in *Drosophila melanogaster*. *J Evol Biol.* (2019) 32:1082–92. doi: 10.1111/jeb.13509
23. Duneau DF, Kondolf HC, Im JH, Ortiz GA, Chow C, Fox MA, et al. The Toll pathway underlies host sexual dimorphism in resistance to both Gram-negative and Gram-positive bacteria in mated Drosophila. *BMC Biol.* (2017) 15:124. doi: 10.1186/s12915-017-0466-3
24. Regan JC, Khericha M, Dobson AJ, Bolukbasi E, Rattanavirotkul N, Partridge L. Sex difference in pathology of the ageing gut mediates the greater response of female lifespan to dietary restriction. *eLife.* (2016) 5:10956. doi: 10.7554/eLife.10956
25. Bateman AJ. Intra-sexual selection in Drosophila. *Heredity.* (1948) 2:349–68.
26. Bonduriansky R, Chenoweth SF. Intralocus sexual conflict. *Trends Ecol Evol.* (2009) 24:280–8. doi: 10.1016/j.tree.2008.12.005
27. Innocenti P, Morrow EH. The sexually antagonistic genes of *Drosophila melanogaster*. *PLoS Biol.* (2010) 8:e1000335. doi: 10.1371/journal.pbio.1000335
28. Tseng M. Sex–specific response of a mosquito to parasites and crowding. *Proc R Soc Lond B Biol Sci.* (2004) 271:S186–8. doi: 10.1098/rsbl.2003.0139
29. Hoang KP, Teo TM, Ho TX, Le VS. Mechanisms of sex determination and transmission ratio distortion in *Aedes aegypti*. *Parasit Vectors.* (2016) 9:49. doi: 10.1186/s13071-016-1331-x
30. Xue L, Manore CA, Thongsripong P, Hyman JM. Two-sex mosquito model for the persistence of Wolbachia. *J Biol Dyn.* (2017) 11:216–37. doi: 10.1080/17513758.2016.1229051
31. Buchon N, Silverman N, Cherry S. Immunity in *Drosophila melanogaster* — from microbial recognition to whole- organism physiology. *Nat Rev Immunol.* (2014) 14:796–810. doi: 10.1038/nri3763
32. Flatt T, Heyland A, Rus F, Porpiglia E, Sherlock C, Yamamoto R, et al. Hormonal regulation of the humoral innate immune response in *Drosophila melanogaster*. *J Exp Biol.* (2008) 211:2712–24. doi: 10.1242/jeb.014878
33. Regan JC, Brandão AS, Leitão AB, Mantas Dias ÂR, Sucena É, Jacinto A, et al. Steroid hormone signaling is essential to regulate innate immune cells and fight bacterial infection in Drosophila. *PLoS Pathog.* (2013) 9:e1003720. doi: 10.1371/journal.ppat.1003720
34. Bakalov VK, Gutin L, Cheng CM, Zhou J, Sheth P, Shah K, et al. Autoimmune disorders in women with turner syndrome and women with karyotypically normal primary ovarian insufficiency. *J Autoimmun.* (2012) 38:315–21. doi: 10.1016/j.jaut.2012.01.015
35. Hewagama A, Gorelik G, Patel D, Liyanarachchi P, Joseph McCune W, Somers E, et al. Overexpression of X-Linked genes in T cells from women with lupus. *J Autoimmun.* (2013) 41:60–71. doi: 10.1016/j.jaut.2012.12.006
36. Invernizzi P, Miozzo M, Selmi C, Persani L, Battezzati PM, Zuin M, et al. X chromosome monosomy: a common mechanism for autoimmune diseases. *J Immunol.* (2005) 175:575–8. doi: 10.4049/jimmunol.175.1.575
37. Kounatidis I, Chtarbanova S, Cao Y, Hayne M, Jayanth D, Ganetzky B, et al. NF-κB immunity in the brain determines fly lifespan in healthy aging and age-related neurodegeneration. *Cell Rep.* (2017) 19:836–48. doi: 10.1016/j.celrep.2017.04.007
38. Shukla AK, Spurrier J, Kuzina I, Giniger E. Hyperactive innate immunity causes degeneration of dopamine neurons upon altering activity of Cdk5. *Cell Rep.* (2019) 26:131–44.e4. doi: 10.1016/j.celrep.2018.12.025
39. Badinloo M, Nguyen E, Suh W, Alzahrani F, Castellanos J, Klichko VI, et al. Overexpression of antimicrobial peptides contributes to aging through cytotoxic effects in Drosophila tissues. *Arch Insect Biochem Physiol.* (2018) 98:e21464. doi: 10.1002/arch.21464
40. Hill-Burns EM, Clark AG. X-Linked variation in immune response in *Drosophila melanogaster*. *Genetics.* (2009) 183:1477–91. doi: 10.1534/genetics.108.093971
41. Kutch IC, Fedorka KM. Y-linked variation for autosomal immune gene regulation has the potential to shape sexually dimorphic immunity. *Proc R Soc B Biol Sci.* (2015) 282:20151301. doi: 10.1098/rspb.2015.1301
42. Meier A, Chang JJ, Chan ES, Pollard RB, Sidhu HK, Kulkarni S, et al. Sex differences in the Toll-like receptor–mediated response of plasmacytoid dendritic cells to HIV-1. *Nat Med.* (2009) 15:955–9. doi: 10.1038/nm.2004
43. Akuffo H, Hultmark D, Engstöm A, Frohlich D, Kimbrell D. Drosophila antibacterial protein, cecropin A, differentially affects non-bacterial organisms such as Leishmania in a manner different from other amphipathic peptides. *Int J Mol Med.* (1998) 1:77–159.
44. Sinha P, Saxena SK. Changes in amine acid content in tomato as a result of infection with *Rhizopus stolonifer* in presence of *Drosophila busckii*. *Sci Lett.* (1988) 203.
45. Jeune B, Thomas-Orillard M. Beneficial effects of viral infection in Drosophila: an evolutionary model. *Acta Oecol.* (1991) 12:489–508.
46. Vincent CM, Sharp NP. Sexual antagonism for resistance and tolerance to infection in *Drosophila melanogaster*. *Proc R Soc B Biol Sci.* (2014) 281:20140987. doi: 10.1098/rspb.2014.0987
47. Schneider D, Miller WJ, Riegler M. Arthropods shopping for Wolbachia. In: Zchori-Fein E, Bourtzis K, editors. *Manipulative Tenants Bacteria Associated with Arthropods.* Boca Raton, FL: CRC Press-Taylor & Francis Group (2011). p. 149–73.

48. Palmer WH, Medd NC, Beard PM, Obbard DJ. Isolation of a natural DNA virus of *Drosophila melanogaster*, and characterisation of host resistance and immune responses. *PLoS Pathog.* (2018) 14:e1007050. doi: 10.1371/journal.ppat.1007050
49. Le Bourg É. Combined effects of suppressing live yeast and of a cold pretreatment on longevity, aging and resistance to several stresses in *Drosophila melanogaster*. *Biogerontology.* (2010) 11:245–54. doi: 10.1007/s10522-009-9250-2
50. Le Bourg É. The NF-kB like factor DIF has weaker effects on *Drosophila melanogaster* immune defenses than previously thought. *J Comp Physiol B.* (2011) 181:741–50. doi: 10.1007/s00360-011-0567-1
51. Le Bourg É. Fasting can protect young and middle-aged *Drosophila melanogaster* flies against a severe cold stress. *Biogerontology.* (2013) 14:513–29. doi: 10.1007/s10522-013-9458-z
52. Taylor K, Kimbrell D. Host immune response and differential survival of the sexes in Drosophila. *Fly.* (2007) 1:197–204. doi: 10.4161/fly.5082
53. Shahrestani P, Chambers M, Vandenberg J, Garcia K, Malaret G, Chowdhury P, et al. Sexual dimorphism in *Drosophila melanogaster* survival of *Beauveria bassiana* infection depends on core immune signaling. *Sci Rep.* (2018) 8:12501. doi: 10.1038/s41598-018-30527-1
54. Lu H-L, Wang JB, Brown MA, Euerle C, Leger RJS. Identification of Drosophila mutants affecting defense to an entomopathogenic fungus. *Sci Rep.* (2015) 5:12350. doi: 10.1038/srep12350
55. Chowdhury M, Li C-F, He Z, Lu Y, Liu X-S, Wang Y-F, et al. Toll family members bind multiple Spätzle proteins and activate antimicrobial peptide gene expression in Drosophila. *J Biol Chem.* (2019) 294:10172–81. doi: 10.1074/jbc.RA118.006804
56. Franchet A, Niehus S, Caravello G, Ferrandon D. Phosphatidic acid as a limiting host metabolite for the proliferation of the microsporidium Tubulinosema ratisbonensis in Drosophila flies. *Nat Microbiol.* (2019) 4:645–55. doi: 10.1038/s41564-018-0344-y
57. Bastos RG, Howard ZP, Hiroyasu A, Goodman AG. Host and bacterial factors control susceptibility of *Drosophila melanogaster* to *Coxiella burnetii* infection. *Infect Immun.* (2017) 85:e00218-17. doi: 10.1128/IAI.00218-17
58. Kutch IC, Fedorka KM. A test for Y-linked additive and epistatic effects on surviving bacterial infections in *Drosophila melanogaster*. *J Evol Biol.* (2017) 30:1400–8. doi: 10.1111/jeb.13118
59. Gupta V, Stewart CO, Rund SSC, Monteith KM, Vale PF. Costs and benefits of sublethal Drosophila C virus infection. *J Evol Biol.* (2017) 30:1325–35. doi: 10.1111/jeb.13096
60. Martins NE, Faria VG, Nolte V, Schlötterer C, Teixeira L, Sucena É, et al. Host adaptation to viruses relies on few genes with different cross-resistance properties. *Proc Natl Acad Sci USA.* (2014) 111:5938–43. doi: 10.1073/pnas.1400378111
61. Vale PF, Jardine MD. Sex-specific behavioural symptoms of viral gut infection and Wolbachia in *Drosophila melanogaster*. *J Insect Physiol.* (2015) 82:28–32. doi: 10.1016/j.jinsphys.2015.08.005
62. Thomson TC, Schneemann A, Johnson J. Oocyte destruction is activated during viral infection. *Genesis.* (2012) 50:453–65. doi: 10.1002/dvg.22004
63. Gomariz-Zilber E, Jeune B, Thomas-Orillard M. Limiting conditions of the horizontal transmission of the Drosophila C virus in its host (*D. melanogaster*). *Acta Oecol.* (1998) 19:125–37. doi: 10.1016/S1146-609X(98)80016-7
64. Wayne ML, Blohm GM, Brooks ME, Regan KL, Brown BY, Barfield M, et al. The prevalence and persistence of sigma virus, a biparentally transmitted parasite of *Drosophila melanogaster*. *Evol Ecol Res.* (2011) 13:323–45.
65. Carpenter J, Hutter S, Baines JF, Roller J, Saminadin-Peter SS, Parsch J, et al. The transcriptional response of *Drosophila melanogaster* to infection with the sigma virus (Rhabdoviridae). *PLoS ONE.* (2009) 4:e6838. doi: 10.1371/journal.pone.0006838
66. Tzou P, Ohresser S, Ferrandon D, Capovilla M, Reichhart J-M, Lemaitre B, et al. Tissue-specific inducible expression of antimicrobial peptide genes in Drosophila surface epithelia. *Immunity.* (2000) 13:737–48. doi: 10.1016/S1074-7613(00)00072-8
67. Ferrandon D, Jung AC, Criqui M-C, Lemaitre B, Uttenweiler-Joseph S, et al. A drosomycin–GFP reporter transgene reveals a local immune response in Drosophila that is not dependent on the toll pathway. *EMBO J.* (1998) 17:1217–27. doi: 10.1093/emboj/17.5.1217
68. Ryu J-H, Nam K-B, Oh C-T, Nam H-J, Kim S-H, Yoon J-H, et al. The homeobox gene caudal regulates constitutive local expression of antimicrobial peptide genes in Drosophila epithelia. *Mol Cell Biol.* (2004) 24:172–85. doi: 10.1128/MCB.24.1.172-185.2004
69. Samakovlis C, Kylsten P, Kimbrell DA, Engström A, Hultmark D. The andropin gene and its product, a male-specific antibacterial peptide in *Drosophila melanogaster*. *EMBO J.* (1991) 10:163–9. doi: 10.1002/j.1460-2075.1991.tb07932.x
70. Chintapalli VR, Terhzaz S, Wang J, Bratty MA, Watson DG, Herzyk P, et al. Functional correlates of positional and gender-specific renal asymmetry in Drosophila. *PLoS ONE.* (2012) 7:e32577. doi: 10.1371/journal.pone.0032577
71. Tang H, Kambris Z, Lemaitre B, Hashimoto C. A serpin that regulates immune melanization in the respiratory system of Drosophila. *Dev Cell.* (2008) 15:617–26. doi: 10.1016/j.devcel.2008.08.017
72. Levin TC, Malik HS. Rapidly evolving toll-3/4 genes encode male-specific toll-like receptors in Drosophila. *Mol Biol Evol.* (2017) 34:2307–23. doi: 10.1093/molbev/msx168
73. Tauszig S, Jouanguy E, Hoffmann JA, Imler J-L. Toll-related receptors and the control of antimicrobial peptide expression in Drosophila. *Proc Natl Acad Sci USA.* (2000) 97:10520–5. doi: 10.1073/pnas.180130797
74. Reichhart JM, Georgel P, Meister M, Lemaitre B, Kappler C, Hoffmann JA. Expression and nuclear translocation of the rel/NF-kappa B-related morphogen dorsal during the immune response of Drosophila. *Comptes Rendus Académie Sci Sér III Sci Vie.* (1993) 316:1218–24.
75. Bhattacharya A, Steward R. The Drosophila homolog of NTF-2, the nuclear transport factor-2, is essential for immune response. *EMBO Rep.* (2002) 3:378–83. doi: 10.1093/embo-reports/kvf072
76. Rera M, Clark RI, Walker DW. Intestinal barrier dysfunction links metabolic and inflammatory markers of aging to death in Drosophila. *Proc Natl Acad Sci USA.* (2012) 109:21528–33. doi: 10.1073/pnas.1215849110
77. Clark RI, Salazar A, Yamada R, Fitz-Gibbon S, Morselli M, Alcaraz J, et al. Distinct shifts in microbiota composition during drosophila aging impair intestinal function and drive mortality. *Cell Rep.* (2015) 12:1656–67. doi: 10.1016/j.celrep.2015.08.004
78. Vale PF, Jardine MD. Infection avoidance behavior: viral exposure reduces the motivation to forage in female *Drosophila melanogaster*. *Fly.* (2017) 11:3–9. doi: 10.1080/19336934.2016.1207029
79. Meister M, Braun A, Kappler C, Reichhart J-M, Hoffmann JA. Insect immunity. A transgenic analysis in Drosophila defines several functional domains in the diptericin promoter. *EMBO J.* (1994) 13:5958–66.
80. Gendrin M, Welchman DP, Poidevin M, Hervé M, Lemaitre B. Long-range activation of systemic immunity through peptidoglycan diffusion in Drosophila. *PLoS Pathog.* (2009) 5:e1000694. doi: 10.1371/journal.ppat.1000694
81. Le Bourg É. A cold stress applied at various ages can increase resistance to heat and fungal infection in aged *Drosophila melanogaster* flies. *Biogerontology.* (2011) 12:185–93. doi: 10.1007/s10522-010-9309-0
82. Bashir-Tanoli S, Tinsley MC. Immune response costs are associated with changes in resource acquisition and not resource reallocation. *Funct Ecol.* (2014) 28:1011–9. doi: 10.1111/1365-2435.12236
83. Wang JB, Lu H-L, Leger RJS. The genetic basis for variation in resistance to infection in the *Drosophila melanogaster* genetic reference panel. *PLoS Pathog.* (2017) 13:e1006260. doi: 10.1371/journal.ppat.1006260
84. Bourtzis K, O'Neill S. Wolbachia infections and arthropod reproduction Wolbachia can cause cytoplasmic incompatibility, parthenogenesis, and feminization in many arthropods. *Bioscience.* (1998) 48:287–93. doi: 10.2307/1313355
85. Merçot H, Charlat S. Wolbachia infections in *Drosophila Melanogaster* and *D. simulans*: polymorphism and levels of cytoplasmic incompatibility. *Genetica.* (2004) 120:51–9. doi: 10.1023/B:GENE.0000017629.31383.8f
86. Cook PE, McGraw EA. Wolbachia pipientis: an expanding bag of tricks to explore for disease control. *Trends Parasitol.* (2010) 26:373–5. doi: 10.1016/j.pt.2010.05.006
87. Maistrenko OM, Serga SV, Vaiserman AM, Kozeretska IA. Effect of Wolbachia infection on aging and longevity-associated genes in Drosophila. In: Vaiserman AM, Moskalev AA, Pasyukova EG, editors. *Life Extension: Lessons from Drosophila Healthy Ageing and*

Longevity. Cham: Springer International Publishing (2015). p. 83–104. doi: 10.1007/978-3-319-18326-8_4
88. Valanne S, Wang J-H, Rämet M. The Drosophila toll signaling pathway. *J Immunol.* (2011) 186:649–56. doi: 10.4049/jimmunol.1002302
89. Myllymäki H, Valanne S, Rämet M. The Drosophila Imd signaling pathway. *J Immunol.* (2014) 192:3455–62. doi: 10.4049/jimmunol.1303309
90. Vaz F, Kounatidis I, Covas G, Parton RM, Harkiolaki M, Davis I, et al. Accessibility to peptidoglycan is important for the recognition of gram-positive bacteria in Drosophila. *Cell Rep.* (2019) 27:2480–92.e6. doi: 10.1016/j.celrep.2019.04.103
91. Buchanan JL, Meiklejohn CD, Montooth KL. Mitochondrial dysfunction and infection generate immunity–fecundity tradeoffs in Drosophila. *Integr Comp Biol.* (2018) 58:591–603. doi: 10.1093/icb/icy078
92. Short SM, Lazzaro BP. Female and male genetic contributions to post-mating immune defence in female *Drosophila melanogaster*. *Proc R Soc B Biol Sci.* (2010) 277:3649–57. doi: 10.1098/rspb.2010.0937
93. Schwenke RA, Lazzaro BP. Juvenile hormone suppresses resistance to infection in mated female *Drosophila melanogaster*. *Curr Biol.* (2017) 27:596–601. doi: 10.1016/j.cub.2017.01.004
94. Yanagawa A, Guigue AMA, Marion-Poll F. Hygienic grooming is induced by contact chemicals in *Drosophila melanogaster*. *Front Behav Neurosci.* (2014) 8:254. doi: 10.3389/fnbeh.2014.00254
95. Yanagawa A, Chabaud M-A, Imai T, Marion-Poll F. Olfactory cues play a significant role in removing fungus from the body surface of *Drosophila melanogaster*. *J Invertebr Pathol.* (2018) 151:144–50. doi: 10.1016/j.jip.2017.11.011
96. Caragata EP, Real KM, Zalucki MP, McGraw EA. Wolbachia infection increases recapture rate of field-released *Drosophila melanogaster*. *Symbiosis.* (2011) 54:55. doi: 10.1007/s13199-011-0124-4
97. Toda H, Williams JA, Gulledge M, Sehgal A. A sleep-inducing gene, nemuri, links sleep and immune function in Drosophila. *Science.* (2019) 363:509. doi: 10.1126/science.aat1650
98. Howick VM, Lazzaro BP. Genotype and diet shape resistance and tolerance across distinct phases of bacterial infection. *BMC Evol Biol.* (2014) 14:56. doi: 10.1186/1471-2148-14-56
99. Kurz CL, Charroux B, Chaduli D, Viallat-Lieutaud A, Royet J. Peptidoglycan sensing by octopaminergic neurons modulates Drosophila oviposition. *Elife.* (2017) 6:e21937. doi: 10.7554/eLife.21937
100. Masuzzo A, Manière G, Viallat-Lieutaud A, Avazeri É, Zugasti O, Grosjean Y, et al. Peptidoglycan-dependent NF-κB activation in a small subset of brain octopaminergic neurons controls female oviposition. *eLife.* (2019) 8:e50559. doi: 10.7554/eLife.50559
101. Kelsey EM, Luo X, Brückner K, Jasper H. Schnurri regulates hemocyte function to promote tissue recovery after DNA damage. *J Cell Sci.* (2012) 125:1393–400. doi: 10.1242/jcs.095323
102. Kleinhesselink K, Conway C, Sholer D, Huang I, Kimbrell DA. Regulation of hemocytes in Drosophila requires dappled Cytochrome b5. *Biochem Genet.* (2011) 49:329–51. doi: 10.1007/s10528-010-9411-7
103. Nakhleh J, El Moussawi L, Osta MA. The melanization response in insect immunity. In: Ligoxygakis P. editor. *Advances in Insect Physiology.* Elsevier (2017). p. 83–109.
104. Nappi AJ, Poirié M, Carton Y. Chapter 4: The role of melanization and cytotoxic by-products in the cellular immune responses of Drosophila against parasitic wasps. In: Prevost G. editor. *Advances in Parasitology.* Elsevier (2009). p. 99–121. doi: 10.1016/S0065-308X(09)70004-1
105. Dudzic J, Kondo S, Ueda R, Bergman CM, Lemaitre B. Drosophila innate immunity: regional and functional specialization of prophenoloxidases. *BMC Biol.* (2015) 13:81. doi: 10.1186/s12915-015-0193-6
106. Dudzic J, Hanson MA, Iatsenko I, Kondo S, Lemaitre B. More than black or white: melanization and toll share regulatory serine proteases in Drosophila. *Cell Rep.* (2019) 27:1050–61.e3. doi: 10.1016/j.celrep.2019.03.101
107. Binggeli O, Neyen C, Poidevin M, Lemaitre B. Prophenoloxidase activation is required for survival to microbial infections in Drosophila. *PLoS Pathog.* (2014) 10:e1004067. doi: 10.1371/journal.ppat.1004067
108. Ming M, Obata F, Kuranaga E, Miura M. Persephone/Spätzle pathogen sensors mediate the activation of Toll receptor signaling in response to endogenous danger signals in apoptosis-deficient Drosophila. *J Biol Chem.* (2014) 289:7558–68. doi: 10.1074/jbc.M113.543884
109. Issa N, Guillaumot N, Lauret E, Matt N, Schaeffer-Reiss C, Dorsselaer AV, et al. The circulating protease persephone is an immune sensor for microbial proteolytic activities upstream of the Drosophila toll pathway. *Mol Cell.* (2018) 69:539–50.e6. doi: 10.1016/j.molcel.2018.01.029
110. Hedengren M, Borge K, Hultmark D. Expression and evolution of the drosophila attacin/diptericin gene family. *Biochem Biophys Res Commun.* (2000) 279:574–81. doi: 10.1006/bbrc.2000.3988
111. Junell A, Uvell H, Davis MM, Edlundh-Rose E, Antonsson Å, Pick L, Engström Y. The POU transcription factor drifter/ventral veinless regulates expression of Drosophila immune defense genes. *Mol Cell Biol.* (2010) 30:3672–84. doi: 10.1128/MCB.00223-10
112. Merkling SH, Bronkhorst AW, Kramer JM, Overheul GJ, Schenck A, Rij RPV. The epigenetic regulator G9a mediates tolerance to RNA virus infection in Drosophila. *PLoS Pathog.* (2015) 11:e1004692. doi: 10.1371/journal.ppat.1004692
113. Gupta, Vale PF. Nonlinear disease tolerance curves reveal distinct components of host responses to viral infection. *R Soc Open Sci.* (2017) 4:170342. doi: 10.1098/rsos.170342
114. Kubiak M, Tinsley MC. Sex-specific routes to immune senescence in *Drosophila melanogaster*. *Sci Rep.* (2017) 7:10417. doi: 10.1038/s41598-017-11021-6
115. Le Bourg É, Massou I, Gobert V. Cold stress increases resistance to fungal infection throughout life in *Drosophila melanogaster*. *Biogerontology.* (2008) 10:613. doi: 10.1007/s10522-008-9206-y
116. Le Rohellec M, Le Bourg É. Contrasted effects of suppressing live yeast from food on longevity, aging and resistance to several stresses in *Drosophila melanogaster*. *Exp Gerontol.* (2009) 44:695–707. doi: 10.1016/j.exger.2009.08.001
117. Akhouayri I, Turc C, Royet J, Charroux B. Toll-8/Tollo negatively regulates antimicrobial response in the Drosophila respiratory epithelium. *PLoS Pathog.* (2011) 7:e1002319. doi: 10.1371/journal.ppat.1002319
118. Peng J, Zipperlen P, Kubli E. Drosophila sex-peptide stimulates female innate immune system after mating via the Toll and Imd pathways. *Curr Biol.* (2005) 15:1690–94. doi: 10.1016/j.cub.2005.08.048
119. Winterhalter WE, Fedorka KM. Sex-specific variation in the emphasis, inducibility and timing of the post-mating immune response in *Drosophila melanogaster*. *Proc R Soc B Biol Sci.* (2009) 276:1109–17. doi: 10.1098/rspb.2008.1559
120. Lung O, Kuo L, Wolfner MF. Drosophila males transfer antibacterial proteins from their accessory gland and ejaculatory duct to their mates. *J Insect Physiol.* (2001) 47:617–22. doi: 10.1016/S0022-1910(00)00151-7
121. McGettigan J, McLennan RKJ, Broderick KE, Kean L, Allan AK, Cabrero P, et al. Insect renal tubules constitute a cell-autonomous immune system that protects the organism against bacterial infection. *Insect Biochem Mol Biol.* (2005) 35:741–54. doi: 10.1016/j.ibmb.2005.02.017
122. Ha E-M, Oh C-T, Bae YS, Lee W-J. A direct role for dual oxidase in Drosophila gut immunity. *Science.* (2005) 310:847–50. doi: 10.1126/science.1117311
123. Buchon N, Broderick NA, Lemaitre B. Gut homeostasis in a microbial world: insights from *Drosophila melanogaster*. *Nat Rev Microbiol.* (2013) 11:615–26. doi: 10.1038/nrmicro3074
124. Hudry B, de Goeij E, Mineo A, Gaspar P, Hadjieconomou D, Studd C, et al. Sex differences in intestinal carbohydrate metabolism promote food intake and sperm maturation. *Cell.* (2019) 178:901–18.e16. doi: 10.1016/j.cell.2019.07.029
125. Hudry B, Khadayate S, Miguel-Aliaga I. The sexual identity of adult intestinal stem cells controls organ size and plasticity. *Nature.* (2016) 530:344–8. doi: 10.1038/nature16953
126. Regan JC, Lu Y-X, Bolukbasi E, Khericha M, Partridge L. Ras inhibition by trametinib treatment in Drosophila attenuates gut pathology in females and extends lifespan in both sexes. *bioRxiv*. (2018) 356295. doi: 10.1101/356295
127. Lindberg BG, Tang X, Dantoft W, Gohel P, Esfahani SS, Lindvall JM, Engström Y. Nubbin isoform antagonism governs Drosophila intestinal immune homeostasis. *PLoS Pathog.* (2018) 14:e1006936. doi: 10.1371/journal.ppat.1006936
128. Dantoft W, Davis MM, Lindvall JM, Tang X, Uvell H, Junell A, et al. The Oct1 homolog Nubbin is a repressor of NF-κB-dependent immune gene

expression that increases the tolerance to gut microbiota. *BMC Biol.* (2013) 11:99. doi: 10.1186/1741-7007-11-99
129. Martino M, Ma D, Leulier F. Microbial influence on Drosophila biology. *Curr Opin Microbiol.* (2017) 38:165–70. doi: 10.1016/j.mib.2017.06.004
130. Benoit JB, Vigneron A, Broderick NA, Wu Y, Sun JS, Carlson JR, et al. Symbiont-induced odorant binding proteins mediate insect host hematopoiesis. *elife.* (2017) 6:e19535. doi: 10.7554/eLife.19535
131. Sansone CL, Cohen J, Yasunaga A, Xu J, Osborn G, Subramanian H, et al. Microbiota-dependent priming of antiviral intestinal immunity in Drosophila. *Cell Host Microbe.* (2015) 18:571–81. doi: 10.1016/j.chom.2015.10.010
132. Han G, Lee HJ, Jeong SE, Jeon CO, Hyun S. Comparative analysis of *Drosophila melanogaster* gut microbiota with respect to host strain, sex, and age. *Microb Ecol.* (2017) 74:207–16. doi: 10.1007/s00248-016-0925-3
133. Wong AC-N, Dobson AJ, Douglas AE. Gut microbiota dictates the metabolic response of Drosophila to diet. *J Exp Biol.* (2014) 217:1894–901. doi: 10.1242/jeb.101725
134. Blum JE, Fischer CN, Miles J, Handelsman J. Frequent replenishment sustains the beneficial microbiome of *Drosophila melanogaster*. *mBio.* (2013) 4:e00860-13. doi: 10.1128/mBio.00860-13
135. Resnik-Docampo M, Koehler CL, Clark RI, Schinaman JM, Sauer V, Wong DM, et al. Tricellular junctions regulate intestinal stem cell behaviour to maintain homeostasis. *Nat Cell Biol.* (2017) 19:52–9. doi: 10.1038/ncb3454
136. Salazar AM, Resnik-Docampo M, Ulgherait M, Clark RI, Shirasu-Hiza M, Jones DL, et al. Intestinal snakeskin limits microbial dysbiosis during aging and promotes longevity. *iScience.* (2018) 9:229–43. doi: 10.1016/j.isci.2018.10.022
137. Fabian DK, Garschall K, Klepsatel P, Santos-Matos G, Sucena É, Kapun M, et al. Evolution of longevity improves immunity in Drosophila. *Evol Lett.* (2018) 2:567–79. doi: 10.1002/evl3.89
138. Odnokoz O, Nakatsuka K, Klichko VI, Nguyen J, Solis LC, Ostling K, et al. Mitochondrial peroxiredoxins are essential in regulating the relationship between Drosophila immunity and aging. *Biochim Biophys Acta Mol Basis Dis.* (2017) 1863:68–80. doi: 10.1016/j.bbadis.2016.10.017
139. Wilson RH, Lai CQ, Lyman RF, Mackay TFC. Genomic response to selection for postponed senescence in Drosophila. *Mech Ageing Dev.* (2013) 134:79–88. doi: 10.1016/j.mad.2012.11.003
140. Le Bourg É, Malod K, Massou I. The NF-κB-like factor DIF could explain some positive effects of a mild stress on longevity, behavioral aging, and resistance to strong stresses in *Drosophila melanogaster*. *Biogerontology.* (2012) 13:445–55. doi: 10.1007/s10522-012-9389-0
141. Henten AMV, Loeschcke V, Pedersen JG, Leisner JJ, Sarup P. Injuries can prolong lifespan in *Drosophila melanogaster* males. *Biogerontology.* (2016) 17:337–46. doi: 10.1007/s10522-015-9616-6
142. Ramsden S, Cheung YY, Seroude L. Functional analysis of the Drosophila immune response during aging. *Aging Cell.* (2008) 7:225–36. doi: 10.1111/j.1474-9726.2008.00370.x
143. Sanchez Bosch P, Makhijani K, Herboso L, Gold KS, Baginsky R, Woodcock KJ, et al. Adult Drosophila lack hematopoiesis but rely on a blood cell reservoir at the respiratory epithelia to relay infection signals to surrounding tissues. *Dev Cell.* (2019) 51:787–803. doi: 10.1016/j.devcel.2019.10.017
144. Camus MF, Fowler K, Piper MW, Reuter M. Sex and genotype effects on nutrient-dependent fitness landscapes in *Drosophila melanogaster*. *Proc R Soc B Biol Sci.* (2017) 284:20172237. doi: 10.1098/rspb.2017.2237
145. Camus MF, Huang C-C, Reuter M, Fowler K. Dietary choices are influenced by genotype, mating status, and sex in *Drosophila melanogaster*. *Ecol Evol.* (2018) 8:5385–93. doi: 10.1002/ece3.4055
146. Camus MF, Piper MD, Reuter M. Sex-specific transcriptomic responses to changes in the nutritional environment. *eLife.* (2019) 8:e47262. doi: 10.7554/eLife.47262
147. Amur S, Parekh A, Mummaneni P. Sex differences and genomics in autoimmune diseases. *J Autoimmun.* (2012) 38:J254–65. doi: 10.1016/j.jaut.2011.12.001
148. Zuk M, Stoehr AM. Immune defense and host life history. *Am Nat.* (2002) 160:S9–22. doi: 10.1086/342131
149. Hamilton WD, Zuk M. Heritable true fitness and bright birds: a role for parasites? *Science.* (1982) 218:384–7. doi: 10.1126/science.7123238
150. Remolina SC, Chang PL, Leips J, Nuzhdin SV, Hughes KA. Genomic basis of aging and life-history evolution in *Drosophila Melanogaster*. *Evolution.* (2012) 66:3390–403. doi: 10.1111/j.1558-5646.2012.01710.x
151. Cowley DE, Atchley WR. Quantitative genetics of *Drosophila Melanogaster*. II. Heritabilities and genetic correlations between sexes for head and thorax traits. *Genetics.* (1988) 119:421–33.
152. Cowley DE, Atchley WR, Rutledge JJ. Quantitative genetics of *Drosophila Melanogaster*. I. Sexual dimorphism in genetic parameters for wing traits. *Genetics.* (1986) 114:549–66.
153. Mackay TFC. The genetic architecture of quantitative traits. *Annu Rev Genet.* (2001) 35:303–39. doi: 10.1146/annurev.genet.35.102401.090633
154. Mallet MA, Chippindale AK. Inbreeding reveals stronger net selection on *Drosophila melanogaster* males: implications for mutation load and the fitness of sexual females. *Heredity.* (2011) 106:994–1002. doi: 10.1038/hdy.2010.148
155. Morrow EH, Stewart AD, Rice WR. Assessing the extent of genome-wide intralocus sexual conflict via experimentally enforced gender-limited selection. *J Evol Biol.* (2008) 21:1046–54. doi: 10.1111/j.1420-9101.2008.01542.x
156. Sharp NP, Agrawal AF. Male-biased fitness effects of spontaneous mutations in *Drosophila Melanogaster*. *Evolution.* (2013) 67:1189–95. doi: 10.1111/j.1558-5646.2012.01834.x
157. Lemos B, Branco AT, Hartl DL. Epigenetic effects of polymorphic Y chromosomes modulate chromatin components, immune response, and sexual conflict. *Proc Natl Acad Sci USA.* (2010) 107:15826–31. doi: 10.1073/pnas.1010383107
158. Rice WR. Sex chromosomes and the evolution of sexual dimorphism. *Evolution.* (1984) 38:735–42. doi: 10.1111/j.1558-5646.1984.tb00346.x
159. Eshel I, Hamilton WD. Parent—offspring correlation in fitness under fluctuating selection. *Proc R Soc Lond B Biol Sci.* (1984) 222:1–14. doi: 10.1098/rspb.1984.0046
160. Andersen SO. Insect cuticular sclerotization: a review. *Insect Biochem Mol Biol.* (2010) 40:166–78. doi: 10.1016/j.ibmb.2009.10.007
161. Alekseyenko OV, Chan Y-B, Li R, Kravitz EA. Single dopaminergic neurons that modulate aggression in Drosophila. *Proc Natl Acad Sci USA.* (2013) 110:6151–6. doi: 10.1073/pnas.1303446110
162. Neckameyer WS. Dopamine and mushroom bodies in Drosophila: experience-dependent and -independent aspects of sexual behavior. *Learn Mem.* (1998) 5:157–65. doi: 10.1101/lm.5.1.157
163. Neckameyer WS. Dopamine modulates female sexual receptivity in *Drosophila Melanogaster*. *J Neurogenet.* (1998) 12:101–14. doi: 10.3109/01677069809167259
164. Massey JH, Chung D, Siwanowicz I, Stern DL, Wittkopp PJ. The yellow gene influences Drosophila male mating success through sex comb melanization. *eLife.* (2019) 8:e49388. doi: 10.7554/eLife.49388
165. Mackay TFC, Lyman RF. Drosophila bristles and the nature of quantitative genetic variation. *Philos Trans R Soc B Biol Sci.* (2005) 360:1513–27. doi: 10.1098/rstb.2005.1672
166. Anh NTT, Nishitani M, Harada S, Yamaguchi M, Kamei K. Essential role of duox in stabilization of Drosophila wing. *J Biol Chem.* (2011) 286:33244–51. doi: 10.1074/jbc.M111.263178
167. Davis MM, Primrose DA, Hodgetts RB. A member of the p38 mitogen-activated protein kinase family is responsible for transcriptional induction of Dopa decarboxylase in the epidermis of *Drosophila melanogaster* during the innate immune response. *Mol Cell Biol.* (2008) 28:4883–95. doi: 10.1128/MCB.02074-07
168. Danchin E, Nöbel S, Pocheville A, Dagaeff A-C, Demay L, Alphand M, et al. Cultural flies: conformist social learning in fruitflies predicts long-lasting mate-choice traditions. *Science.* (2018) 362:1025–30. doi: 10.1126/science.aat1590
169. Mery F, Varela SAM, Danchin É, Blanchet S, Parejo D, Coolen I, et al. Public versus personal information for mate copying in an invertebrate. *Curr Biol.* (2009) 19:730–4. doi: 10.1016/j.cub.2009.02.064
170. Friberg U, Arnqvist G. Fitness effects of female mate choice: preferred males are detrimental for *Drosophila melanogaster* females. *J Evol Biol.* (2003) 16:797–811. doi: 10.1046/j.1420-9101.2003.00597.x
171. Folstad I, Karter AJ. Parasites, bright males, and the immunocompetence handicap. *Am Nat.* (1992) 139:603–22.

172. Foo YZ, Nakagawa S, Rhodes G, Simmons LW. The effects of sex hormones on immune function: a meta-analysis. *Biol Rev.* (2017) 92:551–71. doi: 10.1111/brv.12243
173. Grossman CJ. Interactions between the gonadal steroids and the immune system. *Science.* (1985) 227:257–61. doi: 10.1126/science.3871252
174. Moore SL, Wilson K. Parasites as a viability cost of sexual selection in natural populations of mammals. *Science.* (2002) 297:2015–8. doi: 10.1126/science.1074196
175. Nunn CL, Lindenfors P, Pursall ER, Rolff J. On sexual dimorphism in immune function. *Philos Trans R Soc B Biol Sci.* (2009) 364:61–9. doi: 10.1098/rstb.2008.0148
176. Zuk M. Reproductive strategies and disease susceptibility: an evolutionary viewpoint. *Parasitol Tdy.* (1990) 6:231–3. doi: 10.1016/0169-4758(90)90202-F
177. Rolff J. Bateman's principle and immunity. *Proc R Soc Lond B Biol Sci.* (2002) 269:867–72. doi: 10.1098/rspb.2002.1959
178. Rus F, Flatt T, Tong M, Aggarwal K, Okuda K, Kleino A, et al. Ecdysone triggered PGRP-LC expression controls Drosophila innate immunity. *EMBO J.* (2013) 32:1626–38. doi: 10.1038/emboj.2013.100
179. McKean KA, Nunney L. Bateman's principle and immunity: phenotypically plastic reproductive strategies predict changes in immunological sex differences. *Evolution.* (2005) 59:1510–7. doi: 10.1554/04-657
180. McKean KA, Nunney L. Increased sexual activity reduces male immune function in *Drosophila melanogaster*. *Proc Natl Acad Sci USA.* (2001) 98:7904–9. doi: 10.1073/pnas.131216398
181. Fisher RA. *The Genetical Theory of Natural Selection*. Oxford, UK: Oxford University Press (1930).
182. Lande R. Sexual dimorphism, sexual selection, and adaptation in polygenic characters. *Evolution.* (1980) 34:292–305. doi: 10.1111/j.1558-5646.1980.tb04817.x
183. Connallon T, Knowles LL. Intergenomic conflict revealed by patterns of sex-biased gene expression. *Trends Genet.* (2005) 21:495–9. doi: 10.1016/j.tig.2005.07.006
184. Zuk M. The sicker sex. *PLoS Pathog.* (2009) 5:e1000267. doi: 10.1371/journal.ppat.1000267
185. Klein SL. Hormonal and immunological mechanisms mediating sex differences in parasite infection. *Parasite Immunol.* (2004) 26:247–64. doi: 10.1111/j.0141-9838.2004.00710.x
186. Perch M, Sodemann M, Jakobsen MS, Valentiner-Branth P, Steinsland H, Fischer TK, et al. Seven years' experience with *Cryptosporidium parvum* in Guinea-Bissau, West Africa. *Ann Trop Paediatr.* (2001) 21:313–8. doi: 10.1080/07430170120093490
187. Duneau DF, Ebert D. Host sexual dimorphism and parasite adaptation. *PLoS Biol.* (2012) 10:e1001271. doi: 10.1371/journal.pbio.1001271
188. Úbeda F, Jansen VA. The evolution of sex-specific virulence in infectious diseases. *Nat Commun.* (2016) 7:13849. doi: 10.1038/ncomms13849
189. Kelly CD, Stoehr AM, Nunn C, Smyth KN, Prokop ZM. Sexual dimorphism in immunity across animals: a meta-analysis. *Ecol Lett.* (2018) 21:1885–94. doi: 10.1111/ele.13164
190. Serbus LR, White PM, Silva JP, Rabe A, Teixeira L, Albertson R, et al. The impact of host diet on Wolbachia titer in Drosophila. *PLoS Pathog.* (2015) 11:e1004777. doi: 10.1371/journal.ppat.1004777
191. Ponton F, Wilson K, Holmes A, Raubenheimer D, Robinson KL, Simpson SJ. Macronutrients mediate the functional relationship between Drosophila and Wolbachia. *Proc R Soc B Biol Sci.* (2015) 282:20142029. doi: 10.1098/rspb.2014.2029
192. Ponton F, Morimoto J, Robinson K, Kumar SS, Cotter S, Wilson K, et al. Macronutrients modulate resistance to infection and immunity in Drosophila. *bioRxiv.* (2018) 498493. doi: 10.1101/498493
193. Anagnostou C, LeGrand EA, Rohlfs M. Friendly food for fitter flies? – Influence of dietary microbial specieson food choice and parasitoid resistance in Drosophila. *Oikos.* (2010) 119:533–41. doi: 10.1111/j.1600-0706.2009.18001.x
194. Dinh H, Mendez V, Tabrizi ST, Ponton F. Macronutrients and infection in fruit flies. *Insect Biochem Mol Biol.* (2019) 110:98–104. doi: 10.1016/j.ibmb.2019.05.002
195. Galenza A, Hutchinson J, Campbell SD, Hazes B, Foley E. Glucose modulates Drosophila longevity and immunity independent of the microbiota. *Biol Open.* (2016) 5:165–73. doi: 10.1242/bio.015016
196. Regan JC, Froy H, Walling CA, Moatt JP, Nussey DH. Dietary restriction and insulin-like signalling pathways as adaptive plasticity: a synthesis and re-evaluation. *Funct Ecol.* (2019) 34. doi: 10.1111/1365-2435.13418
197. Graze RM, Tzeng R-Y, Howard TS, Arbeitman MN. Perturbation of IIS/TOR signaling alters the landscape of sex-differential gene expression in Drosophila. *BMC Genomics.* (2018) 19:893. doi: 10.1186/s12864-018-5308-3
198. DiAngelo JR, Bland ML, Bambina S, Cherry S, Birnbaum MJ. The immune response attenuates growth and nutrient storage in Drosophila by reducing insulin signaling. *Proc Natl Acad Sci USA.* (2009) 106:20853–8. doi: 10.1073/pnas.0906749106
199. Karpac J, Younger A, Jasper H. Dynamic coordination of innate immune signaling and insulin signaling regulates systemic responses to localized DNA damage. *Dev Cell.* (2011) 20:841–54. doi: 10.1016/j.devcel.2011.05.011
200. Weiss BL, Wang J, Maltz MA, Wu Y, Aksoy S. Trypanosome infection establishment in the tsetse fly gut is influenced by microbiome-regulated host immune barriers. *PLoS Pathog.* (2013) 9:e1003318. doi: 10.1371/journal.ppat.1003318
201. Jupatanakul N, Sim S, Dimopoulos G. The insect microbiome modulates vector competence for arboviruses. *Viruses.* (2014) 6:4294–313. doi: 10.3390/v6114294
202. Pune T, Kenny N, Eyles D, Moreira LA, O'Neill SL, Asgari S. Infection with the wMel and wMelPop strains of Wolbachia leads to higher levels of melanization in the hemolymph of *Drosophila melanogaster*, *Drosophila simulans* and *Aedes aegypti*. *Dev Comp Immunol.* (2011) 35:360–5. doi: 10.1016/j.dci.2010.11.007
203. Gonzalez EA, Garg A, Tang J, Nazario-Toole AE, Wu LP. A Glutamate-dependent redox system in blood cells is integral for phagocytosis in *Drosophila melanogaster*. *Curr Biol.* (2013) 23:2319–24. doi: 10.1016/j.cub.2013.09.061
204. Teixeira L, Ferreira Á, Ashburner M. The bacterial symbiont Wolbachia induces resistance to RNA viral infections in *Drosophila melanogaster*. *PLoS Biol.* (2008) 6:e1000002. doi: 10.1371/journal.pbio.1000002
205. Gupta V, Vasanthakrishnan RB, Siva-Jothy J, Monteith KM, Brown SP, Vale PF. The route of infection determines Wolbachia antibacterial protection in Drosophila. *Proc R Soc B Biol Sci.* (2017) 284:20170809. doi: 10.1098/rspb.2017.0809
206. Salz HK, Erickson JW. Sex determination in Drosophila: the view from the top. *Fly.* (2010) 4:60–70. doi: 10.4161/fly.4.1.11277
207. Wu B, Ma L, Zhang E, Du J, Liu S, Price J, et al. Sexual dimorphism of sleep regulated by juvenile hormone signaling in Drosophila. *PLoS Genet.* (2018) 14:e1007318. doi: 10.1371/journal.pgen.1007318

Conflict of Interest: The authors declare that the research was conducted in the absence of any commercial or financial relationships that could be construed as a potential conflict of interest.

frontiers in Immunology

ORIGINAL RESEARCH
published: 04 March 2020
doi: 10.3389/fimmu.2020.00362

Viral Infection and Stress Affect Protein Levels of Dicer 2 and Argonaute 2 in *Drosophila melanogaster*

*Alessandro Torri, Vanesa Mongelli†, Juan A. Mondotte† and Maria-Carla Saleh**

Viruses and RNA Interference Unit, CNRS Unité Mixte de Recherche, Institut Pasteur, Paris, France

The small interfering RNA (siRNA) pathway of *Drosophila melanogaster*, mainly characterized by the activity of the enzymes Dicer 2 (Dcr-2) and Argonaute 2 (Ago-2), has been described as the major antiviral immune response. Several lines of evidence demonstrated its pivotal role in conferring resistance against viral infections at cellular and systemic level. However, only few studies have addressed the regulation and induction of this system upon infection and knowledge on stability and turnover of the siRNA pathway core components transcripts and proteins remains scarce. In the current work, we explore whether the siRNA pathway is regulated following viral infection in *D. melanogaster*. After infecting different fly strains with two different viruses and modes of infection, we observed changes in Dcr-2 and Ago-2 protein concentrations that were not related with changes in gene expression. This response was observed either upon viral infection or upon stress-related experimental procedure, indicating a bivalent function of the siRNA system operating as a general gene regulation rather than a specific antiviral system.

Keywords: RNA interference, insect immunity, gene regulation, viral infection, antiviral response, protein regulation

OPEN ACCESS

Edited by:
Dan Hultmark,
Umeå University, Sweden

Reviewed by:
Hai-peng Liu,
Xiamen University, China
Ioannis Eleftherianos,
George Washington University, United States

***Correspondence:**
Maria-Carla Saleh
carla.saleh@pasteur.fr

†These authors have contributed equally to this work

Specialty section:
This article was submitted to Comparative Immunology, a section of the journal Frontiers in Immunology

Received: *26 November 2019*
Accepted: *14 February 2020*
Published: *04 March 2020*

Citation:
Torri A, Mongelli V, Mondotte JA and Saleh M-C (2020) Viral Infection and Stress Affect Protein Levels of Dicer 2 and Argonaute 2 in Drosophila melanogaster. Front. Immunol. 11:362. doi: 10.3389/fimmu.2020.00362

INTRODUCTION

RNA interference (RNAi) is a defensive and gene regulatory process based in sequence homology among nucleic acids (1–3). Small RNAs (sRNAs) are produced and used as guides to target complementary DNA or RNA sequences (4, 5). Three main sRNA pathways are described to date, differing in the origin and biogenesis of the double-stranded sRNAs and their molecular function: the micro RNA pathway (miRNA), the small interfering RNA pathway (siRNA), and the Piwi-interacting RNA pathway (piRNA) (6).

In the siRNA pathway, the ribonuclease Dicer 2 (Dcr-2) recognizes and dices double stranded RNA molecules of exogenous (virus) or endogenous (cellular) origin, producing 21-nucleotide length siRNA duplexes that are loaded into the protein Argonaute 2 (Ago-2) within the RNA-induced silencing complex (RISC). Once loaded, the siRNA duplexes are unwound and only one RNA strand is used by Ago-2 to target and slice the complementary RNA. Two Dcr-2 cofactors are indispensable for siRNA production and correct loading into RISC: LOQS and R2D2 (4, 6).

The siRNA pathway is considered the most ancient and at the origin of the RNAi phenomenon. Its main components (Argonaute-Piwi, Dicer-like, and RNA-dependent RNA Polymerase proteins) are supposed to have been already present in the last common ancestor of eukaryotes (7).

In *Drosophila melanogaster* the siRNA pathway acts as the main antiviral immune response (8) and is also involved in somatic defense against transposons (9). However, the fact that several siRNAs target cellular mRNAs (7, 10) and repress the expression of specific genes (11), suggests that it may also play a role in the regulation of gene expression.

Much effort has been dedicated to studying the RNAi mechanism and pathways, but despite several advancements, not much is known about their regulation (12). Previous studies reported that the mRNA expression of the core components of the siRNA pathway (Dcr-2 and Ago-2 among others) are induced by double stranded RNA (dsRNA) in *Acyrthosiphon pisum* (13), *Manduca sexta* (14), and *Blatella germanica* (15) through a yet unknown mechanism. This induction has also been shown upon viral infection in *Bombus terrestris* (16), *Apis mellifera* (17) and *D. melanogaster* (18). However, in *Apis mellifera* this phenomenon seems to be virus-specific (19) and in *D. melanogaster* the induction was observed upon injection of Zika virus, an arbovirus for which the fruit fly is not a natural host (18). In addition, a study in *D. melanogaster* (20) showed increased levels of *Ago-2* and *Dcr-2* in flies constitutively expressing an active form of dFOXO, establishing a link between stress response and RNAi regulation. However, knowledge on regulation, stability, and turnover of the siRNA pathway core genes and proteins remains scarce.

Here we explore whether the siRNA pathway is regulated at the transcriptional and/or at the translational level following viral infection in *D. melanogaster*. We analyzed the expression of transcripts and proteins for *Dcr-2* and *Ago-2* in three different fly strains infected with Drosophila C Virus (DCV) and Flock House Virus (FHV) by two different modes of delivery, injection and oral infection. Our results show a complex and previously undescribed mechanism of regulation of the siRNA pathway at the protein level independent of fly strain, gene expression and mode of infection.

MATERIALS AND METHODS

Fly Strains and Husbandry

The *D. melanogaster* fly lines used were the following: w^{1118}, *Oregon-R,* and *yw*. Fly stocks harbor the sensitive allele of Pastrel 3L:7350895 (Thr). Flies were reared on a standard cornmeal diet (Bloomington) at a constant temperature of 25°C and kept under a 12:12 photoperiod. All fly lines were cleaned of possible chronic infections (viruses and *Wolbachia*). In addition, fly stocks were analyzed by RT-PCR with pairs of primers specific for CrPV, DAV, DXV, DCV, FHV, and NoraV to confirm that they were not persistently infected by these viruses.

Virus Production and Titration

DCV stock was prepared in w^{1118} flies. Flies were injected intrathoracically with 500 TCID50 per fly. When mortality started, flies were anesthetized and squashed in PBS (3 flies per 100 µl of PBS). The extract was frozen at −80°C, thawed and centrifuged for 15 min at 15,000 × g at 4°C. The supernatant was recovered and filtered to eliminate bacteria, aliquoted, and stored at −80°C.

FHV stock was prepared on low-passage S2 cells. When the cytopathic effect started, the supernatant was harvested and centrifuged.

Both stocks were titrated in S2 cells. Titers were measured by end-point dilution method and expressed as 50% Tissue culture Infective Dose ($TCID_{50}$). DCV stock: $1{,}18 \times 10^{10}$ $TCID_{50}$/ml, FHV stock: 5×10^9 $TCID_{50}$/ml).

Viral Infections

Injections: flies were injected intrathoracically using a nanoject (Nanoject II apparatus; Drummond Scientific) with 50 nL of a viral suspension of 10 $TCID_{50}$ of Drosophila C virus or 100 $TCID_{50}$ of Flock house virus in 10 mM Tris, pH 7. An injection of the same volume of 10 mM Tris, pH 7 served as a mock-infected control. Infected flies were kept at 25°C and changed to fresh vials every 2 days.

Oral infections: flies were starved during 5 h in an empty tube. Then, flies were transferred to a tube containing a Whatman filter paper in the bottom embedded in a mix of viral stock in PBS (10% viral stock, 35% sucrose and 2% of blue dye). After 16 h, only the flies having a blue-belly (corresponding to blue dye in the gut due to ingestion) were placed in new media tubes, kept at 25°C and changed to fresh vials every 2 days.

General Experimental Design

For all the experiments, 4- to 7-day old adult female flies were used. For each experimental condition, flies were divided in two pools: one pool was used for viral titration and RNA extraction, and the other one for protein extraction. For every experiment presented, the analyses were based on three biological replicates. In **Figure 2**, 16 biological replicates were performed (except w^{1118} in **Figure 2B**, $n = 15$). For western blots, only biological replicates were used. For RT-qPCR, three technical replicates per condition and per biological replicate were used.

Survival Assays

Mortality of infected flies was measured daily by counting the number of dead flies in each test tube. Three biological replicates of 60 flies each were done per condition. Fly mortality at day 1 was attributed to damage invoked by injection and/or manipulation procedure, and excluded from further analyses.

RNA Extractions and RT-qPCR

For each time point and condition, total RNA was extracted from a pool of 4–12 flies depending on the biological replicate. Each pool was homogenized in 300 µl of PBS and 100 µl were used to perform RNA extractions using TRIzol reagent (Invitrogen).

The first-strand cDNAs were produced from 400 ng of RNA using Maxima H Minus First Strand cDNA Synthesis Kit with dsDNase (Thermo Scientific) according to the manufacturer's instructions. For each sample, a negative control without the reverse transcriptase enzyme was performed, in order to check for potential genomic DNA contamination. Roche Universal Sybr Green Master Mix (Rox) was used for qPCR. The sequences of the primers used were:

Ago-2 F primer: 5′-GTGGTTTACACGCCTCCTCA-3′
Ago-2 R primer: 5′-GGGTAGTTGCGACTGTGGAA-3′

Dcr-2 F primer: 5′-GGGTGAACAGGGAGTGGATG-3′
Dcr-2 R primer: 5′-CAAAAAGACCTGGGCTGTGC-3′
Quantification was normalized to that of mRNA encoding the endogenous ribosomal protein Rp49 as previously reported (21). Data were calculated using the ΔΔCt method to compute relative gene expression. For each sample, 3 technical replicates plus 1 RT negative control were included in the qPCR plate. qPCR was performed in 384-well plates with a final volume of 10 µl with QuantStudio 7 Flex Real-Time PCR System (Applied Biosystems). The following program was used: Hold stage 50°C for 2 min, 95°C for 10 min. PCR stage: 40 cycles of 95°C for 15 s, 60°C for 1 min. A melt curve to confirm the specificity of the reaction was performed.

Protein Extraction, Western Blot, and Protein Quantification

For each time point and condition, total proteins were extracted from pools of 4–8 flies, depending on the biological replicate, using 200 µl NP40 Buffer: 20 mM HEPES-KOH buffer pH 7.5; 100 mM KCl; 5% Glycerol; 0.05% NP40; 1 mM DTT (freshly added) and 1x complete, EDTA-Free Protease Inhibitor Cocktail (Roche) (freshly added). Each pool was homogenized with a pestle, centrifuged at 12,000 × g for 10 min and the supernatant was recovered and stored at −80°C. Ten microliters of each protein extract were ran in SDS-PAGE using Mini-PROTEAN TGX Stain-free gels 4–20% (BIO-RAD) according to the manufacturer's instructions. The gels were then activated for image acquisition using Molecular Imager Gel Doc XR+ (BIO-RAD) and the transfer was performed using Trans-Blot Turbo Transfer Pack nitrocellulose membranes and Trans-Blot Turbo Transfer System (BIO-RAD). The image acquisition of the total amount of proteins transferred was performed with Molecular Imager Gel Doc XR+ (BIO-RAD). For the immunoblots, the following primary antibodies were used: Anti-Dcr-2 Abcam AB4732 (1:1000); Anti-Ago-2 Siomi 9D6 (non-commercial antibody, 1:15) kindly provided by Haruhiko Siomi. The secondary antibodies were HRP-linked: anti-rabbit GE Healthcare NA9340V (1:10000); anti-mouse Abcam AB6728 (1:10000). The antibodies were diluted in a solution of PBS-BSA 3%, TWEEN 20 0.3%. Membranes were incubated overnight at 4°C with the primary antibodies, washed

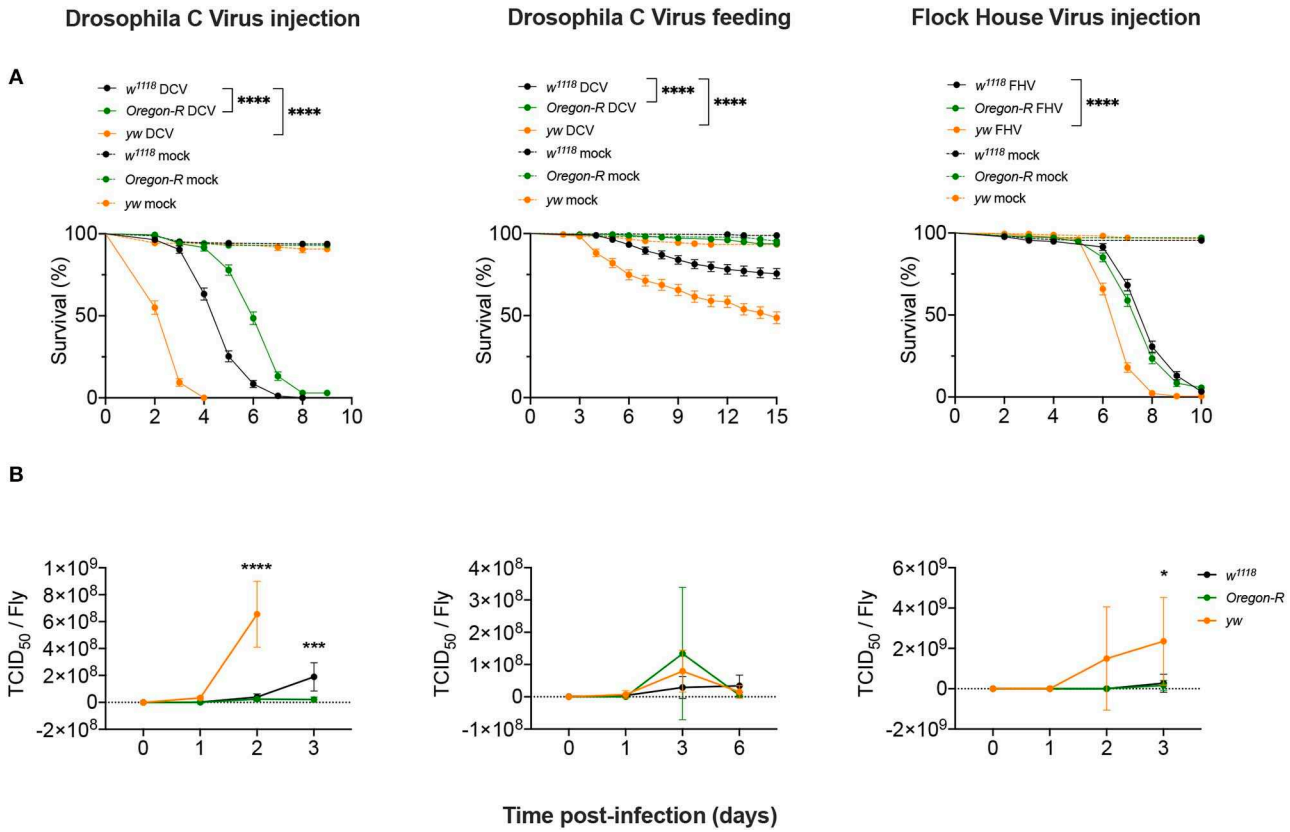

FIGURE 1 | Susceptibility to viral infections. **(A)** w^{1118}, *Oregon-R* and *yw* adult flies were intrathoracically injected with 10 $TCID_{50}$ of DCV (Left panel), 100 $TCID_{50}$ of FHV (Right panel), or orally infected with a solution of sucrose and blue dye containing 1.18×10^{10} $TCID_{50}$ of DCV (Middle panel). Mock controls were injected or fed with Tris buffer. Survival was determined daily. Each curve represents three independent biological experiments of 60 flies each. Survival curves were compared by log-rank (Mantel-Cox) test (****$P < 0.0001$). **(B)** w^{1118}, *Oregon-R* and *yw* viral titers over time. Each time point represents mean and SD of three different biological replicates composed of a pool of 4–12 flies. The infection conditions were the same as described in **(A)**. Controls were negative and are not shown in the figure. Each time point was compared to each other by two-way ANOVA followed by Sidak's multiple comparisons test (*$P < 0.05$; ***$P < 0.0002$).

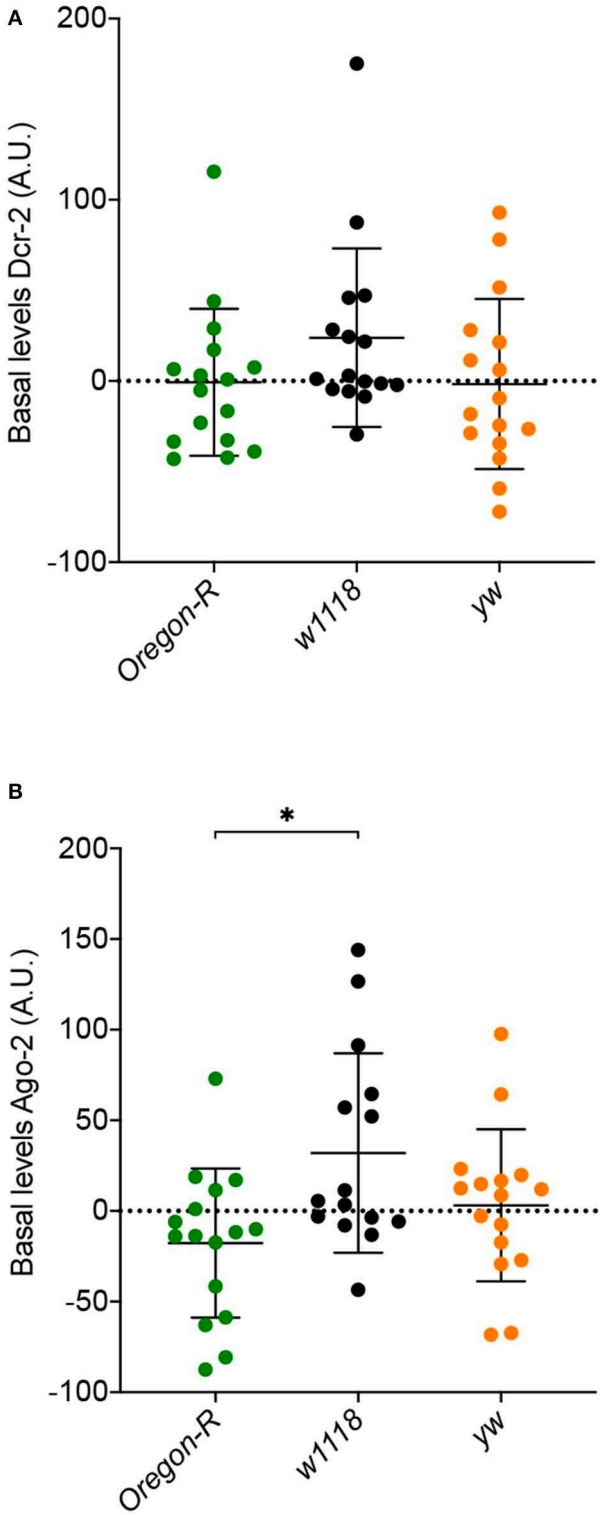

FIGURE 2 | Basal expression levels of core RNAi proteins in *Oregon-R*, w^{1118}, and *yw* flies determined by western blot (quantification and normalization are detailed in Materials and Methods). **(A)** Dcr-2 basal levels. **(B)** Ago-2 basal levels. Each dot represents a biological replicate composed of a pool of 5 flies. A.U. indicates arbitrary units. *Indicates significant differences among *Drosophila* strains using Mann–Whitney test ($P = 0.0106$).

3 times for 5 min with PBS-TWEEN 20 0.3%, incubated with secondary antibodies 1 h at room temperature and washed again 3 times for 5 min with PBS-TWEEN 20 0.3% before adding the ECL (SuperSignal West Pico Plus Chemiluminescent substrate—Thermo Scientific). The image acquisitions were performed with MyECL Imager (Thermo Scientific). The intensities of the bands corresponding to Dcr-2 and Ago-2 were normalized with the total amount of protein in their respective lanes using ImageStudioLite (LI-COR Biosciences) (**Supplementary Figures 1**, **2**).

In order to compare results from different experiments, two types of normalization were employed. To study differences in the relative protein expression, all the data were normalized with the mock-infected time point 0 (**Figures 5**, **6**). To analyze non-relative protein levels, all data were corrected for the experimental effect as previously shown (21). This procedure transforms the raw values into their deviation from the experimental mean, and the resulting adjusted values are centered on zero (**Figures 2**, **7**).

Statistical Analysis

All statistical analyses were performed with Prism 8—GraphPad. The following statistical tests were used: for grouped tables with two grouping variables, two-way ANOVA followed by Sidak's multiple comparisons test; for table with one grouping variable, the Mann-Whitney test; for survival curves, the log-rank (Mantel-Cox) test; to calculate the probability of deviations from a theoretically expected distribution, the binomial test.

RESULTS

Different *D. melanogaster* Strains Differ in Their Susceptibility to Viral Infections

To study the regulation of the siRNA pathway during viral infections we used different *D. melanogaster* strains, viruses and modes of infection in order to establish the commonality of the response. We challenged w^{1118}, *Oregon-R*, and *yw D. melanogaster* strains in two different infection conditions: (1) injection of Drosophila C Virus [DCV; (+)ssRNA *Dicistroviridae*], a natural Drosophila pathogen; and of Flock House Virus [FHV; bisegmented (+)ssRNA, *Nodaviridae*], a non-natural fly pathogen used as a control; and (2) oral infection by feeding with DCV. Survival curves showed that after DCV infection by injection, w^{1118} flies had an intermediate survival rate compared to *yw* flies that were more susceptible, whereas *Oregon-R* were more resistant (**Figure 1A**). Injection of DCV resulted in the death of all flies at 8 days post-infection (dpi) for w^{1118} and 4 dpi for *yw* flies, while 97% of *Oregon-R* flies died at 9 dpi (**Figure 1A**, left panel). In flies orally infected with DCV, the proportions of mortality 15 days after infection were of ∼25% for w^{1118}, ∼50% for *yw*, and ∼6% for *Oregon-R* strains (**Figure 1A**, middle panel). Upon FHV injection, *yw* were still the most susceptible flies, with ∼35% mortality at day 6 compared with ∼9% for w^{1118} and ∼15% for *Oregon-R* (**Figure 1A**, right panel). We then

measured viral loads by $TCID_{50}$ for all tested conditions at 0 dpi (15 min post-injection or 16 h post-feeding) and at 3 further times post-infection (**Figure 1B** and **Supplementary Table 1**). Following virus injection, both DCV and FHV reached higher titers in *yw* flies than w^{1118} and *Oregon-R* flies at 2 dpi and 3 dpi, respectively, while DCV accumulated to higher levels at 3 days post-injection in w^{1118} flies compared with *Oregon-R* (**Figure 1B** and **Supplementary Table 1**). However, no significant differences in DCV titers were found between the different fly strains during oral infections (**Figure 1B** and **Supplementary Table 1**). Taken together, these results show that these fly strains differ in their susceptibility to viral infections and that there is a correlation between the increase of viral loads and mortality (**Figure 1B** and **Supplementary Table 1**), indicating that flies are dying due to the physiological burden imposed by the infection.

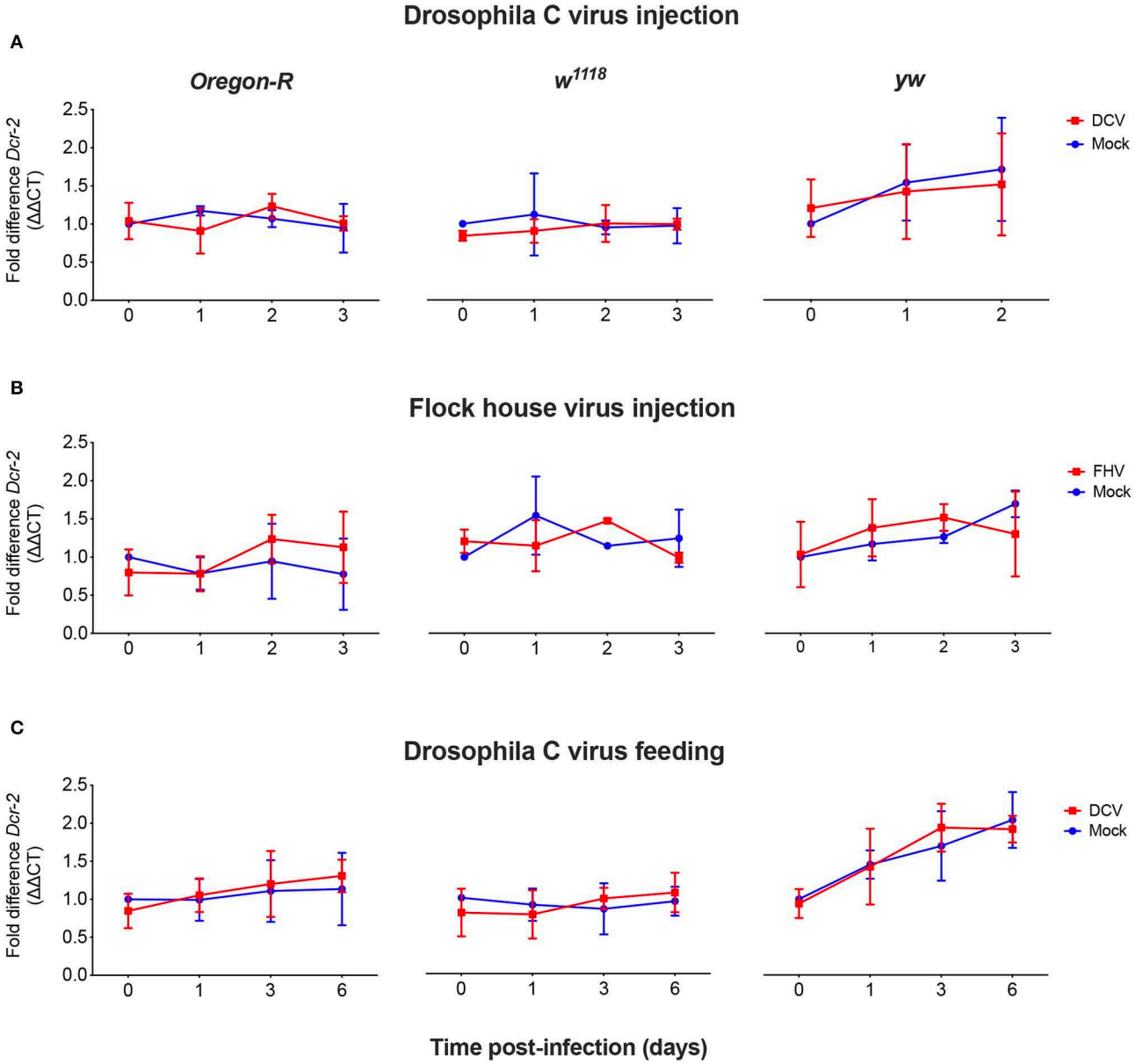

FIGURE 3 | Relative *Dcr-2* mRNA expression levels after viral infection. *Oregon-R*, w^{1118}, and *yw* adult flies were intrathoracically injected with 10 $TCID_{50}$ of DCV **(A)**, 100 $TCID_{50}$ of FHV **(B)**, or orally infected with a solution of sucrose and blue dye containing 1.18×10^{10} $TCID_{50}$ of DCV **(C)**. Mock controls were injected or fed with Tris buffer. Numbers in x-axis represent days post-infection. Time point 0 corresponds to 15 min post-injection in **(A,B)** and 16 h post-feeding in **(C)**. Each curve represents three biological independent experiments with three technical replicates each. In each condition and for each time point, the cDNA from pools of 4–12 flies was used to quantify the expression levels of *Dcr-2* by qPCR. Each data was normalized with the time point 0 of the mock infected. No statistical significance in *Dcr-2* transcript accumulation due to viral infection was found. $n = 3$, mean ± SD, two-way ANOVA followed by Sidak's multiple comparisons test.

Basal Levels of Dcr-2 and Ago-2 Proteins Do Not Account for the Variation in Susceptibility to Viral Infection

We next asked if the differences in susceptibility and viral accumulation observed between w^{1118}, *Oregon-R* and *yw* flies might be due to differences in the basal levels of the siRNA pathway core proteins, Dcr-2 and Ago-2, before viral infection. To address this question, we measured the levels of these proteins in the three Drosophila strains by western blot. Dcr-2 basal levels were similar between strains (**Figure 2A**). A significant increase in Ago-2 basal levels between w^{1118} and *Oregon-R* (**Figure 2B**) was observed, but it cannot explain the difference in susceptibility to virus infection observed for these strains. Taken together, these results show that the basal levels of Dcr-2 and Ago-2 do not play a critical role in fly survival and in the control of viral infections.

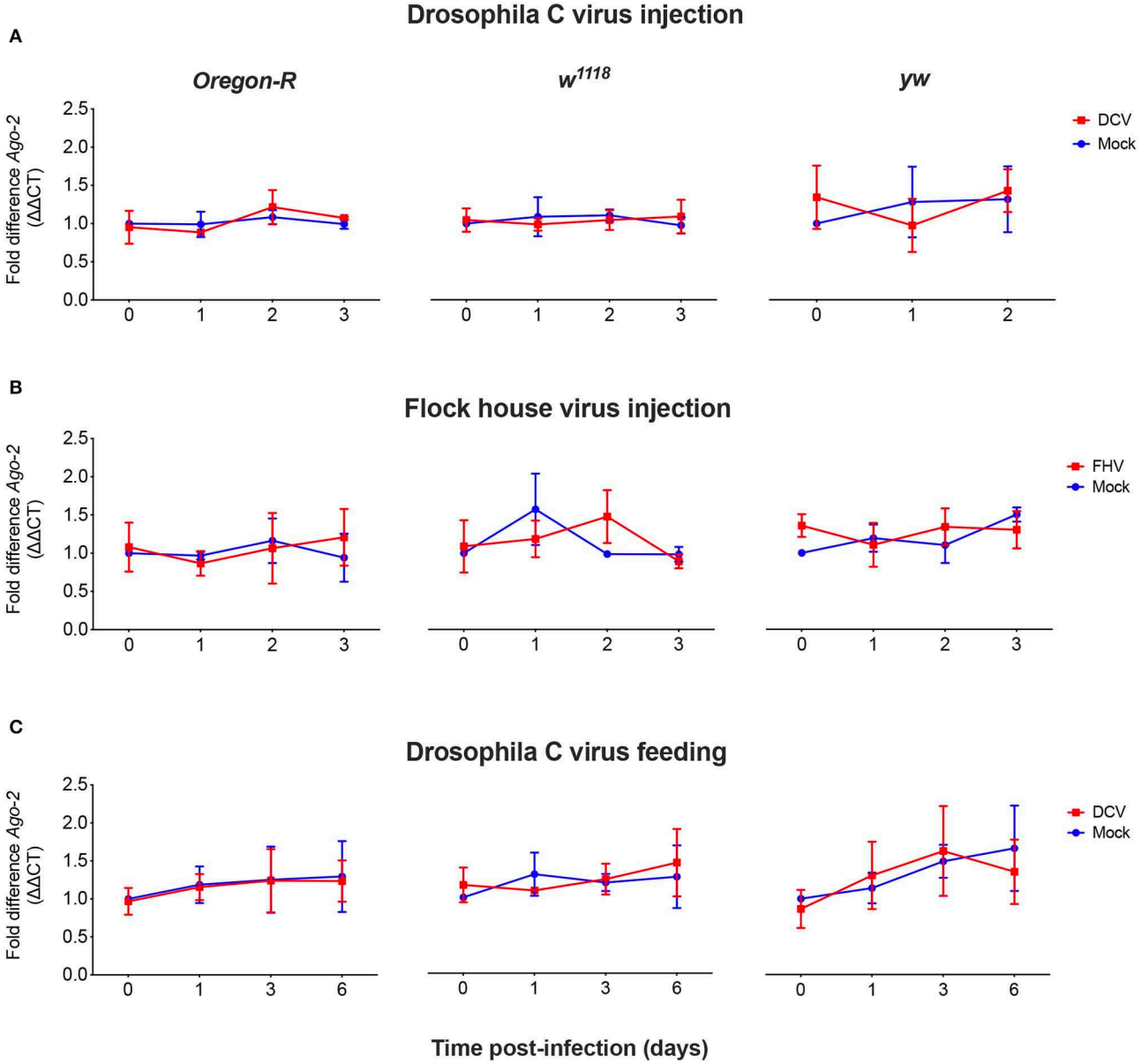

FIGURE 4 | Relative *Ago-2* mRNA expression levels after viral infection. *Oregon-R*, w^{1118} and *yw* adult flies were intrathoracically injected with 10 $TCID_{50}$ of DCV **(A)**, 100 $TCID_{50}$ of FHV **(B)**, or orally infected with a solution of sucrose and blue dye containing 1.18×10^{10} $TCID_{50}$ of DCV **(C)**. Mock controls were injected or fed with Tris buffer. Numbers in x-axis represent days post-infection. Time point 0 corresponds to 15 min post-injection in **(A,B)** and 16 h post-feeding in **(C)**. Each curve represents three biological independent experiments with three technical replicates each. In each condition and for each time point, the cDNA from pools of 4–12 flies was used to quantify the expression levels of *Ago-2* by qPCR. Each data was normalized with the time point 0 of the mock infected. No statistical significance in Ago-2 transcript accumulation due to the viral infection was found. $n = 3$, mean ± SD, two-way ANOVA followed by Sidak's multiple comparisons test.

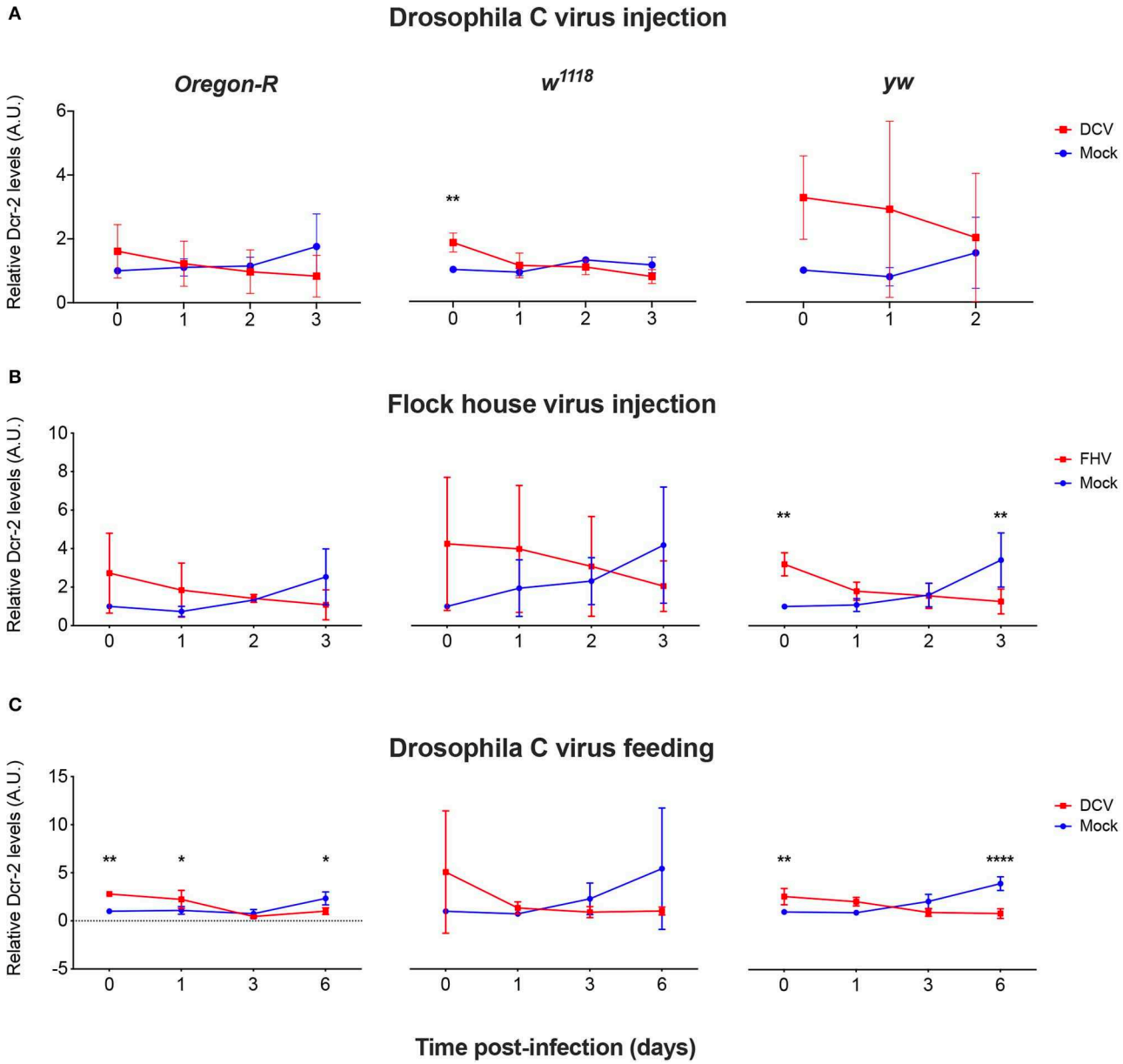

FIGURE 5 | Relative Dcr-2 protein expression levels after viral infection. *Oregon-R*, w^{1118}, and *yw* adult flies were intrathoracically injected with 10 $TCID_{50}$ of DCV **(A)**, 100 $TCID_{50}$ of FHV **(B)**, or orally infected with a solution of sucrose and blue dye containing 1.18×10^{10} $TCID_{50}$ of DCV **(C)**. Mock controls were injected or fed with Tris buffer. Numbers in x-axis represent days post-infection. Time point 0 corresponds to 15 min post-injection in **(A,B)** and 16 h post-feeding in **(C)**. Each curve represents three independent biological experiments. In each condition and for each time point, total protein extraction from pools of 4–8 flies was used to quantify the expression levels of Dcr-2 by western blot. Each band corresponding to Dcr-2 was normalized with the total amount of protein of its lane and each set of data was normalized with the time point 0 of the negative control. Relative levels of Dcr-2 in infected flies at time point 0 were higher compared with the control. A.U. indicates arbitrary units. $n = 3$; mean ± SD, two-way ANOVA followed by Sidak's multiple comparisons test (*$P < 0.05$, **$P < 0.01$, ****$P < 0.0001$).

Viral Infection Does Not Change *Dcr-2* and *Ago-2* Gene Expression Levels

As we did not observe a correlation between Dcr-2 and Ago-2 proteins basal levels and infection outcomes in the *D. melanogaster* strains tested, we wanted to explore if a difference in gene expression would be noticeable as a result of the viral infection. We evaluated the mRNA expression levels of *Dcr-2*, *Ago-2,* and *rp49* (housekeeping gene) by qPCR at four time points post-infection. The mRNA was extracted from the same pools of flies used in **Figure 1B**. We did not observe any significant difference in *Dcr-2* (**Figure 3**) and *Ago-2* (**Figure 4**) mRNA levels of infected flies compared with mock infected flies, independent of the fly strain, virus or mode of infection used.

Viral Infection Induces an Immediate Change in Dcr-2 and Ago-2 Protein Levels

To explore if mRNA expression levels correlate with proteins levels upon viral infection, we quantified the expression of Dcr-2 and Ago-2 proteins. Proteins were extracted from flies that were biological replicates to **Figures 1B**, **3**, **4** and the presence and quantity of Dcr-2 and Ago-2 were analyzed by western blot. After normalization with the time point 0 of the mock-infected condition (see Materials and Methods for details on normalization protocol and **Supplementary Figures 1**, **2**), Dcr-2 levels showed a relative increase in virus infected flies at the time point 0 (15 min post-injection or 16 h post-feeding) independently of the fly strain, virus and mode of infection used (**Figure 5**). These increments were statistically significant for w^{1118} injected with DCV (**Figure 5A**), for *yw* injected with FHV (**Figure 5B**), and for *Oregon-R* and *yw* orally infected with DCV (**Figure 5C**). These significant increases in Dcr-2 protein expression were not observed throughout all the conditions; however, in the 27 western blots performed (3 biological replicates × 3 fly strains × 3 different modes of infection), 26 of them showed higher Dcr-2 levels in infected flies than in the mock infected control. The probability that this phenomenon is due to a random effect is only 0.00002% (binomial test assuming that, during a random phenomenon, the probability to be higher or lower with respect to the control is the same). On the contrary, at the last time point (3 days post-infection for injection and 6 days post-infection for feeding) we found that Dcr-2 protein relative levels in infected flies were lower compared to the mock-infected flies. This decrease was statistically significant for *yw* injected with FHV (**Figure 5B**), and for *Oregon-R* and *yw* orally infected with DCV (**Figure 5C**). In injected flies, we found this pattern in 14 of 15 experiments with a probability of 0.004% for this phenomenon to be due to a random effect. In orally infected flies, we found this pattern in 9 of 9 experiments, with a probability of 0.2%. Due to the limited amount of anti-Ago-2 antibody in our possession (non-commercial antibody), we chose to perform the analysis for Ago-2 protein levels only in the w^{1118} strain. We observed the same trend as for Dcr-2, but without significant differences (**Figure 6**). From a total of 7 western blots performed, we found higher relative levels of Ago-2 7 times for the time point 0, with respect to mock infected flies, with a probability of 0.78% (binomial test) that this is due to a random effect.

Altogether, the results show that Dcr-2 and Ago-2 protein levels change promptly upon virus infection.

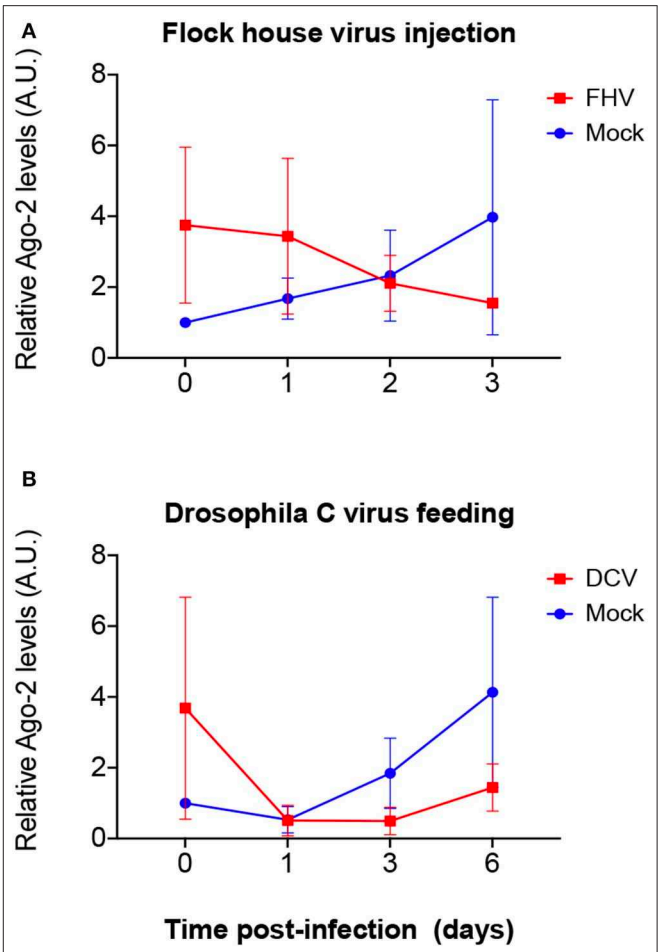

FIGURE 6 | Relative Ago-2 protein expression levels after viral infection. w^{1118} adult flies were intrathoracically injected with 100 $TCID_{50}$ of FHV **(A)** or orally infected with a solution of sucrose and blue dye containing 1.18×10^{10} $TCID_{50}$ of DCV **(B)**. Mock controls were injected or fed with Tris buffer. Numbers in x-axis represent days post infection. Time point 0 corresponds to 15 min post-injection in **(A)** and 16 h post-feeding in **(B)**. Each curve represents three independent biological experiments. In each condition and for each time point, the total protein extract from pools of 4–8 flies was used to quantify the expression levels of Ago-2 by western blot. Each band corresponding to Ago-2 was normalized with the total amount of protein of its lane and each set of data was normalized with the time point 0 of the negative control. Relative levels of Ago-2 in infected flies at time point 0 were higher compared with the control but without statistical significance. A.U. indicates arbitrary units. $n = 3$; mean ± SD; two-way ANOVA followed by Sidak's multiple comparisons test.

Viral Presence, as Well as Infection Procedure Related-Stress, Induce a Change in Dcr-2 Protein Accumulation

The data shown in **Figure 5** correspond to Dcr-2 protein levels relative to the mock-infected time point 0. Therefore, we cannot differentiate if the change observed is due to an absolute Dcr-2 increase after the infection or to an absolute Dcr-2 decrease in the control flies due to the stress caused by the experimental procedure (injury in the case of injection, and starvation in the case of feeding—see modes of infection in Materials and Methods). To answer this question, we compared the absolute protein levels for each time point with the basal level of the non-injected control flies from **Figure 2**. Since we observed the same effect on DCV and FHV injected flies, we pooled the data of all infected flies. We then analyzed the absolute levels of Dcr-2 among strains for each time point. As expected, we did not observe any strain-dependent difference in the levels of Dcr-2 (**Figure 7A**), in agreement with the results reported in **Figure 2**. This allowed us to pool each treatment condition (mock infected, virus infected and non-injected) to analyze the absolute levels of Dcr-2 across time and independently of the fly strain.

Figure 7B shows that, at time 0, Dcr-2 levels in mock-infected flies rapidly decrease compared to the non-injected control. In contrast, injection of virus increased the level of Dcr-2 protein. At 3 days post-infection, the tendency reversed with increased levels of Dcr-2 in mock-infected flies and decreased levels in virus-infected flies. The same analysis was performed for flies infected by feeding. **Figure 7C** shows the same trend with a prompt increase of Dcr-2 protein levels upon virus ingestion and a later decrease. We did not observe a significant decrease of Dcr-2 levels during mock infection at time point 0, but we did find a significant increase for the time point 3. This indicates that starvation, as well as injection, induces a change in the regulation of Dcr-2.

Altogether, these results put in evidence a change of Dcr-2 protein levels that is not only dependent on virus infection but also on infection procedure-related stress. While virus infection rapidly induces an increment of Dcr-2 protein concentration, the infection procedure-related stress immediately decreases Dcr-2 protein levels. The increase of Dcr-2 protein during viral infection is strong enough to mask the decrease produced by stress.

DISCUSSION

Biological systems are composed of two features: pathways and mechanisms (22). Pathways describe the flow of entities or information along space and time; mechanisms describe indirectly the reason these pathways exist. Studying pathways or mechanisms implies studying two different things. In the case of RNAi, if we consider the hierarchical scale that includes the entire RNAi phenomenon, studying the pathway means to study the components of such pathway, the causal way they interact and the flow of these interactions until reaching the "interference" event, which it is relevant to a variety of outcomes. Studying the mechanism means to study how such a pathway works, how it is controlled and regulated, how it is induced or repressed, and for what specific outcome (22). Dcr-2 and Ago-2 are the best characterized enzymes involved in the insect antiviral siRNA pathway. Several lines of evidence demonstrated the pivotal role of this molecular process as the major antiviral response at cellular and systemic level, against both natural and unnatural *D. melanogaster* viruses (23–28). Nevertheless, we still have a scarce comprehension of the biological implication of the siRNA pathway in gene regulation (11) and in trans-kingdom communication (29–31). A comprehensive understanding of the regulation of the siRNA-mediated response upon different biotic and abiotic stimuli, from virus infection and cellular stress to environmental cues, could shed light on the global role that this pathway plays in the organism. As said by Cornish-Bowden et al. (32), "Only through the understanding of the whole can we understand the functions of the parts".

In this work, we focused on the response of the core components of the siRNA pathway at the transcriptional and translational levels upon viral infection in *D. melanogaster* using three fly strains, two modes of infection and natural and unnatural viral pathogens.

We observed a strain-dependent susceptibility to viral infections; *yw* flies were more susceptible to viral infections than w^{1118} and *Oregon-R* flies in all experimental conditions. In agreement with our previous work (21), the mortality after oral infection with DCV was lower with respect to mortality following viral injection. Previous studies reported differences in the immune response of the most common laboratory strains of *D. melanogaster* used in immunity research (33, 34). For example, Okado et al. (33) show that these strains differ in susceptibility to infection, as well as differences in bacterial load and antimicrobial peptides expression profile upon infection with *Lysteria*. In addition, upon bacterial infection with *E. coli*, *M. luteus,* and *E. faecalis*, *yw* displays higher mortality in comparison with other strains (34). Since *yw* fat storage levels decreased during bacterial infection without increases in bacterial load, the authors concluded that the *yw* strain was less tolerant to bacterial infection rather than less resistant (34). As we observed a significant increment of viral load in *yw* flies that correlated with a lower percentage of survival, we cannot advance the hypothesis of a change in tolerance. Nevertheless, several studies highlight a link between metabolism changes and viral resistance in *Drosophila* (18, 35, 36); therefore we do not exclude the involvement of metabolism as an explanation for the different survival trends we noticed among strains.

Previous studies demonstrated that viral infections trigger *Dcr-2* and *Ago-2* mRNA expression in *Apis mellifera* and *Bombus terrestris* (37), and several authors suggested that this induction might be an essential feature to deal against infections in insects (13–15). For these reasons, we hypothesized that variations in *Dcr-2* and *Ago-2* expression levels upon viral infection could explain the difference in mortality between strains. Interestingly, we did not observe changes in transcript expression levels for *Dcr-2* and *Ago-2* in any strain and for any virus and mode of infection. Our results agree with previous *D. melanogaster* studies [reviewed in (38)] that showed that RNAi genes do not alter their expression level after infection with DCV. Interestingly, a recent study in which *D. melanogaster* is used as a model to investigate Zika virus-insect interactions, showed an increased level of *Dcr-2* and *Ago-2* transcripts after infection (18). As previously showed for *A. mellifera* (19), the regulation of *Dcr-2* and *Ago-2* expression may be virus-dependent. A broader study including other model viruses from several Baltimore classes should shed light on whether the absence of changes in transcript expression levels, and mainly of induction of Dcr-2 and Ago-2 proteins, is a general response against infections with natural viruses in *D. melanogaster*.

It is well established that there is not always a direct correlation between mRNA and protein levels (39, 40), and that translational and post-translational regulation and degradation of proteins play a pivotal role in determining protein levels (41). In the current work we showed that, although their transcripts remain unchanged, Dcr-2 and Ago-2 protein levels change after injection-related stress and viral infection. Injection with a sterile solution causes a rapid Dcr-2 level decrease, detectable within minutes and possibly related to a stall in protein translation and/or an increase in protein degradation. Although the actual mechanism is still unknown, similar processes of rapid decrease

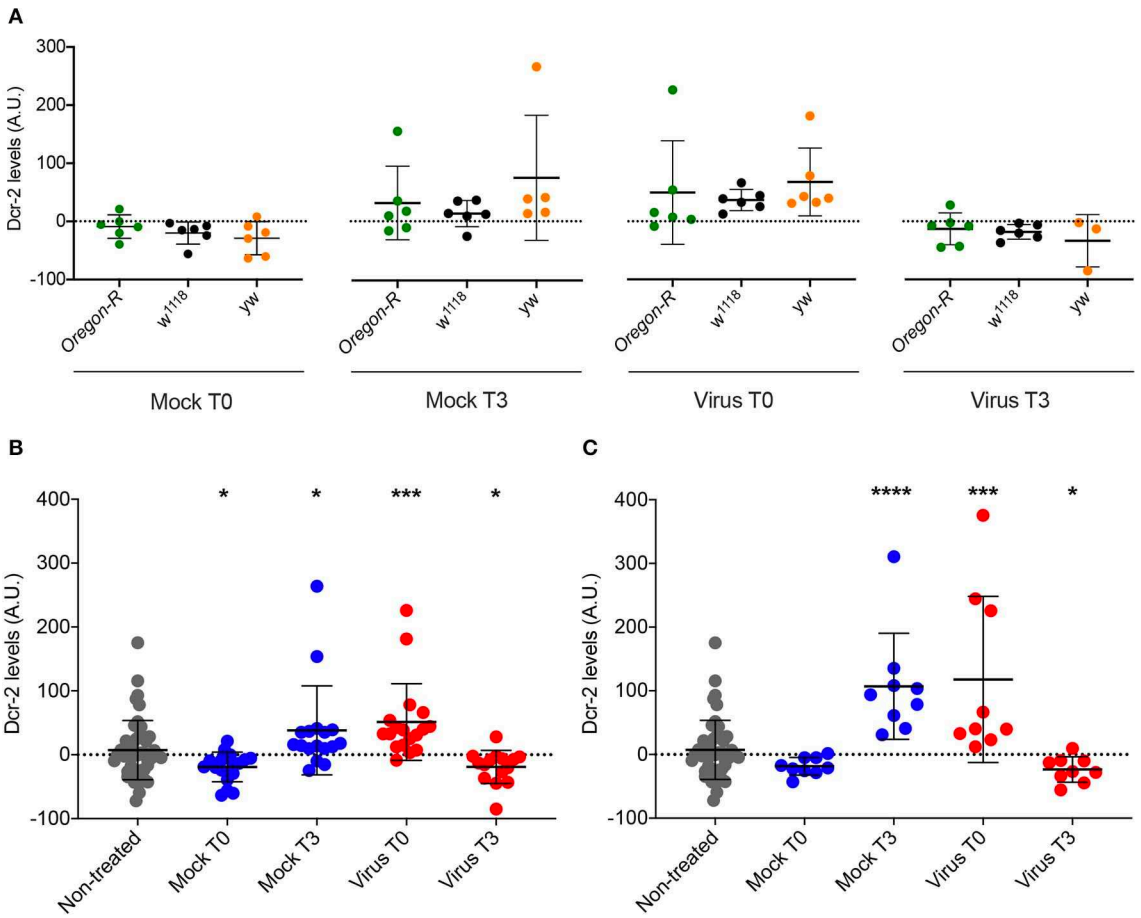

FIGURE 7 | Comparison of Dcr-2 protein expression levels. **(A)** Dcr-2 levels for 2 time points after mock and virus infection. For each time point, Dcr-2 levels were compared between *Oregon-R*, w^{1118}, and *yw* flies (Virus indicates flies injected with DCV or FHV). Each dot indicates a biological replicate composed of a pool of 4–8 flies. No significant differences were observed between the strains inside each time point. Mean ± SD are represented. Analysis performed using the Mann–Whitney test, $n = 6$ except *yw* Mock T3 $n = 5$ and *yw* Virus T3 $n = 3$. **(B)** Dcr-2 levels along time (days post injection); Mock T0 = Mock-control at time point 0; Mock T3 = Mock-control at time point 3; Virus T0 = Virus infection at time point 0; Virus T3 = Virus infection at time point 3. Analysis performed using the Mann–Whitney test; all groups are compared with non-treated. Non-treated $n = 48$, Injected $n = 18$ except *yw* Mock T3 $n = 17$ and *yw* Virus T3 $n = 15$, mean ± SD, ($^*P \leq 0.025$, $^{***}P < 0.0003$). **(C)** Dcr-2 levels along time upon feeding; Mock T0 = Mock-control at time point 0; Mock T3 = Mock-control at time point 3; Virus T0 = Virus infection at time point 0; Virus T3 = Virus infection at time point 3. A.U. indicates arbitrary units. Analysis performed using the Mann-Whitney test; all groups are compared with non-treated. Non-treated $n = 48$, fed $n = 9$, mean ± SD ($^*P \leq 0.025$, $^{***}P = 0.0003$, $^{****}P < 0.0001$).

in protein levels are reported in the literature (42, 43) and can be associated with gene regulation (44). For example, the stimulation with 10 ng/ml of TNF-α induces a fast degradation of IκBα (the NF-κB inhibitor) with a half-life of 16 min (44). On the contrary, we observe that injection with virus leads to an increase of Dcr-2 levels. This suggests that the flies can "sense" the presence of a virus early before the beginning of viral replication, possibly via specific pattern recognition receptors, an assumption previously hypothesized (45, 46) and recently reinforced by results showing that injection of heat-inactivated Zika virus induces certain antiviral immune mechanisms (18). The increase of protein concentration without change in gene expression may be achieved by blocking protein degradation and/or increasing protein translation in a mechanism known as "*translation on demand*" (40). This molecular process seems to play an important role in protein regulation in yeast and other organisms, including mammals (40, 47, 48). For Dcr-2, the aftermath of this increase was a progressive reduction in protein levels over time that correlates with an increase in viral replication. Two non-exclusive explanations may account for this: (1) the DCV and FHV viral suppressors of RNAi (8) trigger the degradation of Dcr-2 and Ago-2 in a similar fashion to that observed for Cricket Paralysis Virus (CrPV) (49); (2) the later activation of other unknown immunological processes to fight viral infection inhibits Dcr-2 and Ago-2 from being produced.

Several lines of evidence demonstrate that immunological responses can be virus-specific. The fact that other pathways can be more effective than RNAi in counteracting viral infection has been proposed for the case of *B. terrestris* infected with Israeli Acute Paralysis virus and Slow Bee Paralysis virus (16). We have previously demonstrated that RNAi is not necessary for the clearance of viruses after oral infection (21). Other

works showed that the antiviral RNAi is ineffective against virus in the midgut of *Aedes aegypti* (50) or in certain basal metazoans (51). Altogether these results highlight the fact that other biological processes may be more effective than, or work together with, the siRNA pathway to reach an effective antiviral response.

CONCLUSIONS

In our work we showed that the key components of the antiviral siRNA pathway in *D. melanogaster*, Dcr-2 and Ago-2, are not induced at the mRNA level upon viral infection, but that their regulation occurs at the protein level through an unknown mechanism reminiscent of translation on demand. This response is independent of the mode of infection, the virus, and the fly strain, and is not related to differences in susceptibility to viral infection among strains. We also reported the bivalent aspect of this regulation, which acts as a general gene regulation mechanism (during infection procedure-related stress) and as an antiviral response (during viral infection), possibly activated via early recognition of viral motifs by unknown pattern recognition receptors.

DATA AVAILABILITY STATEMENT

The raw data supporting the conclusions of this article will be made available by the authors, without undue reservation, to any qualified researcher.

AUTHOR CONTRIBUTIONS

Conceptualization: AT, VM, JM, and M-CS. Methodology and investigation: AT, VM, and JM. Resources: M-CS. Formal analysis and writing—original draft preparation: AT. Writing—review and editing: VM, JM, and M-CS.

FUNDING

This research was funded by the European Research Council (FP7/2013-2019 ERC CoG 615220) and the French Government's Investissement d'Avenir program, Laboratoire d'Excellence Integrative Biology of Emerging Infectious Diseases (grant ANR-10-LABX-62-IBEID) to M-CS.

ACKNOWLEDGMENTS

We thank all members of the Saleh lab for discussion, Mariana Ferrari, Thomas Pradeau, Marco Vignuzzi, and Louis Lambrechts for critical reading and editing of the manuscript, Maxime Rotival for advice with statistical analysis, and Kathryn Rozen-Gagnon for advice in the use of anti-Ago 2 antibody.

SUPPLEMENTARY MATERIAL

The Supplementary Material for this article can be found online at: https://www.frontiersin.org/articles/10.3389/fimmu.2020.00362/full#supplementary-material

REFERENCES

1. Mello CC, Darryl CJ. Revealing the world of RNA interference. *Nature*. (2004) 431:338–42. doi: 10.1038/nature02872
2. Mello CC. Return to the RNAi world: rethinking gene expression and evolution. *Cell Death Differ*. (2007) 14:2013–20. doi: 10.1038/sj.cdd.4402252
3. Claycomb JM. Ancient endo-siRNA pathways reveal new tricks. *Curr Biol*. (2014) 24:R703–15. doi: 10.1016/j.cub.2014.06.009
4. Azlan A, Dzaki N, Azzam G. Argonaute: the executor of small RNA function. *J Genet Genomics*. (2016) 43:481–94. doi: 10.1016/j.jgg.2016.06.002
5. Koonin EV. Evolution of RNA- and DNA-guided antivirus defense systems in prokaryotes and eukaryotes: common ancestry vs convergence. *Biol Direct*. (2017) 12:1–14. doi: 10.1186/s13062-017-0177-2
6. Mongelli V, Saleh M-C. Bugs are not to be silenced: small RNA pathways and antiviral responses in insects. *Annu Rev Virol*. (2016) 3:573–89. doi: 10.1146/annurev-virology-110615-042447
7. Calcino AD, Fernandez-Valverde SL, Taft RJ, Degnan BM. Diverse RNA interference strategies in early-branching metazoans. *BMC Evol Biol*. (2018) 18:1–13. doi: 10.1186/s12862-018-1274-2
8. Mussabekova A, Daeffler L, Imler JL. Innate and intrinsic antiviral immunity in Drosophila. *Cell Mol Life Sci*. (2017) 74:2039–54. doi: 10.1007/s00018-017-2453-9
9. Chung WJ, Okamura K, Martin R, Lai EC. Endogenous RNA interference provides a somatic defense against Drosophila transposons. *Curr Biol*. (2008) 18:795–802. doi: 10.1016/j.cub.2008.05.006
10. Ghildiyal M, Seitz H, Horwich MD, Li C, Du T, Lee S, et al. Endogenous siRNAs derived from transposons and mRNAs in Drosophila somatic cells. *Science*. (2008) 320 :1077 LP—81. doi: 10.1126/science.1157396
11. Czech B, Malone CD, Zhou R, Stark A, Schlingeheyde C, Dus M, et al. An endogenous small interfering RNA pathway in Drosophila. *Nature*. (2008) 453:798–802. doi: 10.1038/nature07007
12. Kurzynska-Kokorniak A, Koralewska N, Pokornowska M, Urbanowicz A, Tworak A, Mickiewicz A, et al. The many faces of Dicer: the complexity of the mechanisms regulating Dicer gene expression and enzyme activities. *Nucleic Acids Res*. (2015) 43:4365–80. doi: 10.1093/nar/gkv328
13. Ye C, An X, Jiang Y, Ding BY, Shang F, Christiaens O, et al. Induction of RNAi core Machinery's gene expression by exogenous dsRNA and the effects of pre-exposure to dsRNA on the Gene Silencing Efficiency in the Pea Aphid (*Acyrthosiphon pisum*). *Front Physiol*. (2019) 10:906. doi: 10.3389/fphys.2018.01906
14. Garbutt JS, Reynolds SE. Induction of RNA interference genes by double-stranded RNA; implications for susceptibility to RNA interference. *Insect Biochem Mol Biol*. (2012) 42:621–8. doi: 10.1016/j.ibmb.2012.05.001
15. Lozano J, Gomez-Orte E, Lee HJ, Belles X. Super-induction of Dicer-2 expression by alien double-stranded RNAs: an evolutionary ancient response to viral infection? *Dev Genes Evol*. (2012) 222:229–35. doi: 10.1007/s00427-012-0404-x
16. Niu J, Smagghe G, De Coninck DIM, Van Nieuwerburgh F, Deforce D, Meeus I. *In vivo* study of Dicer-2-mediated immune response of the small interfering RNA pathway upon systemic infections of virulent and avirulent viruses in *Bombus terrestris*. *Insect Biochem Mol Biol*. (2016) 70:127–37. doi: 10.1016/j.ibmb.2015.12.006
17. Galbraith DA, Yang X, Niño EL, Yi S, Grozinger C. Parallel epigenomic and transcriptomic responses to viral infection in honey bees (*Apis mellifera*). *PLoS Pathog*. (2015) 11:e1004713. doi: 10.1371/journal.ppat.1004713
18. Harsh S, Ozakman Y, Kitchen SM, Paquin-Proulx D, Nixon DF, Eleftherianos I. Dicer-2 regulates resistance and maintains homeostasis against zika virus infection in Drosophila. *J Immunol*. (2018) 201:3058–72. doi: 10.4049/jimmunol.1800597
19. Ryabov EV, Wood GR, Fannon JM, Moore JD, Bull JC, Chandler D, et al. A virulent strain of Deformed Wing Virus (DWV) of honeybees (*Apis mellifera*)

prevails after varroa destructor-mediated, or *in vitro*, transmission. *PLoS Pathog.* (2014) 10:e1004230. doi: 10.1371/journal.ppat.1004230
20. Spellberg MJ, Marr MT. FOXO regulates RNA interference in Drosophila and protects from RNA virus infection. *Proc Natl Acad Sci USA*. (2015) 112:14587–92. doi: 10.1073/pnas.1517124112
21. Mondotte JA, Gausson V, Frangeul L, Blanc H, Lambrechts L, Saleh M-C. Immune priming and clearance of orally acquired RNA viruses in Drosophila. *Nat Microbiol.* (2018) 3:1394–403. doi: 10.1038/s41564-018-0265-9
22. Ross LN. Causal concepts in biology: how pathways differ from mechanisms and why it matters. *Br J Philos Sci.* (2018) axy078. doi: 10.1093/bjps/axy078
23. Li H, Li WX, Ding SW. Induction and suppression of RNA silencing by an animal virus. *Science.* (2002) 296:1319–21. doi: 10.1126/science.1070948
24. Galiana-Arnoux D, Dostert C, Schneemann A, Hoffmann JA, Imler JL. Essential function *in vivo* for Dicer-2 in host defense against RNA viruses in Drosophila. *Nat Immunol.* (2006) 7:590–7. doi: 10.1038/ni1335
25. Van Rij RP, Saleh MC, Berry B, Foo C, Houk A, Antoniewski C, et al. The RNA silencing endonuclease Argonaute 2 mediates specific antiviral immunity in *Drosophila melanogaster*. *Genes Dev*. (2006) 20:2985–95. doi: 10.1101/gad.1482006
26. Zambon RA, Vakharia VN, Wu LP. RNAi is an antiviral immune response against a dsRNA virus in *Drosophila melanogaster*. *Cell Microbiol*. (2006) 8:880–9. doi: 10.1111/j.1462-5822.2006.00688.x
27. Saleh M, Tassetto M, van Rij RP, Goic B, Gausson V, Berry B, et al. Antiviral immunity in Drosophila requires systemic RNA interference spread. *Nature*. (2009) 458:346–50. doi: 10.1038/nature07712
28. Kemp C, Mueller S, Goto A, Barbier V, Paro S, Bonnay F, et al. Broad RNA interference–mediated antiviral immunity and virus-specific inducible responses in Drosophila. *J Immunol.* (2013) 190:650–8. doi: 10.4049/jimmunol.1102486
29. Sarkies P, Miska EA. Is there social RNA? *Science.* (2013) 341:467–8. doi: 10.1126/science.1243175
30. Knip M, Constantin ME, Thordal-Christensen H. Trans-kingdom cross-talk: small RNAs on the move. *PLoS Genet.* (2014) 10:e1004602. doi: 10.1371/journal.pgen.1004602
31. Duval M, Cossart P, Lebreton A. Mammalian microRNAs and long noncoding RNAs in the host-bacterial pathogen crosstalk. *Semin Cell Dev Biol*. (2017) 65:11–9. doi: 10.1016/j.semcdb.2016.06.016
32. Cornish-Bowden A, Cárdenas ML, Letelier JC, Soto-Andrade J, Abarzúa FG. Understanding the parts in terms of the whole. *Biol Cell*. (2004) 96:713–7. doi: 10.1016/j.biolcel.2004.06.006
33. Okado K, Shinzawa N, Aonuma H, Nelson B, Fukumoto S, Fujisaki K, et al. Rapid recruitment of innate immunity regulates variation of intracellular pathogen resistance in Drosophila. *Biochem Biophys Res Commun.* (2009) 379:6–10. doi: 10.1016/j.bbrc.2008.11.097
34. Eleftherianos I, More K, Spivack S, Paulin E, Khojandi A, Shukla S. Nitric oxide levels regulate the immune response of *Drosophila melanogaster* reference laboratory strains to bacterial infections. *Infect Immun.* (2014) 82:4169–81. doi: 10.1128/IAI.02318-14
35. Arnold PA, Johnson KN, White CR. Physiological and metabolic consequences of viral infection in *Drosophila melanogaster*. *J Exp Biol*. (2013) 216:3350–7. doi: 10.1242/jeb.088138
36. Merkling SH, Riahi H, Overheul GJ, Schenck A, van Rij RP. Peroxisome-associated Sgroppino links fat metabolism with survival after RNA virus infection in Drosophila. *Sci Rep*. (2019) 9:1–12. doi: 10.1038/s41598-019-38559-x
37. McMenamin AJ, Daughenbaugh KF, Parekh F, Pizzorno MC, Flenniken ML. Honey bee and bumble bee antiviral defense. *Viruses*. (2018) 10:1–22. doi: 10.3390/v10080395
38. Teixeira L. Whole-genome expression profile analysis of *Drosophila melanogaster* immune responses. *Brief Funct Genomics*. (2012) 11:375–86. doi: 10.1093/bfgp/els043
39. Schwanhüusser B, Busse D, Li N, Dittmar G, Schuchhardt J, Wolf J, et al. Global quantification of mammalian gene expression control. *Nature*. (2011) 473:337–42. doi: 10.1038/nature10098
40. Liu Y, Beyer A, Aebersold R. On the dependency of cellular protein levels on mRNA abundance. *Cell*. (2016) 165:535–50. doi: 10.1016/j.cell.2016.03.014
41. Vogel C, Marcotte EM. Insights into the regulation of protein abundance from proteomic and transcriptomic analyses. *Nat Rev Genet*. (2012) 13:227–32. doi: 10.1038/nrg3185
42. Spruessel A, Steimann G, Jung M, Lee SA, Carr T, Fentz AK, et al. Tissue ischemia time affects gene and protein expression patterns within minutes following surgical tumor excision. *Biotechniques*. (2004) 36:1030–7. doi: 10.2144/04366RR04
43. Joilin G, Guévremont D, Ryan B, Claudianos C, Cristino AS, Abraham WC, et al. Rapid regulation of microRNA following induction of long-term potentiation *in vivo*. *Front Mol Neurosci.* (2014) 7:98. doi: 10.3389/fnmol.2014.00098
44. Turner DA, Paszek P, Woodcock DJ, Nelson DE, Horton CA, Wang Y, et al. Physiological levels of TNFα stimulation induce stochastic dynamics of NF-κB responses in single living cells. *J Cell Sci*. (2010) 123:2834–43. doi: 10.1242/jcs.069641
45. Lemaitre B, Hoffmann J. The host defense of *Drosophila melanogaster*. *Annu Rev Immunol*. (2007) 25:697–743. doi: 10.1146/annurev.immunol.25.022106.141615
46. Lamiable O, Imler J-L. Induced antiviral innate immunity in Drosophila. *Curr Opin Microbiol.* (2014) 20:62–8. doi: 10.1016/j.mib.2014.05.006
47. Beyer A, Hollunder J, Nasheuer H-P, Wilhelm T. Post-transcriptional expression regulation in the yeast *Saccharomyces cerevisiae* on a genomic scale. *Mol Cell Proteomics*. (2004) 3:1083–92. doi: 10.1074/mcp.M400099-MCP200
48. Jovanovic M, Rooney MS, Mertins P, Przybylski D, Chevrier N, Satija R, et al. Dynamic profiling of the protein life cycle in response to pathogens. *Science.* (2015) 347:1259038. doi: 10.1126/science.1259038
49. Nayak A, Kim DY, Trnka MJ, Kerr CH, Lidsky PV, Stanley DJ, et al. A viral protein restricts Drosophila RNAi immunity by regulating argonaute activity and stability. *Cell Host Microbe. (2018)* 24:542–57.e9. doi: 10.1016/j.chom.2018.09.006
50. Olmo RP, Ferreira AGA, Izidoro-Toledo TC, Aguiar ERGR, de Faria IJS, de Souza KPR, et al. Control of dengue virus in the midgut of *Aedes aegypti* by ectopic expression of the dsRNA-binding protein Loqs2. *Nat Microbiol.* (2018) 3:1385–93. doi: 10.1038/s41564-018-0268-6
51. Waldron FM, Stone GN, Obbard DJ. Metagenomic sequencing suggests a diversity of RNA interference-like responses to viruses across multicellular eukaryotes. *PLoS Genet*. (2018) 14:e1007533. doi: 10.1101/166488

Conflict of Interest: The authors declare that the research was conducted in the absence of any commercial or financial relationships that could be construed as a potential conflict of interest.

frontiers in Immunology

REVIEW
published: 25 March 2020
doi: 10.3389/fimmu.2020.00521

Drosophila as a Model System to Investigate the Effects of Mitochondrial Variation on Innate Immunity

Tiina S. Salminen[1,2] and Pedro F. Vale[1]*

[1] School of Biological Sciences, Institute of Evolutionary Biology, The University of Edinburgh, Edinburgh, United Kingdom,
[2] Faculty of Medicine and Health Technology, Tampere University, Tampere, Finland

Understanding why the response to infection varies between individuals remains one of the major challenges in immunology and infection biology. A substantial proportion of this heterogeneity can be explained by individual genetic differences which result in variable immune responses, and there are many examples of polymorphisms in nuclear-encoded genes that alter immunocompetence. However, how immunity is affected by genetic polymorphism in an additional genome, inherited maternally inside mitochondria (mtDNA), has been relatively understudied. Mitochondria are increasingly recognized as important mediators of innate immune responses, not only because they are the main source of energy required for costly immune responses, but also because by-products of mitochondrial metabolism, such as reactive oxygen species (ROS), may have direct microbicidal action. Yet, it is currently unclear how naturally occurring variation in mtDNA contributes to heterogeneity in infection outcomes. In this review article, we describe potential sources of variation in mitochondrial function that may arise due to mutations in vital nuclear and mitochondrial components of energy production or due to a disruption in mito-nuclear crosstalk. We then highlight how these changes in mitochondrial function can impact immune responses, focusing on their effects on ATP- and ROS-generating pathways, as well as immune signaling. Finally, we outline how being a powerful and genetically tractable model of infection, immunity and mitochondrial genetics makes the fruit fly *Drosophila melanogaster* ideally suited to dissect mitochondrial effects on innate immune responses to infection.

Keywords: *Drosophila melanogaster*, cybrid, infection, innate immunity, mitochondria, mtDNA, oxidative phosphorylation, reactive oxygen species

OPEN ACCESS

Edited by:
Nicolas Bertho, INRA Biologie, Épidémiologie et Analyse de Risque en Santé Animale (BIOEPAR), France

Reviewed by:
Kristi L. Montooth, University of Nebraska-Lincoln, United States
Javier Santander, Memorial University of Newfoundland, Canada

****Correspondence:***
Tiina S. Salminen
tiina.susanna.salminen@gmail.com; tiina.s.salminen@tuni.fi

Specialty section:
This article was submitted to Comparative Immunology, a section of the journal Frontiers in Immunology

Received: *23 October 2019*
Accepted: *06 March 2020*
Published: *25 March 2020*

Citation:
Salminen TS and Vale PF (2020) Drosophila as a Model System to Investigate the Effects of Mitochondrial Variation on Innate Immunity. Front. Immunol. 11:521. doi: 10.3389/fimmu.2020.00521

INTRODUCTION

Understanding why individuals vary in their response to infection is one of the major challenges in immunology (1, 2). This variation may arise from differences in host age (3), sex (4), nutrition or environmental stressors (5), and genetic variation present in immune related genes (2). Experimental immunology – mainly in model systems such as mice, zebra fish and fruit flies – has been successful in identifying the major immune pathways (*Drosophila* innate immunity summarized in **Box 1**) (6–8). Quantitative genetic and genomic approaches have identified

BOX 1 | *Drosophila* innate immunity in a nutshell. *Drosophila* has been extensively utilized as a model system for innate immunity and it has led to many breakthrough in immunity field (6, 114, 115). *Drosophila* does not possess acquired/adaptive immunity and it relies on humoral and cell-mediated innate immunity for its defense against pathogens, such as bacteria, viruses, fungi, and parasites. Immune mechanisms against these invaders include activation of appropriate signal transduction pathways depending on the invading microbe, involving production of antimicrobial peptides (AMPs), phagocytosis of microbes, wound closure, and a melanization cascade involved in the encapsulation of foreign elements. Similar first-line innate immune defense mechanisms can be found from plants to humans.

Humoral Innate Immunity: In *Drosophila*, the humoral innate immune response to bacterial pathogens is characterized by the production and release of a cocktail of AMPs into the hemolymph. This response is driven by two evolutionarily conserved and largely independent pathways, Immune deficiency (IMD) and Toll pathways (116). The Toll pathway is induced by bacteria containing LYS-type peptidoglycan in their cell walls (mainly Gram-positive bacteria), while the IMD pathway is induced by DAP-type peptidoglycan (mainly Gram-negative) bacteria. These pathways culminate in the translocation of NF-κB dimers to the nucleus leading to infection-specific upregulation of AMPs targeted to clear the infection (117–119). The response to viral pathogens replicating within the host cells involves both the Janus kinase/signal transducers and activators of transcription (JAK-STAT) pathway (118, 120), RNA interference (RNAi) and antiviral effector molecules (121, 122). Viral infections involve cell-mediated responses like apoptosis and autophagy and humoral responses such as the expression of anti-viral genes, some of which overlap with genes induced upon bacterial and fungal infections, indicating the involvement of the NF-κB signaling upon viral infections. The response to fungal invaders includes both humoral and cellular arms of immunity and involves the expression of AMPs mainly via the Toll pathway.

Cell-Mediated Innate Immunity: In *Drosophila*, the cell-mediated innate immune system consists of hemocytes (blood cells) and is induced by epithelial damage and detection of foreign particles in the hemocoel. Hemocytes function in sealing of epithelial wounds, encapsulating and terminating parasites and engulfing apoptotic corpses [reviewed in (123)]. In *Drosophila* there are three major lineages of hemocytes: plasmatocytes (phagocytic), crystal cells (melanization) and lamellocytes (encapsulation). Plasmatocytes comprise the majority of the circulating hemocyte population and are responsible for the engulfment of small particles, participate in the encapsulation of foreign material and are able to trigger the systemic humoral immune response to secrete AMPs. Crystal cells usually make up less than 5% of the larval circulating hemocytes. Crystal cells contain prophenol oxidase which active form phenol oxidase is involved in the melanization cascade when the crystal cells rupture in response to immune activation (123). In uninfected larvae, the lamellocytes can be present in small numbers in the late third instar stage, otherwise healthy larvae do not contain them. Lamellocytes are produced upon invasion of parasitoid wasps and they form a multilayer capsule around the invading parasitic egg, with the help of plasmatocytes and crystal cells (124). Eventually the capsule is melanized and elevated levels of ROS terminate the intruder (125).

polymorphisms in genes underlying these mechanisms, and these explain some of the variation in infection outcomes (9–12). While most of this work has focused on genetic variation in the nuclear genome, metazoan organisms have an additional genome, inherited maternally inside mitochondria (mtDNA). More than functioning as the powerhouses of the cell, a growing body of work in the last decade has shown that mitochondria play an important role in inflammation and immunity and contribute to the host response to infection (13–18).

Here, we propose that the fruit fly (*Drosophila melanogaster)* offers an ideal model system to investigate the role of mitochondrial variation and mito-nuclear crosstalk in innate immunity. We start by discussing the sources of variation in mitochondrial function, using examples of mutations of nDNA and mtDNA encoded genes that have been shown to affect organismal phenotypes through changes in mitochondrial metabolism and signaling. This is followed by emphasizing the emerging role of mitochondria in immune responses through mitochondrial metabolites and by-products of mitochondrial metabolism, such as ROS. Finally, we describe methodology to investigate the role of mito-nuclear crosstalk and mtDNA variation in immunity in *Drosophila*. We emphasize how the use of cytoplasmic hybrid (cybrid) models allows to distinguish the effect of mtDNA variation from that arising from the nuclear genome. We conclude by highlighting the benefits of the cybrid model to further our understanding of mito-nuclear effects on heterogenous immune responses.

Abbreviations: AMP, antimicrobial peptide; ATP, adenosine triphosphate; DAMP, danger-associated molecular pattern; ETC, electron transport chain; IMD, immune deficiency; mt-aaRS, mitochondrial aminoacyl-tRNA synthetase; mtDNA, mitochondrial DNA; mtROS, mitochondrial reactive oxygen species; nDNA, nuclear DNA; NF-κB, nuclear factor kappa-light-chain-enhancer of activated B cells; OXPHOS, oxidative phosphorylation; ROS, reactive oxygen species.

SOURCES OF MITOCHONDRIAL VARIATION

Mitochondrial function depends on ∼1200 – 1500 proteins, the majority of which are encoded by the nuclear genome and transported to the mitochondria (19). Cellular energy production relies on mitochondria to produce ATP via oxidative phosphorylation (OXPHOS). OXPHOS requires the coordinated function of multiple protein subunits encoded by both the nuclear and mitochondrial genomes (nDNA and mtDNA, respectively – **Box 2**), and therefore both anterograde (from nucleus to mitochondria) and retrograde (from mitochondria to nucleus) signaling is required for optimal mitochondrial function. Mitochondrial variation arising from either nDNA or mtDNA can affect the transcription and translation of the mitochondrial proteins, signaling between the two genomes and through changes in the direct physical interactions among the OXPHOS components originating from the two genomes, ultimately affecting the function of mitochondria. Mitochondrial variation shows multiple mode of inheritance. When this variation originates from mtDNA it is maternally inherited and has a potential to become heteroplasmic even within mitochondria, and when originating from nuclear genome it can be X-linked, autosomal dominant, autosomal recessive or *de novo*. Here, we discuss potential sources of mitochondrial variation with examples of known nuclear and mitochondrial mutations that could also lead to variation in immune responses.

Variation Arising From the Nuclear Genome

The vast majority of the proteins that are required for mitochondrial functions are encoded by the nuclear genome, translated in the cytosol and transported to mitochondria via mitochondrial targeting sequence which is removed upon entry into mitochondria. These proteins include the replication,

BOX 2 | Mito-nuclear crosstalk is required for mitochondrial functions. Mitochondria are cellular organelles of eukaryotic cells that are thought to have originated by endosymbiotic phagocytosis of an oxygen-converting α-proteobacterium by archaebacterium (19, 126). The primary function of mitochondria is to produce ATP through oxidative phosphorylation (OXPHOS) complexes I-V, and mitochondrial matrix is also the site of tricarboxylic acid cycle. Mitochondria contains multiple copies of a circular mtDNA (mtDNA copy number) distinct from that of the nuclear genome (**Figure 1**). Majority of the mtDNA genes required for aerobic energy production through OXPHOS have been shifted to the nuclear chromosomes and the remaining mitochondrial genome in most metazoans encodes for 37 genes, all crucial in OXPHOS. From these, 13 are polypeptide subunits of four of the five OXPHOS complexes, with the majority of the polypeptides encoded by nDNA (**Figure 1B**). Mitochondria contains its own translational system and the mtDNA encodes two rRNA and 22 tRNA genes as the mt-aaRS genes are encoded by the nuclear genome. Beside the 84 nDNA genes functioning in OXPHOS, around 1200-1500 nDNA encoded polypeptides are imported to and assembled within mitochondria, required for the various mitochondrial functions (**Figure 1A**). Nucleus and the mitochondria maintain a bidirectional regulation where the nuclear genome can signal to the mitochondria (anterograde signaling) for example to increase mitochondrial respiration. Mitochondria can signal (retrograde signaling) for example to induce cell death by releasing cytochrome c, or by controlling mitochondrial fusion and fission by AMP-activated protein kinase (57).

transcription and translation machineries for mtDNA and the 84 polypeptide subunits needed for OXPHOS (summarized in **Box 2**). Mutations in nDNA directly affecting OXPHOS complex genes have been reviewed in (20). Maintenance genes of mitochondrial functions include regulatory genes of mitochondrial and cytosolic nucleotide pools to maintain balanced supply of mitochondrial dNTPs, involved with mtDNA nucleoid packaging, carrier proteins required for metabolite and cofactor transport across cellular and mitochondrial membranes, genes for mitochondrial lipid and membrane homeostasis, and mitochondrial fission/fusion and cristae organization [reviewed in (21)].

Mutations in mtDNA maintenance genes (replication and repair pathways and mtDNA nucleoid packaging) have been shown to cause mtDNA deletions, point mutations and even depletion (22). The most important mtDNA maintenance gene is the *DNA polymerase gamma* (*POLG*) which is responsible for the replication of the mtDNA. Almost 200 *POLG* mutations have been reported and these are the most common causes of mitochondrial disease. Mutations in *POLG* have been shown to cause large scale deletions and various other mutations to the mtDNA due to replication and/or repair machinery malfunctions and these have been connected to many mitochondrial diseases such as Alper's syndrome, parkinsonism and multiple other neurodegenerative disorders (23). *POLG* was mutated in *Drosophila* to create a proofreading-deficient form resulting to drastically increased somatic mtDNA mutation frequency and mitochondrial dysfunction, which manifested as a shortened lifespan, a progressive locomotor deficit and a loss of dopaminergic neurons (24).

Regulation of OXPHOS gene transcription is tightly coordinated and must be able to establish efficient oxidative metabolism fulfilling the cell's changing energy requirements. Components of the transcription machinery are encoded by the nuclear genome and have been reviewed in (25). Mossman et al., showed that in *D. melanogaster* cybrid lines the transcription of nuclear encoded mitochondrial genes were affected by mtDNA variation, indicating a retrograde signaling effect in transcription regulation (26). Hence, mutations in the transcription machinery can have a wide impact on the function of mitochondria, and variation in the mtDNA genes can affect the overall transcription efficiency of OXPHOS components, possibly also affecting their translation.

All proteins involved in mtDNA translation (27) are encoded by nuclear genes, involving ribosomal proteins, mt-aaRSs, tRNA modifying enzymes, and translation factors. Mutations in these genes have been shown to cause mitochondrial diseases due to dysfunction in the protein-synthesis machinery (27). mt-aaRSs are transported to mitochondria to catalyze an amino acid attachment to its complementary tRNA in aminoacylation reaction for translation of the thirteen mitochondrial proteins. All ribosomal RNAs and the transfer RNAs required for the translation of the mitochondrial proteins are encoded by the mtDNA (**Figure 1**). Hence, nuclear encoded components of the translation machinery need to be able to recognize mitochondrial counterparts for the production of mitochondrial proteins. mt-aaRS genes are central to cellular energy production and mutations in these can lead to variable disease phenotypes depending on the affected tissues and the energy demands of the cells in those tissue types (28). Mutations in both mt-tRNAs and mt-aaRSs can lead to disease and the clinical presentation has been shown to be highly specific to the affected mt-aaRS [reviewed in (29)]. However, diversity of pathologies is higher for mt-tRNA mutations than mt-aaRSs, possibly due to random distribution of heteroplasmic populations of mtDNA copies during mitotic segregation (28). In *Drosophila simulans* a variant of tyrosyl-tRNA synthetase interacts epistatically with a mitochondrially encoded $tRNA^{Tyr}$ variant, leading to decrease in the activities of OXPHOS complexes I, III, and IV (30). At the organismal level this manifests as developmental delay, compromised bristle formation and decreased fecundity (30).

In *D. melanogaster*, a *tko* mutant (tko^{25t}) carries a missense mutation in nuclear encoded mitoribosomal protein S12 causing a decrease in smaller ribosomal subunits. This causes decreased activity levels of all four OXPHOS complexes that contain mitochondrial encoded proteins (**Figure 1**), ultimately manifesting as developmental delay, temporary paralysis followed from vigorous shaking (bang sensitivity) and sensitivity to antibiotics and high sugar diet as well as impaired courtship behavior and hearing (31, 32). Similar defects have been found in fibroblasts of patients with antenatal encephalopathy caused by mutations in the *MRPS22* gene coding mitochondrial ribosomal protein, which result in a reduction of 12s rRNA (33).

Variation Arising From the Mitochondrial Genome

The effect of the mitochondrial genome variation on innate immunity is intriguing as mtDNA does not follow the traditional Mendelian inheritance because it is inherited uniparentally

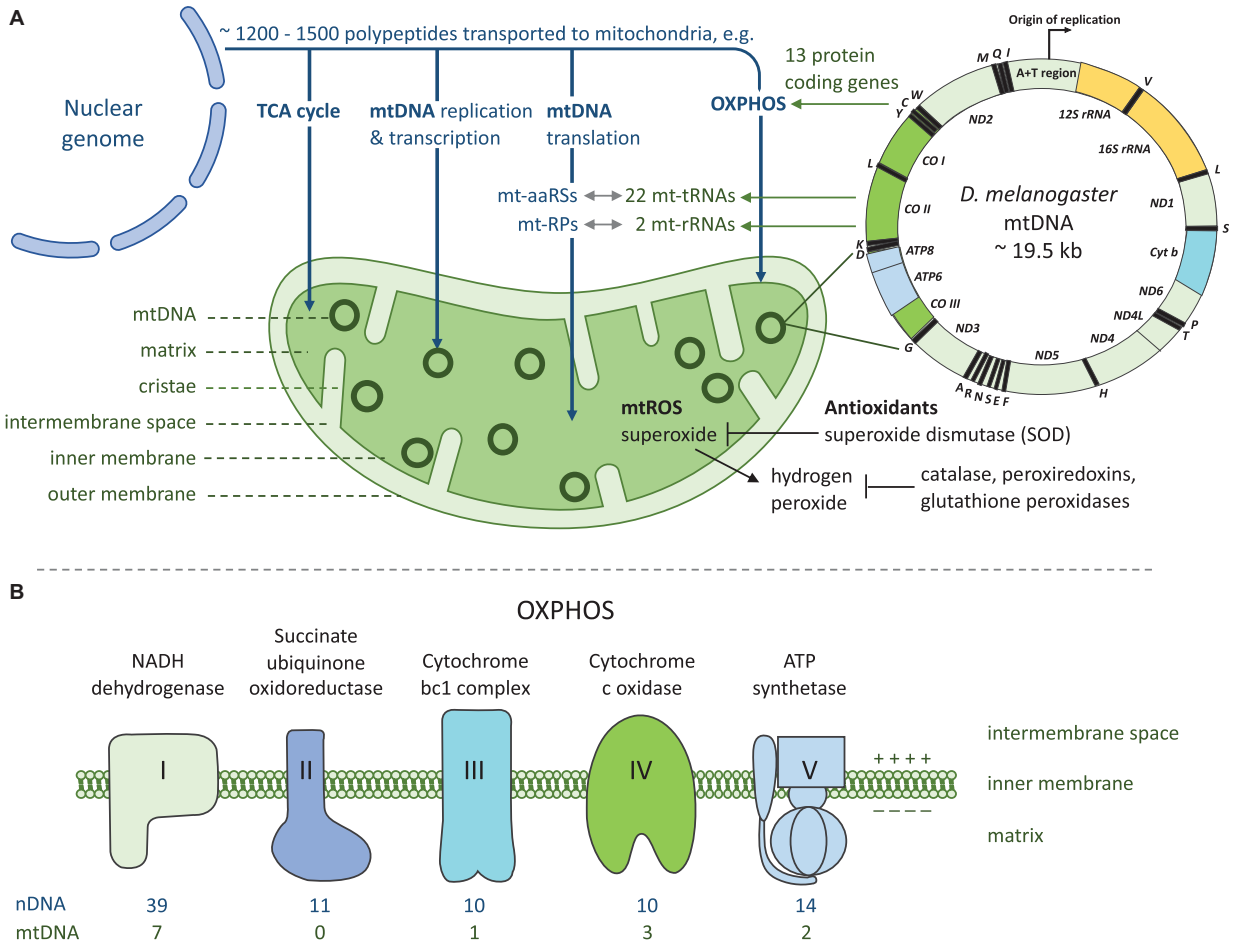

FIGURE 1 | Mito-nuclear crosstalk in mitochondrial functions and energy production. **(A)** Mitochondria rely on coordinated functions of nuclear and mitochondrial genomes. Vast majority of the genes required for mitochondrial functions are encoded by the nuclear genome. These proteins are translated in the cytoplasmic compartment and transported into the mitochondrion post-translationally with a mitochondrial targeting signal. Products of both genomes are required for producing cellular energy in the form of ATP through OXPHOS. As a by-product of OXPHOS mitochondria produces reactive oxygen species (ROS) which are detoxified by antioxidants. mt-aaRSs, mitochondrial aminoacyl-tRNA synthetases; mt-RPs, mitochondrial ribosomal proteins. **(B)** OXPHOS takes place at the inner mitochondrial membrane and it comprises five enzyme complexes. Both nuclear and mitochondrial encoded proteins are required for OXPHOS complexes I and III-V, as complex II contains only nuclear encoded subunits. Complexes I-IV and two electron carriers form the respiratory chain which generates a proton gradient used by complex V to generate ATP.

through the maternal lineage. The mitochondrial genome contains 37 genes, from which 13 encode polypeptides, two rRNA genes and 22 tRNA genes (**Box 2** and **Figure 1A**) and pathogenic mutations have been reported in all 37 mtDNA genes (34). mtDNA is subjected to much higher mutation rates than the nuclear genome and the mutation rate varies between species (35, 36). Besides mutations of the mtDNA replication and repair machinery, higher mutation rate of mtDNA is affected by the production of ROS within mitochondria as by-product of the OXPHOS. This can lead to a cycle in which ROS causes DNA damage, which in turn leads to dysregulation of respiration and accumulation of mutations.

Each cell contains numerous mitochondria and each mitochondrion may contain from a few to dozens of copies of mtDNA (the mtDNA copy number). Hence a given cell of a specific tissue type may contain thousands of copies of mtDNA and only one copy of nDNA. Unlike nDNA, mtDNA is not packed by histones but packed into protein-DNA complexes called nucleoids (37). *Drosophila* mtDNA contains one large A + T rich non-coding region (38), which in humans is called the D-loop. In both *Drosophila* and humans, the non-coding region is the starting point of mtDNA replication (39). Hence, variation in this region might cause changes in the mtDNA replication and have an effect on the mtDNA copy number content (40) and ultimately in energy production. mtDNA copy number is usually higher in tissues that have high energy demand such as brain, skeletal, and cardiac muscle tissues (41) and mtDNA mutations in these tissues can possibly lead to more pronounced phenotypes.

Besides heritable mtDNA mutations occurring in the germ line of the maternal lineage, the mtDNA of both females and males are subjected to spontaneous somatic mutations.

mtDNA genetics is complicated due to its multi-copy nature. mtDNA mutations within a single cell (and even within a single mitochondria) can be either heteroplasmic due to a mix of mutated and wild type mtDNA, or homoplasmic where all mtDNAs contain either the mutated or the wild type form. In a heteroplasmic mutation the proportion of mutated mtDNA needs to exceed a certain threshold for the mutation to manifest. This can be due to the wild type mtDNA not being able to compensate the defect at that point. The threshold is also likely to be dependent on the mutation type and environmental effectors. Nuclear genotypes may also have variation in their ability to dampen or amplify the effects of specific deleterious mitochondrial mutations, which often demonstrate incomplete penetrance (42).

mtDNA mutations have been linked to various human diseases (43). In Leber hereditary optic neuropathy (LHON) the patient suffers from a loss of vision and the mtDNA mutations causing it are mostly considered homoplasmic (44). However, even though all the offspring of a homoplasmic mother inherits the LHON, only 50% of males and 10% of females develop the disease, showing that predicting the way the mtDNA mutation manifests, is difficult due to mito-nuclear crosstalk. Also, environmental factors can cause changes in the mtDNA mutation manifestation, as in the case of mtDNA encoded homoplasmic ribosomal RNA (RNR1) mutation that causes deafness early on in childhood. Specific antibiotics are associated with the manifestations of the clinical symptoms of the RNR1 mutation (45). Due to the complexity of the crosstalk of the two genomes and environmental factors, possible physiological compensations and the amplifying or dampening effects originating from nuclear genome variation and compatibility with the mtDNA, it is difficult to predict how the mtDNA mutations will eventually manifest themselves.

Disruption of Mito-Nuclear Crosstalk

The optimal functioning of mitochondria relies on the correct transcription and translation of genes involved in respiration, and as mentioned above, these genes are found on both the nuclear and mitochondrial genomes. Several signaling pathways between the nucleus and mitochondria have been uncovered recently (46). Mutations in either nDNA or mtDNA have the potential to disrupt the crosstalk between mitochondrial and nuclear proteins, and can therefore disrupt efficient gene transcription and translation (30), with consequences for metabolic rates (47), aging (48) and sperm competitiveness (49), which ultimately have detrimental effects on organismal fitness (50). Evidence for these detrimental effects is especially clear in hybrids between closely related species or between divergent populations within species, where long-term coevolution between the nuclear and mitochondrial genomes has been broken up, resulting in novel combinations of nuclear and mitochondrial genomes (51, 52). For example, hybrids of the marine copepod *Tigriopus* show reduced activity of OXPHOS Complex IV (cytochrome c oxidase) because of the breakup of coevolved nuclear and mitochondrial-encoded subunits of the Complex IV (51). This mismatch between nuclear and mitochondrial genes is thought to be a strong selection pressure for the fixation of compensatory mutations in nuclear-encoded OXPHOS subunits (53).

Mito-nuclear interactions can also have strong effects on the outcome of infection. In *Drosophila*, a mito-nuclear incompatibility resulted in energetically compromised flies that were more susceptible to infection by a bacterial pathogen (54). Salminen et al., identified an OXPHOS Complex III mutation $D_{21}N$ in *D. melanogaster* mitochondrial *CYTB* gene, that was shown to cause larval stage melanotic nodules in a healthy nuclear background (6%) and a significant increase (56%) of melanotic nodules when the mitotype was introgressed into a tko^{25t} nuclear background (55). Formation of melanotic nodules is considered a sign of activated cell mediated innate immunity, and it usually involves the proliferation and aggregation of hemocytes, *Drosophila* blood cells (56). Furthermore, *CYTB* mutation bearing mitotype in a tko^{25t} nuclear background caused 100% pupal lethality, which is a first report of synthetic lethality between nuclear-mitochondrial interaction within a metazoan species (55).

MITOCHONDRIAL VARIATION CAN AFFECT INFECTION OUTCOME

The role of mitochondria in the response to infection is central, impacting multiple functions. First, intermediates of the mitochondrial tricarboxylic acid (TCA) cycle have a signaling function in innate immune responses. Second, mitochondria generate energy by producing ATP during OXPHOS (**Box 2** and **Figure 1B**), and given the elevated energetic requirements of immunity, we may expect variation in mitochondrial functions to result in changes in ATP production, thereby generating heterogeneity in the response to infection. Third, mitochondrial metabolism may further promote protection against pathogens by producing ROS, with direct antimicrobial action. Finally, in mammalian models of immunity, damaged mtDNA has been shown to act as DAMP triggering inflammatory responses akin to those seen during infection. There is therefore increasing evidence that mitochondrial functions contribute to the host response to infection.

Mitochondrial TCA Cycle Metabolites With Immune Signaling Functions

Mitochondrial tricarboxylic acid cycle (TCA, also called Krebs cycle and citric acid cycle) consists of a series of reactions where substrates originating from carbohydrates, fats and proteins have been fed into it and the metabolites from the cycle are transported into cytosol as building blocks for macromolecules or energy is released through the oxidation of acetyl-CoA. However, metabolites in the TCA cycle have also been shown to be involved in regulation of chromatin modifications, DNA methylation and post-translational modifications of proteins [reviewed in (57)]. Intermediates and derivatives of the TCA cycle have been shown to have non-metabolic signaling functions, in addition to their more conventional role as metabolites associated with bioenergetics (58). Non-metabolic functions of

the TCA cycle intermediates succinate, itaconate, fumarate, 2-hydroxyglutarate and acetyl-CoA play a role in inflammation, and immune cell activation (58). For example, succinate is a pro-inflammatory metabolite as its production is enhanced during inflammation (59) and it acts as a signal from mitochondria to the cytosol to induce the expression of pro-inflammatory genes and increases the levels of antioxidant superoxide as a proinflammatory redox signal (60). Succinate has also been shown to accumulate in lipopolysaccharide treated macrophages (59). Itaconate on the other hand is endogenous protective and anti-inflammatory molecule that negatively regulates the inflammatory response and cytokine production (61–63) and also has direct antibacterial effects (64). TCA cycle intermediates have also been connected to epigenetic signaling (58). For example, fumarate has a role as an epigenetic inflammatory signal. Arts et al., showed that the accumulation of fumarate in immune activated monocytes was needed for trained immunity by enhancing cytokine production upon re-activation with lipopolysaccharide (65). Further, Acetyl-CoA has been shown to drive histone acetylation which can have profound impact on immune cell function (66). To summarize, mitochondrial variation may impact infection outcomes via their effect on TCA cycle products that have immune signaling functions.

Changes in ATP Production

Mitochondria generate energy by producing ATP during OXPHOS (**Box 2**), and given the elevated energetic requirements of immunity, we may expect variation in mitochondrial function to result in changes in ATP production, thereby generating heterogeneity in the response to infection (54). Mutations in any of the nuclear or mitochondrial encoded OXPHOS complexes or in nuclear genes affecting replication, transcription or translation of mtDNA can affect the total electron transfer chain outcome, potentially causing a decrease in the total production of ATP. Severely decreased ATP synthesis is an obvious problem for cells with constant high energy demands such as cardiomyocytes and neurons (67) and decreased ATP synthesis can also increase the AMP/ATP ratio that can lead to activation of AMP-activated protein kinase and multiple signaling pathways (46). We might therefore expect mutations in nuclear or mitochondrial encoded components that cause a reduction in ATP to result in a decrease of immune cell function.

Role of ROS in Immune Responses

Reactive oxygen species are a group of reactive molecules and free radicals derived from molecular oxygen which are now known to have a role in cellular homeostasis (68). Elevated levels of ROS can cause oxidative stress, cellular-, and DNA damage in eukaryotic cells. Mutations in nuclear or mitochondrial genes encoding the protein subunits of OXPHOS complexes I and III can cause a decrease or an increase in ROS production, depending on the mutation. One of the most evident roles of mitochondrial functions in innate immunity is the production of ROS by leakage from mitochondrial ETC. The majority of ROS are produced during mitochondrial ETC (mtROS), and some by oxidoreductase enzymes such as NADPH oxidase, a multicomponent membrane bound enzyme complex. Common ROS include superoxide (O^-_2), hydrogen peroxide (H_20_2), hydroxyl radical (OH), hydroxide ion (OH^-) and nitric oxide (NO). Prolonged oxidative stress is harmful and so detoxification of ROS via scavenging enzymes and antioxidants is vital. Therefore, mutations in the nuclear encoded antioxidants that are targeted to detoxify ROS, can also have an impact on immune response. Antioxidant superoxide dismutase (SOD) is transported to mitochondria where it converts superoxide to hydrogen peroxide. Hydrogen peroxide outside mitochondria is converted to water and oxygen with the help of catalase, peroxiredoxins and glutathione peroxidases (**Figure 1**).

mtROS is produced in all cell types that contain mitochondria and it has been connected to regulation of signaling pathways (69), apoptosis (70), inflammation (71), cellular adaptation to hypoxia (72), cellular differentiation (73), and autophagy (74). In addition to the regulative role of mtROS, a growing body of evidence has highlighted the role of ROS as a target of regulation of immune signaling pathways (14, 75). mtROS serves several roles within both the humoral and cell-mediated arms of innate immunity, including direct elimination of pathogens through its microbicidal effects. However, it is still unclear what is the exact mechanism of the bactericidal effect of mtROS upon bacterial infection as the effect seem to be the type of ROS and pathogen specific [reviewed in (68)] and aligns with the increased heterogeneity of the innate immune response.

Alongside its role in promoting bacterial clearance, mtROS also functions in signaling for hemocyte proliferation and differentiation in *Drosophila* and has been identified as an essential signaling molecule in *Drosophila's* cellular immune response to parasitoid infection (76). ROS plays a likely role as a key signaling molecule within the *Drosophila* lymph gland as it has been suggested to prime the quiescent hemocyte progenitors within the lymph gland for differentiation (77). It has been shown that reduction of ROS significantly retards progenitor differentiation whereas upregulation of ROS via OXPHOS Complex I disruption produces a phenotype with a significantly higher hemocyte population (77).

Transmitochondrial cell lines can be created by combining enucleated cells that contain the mtDNA of interest with cells that lack their mtDNA (78). Data obtained from transmitochondrial cell lines suggest that mtDNA variants on a controlled nuclear background can alter ROS levels of cells (79). Organismal cybrids have also been shown to differ in OXPHOS parameters (34) and effect of mtDNA variation on altered ROS production has been studied in *Drosophila in vivo*, showing that specific mtDNA variants can elevate ROS production (80).

Cytosolic mtDNA as a Danger Signal

During infection, elevated levels of ROS can cause mitochondrial and cellular damage resulting mtDNA leakage. Due to the evolutionary origin of mitochondria it harbors resemblance to bacterial DNA making it appear non-self. mtDNA is surrounded by a double-membrane structure and membrane damage could lead to leakage of mtDNA outside mitochondria and elicit self-derived immune activation. When mtDNA is located outside mitochondria in the cytoplasm of the cell or in extracellular space,

it can trigger immune responses by directly engaging the host's innate immune pattern-recognition receptors (PRRs) [reviewed in (81)]. PRRs are conserved receptors that recognize viral, bacterial and fungal particles as well as molecules released from injured cells. The release of mtDNA outside of mitochondria can occur from dying cells, during injury, cellular stress or infection, and mtDNA outside of mitochondria engages PRRs and functions as damage-associated molecular pattern (DAMP) leading to enhancement of pro-inflammatory responses (71). In mammalian models of immunity, inflammasomes are innate immune related signaling complexes that monitor the cytosolic compartment of the cell and are involved in the secretion of cytokines upon infection and recognition of DAMPs (81). Altered mitochondrial dynamics, production of mROS and release of mtDNA outside mitochondria have all been linked to inflammasome activation (82). In mammalian system extracellular circulatory mtDNA has been shown to act as an endogenous Toll-like receptor TLR9 agonist and been connected to many TLR9- dependent inflammatory diseases (81). Cytosolic mtDNA (83) as well as cytosolic double-stranded RNA created during bidirectional transcription of mtDNA (84) has been shown to trigger antiviral responses in human.

USING *DROSOPHILA* TO STUDY MITOCHONDRIAL VARIATION AND MITO-NUCLEAR INTERACTIONS IN IMMUNITY

Mitochondrial function and the content of the mitochondrial genome are highly conserved among metazoans e.g., between humans and the fruit fly *D. melanogaster* and the latter has been widely used to model human mitochondrial diseases [reviewed in (85)]. Besides studying the naturally occurring variation of nuclear genes affecting mitochondrial function, i.e., mtDNA replication, transcription and translation as well as polypeptides needed for TCA and OXPHOS, it is possible to exploit the highly sophisticated genetic toolbox that exists for *D. melanogaster*. With the binary gene expression systems, such as GAL4-UAS, one can modify the expression of a desired gene within a specific tissue within a specific time, providing a route to investigate the effect of specific genes in chosen tissues on a given phenotype (86). For example, overexpression and gene knock-down methods could allow the modification of the gene expression of nuclear encoded genes that are transported to mitochondria, hence altering the mitochondrial function, assuming that the mitochondrial import stage does not dampen the effect of genetic modification.

Another approach to study mitochondrial variation is to focus on naturally occurring variation in mtDNA. Investigating the effect of mtDNA mutations is complicated by cross-talk between the mitochondria and the nucleus of a cell, with nuclear genes generally responsible for controlling mitochondrial activity. With the cytoplasmic hybrid, aka. cybrid model, specific mtDNAs can be introgressed onto controlled nuclear backgrounds, making it possible to focus on the effects arising from the mitochondrial genome (**Figure 2**). It is presently not possible to genetically target and modify the gene expression of specific mtDNA genes, and so the cybrid model relies on using natural mtDNA variants found through different genetic screens. However, there are methods for creating random mutations to mtDNA genome such as using *POLG* mutants (87, 88) or to more specific regions with targeted restriction enzymes (89).

By generating transmitochondrial cybrid cells, it is possible to study the effects of mtDNA variation at the cellular level (78). This *in vitro* approach has been used previously to investigate the cellular effects of mtDNA polymorphism associated with an aggressive form of breast cancer (90). Similarly, Bellizzi et al., hypothesized that the transcription of stress-responder nuclear genes can be modulated according to the mtDNA variability. They showed that osteosarcoma cells depleted of their own mitochondria and repopulated with different ones, modulated the expression of cytokines and cytokine receptors due to the variability of the mtDNA (91).

The effects of mtDNA variation at the organismal level may vary significantly from what can be inferred from cellular level. The transmitochondrial *in vitro* method is limited in investigating the impact of mtDNA variation affecting an entire organism, for example upon environmental stress, limited diet or when fighting infection. However, *D. melanogaster* offers a feasible way of creating and utilizing cybrid strains for *in vivo* experiments of the effects of mtDNA variation at the organismal level (26, 30, 50), as well as quantifying the effects of mtDNA, nDNA and their interaction. Given the ease with which flies can be sampled from natural populations, options of screening the mtDNA variation by sequencing and crossing and breeding the lines in constant laboratory conditions, *Drosophila* cybrid lines offer a unique opportunity to disentangle variation in immunity arising from mtDNA polymorphism from the more commonly investigated variation in nuclear-encoded genes associated with canonical immune pathways.

There are three ways of creating cybrids and two of them, repeated backcrossing and using balancer chromosomes, are common methods in *Drosophila*, explained in detail below and in **Figure 2**. In the third method, Mitochondrial Replacement Therapy (MRT), mtDNA is introduced directly to a novel nuclear environment. In MRT the nucleus of a mtDNA mutation bearing female is transferred to an enucleated egg of a mitochondrially healthy donor (92). To date, MRT has been performed in two other mammalian species beside humans, in macaques (93) and mice (94, 95).

Generating *Drosophila* Cybrids by Repeated Backcrossing

Because mtDNA is inherited uniparentally through the mother, the chosen donor mtDNA can be introgressed onto wanted nuclear background by multiple generations of backcrossing (**Figure 2A**). In the first cross the virgin females containing the donor mtDNA are crossed with males containing the wanted nuclear background, resulting in progeny with 100% maternal mtDNA, 50% maternal nDNA and 50% paternal nDNA. This is followed by a series of crosses where the virgin females of each

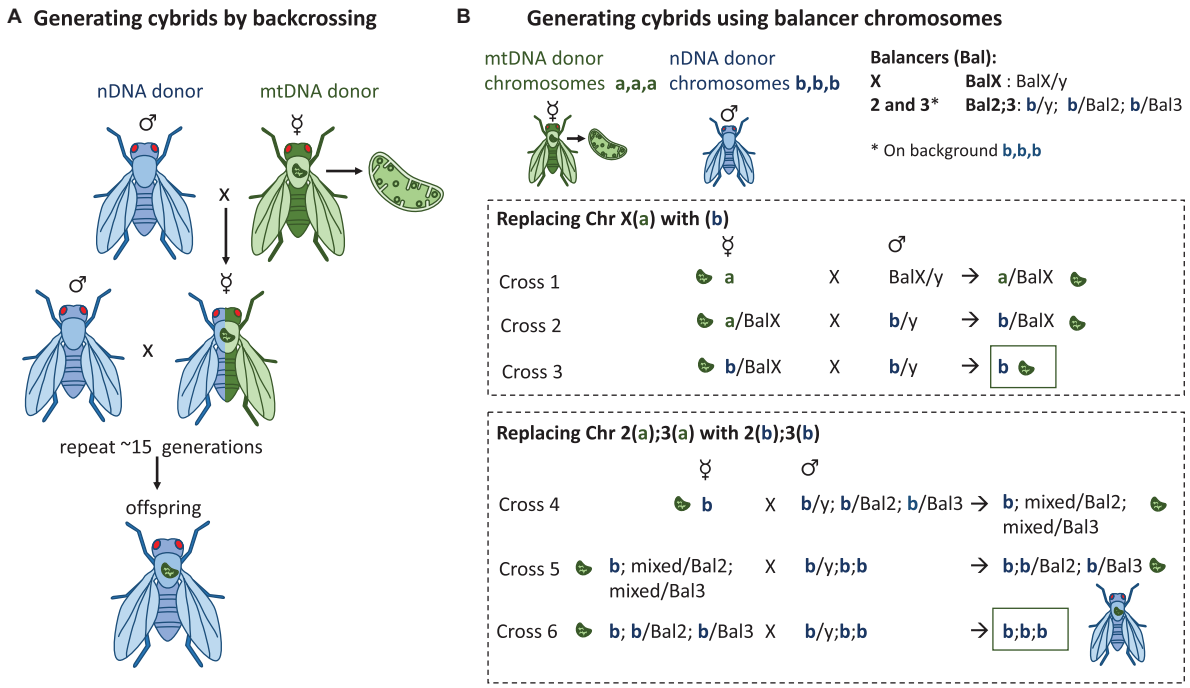

FIGURE 2 | Methods to generate *Drosophila in vivo* cybrid lines. **(A)** Repeated backcrossing. The chosen mtDNA variant is added during the first cross where the virgin females from the mtDNA donor strain are crossed with the males of the nuclear donor strain. Virgin females of the following progeny are crossed again with the males of the nuclear donor strain. This will be repeated for >15 generations, after which the cybrid progeny contain the wanted mtDNA variant on a nuclear background that in theory is the same as the one in the nuclear donor strain. This method also has the potential to reveal possible mito-nuclear epistasis during the course of the backcrossing. **(B)** Balancer chromosome method. *Drosophila* males do not go through recombination, whereas in females the recombination can be controlled with the balancer chromosomes which do not recombine with the normal chromosome homologs during meiotic prophase. The presence of balancer chromosomes in the progeny can be recognized by the dominant marker mutations that the balancers carry, e.g., mutations affecting eye shape, body color, or wing morphology. If the progeny do not have the balancer, it has the normal homolog of the wanted chromosome. Three (labeled here a,a,a or b,b,b) of the four *D. melanogaster* chromosomes can be replaced to contain the genetic content of the wanted nuclear donor strain by using the balancer chromosome method. The mtDNA from the maternal donor strain is introgressed to the strain during the first cross and the chromosome content is replaced chromosome at a time by using the correct progeny of the previous cross. For clarity, chromosomes 2 and 3 have not been marked to the cross where the X(a) is replaced with the X(b).

generation are crossed with males of the nuclear donor strain. With each cross, the proportion of paternal nDNA increases by 50% from the previous generation, meaning that in theory, after 10 generations of backcrossing, less than 0.1% of the maternal nDNA should be present. An important caveat to introgression by repeated backcrossing is that although in theory only 10 generations should be required to obtain a line over 99.9% of the paternal nuclear genome, in practice this value will be lower due to strong linkage disequilibrium between loci that have a close genetic distance (called linkage drag) (96). From a mapping perspective this linkage can be advantageous, but the backcrossing approach has the potential to select for compatible nuclear partners, masking true incompatibilities (also lethal combinations). The number of generations of backcrossing required to break linkage between two loci will therefore depend on the genetic distance such that the number of backcrosses $N = Log(1\text{-}r)(1\text{-}P)$ where r is the recombination frequency, and P is the probability of separation (97). For example, for two loci separated by a 20 cM interval, at least 17 generations of backcrossing are required to have a 95% certainty of a crossover event (97). However, even after multiple generations of backcrossing, some loci are likely to never recombine if they result in strongly deleterious or even lethal phenotypes, and such loci will remain a source of residual heterozygosity regardless of the number of generations of backcrossing.

This method has been used in *D. melanogaster* experiments to study the effect of mito-nuclear interactions on mtDNA copy number, respiration, development time and weight (40) as well as in experiments where the effect of mtDNA variants on mitochondrial diseases has been assayed in combination with the balancer chromosome method (55, 98). The method has been also employed in other insect species where the use of balancer chromosomes is not possible, where the effect of mito-nuclear crosstalk has been studied on traits such as metabolism and aging in *D. simulans* (99), metabolic rate in *Drosophila subobscura* (100), and personality (101), bioenergetics, aging, life history traits (102), and male mating costs (47) in seed beetles.

Utilizing *Drosophila* Balancer Chromosomes

Drosophila has four chromosomes that include the X/Y sex chromosome pair and autosomal chromosomes 2, 3, and 4.

The fourth chromosome is very small, contains only around 80 genes (103) and does not recombine. The genetic tool box developed for *D. melanogaster* allows the replacement of the entire chromosomes with the wanted content of specific strains or mutation. This is done with the help of balancer chromosomes. Balancer chromosomes (104) are multiply inverted and scrambled chromosomes that are not able to undergo crossover with their normal chromosome homologs. They also contain genetic markers that enable the recognition of their segregation. As the small chromosome *4* does not go through crossing over there are no balancers designed for this chromosome. Nuclear genomes can be constructed by replacing the chromosomes in multiple crosses in a properly planned crossing scheme, and eventually controlling the nuclear genome (**Figure 2B**). For creating *Drosophila* lines that contain the wanted mtDNA variant on a controlled nuclear background, the first cross includes the mtDNA donor females after which the wild-type chromosomes will be replaced one by one with the wanted isogenic chromosomes [crossing scheme explained e.g., in (30, 105, 106)]. This method has been utilized to study the effect of mtDNA variation and mito-nuclear interaction on aging (105), sex differences in aging, respiration and fertility (107, 108), starvation resistance, lipid proportion and physical activity (106) as well as ROS production and mtDNA copy number (109).

CONCLUSION AND FUTURE PERSPECTIVES

Drosophila has contributed significantly for our understanding of mitochondrial variation in both mitochondrial diseases and in immunity. Here we have highlighted strengths of this experimental powerhouse and described approaches that will link these two important fields to address the question how mitochondrial variation and specifically mtDNA variation affect innate immune functions. This is significant because a number of mitochondrial mutations have been associated with increased susceptibility to infection in humans (110, 111) and recent genetic screens have revealed vast variation in *Drosophila* mtDNA (112). The *Drosophila* model will also be relevant in the context of mitochondrial replacement therapy as a tool to test for potential incompatibilities that may result from specific mito-nuclear combinations (113). Given the homology between vertebrate and invertebrate innate immunity (114), the *Drosophila* model has the translational potential to generate novel candidate genes originating from mitochondrial sources of disease susceptibility and resistance, and for development of new therapeutic targets.

AUTHOR CONTRIBUTIONS

TS and PV wrote the manuscript.

FUNDING

TS was supported by an Academy of Finland Fellowship (grants 322732 and 32879). PV was supported by a Leverhulme Trust Research Project Grant RPG-2018-369, a Branco Weiss Fellowship (https://brancoweissfellowship.org/), and a Chancellor's Fellowship (School of Biological Sciences, University of Edinburgh).

REFERENCES

1. Lloyd-Smith JO, Schreiber SJ, Kopp PE, Getz WM. Superspreading and the effect of individual variation on disease emergence. *Nature*. (2005) 438:355–9. doi: 10.1038/nature04153
2. Brodin P, Davis MM. Human immune system variation. *Nat Rev Immunol*. (2017) 17:21–9. doi: 10.1038/nri.2016.125
3. Pawelec G. Age and immunity: what is "immunosenescence"? *Exp Gerontol*. (2018) 105:4–9. doi: 10.1016/j.exger.2017.10.024
4. Lotter H, Altfeld M. Sex differences in immunity. *Semin Immunopathol*. (2019) 41:133–5. doi: 10.1007/s00281-018-00728-x
5. Martin LB. Stress and immunity in wild vertebrates: timing is everything. *Gen Comp Endocrinol*. (2009) 163:70–6. doi: 10.1016/j.ygcen.2009.03.008
6. Lemaitre B, Hoffmann J. The host defense of *Drosophila melanogaster*. *Annu Rev Immunol*. (2007) 25:697–743. doi: 10.1146/annurev.immunol.25.022106.141615
7. Tao L, Reese TA. Making mouse models that reflect human immune responses. *Trends Immunol*. (2017) 38:181–93. doi: 10.1016/j.it.2016.12.007
8. Renshaw SA, Trede NS. A model 450 million years in the making: zebrafish and vertebrate immunity. *Dis Model Mech*. (2012) 5:38–47. doi: 10.1242/dmm.007138
9. Barreiro LB, Quintana-Murci L. From evolutionary genetics to human immunology: how selection shapes host defence genes. *Nat Rev Genet*. (2010) 11:17–30. doi: 10.1038/nrg2698
10. Timmann C, Thye T, Vens M, Evans J, May J, Ehmen C, et al. Genome-wide association study indicates two novel resistance loci for severe malaria. *Nature*. (2012) 489:443–6. doi: 10.1038/nature11334
11. McLaren PJ, Coulonges C, Bartha I, Lenz TL, Deutsch AJ, Bashirova A, et al. Polymorphisms of large effect explain the majority of the host genetic contribution to variation of HIV-1 virus load. *Proc Natl Acad Sci USA*. (2015) 112:14658–63. doi: 10.1073/pnas.1514867112
12. Tian C, Hromatka BS, Kiefer AK, Eriksson N, Noble SM, Tung JY, et al. Genome-wide association and HLA region fine-mapping studies identify susceptibility loci for multiple common infections. *Nat Commun*. (2017) 8:599. doi: 10.1038/s41467-017-00257-5
13. Arnoult D, Carneiro L, Tattoli I, Girardin SE. The role of mitochondria in cellular defense against microbial infection. *Semin Immunol*. (2009) 21:223–32. doi: 10.1016/j.smim.2009.05.009
14. West AP, Shadel GS, Ghosh S. Mitochondria in innate immune responses. *Nat Rev Immunol*. (2011) 11:389–402. doi: 10.1038/nri2975
15. Cloonan SM, Choi AM. Mitochondria: commanders of innate immunity and disease? *Curr Opin Immunol*. (2012) 24:32–40. doi: 10.1016/j.coi.2011.11.001
16. Weinberg SE, Sena LA, Chandel NS. Mitochondria in the regulation of innate and adaptive immunity. *Immunity*. (2015) 42:406–17. doi: 10.1016/j.immuni.2015.02.002
17. Fang C, Wei X, Wei Y. Mitochondrial DNA in the regulation of innate immune responses. *Protein Cell*. (2016) 7:11–6. doi: 10.1007/s13238-015-0222-9
18. Mills EL, Kelly B, O'Neill LAJ. Mitochondria are the powerhouses of immunity. *Nat Immunol*. (2017) 18:488–98. doi: 10.1038/ni.3704
19. Scheffler IE. *Mitochondria*. Hoboken, NJ: John Wiley & Sons. (2011).
20. Zeviani M, Spinazzola A, Carelli V. Nuclear genes in mitochondrial disorders. *Curr Opin Genet Dev*. (2003) 13:262–70. doi: 10.1016/S0959-437X(03)00052-2

21. Frazier AE, Thorburn DR, Compton AG. Mitochondrial energy generation disorders: genes, mechanisms, and clues to pathology. *J Biol Chem*. (2019) 294:5386–95. doi: 10.1074/jbc.R117.809194
22. El-Hattab AW, Craigen WJ, Scaglia F. Mitochondrial DNA maintenance defects. *Biochim Biophys Acta Mol Basis Dis*. (2017) 1863:1539–55. doi: 10.1016/j.bbadis.2017.02.017
23. Cohen BH, Chinnery PF, Copeland WC. POLG-related disorders. In: Adam MP, Ardinger HH, Pagon RA, Wallace SE, Bean LJ, Stephens K, et al. editors. *GeneReviews*. Seattle, WA: University of Washington. (2019).
24. Samstag CL, Hoekstra JG, Huang C-H, Chaisson MJ, Youle RJ, Kennedy SR, et al. Deleterious mitochondrial DNA point mutations are overrepresented in *Drosophila* expressing a proofreading-defective DNA polymerase γ. *PLoS Genet*. (2018) 14:e1007805. doi: 10.1371/journal.pgen.1007805
25. Rebelo AP, Dillon LM, Moraes CT. Mitochondrial DNA transcription regulation and nucleoid organization. *J Inherit Metab Dis*. (2011) 34:941–51. doi: 10.1007/s10545-011-9330-8
26. Mossman JA, Biancani LM, Zhu C, Rand DM. Mitonuclear epistasis for development time and its modification by diet in *Drosophila*. *Genetics*. (2016) 203:463–84. doi: 10.1534/genetics.116.187286
27. Jacobs HT, Turnbull DM. Nuclear genes and mitochondrial translation: a new class of genetic disease. *Trends Genet*. (2005) 21:312–4. doi: 10.1016/j.tig.2005.04.003
28. Sissler M, González-Serrano LE, Westhof E. Recent advances in mitochondrial aminoacyl-tRNA synthetases and disease. *Trends Mol Med*. (2017) 23:693–708. doi: 10.1016/j.molmed.2017.06.002
29. Konovalova S, Tyynismaa H. Mitochondrial aminoacyl-tRNA synthetases in human disease. *Mol Genet Metab*. (2013) 108:206–11. doi: 10.1016/j.ymgme.2013.01.010
30. Meiklejohn CD, Holmbeck MA, Siddiq MA, Abt DN, Rand DM, Montooth KL. An incompatibility between a mitochondrial tRNA and its nuclear-encoded tRNA synthetase compromises development and fitness in *Drosophila*. *PLoS Genet*. (2013) 9:e1003238. doi: 10.1371/journal.pgen.1003238
31. Toivonen JM, O'Dell KMC, Petit N, Irvine SC, Knight GK, Lehtonen M, et al. Technical knockout, a *Drosophila* model of mitochondrial deafness. *Genetics*. (2001) 159:241–54.
32. Kemppainen E, George J, Garipler G, Tuomela T, Kiviranta E, Soga T, et al. Mitochondrial dysfunction plus high-sugar diet provokes a metabolic crisis that inhibits growth. *PLoS One*. (2016) 11:e0145836. doi: 10.1371/journal.pone.0145836
33. Saada A, Shaag A, Arnon S, Dolfin T, Miller C, Fuchs-Telem D, et al. Antenatal mitochondrial disease caused by mitochondrial ribosomal protein (MRPS22) mutation. *J Med Genet*. (2007) 44:784–6. doi: 10.1136/jmg.2007.053116
34. Alston CL, Rocha MC, Lax NZ, Turnbull DM, Taylor RW. The genetics and pathology of mitochondrial disease. *J Pathol*. (2017) 241:236–50. doi: 10.1002/path.4809
35. Montooth KL, Rand DM. The spectrum of mitochondrial mutation differs across species. *PLoS Biol*. (2008) 6:e213. doi: 10.1371/journal.pbio.0060213
36. Nabholz B, Glémin S, Galtier N. Strong variations of mitochondrial mutation rate across mammals–the longevity hypothesis. *Mol Biol Evol*. (2008) 25:120–30. doi: 10.1093/molbev/msm248
37. Spelbrink JN. Functional organization of mammalian mitochondrial DNA in nucleoids: history, recent developments, and future challenges. *IUBMB Life*. (2010) 62:19–32. doi: 10.1002/iub.282
38. Lewis DL, Farr CL, Farquhar AL, Kaguni LS. Sequence, organization, and evolution of the A+T region of *Drosophila melanogaster* mitochondrial DNA. *Mol Biol Evol*. (1994) 11:523–38.
39. Falkenberg M. Mitochondrial DNA replication in mammalian cells: overview of the pathway. *Essays Biochem*. (2018) 62:287–96. doi: 10.1042/EBC20170100
40. Salminen TS, Oliveira MT, Cannino G, Lillsunde P, Jacobs HT, Kaguni LS. Mitochondrial genotype modulates mtDNA copy number and organismal phenotype in *Drosophila*. *Mitochondrion*. (2017) 34:75–83. doi: 10.1016/j.mito.2017.02.001
41. D'Erchia AM, Atlante A, Gadaleta G, Pavesi G, Chiara M, De Virgilio C, et al. Tissue-specific mtDNA abundance from exome data and its correlation with mitochondrial transcription, mass and respiratory activity. *Mitochondrion*. (2015) 20:13–21. doi: 10.1016/j.mito.2014.10.005
42. Giordano C, Iommarini L, Giordano L, Maresca A, Pisano A, Valentino ML, et al. Efficient mitochondrial biogenesis drives incomplete penetrance in Leber's hereditary optic neuropathy. *Brain J Neurol*. (2014) 137:335–53. doi: 10.1093/brain/awt343
43. Tuppen HAL, Blakely EL, Turnbull DM, Taylor RW. Mitochondrial DNA mutations and human disease. *Biochim Biophys Acta Bioenerg*. (2010) 1797:113–28. doi: 10.1016/j.bbabio.2009.09.005
44. Man PYW, Griffiths PG, Brown DT, Howell N, Turnbull DM, Chinnery PF. The epidemiology of leber hereditary optic neuropathy in the North East of England. *Am J Hum Genet*. (2003) 72:333–9. doi: 10.1086/346066
45. Prezant TR, Agapian JV, Bohlman MC, Bu X, Oztas S, Qiu W, et al. Mitochondrial ribosomal RNA mutation associated with both antibiotic-induced and non-syndromic deafness. *Nat Genet*. (1993) 4:289–94.
46. Quirós PM, Mottis A, Auwerx J. Mitonuclear communication in homeostasis and stress. *Nat Rev Mol Cell Biol*. (2016) 17:213–26. doi: 10.1038/nrm.2016.23
47. Immonen E, Rönn J, Watson C, Berger D, Arnqvist G. Complex mitonuclear interactions and metabolic costs of mating in male seed beetles. *J Evol Biol*. (2016) 29:360–70. doi: 10.1111/jeb.12789
48. Immonen E, Collet M, Goenaga J, Arnqvist G. Direct and indirect genetic effects of sex-specific mitonuclear epistasis on reproductive ageing. *Heredity*. (2016) 116:338–47. doi: 10.1038/hdy.2015.112
49. Dowling DK, Friberg U, Arnqvist G. A comparison of nuclear and cytoplasmic genetic effects on sperm competitiveness and female remating in a seed beetle. *J Evol Biol*. (2007) 20:2113–25. doi: 10.1111/j.1420-9101.2007.01433.x
50. Montooth KL, Meiklejohn CD, Abt DN, Rand DM. Mitochondrial–nuclear epistasis affects fitness within species but does not contribute to fixed incompatibilities between species of *Drosophila*. *Evolution*. (2010) 64:3364–79. doi: 10.1111/j.1558-5646.2010.01077.x
51. Ellison CK, Burton RS. Disruption of mitochondrial function in interpopulation hybrids of *Tigriopus californicus*. *Evolution*. (2006) 60:1382–91. doi: 10.1111/j.0014-3820.2006.tb01217.x
52. Lee-Yaw JA, Jacobs CGC, Irwin DE. Individual performance in relation to cytonuclear discordance in a northern contact zone between long-toed salamander (*Ambystoma macrodactylum*) lineages. *Mol Ecol*. (2014) 23:4590–602. doi: 10.1111/mec.12878
53. Osada N, Akashi H. Mitochondrial-nuclear interactions and accelerated compensatory evolution: evidence from the primate cytochrome C oxidase complex. *Mol Biol Evol*. (2012) 29:337–46. doi: 10.1093/molbev/msr211
54. Buchanan JL, Meiklejohn CD, Montooth KL. Mitochondrial dysfunction and infection generate immunity–fecundity tradeoffs in *Drosophila*. *Integr Comp Biol*. (2018) 58:591–603. doi: 10.1093/icb/icy078
55. Salminen TS, Cannino G, Oliveira MT, Lillsunde P, Jacobs HT, Kaguni LS. Lethal interaction of nuclear and mitochondrial genotypes in *Drosophila melanogaster*. *G3 (Bethesda)*. (2019) 9:2225–34. doi: 10.1534/g3.119.400315
56. Minakhina S, Steward R. Melanotic mutants in *Drosophila*: pathways and phenotypes. *Genetics*. (2006) 174:253–63. doi: 10.1534/genetics.106.061978
57. Martínez-Reyes I, Chandel NS. Mitochondrial TCA cycle metabolites control physiology and disease. *Nat Commun*. (2020) 11:102. doi: 10.1038/s41467-019-13668-3
58. Ryan DG, Murphy MP, Frezza C, Prag HA, Chouchani ET, O'Neill LA, et al. Coupling Krebs cycle metabolites to signalling in immunity and cancer. *Nat Metab*. (2019) 1:16–33. doi: 10.1038/s42255-018-0014-7
59. Tannahill GM, Curtis AM, Adamik J, Palsson-Mcdermott EM, McGettrick AF, Goel G, et al. Succinate is an inflammatory signal that induces IL-1β through HIF-1α. *Nature*. (2013) 496:238–42. doi: 10.1038/nature11986
60. Mills EL, Kelly B, Logan A, Costa ASH, Varma M, Bryant CE, et al. Succinate dehydrogenase supports metabolic repurposing of mitochondria to drive inflammatory macrophages. *Cell*. (2016) 167:457–70.e13. doi: 10.1016/j.cell.2016.08.064
61. Lampropoulou V, Sergushichev A, Bambouskova M, Nair S, Vincent EE, Loginicheva E, et al. Itaconate links inhibition of succinate dehydrogenase with macrophage metabolic remodeling and regulation of inflammation. *Cell Metab*. (2016) 24:158–66. doi: 10.1016/j.cmet.2016.06.004

62. Bambouskova M, Gorvel L, Lampropoulou V, Sergushichev A, Loginicheva E, Johnson K, et al. Electrophilic properties of itaconate and derivatives regulate the IκBζ-ATF3 inflammatory axis. *Nature*. (2018) 556:501–4. doi: 10.1038/s41586-018-0052-z
63. Mills EL, Ryan DG, Prag HA, Dikovskaya D, Menon D, Zaslona Z, et al. Itaconate is an anti-inflammatory metabolite that activates Nrf2 via alkylation of KEAP1. *Nature*. (2018) 556:113–7. doi: 10.1038/nature25986
64. McFadden BA, Purohit S. Itaconate, an isocitrate lyase directed inhibitor in *Pseudomonas indigofera*. *J Bacteriol*. (1977) 131:136–44.
65. Arts RJW, Novakovic B, ter Horst R, Carvalho A, Bekkering S, Lachmandas E, et al. Glutaminolysis and fumarate accumulation integrate immunometabolic and epigenetic programs in trained immunity. *Cell Metab*. (2016) 24:807–19. doi: 10.1016/j.cmet.2016.10.008
66. Kurdistani SK, Grunstein M. Histone acetylation and deacetylation in yeast. *Nat Rev Mol Cell Biol*. (2003) 4:276–84. doi: 10.1038/nrm1075
67. Smeitink JA, Zeviani M, Turnbull DM, Jacobs HT. Mitochondrial medicine: a metabolic perspective on the pathology of oxidative phosphorylation disorders. *Cell Metab*. (2006) 3:9–13. doi: 10.1016/j.cmet.2005.12.001
68. Dan Dunn J, Alvarez LA, Zhang X, Soldati T. Reactive oxygen species and mitochondria: a nexus of cellular homeostasis. *Redox Biol*. (2015) 6:472–85. doi: 10.1016/j.redox.2015.09.005
69. Shadel GS, Horvath TL. Mitochondrial ROS signaling in organismal homeostasis. *Cell*. (2015) 163:560–9. doi: 10.1016/j.cell.2015.10.001
70. Bender T, Martinou JC. Where killers meet-permeabilization of the outer mitochondrial membrane during apoptosis. *Cold Spring Harb Perspect Biol*. (2013) 5:a011106. doi: 10.1101/cshperspect.a011106
71. Blaser H, Dostert C, Mak TW, Brenner D. TNF and ROS crosstalk in inflammation. *Trends Cell Biol*. (2016) 26:249–61. doi: 10.1016/j.tcb.2015.12.002
72. Guzy RD, Schumacker PT. Oxygen sensing by mitochondria at complex III: the paradox of increased reactive oxygen species during hypoxia. *Exp Physiol*. (2006) 91:807–19. doi: 10.1113/expphysiol.2006.033506
73. Mandal S, Lindgren AG, Srivastava AS, Clark AT, Banerjee U. Mitochondrial function controls proliferation and early differentiation potential of embryonic stem cells. *Stem Cells*. (2011) 29:486–95. doi: 10.1002/stem.590
74. Chen Y, Azad MB, Gibson SB. Superoxide is the major reactive oxygen species regulating autophagy. *Cell Death Differ*. (2009) 16:1040–52. doi: 10.1038/cdd.2009.49
75. Bulua AC, Simon A, Maddipati R, Pelletier M, Park H, Kim KY, et al. Mitochondrial reactive oxygen species promote production of proinflammatory cytokines and are elevated in TNFR1-associated periodic syndrome (TRAPS). *J Exp Med*. (2011) 208:519–33. doi: 10.1084/jem.20102049
76. Meister M, Ferrandon D. Immune cell transdifferentiation: a complex crosstalk between circulating immune cells and the haematopoietic niche. *EMBO Rep*. (2012) 13:3–4. doi: 10.1038/embor.2011.238
77. Owusu-Ansah E, Banerjee U. Reactive oxygen species prime *Drosophila* haematopoietic progenitors for differentiation. *Nature*. (2009) 461:537–41. doi: 10.1038/nature08313
78. Vithayathil SA, Ma Y, Kaipparettu BA. Transmitochondrial cybrids: tools for functional studies of mutant mitochondria. *Methods Mol Biol*. (2012) 837:219–30. doi: 10.1007/978-1-61779-504-6_15
79. Ishikawa K, Takenaga K, Akimoto M, Koshikawa N, Yamaguchi A, Imanishi H, et al. ROS-generating mitochondrial DNA mutations can regulate tumor cell metastasis. *Science*. (2008) 320:661–4. doi: 10.1126/science.1156906
80. Matoo OB, Julick CR, Montooth KL. Genetic variation for ontogenetic shifts in metabolism underlies physiological homeostasis in *Drosophila*. *Genetics*. (2019) 212:537–52. doi: 10.1534/genetics.119.302052
81. West AP, Shadel GS. Mitochondrial DNA in innate immune responses and inflammatory pathology. *Nat Rev Immunol*. (2017) 17:363–75. doi: 10.1038/nri.2017.21
82. Elliott EI, Sutterwala FS. Initiation and perpetuation of NLRP3 inflammasome activation and assembly. *Immunol Rev*. (2015) 265:35–52. doi: 10.1111/imr.12286
83. West AP, Khoury-Hanold W, Staron M, Tal MC, Pineda CM, Lang SM, et al. Mitochondrial DNA stress primes the antiviral innate immune response. *Nature*. (2015) 520:553–7. doi: 10.1038/nature14156
84. Dhir A, Dhir S, Borowski LS, Jimenez L, Teitell M, Rötig A, et al. Mitochondrial double-stranded RNA triggers antiviral signalling in humans. *Nature*. (2018) 560:238–42. doi: 10.1038/s41586-018-0363-0
85. Sánchez-Martínez A, Luo N, Clemente P, Adán C, Hernández-Sierra R, Ochoa P, et al. Modeling human mitochondrial diseases in flies. *Biochim Biophys Acta*. (2006) 1757:1190–8. doi: 10.1016/j.bbabio.2006.05.008
86. Caygill EE, Brand AH. The GAL4 system: a versatile system for the manipulation and analysis of gene expression. *Methods Mol Biol*. (2016) 1478:33–52. doi: 10.1007/978-1-4939-6371-3_2
87. Spelbrink JN, Toivonen JM, Hakkaart GAJ, Kurkela JM, Cooper HM, Lehtinen SK, et al. *In Vivo* functional analysis of the human mitochondrial DNA polymerase POLG expressed in cultured human cells. *J Biol Chem*. (2000) 275:24818–28. doi: 10.1074/jbc.M000559200
88. Ahlqvist KJ, Hämäläinen RH, Yatsuga S, Uutela M, Terzioglu M, Götz A, et al. Somatic progenitor cell vulnerability to mitochondrial DNA mutagenesis underlies progeroid phenotypes in polg mutator mice. *Cell Metab*. (2012) 15:100–9. doi: 10.1016/j.cmet.2011.11.012
89. Xu H, DeLuca SZ, O'Farrell PH. Manipulating the metazoan mitochondrial genome with targeted restriction enzymes. *Science*. (2008) 321:575–7. doi: 10.1126/science.1160226
90. Kulawiec M, Owens KM, Singh KK. MtDNA G10398A variant in African-American women with breast cancer provides resistance to apoptosis and promotes metastasis in mice. *J Hum Genet*. (2009) 54:647–54. doi: 10.1038/jhg.2009.89
91. Bellizzi D, Cavalcante P, Taverna D, Rose G, Passarino G, Salvioli S, et al. Gene expression of cytokines and cytokine receptors is modulated by the common variability of the mitochondrial DNA in cybrid cell lines. *Genes Cells*. (2006) 11:883–91. doi: 10.1111/j.1365-2443.2006.00986.x
92. Wolf DP, Mitalipov N, Mitalipov S. Mitochondrial replacement therapy in reproductive medicine. *Trends Mol Med*. (2015) 21:68–76. doi: 10.1016/j.molmed.2014.12.001
93. Tachibana M, Sparman M, Sritanaudomchai H, Ma H, Clepper L, Woodward J, et al. Mitochondrial gene replacement in primate offspring and embryonic stem cells. *Nature*. (2009) 461:367–72. doi: 10.1038/nature08368
94. Sato A, Kono T, Nakada K, Ishikawa K, Inoue SI, Yonekawa H, et al. Gene therapy for progeny of mito-mice carrying pathogenic mtDNA by nuclear transplantation. *Proc Natl Acad Sci USA*. (2005) 102:16765–70. doi: 10.1073/pnas.0506197102
95. Wang T, Sha H, Ji D, Zhang HL, Chen D, Cao Y, et al. Polar body genome transfer for preventing the transmission of inherited mitochondrial diseases. *Cell*. (2014) 157:1591–604. doi: 10.1016/j.cell.2014.04.042
96. Peng T, Sun X, Mumm RH. Optimized breeding strategies for multiple trait integration: I. Minimizing linkage drag in single event introgression. *Mol Breed*. (2014) 33:89–104. doi: 10.1007/s11032-013-9936-7
97. Kooke R, Wijnker E, Keurentjes JJB. Backcross populations and near isogenic lines. *Methods Mol Biol*. (2012) 871:3–16. doi: 10.1007/978-1-61779-785-9_1
98. Chen S, Oliveira MT, Sanz A, Kemppainen E, Fukuoh A, Schlicht B, et al. A cytoplasmic suppressor of a nuclear mutation affecting mitochondrial functions in *Drosophila*. *Genetics*. (2012) 192:483–93. doi: 10.1534/genetics.112.143719
99. Ballard JWO. *Drosophila simulans* as a novel model for studying mitochondrial metabolism and aging. *Exp Gerontol*. (2005) 40:763–73. doi: 10.1016/j.exger.2005.07.014
100. Kurbalija Novičić Z, Immonen E, Jelić M, AnĐelković M, Stamenković-Radak M, Arnqvist G. Within-population genetic effects of mtDNA on metabolic rate in *Drosophila subobscura*. *J Evol Biol*. (2015) 28:338–46. doi: 10.1111/jeb.12565
101. Løvlie H, Immonen E, Gustavsson E, Kazancioğlu E, Arnqvist G. The influence of mitonuclear genetic variation on personality in seed beetles. *Proc R Soc Lond B Biol Sci*. (2014) 281:20141039. doi: 10.1098/rspb.2014.1039
102. Đorđević M, Stojković B, Savković U, Immonen E, Tucić N, Lazarević J, et al. Sex-specific mitonuclear epistasis and the evolution of mitochondrial bioenergetics, ageing, and life history in seed beetles. *Evolution*. (2017) 71:274–88. doi: 10.1111/evo.13109
103. Riddle NC, Elgin SCR. The *Drosophila* dot chromosome: where genes flourish amidst repeats. *Genetics*. (2018) 210:757–72. doi: 10.1534/genetics.118.301146

104. Muller HJ. Genetic variability, twin hybrids and constant hybrids, in a case of balanced lethal factors. *Genetics*. (1918) 3:422–99.
105. Clancy DJ. Variation in mitochondrial genotype has substantial lifespan effects which may be modulated by nuclear background. *Aging Cell*. (2008) 7:795–804. doi: 10.1111/j.1474-9726.2008.00428.x
106. Aw WC, Correa CC, Clancy DJ, Ballard JWO. Mitochondrial DNA variants in *Drosophila melanogaster* are expressed at the level of the organismal phenotype. *Mitochondrion*. (2011) 11:756–63. doi: 10.1016/j.mito.2011.06.012
107. Camus MF, Wolf JBW, Morrow EH, Dowling DK. Single nucleotides in the mtDNA sequence modify mitochondrial molecular function and are associated with sex-specific effects on fertility and aging. *Curr Biol*. (2015) 25:2717–22. doi: 10.1016/j.cub.2015.09.012
108. Wolff JN, Pichaud N, Camus MF, Côté G, Blier PU, Dowling DK. Evolutionary implications of mitochondrial genetic variation: mitochondrial genetic effects on OXPHOS respiration and mitochondrial quantity change with age and sex in fruit flies. *J Evol Biol*. (2016) 29:736–47. doi: 10.1111/jeb.12822
109. Correa CC, Aw WC, Melvin RG, Pichaud N, Ballard JWO. Mitochondrial DNA variants influence mitochondrial bioenergetics in *Drosophila melanogaster*. *Mitochondrion*. (2012) 12:459–64. doi: 10.1016/j.mito.2012.06.005
110. Angajala A, Lim S, Phillips JB, Kim J-H, Yates C, You Z, et al. Diverse roles of mitochondria in immune responses: novel insights into immunometabolism. *Front Immunol*. (2018) 9:1605. doi: 10.3389/fimmu.2018.01605
111. Kapnick SM, Pacheco SE, McGuire PJ. The emerging role of immune dysfunction in mitochondrial diseases as a paradigm for understanding immunometabolism. *Metabolism*. (2018) 81:97–112. doi: 10.1016/j.metabol.2017.11.010
112. Bevers RPJ, Litovchenko M, Kapopoulou A, Braman VS, Robinson MR, Auwerx J, et al. Mitochondrial haplotypes affect metabolic phenotypes in the *Drosophila* genetic reference panel. *Nat Metab*. (2019) 1:1226–42. doi: 10.1038/s42255-019-0147-3
113. Eyre-Walker A. Mitochondrial replacement therapy: are mito-nuclear interactions likely to be a problem? *Genetics*. (2017) 205:1365–72. doi: 10.1534/genetics.116.196436
114. Buchon N, Silverman N, Cherry S. Immunity in *Drosophila melanogaster*–from microbial recognition to whole-organism physiology. *Nat Rev Immunol*. (2014) 14:796–810. doi: 10.1038/nri3763
115. Rosetto M, Engström Y, Baldari CT, Telford JL, Hultmark D. Signals from the IL-1 receptor homolog, Toll, can activate an immune response in a *Drosophila* hemocyte cell line. *Biochem Biophys Res Commun*. (1995) 209:111–6. doi: 10.1006/bbrc.1995.1477
116. Tanji T, Hu X, Weber ANR, Ip YT. Toll and IMD pathways synergistically activate an innate immune response in *Drosophila melanogaster*. *Mol Cell Biol*. (2007) 27:4578–88. doi: 10.1128/MCB.01814-06
117. Valanne S, Wang J-H, Ramet M. The *Drosophila* Toll signaling pathway. *J Immunol*. (2011) 186:649–56. doi: 10.4049/jimmunol.1002302
118. Myllymaki H, Valanne S, Ramet M. The *Drosophila* Imd signaling pathway. *J Immunol*. (2014) 192:3455–62. doi: 10.4049/jimmunol.1303309
119. Hanson MA, Dostálová A, Ceroni C, Poidevin M, Kondo S, Lemaitre B. Synergy and remarkable specificity of antimicrobial peptides in vivo using a systematic knockout approach. *eLife*. (2019) 8:e44341. doi: 10.7554/eLife.44341
120. Dostert C, Jouanguy E, Irving P, Troxler L, Galiana-Arnoux D, Hetru C, et al. The Jak-STAT signaling pathway is required but not sufficient for the antiviral response of *Drosophila*. *Nat Immunol*. (2005) 6:946–53. doi: 10.1038/ni1237
121. Zambon RA, Vakharia VN, Wu LP. RNAi is an antiviral immune response against a dsRNA virus in *Drosophila melanogaster*. *Cell Microbiol*. (2006) 8:880–9. doi: 10.1111/j.1462-5822.2006.00688.x
122. Obbard DJ, Gordon KHJ, Buck AH, Jiggins FM. The evolution of RNAi as a defence against viruses and transposable elements. *Philos Trans R Soc Lond B Biol Sci*. (2009) 364:99–115. doi: 10.1098/rstb.2008.0168
123. Parsons B, Foley E. Cellular immune defenses of *Drosophila melanogaster*. *Dev Comp Immunol*. (2016) 58:95–101. doi: 10.1016/j.dci.2015.12.019
124. Anderl I, Vesala L, Ihalainen TO, Vanha-aho L-M, Andó I, Rämet M, et al. Transdifferentiation and proliferation in two distinct hemocyte lineages in *Drosophila melanogaster* larvae after wasp infection. *PLoS Pathog*. (2016) 12:e1005746. doi: 10.1371/journal.ppat.1005746
125. Nappi AJ, Vass E. Cytotoxic reactions associated with insect immunity. *Adv Exp Med Biol*. (2001) 484:329–48.
126. Poole AM, Gribaldo S. Eukaryotic origins: how and when was the mitochondrion acquired? *Cold Spring Harb Perspect Biol*. (2014) 6:a015990. doi: 10.1101/cshperspect.a015990

Conflict of Interest: The authors declare that the research was conducted in the absence of any commercial or financial relationships that could be construed as a potential conflict of interest.

frontiers in Immunology

ORIGINAL RESEARCH
published: 27 March 2020
doi: 10.3389/fimmu.2020.00520

Molecular and Functional Analysis of Pore-Forming Toxin Monalysin From Entomopathogenic Bacterium *Pseudomonas entomophila*

Saori Nonaka[1†], Emil Salim[1,2†], Koki Kamiya[3,4*], Aki Hori[1], Firzan Nainu[1,5], Rangga Meidianto Asri[1,5], Ayu Masyita[1,5], Takumi Nishiuchi[6], Shoji Takeuchi[3,7], Noriyuki Kodera[8*] and Takayuki Kuraishi[1*]

[1] Faculty of Pharmacy, Institute of Medical, Pharmaceutical and Health Sciences, Kanazawa University, Kanazawa, Japan, [2] Faculty of Pharmacy, Universitas Sumatera Utara, Medan, Indonesia, [3] Kanagawa Institute of Industrial Science and Technology, Kawasaki, Japan, [4] Graduate School of Science and Technology, Gunma University, Maebashi, Japan, [5] Faculty of Pharmacy, Universitas Hasanuddin, Makassar, Indonesia, [6] Institute for Gene Research, Kanazawa University, Kanazawa, Japan, [7] Department of Mechano-Informatics, Graduate School of Information Science and Technology, The University of Tokyo, Tokyo, Japan, [8] WPI Nano Life Science Institute, Kanazawa University, Kanazawa, Japan

OPEN ACCESS

Edited by:
Laura Vesala,
Tampere University, Finland

Reviewed by:
Rebecca M. McQuade,
University of Arizona, United States
Kwang-Zin Lee,
Fraunhofer Society (FHG), Germany

***Correspondence:**
Koki Kamiya
kamiya@gunma-u.ac.jp
Noriyuki Kodera
nkodera@staff.kanazawa-u.ac.jp
Takayuki Kuraishi
tkuraishi@staff.kanazawa-u.ac.jp

[†] These authors share first authorship

Specialty section:
This article was submitted to Comparative Immunology, a section of the journal Frontiers in Immunology

Received: 29 November 2019
Accepted: 06 March 2020
Published: 27 March 2020

Citation:
Nonaka S, Salim E, Kamiya K, Hori A, Nainu F, Asri RM, Masyita A, Nishiuchi T, Takeuchi S, Kodera N and Kuraishi T (2020) Molecular and Functional Analysis of Pore-Forming Toxin Monalysin From Entomopathogenic Bacterium Pseudomonas entomophila. Front. Immunol. 11:520. doi: 10.3389/fimmu.2020.00520

Pseudomonas entomophila is a highly pathogenic bacterium that infects insects. It is also used as a suitable model pathogen to analyze *Drosophila's* innate immunity. *P. entomophila's* virulence is largely derived from Monalysin, a β-barrel pore-forming toxin that damages *Drosophila* tissues, inducing necrotic cell death. Here we report the first and efficient purification of endogenous Monalysin and its characterization. Monalysin is successfully purified as a pro-form, and trypsin treatment results in a cleaved mature form of purified Monalysin which kills *Drosophila* cell lines and adult flies. Electrophysiological measurement of Monalysin in a lipid membrane with an on-chip device confirms that Monalysin forms a pore, in a cleavage-dependent manner. This analysis also provides a pore-size estimate of Monalysin using current amplitude for a single pore and suggests lipid preferences for the insertion. Atomic Force Microscope (AFM) analysis displays its structure in a solution and shows that active-Monalysin is stable and composed of an 8-mer complex; this observation is consistent with mass spectrometry data. AFM analysis also shows the 8-mer structure of active-Monalysin in a lipid bilayer, and real-time imaging demonstrates the moment at which Monalysin is inserted into the lipid membrane. These results collectively suggest that endogenous Monalysin is indeed a pore-forming toxin composed of a rigid structure before pore formation in the lipid membrane. The endogenous Monalysin characterized in this study could be a desirable tool for analyzing host defense mechanisms against entomopathogenic bacteria producing damage-inducing toxins.

Keywords: innate immunity, *Drosophila*, pore-forming toxin, atomic force microscope, Monalysin

INTRODUCTION

The innate immune system is the front line of defense against microbial infection in metazoan animals (1). Innate immune cells can sense infectious threats either by pathogen-associated molecular patterns (PAMPs) or damage-associated molecular patterns (DAMPs) (1–3): pathogen-specific molecules such as peptidoglycans utilized by microbes as an essential substance of their life (1), or host-derived molecules that are normally kept inside in their cells but released because of the tissue damage by infection (2), respectively. The recognition and signaling mechanisms involving PAMPs are relatively well-studied. In *Drosophila*, humoral innate immunity relies on distinct signaling pathways, the Toll pathway and immune deficiency (IMD) pathway (4, 5). The Toll pathway is responsible for infectious threats from fungi or Gram-positive bacteria, and it senses fungal β-glucans or bacterial Lysine (Lys)-type peptidoglycans with a pattern recognition receptor PGRP-SA/GNBP1 complex or GNBP3 in the hemolymph (6–9). PAMPs recognition by those receptors stimulates serine protease cascades in the hemolymph, which produces a cleaved form of the cytokine-like protein Spätzle (Spz), a ligand of a Toll receptor (10). An activated Toll receptor transmits a signal to NF-κB Dif and/or Dorsal through a dMyd88-Tube-Pelle complex, producing antimicrobial factors such as the antifungal peptide Drosomycin (11, 12). The IMD pathway is another NF-κB pathway that recognizes Diaminopimelic acid (DAP)-type peptidoglycans released from Gram-negative bacteria (13), eventually triggering the translocation of Relish to the nucleus and inducing the expression of genes that encode antimicrobial proteins, including Diptericin (14). In contrast to a PAMPs-initiated innate immunity, DAMPs-mediated innate immune mechanisms in terms of an infectious situation have not been well-characterized yet. In flies, protease cascade upstream of a Toll receptor is partly involved in DAMPs recognition. For example, fungal proteases could potentiate the serine protease cascade through Persephone (15–17). Additionally, entomopathogenic nematodes damage epithelial cells and/or cuticles and degrade basement membrane (BM). Clotting and components from disrupted BM seem to have a protective function against nematode infection (18, 19). However, the whole picture of damage-induced innate immunity is far from understood.

Pseudomonas entomophila is an entomopathogenic, Gram-negative bacterium that was originally isolated from a wild fly sampled in Guadeloupe in the Caribbean (20). *P. entomophila* displays pathogenicity by oral infection, and the bacteria are widely used as a tool to examine gut innate immune responses (20). Recently, *P. entomophila* has also been used in a systemic infection model (21). In the gut, *P. entomophila* infection imposes severe damage via a reactive oxygen species, produced by host cells and a pore-forming toxin (PFT) from the bacteria, generally inhibiting translation in the intestine and thus blocking epithelium renewal (22). The virulence of *P. entomophila* is under the control of a GacS/GacA two component system (20). One of the main effector molecules in this system is a PFT, Monalysin. Monalysin is secreted as a pro-toxin that is cleaved by proteases, such as AprA in *P. entomophila,* to become fully active (23). *Drosophila* adults combat these effectors using a cross-linked drosocrystallin (dcy) protein, which works as physical barrier blocking the permeation of macromolecules (>500 kDa) in the peritrophic matrix (24, 25). Cleaved Monalysin shows cytotoxic activity, probably by forming pores in the plasma membrane of host cells, leading to disrupted membrane permeability and cell death (23). The secondary structure prediction of the membrane-spanning domain indicates that Monalysin is a PFT of the β type (23). Leone et al. reported that X-ray crystallography and cryo-electron microscopy, with recombinant Monalysin produced in *E. coli,* revealed its 3D structure and its putative mechanism during pore formation in the lipid membrane (26). The recombinant Monalysin is an 18-mer complex composed of two disk-shaped nonamers held together by the N-terminal swapping of the pro-peptides. The membrane-spanning region of pro-Monalysin is fully buried in the center of the ring or torus, and, perhaps during activation upon cleavage, the two disk-shaped nonamers dissociate to leave the transmembrane segments that attach to the target membrane, undergo conformational changes, and form the pore.

In order to study the interaction between the host and entomopathogenic bacteria producing damage-inducing toxins, well-characterized purified Monalysin may be a useful tool. Besides, pore-forming proteins such as Monalysin may potentially be developed as biological control agents against insects (e.g., Cry toxin) (27–29), as well as biological "nanopores" that are used as a detector for single-molecule (e.g., α-hemolysin) (30). In that sense, endogenous Monalysin purified from *P. entomophila* could provide more precise insight of its protein function, rather than using the recombinant protein generated by *E. coli* that may have distinct intracellular environment from *P. entomophila,* which potentially gives rise to a different subunit composition of the protein and thereby could influence the structural and functional features of the molecule. Additionally, a detailed analysis of the structure of the native pore-forming protein and its dynamics in solution and in lipid membrane would serve basic information for various applications. In this study, we succeeded in purifying native endogenous Monalysin from *P. entomophila* with killing activity in *Drosophila* cell line and adult flies. We also characterized its structure and function using electrophysiological measurements and a high-speed atomic force microscope (HS-AFM).

MATERIALS AND METHODS

Bacteria Stocks, Other Materials, and Cell Culture

P. entomophila wild-type strain L48 and a Monalysin mutant *mnl* were kindly provided by Dr. B. Lemaitre. 1,2-Dioleoyl-*sn*-glycero-3-phosphocholine (DOPC), 1,2-dioleoyl-*sn*-glycero-3-phospho-L-serine (DOPS), 1,2-dioleoyl-*sn*-glycero-3-phosphoethanolamine (DOPE), and 1,2-dioleoyl-*sn*-glycero-3-phosphoethanolamine-*N*-(cap-biotinyl) (biotin-cap-DOPE) were purchased from Avanti Polar Lipids. n-decane was purchased from Sigma-Aldrich. S2 cells from *Drosophila* hemocytes were maintained at 25°C in

Schneider's *Drosophila* medium (Thermo Fisher SCIENTIFIC) containing 10% (v/v) heat-inactivated FBS, 100 units/mL penicillin, and 100 μg/mL streptomycin.

Purification of Pro-Monalysin

P. entomophila was grown in LB at 29°C overnight, and was collected by centrifugation at 8,700 × g at 4°C for 15 min. The cell pellets were washed with PBS and lysed in PBS containing 2% (w/v) CHAPS. Cells were sonicated at 4°C overnight, filtrated with a 70 μm Cell Strainer (BD Falcon), and centrifuged at 9,000 × g at 4°C for 20 min to remove insoluble pellets. The collected supernatant was diluted 10 times with PBS, filtrated with a 0.22 μm filter (Corning), and dialyzed with PBS for 9 h to exchange the solvent. Total lysate (*P. entomophila* extracts) was performed by ammonium sulfate precipitation (25–50%). The pellet was dissolved in 20 mM Tris-HCl, pH8.0 and dialyzed against the same buffer for 9 h to remove salts. The dialysate was then subjected to anion exchange chromatography with a HiTrap Q HP column (GE Healthcare), pre-equilibrated in 20 mM Tris-HCl, pH8.0 and then eluted with a linear gradient 0 to 1 M NaCl dissolved in 20 mM Tris-HCl, pH8.0 at a flow rate of 1 mL/min for 30 min. After a cell viability assay, the fractions with cytotoxic activity were harvested and concentrated by ammonium precipitation (50%). The pellet was dissolved in 10 mM sodium phosphate buffer, pH 7.4, containing 140 mM NaCl, and then subjected to gel filtration chromatography with a Superdex 200 Increase 10/300 GL column (GE Healthcare), pre-equilibrated in a 10 mM Sodium phosphate buffer, pH 7.4, containing 140 mM NaCl, and then eluted with the same buffer at a flow rate of 0.75 mL/min. The peak eluted at 13–14 min (molecular weight: around 460 kDa) was collected and analyzed by SDS-PAGE. The gel was stained with Coomassie Brilliant Blue (Kanto Chemical Co., Inc.) to check the purity. The 30 kDa band was excised and analyzed by mass spectrometry. The molecular weight of each peak in gel filtration chromatography was estimated by loading Gel filtration Calibration Kit HMW (GE Healthcare) in the same column. Protein concentrations of fractions were measured by a Lowry method with Bio-Rad DC protein assay kit (Bio-Rad). In the trypsin treatment to get active-Monalysin, trypsin was added to purified pro-Monalysin (175 μg) at 0.2 mg/mL and incubated at 25°C for 10 min, followed by a Protease Inhibitor Cocktail for General Use (nacalai tesque, Cat# 04080-11) was added. To completely degrade Monalysin, trypsin was added to pro-Monalysin (10 μg) at a concentration of 0.2 mg/mL and incubated at 37°C for 58 h.

Mass Spectrometry

To identify the protein in the cytotoxic fraction, MALDI-TOF MS/MS analysis was performed at the Institute for Gene Research, Advanced Science Research Center, Kanazawa University, using a tandem mass spectrometer (4,800 plus MALDI TOF/TOF™ Analyzer [Sciex]) with 2,5-dihydroxybenzoic acid (DHB) as a matrix as described in Asano and Nishiuchi (31). Briefly, a cytotoxic fraction was loaded on an SDS-acrylamide gel, and a 30 kDa band was excised and in-gel digested with trypsin. The digested peptides were analyzed by MALDI-TOF/TOF. The data was subjected to the Protein Pilot ver.4.0 (Sciex) against the *Pseudomonas entomophila* (NCBI, Tax ID 312306) protein database (2017-8-23). To determine the molecular weight of the active-Monalysin multimer, MALDI-TOF analysis was performed using the UltrafleXtreme MALDI TOF/TOF Analyzer (Bruker Daltonix) at Fukui Prefectural University with sinapic acid (SA) as a matrix. First, areas on the MALDI plates were coated with the SA solution. Then, the mixture of active-Monalysin with SA was dropped onto the SA-coated spots. Each spot was analyzed to obtain the molecular weight by MALDI-TOF (ultrafleXtreme). The results from several measurements were integrated via analysis software version 4.1.2.

Cell Viability Assay

S2 cells (1.5–8.0 × 10^5 cell in 100 μL) were inoculated in a 96-well plate. 10 μL of *P. entomophila* extract or collected fractions after chromatography, purified pro-Monalysin (1.5 μg/mL), active-Monalysin (1.5 μg/mL), or trypsin (3.8 × 10^{-2} μg/mL) were added and incubated at 25°C for 12–18 h. Cell viability was monitored by luminescence from a CellTiter-Glo Luminescent Cell Viability Assay (Promega) with a Spark 10 M (TECAN). Cell viability is expressed as a relative value, with luminescence in cells incubated with the buffer (negative control) being 100%. To measure total activity, cell viability, after incubation with serial diluted fractions, was examined and total activity was calculated as 1 unit corresponding to activity that yields 70% cell viability. Specific activity was expressed as total activity divided by total protein (mg).

Caspase-3/7 Activity Assay

S2 cells (1.5 × 10^5 cell in 100 μL) were inoculated onto a 96-well plate. Cycloheximide and active-Monalysin were added at 1.5 μg/mL and incubated at 25°C for 6, 12, 18, and 24 h. Caspase-3/7 activity was monitored by luminescence from a Caspase-Glo 3/7 Assay (Promega) using a Synergy HTX (BioTek).

Monalysin Injection and Survival Assay

Oregon R flies (*Drosophila melanogaster*, females, 3–7 days after eclosion) were injected with a pro-Monalysin, active-Monalysin, or degraded-Monalysin solution (1 mg/mL) into their hemolymph by micro-injection (70 nL per fly), and kept at 25°C. Surviving flies were counted at 1 h after injection. For dose-dependent analysis, flies were injected with active-Monalysin solution (3–30 μg/mL), and surviving flies were monitored every 12 h for 60 h.

Total RNA Extraction and Real-Time PCR

Oregon R flies (*Drosophila melanogaster*, female, 3–7 days after eclosion) were injected with an active-Monalysin, degraded-Monalysin solution (50 μg/mL), or 1,000 times dilution of heat-killed *E. coli* into their hemolymph and kept at 25°C for 3, 6, 20 h. To obtain the heat-killed *E. coli*, overnight culture of *E. coli* (DH5α) without dilution were heated at 100°C for 30 min, sonicated for 10 min, and then diluted with water. To quantify the *Drosomycin* (*Drs*), total RNA of the collected flies was isolated with Sepasol-RNA I Super G (nacalai tesque) and used for cDNA synthesis with ReverTra Ace reverse transcriptase (TOYOBO) and oligo (dT)12–18 primers. To quantify the *Diptericin* (*Dpt*),

puckered (*puc*), and *Turandot A* (*TotA*), isolated RNA were subjected to DNase treatment (Promega, M6101), followed by cDNA synthesis with ReverTra Ace reverse transcriptase (TOYOBO) and oligo (dT)12–18 primers. Quantitative real-time PCR (RT-qPCR) was performed using a LightCycler 480 (Roche Diagnostics). *rpL32* was used as an internal control. The following primers were used for RT-qPCR: *Drs* forward, TTGTT CGCCCTCTTCGCTGTCCT; *Drs* reverse, GCATCCTTCGCAC CAGCACTTCA; *Dpt* forward, GTTCACCATTGCCGTCGCC TTAC; *Dpt* reverse, CCCAAGTGCTGTCCATATCCTCC; *puc* forward, GGCCTACAAGCTGGTGAAAG; *puc* reverse, AGTTCAGATTGGGCGAGATG; *TotA* forward, CCAAAATGAATTCTTCAACTGCT; *TotA* reverse, GAATAGCCCATGCATAGAGGAC; *rpL32* forward, AGA TCGTGAAGAAGCGCACCAAG; *rpL32* reverse, CACCAG GAACTTCTTGAATCCGG.

Immunohistochemistry

For oral ingestion of Monalysin, dcy^1 flies (Bloomington #26106, females, 3–7 days after eclosion) obtained from the Bloomington *Drosophila* Stock Center were starved for 2 h at 29°C, then placed in a fly vial with the food solution. The food solution consisted in a mixture of active-Monalysin solution (4 mg/mL) and 5 % sucrose (1:1), which was added to a filter disk that completely covered the surface of the standard fly medium. Flies were kept at 29°C for 8 h, after which their guts were dissected out. Antibody staining was performed as previously described by Kenmoku et al. (32) with 1:200 rabbit anti-PH3 (Cell Signaling, Cat #9701), 1:50 mouse anti-Dlg (Developmental Studies Hybridoma Bank), and 1:200 Alexa 555-coupled and Alexa 488-coupled secondary antibodies (Thermo Fisher SCIENTIFIC). Nuclei were stained by 0.1 μg/mL of 4',6-diamidino-2-phenylindole (DAPI). Samples were visualized with a LSM710 confocal microscope (Carl Zeiss) or observed using a conventional fluorescent microscope and images were reconstructed using Photoshop (Adobe).

SLP Assay for Purified Monalysin

To examine the contamination level of peptidoglycan, 10 μL of 0.001–1 mg/mL pro-Monalysin, active-Monalysin and degraded Monalyin were incubated with 40 μL of Silkworm Larvae Plasma (SLP) reagent (Wako) at 25°C for 30 min in a 96-well plate. The SLP reagent contains all factors involved in the prophenoloxidase cascade system triggered by peptidoglycans, which consequently activates prophenoloxidase. The activated prophenoloxidase then oxidizes 3,4-dihydroxyphenylalanine (DOPA) in the substrate, thus forming a black melanin pigment. The amount of peptidoglycan was monitored as the blackness of the mixture visually. As a positive control, several dilution (1/10, $1/10^2$, $1/10^3$, $1/10^4$) of heat-killed *E. coli* solution were subjected to the same test.

Ion Current Measurement of Monalysin Using a Bilayer Lipid Membrane (BLM) Chip With 16 Separate Channels

One microliter of pro-Monalysin solution (1.5 mg/mL) was added to 0.1 μL of trypsin (0.25 % [w/v]). The mixture was incubated for 10 min at room temperature (∼23°C). To form a planar BLM, using the droplet contact method; 3.7 μl of lipid dissolved in *n*-decane (20 mg/mL dioleoylphosphatidylcholine [DOPC] or dioleoylphosphatidylcholine, dioleoylphosphatidylserine, and dioleoylphatidylethanolamine [DOPC/DOPS/DOPE] [molar ratio of 7:2:1]) was added to each double well on a BLM chip with 16 separate channels (16-ch). Twenty one microliter of buffer solution (20 mM Tris-HCl/ 150 mM NaCl [pH 8.8]) containing 0.015 mg/mL of Monalysin solution was added to each double well. The planar BLM was formed at the macroapertures. The Monalysin's current signals were recorded using a multichannel patch clamp amplifier with a 1-kHz low-pass filter at a sampling frequency of 5 kHz (Tecella JET). The measurement temperature was 23 ± 1°C. Current analysis was performed using the pCLAMP software program (molecular devices).

Atomic Force Microscopy

AFM imaging was performed in a solution at room temperature (24–26°C), using a laboratory-built high-speed AFM setup (33) as described in Uchihashi et al. (34). For AFM substrates, two types were used: the flat muscovite mica substrate and the polydimethylsiloxane (PDMS) substrate with controlled convex shapes (ca. 50 nm) (35). Either a mica disc (1.5 mm in diameter and ∼0.05 mm in thickness) or a PDMS disk (2 mm in diameter and ∼0.02 mm in thickness) was glued on a glass sample stage (2 mm in diameter and height) by epoxy. A freshly cleaved mica surface was prepared by removing the top layers of mica using Scotch tape. The PDMS surface was hydrophilized by a plasma ion bomber (PIB-10, Vacuum Device) set to hard mode for 3 min. The glass stage with either substrate was attached to the top of a Z-scanner by a drop of nail polish, on which a drop (2 μL) of sample solution (either 0.1 mg/mL Monalysin or 0.1 mg/mL liposome) was deposited. The liposome solution was prepared as previously described (34), and the lipid composition was DOPC:DOPS:biotin-cap-DOPE = 7:2:1 (w/w). After incubation for 3–5 min, the substrate surface was rinsed with 20 μL of the observation buffer to remove floating samples. The sample stage was then immersed in a liquid cell containing ∼60 μL of the observation buffer. AFM imaging was carried out in tapping mode, using small cantilevers (BLAC10DS-A2, Olympus), with a resonant frequency of ∼0.5 MHz in water, a quality factor of ∼1.3 in water, and a spring constant of ∼0.08 N/m. The cantilever's free oscillation amplitude A_0 and set-point amplitude A_s were set at 1–2 nm and $\sim 0.9 \times A_0$, respectively. In some experiments, high tapping forces were applied to the samples by reducing A_s, and a protein solution containing either Monalysin or trypsin (5 μL) was injected in the observation buffer during high-speed atomic force microscopy (HS-AFM) imaging. The imaging rate, scan size, and the pixel size for each AFM image are described in figure legends.

Analysis of AFM Images

AFM images were pretreated for analysis by a low-pass filter to remove spike noise and a flatten filter to make the overall xy-plane flat, using a laboratory built software as described in Ngo et al. (36). The molecule heights were measured semi-automatically using the following steps. First, the most probable

highest point near the highest point of the molecule was selected manually. Second, the actual highest point was determined automatically by searching a 10 × 10-pixel area (typically 10 × 10 nm^2) around the selected point. The surface area occupied by the specific molecular species was analyzed by ImageJ using binarized images. The binarized images were obtained by setting a threshold height. The threshold heights were 8 nm for the double-ring complex of pro-Monalysin and 4 nm for the single-ring complex of pro- and active-Monalysin, respectively.

Statistical Analysis

Statistical analyses were performed by a Student's *t*-test or log-rank test, and $P < 0.05$ were considered significant.

RESULTS

Purification of Endogenous Monalysin Protein From *P. entomophila*

In our previous study, we demonstrated that an extract from *P. entomophila*, prepared by sonication of the bacterial cells with detergent, followed by membrane-filtration, is fatal to adult flies if ingested (24). To examine whether *P. entomophila* extract acts as source for the purification of endogenous Monalysin, we tested whether *P. entomophila* extract had Monalysin-derived cytotoxic activity. *P. entomophila* extract was simply added to the *Drosophila* embryonic hemocyte-derived S2 cell culture, and we found that, after 12 h of incubation, almost all cells lost their normal morphology and fell apart (**Figure 1A**). A CellTiter-Glo Luminescent Cell Viability Assay, which measures cellular ATP, indicated that the S2 cells were dying (**Figure 1B**).

Next, we performed the cytotoxic assay, using an extract from a Monalysin-deficient strain of *P. entomophila* to know whether *P. entomophila* extract-induced cell death depends on Monalysin. We found that an extract from a Monalysin-deficient strain showed less cytotoxicity than that of a wild type (**Figures 1A,B**). This indicates that a *P. entomophila* extract contains Monalysin toxin, and that endogenous Monalysin could be purified using the extract. Furthermore, we expected that this cytotoxic assay could be used to find fractions containing Monalysin in each purification step. We attempted its purification in this way (**Figure 1C**, **Table 1**). First, a *P. entomophila* extract or total lysate were precipitated with ammonium sulfate to reduce the extract volume. The precipitate was suspended with a Tris buffer, subjected to a column for anion exchange chromatography, and eluted by a linear gradient of 0 to 1 M NaCl. The active fraction (Fraction III) was subjected to an ammonium sulfate precipitation again and suspended with a phosphate buffer (Fraction IV). Fraction IV was subjected to a column for gel filtration chromatography, and several sub-fractions were collected. A CellTiter-Glo Luminescent Cell Viability Assay showed that only sub-fraction 1 contained cytotoxic activity (**Figure 1E**). The recovered activity of this final fraction (Fraction V in **Table 1** and **Figure 1C**, sub-fraction 1 in **Figures 1D,E**) was 6% that of the starting total lysate of *P. entomophila*. The specific activity increased 14-fold (**Table 1**). The chromatogram of the final fraction (Fraction V in **Table 1** and **Figure 1C**, sub-fraction 1 in **Figures 1D,E**) showed a sharp single peak around 460 kDa and gave a single band with a molecular mass of 30 kDa on an SDS-PAGE (**Figure 1F**), which is the estimated size of the pro-form of Monalysin monomer. Mass spectrometric analysis of the single band resulted in specific amino acid sequences of Monalysin (data not shown). From these results, we concluded that Monalysin, as a pro-form, was purified as a homogeneity from the wild type *P. entomophila*. Note that the molecular mass estimated by gel filtration (460 kDa), that of the multimer of Monalysin, was slightly smaller than the estimate found in previous literature (26).

Pro-Monalysin is considered to undergo proteolytic cleavage by AprA, a protease secreted by *P. entomophila*, in order to be fully activated as a toxin (23). Leone et al. showed that trypsin cleavage of recombinant pro-Monalysin recapitulated the proteolysis by AprA (26). Thus, we performed trypsin cleavage on our purified endogenous Monalysin to see whether it transforms from a pro-form to an active-form. SDS-PAGE analysis showed that 30 kDa of pro-Monalysin monomer was cleaved to 27 kDa of monomer, as previously reported (**Figure 2A**). Hereafter, we refer to trypsin-treated endogenous pro-Monalysin as active-Monalysin since the cleaved form exhibited much higher cytotoxic activity than the pro-form (**Figure 2B**). Note that the trypsin in active-Monalysin did not show cytotoxic activity (**Supplementary Figure 1**). A lethal concentration of 50% (LC_{50}) of pro- and active-Monalysin was estimated from **Figure 2B** as 1.4 and 3.1 μg/mL, respectively (**Figure 2C**), which suggested that pro-Monalysin is also toxic to S2 cells. We interpreted this to mean that pro-Monalysin has cytotoxic activity without trypsin treatment because it can undergo proteolysis with some proteases of S2 cells in a cultured medium or on the cell surface, since the pore formation efficiency of pro-Monalysin in artificial membranes is much lower than active-Monalysin (**Figure 3B**). This cell death induced by active-Monalysin appears to be necrotic rather than apoptotic, as the cells did not show caspase-3/7 activation, while cells treated with cycloheximide (reported to induce typical apoptosis in S2 cells) showed significant induction of the caspase-3/7 activity [(37); **Figure 2D**]. These results are consistent with cell death induced by Monalysin produced in *E. coli* described in Opota et al. (23).

To confirm whether purified Monalysin had toxic activity *in vivo*, we injected Monalysin into adult hemolymphs. **Figure 2E** shows that active-Monalysin killed adult flies more efficiently than pro-Monalysin and degraded-Monalysin that is digested by trypsin for a long time to be fully decayed (**Supplementary Figure 2**), and the insecticidal effect of active-Monalysin has a dose-dependent effect (**Figure 2F**). Furthermore, the analysis of *dcy* mutant guts fed with active-Monalysin revealed that the number of mitotic stem cells using phospho-histone H3 (PH3) staining (38)—an indicator of gut repair after damage—increased after ingestion of active-Monalysin (**Supplementary Figure 3A**). In addition, an immunostaining of the septate junction marker Discs large (Dlg) (39) and nuclear staining in flies after oral injection of active-Monalysin showed disrupted organization of the epithelial cells (**Supplementary Figure 3B**), implying that Monalysin could damage the flies' intestines. Collectively, these results suggest that purified Monalysin has toxic activity *in vivo*.

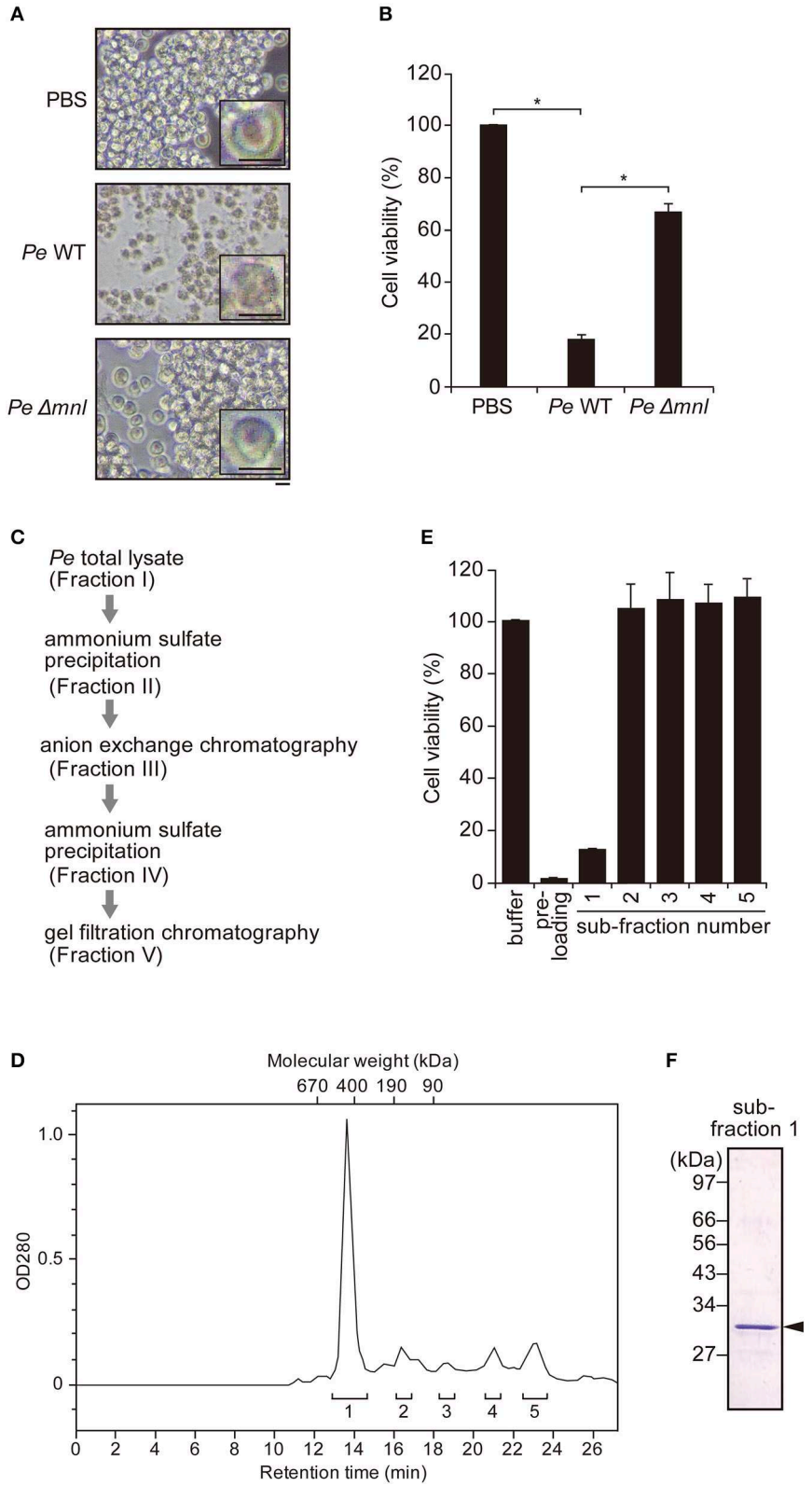

FIGURE 1 | Purification of endogenous pro-Monalysin from *P. entomophila.* **(A)** Phase contrast images of S2 cells after incubation with PBS, wild type (*Pe* WT) or Monalysin-deficient strain (*Pe* Δ*mnl*) of *P. entomophila* extracts (15 μg protein/8 × 10^5 cells in 100 μL) for 12 h. Magnification images are shown in the square on the right side. Scale bar; 20 μm. The space around the S2 cells after incubation with *Pe* WT extracts appears whiter than others, due to cell debris. **(B)** S2 cells were

(Continued)

FIGURE 1 | incubated with *Pe* WT or *Pe* Δ*mnl* total lysates (15 μg protein/8 × 10^5 cells in 100 μL) for 12 h. Cell viability was monitored as luminescence by a CellTiter-Glo Luminescent Cell Viability Assay. Cell viability is shown relative to luminescence in cells that were incubated with PBS, taken as 100%. The means ± S.E. obtained with the data from triplicate samples, are presented (*$P < 0.05$, as determined by a Student's *t*-test). **(C)** The purification step of endogenous pro-Monalysin. A HiTrap Q HP column and a Superdex 200 Increased 10/30 L GL column were used in anion exchange chromatography and gel filtration chromatography, respectively. **(D)** Chromatogram of gel filtration chromatography. Eluted proteins were detected by measuring OD_{280}. The retention time was the time passed after loading the sample into the column. The molecular weight of each retention time was estimated by loading Gel filtration Calibration Kit HMW (GE Healthcare) in the same column. The estimated molecular mass was around 460 kDa for the first eluted peak. Pre-loading indicates a fraction before loading to column for gel filtration chromatography (that is, it is the same Fraction IV in **Table 1**). Brackets and numbers were collected fractions and sub-fraction numbers, respectively. **(E)** S2 cells were incubated with each fraction obtained from gel filtration chromatography for 12 h. Cell viability was monitored as luminescence by a CellTiter-Glo Luminescent Cell Viability Assay. Cell viability is shown relative to luminescence in cells incubated with an elution buffer, taken as 100%. The means ± S.E. obtained with the data from triplicate samples, are presented. **(F)** SDS-PAGE analysis of fraction 1. The gel was stained with Coomassie Brilliant Blue. The arrowhead indicates a pro-Monalysin monomer (30 kDa). The numbers on the left side indicate molecular weight.

TABLE 1 | Purification of pro-Monalysin.

Fraction		Total protein (mg)	Total activity[a] (units)	Specific activity[b] (units/mg protein)	Purification (fold)	Yield (%)
I	Total lysate	3.5	3.1×10^3	8.7×10^2	1.0	100
II	25–50% $(NH4)_2SO_4$ ppt[c]	2.6	1.7×10^3	6.8×10^2	0.78	57
III	Anion exchange HPLC	2.3×10^{-1}	1.6×10^3	7.0×10^3	8.0	52
IV	0–50% $(NH4)_2SO_4$ ppt	6.0×10^{-2}	4.7×10^2	8.4×10^3	9.7	16
V	Gel filtration HPLC	2.0×10^{-2}	1.8×10^2	1.2×10^4	14	6

[a] *Total activity was calculated as 1 unit corresponding to activity that yields 70% cell viability.*
[b] *Specific activity indicates total activity divided by total protein.*
[c] *ppt: precipitate.*

We also examined whether Monalysin injections could induce antimicrobial peptides (AMP) and stress gene expressions in adult flies, as tissue damage could induce infection-independent humoral innate immunity. Real-time quantitative PCR (RT-qPCR) analysis suggested that the expression of *Drosomycin* (*Drs*) and *Turandot A* (*TotA*), a read-out of the activation of the JAK-STAT pathway, was significantly induced by the injection of active-Monalysin (**Supplementary Figures 4A,D**). This suggests that Monalysin activates the innate immune and stress pathways, possibly through the Toll and/or JAK-STAT pathways. Monalysin injection, however, did not induce *Diptericin* (*Dpt*) and *puckered* (*puc*) gene expression, a read-out of the activation of the IMD pathway and Jun-N-terminal kinase (JNK) pathway (**Supplementary Figures 4B,C**). *P. entomophila* is a Gram-negative bacterium which does not contain the Lys-type peptidoglycan recognized by the Toll pathway. In addition, degraded-Monalysin did not induce *Drs* and *TotA* expression (**Supplementary Figures 4A,D**) and a peptidoglycan-contamination test using Silkworm Larvae Plasma (SLP). Reagent did not show significant contamination of peptidoglycans, which normally activate innate immunity, in active-Monalysin (**Supplementary Figures 4E,F**). These results might exclude the possibility that contamination of some PAMPs activates humoral immunity and imply that tissue damage induced by Monalysin might induce a humoral innate immune response and stress response in adult *Drosophila*. Taken together, these results show we succeeded to purify endogenous Monalysin, which has a toxic and damage-inducing activity in *Drosophila*.

Electrophysiological Characterization of Monalysin as a Pore-Forming Toxin

We next sought to confirm that endogenous Monalysin indeed functions as a PFT and characterize its mode-of-action by functional analysis. To monitor pore formation on the lipid membrane, we adopted an "on-chip lipid bilayer system," which was composed of a parallel ion current recording device with 16 separate channels (16-ch) of artificial planar BLM wells, where the bilayers in the wells were formed based on the droplet contact method (**Figure 3A**) (40). First, we observed the formation of Monalysin nanopores onto lipid bilayers via the electrophysiological analysis of an artificial cell membrane. We obtained stepwise signals specific to nanopore-containing proteins in the solution containing the active-Monalysin (**Figure 3B**, left). A total of 723 stepwise signals for active-Monalysin on the DOPC lipid bilayer were observed for 30 min using a 16-ch device ($N = 2$). On the other hand, in case of the pro-Monalysin, 35 stepwise signals were observed for 30 min using a 16-ch device ($N = 2$) (**Figure 3B**, right). These results suggest that the trypsin-treated active-Monalysins were more vigorously reconstituted into the lipid bilayer and formed nanopores within it.

Next, we investigated the appearance of the active-Monalysin on lipid bilayers composed of DOPC and DOPC/DOPS/DOPE (mol ratio of 7:2:1). The formation of the Monalysin nanopores in the lipid bilayers was more occurrent on the DOPC lipid bilayer (723 stepwise signals) than the DOPC/DOPS/DOPE lipid bilayer (349 stepwise signals) (**Figure 3C**). We found two amplitude peaks for the active-Monalysin-specific stepwise

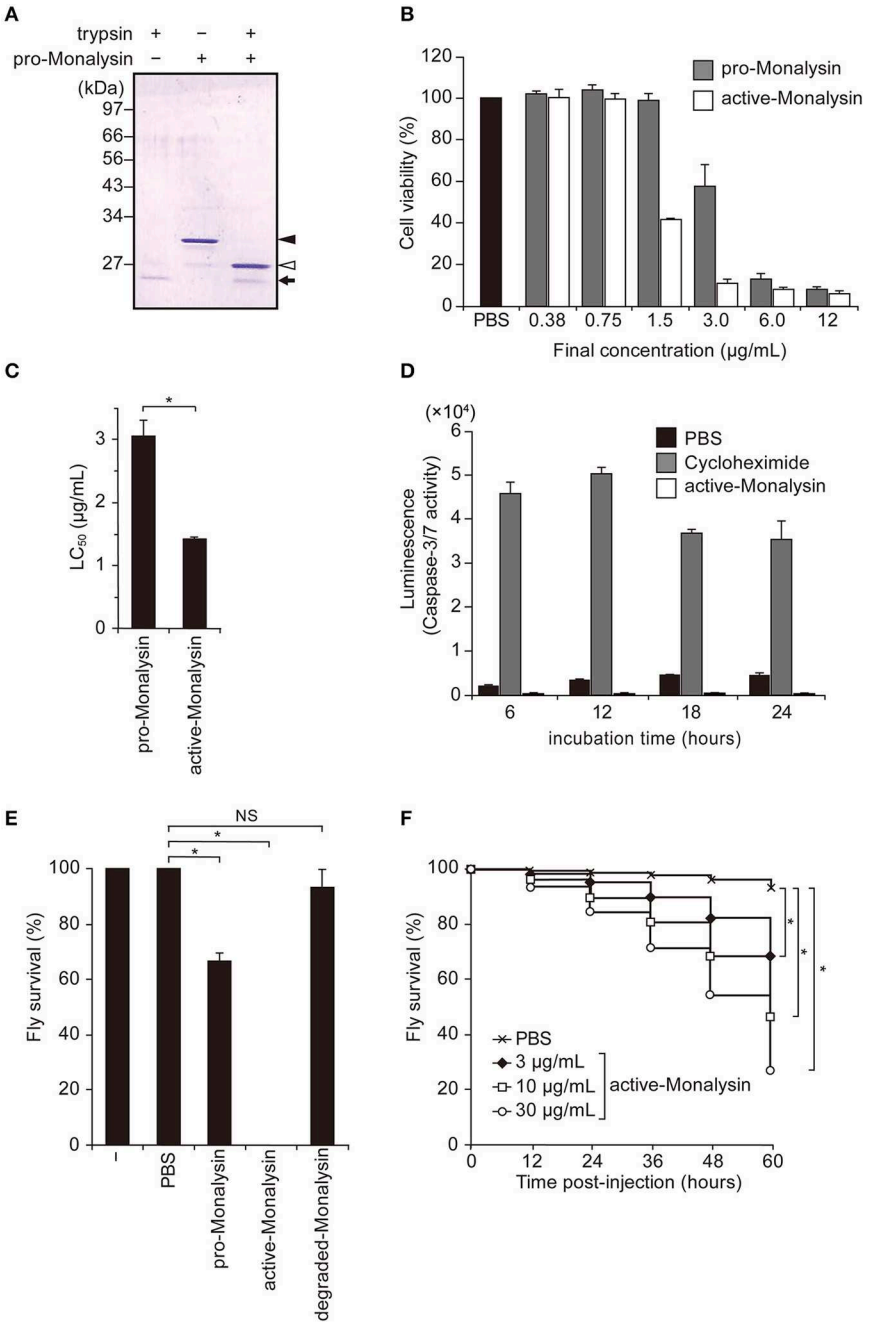

FIGURE 2 | Trypsin treatment transforms purified pro-Monalysin into its active-form. **(A)** A SDS-PAGE analysis of purified pro-Monalysin before and after trypsin treatment. The gel was stained with Coomassie Brilliant Blue. Trypsin was incubated with purified pro-Monalysin at 0.2 mg/mL for 10 min. Closed and open arrowheads indicate a pro-Monalysin monomer (30 kDa) and an active-Monalysin monomer (27 kDa), respectively. The arrow indicates trypsin. **(B)** Cell viability after incubation with pro-Monalysin and active-Monalysin. S2 cells (1.5×10^5 cells in 100 μL) were incubated with the indicated concentration of pro-Monalysin or active-Monalysin for 18 h, cell viability was measured via a CellTiter-Glo Luminescent Cell Viability Assay. Cell viability is shown, relative to luminescence in cells incubated with PBS, taken as 100%. **(C)** LC_{50} of pro-Monalysin and active-Monalysin. LC_{50} was estimated from data in the **B**. The means ± S.E. obtained with the data from triplicate samples are presented (*$P < 0.05$, as determined by a Student's *t*-test). **(D)** Caspase-3/7 activity in cells after incubation with active-Monalysin. S2 cells (1.5×10^5 cell in 100 μL) were incubated with active-Monalysin or Cycloheximide (an apoptosis inducer) at 1.5 μg/mL for the indicated time. Caspase-3/7 activity was measured as luminescence using a Caspase-Glo 3/7 Assay. The means ± S.E. obtained with the data from duplicate samples in two independent experiments **(E)** Survival analysis of adult flies upon injection with pro-Monalysin, active-Monalysin, or degraded-Monalysin (1 mg/mL) into their hemolymph for 1 h (*$P < 0.05$; NS, not significant, as determined by a Student's *t*-test). The minus indicates un-injected flies. The means ± S.E. were obtained with the data from three vials (10 flies/each). The data represents two independent experiments**. (F)** Survival analysis of adult flies upon injection with active-Monalysin (3–30 μg/mL) at indicated time points (*$P < 0.0001$, as determined by a log-rank test).

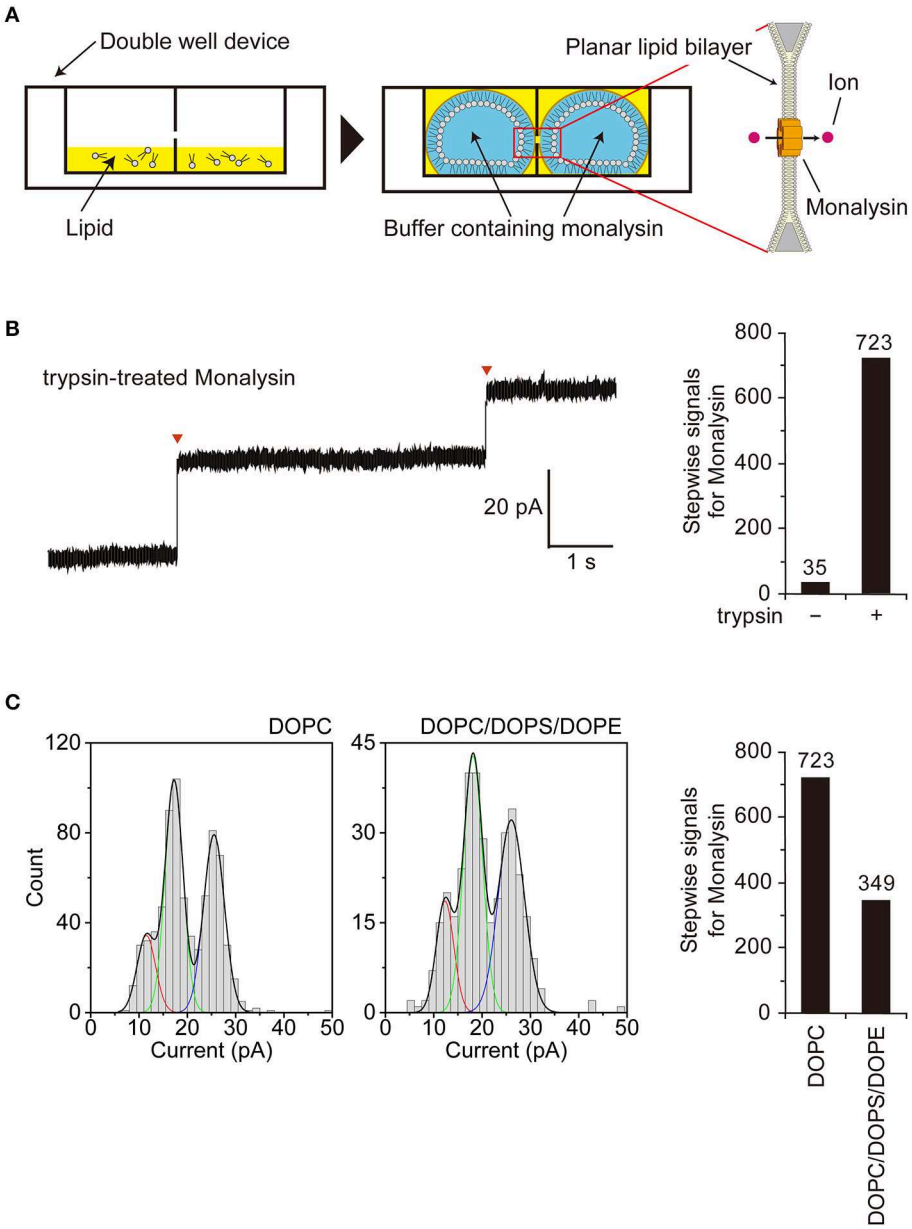

FIGURE 3 | Characterization of Monalysin as a pore-forming toxin using electrophysiological measurements. **(A)** Experimental design for monitoring Monalysin pore formation. A buffer containing Monalysin was supplied to a planar bilayer lipid membrane, prepared by the droplet contact method, and pore formation was monitored by recording ion current signals. **(B)** Typical current trace of the Monalysin, which was digested by trypsin. Applied potential: +100 mV (left). Red triangles represent the detections of a single Monalysin nanopore within the BLM. Total stepwise signals of Monalysin, with or without trypsin treatment, on the DOPC lipid bilayer were shown. Signals for Monalysin were observed for 30 min using a 16-ch device (right). **(C)** Current-amplitude histogram of the Monalysin onto lipid bilayers composed of DOPC and DOPC/DOPS/DOPE (mol ratio of 7:2:1) using a 16-ch device. Applied potential: +100 mV (left). Total signals of Monalysin on the DOPC and DOPC/DOPS/DOPE lipid bilayer were shown. Signals for Monalysin were observed for 30 min using a 16-ch device (right). The curve represents a multipeak Gaussian fitting ($P < 0.05$, F-test, respectively): the red, green and blue curves show the first, second and third Gaussian peak, respectively, and the black curves represent the sum of the three Gaussian curves.

signals in each case: 1.5 ± 1.9 pA, 17.3 ± 1.9 pA, and 25.5 ± 2.2 pA (mean ± S.D.) for the DOPC lipid bilayer, and 12.3 ± 1.8 pA, 18.1 ± 2.0 pA, and 26.1 ± 2.7 pA (mean ± S.D.) for the DOPC/DOPS/DOPE lipid bilayer (**Figure 3C**, left). The amplitude peaks of the active-Monalysin signals in case of the DOPC and DOPC/DOPS/DOPE bilayers showed no significant differences. We estimated the diameters of the active-Monalysin nanopores from the amplitude of the active-Monalysin signals and buffer conductance, in accordance with the method described in Gutsmann et al. (41). The diameters

of the active-Monalysin nanopores were estimated, using the amplitude peaks, to be 0.74 ± 0.30 nm, 0.91 ± 0.30 nm, and 1.10 ± 0.32 nm (mean ± S.D.) in case of the DOPC lipid bilayer, and 0.77 ± 0.30 nm, 0.77 ± 0.29 nm, 0.93 ± 0.31 nm, and 1.12 ± 0.36 nm (mean ± S.D.) in case of the DOPC/DOPS/DOPE lipid bilayer. In summary, Monalysin appears to insert itself preferably within a lipid bilayer with high ratio of PC, and forms pores measuring around 0.7–1 nm, regardless of the lipid composition.

Atomic Force Microscope Analysis for the Structure of Monalysin in Solution

Gel filtration chromatography of endogenous Monalysin indicates that Monalysin forms a stable pore-forming complex before activation and membrane interaction, as previously suggested (26). However, based on the gel filtration analysis, it seems that the molecular weight of a Monalysin complex is slightly smaller than that of a previous 18-mer model of Monalysin. Data from an MALDI-TOFMS analysis is in line with this estimate. We detected a possible molecular ion peak of active-Monalysin multimers, whose m/z was 217932.23. This value was very close to the molecular weight of an 8-mer active-complex expected from the amino acid sequences, 213160.4 Da (**Supplementary Figure 5**). Revealing the structure of native Monalysin in solution and lipid membrane, particularly its dynamic nature, is essential to understand its detailed molecular function and use to evaluate innate immunity mechanisms in flies, as well as to develop biological control agents against insects and biological nanopores. To this end, we employed HS-AFM that enabled dynamic real-time observations of macromolecules at nanometer resolutions, which are not feasible with other methods (42, 43), and had recent achievements of revealing the dynamic structures of pore-forming proteins (44–47).

First, we observed pro-Monalysin in the PBS buffer on a mica surface. The experimental setup is shown in **Figure 4A**. As shown in **Figure 4B**, molecules with a uniform height covered the mica surface. At smaller scan sizes, trefoil-shaped molecules were seen (**Figure 4C**, **Supplementary Movie 1**). Importantly, the molecule corresponding to each leaf of the trefoil dissociated from, and re-bound to, a trefoil-shaped molecule (**Figure 4C**, 9.75, and 10.25 s), indicating that one particle in the trefoil-shaped molecule is the minimum unit of pro-Monalysin. Note that pro-Monalysin occasionally forms a trimer of the minimum unit in the solution. Hereafter, we refer to this minimum unit of pro-Monalysin as pro-form. The pro-form height was 14.0 ± 0.9 nm (mean ± S.D) (**Figures 4D,E**). The center-to-center distance between the adjacent pro-forms in the trefoil-shaped molecule was 11.3 ± 1.7 nm (**Figure 4F**). This result suggests that this distance corresponds to the maximal pro-form diameter, which is slightly smaller than the reported value of recombinant Monalysin (∼14 nm) (26). We did not confirm the presence of the reported pore structure on the center of the pro-form. This is because the pro-form moved faster than the AFM scanning speed.

Next, we observed active-Monalysin in the PBS buffer on a mica surface. As shown in **Supplementary Figure 6A**, no trefoil-shaped molecules were observed, but molecules with a similar width to that of the pro-form were rapidly moving on the mica surface (**Supplementary Movie 2**). The striking difference from the pro-form was that the height of the molecules was 5.1 ± 0.3 nm (**Supplementary Figures 6B,C**), which is less than half of the pro-form. This result is consistent with the idea that pro-Monalysin, double-stacked disk-like oligomers, dissociates into two disk-shaped oligomers upon proteolytic cleavage (26). This suggests that we could observe the active-form of Monalysin. However, the presence of the central pore could not be confirmed as the molecules moved rapidly.

Use of a low salt buffer (30 mM NaCl, 10 mM Sodium phosphate, pH 7.0) as an observation buffer induced strong immobilization of Monalysin oligomers on the mica surface, allowing us to image the molecular feature at a high spatial resolution. As shown in **Figure 4G**, oligomers with a central pore were clearly visualized by the AFM even at somewhat larger scan sizes. The height was 5.3 ± 0.3 nm (mean ± S.D.) (**Figures 4H,I**), identical to that obtained under the PBS buffer. The central pore had an aperture diameter of ∼3 nm (**Figure 4H**), consistent with the previous report (26). The center-to-center distance between the adjacent active-forms was 11.4 ± 0.9 nm (**Figure 4J**), indicating that the maximal diameter of the active-form is identical to that of the pro-form. This result is consistent with no significant change induced in the outer diameters of Monalysin upon protease activation (26). At smaller scan sizes, the sub-unit stoichiometry was directly resolved (**Figure 4K**, **Supplementary Movie 3**). Unexpectedly, the active-Monalysin was composed of eight sub-units and formed a disk-shaped octamer, in contrast to the crystalline structure of recombinant pro-Monalysin (26), which suggests nonameric (9-mer) composition.

We next visualized the conversion of pro-Monalysin to active-Monalysin after trypsin treatment in the PBS buffer. The video shows that, in a trypsin-concentration dependent manner, almost all molecules with a height of ∼14 nm were converted into molecules with a height of ∼5 nm over time (**Figure 5**, **Supplementary Movie 4**). Interestingly, we noticed that, by applying stronger tapping forces, the pro-form with a height of ∼14 nm can be changed into molecules with a height of ∼5 nm without trypsin treatment. Indeed, this change occurred depending on the strength of the tapping force (**Supplementary Figures 7A–C**, **Supplementary Movie 5**). When A_{sp}/A_0 were set at 0.5, this height change was seen for almost all the pro-form molecules after 60 s. The average tapping force in this imaging condition is estimated to be 53 ± 17 pN, using the nominal values of $A_0 = 2.0 \pm 0.2$ nm, $k_c = 80 \pm 20$ pN/nm, and $Q_c = 1.3 \pm 0.2$. In contrast, under the typical imaging conditions using A_{sp}/A_0 of more than 0.8, giving an average tapping force of $<37 \pm 17$ pN, this height alteration was not seen at all, even after 60 s. These results strongly suggest that the pro-Monalysin height change seen in the trypsin treatment is induced by the proteolytic cleavage, not by the mechanical perturbations. Thus, the results seen in **Figure 5** are direct evidence that trypsin treatment effectively digests a portion of pro-Monalysin and produces the active-forms by dissociating the doubly stacked disks. Note that the active-forms can withstand an average tapping force of ∼50

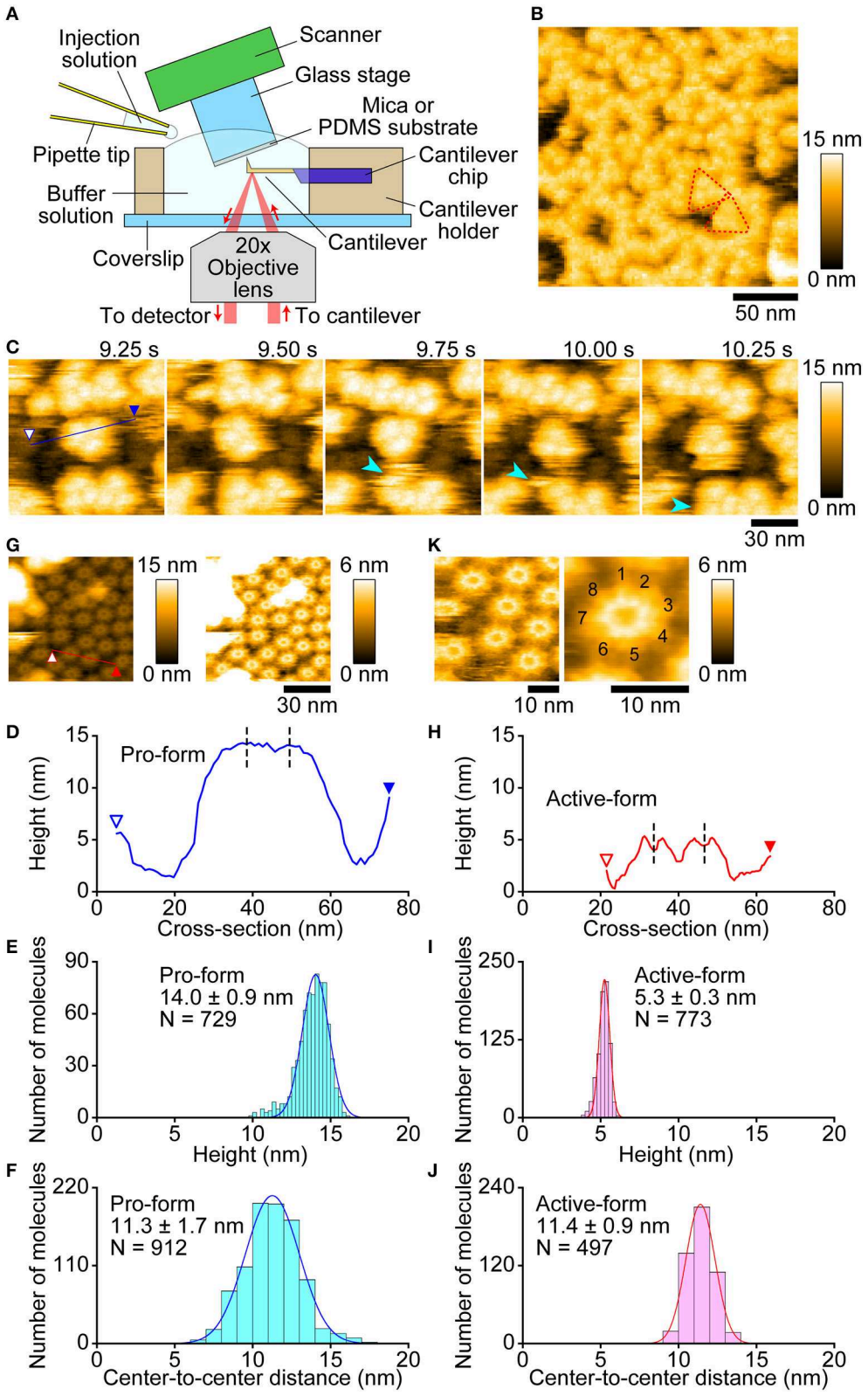

FIGURE 4 | Molecular features of pro- and active-Monalysin on a mica surface visualized by AFM. **(A)** Experimental design for AFM analysis. Samples were absorbed into a substrate surface and imaged by a probe-tip attached at the end of a cantilever. In some experiments, the injection solution was added to the buffer solution during AFM imaging. **(B)** A wide-area image of pro-Monalysin. Typical trefoil-shaped molecules are encircled by red dashed-lines. The scanning area was 200 × 200

(Continued)

FIGURE 4 | nm^2 with 100 × 100 pixels, and the imaging rate was 330 ms/frame. **(C)** Successive AFM images of pro-Monalysin (see **Supplementary Movie 1**). The light blue arrowhead shows that a pro-form detaches from, and binds to, a trefoil-shaped molecule. The scanning area was 100 × 100 nm^2 with 100 × 100 pixels and the imaging rate was 250 ms/frame. **(G)** A wide-area image of active-Monalysin. Two different height scale images are shown. Bright spots are some adsorbed debris. The scanning area was 80 × 80 nm^2 with 160 × 160 pixels and the imaging rate was 330 ms/frame. **(K)** Small-area image of active-Monalysin (see **Supplementary Movie 3**). The scanning area was 40 × 40 nm^2 with 120 × 120 pixels, and the imaging rate was 150 ms/frame. The right image is an averaged image using four successive images. **(D,H)** A cross-section analysis of pro- and active-Monalysin. The sections are from the blue and red lines drawn on the images in **C,G**. Each dashed line indicates the center position of a molecule used in the analysis of **F,J**. **(E,I)** Height distributions of pro- and active-Monalysin. **(F,J)** Center-to-center distance distributions of pro- and active-Monalysin. All distributions were fitted by single-Gaussian curve.

pN (**Supplementary Figures 7D,E**, **Supplementary Movie 6**). In addition, the height alternation of the pro-form from 14 to 5 nm was also induced just when the molecules were strongly immobilized on the mica surface under the low salt buffer (**Supplementary Figure 8**, **Supplementary Movie 7**). These results suggest that the intramolecular interactions supporting the disk-shaped octamer structure are strong, while the disk-disk interaction is relatively weak and perhaps only sustained by the interaction of amino acid residues removed during protease activation. However, it remains an open question whether the force-indeed molecules from the pro-form with a height of ∼5 nm are active and can form nanopores within the cell membrane. Importantly, the pro-Monalysin, not activated by trypsin treatment, strongly immobilized on the mica surface formed the disk-shaped octamer with the central pore (**Supplementary Figure 8B**). Consistent with the previous report (26), this result suggests that the central pore is already formed in the doubly stacked disks of the pro-Monalysin in solution.

Real-Time Dynamics of Monalysin Insertion Into a Lipid Bilayer

We next visualized the insertion events of the active-Monalysin into a lipid membrane (**Figure 6**). A lipid membrane composed of a mixture of phospholipids of DOPC/DOPS/biotin-cap-DOPE was formed on the surface of PDMS (35). The active-Monalysin was then added into the observation buffer to be monitored. HS-AFM video showed that the active-Monalysin was inserted into the lipid membrane without significant structural change (**Figure 6**, **Supplementary Movie 8**). The active-form height was 6.1 ± 0.7 nm (mean ± S.D.) from the surface of lipid membrane (**Figures 6B,C**), which is slightly higher than that seen in the active-form on mica. At smaller scan sizes, the sub-unit stoichiometry was directly resolved to be 8-mer (**Figure 6D**, **Supplementary Movie 9**). These results collectively suggest that endogenous pro-Monalysin is a 16-mer complex, separated by protease into 8-mer active complexes, and the 8-mer active complex is inserted into the lipid membrane as they are.

Interestingly, Monalysin was preferentially inserted into the edge of the lipid membrane (**Figure 6E**). This implies that Monalysin prefers to be inserted in highly curved parts of the membrane. Consistent with this, we observed many insertions of active-Monalysin into the liposome (**Supplementary Figure 9A**, **Supplementary Movie 10**), while no insertion was seen into the lipid membrane formed on the mica surface (**Supplementary Figure 9E**). The surface roughness of the lipid bilayer formed on the PDMS and mica surfaces were 0.51 ± 0.08 nm and 0.13 ± 0.05 nm, respectively. These results indicate that the active-Monalysin can recognize such difference in the surface roughness of lipid membrane and make a drastic difference in the membrane insertion. Interestingly, the liposome placed on the mica surface was distorted and deformed into a disc shape (∼13 nm in height and ∼80 nm in width) rather than a spherical shape (**Supplementary Figure 9B**), and all Monalysin molecules were located on the outer periphery of the disc (see the blue arrowheads in **Supplementary Figure 9A**). This suggests that the active-form can spontaneously migrate to highly curved sites on the lipid membrane. In addition, we found that the active-Monalysin which have been reconstituted with liposome has two height states of 5.9 ± 0.5 and 7.3 ± 0.4 nm (**Supplementary Figures 9C,D**). Considering that the height of the active-form inserted into the lipid membrane formed on the PDMS is ∼6 nm, the active molecule inserted into the curved membrane may have a height of ∼7 nm, and the molecules with the height of ∼7 nm seen in **Supplementary Figures 9C,D** are presumably in a molecular state before height transition from ∼7 to ∼6 nm.

DISCUSSION

In this study, we reported, for the first time, on the purification of endogenous pro-Monalysin from entomopathogenic bacteria *P. entomophila*. Purified pro-Monalysin is activated by trypsin treatment, which is confirmed by electrophysiological analysis with an artificial lipid membrane. The pro-form is stable for more than a month at 4°C (data not shown), and active-form produced by trypsin treatment had cytotoxic activity in *Drosophila* cell line and adult flies. In particular, we examined the distinct structure and dynamics of endogenous Monalysin in solution and within the lipid membrane using HS-AFM and revealed the stability of the active-octamer structure. This study suggests that endogenous Monalysin is one of the best model toxins from entomopathogenic bacteria. Additionally, information on pore size estimated by electrophysiological analysis is useful for the potential development of biological nanopores from endogenous Monalysin.

We purified pro-Monalysin based on cytotoxic activity from cell pellets of *P. entomophila*, not from a culture supernatant, meaning that a large amount of Monalysin is kept inside the cells as an assembled pro-form. The diameters of pro-Monalysin and active-Monalysin, estimated from HS-AFM analysis, are ∼11 nm and their heights are ∼14 and 5–7 nm, respectively. Both sizes are too large to be secreted by *P. entomophila's* secretion system. It has type I and II secretion systems with secretion pore diameters that are generally <5 nm (48–50). Since *P. entomophila*

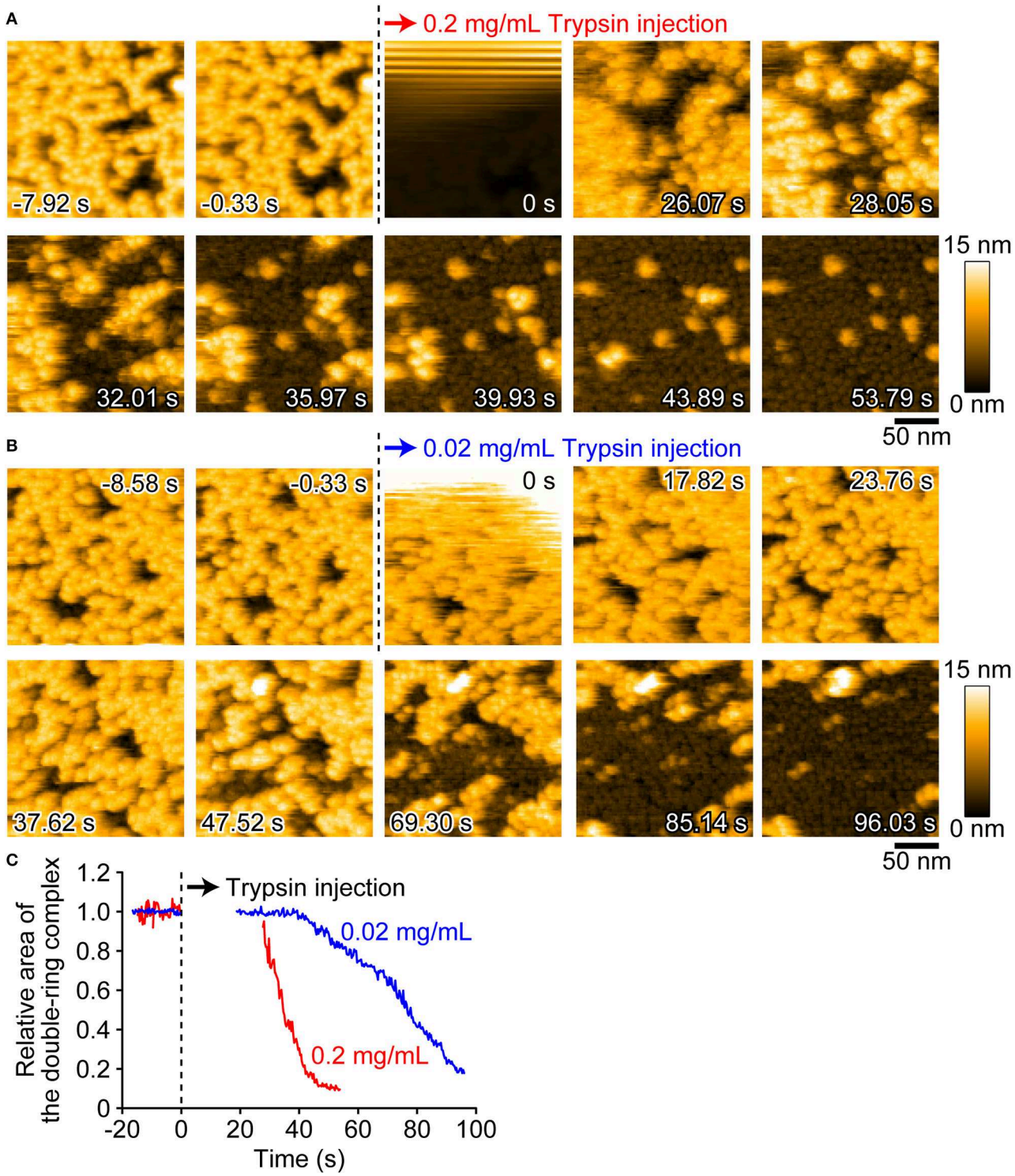

FIGURE 5 | AFM images showing the height conversion of pro-Monalysin upon trypsin treatment. **(A,B)** Successive AFM images before and after trypsin injection (**Supplementary Movie 4**). The scanning area was 200 × 200 nm^2 with 100 × 100 pixels, and the imaging rate was 330 ms/frame. At 0 s, a drop of trypsin solution was injected in the observation buffer. The final concentrations of trypsin in the observation buffer were 0.2 mg/mL for **A** and 0.02 mg/mL for **B**, respectively. After injection, the height conversion was gradually seen. **(C)** The time course of the relative area of the double-ring complex of pro-Monalysin before and after trypsin injection. The average coverage area before trypsin injection is set to 1. The time course after injection is missing for 20–30 s. This is because the AFM images during this term were disturbed, and the area measurements cannot be performed.

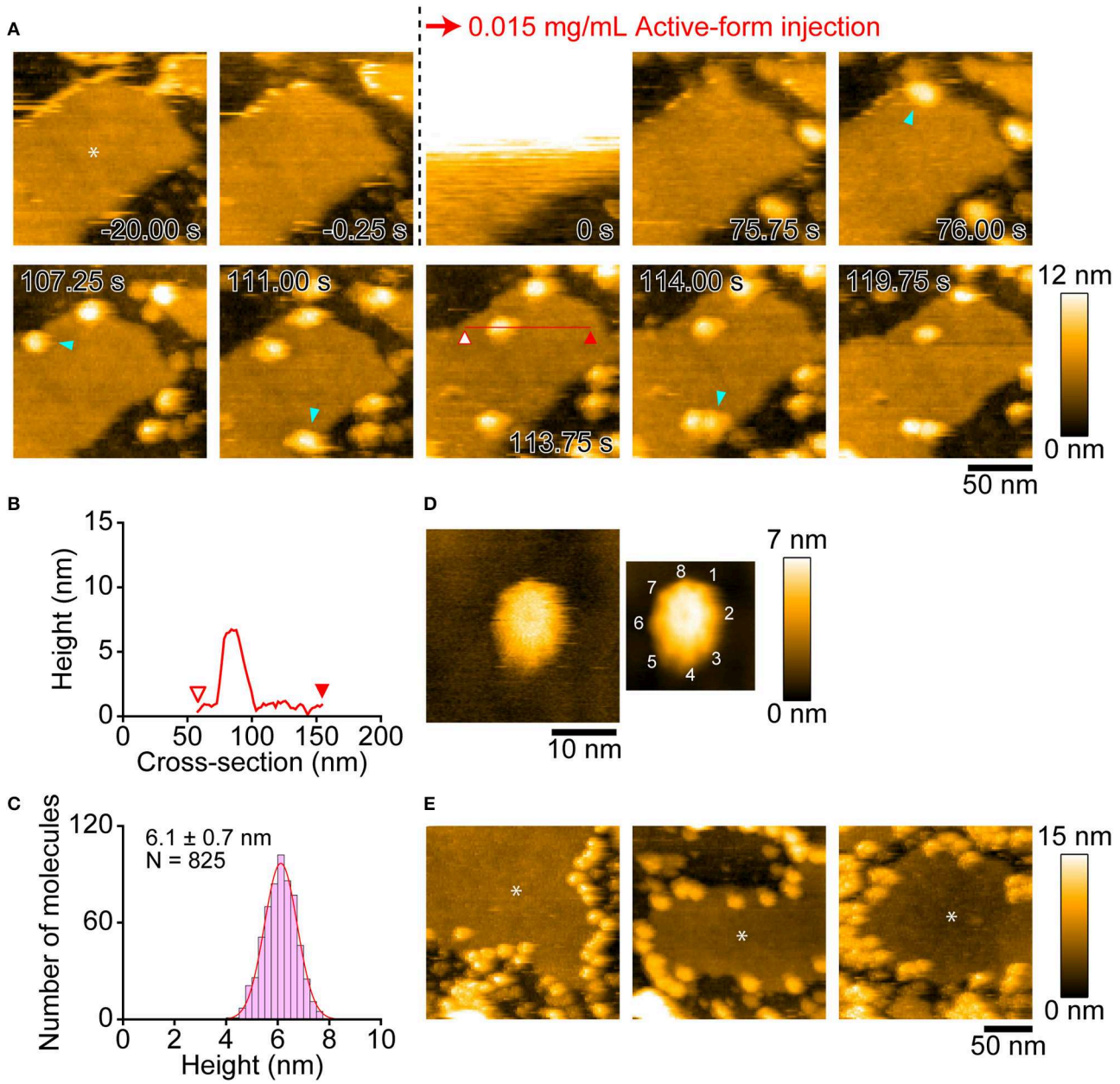

FIGURE 6 | AFM images showing insertion of active-Monalysin onto lipid membrane formed on the PDMS surface. **(A)** Successive AFM images before and after active-Monalysin injection (**Supplementary Movie 8**). Dark area represents the PDMS surface, while slightly bright area represents the lipid membrane surface (see the asterisk in the first image). The scanning area was 150 × 150 nm^2 with 80 × 80 pixels, and the imaging rate was 250 ms/frame. At 0 s, a drop of active-Monalysin solution was injected in the observation buffer. The final concentrations of active-Monalysin in the observation buffer were 0.015 mg/mL. After injection, the active-Monalysin were gradually inserted on the lipid bilayer (see the light blue arrowheads). **(B)** A cross-section analysis of active-Monalysin inserted in the lipid bilayer. The section is from the red line drawn on the image in **A**. **(C)** Height distributions of active-Monalysin inserted in the lipid bilayer. The distribution was fitted by single-Gaussian curve. **(D)** Small-area image of active-Monalysin inserted in the lipid bilayer (**Supplementary Movie 9**). The scanning area was 30 × 30 nm^2 with 150 × 150 pixels, and the imaging rate was 330 ms/frame. The right image is an averaged image using 20 successive images. **(E)** AFM image gallery showing that the active-Monalysin are preferentially inserted into the edge of lipid bilayer. Asterisk marks represent the lipid bilayer areas. The scanning area was 200 × 200 nm^2 with 100 × 100 pixels, and the imaging rate was 330 ms/frame.

tends to undergo autolysis, particularly at temperatures over 30°C, some *P. entomophila* may have been lysed in the host's intestine. In this case, pro-Monalysin was released from the dead bacteria and digested by bacterial proteases such as AprA, or perhaps also by host proteases, to become its active-form. We also observed that the trefoil-shaped structure of 16-mer

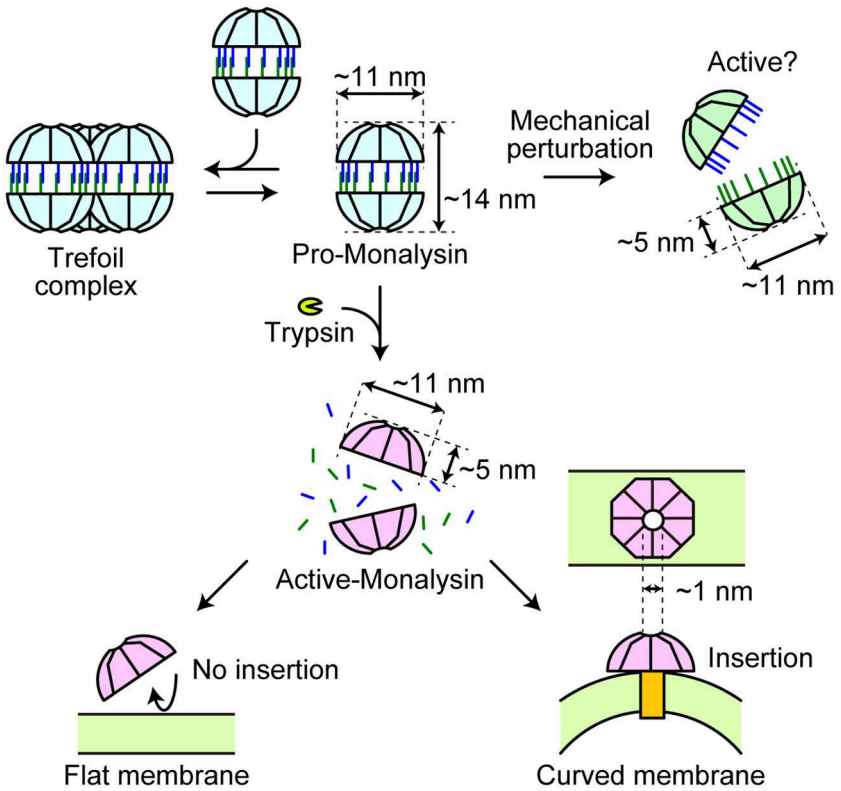

FIGURE 7 | A model of Monalysin activation for pore formation. Endogenous pro-Monalysin presents a 16-mer complex and occasionally forms a trefoil-shaped structure composed of trimer complex in the PBS buffer when its concentration is high enough. After trypsin treatment or mechanical perturbation, the double-stacked disk-like 16-mer complex dissociates into two disk-shaped 8-mer complexes. The 8-mer complex of active-Monalysin, in turn, preferentially inserts itself into the curved lipid membrane and forms nanopores (pore size = 1 nm).

pro-Monalysin composes the trimer complex in the PBS buffer when the concentration of pro-Monalysin is high enough. By making a trimer complex, the cleavage site for proteolytic activation of pro-Monalysin might be hidden and prevented from being an active-form in *P. entomophila*. Sub-cellular localization and estimated concentration of pro-Monalysin in *P. entomophila* should be investigated in a future study.

The most well-characterized PFTs that damage insect tissue are probably Cry toxins from *Bacillus thuringiensis*, a Gram-positive bacterium commonly used as a biological pesticide (27). Cry toxins represent a large family, consisting of more than 350 different members, yet their common features as toxins are essentially the same (27). They form crystalline inclusions after production, are solubilized, undergo partial cleavage by proteases in digestive juice, and are activated after ingestion. The activated Cry toxin is considered a monomer and then forms a pore on the cell membrane of midgut epithelial cells, following specific interactions with a receptor(s), resulting in cell lysis and destruction of midgut tissue (27, 28). However, our study showed that endogenous Monalysin was composed of a pore-forming multimer from the beginning and demonstrates a receptor-independent insertion into the lipid membrane. Importantly, since Cry toxins show target specificity of insect species through selective toxin-receptor interactions, one needs to employ a genetic trick when using them on flies, e.g., overexpression of the Cry1Aa receptor and the application of Cry1Aa thereafter (29). Thus, if one seeks to impose tissue damage in a non-specific manner, Monalysin injection or ingestion would be a simple method. Indeed, our study showed that injection of endogenous Monalysin, through a standard procedure, effectively killed adult flies and induced an innate immune response. This study provides a theoretical basis for the use of endogenous Monalysin toxins as a tool for studying injury-induced innate immunity in the context of microbial infections. Note that endogenous Monalysin can be purified milligram order from 1 L of bacterial culture, suggesting its versatility within a range of experiments.

Our HS-AFM analysis revealed real-time dynamics of Monalysin in action (**Figure 7**). Pro-Monalysin purified from *P. entomophila* showed a relatively scissile 16-mer complex (though stable enough during the purification step and storage), in contrast to the 18-mer structure of recombinant Monalysin prepared from *E. coli*. A 16-mer model of our endogenous Monalysin is consistent with gel filtration chromatography and MALDI-TOFMS analysis. This discrepancy might be derived from the different techniques, or the hosts, used to express Monalysin. Alternatively, pore-forming toxins tend to compose different subunit stoichiometry in solution than in crystal. Indeed, α-hemolysin had been suggested to form heptamer by

X-ray crystallography, though an AFM analysis indicated that α-hemolysin composes hexameric stoichiometry (51). This report and our current study may imply that pore-forming toxins, in general, could form two different energetically stable oligomers in different conditions. By using endogenous Monalysin, it would be interesting to solve crystal structure or to perform cryo-EM in the future study.

Activated-Monalysin obtained by trypsin treatment has an 8-mer constitution and roughly halves in height, indicating that pro-Monalysin is half dissociated into an 8-mer pair well before insertion. It penetrates and forms pores in the lipid bilayer without profound structural change. Notably, Monalysin was preferentially inserted into the edge of the lipid membrane, implying that Monalysin could recognize the target membrane's curvature. Eukaryotic cells possess local membrane subdomains, some of which have high curved areas, such as the tip of filopodia and the area of endocytosis or exocytosis. Those subregions have important biological functions for cell movement, intracellular communication, and signaling (52). Phagocytosing immune cells, such as macrophages, extend a lot of filopodia, particularly upon immune activation. Monalysin or its relatives might preferentially target those cells and/or important biological membrane regions. Additionally, a possible entry site of Monalysin is the tip of microvilli of enterocytes in the fly's intestinal epithelium, as previous studies have reported that Monalysin killed adult flies after oral infection through gut injury (23). Furthermore, electrophysiological analysis revealed that Monalysin inserts itself most commonly within lipid bilayers with high ratio of PC. The chemical nature of lipids determines how the lipids bundle side-by-side in a monolayer and thereby influences the monolayer curvature. For example, lysophospholipids form positively curved monolayers; PC build nearly flat monolayers; and DOPE assemble negatively curved monolayers (53). Notably, upon cell activation, some of the membrane phospholipids are metabolized into eicosanoids and lysophospholipids (54). Active-Monalysin may prefer to insert a highly bent portion of the plasma membrane with a large amount of lysophospholipids produced upon a cell signaling event. From this point of view, not only local membrane subdomains, but also some specific cell types and/or cell activation status could be the insertion target of active-Monalysin. And then, these characteristics might determine host and position specificity where Monalysin shows toxicity. More detailed analysis to find more specific lipid preference and the optimal radius of curvature for Monalysin insertion shall be conducted *in vitro* and *in vivo*. Further studies on endogenous Monalysin are required to answer questions concerning the precise mode-of-action during pore formation in the target membrane.

DATA AVAILABILITY STATEMENT

All datasets generated for this study are included in the article/**Supplementary Material**.

AUTHOR CONTRIBUTIONS

NK and TK: conceptualization. SN, KK, NK, and TK: formal analysis and writing—original draft. SN, ES, KK, AH, FN, RA, AM, TN, ST, NK, and TK: investigation. SN, ES, KK, AH, ST, NK, and TK: funding acquisition. All authors writing—review and editing.

FUNDING

This work was supported by a JSPS KAKENHI Grant and an AMED Grant for TK, an Indonesia Endowment Fund for Education (LPDP) and Ministry of Research, Technology and Higher Education of the Republic of Indonesia (BUDI-LN Scholarship) and the Sasakawa Scientific Research Grant for ES, The Mochida Memorial Foundation for Medical and Pharmaceutical Research for SN, the Kao Foundation for Arts and Sciences for AH, JSPS KAKENHI Grant (15H04360 and 18H05269) and JST CREST (JPMJCR1762) for NK.

ACKNOWLEDGMENTS

We thank Dr. Bruno Lemaitre for strains of *P. entomophila* and antibody against Monalysin. We also thank the Bloomington *Drosophila* Stock Center and Developmental Studies Hybridoma Bank for providing us with the flies and antibodies, respectively. We are grateful to Drs. Shoichiro Kurata and Yoshinobu Nakanishi for our discussions. We acknowledge the technical support in the electrophysiological characterization of Monalysin provided by Ms Y. Yatomi, and the technical support for the HS-AFM from Drs. Toshio Ando and Takayuki Uchihashi. The authors would like to thank Enago (www.enago.jp) for the English language review.

SUPPLEMENTARY MATERIAL

The Supplementary Material for this article can be found online at: https://www.frontiersin.org/articles/10.3389/fimmu.2020.00520/full#supplementary-material

REFERENCES

1. Akira S, Uematsu S, Takeuchi O. Pathogen recognition and innate immunity. *Cell*. (2006) 124:783–801. doi: 10.1016/j.cell.2006.02.015
2. Chen GY, Nunez G. Sterile inflammation: sensing and reacting to damage. *Nat Rev Immunol*. (2010) 10:826–37. doi: 10.1038/nri2873
3. Venereau E, Ceriotti C, Bianchi ME. DAMPs from cell death to new life. *Front Immunol*. (2015) 6:422. doi: 10.3389/fimmu.2015.00422
4. Lemaitre B, Hoffmann J. The host defense of *Drosophila* melanogaster. *Annu Rev Immunol*. (2007) 25:697–743. doi: 10.1146/annurev.immunol.25.022106.141615
5. Myllymaki H, Valanne S, Ramet M. The *Drosophila* imd signaling pathway. *J Immunol*. (2014) 192:3455–62. doi: 10.4049/jimmunol.1303309
6. Valanne S, Wang JH, Ramet M. The *Drosophila* toll signaling pathway. *J Immunol*. (2011) 186:649–56. doi: 10.4049/jimmunol.1002302

7. Gobert V, Gottar M, Matskevich AA, Rutschmann S, Royet J, Belvin M, et al. Dual activation of the *Drosophila* toll pathway by two pattern recognition receptors. *Science*. (2003) 302:2126–30. doi: 10.1126/science.1085432
8. Michel T, Reichhart JM, Hoffmann JA, Royet J. *Drosophila* toll is activated by gram-positive bacteria through a circulating peptidoglycan recognition protein. *Nature*. (2001) 414:756–9. doi: 10.1038/414756a
9. Gottar M, Gobert V, Matskevich AA, Reichhart JM, Wang C, Butt TM, et al. Dual detection of fungal infections in *Drosophila* via recognition of glucans and sensing of virulence factors. *Cell*. (2006) 127:1425–37. doi: 10.1016/j.cell.2006.10.046
10. Parthier C, Stelter M, Ursel C, Fandrich U, Lilie H, Breithaupt C, et al. Structure of the Toll-Spatzle complex, a molecular hub in *Drosophila* development and innate immunity. *Proc Natl Acad Sci USA*. (2014) 111:6281–6. doi: 10.1073/pnas.1320678111
11. Sun H, Bristow BN, Qu G, Wasserman SA. A heterotrimeric death domain complex in toll signaling. *Proc Natl Acad Sci USA*. (2002) 99:12871–6. doi: 10.1073/pnas.202396399
12. Lindsay SA, Wasserman SA. Conventional and non-conventional *Drosophila* toll signaling. *Dev Comp Immunol*. (2014) 42:16–24. doi: 10.1016/j.dci.2013.04.011
13. Kleino A, Silverman N. The *Drosophila* IMD pathway in the activation of the humoral immune response. *Dev Comp Immunol*. (2014) 42:25–35. doi: 10.1016/j.dci.2013.05.014
14. Paquette N, Broemer M, Aggarwal K, Chen L, Husson M, Erturk-Hasdemir D, et al. Caspase-mediated cleavage, IAP binding, and ubiquitination: linking three mechanisms crucial for *Drosophila* NF-kappaB signaling. *Mol Cell*. (2010) 37:172–82. doi: 10.1016/j.molcel.2009.12.036
15. El Chamy L, Leclerc V, Caldelari I, Reichhart JM. Sensing of danger signals and pathogen-associated molecular patterns defines binary signaling pathways upstream of Toll. *Nat Immunol*. (2008) 9:1165–70. doi: 10.1038/ni.1643
16. Ming M, Obata F, Kuranaga E, Miura M. Persephone/spatzle pathogen sensors mediate the activation of toll receptor signaling in response to endogenous danger signals in apoptosis-deficient *Drosophila*. *J Biol Chem*. (2014) 289:7558–68. doi: 10.1074/jbc.M113.543884
17. Issa N, Guillaumot N, Lauret E, Matt N, Schaeffer-Reiss C, Van Dorsselaer A, et al. The circulating protease persephone is an immune sensor for microbial proteolytic activities upstream of the *Drosophila* toll pathway. *Mol Cell*. (2018) 69:539–50. doi: 10.1016/j.molcel.2018.01.029
18. Arefin B, Kucerova L, Dobes P, Markus R, Strnad H, Wang Z, et al. Genome-wide transcriptional analysis of *Drosophila* larvae infected by entomopathogenic nematodes shows involvement of complement, recognition and extracellular matrix proteins. *J Innate Immun*. (2014) 6:192–204. doi: 10.1159/000353734
19. Hyrsl P, Dobes P, Wang Z, Hauling T, Wilhelmsson C, Theopold U. Clotting factors and eicosanoids protect against nematode infections. *J Innate Immun*. (2011) 3:65–70. doi: 10.1159/000320634
20. Vodovar N, Vinals M, Liehl P, Basset A, Degrouard J, Spellman P, et al. *Drosophila* host defense after oral infection by an entomopathogenic pseudomonas species. *Proc Natl Acad Sci USA*. (2005) 102:11414–9. doi: 10.1073/pnas.0502240102
21. Martins NE, Faria VG, Teixeira L, Magalhaes S, Sucena E. Host adaptation is contingent upon the infection route taken by pathogens. *PLoS Pathog*. (2013) 9:e1003601. doi: 10.1371/journal.ppat.1003601
22. Chakrabarti S, Liehl P, Buchon N, Lemaitre B. Infection-induced host translational blockage inhibits immune responses and epithelial renewal in the *Drosophila* gut. *Cell Host Microbe*. (2012) 12:60–70. doi: 10.1016/j.chom.2012.06.001
23. Opota O, Vallet-Gely I, Vincentelli R, Kellenberger C, Iacovache I, Gonzalez MR, et al. Monalysin, a novel β-pore-forming toxin from the *Drosophila* pathogen *Pseudomonas entomophila*, contributes to host intestinal damage and lethality. *PLoS Pathog*. (2011) 7:e1002259. doi: 10.1371/journal.ppat.1002259
24. Kuraishi T, Binggeli O, Opota O, Buchon N, Lemaitre B. Genetic evidence for a protective role of the peritrophic matrix against intestinal bacterial infection in *Drosophila* melanogaster. *Proc Natl Acad Sci USA*. (2011) 108:15966–71. doi: 10.1073/pnas.1105994108
25. Shibata T, Maki K, Hadano J, Fujikawa T, Kitazaki K, Koshiba T, et al. Crosslinking of a peritrophic matrix protein protects gut epithelia from bacterial exotoxins. *PLoS Pathog*. (2015) 11:e1005244. doi: 10.1371/journal.ppat.1005244
26. Leone P, Bebeacua C, Opota O, Kellenberger C, Klaholz B, Orlov I, et al. X-ray and cryo-electron microscopy structures of monalysin pore-forming toxin reveal multimerization of the pro-form. *J Biol Chem*. (2015) 290:13191–201. doi: 10.1074/jbc.M115.646109
27. Jurat-Fuentes JL, Crickmore N. Specificity determinants for cry insecticidal proteins: insights from their mode of action. *J Invertebr Pathol*. (2017) 142:5–10. doi: 10.1016/j.jip.2016.07.018
28. Bravo A, Gómez I, Porta H, García-Gómez BI, Rodriguez-Almazan C, Pardo L, et al. Evolution of *Bacillus thuringiensis* cry toxins insecticidal activity. *Microb Biotechnol*. (2013) 6:17–26. doi: 10.1111/j.1751-7915.2012.00342.x
29. Obata F, Tanaka S, Kashio S, Tsujimura H, Sato R, Miura M. Induction of rapid and selective cell necrosis in *Drosophila* using *Bacillus thuringiensis* cry toxin and its silkworm receptor. *BMC Biol*. (2015) 13:48. doi: 10.1186/s12915-015-0160-2
30. Jetha NN, Wiggin M, Marziali A. Forming an alpha-hemolysin nanopore for single-molecule analysis. *Methods Mol Biol*. (2009) 544:113–27. doi: 10.1007/978-1-59745-483-4_9
31. Asano T, Nishiuchi T. Comparative analysis of phosphoprotein expression using 2D-DIGE. *Methods Mol Biol*. (2011) 744:225–33. doi: 10.1007/978-1-61779-123-9_16
32. Kenmoku H, Ishikawa H, Ote M, Kuraishi T, Kurata S. A subset of neurons controls the permeability of the peritrophic matrix and midgut structure in *Drosophila* adults. *J Exp Biol*. (2016) 219:2331–9. doi: 10.1242/jeb.122960
33. Ando T, Uchihashi T, Fukuma T. High-speed atomic force microscopy for nano-visualization of dynamic biomolecular processes. *Prog Surf Sci*. (2008) 83:337–437. doi: 10.1016/j.progsurf.2008.09.001
34. Uchihashi T, Kodera N, Ando T. Guide to video recording of structure dynamics and dynamic processes of proteins by high-speed atomic force microscopy. *Nat Protoc*. (2012) 7:1193–206. doi: 10.1038/nprot.2012.047
35. Uchihashi T, Watanabe H, Kodera N. Optimum substrates for imaging biological molecules with high-speed atomic force microscopy. *Methods Mol Biol*. (2018) 1814:159–79. doi: 10.1007/978-1-4939-8591-3_10
36. Ngo KX, Kodera N, Katayama E, Ando T, Uyeda TQ. Cofilin-induced unidirectional cooperative conformational changes in actin filaments revealed by high-speed atomic force microscopy. *Elife*. (2015) 4:e04806. doi: 10.7554/eLife.04806.033
37. Manaka J, Kuraishi T, Shiratsuchi A, Nakai Y, Higashida H, Henson P, et al. Draper-mediated and phosphatidylserine-independent phagocytosis of apoptotic cells by *Drosophila* hemocytes/macrophages. *J Biol Chem*. (2004) 279:48466–76. doi: 10.1074/jbc.M408597200
38. Obata F, Tsuda-Sakurai K, Yamazaki T, Nishio R, Nishimura K, Kimura M, et al. Nutritional control of stem cell division through S-adenosylmethionine in *Drosophila* intestine. *Dev Cell*. (2018) 44:741–51. doi: 10.1016/j.devcel.2018.02.017
39. Buchon N, Broderick NA, Kuraishi T, Lemaitre B. *Drosophila* EGFR pathway coordinates stem cell proliferation and gut remodeling following infection. *BMC Biol*. (2010) 8:152. doi: 10.1186/1741-7007-8-152
40. Funakoshi K, Suzuki H, Takeuchi S. Lipid bilayer formation by contacting monolayers in a microfluidic device for membrane protein analysis. *Anal Chem*. (2006) 78:8169–74. doi: 10.1021/ac0613479
41. Gutsmann T, Heimburg T, Keyser U, Mahendran KR, Winterhalter M. Protein reconstitution into freestanding planar lipid membranes for electrophysiological characterization. *Nat Protoc*. (2015) 10:188–98. doi: 10.1038/nprot.2015.003
42. Ando T, Uchihashi T, Scheuring S. Filming biomolecular processes by high-speed atomic force microscopy. *Chem Rev*. (2014) 114:3120–88. doi: 10.1021/cr4003837
43. Ando T, Kodera N, Takai E, Maruyama D, Saito K, Toda A. A high-speed atomic force microscope for studying biological macromolecules. *Proc Natl Acad Sci USA*. (2001) 98:12468–72. doi: 10.1073/pnas.211400898
44. Czajkowsky DM, Hotze EM, Shao Z, Tweten RK. Vertical collapse of a cytolysin prepore moves its transmembrane beta-hairpins to the membrane. *EMBO J*. (2004) 23:3206–15. doi: 10.1038/sj.emboj.7600350
45. Yilmaz N, Yamada T, Greimel P, Uchihashi T, Ando T, Kobayashi T. Real-time visualization of assembling of a sphingomyelin-specific toxin on planar lipid membranes. *Biophys J*. (2013) 105:1397–405. doi: 10.1016/j.bpj.2013.07.052

46. Leung C, Dudkina NV, Lukoyanova N, Hodel AW, Farabella I, Pandurangan AP, et al. Stepwise visualization of membrane pore formation by suilysin, a bacterial cholesterol-dependent cytolysin. *Elife*. (2014) 3:e04247. doi: 10.7554/eLife.04247.021
47. Ni T, Jiao F, Yu X, Aden S, Ginger L, Williams SI, et al. Structure and mechanism of bactericidal mammalian perforin-2, an ancient agent of innate immunity. *Sci Adv*. (2020) 6:eaax8286. doi: 10.1126/sciadv.aax8286
48. Vodovar N, Vallenet D, Cruveiller S, Rouy Z, Barbe V, Acosta C, et al. Complete genome sequence of the entomopathogenic and metabolically versatile soil bacterium *Pseudomonas entomophila. Nat Biotechnol*. (2006) 24:673–9. doi: 10.1038/nbt1212
49. Kim JS, Song S, Lee M, Lee S, Lee K, Ha NC. Crystal structure of a soluble fragment of the membrane fusion protein HlyD in a type I secretion system of gram-negative bacteria. *Structure*. (2016) 24:477–85. doi: 10.1016/j.str.2015.12.012
50. Hay ID, Belousoff MJ, Lithgow T. Structural basis of type 2 secretion system engagement between the inner and outer bacterial membranes. *mBio*. (2017) 8:e01344–17. doi: 10.1128/mBio.01344-17
51. Czajkowsky DM, Sheng S, Shao Z. Staphylococcal alpha-hemolysin can form hexamers in phospholipid bilayers. *J Mol Biol*. (1998) 276:325–30. doi: 10.1006/jmbi.1997.1535
52. McMahon HT, Boucrot E. Membrane curvature at a glance. *J Cell Sci*. (2015) 128:1065–70. doi: 10.1242/jcs.114454
53. Graham TR, Kozlov MM. Interplay of proteins and lipids in generating membrane curvature. *Curr Opin Cell Biol*. (2010) 22:430–6. doi: 10.1016/j.ceb.2010.05.002
54. Hla T, Lee MJ, Ancellin N, Paik JH, Kluk MJ. Lysophospholipids–receptor revelations. *Science*. (2001) 294:1875–8. doi: 10.1126/science.1065323

Conflict of Interest: The authors declare that the research was conducted in the absence of any commercial or financial relationships that could be construed as a potential conflict of interest.

frontiers in Immunology

ORIGINAL RESEARCH
published: 08 July 2020
doi: 10.3389/fimmu.2020.01419

Origins of Metabolic Pathology in *Francisella*-Infected *Drosophila*

Crystal M. Vincent, Carolina J. Simoes da Silva, Ashima Wadhawan and Marc S. Dionne**

MRC Centre for Molecular Bacteriology and Infection and Department of Life Sciences, Imperial College London, London, United Kingdom

The origins and causes of infection pathologies are often not understood. Despite this, the study of infection and immunity relies heavily on the ability to discern between potential sources of pathology. Work in the fruit fly has supported the assumption that mortality resulting from bacterial invasion is largely due to direct host-pathogen interactions, as lower pathogen loads are often associated with reduced pathology, and bacterial load upon death is predictable. However, the mechanisms through which these interactions bring about host death are complex. Here we show that infection with the bacterium *Francisella novicida* leads to metabolic dysregulation and, using treatment with a bacteriostatic antibiotic, we show that this pathology is the result of direct interaction between host and pathogen. We show that mutants of the immune deficiency immune pathway fail to exhibit similar metabolic dysregulation, supporting the idea that the reallocation of resources for immune-related activities contributes to metabolic dysregulation. Targeted investigation into the cross-talk between immune and metabolic pathways has the potential to illuminate some of this interaction.

Keywords: *Drosophila*, *Francisella*, metabolism, pathophysiology, immune response

OPEN ACCESS

Edited by:
Susanna Valanne, Tampere University, Finland

Reviewed by:
Edan Foley, University of Alberta, Canada
Elodie Ramond, Institut National de la Santé et de la Recherche Médicale (INSERM), France

****Correspondence:***
Crystal M. Vincent
crystal.vincent@imperial.ac.uk
Marc S. Dionne
m.dionne@imperial.ac.uk

Specialty section:
This article was submitted to Comparative Immunology, a section of the journal Frontiers in Immunology

Received: *25 November 2019*
Accepted: *02 June 2020*
Published: *08 July 2020*

Citation:
Vincent CM, Simoes da Silva CJ, Wadhawan A and Dionne MS (2020) Origins of Metabolic Pathology in Francisella-Infected Drosophila. Front. Immunol. 11:1419. doi: 10.3389/fimmu.2020.01419

INTRODUCTION

Infection phenotypes can result from direct interactions between host and pathogen, or indirect interactions which often take the form of trade-offs with, or damage caused by, the host's immune response (1–4). The deleterious effects of immune activity are most often described in the context of an unfettered immune response and the resultant "costs" of said activation [e.g., decreased lifespan (5–7)], or, the by-products of immune effectors [e.g., biochemical interactions; pleiotropic signaling cascades (8–11)].

While the contribution of the host's immune response to infection pathology is acknowledged, a majority of studies focus on pathogen-derived infection phenotypes. Studying direct host-pathogen interactions allows researchers to be on the frontline of infection, dissecting each play and counter-play as host and pathogen battle, often resulting in either elimination of the invader, or death of the host. Work in the fruit fly has supported the assumption that mortality resulting from bacterial invasion is largely due to direct host-pathogen interactions, as lower pathogen loads are often associated with reduced pathology, and bacterial load upon death is predictable (12–14).

Drosophila melanogaster has been used as a model for host-pathogen interactions due to its experimental tractability (10, 15–18). One emergent and exciting field of work is focused on the interaction between infection and host metabolism. Work from our lab and others has identified a number of regulatory factors that play roles in both immune and metabolic activity (10, 11, 19).

For example, infection with the intracellular bacterium *Mycobacterium marinum* leads to a wasting phenotype, with flies losing both glycogen and triglyceride stores over the course of infection (20). This wasting phenotype is mediated, in part, by impaired insulin signaling.

Here we explore the interaction between pathogenesis, immunity and metabolic function. The bacteriostatic antibiotic doxycycline, a close analog of tetracycline, is a standard treatment for infection with *Francisella tularensis* (21). Flies infected with the Gram-negative intracellular bacterium *Francisella novicida* die within 6 days of infection (22). In these infections, the greatest pathogen loads are observed immediately prior to death (22). We show that *F. novicida*—infected flies treated with tetracycline maintain live bacteria at loads less than the initial inoculum and exhibit no difference in survival with their PBS-injected controls. These results suggest that factors dependent on bacterial proliferation contribute to mortality during infection. We find that the metabolic dysregulation observed during this infection is dependent on bacterial load, and we distinguish between immune-derived and pathogen-driven pathology using immune deficient hosts.

MATERIALS AND METHODS

General Experimental Procedures

We used w^{1118}; and w^{1118}; imd^{10191} flies in this study. The w^{1118}; imd^{10191} line is a mutant of the immune deficiency pathway (*imd*); it has a 26-nucleotide deletion that frameshifts the protein at amino acid 179, which is the beginning of the death domain (23). Male flies were collected following eclosion and kept in same-sex vials for 5 to 9 days in groups of 20. Flies were maintained on a standard sugar-yeast diet (10% yeast, 8% fructose, 2% polenta, 0.8% agar, supplemented with 0.75% propionic acid and 0.075% nipagin) at 25°C. Injections were carried out using a pulled-glass capillary needle and a Picospritzer injector system. Flies given tetracycline were transferred to 0.04% tetracycline food (same recipe as above, supplemented with powdered Tetracycline≥98.0% (NT), 87128 Sigma-Aldrich) 6 h after injection. We transferred flies onto tetracycline 6 h post injection for two reasons: first, we wanted to simulate normal usage of antibiotics, and therefore did not administer tetracycline prior to the establishment of infection; second, preliminary studies showed that flies transferred to tetracycline food at 6 and 24 h post infection had similar survival (**Supplementary Figure 1**). We chose to administer tetracycline at 6 h to allow more time to assay pathology in the shorter-lived imd^{10191} mutants.

Bacteria were grown from single colonies overnight at 37°C in a shaking incubator. Wild-type *Francisella novicida* (U112) and tetracycline resistant *Francisella novicida* (U112 pKK219-GFP) were grown in Tryptic Soy Broth supplemented with 5% cysteine. U112 pKK219 cultures were additionally supplemented with 0.1 % tetracycline. Each fly was injected with 50 nl of bacterial culture diluted to $OD_{600} = 0.1$ in PBS. As infection (bacteria) and wounding controls, we had flies that were injected with sterile PBS and anesthetized but otherwise unmanipulated, respectively.

Survival Assays

Survival experiments were performed at 29°C with 15–25 flies/vial. Survival was monitored daily and flies were "tipped" into fresh vials every 3 days; this method for transferring flies permits the provisioning of fresh food without anesthesia.

Bacterial Quantification

For each sample, at the timepoint specified, 1 fly was homogenized in a 100 µl of Tris-EDTA, 1% Proteinase K (NEB, P8107S) solution. Homogenates were incubated for 3 h at 55°C followed by a ten-minute incubation at 95°C. Following incubation, we performed our qPCR protocol as outlined below to determine the number of bacterial colony forming units (CFU). Methods used to estimate bacterial load upon death (BLUD) are described elsewhere (12); briefly, we collected flies within 30 min of death and processed samples as above. Preliminary experiments showed that quantification via qPCR yields similar results to plating (mean CFU: plating−1850, qPCR−2204, **Supplementary Figure 2**). As such, we are confident that this method of quantification provides a good estimate of bacterial number.

Gene Expression—Quantitative Reverse Transcription PCR

For each sample, three flies were homogenized in 100 µl of the single-step RNA isolation reagent TRI Reagent (Sigma), followed by a chloroform extraction and precipitation in isopropanol. The resultant pellet was then washed with 70% ethanol. Pellets were resuspended and subjected to DNase treatment. Revertaid M-MuLV reverse transcriptase and random hexamers (Thermo Scientific) were used to carry out cDNA synthesis. Five-microliter of each cDNA sample was put into a "neat" standard tube; this tube was later used to generate standards which would be used to generate a standard curve for each gene. Each cDNA sample was diluted and this diluted sample used for analysis.

We used qPCRBIO SyGreen Mix for qRT-PCR. The cycling conditions were as follows: Hold 95°C for 10 min, then 45 cycles of 95°C for 15 s, 59°C for 30 s, 72°C for 30 s, followed by a melting curve. To gain a general picture of AMP activity, we assayed a subset of antimicrobial peptides which we have found to be strongly induced during *F. novicida* infection (**Table 1**). Gene expression was calculated based on the standard curve generated during each run, normalized to the value of our housekeeping gene, *RPL1*. Samples from PBS and infected treatments were then divided by the mean value of their uninfected controls to generate expression values relative to uninfected flies. All gene expression experiments were repeated at least twice, with four or more biological replicates per experiment.

Measurement of Glucose and Glycogen Levels

Each sample contained three flies that were homogenized in 75 µl of TE + 0.1% Triton X-100 (Sigma Aldrich), and stored at −80°C. Prior to the assay, samples were incubated for 5 min at 65°C. Following incubation, 10 µl from each sample was loaded

TABLE 1 | Primer sequences used for qRT-PCR.

Gene	Forward	Reverse
AttA	5′- cacaatgtggtgggtcagg−3′	5′- ggcaccatgaccagcatt−3′
Dpt	5′- accgcagtacccactcaatc−3′	5′- cccaagtgctgtccatatcc−3′
Dro	5′- ccatcgaggatcacctgact−3′	5′- ctttaggcgggcagaatg−3′
Mtk	5′- tcttggagcgatttttctgg−3′	5′- tctgccagcactgatgtagc−3′
Rpl1	5′- tccaccttgaagaagggcta−3′	5′- ttgcggatctcctcagactt−3′
U112_lglD	5′- aggataagacctgtctgca−3′	5′- ggttaagcaccgcaagctat−3′

into 3-wells of a 96-well plate. Each well was designated to serve as a measurement for either: control (10 μl sample + 190 μl H_20), glucose [10 μl sample + 190 μl glucose reagent (Sentinel Diagnostics)], or glycogen [10 μl sample + 190 μl glucose reagent + amyloglucosidase (Sigma Aldrich)]. A standard curve was generated by serially diluting a glucose sample of known concentration and adding 190 μl of glucose reagent to 10 μl of each standard. Standards were always run at the same time and in the same plate as samples. Plates were incubated for 1.5–2 h at 37°C following which the absorbance for each well at 492 nm was determined using a plate reader.

Measurement of Triglyceride Levels

Triglycerides were measured using Thin Layer Chromatography (TLC) assays as described elsewhere (24). Briefly, each sample consisted of eight flies; flies were placed in microcentrifuge tubes and stored at −80°C until the time of analysis. To perform the TLC assay, samples were removed from the −80°C freezer and spun down (3 min at 13,000 rpm at 4°C) in 100 μl of a 3:1 (v/v) mix of chloroform and methanol. Flies were then homogenized and subjected to a further "quick spin." Standards were generated using lard dissolved in the same chloroform: methanol solution. We loaded 2 μl of each standard and 20 μl of each sample onto a silica gel glass plate (Millipore). Plates were then placed into a chamber pre-loaded with solvent (a 4:1 (v/v) mix of hexane and ethyl ether) and left to run until the solvent reached a point 1 cm short of the edge of the plate. Plates were then removed from the chamber, allowed to dry, and stained with CAM solution (24). Plates were baked at 80°C for 15–25 min and imaged using a scanner. Triglyceride was quantified in Image J using the Gel Analysis tool.

Statistical Analysis

All data were analyzed in R Studio with R version 3.5.1. Survival data were analyzed using pairwise comparisons Log-Rank tests. BLUD assay correlations were computed by Pearson's correlation. For all other assays, we first tested for normality of data which dictated whether an ANOVA, *t*-test, Kruskal—Wallis analysis of variance, or Wilcoxon test was used to calculate differences between treatments. When appropriate, we performed *post-hoc* Tukey or Dunn analyses to identify specific differences between treatments. All assays were repeated at least twice with the number of biological replicates as indicated.

RESULTS

Effect of Tetracycline During *F. novicida* Infection on w^{1118} Flies

Infected w^{1118} flies given tetracycline lived 4.3x longer than flies kept on normal food (median survival of infected flies: normal food−4 d; tetracycline−17.5 d; **Figure 1A**) and similar survival to their PBS controls (median survival of tetracycline-fed flies: PBS−16 d; *F. novicida*−17.5 d; **Figure 1A**, **Supplementary Table 1**). Flies injected with PBS and fed tetracycline lived significantly longer than their normal food controls, while the opposite was true in uninfected flies (median survival; Uninfected: normal food−27 d, tetracycline−23 d; PBS: normal food−11 d, tetracycline−16 d; **Figure 1A**). As tetracycline is a bacteriostatic antibiotic and thus prevents bacteria from proliferating rather than actively killing bacterial cells (21), we assayed bacterial load over the course of infection in tetracycline-fed and normal food flies. Confirming our preliminary findings, flies kept on normal food exhibited an exponential increase in bacterial numbers over the first 3 days of infection, while flies given tetracycline maintained a low level of bacteria (**Figure 1B**). Bacterial load differed significantly between normal food and tetracycline flies for all time points beyond 24 h. Furthermore, bacterial loads in normal food flies differed significantly between all consecutive time points apart from days 1 and 2. For tetracycline-fed flies, there was a significant increase in bacterial load between day 3 and day 5, but no difference between days 1 and 3, nor days 5 and 11 (**Figure 1B**).

Because pathogen detection is required for the initiation of the antimicrobial peptide (AMP) response (25–27), we sought to determine how the changing bacterial load on normal food, and the static load on tetracycline food, were affecting AMP expression. We found that 24 h post-infection, AMP expression did not differ between flies given tetracycline and those on normal food (**Figure 1C**, **Supplementary Figure 3**). This finding was unsurprising as bacterial loads did not differ significantly between the two groups at this time. In contrast, by 72 h post-infection, all four of the AMPs measured had greater induction in normal food flies compared to tetracycline-fed (**Figure 1D**).

Having confirmed that infection with *F. novicida* is lethal, and characterized by rapid bacterial proliferation and AMP induction, we wanted to determine if *F. novicida* infection had any effect on host metabolism. Infected tetracycline-fed flies live longer, have lower bacterial loads, and reduced AMP induction; thus, we anticipated that the metabolism of these flies would not be affected in the same way as flies that were not given tetracycline. However, we found that flies infected with the non-lethal pathogen *Micrococcus luteus* exhibit metabolic dysregulation similar to what we here observe, suggesting that this phenotype is independent of moribundity [**Supplementary Figure 4**, (28)]. During the early stages of infection, there was no effect of tetracycline or infection on metabolism (**Figures 1E,F**). However, by 72 h post-infection, infected flies kept on normal food had significantly higher levels of glucose, as well as depleted glycogen and triglyceride stores. Infection did not affect glucose, glycogen, or triglyceride levels in tetracycline-fed flies (**Figures 1F,G**). Collectively,

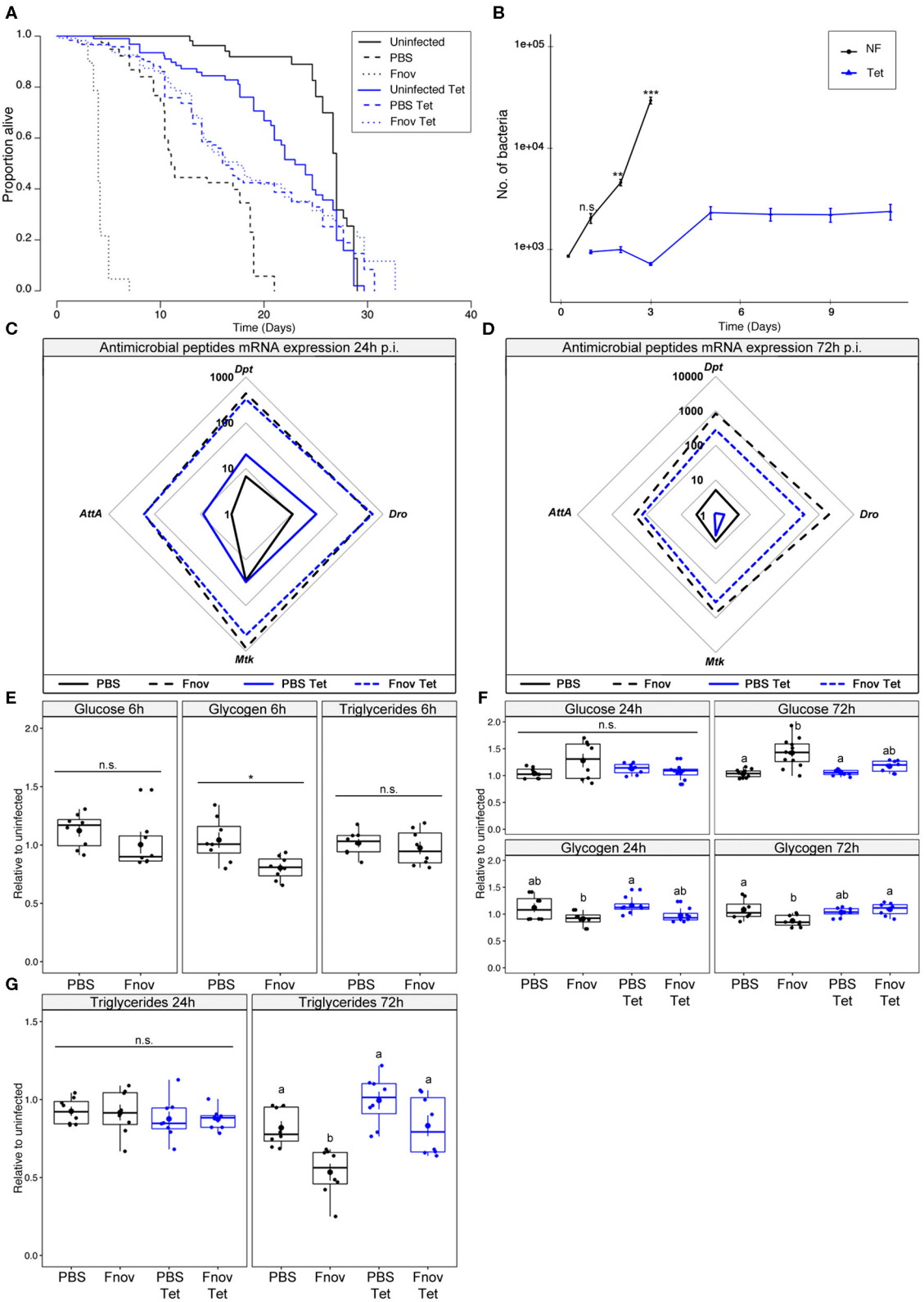

FIGURE 1 | Tetracycline alleviates pathology associated with *F. novicida* infection. Five to nine days old adult w^{1118} flies infected with *F. novicida* (OD_{600} = 0.1, or ~1,000 bacteria). Animals fed tetracycline were switched to tetracycline food 6 h post-infection. In all plots, black and blue tracings represent normal and tetracycline

(Continued)

FIGURE 1 | food, respectively. Significance codes: *** < 0.001, ** < 0.01, * < 0.05. Survival **(A)** *F. novicida* -infection is represented by dotted lines. Uninfected and PBS controls are represented by solid and dashed lines, respectively. Infected, tetracycline-fed flies live 4.3x longer than flies kept on normal food. Median survival of infected flies: tetracycline−17.5 d; normal food−4 d (Log-Rank = 745.6, df = 5, $n = 602$, $p \leq 2e\text{-}16$). Survivals were repeated 2 or 3 times with 20 flies/treatment/repeat. A full-factorial report of statistics can be found in **Supplementary Table 1**. Bacterial quantification **(B)** tetracycline-fed flies (Tet) had significantly lower bacterial loads at both 2 and 3 d post infection (Kruskal-Wallis = 112.47, df = 11, $p = 2.2e\text{-}16$; Dunn's *post hoc*: 48 h–$p = 0.001$, 72 h–$p = 2.1e\text{-}11$). A significant increase in bacterial load was observed between days 3 and 5 in tetracycline-fed flies (Dunn's *post hoc*: tetracycline 2d—tetracycline 5 d, $p = 0.008$), but remained constant from that point on. Normal food (NF) flies show an exponential increase in bacterial load throughout infection. Markers indicate means and bars represent SE. Bacterial quantifications were repeated twice, with $n = 8$ samples/treatment/repeat. Spider plots showing antimicrobial peptide transcript levels 24 h **(C)** and 72 h **(D)** post infection. All tracings are relative to uninfected individuals of the same treatment. Solid and dashed lines represent PBS and *F. novicida* injection, respectively. The area contained within the innermost quadrilateral represents induction levels falling between one and ten times that of the uninfected controls. The middle and outer quadrilaterals represent 10–100 and 100–1,000-fold induction, respectively. Antimicrobial peptide assays were repeated twice, with four samples/treatment/repeat. These data are also shown, represented differently, in **Supplementary Figure 3A**. Metabolism **(E)** glucose, glycogen and triglyceride levels are unchanged at an early point (6 h post-infection) of infection. **(F)** Glucose and glycogen levels 24 and 72 h post-infection. Infection led to a significant increase in glucose levels during late infection in normal food flies (Kruskal-Wallis = 20.007, df =3, $p = 1.7e\text{-}04$; Dunn's *post hoc*: normal food PBS—normal food Fnov = 2.6e-04). Glycogen stores were depleted by infection in normal food flies (AOV: df =3, $n = 28$, $F = 4.855$, $p = 7.6e\text{-}03$, Tukey's HSD: normal food PBS—normal food Fnov = 0.015). Groups sharing the same letter are not significantly different. **(G)** Infection led to a significant depletion of triglycerides in infected normal food flies (AOV: df =3, $n = 28$, $F = 11.86$, $p = 3.4e\text{-}05$, Tukey's HSD: normal food PBS—normal food Fnov, $p = 0.006$). Infection did not affect any measure of metabolism in tetracycline-fed flies. Large circular markers indicate means while smaller circles represent individual data points. Horizontal bar within each box represents the median. The bottom and top lines of the box represent the 1st and 3rd quartiles, respectively. Whiskers represent either the maximum and minimum values, or, the maximum and minimum values falling within 1.5x the interquartile range, in which case outliers are indicated. Metabolic assays were repeated 2 or 3 times, with four samples/treatment/repeat.

these data show that tetracycline reduces the pathology of *F. novicida* infection.

Effect of Tetracycline During *F. novicida* Infection on *imd*^{10191} Flies

Mutants of the Imd pathway exhibit poor AMP induction in response to infection with Gram-negative bacteria and impaired survival during infection with *F. novicida* (22, 25, 29, 30), so we did not measure AMPs in these flies. Instead, we tested whether treatment with tetracycline enhances survival in *imd*^{10191} mutants to a level similar to that observed in w^{1118} flies. In addition, as there is an assumed "cost of immunity" (4, 31–33), infection of *imd*^{10191} mutants with *F. novicida* would allow us to determine if part of the observed metabolic dysregulation during infection in w^{1118} is caused by *imd*-dependent immune activation. Any observed differences in metabolism between w^{1118} and *imd*^{10191} flies are unlikely to result from differential resource availability as we found no difference in triglyceride levels between the two (**Supplementary Figure 5**).

Infected *imd*^{10191} flies given tetracycline lived 3.6x longer than flies kept on normal food (median survival of infected flies: tetracycline−11 days; normal food−3 days; **Figure 2A**, **Supplementary Table 2**). In the absence of infection, tetracycline had a slightly positive, though non-significant effect on survival, with uninfected normal food and tetracycline flies having similar median survival times (12 and 13.3 d, respectively).

In contrast to our observation in w^{1118}, tetracycline did not affect survival of PBS-injected *imd*^{10191} mutants. Bacterial load differed significantly between tetracycline and normal food *imd*^{10191} flies for all time points measured (**Figure 2B**). Bacterial load in normal food flies differed significantly between all consecutive time points, but remained constant in tetracycline-fed flies, excluding day 7, where values were significantly higher (**Figure 2B**). As both survival and bacterial proliferation in *imd*^{10191} mutants resembled the overall pattern observed in w^{1118} flies, we tested whether the metabolic dysregulation was also present during this infection. Infection affected neither glucose nor glycogen, independent of whether flies were fed tetracycline (**Figures 2C,D**). Similar to what we observed in w^{1118}, during late-stage infection, flies kept on normal food had significant depletion of triglycerides compared to PBS controls. Triglyceride levels were unaffected by infection in tetracycline-fed flies (**Figure 2E**).

Pathology of Infection With Tetracycline-Resistant *F. novicida*

Flies kept on tetracycline food post-injection showed restricted bacterial growth and failed to exhibit metabolic dysregulation over the course of infection (**Supplementary Figure 6**). To confirm that the absence of metabolic pathology in tetracycline-fed flies was the result of low pathogen loads, rather than tetracycline having a protective effect on host physiology, we repeated all experiments with tetracycline-resistant *F. novicida* (U112 pKK219—GFP, herein referred to as TetR *F. novicida*). Flies infected with TetR *F. novicida* have a median survival of 5 d (**Supplementary Figure 7A**), 1 day longer than infection with wild-type *F. novicida*. We attribute this difference in survival to the decreased growth rate that typically accompanies antibiotic resistance in bacteria [**Supplementary Figure 7B** (34, 35)], despite this difference being marginal at all timepoints assayed *in vivo* (**Figure 3A**). There was no difference in survival between normal food and tetracycline-fed flies infected with TetR *F. novicida*, confirming that the extended lifespan observed in TetR-infected flies (fed tetracycline) is not the result of tetracycline having an unidentified effect on the flies (**Supplementary Figure 7A**).

Tetracycline-resistant *F. novicida* induced AMP expression to levels equal to or greater than that of wild-type bacteria (**Figures 3B,C**). This confirmed that tetracycline alone did not inhibit AMP induction. To ensure that we were looking at a comparable stage of infection, we assayed metabolism at 96 h (24 h prior to death) during *TetR F. novicida* infection, rather

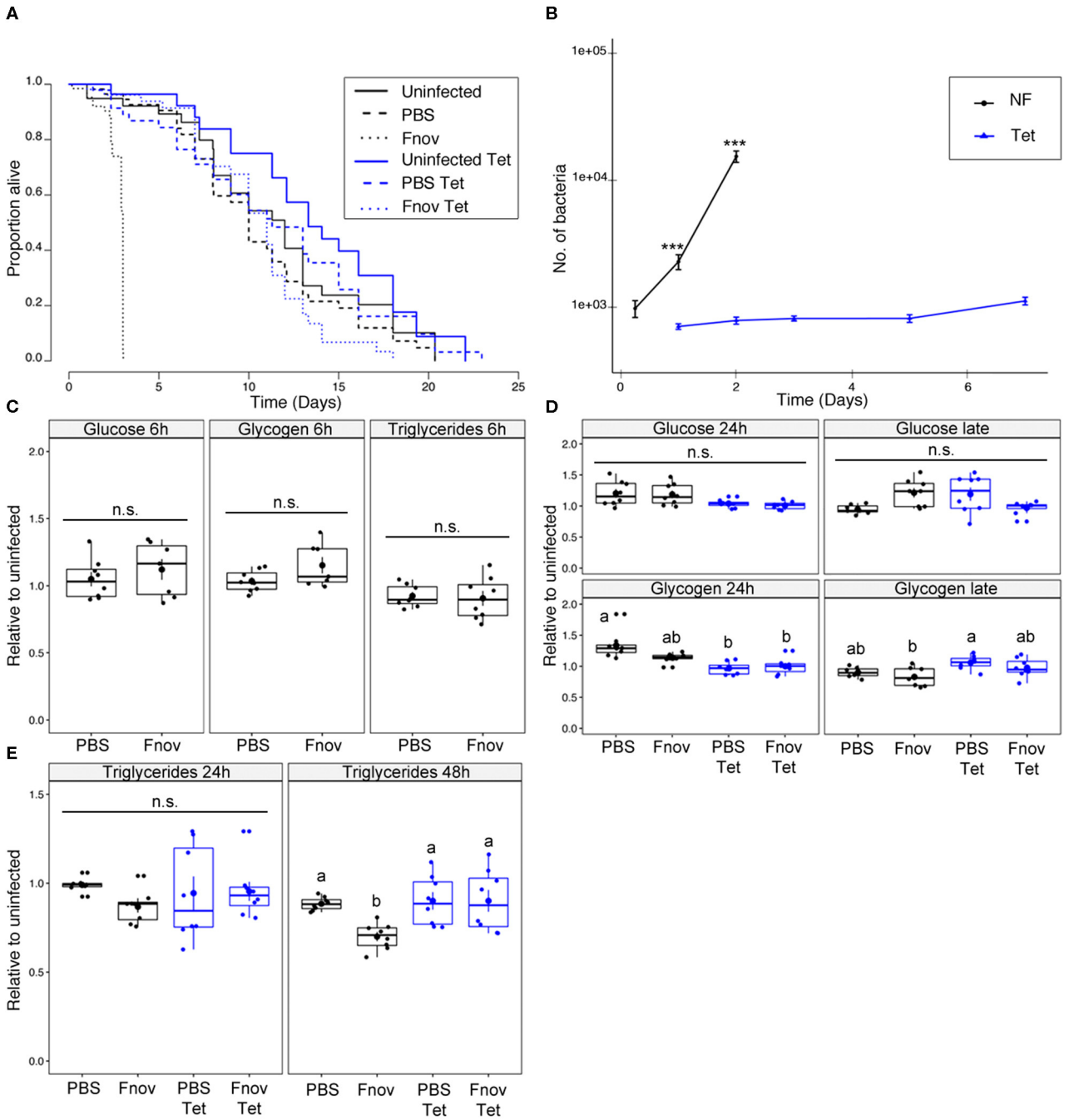

FIGURE 2 | *imd*^{101091} mutants only partly reproduce metabolic phenotype of *F. novicida* infection. Five to nine days old adult *imd*^{10191} flies infected with *F. novicida* (OD_{600} = 0.1, or ~1,000 bacteria). Animals fed tetracycline were switched to tetracycline food 6 h post-infection. In all plots, black and blue tracings represent normal and tetracycline food, respectively. Significance codes: *** < 0.001. Survival **(A)** *F. novicida* -infection is represented by dotted lines. Uninfected and PBS controls are represented by solid and dashed lines, respectively. Infected, tetracycline-fed flies lived 3.6x longer than flies kept on normal food; median survival of infected flies: tetracycline−11 d; normal food−3d (Log-Rank = 314.7, df = 5, n = 602, p ≤ 2e-16). Survivals were repeated 2 or 3 times with 20 flies/treatment/repeat. A full-factorial report of statistics can be found in **Supplementary Table 2**. Bacterial quantification **(B)** tetracycline-fed flies (Tet) have significantly lower bacterial loads both 1 and 2 d post infection (Kruskal-Wallis = 105.03, df = 7, p = 2.2e-16; Dunn's *post hoc*: 24 h–p = 1.3e-06, 48 h–p = 9.2e-11). Normal food (NF) flies show an exponential increase in bacterial load throughout infection. Load in tetracycline-fed flies remained constant throughout infection. Markers indicate means and bars represent SE. Bacterial quantifications were repeated twice, n = 8 samples/treatment/repeat. Metabolism **(C)** glucose, glycogen and triglyceride levels at an early point (6 h post-infection) of infection. **(D)** Glucose and glycogen levels "late" in infection (48 and 72 h for normal food and tetracycline-fed flies, respectively). Neither infection

(Continued)

FIGURE 2 | nor tetracycline affected glucose or glycogen levels. Groups sharing the same letter are not significantly different. **(E)** Infection led to a significant depletion of triglycerides during late infection in normal food flies (AOV: df =3, $n = 28$, $F = 5.48$, $p = 4.3e\text{-}02$, Tukey's HSD: normal food PBS—normal food Fnov, $p = 0.021$). Infection had no effect on tetracycline-fed flies. Large circular markers indicate means while smaller circles represent individual data points. Horizontal bar within each box represents the median. The bottom and top lines of the box represent the 1st and 3rd quartiles, respectively. Whiskers represent either the maximum and minimum values, or, the maximum and minimum values falling within 1.5x the interquartile range, in which case outliers are indicated. Groups sharing the same letter are not significantly different. Metabolic assays were repeated twice, with four samples/treatment/repeat.

than 72 h as with the wild-type *F. novicida*. Neither glucose nor glycogen levels differed between *TetR F. novicida* and wild-type *F. novicida*—infected flies (**Figure 3D**). TetR *F. novicida*—infected flies exhibited metabolic dysregulation mirroring that of wild-type *F. novicida* infections.

We measured bacterial load upon death (BLUD) to determine whether the increased severity of metabolic dysregulation we observe over the course of infection is dependent on bacterial number. We found that BLUD did not differ significantly across treatments (**Figure 4**). Despite exhibiting the least amount of metabolic dysregulation, at their time of death, imd^{10191} flies exhibited the highest pathogen burden, harboring on average, 37 and 59% more bacteria than w^{1118} flies infected with wild-type and TetR *F. novicida*, respectively (*F. novicida*: imd^{10191}—75 938 ± 8757, w^{1118}—55 317 ± 4622; TetR *F. novicida* 47 505 ± 5150; mean ± se). We did not observe a significant correlation between time of death and bacterial load in any infection (**Figure 4**).

DISCUSSION

We have shown that infection with *F. novicida* leads to metabolic dysregulation in w^{1118} flies and that part of this pathology results from a direct interaction between host and pathogen, as pathology increased concomitant with bacterial load. However, activation of the *imd*-derived antimicrobial peptide response also contributes to this phenotype as we found both that: *imd* mutants do not exhibit similar levels of dysregulation, and; w^{1118} flies treated with tetracycline exhibited both a strong induction of AMPs, as well as a trend toward hyperglycaemia and triglyceride depletion (**Figure 1**). Whilst these subtle trends found in tetracycline-treated flies could be attributed to low bacterial loads (rather than immune activation), hyperglycaemia and triglyceride depletion were not seen in tetracycline-treated *imd* mutants, demonstrating that immune costs—rather than bacterial load—were responsible. However, that we do see triglyceride depletion in normal-food *imd* flies, suggests that at least part of this phenotype is pathogen-driven, possibly resulting from host triglyceride usurpation by the bacteria (36–38).

It is still possible that the metabolic pathology we observe is a consequence of *Toll* pathway activation, notwithstanding the fact that most immune activation in this infection is *imd*-dependent. Others have observed that Gram-negative infections can activate the *Toll* pathway (9, 39–41), and Toll pathway activation has been associated with effects on the insulin signaling pathway that could drive the metabolic effects we see in this infection. This possibility—that bacterial sensing via the *Toll* pathway is the critical driver of metabolic pathology in most bacterial infections in *Drosophila,* independent of the specific type of bacterium—is an interesting one for future study.

One further possibility is that *F. novicida* makes direct use of host-derived resources and therefore is responsible for some of the changes in host metabolism we observe. *Francisella* spp. preferentially use glucose as a carbon source (38, 42). It has also been shown that *F. tularensis* cannot use glycogen as a carbon source (43); thus, if glycogen depletion were the result of bacterial consumption of nutrients, the expected pathway would be via bacterial depletion of free sugar triggering host glycogenolysis. We observe that glycogen depletion is accompanied by increases in free sugar, such immunometabolic switches are well-known (44) and have been shown to be instrumental in the provisioning of resources to haemocytes during infection in *D. melanogaster* (45), further suggesting that metabolic demands of the host—rather than pathogen—account for much of the observed effect.

During intracellular replication, *F. novicida* has been shown to metabolize glycerol for gluconeogenesis (38), supporting the possibility that the observed triglyceride depletion was bacterial-driven. However, in *D. melanogaster*, proliferation of *F. novicida* occurs predominantly extracellularly (22), and it is unclear how large of an impact these bacteria could have on host triglyceride levels. None of this precludes the possibility that *F. novicida* triggers host catabolism of endogenous stores to convert them into a form it can use itself. However, the fact that hyperglycaemia and loss of triglyceride and glycogen stores is seen in other bacterial infections, does imply that this reflects an aspect of the host response (20, 46), and the presence of hyperglycaemia in this infection suggests that the amount of sugar being released exceeds the amount consumed by the bacteria.

Finally, the metabolic pathology observed may be part of a moribund phenotype, with an overall worsening of condition as the animal approaches death. However, if this were the case, we would not expect to observe said pathology during infection with non-lethal bacteria like *M. luteus* (**Supplementary Figure 4**). Furthermore, if metabolic dysregulation and bacterial load are decoupled, as should be the case if it is caused by moribundity, we would have expected tetracycline-fed flies to exhibit metabolic dysregulation as this infection persists for several days and activates the immune response to levels comparable to flies fed on normal food.

Together these data indicate that in this infection *imd* activation is necessary, but not sufficient, for metabolic pathology. Tetracycline-fed flies of both genotypes maintain constant metabolite levels, and w^{1118} maintain AMP levels, throughout the duration of the infection (**Supplementary Figure 6**); this may be due in part, to an effect of tetracycline on host physiology and metabolism (47). We found no difference in triglyceride levels between uninfected, normal food flies of the two genotypes (**Supplementary Figure 7**); thus, the differential usage of energy stores between w^{1118} and

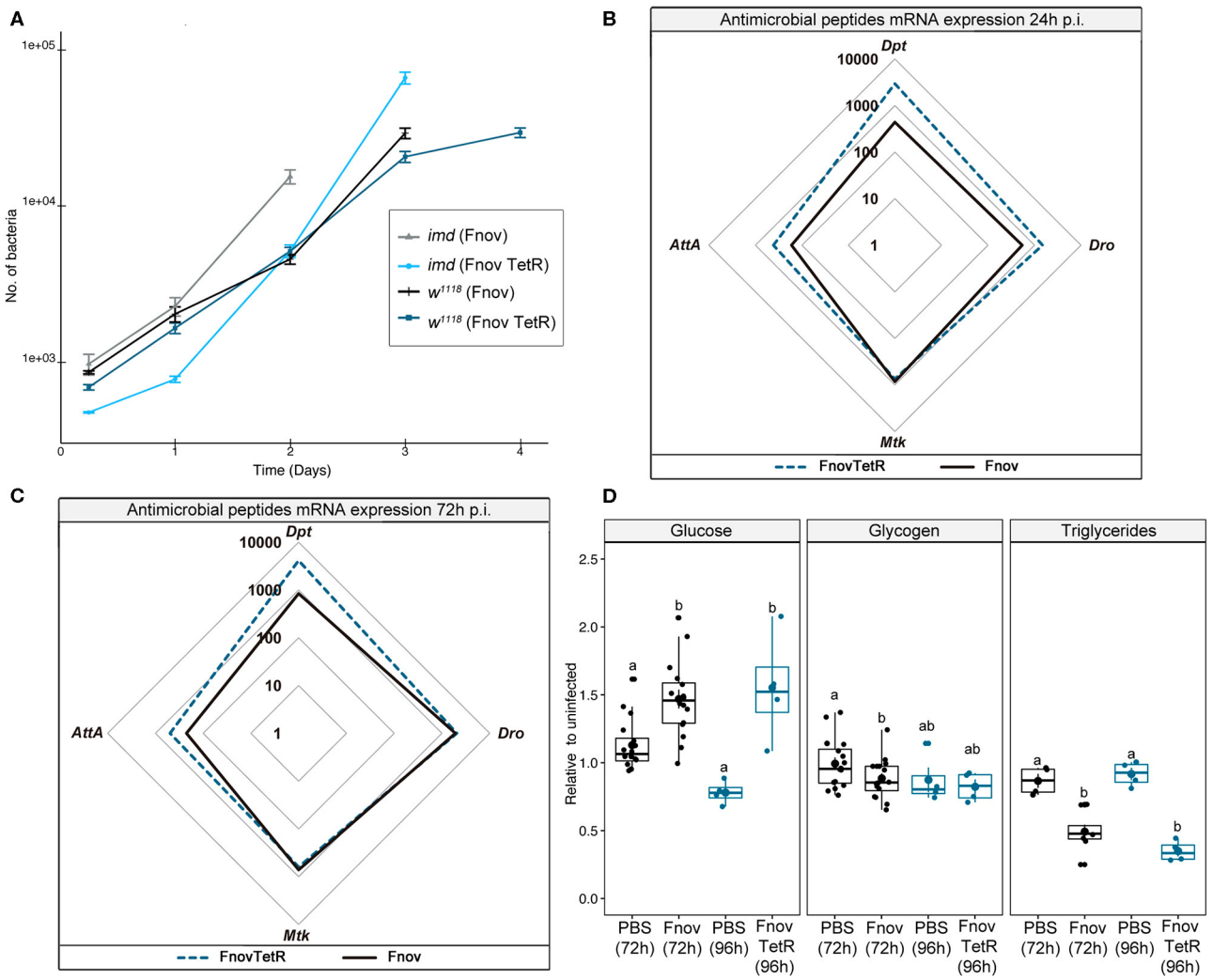

FIGURE 3 | Tetracycline alone is not protective. Five to nine days old adult w^{1118} flies infected with tetracycline resistant *F. novicida* (TetR: $OD_{600} = 0.1$). Tet-R-infected animals were put on tetracycline food at the time of injection. Bacterial quantification **(A)** TetR is indicated in dark blue and light blue, and wild-type *F. novicida* in black and gray, in w^{1118} and imd^{10191} flies, respectively. TetR proliferate at a similar rate to wild-type *F. novicida*. Circular markers indicate means and bars represent SE. Bacterial quantifications were repeated twice, $n = 8$ samples/treatment/repeat. Spider plots showing antimicrobial peptide transcript levels 24 h **(B)** and 72 h **(C)** post-infection. All tracings are relative to uninfected individuals of the same treatment. TetR and wild-type *F. novicida* are indicated in dark blue dashed and solid black lines, respectively. The area contained within the innermost quadrilateral represents induction levels falling between one and ten times that of the uninfected controls. The middle and outer quadrilaterals represent 10–100 and 100–1,000-fold induction, respectively. Antimicrobial peptide assays were repeated twice, with four samples/treatment/repeat. These data are also shown, represented differently, in **Supplementary Figure 3B**. Metabolism **(D)** late-stage infection (normal food−72 h; tetracycline−96 h) glucose, glycogen and triglyceride levels. TetR and wild-type *F. novicida* are indicated in dark blue and black, respectively. Infection with both wild-type and TetR *F. novicida* led to hyperglycaemia and depleted triglycerides, relative to their PBS controls (Glucose: Kruskal-Wallis = 11.98, df = 3, $p = 1.4e\text{-}5$; Dunn's *post hoc*: TetR−$p = 5.3e\text{-}04$, wild-type−$p = 2.8e\text{-}3$; Triglycerides: Kruskal-Wallis = 24.66, df = 3, $p = 3.06e\text{-}6$; Dunn's *post hoc*: TetR−$p = 2.1e\text{-}05$, wild-type−$p = 4.6e\text{-}4$). Glycogen levels were unaffected in the overall model (Kruskal-Wallis = 7.171, df = 3, $p = 6.6e\text{-}2$), but analysis of only wild-type *F. novicida* - infected flies showed reduced glycogen relative to PBS controls (Wilcoxon = 164.5, $p = 3.2e\text{-}2$) whilst TetR *F. novicida* did not (Wilcoxon = 7, $p = 0.8$). Overall, we found no difference across metabolism between the two *F. novicida* strains. Large circular markers indicate means while smaller circles represent individual data points. Horizontal bar within each box represents the median. The bottom and top lines of the box represent the 1st and 3rd quartiles, respectively. Whiskers represent either the maximum and minimum values, or, the maximum and minimum values falling within 1.5x the interquartile range, in which case outliers are indicated. Groups sharing the same letter are not significantly different. Metabolic assays were repeated 2 or 3 times, with four samples/treatment/repeat.

imd^{10191}, is unlikely the result of disparate resource availability. Previous work in our lab suggests that during bacterial infection, flies may disrupt insulin signaling as a means of conserving energy for immune-related activities, leading to metabolic dysregulation (20). In showing that in the absence of *imd*, part of the metabolic phenotype observed during w^{1118} infection cannot be reproduced, the current work supports this supposition. Additionally, as *imd* mutants retain an active Toll response, this

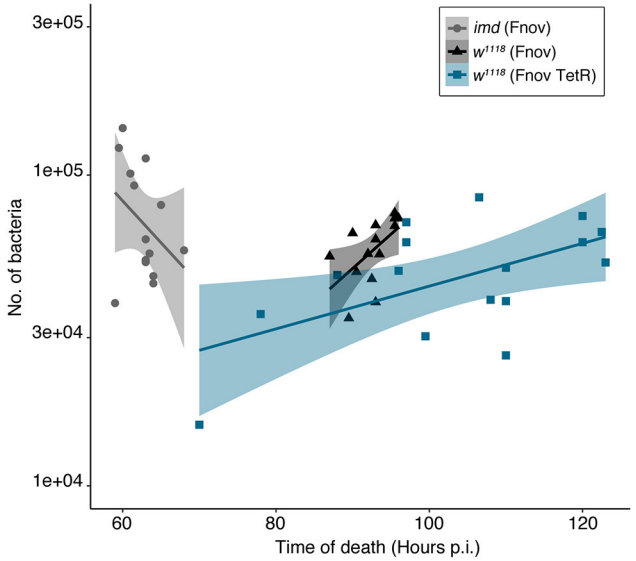

FIGURE 4 | Bacterial load upon death is consistent within and across infections. Bacterial load in flies was measured within 30 min of death. We found that BLUD did not differ significantly across treatments (Kruskal-Wallis = 5.492, df = 2, $p = 0.064$). Time of host death did not correlate with bacterial load in any of the infections assayed (Pearson's correlation: *F. novicida*: imd^{10191} — $t = -1.677$, df = 12, $p = 0.119$, w^{1118} — $t = 0.86363$, df = 13, $p = 0.403$; TetR *F. novicida*: w^{1118} — $t = 1.5432$, df = 15, $p = 0.1436$). imd^{10191} flies had the highest pathogen burden, harboring on average, 37 and 59% more bacteria than w^{1118} flies infected with wild-type and TetR *F. novicida*, respectively (*F. novicida*: imd^{10191} — 75 938 ± 8757, w^{1118} — 55 317 ± 4622; TetR *F. novicida* 47 505 ± 5150; mean ±se). *Francisella novicida* — infected imd^{10191} and w^{1118} flies are indicated in gray and black, respectively. TetR *F. novicida* — infected w^{1118} flies are indicated in blue. Each marker represents an individual fly. Standard error is demarcated by shaded area. BLUD assay was repeated twice, with six to eight samples/treatment/repeat.

also demonstrates that Toll is not—at least entirely—responsible for the observed phenotype.

Flies infected with TetR *F. novicida* and kept on tetracycline-food exhibited near-identical infection pathology—albeit slightly protracted—to wild-type *F. novicida* infection. Interestingly, we found that independent of host and pathogen identity and their interaction, flies had similar pathogen loads at the time of death, despite there being a 1–2 d difference in median survivals (**Figure 4**); this observation further supports the idea that there is a critical bacterial load beyond which hosts cannot survive (12).

The metabolic dysregulation observed during infection is likely the result of several different factors. That multiple bacteria cause some sort of metabolic shift in their hosts suggests that both bacterial and host factors contribute to the phenotype; elucidating the need to understand the different requirements of pathogens and how these are met in a given host. Further investigation into the cross-talk between host immune and metabolic pathways under different infections has the potential to reveal some of this interaction.

DATA AVAILABILITY STATEMENT

All datasets generated for this study are included in the article/**Supplementary Material**.

AUTHOR CONTRIBUTIONS

CV conceived, designed and performed experiments, analyzed data, and wrote the manuscript. CS performed experiments, prepared figures, and edited the manuscript. AW performed experiments and edited the manuscript. MD conceived of experiments and edited the manuscript. All authors contributed to the article and approved the submitted version.

FUNDING

Funders have funded this research by paying salaries (CV, CS, and MD) and consumables but were not involved in the design of this project. Open access fees will be paid via institutional open access funds. This work was supported by MRC Research Grant MR/R00997X/1 and Wellcome Trust Investigator Award 207467/Z/17/Z.

ACKNOWLEDGMENTS

We are grateful to the reviewers whose comments improved the clarity and structure of this manuscript.

SUPPLEMENTARY MATERIAL

The Supplementary Material for this article can be found online at: https://www.frontiersin.org/articles/10.3389/fimmu.2020.01419/full#supplementary-material

REFERENCES

1. Sadd BM, Siva-Jothy MT. Self-harm caused by an insect's innate immunity. *Proc Biol Sci.* (2006) 273:2571–4. doi: 10.1098/rspb.2006.3574
2. McMillan LE, Miller DW, Adamo SA. Eating when ill is risky: immune defense impairs food detoxification in the caterpillar Manduca sexta. *J Exp Biol.* (2018) 221:jeb173336. doi: 10.1242/jeb.173336
3. Okin D, Medzhitov R. Evolution of inflammatory diseases. *Curr Biol.* (2012) 22:R733–40. doi: 10.1016/j.cub.2012.07.029
4. Moret Y, Schmid-Hempel P. Survival for immunity: the price of immune system activation for bumblebee workers. *Science.* (2000) 290:1166–8. doi: 10.1126/science.290.5494.1166
5. Cao Y, Chtarbanova S, Petersen AJ, Ganetzky B. Dnr1 mutations cause neurodegeneration in Drosophila by activating the innate immune response in the brain. *PNAS.* (2013) 110:E1752–60. doi: 10.1073/pnas.1306220110
6. Libert S, Chao Y, Chu X, Pletcher SD. Trade-offs between longevity and pathogen resistance in *Drosophila melanogaster* are mediated by NFκB signaling. *Aging Cell.* (2006) 5:533–43. doi: 10.1111/j.1474-9726.2006.00251.x
7. Fernando MDA, Kounatidis I, Ligoxygakis P. Loss of Trabid, a new negative regulator of the Drosophila Immune-Deficiency pathway at the level of TAK1, reduces life span. *PLoS Genet.* (2014) 10:e1004117. doi: 10.1371/journal.pgen.1004117

8. Shang Y, Smith S, Hu X. Role of Notch signaling in regulating innate immunity and inflammation in health and disease. *Protein Cell.* (2016) 7:159–74. doi: 10.1007/s13238-016-0250-0
9. DiAngelo JR, Bland ML, Bambina S, Cherry S, Birnbaum MJ. The immune response attenuates growth and nutrient storage in Drosophila by reducing insulin signaling. *PNAS.* (2009) 106:20853–58. doi: 10.1073/pnas.0906749106
10. Clark RI, Tan SWS, Péan CB, Roostalu U, Vivancos V, Bronda K, et al. MEF2 is an in vivo immune-metabolic switch. *Cell.* (2013) 155:435–47. doi: 10.1016/j.cell.2013.09.007
11. Sharrock J, Estacio-Gomez A, Jacobson J, Kierdorf K, Southall TD, Dionne MS. fs(1)h controls metabolic and immune function and enhances survival via AKT and FOXO in Drosophila. *Dis Models Mech.* (2019) 12:dmm037259. doi: 10.1242/dmm.037259
12. Duneau D, Ferdy J-B, Revah J, Kondolf H, Ortiz GA, Lazzaro BP, et al. Stochastic variation in the initial phase of bacterial infection predicts the probability of survival in *D. melanogaster*. *eLife.* (2017) 6:e28298. doi: 10.7554/eLife.28298
13. Khalil S, Jacobson E, Chambers MC, Lazzaro BP. Systemic bacterial infection and immune defense phenotypes in *Drosophila melanogaster*. *J Vis Exp*. (2015) 99:e52613. doi: 10.3791/52613
14. Vonkavaara M, Telepnev MV, Rydén P, Sjöstedt A, Stöven S. *Drosophila melanogaster* as a model for elucidating the pathogenicity of Francisella tularensis. *Cell Microbiol.* (2008) 10:1327–38. doi: 10.1111/j.1462-5822.2008.01129.x
15. Dionne MS, Schneider DS. Models of infectious diseases in the fruit fly *Drosophila melanogaster*. *Dis Model Mech.* (2008) 1:43–9. doi: 10.1242/dmm.000307
16. Pandey UB, Nichols CD. Human Disease Models in *Drosophila melanogaster* and the role of the fly in therapeutic drug discovery. *Pharmacol Rev.* (2011) 63:411–36. doi: 10.1124/pr.110.003293
17. Dionne MS, Ghori N, Schneider DS. *Drosophila melanogaster* is a genetically tractable model host for *Mycobacterium marinum*. *Infect Immun.* (2003) 71:3540–50. doi: 10.1128/IAI.71.6.3540-3550.2003
18. Troha K, Buchon N. Methods for the study of innate immunity in *Drosophila melanogaster*. *Wiley Interdiscip Rev Dev Biol.* (2019) 8:e344. doi: 10.1002/wdev.344
19. Péan CB, Schiebler M, Tan SWS, Sharrock JA, Kierdorf K, Brown KP, et al. Regulation of phagocyte triglyceride by a STAT-ATG2 pathway controls mycobacterial infection. *Nat Commun.* (2017) 8:1–11. doi: 10.1038/ncomms14642
20. Dionne MS, Pham LN, Shirasu-Hiza M, Schneider DS. Akt and FOXO dysregulation contribute to infection-induced wasting in Drosophila. *Curr Biol.* (2006) 16:1977–85. doi: 10.1016/j.cub.2006.08.052
21. Chopra I, Roberts M. Tetracycline antibiotics: mode of action, applications, molecular biology, and epidemiology of bacterial resistance. *Microbiol Mol Biol Rev.* (2001) 65:232–60. doi: 10.1128/MMBR.65.2.232-260.2001
22. Moule MG, Monack DM, Schneider DS. Reciprocal analysis of *Francisella novicida* infections of a *Drosophila melanogaster* model reveal host-pathogen conflicts mediated by reactive oxygen and imd-regulated innate immune response. *PLOS Pathog.* (2010) 6:e1001065. doi: 10.1371/journal.ppat.1001065
23. Pham LN, Dionne MS, Shirasu-Hiza M, Schneider DS. A specific primed immune response in Drosophila is dependent on phagocytes. *PLoS Pathog.* (2007) 3:e26. doi: 10.1371/journal.ppat.0030026
24. Al-Anzi B, Sapin V, Waters C, Zinn K, Wyman RJ, Benzer S. Obesity-blocking neurons in Drosophila. *Neuron.* (2009) 63:329–41. doi: 10.1016/j.neuron.2009.07.021
25. Gottar M, Gobert V, Michel T, Belvin M, Duyk G, Hoffmann JA, et al. The Drosophila immune response against Gram-negative bacteria is mediated by a peptidoglycan recognition protein. *Nature.* (2002) 416:640–4. doi: 10.1038/nature734
26. Choe K-M, Werner T, Stöven S, Hultmark D, Anderson KV. Requirement for a peptidoglycan recognition protein (PGRP) in Relish activation and antibacterial immune responses in Drosophila. *Science.* (2002) 296:359–62. doi: 10.1126/science.1070216
27. Tanji T, Ip YT. Regulators of the Toll and Imd pathways in the Drosophila innate immune response. *Trends Immunol.* (2005) 26:193–8. doi: 10.1016/j.it.2005.02.006
28. Nehme NT, Quintin J, Cho JH, Lee J, Lafarge M-C, Kocks C, et al. Relative roles of the cellular and humoral responses in the Drosophila host defense against three Gram-positive bacterial infections. *PLoS ONE.* (2011) 6:e14743. doi: 10.1371/journal.pone.0014743
29. Lemaitre B, Kromer-Metzger E, Michaut L, Nicolas E, Meister M, Georgel P, et al. A recessive mutation, immune deficiency (imd), defines two distinct control pathways in the Drosophila host defense. *Proc Natl Acad Sci USA.* (1995) 92:9465–9. doi: 10.1073/pnas.92.21.9465
30. Kaneko T, Goldman WE, Mellroth P, Steiner H, Fukase K, Kusumoto S, et al. Monomeric and polymeric Gram-negative peptidoglycan but not purified LPS stimulate the Drosophila IMD pathway. *Immunity.* (2004) 20:637–49. doi: 10.1016/S1074-7613(04)00104-9
31. Jacot A, Scheuber H, Brinkhof MWG. Costs of an induced immune response on sexual display and longevity in field crickets. *Evolution.* (2004) 58:2280. doi: 10.1554/03-660
32. Kelly CD. Reproductive and physiological costs of repeated immune challenges in female Wellington tree weta (Orthoptera: Anostostomatidae). *Biol J Linnean Soc.* (2011) 104:38–46. doi: 10.1111/j.1095-8312.2011.01714.x
33. McKean KA, Nunney L. Increased sexual activity reduces male immune function in *Drosophila melanogaster*. *PNAS.* (2001) 98:7904–9. doi: 10.1073/pnas.131216398
34. Wiesch PS zur, Engelstädter J, Bonhoeffer S. Compensation of fitness costs and reversibility of antibiotic resistance mutations. *Antimicrob Agents Chemother.* (2010) 54:2085–95. doi: 10.1128/AAC.01460-09
35. Andersson DI, Hughes D. Antibiotic resistance and its cost: is it possible to reverse resistance? *Nat Rev Microbiol.* (2010) 8:260–71. doi: 10.1038/nrmicro2319
36. Barisch C, Soldati T. Mycobacterium marinum degrades both triacylglycerols and phospholipids from its dictyostelium host to synthesise its own triacylglycerols and generate lipid inclusions. *PLOS Pathog.* (2017) 13:e1006095. doi: 10.1371/journal.ppat.1006095
37. Herker E, Ott M. Emerging Role of lipid droplets in host/pathogen interactions. *J Biol Chem.* (2012) 287:2280–7. doi: 10.1074/jbc.R111.300202
38. Chen F, Rydzewski K, Kutzner E, Häuslein I, Schunder E, Wang X, et al. Differential substrate usage and metabolic fluxes in *Francisella tularensis* Subspecies holarctica and *Francisella novicida*. *Front Cell Infect Microbiol.* (2017) 7:275. doi: 10.3389/fcimb.2017.00275
39. Issa N, Guillaumot N, Lauret E, Matt N, Schaeffer-Reiss C, Van Dorsselaer A, et al. The circulating protease persephone is an immune sensor for microbial proteolytic activities upstream of the Drosophila Toll pathway. *Mol Cell.* (2018) 69:539–50.e6. doi: 10.1016/j.molcel.2018.01.029
40. Roth SW, Bitterman MD, Birnbaum MJ, Bland ML. Innate immune signaling in Drosophila blocks insulin signaling by uncoupling pi(3,4,5)p3 production and akt activation. *Cell Rep.* (2018) 22:2550–6. doi: 10.1016/j.celrep.2018.02.033
41. Lau GW, Goumnerov BC, Walendziewicz CL, Hewitson J, Xiao W, Mahajan-Miklos S, et al. The *Drosophila melanogaster* Toll pathway participates in resistance to infection by the Gram-Negative human pathogen *Pseudomonas aeruginosa*. *Infect Immun.* (2003) 71:4059–66. doi: 10.1128/IAI.71.7.4059-4066.2003
42. Radlinski LC, Brunton J, Steele S, Taft-Benz S, Kawula TH. Defining the metabolic pathways and host-derived carbon substrates required for *Francisella tularensis* intracellular growth. *mBio.* (2018) 9. doi: 10.1128/mBio.01471-18
43. Gyuranecz M, Erdélyi K, Fodor L, Jánosi K, Szépe B, Füleki M, et al. Characterization of *Francisella tularensis* strains, comparing their carbon source utilization. *Zoon Public Health.* (2010) 57:417–22. doi: 10.1111/j.1863-2378.2009.01238.x
44. Traven A, Naderer T. Central metabolic interactions of immune cells and microbes: prospects for defeating infections. *EMBO Rep.* (2019) 20:e47995. doi: 10.15252/embr.201947995

45. Krejčová G, Danielová A, Nedbalová P, Kazek M, Strych L, Chawla G, et al. Drosophila macrophages switch to aerobic glycolysis to mount effective antibacterial defense. *eLife*. (2019) 8:e50414. doi: 10.7554/eLife.50414
46. Chambers MC, Song KH, Schneider DS. Listeria monocytogenes infection causes metabolic shifts in *Drosophila melanogaster*. *PLoS ONE*. (2012) 7:e50679. doi: 10.1371/journal.pone.0050679
47. Chatzispyrou IA, Held NM, Mouchiroud L, Auwerx J, Houtkooper RH. Tetracycline antibiotics impair mitochondrial function and its experimental use confounds research. *Cancer Res*. (2015) 75:4446–s9. doi: 10.1158/0008-5472.CAN-15-1626

Conflict of Interest: The authors declare that the research was conducted in the absence of any commercial or financial relationships that could be construed as a potential conflict of interest.

frontiers in Immunology

REVIEW
published: 22 July 2020
doi: 10.3389/fimmu.2020.01574

Beyond Host Defense: Deregulation of *Drosophila* Immunity and Age-Dependent Neurodegeneration

Srishti Arora and Petros Ligoxygakis**

Laboratory of Cell Biology, Development and Genetics, Department of Biochemistry, University of Oxford, Oxford, United Kingdom

Age-dependent neurodegenerative disorders are a set of diseases that affect millions of individuals worldwide. Apart from a small subset that are the result of well-defined inherited autosomal dominant gene mutations (e.g., those encoding the β-amyloid precursor protein and presenilins), our understanding of the genetic network that underscores their pathology, remains scarce. Genome-wide association studies (GWAS) especially in Alzheimer's disease patients and research in Parkinson's disease have implicated inflammation and the innate immune response as risk factors. However, even if GWAS etiology points toward innate immunity, untangling cause, and consequence is a challenging task. Specifically, it is not clear whether predisposition to de-regulated immunity causes an inadequate response to protein aggregation (such as amyloid or α-synuclein) or is the direct cause of this aggregation. Given the evolutionary conservation of the innate immune response in *Drosophila* and humans, unraveling whether hyperactive immune response in glia have a protective or pathological role in the brain could be a potential strategy in combating age-related neurological diseases.

Keywords: aging, drosophila, neurodegeneration, immunity, immunotherapy

OPEN ACCESS

Edited by:
Susanna Valanne,
Tampere University, Finland

Reviewed by:
Shinya Yamamoto,
Baylor College of Medicine, United States
Edward Giniger,
National Institutes of Health (NIH), United States
Arvind Shukla,
National Institutes of Health (NIH), United States, in collaboration with reviewer EG

****Correspondence:***
Srishti Arora
srishti.arora@bioch.ox.ac.uk
Petros Ligoxygakis
petros.ligoxygakis@bioch.ox.ac.uk

Specialty section:
This article was submitted to Comparative Immunology, a section of the journal Frontiers in Immunology

Received: *13 December 2019*
Accepted: *15 June 2020*
Published: *22 July 2020*

Citation:
Arora S and Ligoxygakis P (2020) Beyond Host Defense: Deregulation of Drosophila Immunity and Age-Dependent Neurodegeneration. Front. Immunol. 11:1574. doi: 10.3389/fimmu.2020.01574

INTRODUCTION

Aging is characterized by the time-dependent deterioration of cellular function and fitness of an organism, accompanied by an increased susceptibility to diseases (1). This decline in function is inexorable, and is a key risk factor for a number of human disease pathologies such as diabetes, cancer, cardiovascular disorders, and neurodegenerative diseases (2). As the world's geriatric population continues to grow at an exceptional rate (3), a substantial economic burden is placed on the healthcare system to deal with the development of age related diseases. Therefore, understanding the mechanism of longevity and identifying targets to improve health during aging is of paramount importance.

Over the last decade there have been a number of attempts to explain the phenomenon of aging (1). Different processes that affect aging can be categorized into nine hallmarks that are shared by aging and age-related diseases (4). These include: altered intercellular communication, stem cell exhaustion, cellular senescence, mitochondrial dysfunction, deregulated nutrient sensing, genomic instability, telomere attrition, loss of proteostasis (protein homeostasis), and epigenetic alterations. These co-occur as an organism ages and are extensively interconnected. However, there are several questions regarding the interconnectedness of these hallmarks. One such question is the role of inflammation and its impact on age-related disorders (5). There is an age-dependent decline in immune response, this phenomenon is termed as "immunosenescence" (6, 7). This

process is marked by a reduction in the adaptive immune response and was initially believed to be a consequence of a progressive rise in low-grade chronic pro inflammatory status known as "inflammageing" (8–10). More precisely, as the thymus releases the last pool of naïve T-cells and that pool gets depleted each time there is an infection, older people (>65) become progressively weaker in their T-cell responses (5–7). Increase in innate immune pro-inflammatory levels has been seen as a "balancing act" to counter adaptive response reduction. Nevertheless, recent studies have observed that the two processes are mutually maintained and affect one another (11). For instance, depletion of adaptive immune cells strengthens the innate immune response causing inflammageing; similarly, the increased innate immune inflammatory mediators leads to a reduction in the number of adaptive immune cells causing immunosenescence. Cumulative studies have also indicated an age-dependent change in the innate immune cell types that leads to an overall decrease in their ability to collaborate in the initiation of the adaptive immune response [reviewed by (6)]. Inflammageing is often a result of non-resolving or sterile inflammation and is thought to be as a possible underlying basis for most age related diseases such as infections, cancer, autoimmune disorders, and chronic inflammatory diseases (12). Additionally, cell senescence in other tissues generates cytokines that signal the necessity for these cells to be removed by macrophages, to avoid what is called "by-stander senescence" propagating in tissues. This further enhances age-dependent systemic pro-inflammatory activity (5–9). The above, happens to everyone in the context of healthy aging. Some however, are "high responders" and develop neurodegeneration. Does predisposition to different levels of immunity influence this? This review focuses on the role of immunity in neurodegenerative disorders. The primary goal is to understand the importance of immune regulation and its role in aging and age-related diseases. We start by exploring the correlation between immunity and neurodegeneration connected to specific disorders. Then we explore the advantages and disadvantages of non-vertebrate animal models in studying aging and neurodegeneration. We continue with a brief introduction to *Drosophila* immune response and central nervous system. Finally, we conclude with studies suggesting a role for the immune system as a modulator of basal levels of age-dependent neurodegeneration and talk about the need to explore the potential role of negative regulators in immunotherapy.

IMMUNITY AND NEURODEGENERATION

While the correlation between inflammation and neurodegeneration is well-known (13), whether inflammation is one of its causes or a consequence remains unclear. Inflammation can be triggered as a *consequence* through the production of apoptotic factors and cytokines signaling during neuronal death However, immune cells produce neurotoxic cytokines that could *cause* death of neurons (14). Initially, the activation of the immune response in the central nervous system (CNS) was believed to be responsible for the elimination of infectious agents and the clearing of debris after injury, suggesting a neuroprotective role of inflammation. A positive role of antimicrobial peptide (AMP) production and aging has been suggested by Loch et al. (15). Genome wide association studies (GWAS) have reported the activation of numerous genes of the inflammatory pathway during aging (16). Age is the greatest risk factor for neurodegenerative disorders and age-related chronic activation of the immune response is a shared feature among many neurodegenerative disorders (17). However, the cause of this sterile inflammation is still unknown.

Studies in animal models indicate the importance of inflammation in several neurodegenerative disease pathologies (18). Altering expression of Cdk5 protein kinase (Cdk5α) leads to disruption in autophagy that in turn leads to upregulation of AMP and age-dependent degeneration of dopamine neurons in *Drosophila* (19). Neuroinflammation has been a crucial factor for the pathogenesis of diseases such as Alzheimer's Disease (AD) (20). Microglia, the resident innate immune cells of the CNS are shown to be chronically activated around these plaques. It is believed that the uncontrolled inflammation of these cells leads to the secretion of multiple neurotoxic factors such as inflammatory mediators and reactive oxygen species by glial cells that aggravate the pathology of the disease (14). It is further demonstrated that mutations in microglial protein TREM2, PLCG2, and ABI3 increase the risk for AD (21). Additionally, molecular and pathological interaction studies have established glial expression of TREM2/TYROBP as a key factor in tau mediated neurodegeneration (22). Activated microglia is suggested as a potential marker to detect AD before the appearance of plaques (23). Additional risk genes for late onset AD connected to microglia and immunity have been identified recently (24). Genetic analysis of these late-onset AD risk genes identified a transcriptional network of 12 largely microglial genes that form a transcriptional network (25). Six of these (*OAS1, LAPTM5, ITGAM, ABI3, PLCG2, SPI1*) have good *Drosophila* homologs expressed in the nervous system (our unpublished observations).

Drosophila models illustrate the importance of the Toll mediated NF-κB response in the neurotoxicity cause by the presence of Aβ42, an isoform of the beta amyloid protein. Down regulation of this immune pathway was shown to reduce the pathological activity of Aβ42 (26). Evidence in both human and animal model studies have illustrated the correlation between inflammation and Parkinson's disease (PD) (27). Mechanisms of neuronal dysfunction such as mitochondrial dysfunction and oxidative stress have been linked to pathogenesis of PD (28). Dopaminergic neurons (DA) in the midbrain are shown to be sensitive to pro inflammatory cytokines, reactive oxygen species, and chemokines such as TNF-α and IFN that exacerbating neuronal lesions (29). Additionally, there is a rich population of microglia in the substantia nigra, which is the region of the brain that shows the most DA neuron loss in PD patients (30). Studies have observed correlation between deposition microglial activation and alpha-synuclein making microglia an attractive therapeutic target (31, 32). However, PD is considered as a condition that is hypothesized to starts in the intestine as

chronic inflammation, then may transfer α-synuclein to the brain through the vagus nerve (33).

Transgenic mice lacking the TNF- receptor demonstrate a reduction in the TH-immunoreactivity after being exposed to MPTP (1-methyl-4-phenyl-1,2,3,6-tetrahydropyridin). Prolonged use of non-steroidal anti-inflammatory drugs such as ibuprofen is shown to reduce risk of PD (27). Consistent with these studies, an increase in circulating cytokines and increased microglial activation have also been linked to early stages of Huntington's disease (34, 35). However, production of pro inflammatory molecules is not just limited to microglia. Other types of glia cells such as astrocytes are also used to investigate the progression of inherited ALS (36). Studying these processes in humans is extremely challenging. Therefore, to explore the processes that govern aging requires accessible model systems that help provide critical insights into the cellular and molecular levels of aging.

ANIMAL MODELS OF AGING

There are several challenges in studying primate subjects in aging research. These include a number of ethical issues, environmental factors, as well as their relatively long lifespan. Consequently, aging researchers have turned to unicellular or small animal models to investigate the genetic and physiological mechanisms related to human aging and longevity. These models allow us to better control for several intrinsic and extrinsic factors such as uniformity in background genetics, large sample sizes, genetic tractability as well as environmental factors such as managed nutrient availability and chemically-defined diets. These conditions make mechanistic analysis easier and ultimately help identify novel pharmaceutical targets. Some of the popular models used in aging research include: the budding yeast (*Saccharomyces cerevisiae*), the nematode worm (*Caenorhabditis elegans*), the fruit fly (*Drosophila melanogaster*), and mouse (*Mus musculus*).

Saccharomyces cerevisiae

Studies in model organism have identified conserved pathways that influence the rate of aging (37). The simplest organism that can be used to study eukaryotic aging is Brewer's yeast or *Saccharomyces cerevisiae*. This single celled living organism shares a number of genes with humans, out of which a significant number carry out the same function in both organisms (38). This includes mechanisms that facilitate pathogen recognition during its vegetative development (18). Fungi possess a class of cytosolic NOD (Nucleotide Oligomerization Domain)- like receptors or NLRs are responsible for self and non-self-recognition. These fungal receptors share homology with the effector domains of several plant or animal NLRs and provide a unique opportunity to explore infectious host-pathogen interactions (39).

Aging in yeast can be studied using two different models. The first, replicative lifespan (RLS) that describes the total number of cell divisions a single mother (virgin) cell undergoes, the second, the chronological lifespan (CLS) that represents the length of time a cell can stay viable in a post mitotic state (40). CLS shows an elevation in DNA damage that is a characteristic that resembles that of post mitotic cellular aging in humans (41). However, both models rely on nutrient availability and negatively affect each other (42). The small genomic size and rapid generation time of 3 h makes yeast a great model for high throughput screening and exploiting genetic interactions that are thought to be involved in human aging (42). It is also used to study the effects of dietary restriction (43), oxidative stress (44), and target of rapamycin (TOR) nutrient response pathway on age related phenotypes (42, 45) Moreover, yeast models are used to study a number of age related diseases including Werner syndrome, (41) Huntington's disease (46), Alzheimer's disease (47), Parkinson's disease (48). The lessons from yeast have given us valuable insights into how stress and aging are modulated in higher organisms. However, yeast lacks the complexity of a higher eukaryotic cell and intercellular interactions that are of major importance in aging and age-related disorders.

Caenorhabditis elegans

Another invaluable model system to study aging is the small nematode worm, *Caenorhabditis elegans. C. elegans* have a short lifespan of about 2–3 weeks at 20°C. This small worm grows to be about a millimeter in length and displays complex behavior such as avoidance behavior when exposed to pathogens. It is compatible with a wide range of genetic techniques including chemical mutagenesis screens, CRISPR, and RNAi. Unlike yeast, it allows us to study tissue-to-tissue communication by tissue-specific transgenic expression and knockdown techniques in a multicellular context. *C. elegans* lack an adaptive immune response and are devoid of any migratory innate immune cells. Instead the protective immune response relies on three lines of defense. The first is avoidance behavior in which the worm can discriminate between different species of bacteria by recognizing odors of specie specific molecules such as cyclic pentadepsipeptide biosurfactant serrawettin W2 produced by *Serratia marcescens* (49). The second line of defense consists of physical barriers. The strong exoskeleton of *C. elegans* is made up of collagen and chitin that creates a physical barrier limiting the entry of potential pathogens. Additionally, a pharyngeal grinder prevents pathogens from accessing the intestines. The third and final line of defense is the humoral response which involves the activation of conserved signaling pathways (including MAP kinase cascades) that leads to the production of several antimicrobial peptides (50, 51).

C. elegans allow us to experimentally demonstrate the roles of several other conserved processes in aging such as caloric restriction, mitochondrial pathways energy metabolism, endocrine signaling, and signal transduction, the stress response, protein translation, and gene expression in aging. (52). At the convergence of immunity and aging, recent studies have shown the role of innate immunity regulated by p38 signaling and the transcription factor ATF-7 as responsible for the lifespan extension caused during dietary restriction (53). However, *C. elegans* are evolutionarily distant from humans and has a very different nervous system organization of just 302 neurons leading to behaviors unique to its lifestyle (54). Nevertheless, studies of neuronal cell death in worms has implicated proteins very closely related to mammalian calpains and cathepsins (55). Calpains

are a family of calcium regulated cysteine proteases that are highly expressed in neurons. They affect a wide range of cellular functions including cell division, proliferation, migration, and death. In neurons, these proteases have been linked to synaptic plasticity and neurodegeneration (56). The calpain mediated cleavage of carbonylated Hsp70.1 due to oxidative stress leads to loss of lysosomal integrity and rupture. Among the contents of the lysosome, a hydrolytic enzyme (cathepsins) is also released that takes over the role of a "death-executing proteases" by degrading several cellular proteins (55, 57). This Calpain-mediated cleavage of Hsp70.1 helps elucidate the importance of proteolysis in neuronal death and serves as a promising target for preventive interventions of neuronal death (57). Thus, at the cellular level, worm genetics can provide new insights into brain cell death.

Mus musculus

While yeast and worms have broadened our understanding into the cellular mechanisms of aging and age-dependent neurodegeneration, they fail to replicate system level neurological changes that occur during human aging. Therefore, mammalian model organisms are essential to unravel these complex mechanisms. What makes the mouse an indispensable model is the easy genetic manipulation, short lifespan, low-cost (compared to other primate models), and considerable similarities with human physiological and cellular function (58). Many mouse models of human aging have been developed and characterized, including models for Werner syndrome (59), Ataxia telangiectasia (60), Alzheimer's (61), and Parkinson's diseases (62). Although the degree of complexity of the mouse brain is lower than that of a human, there are several cellular similarities of the nervous system. They show complex behaviors and are a good tool to measure cognitive changes in neurodegenerative disorders (63).

Studies in mice with Alzheimer's disease have highlighted rapamycin as a valid therapeutic approach for prevention or treatment of AD (64, 65). Mouse models that display lifespan extension and rise in delayed aging phenotypes are in line with the observation that DNA metabolism influences aging. Furthermore, factors such as caloric restriction and defects in genome maintenance have been investigated in mice (66). Li et al. demonstrated the role of chronic high fat diet in mice causes loss of neuronal stem cells in the hypothalamus via IKKβ/NF-κB activation that eventually leads to obesity and pre-diabetes (67). The hypothalamus the neuroendocrine functional center of the body is also responsible for systemic aging though NF-κB signaling (25) and thus provide a potential therapeutic approach to combat age and age related disorders (68). This seems to be an evolutionary conserved component of aging as NF-κB in the brain is a major life span determinant in *Drosophila* as well [(41), see below]. Even though laboratory mice are an admirable model to study some age- related phenotypes, they do not fully mimic the mechanism. Laboratory mice are inbred and age very quickly. They invest more in reproduction and less in somatic maintenance and therefore do not display the trade-off between fecundity and longevity observed in humans. They also do not recapitulate age related disease pathologies as seen in humans (e.g., Werner diseases models and amyloid plaques in AD mice models).

Drosophila melanogaster

Over the last two decades, *Drosophila* has developed as a powerful tool to investigate human disease mechanisms. It has orthologs of ∼65% of all genes causing heritable diseases in humans (69, 70), making it an attractive model organism to address novel lines of inquiry for human diseases (71). Moreover, for every one of these genes, the fly will most of times have one copy while humans will normally have a group of genes with the same function. The fruit fly is small, has a low cost of rearing and is easy to manipulate in the laboratory. It has short generation time of 10 days at 25°C, a relatively short lifespan and produces a large number of eggs which boosts statistical relevance of the data obtained. *Drosophila* shows complex behavioral phenotypes including social aggregation, re-enforced learning as well as sleep activity that help address questions of brain function. Transgenic fly lines can be created using numerous sophisticated genetic and molecular tools such as insertions of P-elements (72) CRISPR, RNAi silencing, tissue specific GAL4-UAS expression system. Additionally, genome-wide genetic screening, genome-wide analyses with deep sequencers, such as RNA-seq and ChIP-seq, and metabolomics analyses allows us to enquire the cellular and molecular mechanisms of aging and age-related diseases. *Drosophila* has been crucial in the discovery and understanding of innate immune signaling and the development of the nervous system. The fly exhibits multiple physiological changes associated with aging and age related diseases such as reduced locomotive ability (73, 74), impaired learning and memory (75), progressive decline in intestinal barrier function (76), increased inflammation (77), reduced reproductive capacity, and altered neuronal function (78, 79). Additionally, several environmental manipulations such as effects of dietary restrictions are easy to observe (80).

The process of development of neurons is conserved from flies to humans. *Drosophila* has a relatively complex nervous system that is separated from the rest of the body with the blood brain barrier built by glial cells and neurons (81). It's CNS contains about 200,000–300,000 neurons can be histologically divided into two distinct regions (82): the neuronal cell cortex, formed by all the neuronal cell bodies, and a synapse dense neuropil, to which all the dendrites and axons project (83). The fly brain is a sophisticated structure that has several sub-structures: including the antennal lobes, the mushroom bodies, the central body complex, the protocerebrum, the optic lobes, the posterior slope, and lateral deutocerebrum. Sensory organs and the musculature send signals to the CNS via peripheral nerves. The neurons in these associated structures are supported with glial cells. Apart from being the resident immune cells for the CNS, glial cells are responsible for maintaining ionic homeostasis, recycling neurotransmitters, and for the formation of the blood brain barrier (83). *Drosophila* glial cells can be largely categorized on the basis of their location and/or morphology. There are six morphologically and molecularly distinct glial subtypes; perineurial glia (PG), subperineurial glia (SPG), cortex glia (CG), ensheathing glia (EG), astrocytes-like glia(ALG), and

wrapping glia (EG in the PNS) (84). The surface of CNS and the peripheral nerves are covered with a thick carbohydrate-rich lamella secreted by perineural glia (PG) and macrophages (85). This PG layer is discontinuous and forms glia–glia pleated septate junctions (pSJs) with subperineural glial cells (SPG) that lie directly below the PG layer. These cells establish the Blood Brain Barrier (BBB) and separate the neuronal elements from the potassium-rich hemolymph. Apart from the BBB, the peripheral nerves have a specialized form of ensheathing glia called wrapping glia, that encloses motor and sensory axons (86). Deeper in the CNS beneath the BBB lie cortex glia, ensheathing glia, and astrocytes-like glia which are closely associated to neurons (87). Cortex glia or cell body associated glia are found within the cell cortex and invade the space between neuronal cell bodies. These cells are in contact with the tracheas and the BBB, suggesting that they are likely responsible to transfer nutrients and gases from the hemolymph to neurons (81). The ensheathing glial cells compartmentalize the brain by forming a sheath around the neuropil (88). These cells are responsible for the phagocytoses of axonal debris (89). As the name suggests astrocyte-like glial cells are functionally and morphologically similar to mammalian astrocytes (90). They are responsible for the maintenance of neurotransmitter homeostasis and in regulating circadian rhythm (91).

Additionally, a large amount of effort has been exerted in creating many distinct *Drosophila* models for a range of neurological disorders such as Parkinson's disease (PD) (92), Alzheimer's disease (AD) (93, 94), and polyglutamine diseases (polyQ) (95, 96). Many of these diseases are caused by abnormal production or accumulation of different proteins such as the accumulation of Lewy bodies in PD, amyloid plaques in AD, and inclusions in polyQ diseases. These protein defects are not normally observed in *Drosophila*. However, they can be artificially produced in flies by introducing human genes into the genome and over expressing them in neurons through the UAS/GAL4 system (97). This is both an advantage and a disadvantage. This technique helps replicate human-like morphological lesions of these diseases and devise screens to genetically identify mutations that suppress the extend of the resulting lesions. However, it is difficult to distinguish the immune responses to such protein build-up from mere non-specific stress responses due to overproduction of an exogenous protein (98).

INTRODUCTION TO *DROSOPHILA* IMMUNITY

The innate immune system, an immune reaction with broad specificity, is an organism's first line of defense. It is centered on receptors, which target conserved features of microbial invaders and expeditiously activate downstream cascade to destroy pathogens (99). In jawed vertebrates and some jawless fishes (lampreys) this activation leads also to the induction of adaptive immunity. Unlike those vertebrate categories however, insects lack an adaptive immune system and therefore rely on a relatively sophisticated set of innate defense responses for their survival. The development and function of these reactions are shown to be shared with higher organisms and can be used to study innate immunity and inflammation in humans (100).

Due to the wide range of genetic manipulation techniques it offers, *Drosophila* has been a powerful model to study innate immunity (101). It utilizes a wide range of actions to form effective barriers against pathogens, first of which is a local immune response. This includes the elimination of incoming pathogens by constitutive secretion of AMPs and by reactive oxygen species (ROS) in barrier epithelia such as gut, genitals, cuticle (102, 103), followed by a cellular response which includes engulfment, entrapment, and melanization of the pathogen (104–106). The final response is marked by the rapid synthesis of antimicrobial peptides (AMPs) in the haemocytes and the fat body. The AMPs are regulated by two signaling pathways: The Toll pathway, which was the first in the family of Toll-like receptors discovered in a wide range of organisms from sea urchins to humans, and the IMD pathway homologous to the tumor necrosis factor receptor 1 (TNFR1) in mammals (107).

The Toll-mediated responses are triggered by bacterial or fungal infection which leads to the activation of two Rel transcription factors, Dif and Dorsal that regulate hundreds of genes [reviewed in (100)] (**Figure 1**). Apart from its role in immunity, the Toll pathway plays a crucial role in the determination of the dorsal-ventral polarity during *Drosophila* early embryogenesis (108, 109). In order to initiate the Toll response, bacterial or fungal pathogens, are sensed by receptors in the form of Peptidoglycan Recognition Proteins (PGRPs; in this case PGRP-SA) or Glucan Binding Proteins (GNBP1, GNBP3) or through cleavage of endogenous proteases (such as Persephone or Psh) (110–112). The next step gives rise to an extracellular proteolytic cascade that culminates in the proteolytic cleavage and activation of the Toll receptor ligand Spatzle (Spz) leading to its activation (113). Spatzle binds to the Toll receptor that recruits MyD88 through its TIR domain, which further interacts with Tube and Pelle through their respective death domains (DD) and promote the phosphorylation of Cactus. Cactus is the *Drosophila* IkB homolog and is bound to Dorsal and/or Dif, inhibiting their activity and nuclear localization. Once degraded, Dorsal and Dif translocates to the nucleus and ultimately leads to the transcription of AMPs and other target genes [reviewed in (114)].

Another evolutionarily conserved singling cascade is the immune deficiency (Imd) pathway (**Figure 1**), the activation of which is achieved with the help of two PGRP receptors namely, PGRP-LC and PCRP-LE. These receptors bind better to DAP-type peptidoglycan present on Gram-negative bacteria and Gram-positive bacilli and trigger a response, that finally leads to the activation of Rel/NF-κB transcription factor Relish (115). The activated PGRP receptors initiates a signaling cascade and recruits a protein complex containing Imd, a death domain protein, dFadd, and Dredd. Dredd is the caspase-8 homolog, is activated by Iap2 (inhibitor of apoptosis 2) and cleaves Imd to reveal a site important for its role as a transient signaling hub. Iap2 then ubiquitnates Imd and recruits Tab2/Tak1 complex to the reaction site that phosphorylates the Drosophila IKK complex (116). Relish is activated by two events: the phosphorylation of

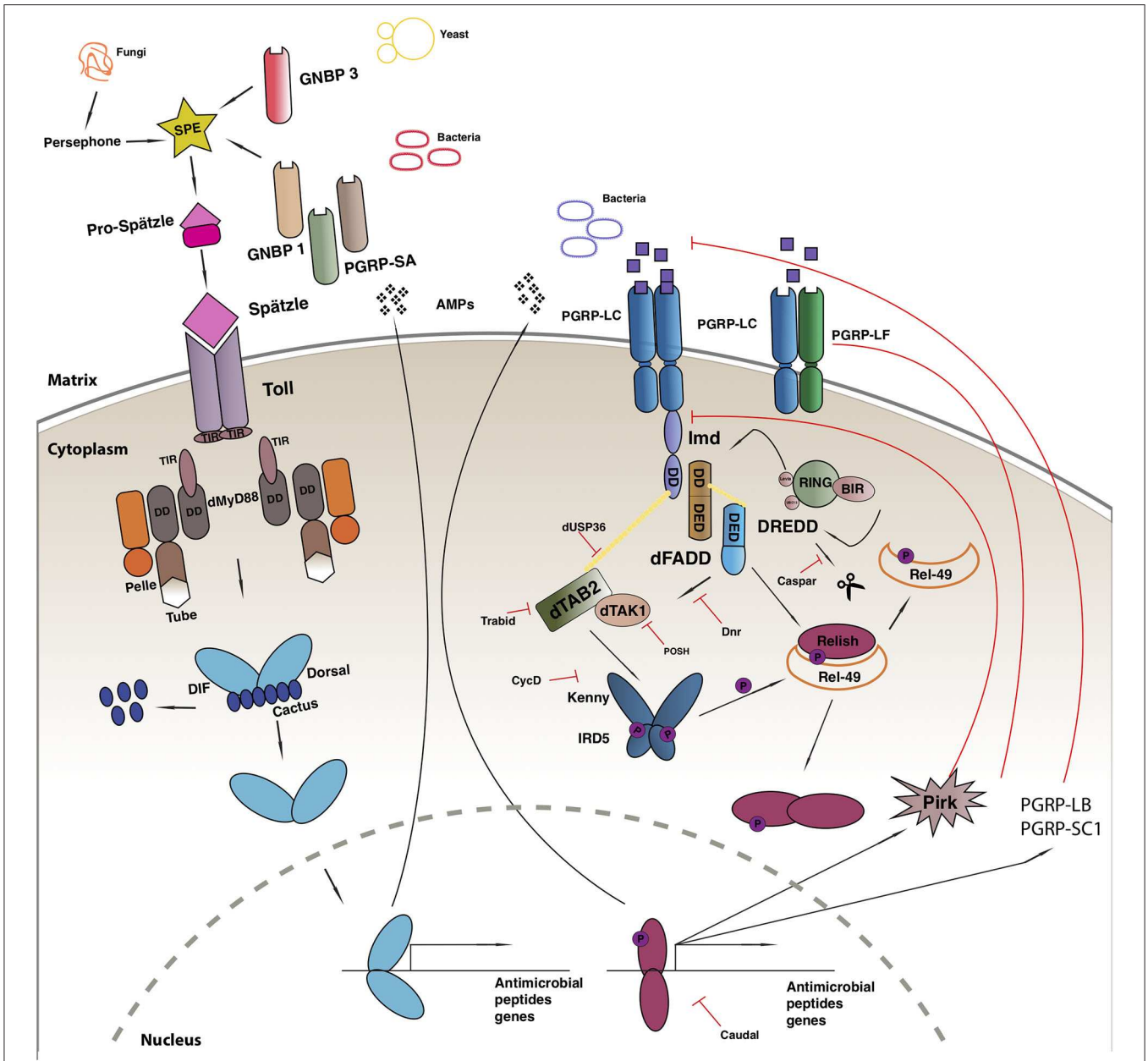

FIGURE 1 | *Drosophila* immune response. Toll pathway (on left) and IMD pathway (on right). See main text for details to the legend.

its *N* terminal by Tab2/Tak1 complex and the cleavage of its *C* terminal ANK repeats domain by Dredd. The activated *N* terminal (Rel-68) enters the nucleus and initiates transcription of AMPs (116).

The improper activation of the immune signaling pathways is associated with inflammation, cancer, and neurodegeneration (77, 117), and leads to developmental defects during ontogenesis (118–120). To prevent the harmful consequences of unwarranted activation, the pathway is firmly regulated by extracellular and intracellular proteins.

Negative Regulation of IMD

The IMD immune response is tightly regulated at many levels, first of which is the dilution of the activating signal. This is done by the secreted PGRP-SC and PGRP—LB amidase that breakdown bacterial peptidoglycan into non-stimulatory fragments in the extracellular matrix (119, 121). On the plasma membrane, the three PGRP-LC isomers interact with each other to suppress spontaneous dimerization and reduce the number of functioning receptors (122). Additionally, PGRP-LF binds with PGRP-LC to form non-signaling heterodimers and down regulate the response (123). Intracellularly, PIMS/pirk/rudra

coimmunoprecipitates with Imd causing a disruption in its association with the cytoplasmic tail of PGRP-LC receptor leading to its the depletion from the membrane. *Pirk* mutant have constitutively activated immune response and are short lived. Moreover, flies over expressing pirk have a reduced Imd response (124–126). Dnr1 inhibits the activity of Dredd caspase by promoting its proteolytic degradation. *Dnr 1* mutants have shorter lifespans and exhibit age-dependent neuropathology (127). The activity of the Dredd caspase is also impaired by Caspar, which inhibit Dredd-dependent modification of Relish and further blocking its translocation to the nucleus (13). The activity of NF-kB is regulated by several ubiquitin-mediated interactions, deregulation of these factors cause chronic inflammation and cancer (128). Further negative regulators of the Imd pathway include SkpA, dUSP36, CYLD, POSH, Trabid, and transglutaminase (TG). *Drosophila* ubiquitin-specific protease 36 (dUSP36) inhibits the K63-polyubiquitinated Imd build up and promotes its degradation (129). It is a negative regulator of the pathways as silencing *dUSP36* constitutively activates the IMD signaling pathway. This activation is lost in germ free flies leading to the hypothesis that this interaction might be microbiome dependent (130). K63-linked ubiquitination of dTAK1 is monitored by another negative regulator of IMD known as Trabid. Flies lacking this protein show a remarkable increase in the amount of the IMD target, Diptericin with a dramatic reduction of the lifespan (131). A further negative regulator of TAK1, POSH (Plenty-of-SH3s) prevents engagement with the JNK scaffold (132). Downstream, the cylidromatosis disease homolog dCYLD interacts with the *Drosophila* IKKγ homolog Kenny and disrupts downstream signaling (133). In its absence, triglyceride and AMP levels increase (133). At the level of Relish finally, SkpA and the proteasome-ubiquitin pathway (134) and Transglutaminase (135) suppress NF-κB activity.

PREDISPOSITION TO AN OVERACTIVE IMMUNITY CAUSES NEURODEGENERATION

Human genetics and animal model research have illustrated the correlation between innate immunity in the brain and the pathogenesis of neurodegenerative disorders (**Table 1**). Increasing amount of evidence suggests that the accumulation of aggregated proteins is only a part of the pathology of neurodegenerative disorders and not the full story [reviewed in (143)]. Increasing evidence suggests the role of the immune system as an aetiological mechanism that influences not only the pathology of the diseases but also modulates basal levels of age dependent neurodegeneration in the context of healthy aging (144).

Loss of Negative Regulation of IMD

Cao et al. illustrated that chronic activation of the immune response in the wild type *Drosophila* brains causes neurodegeneration (127). Flies with loss of function mutations in a Relish repressor gene *dnr-1* show signs of early neurodegeneration and an increase in the number of Relish target genes transcripts in the fly brain. The authors suggest the cause of this neurodegeneration as AMP-associated toxicity caused by constitutive expression or an extremely high level of AMPs present in neurons or glial cells. The study also revealed that the overexpression of AMPs in nervous tissue can cause neurodegeneration and established a causative relationship between neurodegeneration and IMD signaling. However, overexpression of AMPs brings expression to much higher levels than the *dnr-1* mutant and therefore more work is needed to prove this point. Nevertheless, the possibility of a neuroprotective role of negative regulators in neuronal viability is clearly suggested here (127).

A similar result were obtained by Kounatidis et al., who demonstrated an age-dependent increase in NF-kB- controlled immune activity in *Drosophila* in the context of healthy aging (77). Most of it was dependent on the microbiota, as germ free flies had much reduced age-dependent AMP increase compared to conventionally reared insects (77). Nevertheless, there was consistently a 2–4x age-dependent AMP increase in germ free flies as was a clear sterile inflammation in the brain. Moreover, the loss of Trabid, Pirk, and TG in neuronal tissue resulted in shortening of lifespan, locomotion defects, and the formation of brain lesions. This phenotype was rescued once Relish was suppressed in glial cells of these flies. In wild type flies, suppressing *relish* in glial cells resulted in lifespan extension. Therefore, genetic predisposition to higher immune levels with mutation in *trbd*, *pirk*, and *tg* led to early neurodegeneration and curtailed lifespan (77).

Autophagy and Immunity

An interesting connection between autophagy, immunity and neurodegeneration was recently made by the observation that mutants for the Cdk5 protein kinase have increased AMP expression in the brain and loss of dopaminergic neurons. This happens because loss of Cdk5 disrupts autophagy and this results in increased levels of immunity (19). This point is important since autophagy seems to be necessary and sufficient to drive the increase in AMP levels. Given the dysregulation of Cdk5 and innate immunity in human neurodegeneration and the conserved role of this kinase in the regulation of autophagy, this sequence of events is likely to resemble what happens in humans (19). However, the connection between immunity and autophagy remains largely unexplored. One indication is the interaction between Kenny (IKKγ) and the autophagy protein Atg8, which targets Kenny for selective degradation. Loss of Atg8, "releases" Kenny, enhancing IKK signaling, and resulting in chronic IMD induction (145).

Neurodegenerative Disease Models

The Penetrating traumatic brain injury (pTBI) model show a greater expression of AMP genes and an over activation of the innate immune response in both young and older flies (136). The positive interaction between pTBI and aging was further supported by the high expression of Imd negative regulators in older pTBI fly brains. The study indicated that aging exasperates the immune response caused by pTBI and causes neurodegeneration. Additionally Yorkie, a co-activator

TABLE 1 | Summary of papers at the junction of immunity and neurodegeneration in *Drosophila*.

Gene	Immune phenotype	Neurological phenotype	References
pirk/*rudra*/*pims* (loss of function)	Overactivation of IMD	Locomotion, reduced lifespan, brain neurodegeneration	(77)
trabid (loss of function)	Overactivation of IMD	Locomotion, reduced lifespan, brain neurodegeneration	(77)
transglutaminase (loss of function)	Overactivation of IMD	Locomotion, reduced lifespan, brain neurodegeneration	(77)
dnr1 (loss of function)	Overactivation of IMD	Locomotion, reduced lifespan, brain neurodegeneration	(127)
cdk5 (loss of function)	Overactive immunity through reduction of autophagy	Loss of DA neurons	(19)
Toll and IMD activity increases	Overactive immunity	Age-dependent neurodegeneration in a model of pTBI	(136)
yorkie activity	Suppression of IMD and Toll	Reduction of PolyQ-mediated neurodegeneration	(137)
relish (knock-down in DA neurons)	Suppression of IMD	Increased resistance to paraquat, rescue of motility defects and DA neurons in a *Drosophila* model of PD	(138)
relish (loss of function)	Suppression of IMD	Suppression of retinal degeneration in norpA mutants	(139)
draper activity	Glial phagocytosis	Better clearance of Aβ-amyloid	(140)
draper (age-dependent reduction)	Dysfunctional glial-mediated engulfment	Neuronal death	(141)
spz-5 (in neurons)	Activation of Toll-6 in glia	Neuronal death; dying neurons signal to glia	(142)

We only list those showing a causative link between immune activity or immune-related signaling and neurological phenotype.

of Hippo pathway was also shown to reduce polyglutamine (PolyQ)-mediated neurodegeneration by negatively regulating Toll and Imd pathways *via cactus* and *relish*, respectively (137).

Recently, transcription of innate immune genes were observed as the prominent response to paraquat in a *Drosophila* model of PD (138). Interestingly, Relish knock down in dopaminergic neurons conferred resistance to paraquat and rescued both motility defects and loss of dopaminergic neurons. The study indicates that the immune reaction might not be protective and indicate potential drug targets for preventing neuronal loss during PD. Immunity induced neurodegeneration can explain the neurodegenerative phenotypes observed in both *ataxia–telangiectasia mutated (ATM)* gene and retinal degeneration in *norpA* (no receptor potential) mutants (139). Reduction in the ATM kinase activity in the glial cells may be responsible for the increased innate immune response through protein phosphorylation and cause neurodegeneration in these mutants. Furthermore, retinal degeneration in *norpA* mutant flies was shown to be dependent on Relish and Dredd.

Neuroprotective Roles of Immunity

In addition to the role of the long-term heightened IMD signaling in causing neurodegeneration, there is also a neuroprotective aspect of glial signaling components connected to immunity. Ray et al. showed the neuroprotective role of the glial engulfment receptor, Draper, in *Drosophila* model of AD (140). Overexpression of glial *draper* reverses amyloid (Aβ) accumulation along with AD associated behavior phenotypes. They also show that protein degradation pathways are expressed downstream to Draper in response to amyloid accumulation. This supports the theory that glial cells may be responsible for the clearance of neurotoxic amyloid peptides in the brain through a Draper/JNK/STAT92E signaling cascade (140). Draper is also observed to have a significant role in clearance of damaged axons. Purice et al. observed an age-dependent decline in the levels of Draper that causes dysfunctional glial engulfment in older flies (141). Dying neurons activate Toll receptor ligand, Spz, in the cortex glia, that further drives the expression of Draper to ensure efficient clearance of the neuron (142).

Gut-Brain Axis

Recent studies have also focused on the role of gut- brain crosstalk and neurodegeneration. Wu et al. highlighted the effect of enteric infection in AD progression (146). Gut dysbiosis in AD mutant flies caused an increase in haemocyte recruitment to the brain and activation of TNF-JNK mediated neurodegeneration. Neurodegeneration and reduction in lifespan were rescued in flies with genetically depleted Eiger (an activator for JNK

pathway) in the brain, further supporting the hypothesis. Westfall et al. explored how symbiotic and probiotic formulation can influence gut brain signaling and delay the progression of AD (147).

Limitations

Needless to say, no model system is without limitations. It is important to note that like most invertebrate organisms, the fruit fly is evolutionarily distant from humans and does not accurately mimic all the neurodegenerative phenotypes observed in human diseases such as tau aggregates and plaques (148). *Drosophila* lacks an adaptive immune response making it difficult to recapitulate complex changes in the immune response, that might take place during aging. Additionally, the hemolymph of the fly contains primitive hemocytes which cannot undergo DNA rearrangement and somatic hypermutation like mammalian lymphocytes. Unlike mammals, flies do not possess microglia rather, all glial cells can perform microglial tasks; such as engulfing neuronal corpses during development (84). However, this restricts studies that attempt to understand the complicated relationship between the immune system and the relation between neuroprotection and neurodegeneration. Nevertheless, the studies summarized here highlight evidence suggesting that the immune system plays an important role in neurodegenerative disorder in *Drosophila*. Two key contributors to lifespan reduction and neuropathy are overproduction of AMPs and impaired phagocytosis. Even though animal models do not represent the diseases completely (for example in the lack of direct orthologs for the human proteins prone to aggregation in AD or PD), comparative studies of brain development and the innate immune response have demonstrated significant evolutionary conserved mechanisms between vertebrates and invertebrates. Moreover, the deregulation of innate immunity as etiology for neurodegeneration stands in *Drosophila* even in the absence of tau or β-amyloid. There is a large therapeutic potential of immunomodulation and therapeutic immunization (149) to help combat the development of such diseases by screening fast in whole animal models such as the fly. Moreover, since the role of immune activity in microglia and astrocytes in neurodegeneration is well-documented, we could envisage that negative regulators of immunity could be potential candidates for early interventions.

CONCLUSION

The precise mechanism of the development of neurodegenerative diseases is still unknown and this presents a challenge for the development of treatments and therapies. Currently, therapies focus only on treating isolating disease symptoms such as protein accumulation, sleep disturbances, memory loss, or behavioral changes. Additionally, disease modifying therapies are largely unsuccessful and there is need for more drug candidates to enter the pipeline. Since most of the cases of neurodegeneration are only diagnosed after severe neuronal loss. Exploring preclinical symptoms as potential therapy can facilitate the development of treatments for the early symptoms of the disease. Aberrant immune regulation resulting in chronic inflammation long before neurological symptoms manifest themselves may be at the root of these diseases. We believe that *Drosophila* represents an ideal compromise between its relevance to humans and its demographic power and genetic tractability, making it a model of choice for understanding mechanistic aspects of age-related neurodegeneration.

AUTHOR CONTRIBUTIONS

SA wrote the first draft and drew the figures. PL worked on subsequent drafts with SA. All authors contributed to the article and approved the submitted version.

FUNDING

This work was supported by the European Research Council (310912 Droso-Parasite), project grant BB/P00569/1 from the Biological and Biotechnological Sciences Research Council UK and the EP Abraham Cephalosporin Trust Fund Grants CF 319 and 333, all to PL.

ACKNOWLEDGMENTS

We thank all members of the PL's lab for critical reading and comments on the manuscript.

REFERENCES

1. Lipsky MS, King M. Biological theories of aging. *Dis Month.* (2015) 61:460–6. doi: 10.1016/j.disamonth.2015.09.005
2. Ferrucci L, Fabbri E. Inflammageing: chronic inflammation in ageing, cardiovascular disease, and frailty. *Nat Rev Cardiol.* (2018) 15:505–22. doi: 10.1038/s41569-018-0064-2
3. United Nations, Department of Economic and Social Affairs, Population Division. *World Population Prospects 2019: Highlights (ST/ESA/SER.A/423)* (2019).
4. López-Otín C, Blasco MA, Partridge L, Serrano M, Kroemer G. The hallmarks of aging. *Cell.* (2013) 153:1194–217. doi: 10.1016/j.cell.2013.05.039
5. Kennedy BK, Berger SL, Brunet A, Campisi J, Cuervo AM, Epel ES, et al. Geroscience: linking aging to chronic disease. *Cell.* (2014) 159:709–13. doi: 10.1016/j.cell.2014.10.039
6. Solana R, Tarazona R, Gayoso I, Lesur O, Dupuis G, Fulop T. Innate immunosenescence: effect of aging on cells and receptors of the innate immune system in humans. *Semin Immunol.* (2012) 24:331–41. doi: 10.1016/j.smim.2012.04.008
7. Franceschi C, Capri M, Garagnani P, Ostan R, Santoro A, Monti D, et al. Inflammaging. In: Fulop T, Franceschi C, Hirokawa K, Pawelec G, editors. *Handbook of Immunosenescence*. Cham: Springer (2019).
8. Franceschi C, Garagnani P, Parini P, Giuliani C, Santoro A. Inflammaging: a new immune–metabolic viewpoint for age-related diseases. *Nat Rev Endocrinol.* (2018) 14:576–90. doi: 10.1038/s41574-018-0059-4
9. Franceschi C, Capri M, Monti D, Giunta S, Olivieri F, Sevini F, et al. Inflammaging and anti-inflammaging: a systemic perspective on aging and longevity emerged from studies in humans. *Mech Ageing Dev.* (2007) 128:92–105. doi: 10.1016/j.mad.2006.11.016

10. Frank MO, Caceres BA. Inflammaging: a concept analysis. *J Nurse Pract.* (2015) 11:258–61. doi: 10.1016/j.nurpra.2014.08.005
11. Fulop T, Larbi A, Dupuis G, Page A Le, Frost EH, Cohen AA, et al. Immunosenescence and inflamm-aging as two sides of the same coin: friends or Foes? *Front Immunol.* (2018) 8:1960. doi: 10.3389/fimmu.2017.01960
12. Salvioli S, Lanzarini C, Conte M, Pirazzini C, Bacalini MG, Garagnani P, et al. Immune system, cell senescence, aging and longevity - inflamm-aging reappraised. *Curr Pharm Des.* (2013) 19:1675–9. doi: 10.2174/1381612811319090015
13. Kim M, Lee JH, Lee SY, Kim E, Chung J. Caspar, a suppressor of antibacterial immunity in *Drosophila*. *Proc Natl Acad Sci USA.* (2006) 103:16358–63. doi: 10.1073/pnas.0603238103
14. Smith JA, Das A, Ray SK, Banik NL. Role of pro-inflammatory cytokines released from microglia in neurodegenerative diseases. *Brain Res Bull.* (2012) 87:10–20. doi: 10.1016/j.brainresbull.2011.10.004
15. Loch G, Zinke I, Mori T, Carrera P, Schroer J, Takeyama H, et al. Antimicrobial peptides extend lifespan in *Drosophila*. *PLoS ONE.* (2017) 12:e0176689. doi: 10.1371/journal.pone.0176689
16. Jeck WR, Siebold AP, Sharpless NE. Review: a meta-analysis of GWAS and age-associated diseases. *Aging Cell.* (2012) 11:727–31. doi: 10.1111/j.1474-9726.2012.00871.x
17. Xia S, Zhang X, Zheng S, Khanabdali R, Kalionis B, Wu J, et al. An update on inflamm-aging: mechanisms, prevention, and treatment. *J Immunol Res.* (2016) 2016:8426874. doi: 10.1155/2016/8426874
18. Glass CK, Saijo K, Winner B, Marchetto MC, Gage FH. Mechanisms underlying inflammation in neurodegeneration. *Cell.* (2010) 140:918–34. doi: 10.1016/j.cell.2010.02.016
19. Shukla AK, Spurrier J, Kuzina I, Giniger E. Hyperactive innate immunity causes degeneration of dopamine neurons upon altering activity of Cdk5. *Cell Rep.* (2019) 26:131–144.e4. doi: 10.1016/j.celrep.2018.12.025
20. Heneka MT, Carson MJ, Khoury J El, Landreth GE, Brosseron F, Feinstein DL, et al. Neuroinflammation in Alzheimer's disease. *Lancet Neurol.* (2015) 14:388–405. doi: 10.1016/S1474-4422(15)70016-5
21. Dalmasso MC, Brusco LI, Olivar N, Muchnik C, Hanses C, Milz E, et al. Transethnic meta-analysis of rare coding variants in PLCG2, ABI3, and TREM2 supports their general contribution to Alzheimer's disease. *Transl Psychiatry.* (2019) 9:1–6. doi: 10.1038/s41398-019-0394-9
22. Sekiya M, Wang M, Fujisaki N, Sakakibara Y, Quan X, Ehrlich ME, et al. Integrated biology approach reveals molecular and pathological interactions among Alzheimer's Aβ42, Tau, TREM2, and TYROBP in *Drosophila* models. *Genome Med.* (2018) 10:26. doi: 10.1186/s13073-018-0530-9
23. Wright AL, Zinn R, Hohensinn B, Konen LM, Beynon SB, Tan RP, et al. Neuroinflammation and neuronal loss precede Aβ plaque deposition in the hAPP-J20 mouse model of Alzheimer's disease. *PLoS ONE.* (2013) 8:e59586. doi: 10.1371/journal.pone.0059586
24. Salih DA, Bayram S, Guelfi S, Reynolds RH, Shoai M, Ryten M, et al. Genetic variability in response to amyloid beta deposition influences Alzheimer's disease risk. *Brain Commun.* (2019) 1:1–13. doi: 10.1093/braincomms/fcz022
25. Zhang G, Li J, Purkayastha S, Tang Y, Zhang H, Yin Y, et al. Hypothalamic programming of systemic ageing involving IKK-β, NF-κB and GnRH. *Nature.* (2013) 497:211–16. doi: 10.1038/nature12143
26. Tan L, Schedl P, Song HJ, Garza D, Konsolaki M. The Toll→ NFκB signaling pathway mediates the neuropathological effects of the human Alzheimer's Aβ42 polypeptide in *Drosophila*. *PLoS ONE.* (2008) 3:e3966. doi: 10.1371/journal.pone.0003966
27. Kannarkat GT, Boss JM, Tansey MG. The role of innate and adaptive immunity in Parkinson's disease. *J Parkinsons Dis.* (2013) 3:493–514. doi: 10.3233/JPD-130250
28. Dauer W, Przedborski S. Parkinson's disease: mechanisms and models. *Cambridge Companion Philos Biol.* (2007) 39:139–59. doi: 10.1017/CCOL9780521851282.008
29. Herrera AJ, Tomás-Camardiel M, Venero JL, Cano J, Machado A. Inflammatory process as a determinant factor for the degeneration of substantia nigra dopaminergic neurons. *J Neural Transm.* (2005) 112:111–19. doi: 10.1007/s00702-004-0121-3
30. Croisier E, Moran LB, Dexter DT, Pearce RKB, Graeber MB. Microglial inflammation in the parkinsonian substantia nigra: relationship to alpha-synuclein deposition. *J Neuroinflammation.* (2005) 2:1–8. doi: 10.1186/1742-2094-2-14
31. Su X, Maguire-Zeiss KA, Giuliano R, Prifti L, Venkatesh K, Federoff HJ. Synuclein activates microglia in a model of Parkinson's disease. *Neurobiol Aging.* (2008) 29:1690–701. doi: 10.1016/j.neurobiolaging.2007.04.006
32. Alvarez-Erviti L, Couch Y, Richardson J, Cooper JM, Wood MJA. Alpha-synuclein release by neurons activates the inflammatory response in a microglial cell line. *Neurosci Res.* (2011) 69:337–42. doi: 10.1016/j.neures.2010.12.020
33. Kim S, Kwon SH, Kam TI, Panicker N, Karuppagounder SS, Lee S, et al. Transneuronal propagation of pathologic α-synuclein from the gut to the brain models Parkinson's disease. *Neuron.* (2019) 103:627–41.e7. doi: 10.1016/j.neuron.2019.05.035
34. Politis M, Lahiri N, Niccolini F, Su P, Wu K, Giannetti P, et al. Increased central microglial activation associated with peripheral cytokine levels in premanifest Huntington's disease gene carriers. *Neurobiol Dis.* (2015) 83:115–21. doi: 10.1016/j.nbd.2015.08.011
35. Björkqvist M, Wild EJ, Thiele J, Silvestroni A, Andre R, Lahiri N, et al. A novel pathogenic pathway of immune activation detectable before clinical onset in Huntington's disease. *J Exp Med.* (2008) 205:1869–77. doi: 10.1084/jem.20080178
36. Yamanaka K, Chun SJ, Boillee S, Fujimori-Tonou N, Yamashita H, Gutmann DH, et al. Astrocytes as determinants of disease progression in inherited ALS. *Nat Neurosci.* (2008) 11:1–5. doi: 10.1038/nn2047
37. Lees H, Walters H, Cox LS. Animal and human models to understand ageing. *Maturitas.* (2016) 93:18–27. doi: 10.1016/j.maturitas.2016.06.008
38. Kachroo AH, Laurent JM, Yellman CM, Meyer AG, Wilke CO, Marcotte EM. Systematic humanization of yeast genes reveals conserved functions and genetic modularity. *Science.* (2015) 348:921–6. doi: 10.1126/science.aaa0769
39. Uehling J, Deveau A, Paoletti M. Do fungi have an innate immune response? An NLR-based comparison to plant and animal immune systems. *PLoS Pathog.* (2017) 13:e1006578. doi: 10.1371/journal.ppat.1006578
40. Longo VD, Shadel GS, Kaeberlein M, Kennedy B. Replicative and chronological aging in saccharomyces cerevisiae. *Cell Metab.* (2012) 16:18–31. doi: 10.1016/j.cmet.2012.06.002
41. Madia F, Gattazzo C, Wei M, Fabrizio P, Burhans WC, Weinberger M, et al. Longevity mutation in SCH9 prevents recombination errors and premature genomic instability in a Werner/Bloom model system. *J Cell Biol.* (2008) 180:67–81. doi: 10.1083/jcb.200707154
42. Kaeberlein M. Lessons on longevity from budding yeast. *Nature.* (2010) 464:513–19. doi: 10.1038/nature08981
43. Ruetenik A, Barrientos A. Dietary restriction, mitochondrial function and aging: from yeast to humans. *Biochim Biophys Acta Bioenerg.* (2015) 1847:1434–47. doi: 10.1016/j.bbabio.2015.05.005
44. Eleutherio E, Brasil A de A, França MB, de Almeida DSG, Rona GB, Magalhães RSS. Oxidative stress and aging: learning from yeast lessons. *Fungal Biol.* (2018) 122:514–25. doi: 10.1016/j.funbio.2017.12.003
45. Zimmermann A, Hofer S, Pendl T, Kainz K, Madeo F, Carmona-Gutierrez D. Yeast as a tool to identify anti-aging compounds. *FEMS Yeast Res.* (2018) 18:1–16. doi: 10.1093/femsyr/foy020
46. Meriin AB, Zhang X, He X, Newnam GP, Chernoff YO, Sherman MY. Huntingtin toxicity in yeast model depends on polyglutamine aggregation mediated by a prion-like protein Rnq1. *J Cell Biol.* (2002) 157:997–1004. doi: 10.1083/jcb.200112104
47. Moosavi B, Mousavi B, Macreadie IG. Yeast model of amyloid- β and Tau aggregation in Alzheimer's disease. *J Alzheimer's Dis.* (2015) 47:9–16. doi: 10.3233/JAD-150173
48. Sharma N, Brandis KA, Herrera SK, Johnson BE, Vaidya T, Shrestha R, et al. Alpha synuclein budding yeast model. *J Mol Neurosci.* (2006) 28:161–78. doi: 10.1385/JMN:28:2:161
49. Pradel E, Zhang Y, Pujol N, Matsuyama T, Bargmann CI, Ewbank JJ. Detection and avoidance of a natural product from the pathogenic bacterium serratia marcescens by caenorhabditis elegans. *Proc Natl Acad Sci USA.* (2007) 104:2295–300. doi: 10.1073/pnas.0610281104

50. Kim DH, Ewbank JJ. Signaling in the innate immune response. In: *WormBook: The Online Review of C. elegans Biology*. Pasadena, CA: WormBook (2018). p. 2005–18.
51. Dierking K, Yang W, Schulenburg H. Antimicrobial effectors in the nematode *Caenorhabditis elegans*: an outgroup to the arthropoda. *Philos Trans R Soc B Biol Sci.* (2016) 371:20150299. doi: 10.1098/rstb.2015.0299
52. Tissenbaum HA. Using *C. elegans* for aging research. *Invertebr Reprod Dev.* (2015) 59:59–63. doi: 10.1080/07924259.2014.940470
53. Wu Z, Isik M, Moroz N, Steinbaugh MJ, Zhang P, Blackwell TK. Dietary restriction extends lifespan through metabolic regulation of innate immunity. *Cell Metab.* (2019) 29:1192–205.e8. doi: 10.1016/j.cmet.2019.02.013
54. Lee JS, Shih PY, Schaedel ON, Quintero-Cadena P, Rogers AK, Sternberg PW. FMRFamide-like peptides expand the behavioral repertoire of a densely connected nervous system. *Proc Natl Acad Sci USA.* (2017) 114:E10726–35. doi: 10.1073/pnas.1710374114
55. Syntichaki P, Xu K, Driscoll M, Tavernarakis N. Specific aspartyl and calpain proteases are required for neurodegeneration in *C. elegans*. *Nature.* (2002) 419:939–44. doi: 10.1038/nature01108
56. Millet ACM, Ewbank JJ. Immunity in *Caenorhabditis elegans*. *Curr Opin Immunol.* (2004) 16:4–9. doi: 10.1016/j.coi.2003.11.005
57. Yamashima T. Can 'calpain-cathepsin hypothesis' explain alzheimer neuronal death? *Ageing Res Rev.* (2016) 32:169–79. doi: 10.1016/j.arr.2016.05.008
58. Hasty P, Vijg J. Accelerating aging by mouse reverse genetics: a rational approach to understanding longevity. *Aging Cell.* (2004) 3:55–65. doi: 10.1111/j.1474-9728.2004.00082.x
59. Chang S, Multani AS, Cabrera NG, Naylor ML, Laud P, Lombard D, et al. Essential role of limiting telomeres in the pathogenesis of werner syndrome. *Nat Genet.* (2004) 36:877–82. doi: 10.1038/ng1389
60. Barlow C, Hirotsune S, Paylor R, Liyanage M, Eckhaus M, Collins F, et al. Atm-deficient mice: a paradigm of ataxia telangiectasia. *Cell.* (1996) 86:159–71.
61. Meyer-Luehmann M, Spires-Jones TL, Prada C, Garcia-Alloza M, De Calignon A, Rozkalne A, et al. Rapid appearance and local toxicity of amyloid-β plaques in a mouse model of Alzheimer's disease. *Nature.* (2008) 451:720–24. doi: 10.1038/nature06616
62. Meredith GE, Rademacher DJ. MPTP mouse models of Parkinson's disease: an update. *J Parkinsons Dis.* (2011) 1:19–33. doi: 10.3233/JPD-2011-11023
63. Arey RN, Murphy CT. Conserved regulators of cognitive aging: from worms to humans. *Behav Brain Res.* (2017) 322:299–310. doi: 10.1016/j.bbr.2016.06.035
64. Spilman P, Podlutskaya N, Hart MJ, Debnath J, Gorostiza O, Bredesen D, et al. Inhibition of mTOR by rapamycin abolishes cognitive deficits and reduces amyloid-β levels in a mouse model of Alzheimer's disease. *PLoS ONE.* (2010) 5:e9979. doi: 10.1371/journal.pone.0009979
65. Majumder S, Richardson A, Strong R, Oddo S. Inducing autophagy by rapamycin before, but not after, the formation of plaques and tangles ameliorates cognitive deficits. *PLoS ONE.* (2011) 6:e25416. doi: 10.1371/journal.pone.0025416
66. Vanhooren V, Libert C. The mouse as a model organism in aging research: usefulness, pitfalls and possibilities. *Ageing Res Rev.* (2013) 12:8–21. doi: 10.1016/j.arr.2012.03.010
67. Li J, Tang Y, Cai D. IKKβ/NF-κB disrupts adult hypothalamic neural stem cells to mediate a neurodegenerative mechanism of dietary obesity and pre-diabetes. *Nat Cell Biol.* (2012) 14:999–1012. doi: 10.1038/ncb2562
68. Zhang Y, Reichel JM, Han C, Zuniga-hertz JP. Astrocytic process plasticity and IKK b / NF- k B in central control of blood glucose, blood pressure, and body weight. *Cell Metab.* (2017) 25:1091–102. doi: 10.1016/j.cmet.2017.04.002
69. Ugur B, Chen K, Bellen HJ. Drosophila tools and assays for the study of human diseases. *Dis Model Mech.* (2016) 9:235–44. doi: 10.1242/dmm.023762
70. Yamamoto S, Jaiswal M, Charng WL, Gambin T, Karaca E, Mirzaa G, et al. A drosophila genetic resource of mutants to study mechanisms underlying human genetic diseases. *Cell.* (2014) 159:200–14. doi: 10.1016/j.cell.2014.09.002
71. Singh A, Irvine KD. *Drosophila* as a model for understanding development and disease. *Dev Dyn.* (2012) 241:1–2. doi: 10.1002/dvdy.23712
72. Spradling AC, Stern D, Beaton A, Rhem EJ, Laverty T, Mozden N, et al. The berkeley *Drosophila* genome project gene disruption project: single P-element insertions mutating 25% of vital drosophila genes. *Genetics.* (1999) 153:135–77.
73. Gargano JW, Martin I, Bhandari P, Grotewiel MS. Rapid iterative negative geotaxis (RING): a new method for assessing age-related locomotor decline in *Drosophila*. *Exp Gerontol.* (2005) 40:386–95. doi: 10.1016/j.exger.2005.02.005
74. Jones MA, Grotewiel M. *Drosophila* as a model for age-related impairment in locomotor and other behaviors. *Exp Gerontol.* (2011) 46:320–25. doi: 10.1016/j.exger.2010.08.012
75. Tamura T, Chiang AS, Ito N, Liu HP, Horiuchi J, Tully T, et al. Aging specifically impairs amnesiac-dependent memory in *Drosophila*. *Neuron.* (2003) 40:1003–11. doi: 10.1016/S0896-6273(03)00732-3
76. Rera M, Clark RI, Walker DW. Intestinal barrier dysfunction links metabolic and inflammatory markers of aging to death in *Drosophila*. *Proc Natl Acad Sci USA.* (2012) 109:21528–33. doi: 10.1073/pnas.1215849110
77. Kounatidis I, Chtarbanova S, Yang Cao MH, Dhruv Jayanth BG, Ligoxygakis P. NF-kB immunity in the brain determines fly lifespan in healthy aging and age-related neurodegeneration. *Cell Rep.* (2017) 19:836–48. doi: 10.1016/j.celrep.2017.04.007
78. Beaver LM, Gvakharia BO, Vollintine TS, Hege DM, Stanewsky R, Giebultowicz JM. Loss of circadian clock function decreases reproductive fitness in males of drosophila melanogaster. *Proc Natl Acad Sci USA.* (2002) 99:2134–9. doi: 10.1073/pnas.032426699
79. Piper MDW, Partridge L. Drosophila as a model for ageing. *Biochim Biophys Acta Mol Basis Dis.* (2018) 1864:2707–17. doi: 10.1016/j.bbadis.2017.09.016
80. Partridge L, Piper MDW, Mair W. Dietary restriction in *Drosophila*. *Mech Ageing Dev.* (2005) 126:938–50. doi: 10.1016/j.mad.2005.03.023
81. Limmer S, Weiler A, Volkenhoff A, Babatz F, Klämbt C. The *Drosophila* blood-brain barrier: development and function of a glial endothelium. *Front Neurosci.* (2014) 8:365. doi: 10.3389/fnins.2014.00365
82. Lovick JK, Ngo KT, Omoto JJ, Wong DC, Nguyen JD, Hartenstein V. Postembryonic lineages of the *Drosophila* brain: I. Development of the lineage-associated fiber tracts. *Dev Biol.* (2013) 384:228–57. doi: 10.1016/j.ydbio.2013.07.008
83. Kremer MC, Jung C, Batelli S, Rubin GM, Gaul U. The glia of the adult *Drosophila* nervous system. *Glia.* (2017) 65:606–38. doi: 10.1002/glia.23115
84. Freeman MR, Doherty J. Glial cell biology in *Drosophila* and vertebrates. *Trends Neurosci.* (2006) 29:82–90. doi: 10.1016/j.tins.2005.12.002
85. Carlson SD, Juang J-L, Hilgers SL, Garment MB. Blood barriers of the insect. *Annu Rev Entomol.* (2000) 45:151–74. doi: 10.1146/annurev.ento.45.1.151
86. Omoto JJ, Lovick JK, Hartenstein V. Origins of glial cell populations in the insect nervous system. *Curr Opin Insect Sci.* (2016) 18:96–104. doi: 10.1016/j.cois.2016.09.003
87. Yildirim K, Petri J, Kottmeier R, Klämbt C. *Drosophila glia*: few cell types and many conserved functions. *Glia.* (2019) 67:5–26. doi: 10.1002/glia.23459
88. Hartenstein V. Structure and development of glia in *Drosophila*. *Glia.* (2011) 59:1237–52. doi: 10.1002/glia.21162
89. Doherty J, Logan MA, Freeman MR. Ensheathing glia function as phagocytes in the adult *Drosophila* brain. *J Neurosci.* (2009) 29:4768–81. doi: 10.1523/JNEUROSCI.5951-08.2009
90. Barres BA. Perspective the mystery and magic of glia : a perspective on their roles in health and disease. *Neuron.* (2008) 60:430–40. doi: 10.1016/j.neuron.2008.10.013
91. Ng FS, Tangredi MM, Jackson FR. Glial cells physiologically modulate clock neurons and circadian behavior in a calcium-dependent manner. *Curr Biol.* (2011) 21:625–34. doi: 10.1016/j.cub.2011.03.027
92. Lu B, Vogel H. *Drosophila* models of neurodegenerative diseases. *Annu Rev Pathol Mech Dis.* (2009) 4:315–42. doi: 10.1146/annurev.pathol.3.121806.151529
93. Ye Y, Fortini ME. Apoptotic activities of wild-type and Alzheimer's disease-related mutant presenilins in *Drosophila melanogaster*. *J Cell Biol.* (1999) 146:1351–64. doi: 10.1083/jcb.146.6.1351

94. Finelli A, Kelkar A, Song HJ, Yang H, Konsolaki M. A model for studying Alzheimer's Aβ42-induced toxicity in *Drosophila melanogaster*. *Mol Cell Neurosci.* (2004) 26:365–75. doi: 10.1016/j.mcn.2004.03.001
95. McLeod CJ, O'Keefe LV, Richards RI. The pathogenic agent in *Drosophila* models of "polyglutamine" diseases. *Hum Mol Genet.* (2005) 14:1041–48. doi: 10.1093/hmg/ddi096
96. Bilen J, Bonini NM. *Drosophila* as a model for human neurodegenerative disease. *Annu Rev Genet.* (2005) 39:153–71. doi: 10.1146/annurev.genet.39.110304.095804
97. Dabool L, Juravlev L, Hakim-Mishnaevski K, Kurant E. Modeling Parkinson's disease in adult *Drosophila*. *J Neurosci Methods.* (2019) 311:89–94. doi: 10.1016/j.jneumeth.2018.10.018
98. Tickoo S, Russell S. *Drosophila melanogaster* as a model system for drug discovery and pathway screening. *Curr Opin Pharmacol.* (2002) 2:555–60. doi: 10.1016/S1471-4892(02)00206-0
99. Kounatidis I, Ligoxygakis P. *Drosophila* as a model system to unravel the layers of innate immunity to infection. *Open Biol.* (2012) 2:120075. doi: 10.1098/rsob.120075
100. Lemaitre B, Hoffmann J. The host defense of *Drosophila melanogaster*. *Annu Rev Immunol.* (2007) 25:697–743. doi: 10.1146/annurev.immunol.25.022106.141615
101. Neyen C, Bretscher AJ, Binggeli O, Lemaitre B. Methods to study *Drosophila* immunity. *Methods.* (2014) 68:116–28. doi: 10.1016/j.ymeth.2014.02.023
102. Ferrandon D, Jung AC, Criqui MC, Lemaitre B, Uttenweiler-Joseph S, Michaut L, et al. A drosomycin-GFP reporter transgene reveals a local immune response in *Drosophila* that is not dependent on the toll pathway. *EMBO J.* (1998) 17:1217–27. doi: 10.1093/emboj/17.5.1217
103. Liehl P, Blight M, Vodovar N, Boccard F, Lemaitre B. Prevalence of local immune response against oral infection in a *Drosophila/Pseudomonas* infection model. *PLoS Pathog.* (2006) 2:e56. doi: 10.1371/journal.ppat.0020056
104. Tzou P, De Gregorio E, Lemaitre B. How *Drosophila* combats microbial infection: a model to study innate immunity and host-pathogen interactions. *Curr Opin Microbiol.* (2002) 5:102–10. doi: 10.1016/S1369-5274(02)00294-1
105. Ayres JS, Schneider DS. A signaling protease required for melanization in *Drosophila* affects resistance and tolerance of infections. *PLoS Biol.* (2008) 6:2764–73. doi: 10.1371/journal.pbio.0060305
106. Stuart LM, Ezekowitz RA. Phagocytosis and comparative innate immunity: learning on the fly. *Nat Rev Immunol.* (2008) 8:131–41. doi: 10.1038/nri2240
107. Hultmark D. *Drosophila* immunity : paths and patterns. *Curr Opin Immunol.* (2003) 15:12–19. doi: 10.1016/S0952-7915(02)00005-5
108. Anderson KV, Bokla L, Nüsslein-Volhard C. Establishment of dorsal-ventral polarity in the *Drosophila embryo*: the induction of polarity by the toll gene product. *Cell.* (1985) 42:791–8. doi: 10.1016/0092-8674(85)90275-2
109. Lemaitre B, Nicolas E, Michaut L, Reichhart J-M, Hoffmann JA. The dorsoventral regulatory gene cassette spä tzle/Toll/cactus controls the potent antifungal response in *Drosophila* adults. *Cell.* (1996) 86:973–83. doi: 10.1016/S0092-8674(00)80172-5
110. Gottar M, Gobert V, Matskevich AA, Reichhart JM, Wang C, Butt TM, et al. Dual detection of fungal infections in *Drosophila* via recognition of glucans and sensing of virulence factors. *Cell.* (2006) 127:1425–37. doi: 10.1016/j.cell.2006.10.046
111. Issa N, Guillaumot N, Lauret E, Matt N, Schaeffer-Reiss C, Van Dorsselaer A, et al. The circulating protease persephone is an immune sensor for microbial proteolytic activities upstream of the *Drosophila* toll pathway. *Mol Cell.* (2018) 69:539–50.e6. doi: 10.1016/j.molcel.2018.01.029
112. Vaz F, Kounatidis I, Covas G, Parton RM, Harkiolaki M, Davis I, et al. Accessibility to peptidoglycan is important for the recognition of gram-positive bacteria in *Drosophila*. *Cell Rep.* (2019) 27:2480–92.e6. doi: 10.1016/j.celrep.2019.04.103
113. Weber ANR, Tauszig-Delamasure S, Hoffmann JA, Lelièvre E, Gascan H, Ray KP, et al. Binding of the *Drosophila* cytokine spätzle to toll is direct and establishes signaling. *Nat Immunol.* (2003) 4:794–800. doi: 10.1038/ni955
114. Valanne S, Wang J, Rämet M. The *Drosophila* toll signaling pathway. *J Immunol.* (2011) 186:649–56. doi: 10.4049/jimmunol.1002302
115. Kaneko T, Yano T, Aggarwal K, Lim JH, Ueda K, Oshima Y, et al. PGRP-LC and PGRP-LE have essential yet distinct functions in the *Drosophila* immune response to monomeric DAP-type peptidoglycan. *Nat Immunol.* (2006) 7:715–23. doi: 10.1038/ni1356
116. Myllymaki H, Valanne S, Ramet M. The *Drosophila* imd signaling pathway. *J Immunol.* (2014) 192:3455–62. doi: 10.4049/jimmunol.1303309
117. Hoesel B, Schmid JA. The complexity of NF-κB signaling in inflammation and cancer. *Mol Cancer.* (2013) 12:86. doi: 10.1186/1476-4598-12-86
118. Georgel P, Kappler C, Langley E, Gross I, Reichhart J, Hoffmann JA. *Drosophila* immunity. A sequence homologous to mammalian interferon consensus response element enhances the activity of the diptericin promoter. *Nucleic Acids Res.* (1995) 23:1140–45. doi: 10.1093/nar/23.7.1140
119. Bischoff V, Vignal C, Duvic B, Boneca IG, Hoffmann JA, Royet J. Downregulation of the *Drosophila* immune response by peptidoglycan- recognition proteins SC1 and SC2. *PLoS Pathog.* (2006) 2:e14. doi: 10.1371/journal.ppat.0020014
120. Maillet F, Bischoff V, Vignal C, Hoffmann J, Royet J. The *Drosophila* peptidoglycan recognition protein PGRP-LF blocks PGRP-LC and IMD/JNK pathway activation. *Cell Host Microbe.* (2008) 3:293–303. doi: 10.1016/j.chom.2008.04.002
121. Charroux B, Capo F, Peslier S, Chaduli D, Viallat-lieutaud A, Royet J, et al. Cytosolic and secreted peptidoglycan-degrading enzymes in *Drosophila* respectively control local and systemic immune responses to microbiota article cytosolic and secreted peptidoglycan-degrading enzymes in *Drosophila* respectively control local and systemi. *Cell Host Microbe.* (2018) 23:215–28. doi: 10.1016/j.chom.2017.12.007
122. Kaneko T, Silverman N. Bacterial recognition and signalling by the *Drosophila* IMD pathway. *Cell Microbiol.* (2005) 7:461–9. doi: 10.1111/j.1462-5822.2005.00504.x
123. Basbous N, Coste F, Leone P, Vincentelli R, Royet J, Kellenberger C, et al. The *Drosophila* peptidoglycan-recognition protein LF interacts with peptidoglycan-recognition protein LC to downregulate the Imd pathway. *EMBO Rep.* (2011) 12:327–33. doi: 10.1038/embor.2011.19
124. Aggarwal K, Rus F, Vriesema-Magnuson C, Ertürk-Hasdemir D, Paquette N, Silverman N. Rudra interrupts receptor signaling complexes to negatively regulate the IMD pathway. *PLoS Pathog.* (2008) 4:e1000120. doi: 10.1371/journal.ppat.1000120
125. Lhocine N, Ribeiro PS, Buchon N, Wepf A, Wilson R, Tenev T, et al. Article PIMS modulates immune tolerance by negatively regulating *Drosophila* innate immune signaling. *Cell Host Microbe.* (2008) 4:147–58. doi: 10.1016/j.chom.2008.07.004
126. Kleino A, Myllymaki H, Kallio J, Vanha-aho L-M, Oksanen K, Ulvila J, et al. Pirk is a negative regulator of the *Drosophila* imd pathway. *J Immunol.* (2008) 180:5413–22. doi: 10.4049/jimmunol.180.8.5413
127. Cao Y, Chtarbanova S, Petersen AJ, Ganetzky B. Dnr1 mutations cause neurodegeneration in *Drosophila* by activating the innate immune response in the brain. *Proc Natl Acad Sci U S A.* (2013) 110:E1752–60. doi: 10.1073/pnas.1306220110
128. Chen J, Chen ZJ. Regulation of NF-κB by ubiquitination. *Curr Opin Immunol.* (2013) 25:4–12. doi: 10.1016/j.coi.2012.12.005
129. Lee K-Z, Ferrandon D. Negative regulation of immune responses on the fly. *EMBO J.* (2011) 30:988–90. doi: 10.1038/emboj.2011.47
130. Leulier F. Tuning down NF-κB signaling by DUBs: a fly case. *Cell Host Microbe.* (2009) 6:294–6. doi: 10.1016/j.chom.2009.10.002
131. Fernando MDA, Kounatidis I, Ligoxygakis P. Loss of trabid, a new negative regulator of the *Drosophila* immune-deficiency pathway at the level of TAK1, reduces life span. *PLoS Genet.* (2014) 10:e1004117. doi: 10.1371/journal.pgen.1004117
132. Tsuda M, Langmann C, Harden N, Aigaki T. The RING-finger scaffold protein Plenty of SH3s targets TAK1 to control immunity signalling in *Drosophila*. *EMBO Rep.* (2005) 6:1082–7. doi: 10.1038/sj.embor.7400537
133. Tsichritzis T, Gaentzsch PC, Kosmidis S, Brown AE, Skoulakis EM, Ligoxygakis P, et al. A *Drosophila* ortholog of the human cylindromatosis tumor suppressor gene regulates triglyceride content and antibacterial defense. *Development.* (2007) 134:2605–14. doi: 10.1242/dev.02859
134. Khush RS, Cornwell WD, Uram JN, Lemaitre B. A ubiquitin-proteasome pathway represses the *Drosophila* immune deficiency signaling cascade least seven types of antimicrobial peptides that are ac- tive against different classes

of microbes. These pep- tides are synthesized in both surface epithelial ti. *Curr Biol.* (2002) 12:1728–37. doi: 10.1016/S0960-9822(02)01214-9
135. Shibata T, Sekihara S, Fujikawa T, Miyaji R, Maki K, Ishihara T, et al. Transglutaminase-catalyzed protein-protein cross-linking suppresses the activity of the NF-κB-like transcription factor relish. *Sci Signal.* (2013) 6:1–11. doi: 10.1126/scisignal.2003970
136. Sanuki R, Tanaka T, Suzuki F, Ibaraki K, Takano T. Normal aging hyperactivates innate immunity and reduces the medical efficacy of minocycline in brain injury. *Brain Behav Immun.* (2019) 80:427–38. doi: 10.1016/j.bbi.2019.04.023
137. Dubey SK, Tapadia MG. Yorkie regulates neurodegeneration through canonical pathway and innate immune response. *Mol Neurobiol.* (2018) 55:1193–207. doi: 10.1007/s12035-017-0388-7
138. Maitra U, Scaglione MN, Chtarbanova S, O'Donnell JM. Innate immune responses to paraquat exposure in a *Drosophila* model of Parkinson's disease. *Sci Rep.* (2019) 9:12714. doi: 10.1038/s41598-019-48977-6
139. Chinchore Y, Gerber GF, Dolph PJ. Alternative pathway of cell death in *Drosophila* mediated by NF-κB transcription factor relish. *Proc Natl Acad Sci USA.* (2012) 109:E605–12. doi: 10.1073/pnas.1110666109
140. Ray A, Speese SD, Logan MA. Glial draper rescues Aβ toxicity in a *Drosophila* model of Alzheimer's disease. *J Neurosci.* (2017) 37:11881–93. doi: 10.1523/JNEUROSCI.0862-17.2017
141. Purice MD, Speese SD, Logan MA. Delayed glial clearance of degenerating axons in aged *Drosophila* is due to reduced PI3K/Draper activity. *Nat Commun.* (2016) 7:12871. doi: 10.1038/ncomms12871
142. McLaughlin CN, Perry-Richardson JJ, Coutinho-Budd JC, Broihier HT. Dying neurons utilize innate immune signaling to prime glia for phagocytosis during development. *Dev Cell.* (2019) 48:506–22.e6. doi: 10.1016/j.devcel.2018.12.019
143. Labzin LI, Heneka MT, Latz E. Innate immunity and neurodegeneration. *Annu Rev Med.* (2018) 69:437–49. doi: 10.1146/annurev-med-050715-104343
144. Letiembre M, Hao W, Liu Y, Walter S, Mihaljevic I, Rivest S, et al. Innate immune receptor expression in normal brain aging. *Neuroscience.* (2007) 146:248–54. doi: 10.1016/j.neuroscience.2007.01.004
145. Tusco R, Jacomin AC, Jain A, Penman BS, Larsen KB, Johansen T, et al. Kenny mediates selective autophagic degradation of the IKK complex to control innate immune responses. *Nat Commun.* (2017) 8:1–15. doi: 10.1038/s41467-017-01287-9
146. Wu SC, Cao ZS, Chang KM, Juang JL. Intestinal microbial dysbiosis aggravates the progression of Alzheimer's disease in *Drosophila*. *Nat Commun.* (2017) 8:24. doi: 10.1038/s41467-017-00040-6
147. Westfall S, Lomis N, Id SP. A novel synbiotic delays alzheimer's disease onset via combinatorial gut-brain-axis signaling in *Drosophila* melanogaster. *PLoS ONE.* (2019) 14:e0214985. doi: 10.1371/journal.pone.0214985
148. Jeibmann A, Paulus W. *Drosophila* melanogaster as a model organism of brain diseases. *Int J Mol Sci.* (2009) 10:407–40. doi: 10.3390/ijms10020407
149. Benner EJ, Mosley RL, Destache CJ, Lewis TB, Jackson-Lewis V, Gorantla S, et al. Therapeutic immunization protects dopaminergic neurons in a mouse model of Parkinson's disease. *Proc Natl Acad Sci USA.* (2004) 101:9435–40. doi: 10.1073/pnas.0400569101

Conflict of Interest: The authors declare that the research was conducted in the absence of any commercial or financial relationships that could be construed as a potential conflict of interest.

frontiers in Immunology

ORIGINAL RESEARCH
published: 31 July 2020
doi: 10.3389/fimmu.2020.01528

Immune Control of Animal Growth in Homeostasis and Nutritional Stress in *Drosophila*

Preethi P[1], *Ajay Tomar*[1,2], *Sukanya Madhwal*[1,3] *and Tina Mukherjee*[1]*

[1] *Institute for Stem Cell Science and Regenerative Medicine (inStem), Bangalore, India,* [2] *The University of Trans-Disciplinary Health Sciences and Technology, Bangalore, India,* [3] *Manipal Academy of Higher Education, Manipal, India*

A large body of research implicates the brain and fat body (liver equivalent) as central players in coordinating growth and nutritional homeostasis in multicellular animals. In this regard, an underlying connection between immune cells and growth is also evident, although mechanistic understanding of this cross-talk is scarce. Here, we explore the importance of innate immune cells in animal growth during homeostasis and in conditions of nutrient stress. We report that *Drosophila* larvae lacking blood cells eclose as small adults and show signs of insulin insensitivity. Moreover, when exposed to dietary stress of a high-sucrose diet (HSD), these animals are further growth retarded than normally seen in regular animals raised on HSD. In contrast, larvae carrying increased number of activated macrophage-like plasmatocytes show no defects in adult growth when raised on HSD and grow to sizes almost comparable with that seen with regular diet. These observations imply a central role for immune cell activity in growth control. Mechanistically, our findings reveal a surprising influence of immune cells on balancing fat body inflammation and insulin signaling under conditions of homeostasis and nutrient overload as a means to coordinate systemic metabolism and adult growth. This work integrates both the cellular and humoral arm of the innate immune system in organismal growth homeostasis, the implications of which may be broadly conserved across mammalian systems as well.

Keywords: myeloid cells, high sugar, metabolism, inflammation, stress, innate immunity, insulin

OPEN ACCESS

Edited by:
Dan Hultmark,
Umeå University, Sweden

Reviewed by:
Michelle L. Bland,
University of Virginia, United States
Michael J. Williams,
Uppsala University, Sweden

***Correspondence:**
Tina Mukherjee
tinam@instem.res.in

Specialty section:
This article was submitted to Comparative Immunology, a section of the journal Frontiers in Immunology

Received: *12 November 2019*
Accepted: *10 June 2020*
Published: *31 July 2020*

Citation:
P P, Tomar A, Madhwal S and Mukherjee T (2020) Immune Control of Animal Growth in Homeostasis and Nutritional Stress in Drosophila. Front. Immunol. 11:1528. doi: 10.3389/fimmu.2020.01528

INTRODUCTION

The immune system comprises circulating cells and blood-forming tissues whose main function is combating infections. The development of this system is metabolically expensive and often associated with trade-offs with other physiological functions such as reproductive fitness (1, 2) and survival, especially in conditions of nutrition challenge (3). Development of a robust immune system and its impact on animal growth has been described in several studies across animal models. Decreased immune function in flies with increased body mass (4) or improved resistance with reduced competitive ability on a poor diet (5) are some studies illustrating this robust connection. Nevertheless, any understanding of animal growth from the standpoint of immune homeostasis is poorly explored. *Drosophila* is a well-established and a conserved model system for addressing questions pertinent to blood development (6) and mechanisms regulating organismal growth (7) mechanisms. In this study, we have used *Drosophila* to explore the consequences of altering immune homeostasis early in animal life on organismal metabolism and growth control and the implications of nutrient overload in this phenomenon.

Drosophila blood cells akin to vertebrate myeloid cells perform functions central to the maintenance of general animal physiology that includes wound healing response (8), antimicrobial functions (9), hypoxia response (10), innate immunity, and response to wasp-parasitization (11). Of the three different types of blood cells prevailing within the *Drosophila* larvae, the platelet-like crystal cells are implicated in wound healing and hypoxia response, whereas lamellocytes are involved in the response to parasitic wasps. The phagocytic plasmatocytes constitute 95% of the differentiated mature cell type. These phagocytic blood cells, akin to vertebrate macrophages, perform functions relevant for clearance of apoptotic cells and invading particles, neuronal pruning, tissue remodeling, and antimicrobial functions (12). Immune cells in *Drosophila* are derived from immune progenitor cells whose development, much like in vertebrates, is derived from two distinct waves of hematopoiesis: the primitive and the definitive. The primitive wave of hematopoiesis occurs in the early embryonic stage where the first pool of blood precursors gets specified from embryonic head mesoderm (13, 14). These hematopoietic precursors proliferate and differentiate into mature hemocytes and constitute the larval circulatory and sessile pools of blood cells detected in the larvae (15) and later in adult stages (12). Definitive hematopoiesis initiates in a larval hematopoietic organ called the lymph gland, which gets specified at the late stages of embryonic development (13, 14). The lymph gland comprises multipotent undifferentiated blood progenitor cells that proliferate and mature to give rise to differentiated blood cells during larval stages of development. By the early pupal stage, the blood progenitor cells completely differentiate, after which the lymph gland disintegrates to release these mature hemocytes into circulation contributing to immune cells in the adult fly (6, 12). By early pupal stage, blood cells complete differentiation into hemocytes, after which the lymph gland disintegrates to release these cells into circulation in the adult fly.

The cues that regulate blood development and homeostasis in *Drosophila* are of both local as well as systemic origin (6). The systemic cues include environmental (odors and sensory stimulation) (16, 17) and of nutritional origins (18), the latter, more relevant to this study. During blood development, blood progenitor cells directly sense amino acids and insulin to sustain their maintenance. Starvation or loss of insulin signaling results in the differentiation of progenitors and activation of inflammatory responses, recapitulating a diabetic-like condition (18). Nutrient-rich conditions (19) or any change in the physiological state of the developing larvae (3) have been shown to alter immune cell numbers as well. As immune cells undergo functional maturation, the macrophage-like plasmatocytes perform lipid-scavenging functions and exert systemic control on glucose homeostasis and survival on lipid-rich diet (20). Taken together, these studies provide evidence of nutrient-dependent modulation of immune cell development, homeostasis, and signaling. What remain unclear are the underlying contributions of the immune cell changes on animal physiology in modulating nutrient conditions. We hypothesize immune cells as effectors of coordinating metabolic homeostasis under these conditions and they are necessary for organismal homeostasis.

Animal growth is a complex adaptive process that is dependent on extrinsic nutrient conditions, and is intricately linked with cues of both developmental (21, 22) and nutritional origins (7, 23, 24). These cues coordinate a central growth program that ensures animals achieve their size and proportion within their respective developmental time scale (21). This cross-talk is facilitated by long-range signaling molecules originating from the brain and fat body in *Drosophila* to coordinate the scaling of animal size in response to nutrient availability (7) uptake, and utilization (21, 25). Indeed, several recent studies have demonstrated a complex interplay of insulin signaling with innate immune pathways in growth and nutritional homeostasis (26–29). These studies have positioned the fat body as the major organ responsible for sensing and storing nutrients, in addition to its immune effector functions as a central member of the innate immune system.

Cells of the innate immune system also sense microbial load, integrate metabolic inputs, and alter nutrient allocation and organismal growth when performing pathogenic clearance functions (3, 30, 31). These functions are very similar to roles performed by the fat body, and we hypothesize immune cells as regulators of metabolism and organismal metabolic homeostasis not only in conditions of immune challenge but also in homeostasis or modulating nutrient environments. Development of metabolic disorders such as diabetes and obesity with altered immune cell activity and function are in agreement with this idea (32). In this study, we test this hypothesis and observe that blood cells are necessary to coordinate systemic metabolism and animal growth in homeostasis and in conditions of nutrient overload. Loss or gain of blood cells early in larval development affected adult growth. Our experiments suggest a role for blood cells in the control of fat body innate immune homeostasis and insulin sensitivity. These findings indicate that immune cell activity, as opposed to their number, orchestrates organismal growth homeostasis especially in conditions of dietary excess.

RESULTS

Drosophila Larval Blood Cells Function to Control Growth of Adult Flies

We aim to explore non-immune homeostatic functions of mature immune cells. To initiate this investigation, the impact of hemocyte ablation from early *Drosophila* larval stages on larval metabolism and development was assessed. *Hemolectin$^{\Delta}$Gal4 (Hml$^{\Delta}$ >)* (**Figure 1a**) was used as the driver to express the pro-apoptotic gene, *hid* in blood cells. Expressing *UAS-hid* specifically in blood cells leads to killing of a majority of blood cells (**Figures 1b–f**) (33). *UAS-hid* control larvae showed no changes in blood cell numbers or overall larval growth (**Supplementary Figures 1a–c**), confirming that the dramatic loss of immune cells was specific to *UAS-hid* expression and not a consequence of leaky or non-autonomous *UAS-hid* transgene expression. We ensured the specificity of *Hml$^{\Delta}$Gal4* driver line by conducting lineage analysis using G-TRACE (34). This

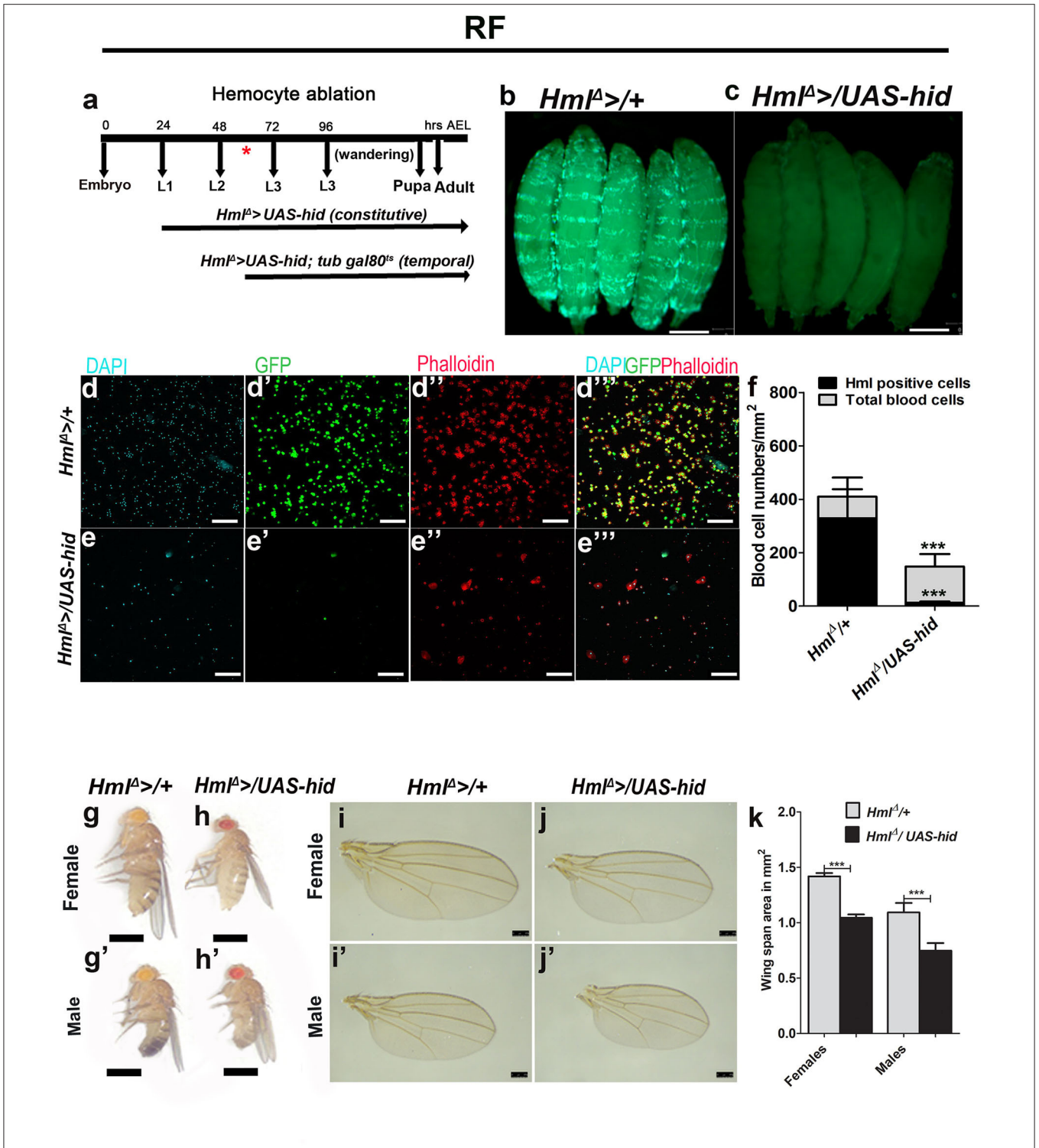

FIGURE 1 | Ablating *Drosophila* larval blood cells leads to adult fly growth defect. In **(b,c,g–h')**, scale bar = 1 mm, **(d–e'')** = 40 μm, and **(i–j')** = 250 μm. RF indicates regular food. In **(f,k)** bar graphs represent mean ± standard deviation (SD). Statistical analysis applied in **(f,k)** is unpaired *t*-test, two-tailed. "*n*" is the total number of larvae analyzed and "*N*" is the total number of repeats. **(a)** Pictorial representation of the constitutive and temporal experiments undertaken using "*Hml*$^{\Delta}$ >" and "*Hml*$^{\Delta}$ >*; tub gal80*^{ts}," respectively. **(b–f)** Overexpression of "hid" in Hml-positive cells (*Hml*$^{\Delta}$ >*UAS-GFP/UAS*-hid) leads to efficient killing of blood cells. **(b)** Control (*Hml*$^{\Delta}$ >*UAS-GFP*) larvae depicting blood cells (Hml, green), **(c)** *Hml*$^{\Delta}$ >*UAS-GFP/UAS*-hid larvae show lack of GFP expression. **(d–e'')** Blood cell characterization in **(d-d'')** control and **(e–e'')** *Hml*$^{\Delta}$ >*UAS-GFP/UAS-hid* larvae reveals reduction in total blood cell numbers, but this does not lead to a complete

(Continued)

FIGURE 1 | loss in blood cells as evident from **(d,e)** DAPI, **(d′,e′)** Hml expression (*Hml*$^{\Delta}$ >*UAS-GFP*), and **(d″,e″)** Phalloidin stainings. **(d′″,e′″)** Merge of all the channels. **(f)** Graphical representation of total and Hml^{+} blood cells in control, *Hml*$^{\Delta}$ >*UAS-GFP*, and *Hml*$^{\Delta}$ >*UAS-GFP/UAS-hid* larvae. Control (*Hml*$^{\Delta}$ >*UAS-GFP/+*) total number of blood cells/mm^2 ($n = 16$, 409.8 ± 149.4) and Hml-GFP positive cells/mm^2 ($n = 16$, 328.8 ± 108.8). *Hml*$^{\Delta}$ >*UAS-GFP/UAS-hid* show significantly less number of total blood cells/mm^2 ($n = 16$,148.3 ± 50.04, ***p-value = 0.0003, in comparison with control total blood cells) and less Hml-GFP-positive cells ($n = 16$, 13.11 ± 4.0, ***p-value < 0.0001 in comparison with control Hml^{+} cells). **(g–k)** Blood cell ablation affects adult growth. **(g–h′)** Representative images showing adult size defect. In comparison with **(g,g′)** control adult (*Hml*$^{\Delta}$ >/+) **(g)** female and **(g′)** male fly, **(h, h′)** *Hml*$^{\Delta}$ >*/UAS-hid* **(h)** female and **(h′)** male adult flies are smaller in size. **(i–j′)** This growth defect is also shown seen in wing span areas. Representative adult wings from **(i,i′)** controls (*Hml*$^{\Delta}$ >/+) and **(j,j′)** *Hml*$^{\Delta}$ >*/UAS-hid* adults. **(k)** Quantification of wingspan areas. *Hml*$^{\Delta}$ >/+ (female $n = 100$, 1.42 ± 0.03, male $n = 1.00$, 1.1 ± 0.08) and *Hml*$^{\Delta}$ >*/UAS-hid* (female $n = 100$, 1.04 ± 0.03 (***p-value < 0.0001), male $n = 100$, 0.74 ± 0.07 (***p-value < 0.0001).

approach confirmed *hid* expression (both in real time and lineage based) in blood cells alone, without any expression detected in other larval tissues (**Supplementary Figures 1d–h″**). *Hml*$^{\Delta}$*Gal4* is seen in differentiating and mature populations of larval immune cells, which are essentially the plasmatocytes (**Supplementary Figures 1i–i″**) (35, 36), making *Hml*$^{\Delta}$*Gal4* a reliable driver line to specifically modulate immune cells and assess systemic changes.

Driving *UAS-hid* with *Hml*$^{\Delta}$ >resulted in an overall reduction in blood cells. We report a dramatic loss of *Hml* positive (*Hml*$^{+}$) hemocytes (**Figures 1b–f**) with a small increase in *Hml* negative (*Hml*$^{-}$) blood cells (**Figures 1d–f**). These results are consistent with published reports (33). Loss of *Drosophila* larval hemocytes using this strategy dramatically affected adult fly sizes (**Figures 1g–h′**). This was not a consequence of any major defect in larval development in *Hml*$^{\Delta}$ >*/UAS-hid* animals (**Figure 1c** compared with **Figure 1b**). However, any minor differences cannot be ruled out. To estimate the degree of adult growth retardation, wing span areas of both female and male flies were measured. We observed a significant reduction in wing span areas of *Hml*$^{\Delta}$ >*/UAS-hid* adults (**Figures 1i–k**), indicating a role for *Hml*$^{+}$ blood cells in animal growth control.

Next, we assessed the temporal requirement of larval blood cells in growth control. To address this, we conducted blood cell ablations at mid L2/early L3 time point. Using the temperature-sensitive form of *Gal80*, the expression of *Hml*$^{\Delta}$ > was regulated to drive *UAS-hid* transgene expression from mid L2 larval time point until wandering L3 after which these animals were dissected (**Supplementary Figure 2a**). While this temporal expression of *UAS-hid* was sufficient to successfully eliminate *Hml*$^{+}$ larval blood cells (**Supplementary Figures 2a–c**), the conditional loss of blood cells post L2 phase of larval development did not result in defective adult growth (**Supplementary Figures 2d–g′**), as assessed by adult fly sizes (**Supplementary Figures 2d–e′**) or wing span areas (**Supplementary Figures 2f–h**). Together, these results show that Hml^{+} cells play a critical role in the systemic control of animal growth at the early phase of the larval development rather than later in larval life.

Blood Cells Regulate Insulin Signaling

Insulin signaling is a central regulator of animal growth (37). To understand the underlying regulation by blood cells in coordinating systemic growth, we undertook an in-depth analysis of insulin signaling in *Hml*$^{\Delta}$ >*/UAS-hid* animals. We first assessed production and expression of different Dilp genes from the insulin producing cells (IPCs) of feeding L3 larvae. Dilp release from the IPCs is dependent on feeding state of the animal. As long as larvae are feeding, Dilps are produced and released from the IPCs. In non-feeding state or in conditions of nutritional deprivation such as starvation, Dilp release is inhibited leading to their accumulation in the IPCs (37). We conducted immunohistochemical and quantitative m*RNA* analysis of Dilp 2 and 5. Compared with control larvae, *Hml*$^{\Delta}$ >*/UAS-hid* animals showed increased Dilp 2 and Dilp 5 peptide expression in the IPCs (**Figures 2a–d**, **Supplementary Figures 3a,b**). To test whether the increase was a consequence of heightened synthesis of Dilp 2 and 5, qRT-PCR analysis was done for *Dilp 2* and *5* m*RNA* levels in feeding L3 larval brain tissues (**Figure 2e**). There was no increase in the levels of mRNA suggesting that the increase observed in Dilp 2 and Dilp 5 peptide expression was most likely a consequence of its accumulation or abrogated release. Blocking Dilp release or its accumulation in the brain IPCs is associated with hyperglycemia, which is a characteristic of reduced insulin signaling. Therefore, we tested readouts of glucose homeostasis, measuring circulating levels of glucose and trehalose as well as whole-animal glucose and glycogen and TAG levels. These biochemical assays were performed on feeding L3 larvae from control and *Hml*$^{\Delta}$ >*/UAS-hid* backgrounds. As reported in conditions of reduced Dilp release, in *Hml*$^{\Delta}$ >*/UAS-hid* animals, a significant increase of glucose and trehalose was observed in the circulating hemolymph (**Figures 2f,g**). Whole-animal glycogen was reduced (**Figure 2h**), whereas glucose levels were upregulated (**Figure 2i**). Further, increased levels of TAG were observed in whole larvae, circulating hemolymph, and fat body (**Figure 2l**). Neutral lipids detected via Nile red staining also confirmed increased TAG accumulation in *Hml*$^{\Delta}$ >*/UAS-hid* fat bodies (**Figures 2j,k**). Lipid droplet size in these fat bodies was comparatively larger than seen in control conditions (**Figures 2j,k**).

Consistent with the biochemical analysis, assessment of downstream readouts of insulin signaling in the fat body also revealed a reduction in insulin signaling. Fat body glucose levels were reduced (**Supplementary Figure 3c**). Expression levels of tGPH, a membrane-associated GFP expression marker whose fluorescence is an indicator of insulin-dependent PI3K activity in living cells (38, 39), showed a reduction in *Hml*$^{\Delta}$ >*/UAS-hid* larval fat bodies (**Figures 2m–o**). Insulin-mediated repression of FoxO nuclear localization and signaling (40) was also affected in *Hml*$^{\Delta}$ >*/UAS-hid* larvae. FoxO protein (detected using antibodies against it), which was detected primarily in the cytoplasm of control fat body tissues, in *Hml*$^{\Delta}$ >*/UAS-hid* larval fat bodies, was nuclear localized (**Figures 2p,q**). Subsequently, we also checked for the mRNA levels of FoxO targets *4EBP*, *InR*,

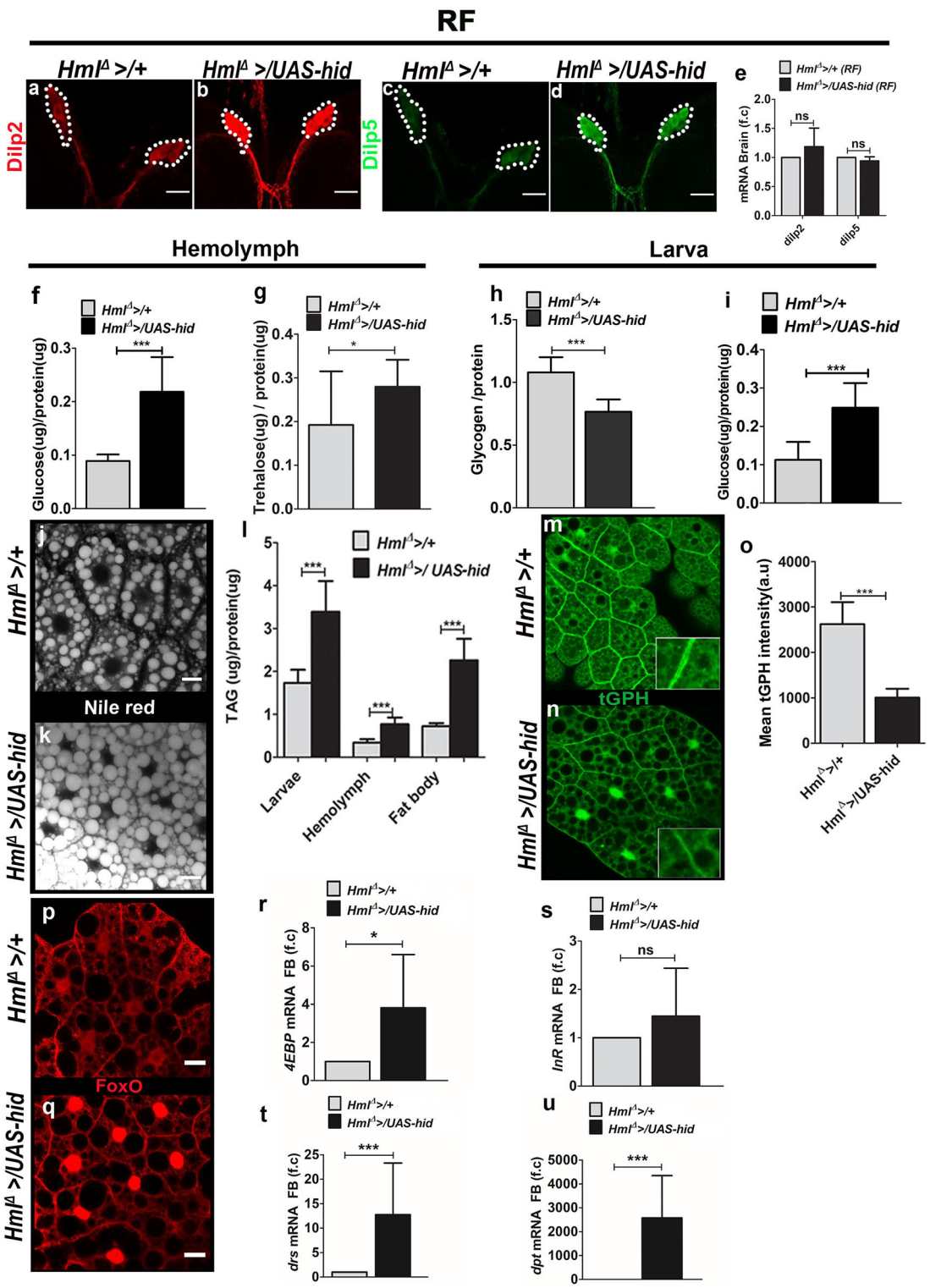

FIGURE 2 | Ablation of Hml^{+} plasmatocytes regulates fat body insulin sensitivity and inflammatory homeostasis. In **(a–d,j,k,p,q),** scale bar = 20 μm. In **(e–i,l,o,r–u)** bar graphs represent mean ± standard deviation (SD). Statistical analysis, unpaired *t*-test, two-tailed in **(e–i,l,o,r–u)**. "n" is the total number of larvae analyzed, RF is regular food, FB is fat body, f.c is fold change, a.u is arbitrary units. **(a–e)** Dilp2 and Dilp5 analysis in feeding L3 larval brains. Immunostainings of **(a,b)** Dilp2 and **(c,d)** Dilp5 peptides. As compared with **(a,c)** control (*Hml*$^{\Delta}$ *>/+)*, **(b,d)** *Hml*$^{\Delta}$ *>/UAS-hid* larval brains reveal increased Dilp2 and Dilp5 peptide expression in insulin-producing cells (IPCs). **(e)** qPCR analysis for *dilp2* and *dilp5* in brain tissue of feeding L3 larvae does not show any change in their relative mRNA expression.

(Continued)

FIGURE 2 | Relative fold change is represented and statistical analysis was performed on $C_t$values (dilp2; Hml^{Δ} >/+, $n = 70$, 4 ± 0.32; Hml^{Δ} >/*UAS-hid*, $n = 80$, 3.77 ± 0.71 and dilp5; Hml^{Δ} >/+, $n = 70$, 9.25 ± 0.18; Hml^{Δ} >/*UAS-hid*, $n = 80$, 9.34 ± 0.29). **(f)** Hemolymph glucose levels. Hml^{Δ} >/+, $n = 78$, 0.09 ± 0.01 and Hml^{Δ} >/*UAS-hid* $n = 78$, 0.22 ± 0.06 (***p-value < 0.0001). **(g)** Hemolymph trehalose levels. Hml^{Δ} >/+, $n = 90$, 0.19 ± 0.10 and Hml^{Δ} >/*UAS-hid*, $n = 72$, 0.28 ± 0.06 (*p-value = 0.0335). **(h)** Whole-larvae glycogen levels. Hml^{Δ} >/+, $n = 6$, 1.08 ± 0.12 and Hml^{Δ} >*UAS hid*, $n = 6$, 0.77 ± 0.1 (***p-value = 0.0006). **(i)** Whole-larvae glucose levels. Hml^{Δ} >/+, $n = 39$, 0.11 ± 0.05 and Hml^{Δ} >/*UAS-hid*, $n = 39$, 0.25 ± 0.06 (***p-value < 0.0001). **(j,k)** Neutral lipid staining (Nile red) in fat bodies of **(j)** Hml^{Δ} >/+ and **(k)** Hml^{Δ} >*UAS-hid*. Compared with control, **(j)** Hml^{Δ} >/+, **(k)** Hml^{Δ} >*UAS-hid* fat bodies show more lipid droplets. **(l)** TAG levels measurement in whole larvae (Hml^{Δ} >/+, $n = 36$, 1.7 ± 0.3 and Hml^{Δ} >*UAS hid*, $n = 36$, 3.4 ± 0.7, ***p-value = 0.0005), hemolymph (Hml^{Δ} >/+, $n = 60$, 0.34 ± 0.08 and Hml^{Δ} >/*UAS-hid*, $n = 66$, 0.77 ± 0.16, ***p-value < 0.0001) and fat body (Hml^{Δ} >/+, $n = 45$, 0.7 ± 0.07 and Hml^{Δ} >/*UAS-hid*, $n = 40$, 2.25 ± 0.5, ***p-value < 0.0001). **(m–o)** tGPH expression in **(m,n)** fat bodies of feeding L3 larvae from **(m)** control (Hml^{Δ} >/+) and **(n)** Hml^{Δ} >/*UAS-hid* backgrounds shows reduced tGPH expression in Hml^{Δ} >/*UAS-hid* condition. **(o)** Quantification of mean tGPH intensities in Hml^{Δ} >/+ ($n = 25$, 2621 ± 486.2) and Hml^{Δ} >/*UAS-hid* ($n = 25$, 1005 ± 196, ***p-value = 0.0001). **(p,q)** FoxO immunostaining in fat bodies of feeding L3larvae from **(p)** control (Hml^{Δ} >/+) and **(q)** Hml^{Δ} </*UAS-hid* backgrounds. As compared with **(p)** control, FoxO is nuclear localized in fat bodies of Hml^{Δ} </*UAS-hid* animals. **(r,s)** Fat body analysis of FoxO target genes. **(r)** *4EBP* and **(s)** *InR* m*RNA* expression. *4EBP* is upregulated in Hml^{Δ} >/*UAS-hid* condition. Relative fold change is represented and statistical analysis was performed on $C_t$values (*4EBP*: Hml^{Δ} >/+, $n = 60$, 2.53 ± 0.91; Hml^{Δ} >/*UAS-hid*, $n = 60$, 1.11 ± 0.45; *p-value = 0.0233 and *InR*; Hml^{Δ} >/+, $n = 60$, 10.15 ± 0.93; Hml^{Δ} >/*UAS-hid*, $n = 60$, 9.99 ± 1.31). **(t,u)** Fat body analysis of inflammatory pathway target genes. **(t)** *drs* and **(u)** *dpt* m*RNA* expression is significantly upregulated in Hml^{Δ} >/*UAS-hid* condition. Relative fold change is represented and statistical analysis was performed on $C_t$values (*drs*: Hml^{Δ} >/+, $n = 60$, 5.40 ± 0.64; Hml^{Δ} >/*UAS-hid*, $n = 60$, 2.29 ± 1.28; ***p-value = 0.0002 and *dpt*: Hml^{Δ} >/+, $n = 60$, 16.79 ± 1.16; Hml^{Δ} >/*UAS-hid*, $n = 60$, 5.78 ± 0.69; ***p-value < 0.0001).

and *tobi* in the fat body by isolating RNA followed by qRT-PCR from control and Hml^{Δ} >/*UAS-hid* conditions. This detected a significant upregulation in the levels of *4EBP* (**Figure 2r**) and mild upregulation of *InR* (**Figure 2s**) in Hml^{Δ} >/*UAS-hid* conditions compared with controls. Together, these data show that the adult growth retardation was a consequence of reduced fat body insulin signaling in Hml^{Δ} >/*UAS-hid* conditions. To determine if these changes were a result of the defect in fat body Akt signaling, we assessed levels of phosphorylated Ser505-Akt. Although immunohistochemical analysis did show a reduction in pAkt level, a quantitative analysis of its expression with respect to total Akt revealed only a minor difference in Hml^{Δ} >/*UAS-hid* animals (**Supplementary Figures 3d–f**). This suggests either Akt independence (41) or phosphorylation at other sites on Akt, which are more sensitive indicators of its function (29) and remains to be addressed.

A strong connection between activation of fat body innate immune signaling leading to loss of insulin sensitivity (42, 43) and animal growth defect is well-established (29). Given the growth defect seen upon loss of immune cells, we asked if immune cell loss led to any changes in fat body innate immune signaling. For this, we investigated Toll and Imd innate immune signaling pathways in fat bodies in control and Hml^{Δ} >/*UAS-hid* conditions. Expression analysis of *drosomycin (drs)*, a Toll pathway target gene, and *diptericin (dpt)*, an Imd pathway target gene, was undertaken by isolating RNA from the fat body of Hml^{Δ} >/*UAS-hid* and control larvae. Compared with expression in controls, Hml^{Δ} >/*UAS-hid* conditioned fat bodies showed a strong upregulation of both *drs* (**Figure 2t**) and *dpt* (**Figure 2u**). This indicated a robust activation of innate immune signaling pathways in the fat body on the loss of Hml^{+} immune cells, implying a role for these cells in moderating activation of inflammatory pathways in the fat body.

Hemocytes Control Tolerance to High-Sucrose Diet

It is known that larvae fed on a high-sucrose diet develop as smaller adults (21). High sugar stress also corresponds with a reduction in immune cell numbers (44). The sugar stress–induced growth defect is a consequence of reduction in fat body insulin signaling (39, 45). Hml^{Δ} >/*UAS-hid* larvae with reduced Hml^{+} immune cells demonstrated a similar growth defect, reduced insulin signaling, elevated fat body inflammation, and hyperglycemia, all of which are characteristic signs of insulin resistance. Hence, it was important to investigate how loss of Hml^{+} immune cells influenced tolerance to additional high sugar dietary stress. To address this, larvae were raised on 25% sucrose, referred to as high-sucrose diet (HSD) in the text. Compared with the growth defect seen in control animals fed on HSD, Hml^{Δ} >/*UAS-hid* animals on HSD showed further growth retardation (**Figures 3a–g**). The growth retardation was also detected when these animals were raised on diet with elevated fructose (**Supplementary Figures 4a–c**). This result showed that the growth defect was a consequence of high dietary sugar induced stress and was not limited to sucrose-enriched diet, suggesting a growth promoting or stress relieving function of Hml^{+} innate immune cells in conditions of high dietary sugar.

To address if any changes in insulin signaling could explain the worsening of growth in Hml^{Δ} >/*UAS-hid* HSD animals, we analyzed different components of insulin signaling, as described in the previous section. Estimation of expression of Dilp2 and 5 peptides (**Figures 3h–k**, **Supplementary Figures 4d,e**) and their m*RNA* levels in the larval brain IPCs (**Figure 3l**) showed no change between Hml^{Δ} >/*UAS-hid* and controls. Biochemical analysis revealed a mild increase in larval hemolymph glucose in Hml^{Δ} >/*UAS-hid* HSD animals (**Figure 3m**), but trehalose levels remained comparable with control HSD larvae (**Figure 3n**). Whole-animal glucose and glycogen failed to detect any changes in their levels (**Figures 3o,p**). Readouts of fat body insulin signaling did not reveal any difference either. Membrane tGPH expression (**Figures 3q–s**), fat body glucose levels (**Supplementary Figure 4f**), phosphorylated S505-Akt levels (**Supplementary Figures 4g,h,k**), nuclear localization of FoxO protein (**Supplementary Figures 4i,j**), and expression of FoxO target genes (**Figures 3t,u** and **Supplementary Figure 4l**) remained comparable between control HSD and Hml^{Δ} >/*UAS-hid* HSD larvae. Thus, the growth defect seen in Hml^{Δ} >/*UAS-hid* HSD animals was not a

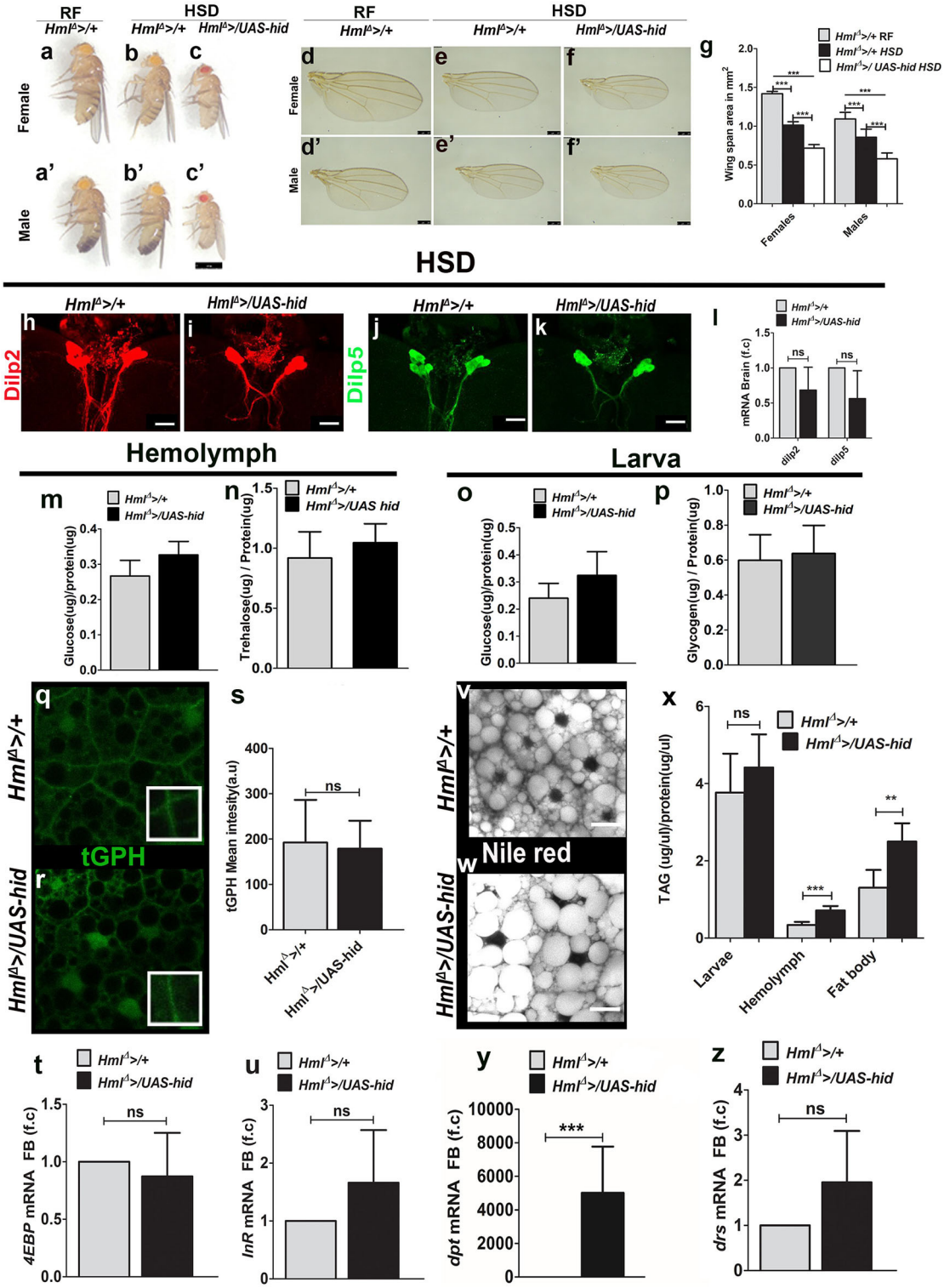

FIGURE 3 | Immune cells are necessary for tolerance to high dietary sugar–induced metabolic stress. Scale bars in **(a–c')** = 1 mm, **(d–f')** = 250 μm, and **(h–k,v,w)** = 20 μm. Bar graphs in **(g,l,m–p,s–u),** and **(x–z)** represent mean ± standard deviation (SD). Statistical analysis in **(g,l,m–p,s–u,x–z)** is unpaired *t*-test, two-tailed and two-way ANOVA comparison in **(g)**. "n" is total number of larvae analyzed, HSD is high sugar diet, RF is regular food, FB is fat body, f.c is fold change, a.u is arbitrary units. **(a–g)** Blood cell ablation worsens HSD induced adult growth defect. Compared with controls (*Hml*$^{\Delta}$ >/+) reared on **(a,a')** RF, **(b,b')** HSD induces a growth retardation which is **(c,c')** worsened in *Hml*$^{\Delta}$ >/*UAS-hid* HSD animals. **(d–g)** Representative images showing adult size defect. In comparison with **(d,d')** *Hml*$^{\Delta}$ >/+

(Continued)

FIGURE 3 | on RF, **(e,e′)** Hml^{Δ} >/+ on HSD show reduction in wing sizes which is further reduced in **(f,f′)** Hml^{Δ} >/*UAS-hid* HSD adults. **(g)** Quantification of wing span areas in: Hml^{Δ} >/+ on RF (female $n = 100$, 1.4 ± 0.03, male $n = 100$, 1.1 ± 0.09) Hml^{Δ} >/+ on HSD (female $n = 100$, 1.0 ± 0.04, ***p-value < 0.0001, male $n = 100$, 0.856 ± 0.1, ***p-value < 0.0001) and Hml^{Δ} >/*UAS-hid* on HSD (female $n = 100$, 0.7 ± 0.04, ***p-value < 0.0001 and male $n = 100$, 0.6 ± 0.08, ***p-value < 0.0001). Two-way ANOVA analysis was performed (females ***p-value < 0.0001 and males ***p-value < 0.0001). **(h–l)** Dilp2 and Dilp5 analysis in feeding L3 larval brains raised on HSD. Immunostainings of **(h,i)** Dilp2 and **(j,k)** Dilp5 peptides in **(h,j)** control (Hml^{Δ} >/+) and **(i,k)** Hml^{Δ} >/*UAS-hid* larval brains do not show any change in their peptide expression in insulin-producing cells (IPCs). **(l)** qPCR analysis for *dilp2* and *dilp5* in brain tissue of feeding L3 larvae does not show any change in their relative mRNA expression. Relative fold change is represented and statistical analysis was performed on $\mathbf{C_t}$values (*dilp2*; Hml^{Δ} >/+, HSD, $n = 100$, 4.86 ± 1.27; Hml^{Δ} >/*UAS-hid*, HSD, $n = 100$, 5.92 ± 1.46 and *dilp5*; Hml^{Δ} >/+, HSD, $n = 100$, 9.15 ± 2.13; Hml^{Δ} >/*UAS-hid*, HSD, $n = 100$, 10.66 ± 2.48). **(m)** Hemolymph glucose levels. Hml^{Δ} >/+, HSD, $n = 42$, 0.27 ± 0.04 and Hml^{Δ} >/*UAS-hid*, HSD, $n = 42$, 0.33 ± 0.04 (*p-value $= 0.0189$). **(n)** Hemolymph trehalose levels. Hml^{Δ} >/+, HSD, $n = 36$, 0.92 ± 0.22, and Hml^{Δ} >/*UAS-hid*, HSD, $n = 36$, 0.28 ± 0.2. **(o)** Whole-larvae glucose levels. Hml^{Δ} >/+, HSD $n = 18$, 0.24 ± 0.05 and Hml^{Δ} >/*UAS-hid* $n = 18$, 0.32 ± 0.09. **(p)** Whole-larvae glycogen levels. Hml^{Δ} >/+, HSD, $n = 13$, 0.6 ± 0.15 and Hml^{Δ} >/*UAS-hid* HSD, $n = 13$, 0.64 ± 0.16. **(q–s)** tGPH expression in **(q,r)** fat bodies of feeding L3 larvae from **(q)** Hml^{Δ} >/+, HSD controls and **(r)** Hml^{Δ} >/*UAS-hid*, HSD backgrounds showed no change in tGPH expression. **(s)** Quantification of mean tGPH intensities in Hml^{Δ} >/+ on HSD ($n = 15$, 192 ± 94) and Hml^{Δ} >/*UAS-hid*, on HSD ($n = 20$, 178 ± 61). **(t,u)** Fat body analysis of FoxO target genes. **(t)** *4EBP* and **(u)** *lnR* m*RNA* expression show no difference. Relative fold change is represented and statistical analysis was performed on $\mathbf{C_t}$values. (*4EBP*: Hml^{Δ} >/+, HSD, $n = 80$, 0.29 ± 0.65; Hml^{Δ} >/*UAS-hid*, HSD, $n = 80$, 0.61 ± 1.18 and *lnR*: Hml^{Δ} >/+, HSD, $n = 80$, 8.97 ± 1.34; Hml^{Δ} >/*UAS-hid*, HSD, $n = 80$, 8.43 ± 1.91). **(v,w)** Neutral lipid (Nile red) staining in fat bodies of larvae raised on HSD. Compared with **(v)** Hml^{Δ} >/+, on HSD **(w)** Hml^{Δ} >/*UAS-hid* HSD animals show increased number of bigger lipid droplets. **(x)** TAG levels measurements in whole larvae (Hml^{Δ} >/+, HSD, $n = 24$, 3.8 ± 1 and Hml^{Δ} >*UAS hid*, HSD, $n = 24$, 4.4 ± 0.86), hemolymph (Hml^{Δ} >/+, HSD, $n = 60$, 0.34 ± 0.08 and Hml^{Δ} >/*UAS-hid*, HSD, $n = 60$, 0.7 ± 0.1, ***p-value < 0.0001), and fat body (Hml^{Δ} >/+, HSD $n = 30$, 1.304 ± 0.5 and Hml^{Δ} >/*UAS-hid*, HSD, $n = 30$, 2.5 ± 0.5, **p-value $= 0.0013$). **(y,z)** qPCR analysis of **(y)** *dpt* and **(z)** *drs* m*RNA* expression in fat body tissue of feeding L3 larvae raised on HSD. Relative fold change is represented and statistical analysis was performed on $\mathbf{C_t}$values (*dpt:* Hml^{Δ} >/+ HSD $n = 80$, 17.96 ± 0.88; Hml^{Δ} >/*UAS-hid*, HSD, $n = 80$, 5.96 ± 0.75; ***p-value < 0.0001 and *drs:* Hml^{Δ} >/+, HSD, $n = 80$, 8.13 ± 0.48; Hml^{Δ} >/*UAS-hid*, HSD, $n = 80$, 7.12 ± 1.11) *indicates signifcant p values.

consequence of any dramatic change in glucose homeostasis or insulin signaling.

Immune cell ablation, however, impacted the TAG levels in these animals. Although overall larval TAG levels remained comparable, hemolymph and fat body TAG levels showed a significant increase in Hml^{Δ} >/*UAS-hid* HSD larvae (**Figure 3x**). Nile red staining of fat bodies confirmed the increase in the TAG levels as well (**Figures 3v,w**). The lipid droplet sizes detected in Hml^{Δ} >/*UAS-hid* HSD fat bodies were comparatively larger than seen in the control tissues (**Figures 3v,w**). Together, these results showed a defect in the fat body lipid metabolism in the Hml^{Δ} >/*UAS-hid* HSD larvae.

We next assessed the status of fat body innate immune signaling in response to immune cell ablation in HSD condition. Interestingly, Hml^{Δ} >/*UAS-hid* animals showed upregulation of Imd target gene, *dpt* (**Figure 3y**), whereas expression of Toll target gene, *drs*, remained comparable with control HSD fat bodies (**Figure 3z**). This suggested specific activation of the Imd pathway on loss of immune cells in HSD condition and was unlike regular dietary state, where loss of Hml^{+} cells led to dramatic upregulation of both Toll and Imd signaling in the fat body. In conditions of dietary excess, such specific modulation of fat body inflammatory signaling (46) and influence on tolerance to metabolic toxicity (47) is reported. Our findings support this notion and implicate Hml^{+} immune cells in moderating this specificity.

Increasing the Number of Activated Blood Cells in *Drosophila* Larvae Rescues the HSD Induced Growth Defect

We next assessed the outcome of increasing immune cell numbers on organismal metabolic state and growth homeostasis. For this, we over-expressed a constitutively active version of PDGF/VEGF-like receptor (Pvr^{act}) in blood cells using Hml^{Δ} > as the driver (Hml^{Δ} >/*UAS* Pvr^{Act}) (48). This genetic manipulation resulted in a dramatic increase in immune cell numbers and specifically of Hml^{+} cells (**Figures 4a–c**, **Supplementary Figures 5a–b′′**). This manipulation leads to the expansion of immune cells that are characteristically similar to the invasive macrophages (49). In regular food conditions, adult flies from this genetic background did not show any effect on growth phenotype and were comparable in size with control adult flies (**Supplementary Figures 5g–k**). This result suggested that although animal growth is sensitive to loss of immune cells (**Figures 1**, **2**), a mere increase in the immune cell numbers did not result in a concomitant increase in animal sizes. These data suggest that immune cells are not directly involved in scaling of animal sizes. Consistent with this notion, insulin signaling remained unaffected in Hml^{Δ} >/*UAS* Pvr^{Act} animals (**Supplementary Figures 5c–f,l–v**).

Next, we explored the influence of increased immune cell numbers on dietary sugar–induced growth defect and tolerance. Compared with immune cell numbers of controls on HSD, Hml^{Δ} >/*UAS* Pvr^{Act} raised on HSD had significantly higher immune cell numbers (**Figure 4d**), but not as dramatic as seen in regular condition (compared with **Figure 4c**). The proportion of Hml^{+} immune cells was specifically increased (**Figure 4c**). Interestingly, the growth defect seen in HSD animals was dramatically restored in Hml^{Δ} >/*UAS* Pvr^{Act} HSD genetic background (**Figures 4e–h**). Their sizes were comparable with sizes seen for controls raised on regular dietary state (**Figures 4g,g′** compared with **Figures 4e,e′**). A similar trend of increased immune cell numbers was also evident with overexpression of wild-type Pvr in Hml^{+} (Hml^{Δ} >/Pvr^{WT}) blood cells (**Supplementary Figures 6a,b,d**). These animals were also significantly larger than HSD controls (**Supplementary Figures 6e–g**), but smaller than Hml^{Δ} >/*UAS* Pvr^{Act} HSD animals (compare **Figure 4h** with **Supplementary Figure 6g**). The difference in growth restoration between Hml^{Δ} >/*UAS* Pvr^{Act} and Hml^{Δ} >/Pvr^{WT} may stem from the extent of increased numbers of activated

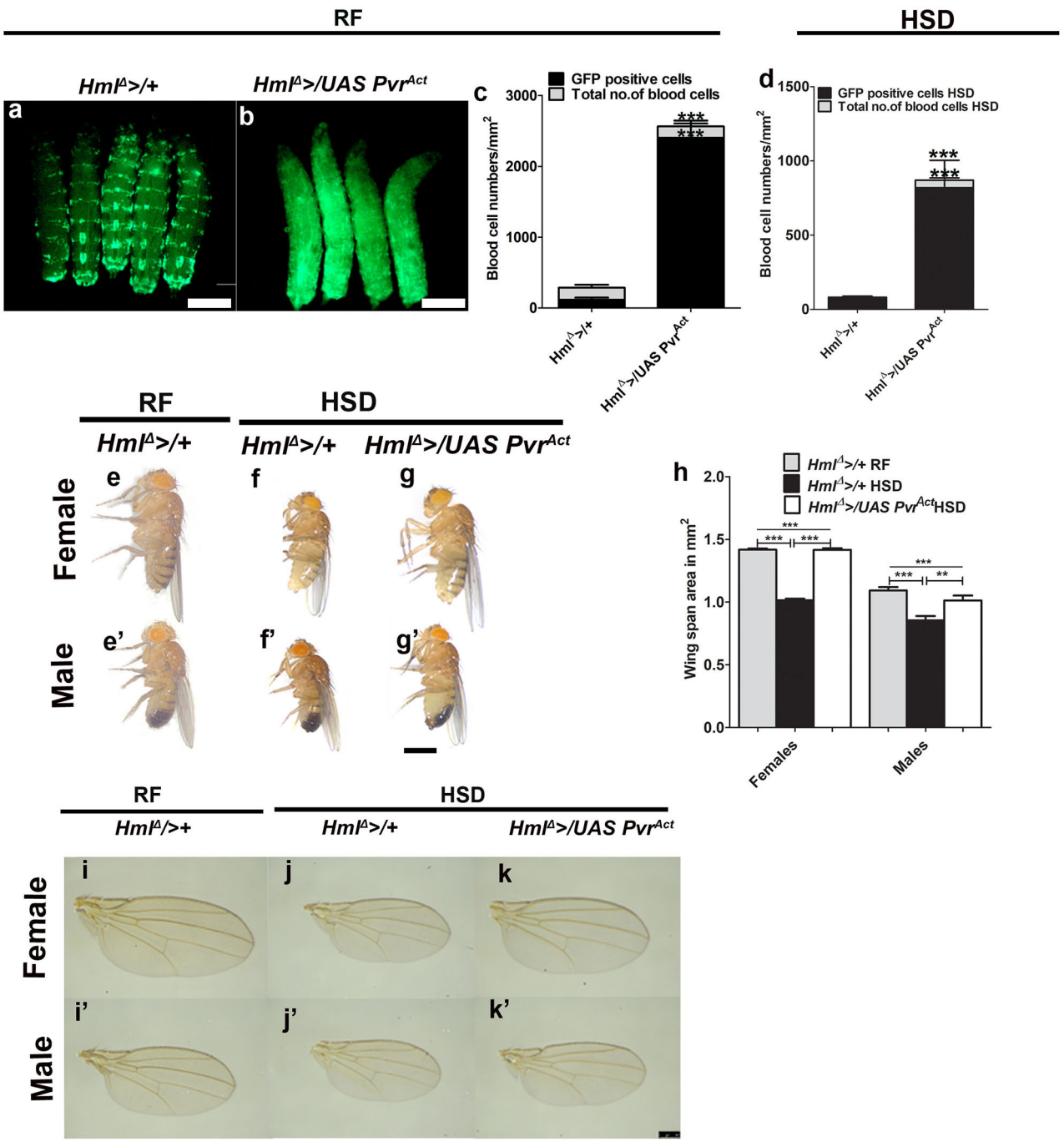

FIGURE 4 | Increased immune cell activity restores adult growth defect seen in high dietary sugar condition. In **(a,b,e–g′),** scale bar = 1 mm, **(i–k′)** = 250 μm. In **(c,d,h)**, bar graphs show mean ± standard deviation (SD) and statistical analysis in these panels is unpaired *t*-test, two-tailed. "*n*" is the total number of larvae analyzed, RF indicates regular food, HSD indicates high sugar diet. **(a–d)** Expressing Pvr^{Act} in blood cells (Hml, green) causes an expansion in their numbers. Compared with **(a)** control (Hml^{Δ} >*UAS-GFP*) larvae, **(b)** Hml^{Δ} >*UAS* Pvr^{Act} animals have more blood cells. Blood cell quantifications on **(c)** RF and **(d)** HSD. **(c)** Hml^{Δ} >/+ on RF (total number of blood cells: $n = 10$, 202.39 ± 26 and Hml^{+} cells, $n = 10$, 117.7 ± 28.3) and Hml^{Δ} >*UAS* Pvr^{Act} on RF (total number of cells: $n = 10$, 2563.15 ± 226.47, ***p-value < 0.0001 and Hml^{+} cells, $n = 10$, 2403.7 ± 200.04, ***p-value < 0.0001). **(d)** Hml^{Δ} >/+ on HSD (total number of blood cells, $n = 10$, 81.4 ± 16 and Hml^{+} cells, $n = 10$, 70 ± 17) and Hml^{Δ} >*UAS* Pvr^{Act} on HSD (total number of blood cells, $n = 10$, 871 ± 189, ***p-value < 0.0001 and Hml^{+} cells, $n = 10$, 819 ± 185, ***p-value < 0.0001). **(e–g′)** Expressing Pvr^{act} in blood cells restores HSD induced adult growth defect. Compared with Hml^{Δ} >/+ reared on **(e,e′)** RF**, (f,f′)** HSD induced growth retardation is **(g,g′)** restored in Hml^{Δ} >*UAS* Pvr^{Act} HSD animals. See quantifications in **(h). (h)** Quantification of wing span areas. Hml^{Δ} >/+ reared on RF (female = 1.4 ± 0.03, $n = 100$; male = 1.1 ± 0.08, $n = 100$), Hml^{Δ} >/+ on HSD (female = 1 ± 0.04, $n = 100$, ***p-value < 0.0001 in comparison with Hml^{Δ} >/+ reared on RF, male 0.9 ± 0.11, $n = 100$, ***p-value < 0.0001 in comparison with Hml^{Δ} >/+ reared on RF) and Hml^{Δ} >*UAS* Pvr^{Act} on

(Continued)

FIGURE 4 | HSD (female = 1.4 ± 0.05, $n = 100$, ***p-value < 0.0001 in comparison with Hml^{Δ} >/+ reared HSD, male 1.01 ± 0.12, $n = 100$, **p-value = 0.0064 in comparison with Hml^{Δ} >/+ reared on HSD). Two-way ANOVA comparison was performed (females ***p-value < 0.0001 and males ***p-value < 0.0001). **(l–k')** Representative wing images of adult flies showing growth restoration of Hml^{Δ} >/UAS Pvr^{Act} adults on HSD. **(i–j')** Hml^{Δ} >/+on **(i,i')** RF and **(j,j')** on HSD and **(k,k')** Hml^{Δ} >/UAS Pvr^{Act} on HSD.

immune cells, which is much higher in Hml^{Δ} >/UAS Pvr^{Act} as opposed to Hml^{Δ} >/Pvr^{WT} (**Figure 4c** compared with **Supplementary Figure 6d**). Importantly, increasing immune cell numbers using other genetic manipulations did not lead to a growth restoration phenotype. Expression of a temperature-sensitive form of shibire, shi^{ts} in Hml^{+} cells (Hml^{Δ} >/UAS shi^{ts}), which also causes a comparable expansion of Hml^{+} immune cells as seen in Hml^{Δ} >/Pvr^{WT} (**Supplementary Figures 6a,c,d**), was insufficient to recover the growth defect of HSD. Contrastingly, Hml^{Δ} >/UAS shi^{ts} HSD animals were smaller and demonstrated growth retardation (**Supplementary Figures 6h–j**). These data suggested immune cell state as a key component in growth control. We conclude that immune cell activity is linked to systemic growth control as opposed to only their numbers being a regulator for growth.

We further tested other dietary sugar–induced stress, such as fructose and glucose, and observed that different sugars had varying effects on growth. Compared with the growth of control animals on sucrose-rich diet, the growth reduction was severe in high-glucose diet, whereas fructose-rich diet showed a mild growth defect (**Supplementary Figures 7a,b**); Hml^{Δ} >/UAS Pvr^{Act} animals were able to restore growth in all conditions. This was not seen in Hml^{Δ} >/UAS shi^{ts} animals. Hml^{Δ} >/UAS Pvr^{Act} condition restored growth in every dietary condition, but at differential capacities. This trend was not evident in Hml^{Δ} >/UAS shi^{ts} animals (**Supplementary Figures 7c–r**). This result further strengthened the importance of immune cell states in moderating dietary stress–induced growth defect.

We assessed the effect of Pvr^{Act} expression in hemocytes on peripheral insulin and inflammatory signaling in HSD condition and observed restoration of certain features of insulin resistance. The accumulation of Dilp2 and Dilp5 peptides normally seen in larval IPCs in control HSD animals was not observed in Hml^{Δ} >/UAS Pvr^{Act} HSD larval brain IPCs (**Figures 5a–d**, **Supplementary Figures 8a,b**). This was a not a consequence of reduction in *Dilp2* and *Dilp5* m*RNA* levels (**Figure 5e**). Biochemical analysis of circulating larval hemolymph glucose and trehalose revealed a reduction in glucose levels, whereas trehalose remained unchanged (**Figures 5f,g**). Whole-animal glycogen was comparatively higher in Hml^{Δ} >/UAS Pvr^{Act} HSD animals as compared with control groups (**Figure 5h**). However, whole-animal glucose levels remained unchanged (**Figure 5i**). These data suggested an improvement in circulating glucose and whole-animal glycogen levels in Hml^{Δ} >/UAS Pvr^{Act} HSD larvae. Lipid measurements, however, showed no change and remained comparable with control HSD conditions (**Figures 5j–l**).

Readouts of peripheral fat body insulin signaling revealed restoration of some of its features. Of these, membrane tGPH levels (**Figures 5m–o**) and FoxO localization (**Figures 5p,q**) were restored in Hml^{Δ} >/UAS Pvr^{Act} HSD larvae. Changes in the expression of FoxO target genes, *4EBP*, *InR*, and *tobi*, were not detected (**Figures 5r,s**, **Supplementary Figure 8g**). pAKT levels also did not increase (**Supplementary Figures 8d–f**). Examining Toll and Imd pathway targets revealed an unexpected upregulation of *drs* (**Figure 5t**) in Hml^{Δ} >/UAS Pvr^{Act} HSD animals, whereas *dpt*, the Imd pathway target gene, remained unchanged (**Figure 5u**). This was unlike the Hml^{Δ} >/UAS *hid* HSD animals where a dramatic upregulation of *dpt* was evident without any change in *drs* expression.

DISCUSSION

Much of our understanding of systemic control of animal growth is generally limited to endocrine organs. In *Drosophila*, the fat body (24), gut (15), and brain are highlighted as predominant nutrient sensors regulating growth (21). Because of nutrient sensing and signaling functions performed by these organs, they have been the primary focus of investigations on growth regulation. The formation of blood cells is also an energy-consuming process and has a metabolic cost on the animal. Immune cells are highly sensitive to nutrient modulation (18, 50). However, the physiological relevance of their increased sensitivity to dietary changes and impact on growth, if any, is poorly understood. Our study demonstrates the influence of immune cells on coordinating systemic metabolism and animal growth. In this regard, two important points emerge from this work: (1) immune cell states rather than their number is an important parameter in growth regulation and (2) immune cells systemically coordinate growth via the regulation of fat body inflammation and insulin signaling. These functions of blood cells support the attainment of proper adult size both in homeostasis and in conditions of sugar excess. While we focus on immune cell–fat body cross-talk, our results do not rule out any direct communication between immune cells and the brain or other organs in coordinating growth. Overall, this study positions innate immune cells as a novel player in organismal metabolic homeostasis and growth control regulation.

Immune Cell/Fat Body Cross-Talk in Animal Growth Control

We find that in homeostatic conditions, modulating immune cell numbers in larval life impacts overall organismal metabolic state and animal growth. The loss of immune cells dramatically reduces adult growth. The metabolic and biochemical assays in these animals resembles features of systemic insulin insensitivity (51). This includes increased circulating TAGs, circulating glucose/trehalose levels with reduced whole-animal glycogen levels. Specifically, fat body metabolism, innate immune signaling, and insulin sensitivity are also affected. Past and recent findings have highlighted immune cell–mediated regulation of

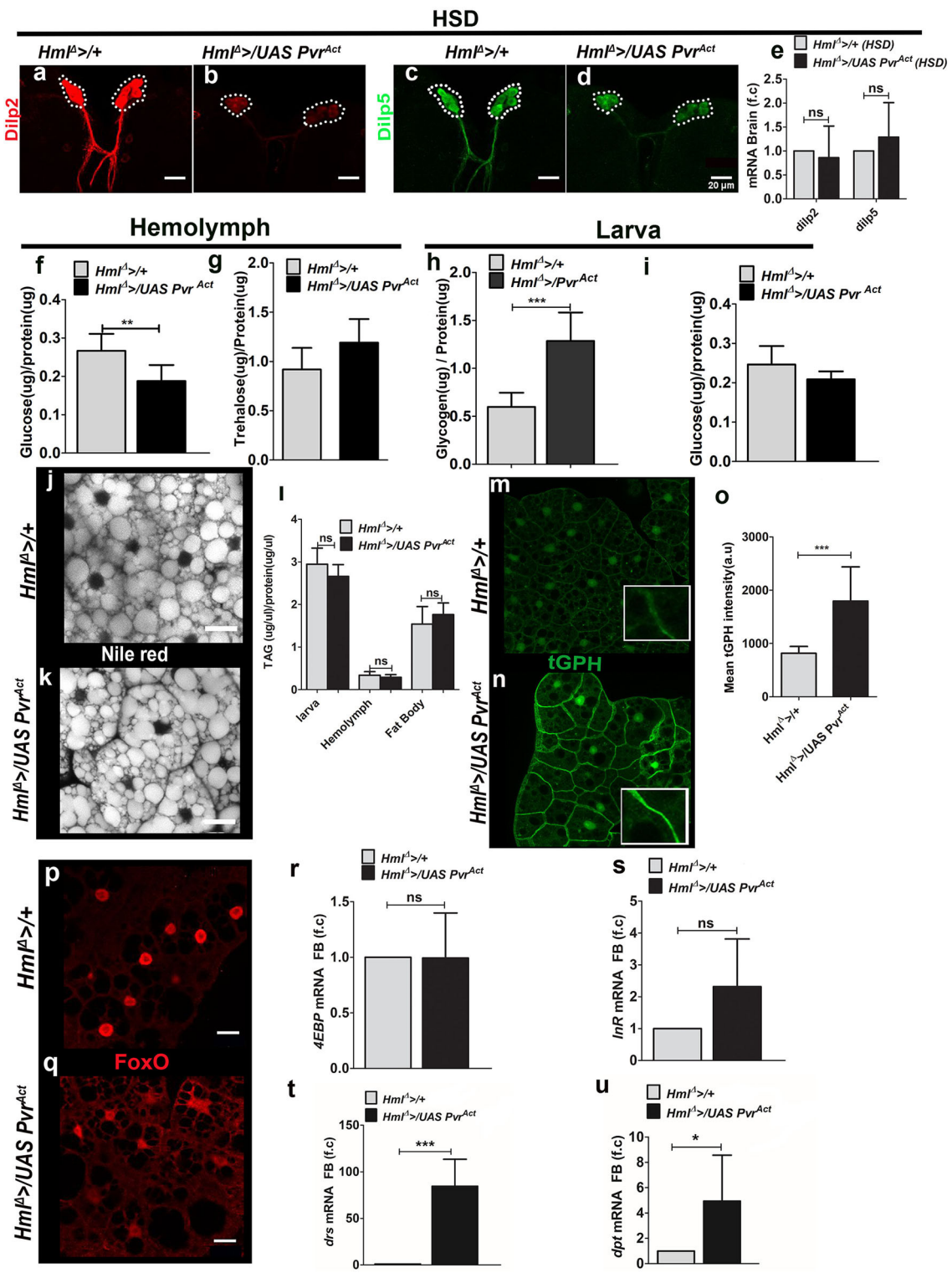

FIGURE 5 | Increased immune cell activity improves fat body insulin sensitivity and tolerance on HSD condition. In **(a–d,m,n,p,q),** scale bar = 20 µm. In **(e–i,l,o,r-u)** bar graphs show mean ± standard deviation (SD) and statistical analysis applied in these panels is unpaired *t*-test, two-tailed. "*n*" is the total number of larvae analyzed, HSD indicates high-sugar diet, a.u is arbitrary units, FB is fat body. **(a–e)** Dilp2 and Dilp5 expression analysis in feeding L3 larvae reared on HSD. **(a–d)** Immunostaining of **(a,b)** Dilp2 and **(c,d)** Dilp5 peptide expression in insulin-producing cells (IPCs) of **(a,c)** control (*Hml*$^{\Delta}$ >/+) on HSD and **(b,d)** *Hml*$^{\Delta}$ >/*UAS Pvr*^{Act} HSD brains show reduced Dilp2 and Dilp5 levels in *Hml*$^{\Delta}$ >/*UAS Pvr*^{Act} condition. **(e)** Relative quantification of *dilp2* and *dilp5*m*RNA* levels showed no change.

(Continued)

FIGURE 5 | Relative fold change is represented and statistical analysis was done using $C_t$values (*dilp2*; Hml^{Δ} >/+, HSD, $n = 100$, 4.86 ± 1.27; Hml^{Δ} >/*UAS* Pvr^{Act}, HSD, $n = 100$, 5.66 ± 1.52 and *dilp5*; Hml^{Δ} >/+, HSD, $n = 100$, 9.15 ± 2.13; Hml^{Δ} >/*UAS* Pvr^{Act}, HSD, $n = 100$, 9.91 ± 1.11). **(f)** Hemolymph glucose levels (Hml^{Δ} >/+, HSD, $n = 42$, 0.27 ± 0.04 and Hml^{Δ} >/*UAS* Pvr^{Act}, HSD, $n = 42$, 0.19 ± 0.4, $^{**}p$-value = 0.0051). **(g)** Hemolymph trehalose levels (Hml^{Δ} > /+ HSD, $n = 36$, 0.92 ± 0.22 and Hml^{Δ} >/*UAS* Pvr^{Act}, HSD, $n = 48$, 1.2 ± 0.2). **(h)** Whole-larvae glycogen levels (Hml^{Δ} >/+, HSD, $n = 13$, 0.6 ± 0.15 and Hml^{Δ} >/*UAS* Pvr^{Act}, HSD, $n = 15$, 1.3 ± 0.3, $^{***}p$-value < 0.0001). **(i)** Whole-larvae glucose levels. (Hml^{Δ} /+, HSD, $n = 18$, 0.25 ± 0.05 and Hml^{Δ} >/*UAS* Pvr^{Act}, HSD, $n = 18$, 0.21 ± 0.02). **(j,k)** Neutral lipid (Nile red) staining in fat bodies of **(j)** Hml^{Δ} >/+ on HSD and **(k)** Hml^{Δ} >/*UAS* Pvr^{Act} on HSD revealed no change in lipid levels. **(l)** TAG measurements in whole larvae (Hml^{Δ} >/+ HSD $n = 18$, 3 ± 0.4 and Hml^{Δ} >/*UAS* Pvr^{Act} $n = 18$, 2.7 ± 0.3), hemolymph (Hml^{Δ} >/+ HSD $n = 60$, 0.34 ± 0.08 and Hml^{Δ} >/*UAS* Pvr^{Act} HSD $n = 60$, 0.3 ± 0.06) and fat body (Hml^{Δ} > + HSD $n = 30$, 1.54 ± 0.41 and Hml^{Δ} >/*UAS* Pvr^{Act} HSD $n = 30$, 1.76 ± 0.3). **(m–o)** tGPH expression in fat bodies of feeding L3 larvae reared on HSD. Compared with **(m)** HSD control (Hml^{Δ} >/+), **(n)** Hml^{Δ} >/*UAS* Pvr^{Act}, HSD animals show restored membrane tGPH expression. **(o)** Mean tGPH intensity quantifications of Hml^{Δ} >/+ on HSD, $n = 15$, 818 ± 126 and Hml^{Δ} >/*UAS* Pvr^{Act} on HSD, $n = 15$, 1796 ± 640 ($^{***}p$-value < 0.0001). **(p,q)** FoxO immunostaining in fat bodies of feeding L3 larvae reared on HSD. Compared with **(p)** nuclear FoxO expression in control (Hml^{Δ} >/+) on HSD, **(q)** Hml^{Δ} >/*UAS* Pvr^{Act}, HSD animals show lesser levels in the nucleus. **(r,s)** Fat body analysis of FoxO target genes. **(r)** *4EBP* and **(s)** *InR* m*RNA* expression. Relative fold change is represented and statistical analysis was done using $C_t$values (*4EBP*: Hml^{Δ} >/+, HSD, $n = 80$, 0.29 ± 0.65 and Hml^{Δ} >/*UAS* Pvr^{Act}, HSD, $n = 80$, 0.39 ± 0.35 and (*InR*: Hml^{Δ} >/+, HSD, $n = 80$, 8.97 ± 1.34 and Hml^{Δ} >/*UAS* Pvr^{Act}, HSD, $n = 80$, 7.98 ± 1.13). **(t,u)** qPCR analysis of **(t)** *drs* and **(u)** *dpt* m*RNA* expression in fat body tissue of feeding L3 larvae raised on HSD. Relative fold change is represented and statistical analysis was performed on C_t values (*drs*: Hml^{Δ} >/+, HSD, $n = 80$, 8.13 ± 0.48 and Hml^{Δ} >/*UAS* Pvr^{Act}, HSD, $n = 80$, 1.81 ± 0.88; $^{***}p$-value < 0.0001 and *dpt*; Hml^{Δ} >/+, HSD, $n = 80$, 17.96 ± 0.88 and Hml^{Δ} >/*UAS* Pvr^{Act}, HSD, $n = 80$, 15.74 ± 0.75 $^{*}p$-value 0.0313).

fat body immune activation and metabolic homeostasis by secreted factors like psidin (52), Upd3 (53), and adenosine (30). These interactions between immune cells and the fat body allow nutrient allocation to regulate animal growth in nutrient overload conditions (53) or in response to infection for an effective immune response (30, 52). Our study suggests a similar cross-talk between immune cells and the fat body in the maintenance of metabolic homeostasis. We posit that immune cell activity modulates fat body insulin signaling, which is central to organismal growth control. Loss of Hml^{+} immune cells corresponds with robust activation of fat body Toll and Imd signaling, indicating increased inflammation. This positions Hml^{+} cells as key regulators of fat body inflammatory homeostasis. Persistent activation of Toll (29) and Imd signaling pathways in the fat body (26, 28) leads to insulin insensitivity, metabolic dysregulation, and growth defect (54). Recently published data by Shin et al. (53) have highlighted a similar role for Hml^{+} cells in systemic control of animal growth by regulating fat body Jak/Stat signaling. Our data strengthen this notion and proposes a model where anti-inflammatory inputs by immune cells function on controlling fat body innate immune homeostasis and insulin sensitivity, thereby contributing to animal growth control (43). In addition, any change of Dilp 2 and Dilp5 production or secretion from the larval brain IPCs on immune cell manipulation cannot be ruled out. This can also lead to a reduction in circulating Dilps and reduced systemic insulin signaling. Whether this is mediated by the fat body (24) or by blood cells directly requires further validation.

However, in conditions of nutrient excess (HSD), the modulation of immune cell numbers on systemic metabolism, fat body inflammation, and its insulin sensitivity does not correlate with the findings in regular dietary conditions. These data are unexpected and indicate that cross-talk between blood cells and the fat body is more complex. Ablation of Hml^{+} blood cells further worsened the adult sizes without differences in insulin sensitivity. Fat body insulin signaling and overall glucose homeostasis were not different from what is observed in control animals raised on HSD. Interestingly, this resulted in preferential activation of the Imd pathway in the fat body, without any change in Toll signaling. On the other hand, increasing the numbers of activated immune cells (Hml^{Δ} >Pvr^{Act}) relieved the symptoms of metabolic stress induced by HSD. Here, signatures of insulin resistance or fat body insulin sensitivity revealed only partial recovery, but the extent of growth restoration observed in these animals was comparable with wild types raised on a regular diet. In these growth-restored animals, a specific activation of fat body Toll signaling was evident. This is possible as activated immune cells are capable of secreting spaztle, the Toll ligand, and drive systemic Toll activation (55, 56). A similar influence of innate immune signaling on growth in nutrient overload is supported by the published literature. Peptidoglycan recognition proteins (PGRPs) are known to activate either Toll or Imd pathways, and their modulation in the fat body differentially influences animal growth. PGRP-SB2 activates the Imd pathway, and its loss in the fat body increases growth and survival on HSD. Although PGRP-SC2 negatively regulates the Imd pathway and positively regulates the Toll pathway, its loss in the fat body reduces animal size on HSD (27).

Together, these data reveal that growth is differentially controlled in dietary excess as opposed to homeostasis and is supported by the independence of animal growth from insulin signaling seen in HSD Hml^{Δ} >*hid* and Hml^{Δ} >Pvr^{Act} conditions. Our data also suggest an additional growth-promoting axis independent of insulin signaling regulated by blood cell activity. Here, we propose a model where immune cells function to balance fat body innate immune activation. This supports fat body nutrient reallocation toward the promotion of animal growth and prevents metabolic toxicity. The additional immune cell/fat body inflammatory axis compensates for reduced fat body insulin signaling in HSD conditions.

Immune Cell State as the Driver of Growth Control

Cross-talk between the fat body and immune cells could either be dependent on immune cell numbers (3) or activity. Our findings reveal the importance of immune cell state to sustain metabolism and growth capacity. The expression of a constitutively active form of Pvr in immune cells resulted in the activation of invasive plasmatocytes (6, 49) and improved

tolerance to dietary excess. Increasing immune cell numbers by overexpression of *shi*^{ts} did not ameliorate the HSD growth defect. On the contrary, *Hml*$^{\Delta}$ >*/UAS shi*^{ts} animals were smaller. Loss of shibire function blocks exocytosis (57, 58); therefore, shibire lacking blood cells are functionally inert, unlike *Pvr*^{Act}-expressing hemocytes, which are more active. Immune cell states are reflective of their internal metabolic activity (25) and signaling capacities (52, 53, 56, 59). The elevated metabolic state of active immune cells may therefore provide an animal with additional means to metabolize nutrients (especially when in excess) and does not require increased immune cell number with inert metabolic states. The immune cell states may be a reflection of changes in immune heterogeneity (25, 53) or internal metabolic states as seen in development (25) or in conditions of stress (20).

A Model of Temporal Control of Immune Cell Function in Regulation of Animal Growth

Immune cell function in growth homeostasis is temporally controlled and is required early, before the 3rd instar. This is inferred from the pronounced deficit in adult growth after loss of immune cells in early stages of larval development and not if immune cells are depleted post 3rd instar. Although larval growth is unchanged after immune cell depletion, subtler changes in larval sizes or weight cannot be ruled out. The reduced adult size may stem from a reduction in cell growth and proliferation (60, 61). This is supported by analysis of cell densities in wing imaginal discs of wandering 3rd instar *Hml*$^{\Delta}$ >*hid* larvae, which showed a reduction in wing disc cell densities with increased spacing between cells (**Supplementary Figures 2i–k**). Suppression of insulin receptor signaling late in development affects body and organ size as opposed to its early role in developmental timing. This transition from the control of developmental timing to growth occurs early in 3rd instar, when larvae reach critical size, post which development can be completed in the absence of food. Consequently, critical size is a key stage in insect development that is established in early 3rd instar larvae and sets the lower limit of final adult size. The mechanisms that measure the critical size and the organs involved in this process are largely unclear. Fat body, imaginal discs are the only predicted critical-size sensing organs thus far. Based on the early immune function apparent from this study, we hypothesize an involvement of immune cells in the assessment of larval critical weight, supported by the evidence of cross-talk in this work. The implication of immune cell/fat body interaction early in larval life could be relevant in the establishment of developmental switches or programs that time the acquisition of critical weight and the temporal shift in insulin signaling to allow growth in non-feeding larval and pupal stages (60). The comparable metabolic and growth phenotypes seen in animals with reduced Inr activity late in larval life with animals depleted for immune cells are in agreement with this hypothesis.

CONCLUSION

The fat body functions to integrate the physiological state of the animal and determine allocation of resources in a context-dependent manner (23). Much like this tissue, immune cells, in addition to their role in sensing infection, are also effective sensors of changes in nutrient levels (3, 20, 62). However, unlike the fat body which is fixed in location, immune cells are mobile and highly dynamic. Their behavior and localization change rapidly in contexts of stress or nutrient modulation (3, 30). Our findings clearly implicate immune cells as central players coordinating global metabolic homeostasis and growth control along with the fat body. This integrates both the cellular and humoral component of the innate immune system, which may have evolved for efficient allocation of resources during infections but is also coopted in development to orchestrate systemic metabolism and growth. Metabolic disorders like diabetes, obesity, and fatty liver in mammals (62) are associated with heightened inflammation and altered immune responses. This exemplifies a connection between immune cells, altered metabolic homeostasis, and disease progression; however, its relevance in development regulation like growth remains unaddressed. Future investigations will be necessary to probe the temporal nature of this cross-talk to reveal mechanistic insights underlying developmental paradigms operating in animal growth and physiology.

METHODS

Drosophila Husbandry, Stocks, Genetics, and Food

The following *Drosophila* stocks were used in this study: *w*^{1118} (wild-type), *Hml*$^{\Delta}$>*UAS-Gfp* (S.Sinenko), *domeMESO-GFP*; *hml-dsRed* (Utpal Banerjee), *Hml*$^{\Delta}$>*Gfp;tub gal 80*^{ts}, *Hml*$^{\Delta}$>*Gfp;tGPH*, *UAS-hid/CyoGFP*, *UAS-Pvr*^{Act} and *UAS-Shi*^{ts} (63), *UAS Pvr* (BL58998), and *Hml*$^{\Delta}$*gal4* (BL30141). All fly stocks were reared on the standard BDSC corn meal agar food medium with yeast supplementation (referred to as the regular food in the article) at 25°C incubator unless specified. The specific composition of the regular food (RF) for 1 L is corn flour, 80 g; D-glucose, 20 g; sugar, 40 g; agar, 8 g; yeast powder, 15 g; propionic acid, 4 mL; Tego (methyl parahydroxy benzoate), 1 g (5 mL ethanol); and orthophosphoric acid, 0.6 mL. For high-sugar diet (HSD), the regular food composition was modified by supplementing the food with 25% sucrose (20 g in 100 mL of standard medium) whereas the composition of the other ingredients remained unchanged. For high-fructose diet (HFD), the regular food composition was modified by supplementing the food with 25% D-fructose (25 g in 100 mL of standard medium) while the composition of the other ingredients remained unchanged. For high-glucose diet (HGD), the regular food composition was modified by supplementing the food with 25% D-glucose (23 g in 100 mL of standard medium) whereas the composition of the other ingredients remained unchanged. All genetic crosses were set up at 25 °C and then transferred to 29°C where they were grown until analysis either as larvae or as adults.

Embryo Collection

Embryo collections were done for 4–6 h at 25°C. This was followed strictly for all experimental crosses. For HSD experiments, the embryos were collected on RF at 25°C after which 40–50 embryos were carefully transferred to HSD and reared at 29°C until analysis. Temperature-sensitive experiments with *tub gal80^{ts}* were carefully monitored to maintain timings for shifting them from a non-permissive (18°C) to permissive (29 °C) temperature. Specifically, for *Hml$^{\Delta}$ >UAS-hid;tub gal80^{ts}*, the embryo collection was conducted at 25°C and shifted to 18°C where they were grown until mid-2nd instar larvae followed by shift to 29°C incubator. For *Hml$^{\Delta}$ >UAS shi^{ts}* experiments after embryo collection, the animals were grown at 29°C until analysis.

Quantification of Adult Growth Phenotype

All adult flies were scored for their body sizes 2 days after eclosion. The animals were scored first by comparing their body sizes against the control *Hml$^{\Delta}$ >/w^{1118}* reared either on regular food or on HSD. The wingspan area of the adult animals was also scored to quantify for growth (64). The wings of flies of interest were plucked, mounted on a slide, and imaged using a bright-field microscope. Female and male wings were mounted separately and analyzed separately. The wingspan areas were calculated using Fiji software. Briefly, the circumference of the wing is marked and area is measured. Only one wing per animal has been analyzed. In every experiment, we analyzed 12–15 animals. This was done with a minimum of 10 repeats.

The wingspan area quantification for genotypes *UAS hid* and *UAS Pvr^{Act}* on RF were carried out together in multiple batches. Hence, the controls are the same in **Figure 1h** and **Supplementary Figure 5k**.

Immunostaining, Immunohistochemistry, and Fluorescence Quantification

For rabbit pAKT (1:400) and rabbit FoxO (1:500) staining, fat bodies from feeding 3rd instar larvae were dissected in 1× PBS, fixed in PBS containing 4% formaldehyde for 20 min at room temperature, and washed in PBS containing 0.1% Triton X-100 (PBT). Tissues were then blocked for 2 h in 0.3% PBT containing 5% NGS. Primary antibodies were incubated overnight at 4°C and secondary antibodies for 2 h at room temperature.

For Dilp 2 (1:400) and Dilp 5 (1:800) stainings, brains were dissected from feeding L3 larvae in 1× PBS. They were fixed in 1× PBS containing 4% formaldehyde for 20 min at room temperature, and extensively washed in 1× PBS containing 0.3% Triton X-100 (PBT). Tissues were then blocked for 2 h in 0.3% PBT containing 5% NGS. Primary antibodies were incubated overnight at 4°C and secondary antibodies for 2 h at room temperature. To quantify Dilp2 and Dilp5 levels, confocal Z series of the IPCs were obtained using a 2-μm step size and identical laser power and scan settings. Fiji software was used to generate sum-intensity 3D projections of the Z stacks (16-bit scanned images) and to measure total fluorescent intensity across the IPCs.

For staining circulating blood cells, 3rd instar larvae were bled on Teflon-coated slides (Immuno-Cell no. 2015 C 30) followed by staining protocol as previously described.

The following secondary antibodies have been used in the study at 1:500 dilution: FITC and Cy3 (Jackson Immuno Research Laboratories). Phalloidin (Sigma-Aldrich no. 94072) was used at 1:100 dilutions to stain cell morphologies and nuclei were visualized using DAPI. Samples were mounted with Vectashield (Vector Laboratories) or 70% glycerol.

Imaging

Immunostained images, blood cell images, and wing Disc images were acquired using Olympus FV3000 confocal microscopy system under a × 20 air or ×40 oil-immersion objective or ×60 oil-immersion objective. Bright-field and larval fluorescence images were obtained on Leica fluorescence stereomicroscope.

Hemocyte Isolation and Quantification

Total blood cells including circulating hemocytes and sessile pool resistant hemocytes were isolated. For this, larvae where mechanically brushed to release the sessile pool resident hemocytes into circulation, and after dissection, the cells still adhering to cuticle were scraped with the forceps as per published protocol (65).

Circulating cell numbers obtained were quantified per larvae. For each genotype, a minimum of 10 larvae were analyzed. Five images per well covering the field of view were obtained under constant magnification. The hemocytes in these views were counted manually to score for DAPI-positive (representing total blood cells), Hml-positive, and Hml-negative cells. The counts are represented as blood cell numbers per square millimeter (53).

Quantification of tGPH

tGPH intensity is quantified using ImageJ software as previously described in (39). Briefly, fat bodies of feeding L3 larvae were imaged using confocal microscopy and average fluorescence was measured in 25 random squared areas (10 × 30 pixels), each covering part of the plasma membrane in different cells.

Nile Red Staining

For lipid droplet staining, wandering L3 larvae were dissected in 1× PBS and fixed in 4% formaldehyde in 1× PBS for 20 min at room temperature. Tissues were then rinsed twice with 1× PBS, incubated for 30 min in a 1:1000 dilution with 70% glycerol of 0.02% Nile red (Sigma—Cat. no. N3013). The tissues were mounted in 70% glycerol with DAPI.

Metabolite Measurements

Glucose, trehalose, and glycogen measurements were done in feeding 3rd instar larvae. Triglyceride measurements were done in wandering 3rd instar larvae.

Glucose and TAG assays were conducted in extracts made from whole larva (1 sample = 3 larvae) and fat body (1 sample = fat body from 5 larvae). These tissues were homogenized in 100 μL of 1× PBS using GENETIX Bead Beater to obtain the extract for glucose or TAG analysis. For hemolymph extracts, bleeds

from six larvae was collected in 100 µL of 1× PBS and centrifuged at 1000 rpm to remove blood cells. The extracted samples were heat inactivated at 70°C for 10 min and then centrifuged at 1000 rpm. The supernatant was collected and subjected to glucose analysis using Sigma GOD-POD kit (GAGO20) or TAG analysis using the Sigma Triglycerides assay reagents (T2449 and F6428) (66).

For hemolymph trehalose assays, we adapted a previously published protocol (66). Briefly, larval hemolymph from six animals was collected in 25 µL of ice-cold 1× PBS and centrifuged at 5,000 rpm for 5 min to remove blood cells. 10 µL of sample was incubated in 25 µL of 0.25 M sodium carbonate at 95°C for 2 h in a thermal cycler, then cooled to room temperature followed by additions of 8 µL of 1 M acetic acid and 66 µL of 0.25 M sodium acetate (pH 5.2) as the digestion buffer. 1 µL of porcine trehalase (Sigma T8778) was added to 40 µL of this mixture and incubated at 37°C overnight. The resulting glucose was analyzed and normalized to protein levels.

The trehalose measurements for genotypes *UAS hid* and *UAS* Pvr^{Act} on RF and HSD were carried out together in multiple batches. Hence, the controls are same in **Figures 5p**, **2g** (RF) and **Figures 3n**, **5g** (HSD).

Whole-larvae glycogen assay was conducted as per the instructions provided along with Glycogen Assay Kit (MAK016) (67). For this one, whole larva was homogenized in 100 µL of 1× PBS. This extract was used for the assay and the amounts were normalized to total protein levels in the same sample.

The glycogen measurements for genotypes *UAS hid* and *UAS* Pvr^{Act} on RF and HSD were carried out together in multiple batches. Hence, **Figures 5o**, **2h** (RF) and **Figures 3p**, **5h** (HSD) share the same controls.

Protein estimation was undertaken using the Thermo Scientific BCA protein assay kit (Cat. no. 23225) and Varioskan LUX Multimode Microplate Reader using skanit software was used to quantify all metabolites.

Cell Density Quantification

Wing disc cell density was quantified by counting the total number of nuclei stained with DAPI in five random regions (430 μm^2 area each) of the wing imaginal disc. This was done for five different wing discs (68).

RNA Extraction and RT-PCR Analysis

RNA extractions from larval fat bodies(20 larvae) and brain (35 larvae) tissues were performed as previously published (69). Briefly, RNA from these samples was extracted using Trizol reagent (Ambion by Life Technologies Cat no. 15596). For RT-PCR, RNA samples were treated with DNase I (Thermo Scientific) and converted to cDNA with SuperScript II (Invitrogen). qPCR was performed using the SYBR Green PCR Master Mix (Applied Biosystems), in the C-1000 Touch Thermal Cycler (BIO-RAD CFX384 Real-Time System) in 384-well plates (Applied Biosystems). At least three biological replicates were used for statistical analysis. The following primers were used to perform qPCR:

List of qPCR primers

Gene	*Primer*	*Reference*
InR	*F–5′-ACTGAACCTCTCGTCAAGGC-3′* *R–5′-GAACCCTCCACGCACTTACA-3′*	*(70)*
tobi	*F–5′-CCACCAAGCGAGACATTTACC-3′* *R–5′-GAGCGGCGTAGTCCATCAC-3′*	*(70)*
4EBP	*F–5′-CCAGGAAGGTTGTCATCTCG-3′* *R–5′-CCAGGAGTGGTGGAGTAGAGG-3′*	*(70)*
dpt	*F–5′-ACCGCAGTACCCACTCAATC-3′* *R–5′-CCCAAGTGCTGTCCATATCC-3′*	*Designed using NCBI primer blast*
drs	*F–5′-GTACTTGTTCGCCCTCTTCG-3′* *R–5′-CTTGCACACACGACGACAG-3′*	*Designed using NCBI primer blast*
rp49	*F–5′-CGGATCGATATGCTAAGCTGT-3′* *R–5′-GCGCTTGTTCGATCCGTA-3′*	*Gifted by Dr. Raghu Padinjat Lab, NCBS*

The mRNA quantifications for genotypes *UAS hid* and *UAS* Pvr^{Act} on HSD were carried out together in multiple batches. Hence, **Figures 3t,u,y,z**, **5r,s,t,u**, **Supplementary Figures 4l, 8g** share the same controls.

Protein Extraction and Western Blot Analysis

Tissues (fat bodies from 20 larvae and brains from 35 larvae) were homogenized with the help of stainless steel beads (Qiagen; 69989) in an EZ-Lyser bead beater (Genetix). Protein extraction was carried out as previously published (69). Protein estimations were done using Bradford Reagent (Sigma B6916). 10% SDS-PAGE and Western blots were performed using standard methods (69). The following antibodies were used: primary antibodies—anti-pAkt (1:1000; rabbit; CST 4054; Ser505), anti-Akt (1:1000; rabbit; CST 9272), and anti-β-tubulin (1:3000; rabbit; Abcam ab6046) and secondary antibodies—anti-rabbit IgG, HRP-linked (CST 7074). Chemiluminescent reagent Western Bright Quantum (Advansta r-03026-c50) was used for detection by iBright FL1000 (Invitrogen). For measurements of pAKT/AKT ratios, the band mean intensities of pAkt and Akt were quantified with the help of Fiji (ImageJ) and corrected for background levels, followed by calculating their ratios from which the fold change was obtained.

The immunoblot quantifications for genotypes *UAS-hid* and *UAS* Pvr^{Act} on HSD were carried out together in multiple batches. Hence, **Supplementary Figures 4k**, **8f** share the same control.

STATISTICAL ANALYSIS

All statistical analysis was performed using Graph Pad Prism 5 and Microsoft Excel 2010. The means were analyzed using two-tailed, unpaired Student *t* test. Two-way ANOVA was performed between wing span areas of Hml^{Δ} >/+ RF, Hml^{Δ} >/+ HSD versus Hml^{Δ} >/*UAS-hid* RF, Hml^{Δ} >/*UAS-hid* HSD (**Figure 3g**)

and Hml^{Δ} >/+ RF, Hml^{Δ} >/+ HSD versus Hml^{Δ} >/*UAS* Pvr^{Act} RF, Hml^{Δ} >/*UAS* Pvr^{Act} HSD (**Figure 4h**).

DATA AVAILABILITY STATEMENT

All datasets generated for this study are included in the article/**Supplementary Material**.

AUTHOR CONTRIBUTIONS

PP and TM conceptualized the project. PP, AT, and SM performed experiments, conducted the formal analysis, and contributed to the writing of the manuscript. TM contributed towards procuring funding to drive this research, overseen the project for its scientific, critical evaluation of the data and manuscript writing and editing. All authors contributed to the article and approved the submitted version.

FUNDING

This study was supported by the DBT-Center of Excellence grant BT/PR13446/COE/34/30/2015, DST-ECR ECR/2015/000390DBT-IYBA 2017, DBT Ramalingaswami Re-entry Fellowship and CEFIPRA awarded to TM.

ACKNOWLEDGMENTS

We thank Pierre Leopold for Dilp2, Dilp5 and FoxO antibodies, Raghu Padinjat lab for primers, Banerjee lab for fly stocks, Angela Giangrande, Shruthi Balachandran for useful comments on the manuscript and necessary discussion inputs and Apurva Sarin and Dasaradhi Palakodeti for critical evaluation of the manuscript. We acknowledge our imaging and fly facility. PP is a Project Assistant and AT and SM are graduate students in the Mukherjee lab.

SUPPLEMENTARY MATERIAL

The Supplementary Material for this article can be found online at: https://www.frontiersin.org/articles/10.3389/fimmu.2020.01528/full#supplementary-material

Supplementary Figure 1 | In **(d–h″),** scale bar = 20 μm. Bar graph in **(c)** shows mean ± standard deviation (SD). Statistical analysis applied in panel **c** is unpaired *t*-test, two-tailed in **(c)**. "*n*" is the total number of larvae analyzed. **(a–c)** *UAS-hid* genetic background does not show any blood cell defect. 3rd instar larval images depicting Hml^{+} blood cells (red, marked with RFP) in **(a)** control (*domeMESO-GFP; hml-dsRed/+*) and **(b)** *domeMESO-GFP; hml-dsRed/UAS-hid* are comparable. **(c)** Blood cell counts/mm^2 in these backgrounds (*domeMESO-GFP; hml-dsRed/w1118*, *n* = 5, 166.5 ± 111.7 and *domeMESO-GFP; hml-dsRed/UAS-hid*, *n* = 5, 165.8 ± 92.7). **(d–i″)** Lineage analysis of Hml^{Δ}*gal4* using GTRACE confirms blood-specific expression. RFP (real-time Hml^{Δ}*gal4* expression) or GFP (lineage-based Hml^{Δ}*gal4* expression) was not detected in **(d–d″)** brain, **(e–e″)** fat body, **(f–f″)** proventriculus, **(g–g″)** leg disc, **(h–h″)** wing disc. **(i–i″)** Both RFP and GFP expression is detected in blood cells.

Supplementary Figure 2 | In **(b,c,d–e′),** scale bar = 1 mm, **(f–g′)** = 250 μm, and **(i,j)** = 20 μm. In **(h**, **k)**, bar graphs show mean ± standard deviation (SD). Statistical analysis in **(h**, **k)** is unpaired *t*-test, two-tailed. "*n*" is the total number of larvae analyzed. **(a)** Shows the pictorial representation of the constitutive and temporal experiments that have been done using Hml^{Δ} > and Hml^{Δ} >*; tub* $gal80^{ts}$, respectively. The red mark indicates the temporal expression of *UAS hid* in blood cells by shifting the larvae from permissive (18°C) to non-permissive temperature (29°C). **(b,c)** Temporal expression of *UAS-hid* in Hml^{+} blood cells (marked by GFP, green) causes a loss of blood cells. Compared with **(b)** control (Hml^{Δ} >*UAS-GFP; tub* $gal80^{ts}$/+), **(c)** Hml^{Δ} >*UAS-GFP; tub* $gal80^{ts}$*/ UAS hid* larvae show no GFP signal. **(d–h)** Temporal expression of *UAS-hid* in Hml^{+} blood cells did not alter adult growth. Representative adult **(d–e′)** fly and **(f–g′)** wing images in **(d, d′, f, f′)** control (Hml^{Δ} >*UAS-GFP; tub* $gal80^{ts}$/+) and **(e,e′,g,g′)** Hml^{Δ} >*UAS-GFP; tub* $gal80^{ts}$*/ UAS hid* show no growth reduction. **(h)** Wingspan area quantifications in Hml^{Δ} >*; tub* $gal80^{ts}$/+ (female *n* = 100, 1.4 ± 0.1, male *n* = 100, 1.05 ± 0.07) and in Hml^{Δ} >*; tub* $gal80^{ts}$*/UAS-hid* (female *n* = 100, 1.3 ± 0.1, male *n* = 100, 1.05 ± 0.09). **(i–k)** Reduced cell density in wing discs of Hml^{Δ} >*/UAS-hid* L3 larvae. Compared with cell density seen in wing discs of **(i)** control (Hml^{Δ} >/+), **(j)** Hml^{Δ} >*/UAS-hid* cell density is reduced. **(k)** Quantified by counting DAPI-positive cells (white). Hml^{Δ} >/+, *n* = 5, 11.24 ± 3, and Hml^{Δ} >*/UAS-hid*, *n* = 5, 4.80 ± 0.60 and (***p*-value = 0.0017).

Supplementary Figure 3 | In **(d,e),** scale bar = 20 μm. In **(a–c**, **g),** bar graphs show mean ± standard deviation (SD) and statistical analysis applied in these panels is unpaired *t*-test, two-tailed. "*n*" is the total number of larvae analyzed, FB is fat body, a.u is arbitrary units, f.c is fold change and RF indicates regular food. **(a)** Quantification of mean intensity of Dilp2 levels of images shown in **Figures 2a,b**. Control, Hml^{Δ} >/+ (*n* = 16, 204.5 ± 149.8) and Hml^{Δ} >*/UAS-hid* (*n* = 14, 1768.8 ± 794.2, ****p*-value < 0.0001). **(b)** Quantification of mean intensity of Dilp5 levels of images shown in **Figures 2c,d**. Control, Hml^{Δ} >/+ (*n* = 16, 234.023 ± 321.72) and Hml^{Δ} >*/UAS-hid* (*n* = 13, 1395.4 ± 1303.9, ***p*-value = 0.0019). **(c)** Fat body glucose levels. Hml^{Δ} >/+ (*n* = 65, 0.095 ± 0.017) and Hml^{Δ} >*/UAS-hid* (*n* = 65, 0.04 ± 0.02, ****p*-value < 0.0001). **(d–f)** Fat body pAKT analysis. **(d,e)** Immunostaining of feeding L3 larval fat bodies with anti-pAKT antibody in **(d)** control, Hml^{Δ} >/+ and **(e)** Hml^{Δ} >*/UAS-hid* backgrounds show reduced pAKT levels in Hml^{Δ} >*/UAS-hid* condition. **(f)** Immunoblot analysis of pAkt/Akt ratio in fat bodies of feeding L3 larvae of control (Hml^{Δ} >/+) and Hml^{Δ} >*/UAS-hid* reveals a small difference (fold change ± SD mentioned in the blots). β-Tubulin was used as the internal loading control. **(g)** Relative fat body m*RNA* levels of *tobi*. Fold change is plotted, and statistical analysis was done using C_t values (Hml^{Δ} >/+, *n* = 60,8.67 ± 3.57 and Hml^{Δ} >*/UAS-hid*, *n* = 60, 10.68 ± 0.75).

Supplementary Figure 4 | In **(a–b′)**, scale bar = 250 μm and **(g–j)** is 20 μm. In **(c–f,l)**, bar graphs show mean ± standard deviation (SD) and statistical analysis applied for these panels is unpaired *t*-test, two tailed. "*n*" is the total number of larvae analyzed, FB is fat body, a.u is arbitrary units, f.c is fold change, HFD is high-fructose diet and HSD is high-sugar diet. **(a–c)** Loss of immune cells affects tolerance to high fructose diet. (**a–b′**) Representative wing images of **(a,a′)** control (Hml^{Δ} >/+) on HFD and **(b,b′)**, Hml^{Δ} >*/UAS-hid* on HFD showing reduction in wing sizes of Hml^{Δ} >*/UAS-hid*, HFD animals. **(c)** Quantification of wingspan areas of Hml^{Δ} >/+ on HFD (female, *n* = 50, 1.4 ± 0.03, male *n* = 120, 1.1 ± 0.08) and Hml^{Δ} >*/UAS-hid* on HFD (female *n* = 120, 1.4 ± 0.06, ****p*-value < 0.0001, compared with Hml^{Δ} >/+ HFD females, male *n* = 120, 1.1 ± 0.06, **p*-value < 0.0333, compared with Hml^{Δ} >/+ males). **(d)** Quantification of mean intensity of Dilp2 expression of representative images shown in **Figures 3h,i**. Control, Hml^{Δ} >/+on HSD (*n* = 9, 2499 ± 561) and Hml^{Δ} >*/UAS-hid* on HSD (*n* = 8, 2681 ± 387.4). **(e)** Quantification of mean intensity of Dilp5expression of representative images shown in **Figures 3j,k**. Control, Hml^{Δ} >/+on HSD (*n* = 10, 1521 ± 425) and Hml^{Δ} >*/UAS-hid* on HSD (*n* = 7, 1463 ± 467). **(f)** Fat body glucose levels. Hml^{Δ} >/+ on HSD (*n* = 30, 0.021 ± 0.019) and Hml^{Δ} >*/UAS-hid* on HSD (*n* = 30, 0.02 ± 0.01). (**g,h**) pAKT immunostaining in fat bodies of feeding L3 larvae on HSD of **(g)** control (Hml^{Δ} >/+) and **(h)** Hml^{Δ} >*/UAS-hid* are comparable. **(i,j)** FoxO immunostaining in fat bodies of feeding L3 larvae on HSD of **(i)** control (Hml^{Δ} >/+) and **(j)** Hml^{Δ} >*/UAS-hid* show similar FoxO nuclear localization. **(k)** Immunoblot analysis of pAkt/Akt ratio in fat bodies of feeding L3 control (Hml^{Δ} >/+) and Hml^{Δ} >*/UAS-hid* larvae raised on HSD show no change. Fold change ± SD mentioned in the blots. β-Tubulin was used as the internal loading control. **(l)** Relative fat body m*RNA* levels of *tobi*. Fold change is plotted, and statistical analysis was done using C_t values (Hml^{Δ} >/+ on HSD, *n* = 80, 11.83 ± 1.32 and Hml^{Δ} >*/UAS-hid* on HSD *n* = 80, 11.69 ± 0.98).

Supplementary Figure 5 | In **(a–f,l–n′,q–s′),** and **(u–u′)** scale bar = 20 μm, **(g–h′)** scale bar = 1 mm, and **(i–j′)** scale bar = 250 μm. In **(k,l–p,t,v)**, bar graphs show mean ± standard deviation (SD) and in these panels statistical analysis applied is unpaired *t*-test, two tailed. "*n*" is the total number of larvae analyzed. a.u is arbitrary unit and RF is regular food. **(a–b′′′)** Characterization of blood cells in Hml^{Δ} >*UAS-GFP/UAS* Pvr^{Act} backgrounds. Compared with blood cells in **(a–a′′′)**

control, *Hml*$^{\Delta}$ >*UAS-GFP*, **(b–b′′′)** *Hml*$^{\Delta}$ >*UAS-GFP/UAS Pvr*^{Act} larvae have increased numbers as evident from increased **(a,b)** DAPI, **(a′,b′)** Hml (*Hml*$^{\Delta}$ >*UAS-GFP)* and **(a″,b″)** phalloidin stainings. **(a′′′,b′′′)** Merge of all the channels. **(c–f)** Immunostainings of **(c,d)** Dilp2 and **(e,f)** Dilp5 in L3 feeding larval brain insulin-producing cells (IPCs). As compared with **(c,e)** control (*Hml*$^{\Delta}$ >/+) on RF, **(d,f)** *Hml*$^{\Delta}$ >*/UAS Pvr*^{Act} on RF, no change in Dilp2 and Dilp5 staining is detected. Quantification of mean intensities in **(l,m)**. **(g–k)** Expression of *UAS Pvr*^{Act} in Hml^{+} blood cells have not altered adult growth on RF. Representative adult **(g–h′)** fly and **(i–j′)** wing images in **(g,g′,i,i′)** control (*Hml*$^{\Delta}$ >/+) and **(h,h′,j,j′)** *Hml*$^{\Delta}$ >*/UAS Pvr*^{Act} show no growth modulation. **(k)** Quantifications of wing span areas of control *Hml*$^{\Delta}$ >/+ on RF (female $n = 100$, 1.4 ± 0.03, male $n = 100$, 1.1 ± 0.08) and *Hml*$^{\Delta}$ >*/UAS Pvr*^{Act} on RF (female $n = 100$, 1.4 ± 0.06, male $n = 100$, 1.1 ± 0.06). **(l)** Mean intensity of Dilp2quantification. Control, *Hml*$^{\Delta}$ >/+ on RF ($n = 9$, 446.88 ± 349.05) and *Hml*$^{\Delta}$ >*/UAS Pvr*^{Act} on RF ($n = 9$, 649.86 ± 678.53). **(m)** Mean intensity of Dilp5 quantification. Control, *Hml*$^{\Delta}$ >/+ on RF ($n = 9$, 411.82 ± 365.73) and *Hml*$^{\Delta}$ >*/UAS Pvr*^{Act} on RF ($n = 8$, 474.98 ± 476.43). **(n)** Glucose levels were measured in whole larvae (*Hml*$^{\Delta}$ >/+, RF, $n = 18$, 0.094 ± 0.036 and *Hml*$^{\Delta}$ >*/UAS Pvr*^{Act}, RF, $n = 15$, 0.08 ± 0.025), hemolymph (*Hml*$^{\Delta}$ >/+, RF, $n = 30$, 0.09 ± 0.014 and *Hml*$^{\Delta}$ >*/UAS Pvr*^{Act} RF, $n = 30$, 0.08 ± 0.03), and fat body (*Hml*$^{\Delta}$ >/+, RF, $n = 30$, 0.08 ± 0.02 and *Hml*$^{\Delta}$ >*/UAS Pvr*^{Act}, RF, $n = 30$, 0.08 ± 0.03). **(o)** Glycogen level measures in whole larvae of *Hml*$^{\Delta}$ >/+, RF ($n = 6$, 1.08 ± 0.12) and *Hml*$^{\Delta}$ >*/UAS Pvr*^{Act}, RF ($n = 6$, 1.46 ± 0.16, ***p-value = 0.0009). **(p)** Hemolymph trehalose levels of *Hml*$^{\Delta}$ >/+, RF ($n = 66$, 0.18 ± 0.05) and *Hml*$^{\Delta}$ >*/UAS Pvr*^{Act}, RF ($n = 66$, 0.17 ± 0.06). **(q–t)** Analysis of fat body insulin signaling in **(q–s)** control (*Hml*$^{\Delta}$ >/+) on RF and (**q′-s′**) *Hml*$^{\Delta}$ >*/UAS Pvr*^{Act} on RF shows no change in **(q,q′)** tGPH expression, quantified in **(t**, **r,r′)** pAKT immunostaining, and **(s,s′)** FoxO expression. **(t)** Mean tGPH intensity quantification of control, *Hml*$^{\Delta}$ >/+ on RF ($n = 25$, 2621 ± 486) and *Hml*$^{\Delta}$ >*/UAS Pvr*^{Act} on RF ($n = 25$, 2875 ± 158). **(u,u′)** Neutral lipid (Nile red) staining in fat bodies of **(u)** *Hml*$^{\Delta}$ >/+ and **(u′)** *Hml*$^{\Delta}$ >*/UAS Pvr*^{Act} on RF are comparable. **(v)** TAG levels measurements in whole larvae (*Hml*$^{\Delta}$ >/+ on RF, $n = 36$, 2.01 ± 0.15 and *Hml*$^{\Delta}$ >*/UAS Pvr*^{Act} on RF, $n = 36$, 1.98 ± 0.3) and hemolymph (*Hml*$^{\Delta}$ >/+ on RF, $n = 48$, 0.37 ± 0.15 and *Hml*$^{\Delta}$ >*/UAS Pvr*^{Act} on RF, $n = 48$, 0.23 ± 0.1).

Supplementary Figure 6 | In **(a–c),** scale bar = 1 mm**, (e–f′,h–i′)** scale bar = 250 μm. In **(d,g,j),** bar graphs show mean ± standard deviation (SD) and in these panels statistical analysis applied is unpaired *t*-test, two tailed. "*n*" is the total number of larvae analyzed, RF indicates regular food and HSD indicates high-sucrose diet. **(a–d)** Larval images showing blood cells (Hml^{+}, GFP, green) in **(a)** control (*Hml*$^{\Delta}$ >/+), **(b)** *Hml*$^{\Delta}$ >*/UAS Pvr*^{WT}, and **(c)** *Hml*$^{\Delta}$ >*/UAS Shi*^{ts}. Expression of *Pvr*^{WT} or *Shi*^{ts} in Hml^{+} cells causes increase in GFP-positive cells, quantified in **(d)**. **(d)** Quantifications of total blood cell numbers and Hml^{+} blood cells in *Hml*$^{\Delta}$ >/+ (total number of blood cells/mm^2, $n = 20$, 203.49 ± 41.20 and GFP-positive cells, $n = 20$, 152.37 ± 42.6), *Hml*$^{\Delta}$ >*/UAS Pvr*^{WT} (total number of blood cells/mm^2, $n = 10$, 403.20 ± 114.54, ***p-value < 0.0001 and GFP-positive cells, $n = 10$, 334.32 ± 76.49, ***p-value < 0.0001), and *Hml*$^{\Delta}$ >*/UAS Shi*^{ts} (total number of blood cells, $n = 16$, 503.40 ± 68.26, ***p-value < 0.0001 and GFP-positive cells $n = 16$, 430.90 ± 68.14, ***p-value < 0.0001). **(e–g)** Increasing immune cell numbers of an activated state restores HSD growth defect. Compared with **(e,e′)** control wing sizes, *Hml*$^{\Delta}$ >/+ on HSD **(f,f′)**, *Hml*$^{\Delta}$ >*UAS Pvr* on HSD showed a significant growth rescue. **(g)** Quantifications of wingspan areas of *Hml*$^{\Delta}$ >/+ on HSD (female $n = 50$, 1.01 ± 0.07, male $n = 50$, 0.9 ± 0.05) and in *Hml*$^{\Delta}$ >*/UAS Pvr*^{WT} on HSD (female $n = 25$, 1.09 ± 0.09, **p-value = 0.0038, male $n = 25$, 1.03 ± 0.05, ***p-value < 0.0001). **(h–j)** Increasing immune cell numbers by expressing *UAS Shi*^{ts} did not restore HSD growth defect. Compared with **(h,h′)** control wing sizes, *Hml*$^{\Delta}$ >/+ on HSD **(i,i′)**, *Hml*$^{\Delta}$ >*UAS Shi*^{ts} showed a significant growth retardation. **(j)** Quantifications of wing span areas of *Hml*$^{\Delta}$ >/+ on HSD (female $n = 50$, 1.0 ± 0.1, male $n = 50$, 0.90 ± 0.11) and in *Hml*$^{\Delta}$ >*/UAS Shi*^{ts} on HSD (female $n = 50$, 0.9 ± 0.09, *p-value = 0.0223, male $n = 50$, 0.78 ± 0.09, **p-value = 0.0031).

Supplementary Figure 7 | In **(c–e,g–i,k–m,o–q)**, scale bar = 250 μm. In **(a,b,f,j,n,r)**, bar graphs show mean ± standard deviation (SD) and statistical analysis applied in these panels is unpaired *t*-test. "*n*" is total number of larvae analyzed, RF is regular food, HSD is high-sucrose diet, HFD is high-fructose diet, and HGD is high-glucose diet. **(a,b)** High-sugar diet causes adult growth retardation. Quantification of wing span areas of **(a)** females (*Hml*$^{\Delta}$ >/+) and **(b)** males (*Hml*$^{\Delta}$ >/+) reared on different sugar diets. *Hml*$^{\Delta}$ >/+ on RF (female $n = 50$, 1.45 ± 0.06 and male $n = 50$, 1.10 ± 0.04), *Hml*$^{\Delta}$ >/+ on HSD (female $n = 50$, 1.01 ± 0.08, ***p-value < 0.0001, compared with RF females and male $n = 50$, 0.84 ± 0.13, ***p-value < 0.0001, compared with RF males), *Hml*$^{\Delta}$ >/+ on HFD (female $n = 50$, 1.13 ± 0.13, ***p-value < 0.0001, compared with RF females and male $n = 50$, 0.84 ± 0.07, ***p-value < 0.0001, compared with RF males), and *Hml*$^{\Delta}$ >/+ on HGD (female $n = 25$, 0.74 ± 0.08, ***p-value < 0.0001, compared with RF females and male $n = 25$, 0.60 ± 0.11, ***p-value < 0.0001, compared with RF males). **(c–r)** Increasing immune cell numbers of an activated state restores growth defect induced by high-sugar diet as represented in wing span sizes. **(c–j)** HFD-induced growth defect seen in **(c,g)** control, *Hml*$^{\Delta}$ >/+ females and males, is restored in **(d,h)** *Hml*$^{\Delta}$ >*/UAS Pvr*^{Act} HSD condition but not restored in **(e,i)** *Hml*$^{\Delta}$ >*/UAS Shi*^{ts} HFD animals. Contrarily, **(e)** *Hml*$^{\Delta}$ >*/UAS Shi*^{ts} HFD females show a significant growth defect. Quantifications of wing span areas in **(f)** females and **(j)** males. **(f)** Wing span areas of *Hml*$^{\Delta}$ >/+ HFD (female $n = 35$, 1.13 ± 0.13), *Hml*$^{\Delta}$ >*/UAS Pvr*^{Act} HFD (female $n = 51$, 1.26 ± 0.08, ***p-value < 0.0001), and *Hml*$^{\Delta}$ >*/UAS Shi*^{ts} HFD (female $n = 25$, 0.99 ± 0.09, ***p-value < 0.0002) all comparisons made with *Hml*$^{\Delta}$ >/+ HFD females. **(j)** Wingspan areas of *Hml*$^{\Delta}$ >/+ HFD (male $n = 25$, 0.84 ± 0.07), *Hml*$^{\Delta}$ >*/UAS Pvr*^{Act} HFD (male $n = 25$, 0.97 ± 0.07, ***p-value < 0.0001), and *Hml*$^{\Delta}$ >*/UAS Shi*^{ts} HFD (male $n = 25$, 0.83 ± 0.07). All comparisons made with *Hml*$^{\Delta}$ >/+ HFD males. **(k–r)** HGD-induced growth defect seen in **(k,o)** control, *Hml*$^{\Delta}$ >/+ females and males, is restored in **(l,p)** *Hml*$^{\Delta}$ >*/UAS Pvr*^{Act} HGD condition but not restored in **(m,q)** *Hml*$^{\Delta}$ >*/UAS Shi*^{ts} HGD animals. Quantifications of wing span areas in **(n)** females and **(r)** males. **(n)** Wing span areas of *Hml*$^{\Delta}$ >/+ HGD (female $n = 25$, 0.74 ± 0.07), *Hml*$^{\Delta}$ >*/UAS Pvr*^{Act} HGD (female $n = 25$, 0.96 ± 0.09, ***p-value < 0.0001) and *Hml*$^{\Delta}$ >*/UAS Shi*^{ts} HGD (female $n = 25$, 0.77 ± 0.06). All comparisons made with *Hml*$^{\Delta}$ >/+ HGD females. **(r)** Wingspan areas of *Hml*$^{\Delta}$ >/+ HGD (male $n = 25$, 0.6 ± 0.11), *Hml*$^{\Delta}$ >*/UAS Pvr*^{Act} HGD (male $n = 25$, 0.9 ± 0.05, ***p-value < 0.0001), and *Hml*$^{\Delta}$ >*/UAS Shi*^{ts} HGD (male $n = 25$, 0.61 ± 0.08). All comparisons made with *Hml*$^{\Delta}$ >/+ HGD males.

Supplementary Figure 8 | In **(d**, **e),** scale bar = 20 μm. In **(a–c,g)**, bar graphs show mean ± standard deviation (SD) and statistical analysis applied in these panels is unpaired *t*-test, two-tailed. "*n*" is the total number of larvae analyzed, a.u is arbitrary unit, FB is fat body, f.c is fold change, and HSD is high-sucrose diet. **(a)** Mean intensity of Dilp2 quantification of representative image shown in **Figures 5a,b**. Control, *Hml*$^{\Delta}$ >/+ on HSD ($n = 5$, 2291 ± 678) and *Hml*$^{\Delta}$ >*/UAS Pvr*^{Act} on HSD ($n = 5$, 1225 ± 578.6, *p-value = 0.0283). **(b)** Mean intensity of Dilp5 quantification of representative image shown in **Figures 5c,d**. Control, *Hml*$^{\Delta}$ >/+ on HSD ($n = 5$, 1310 ± 304) and *Hml*$^{\Delta}$ >*/UAS Pvr*^{Act} on HSD ($n = 5$, 580.3 ± 238.7, **p-value = 0.0029). **(c)** Fat body glucose levels. *Hml*$^{\Delta}$ >/+ on HSD ($n = 35$, 0.02 ± 0.017) and *Hml*$^{\Delta}$ >*/UAS Pvr*^{Act} on HSD ($n = 35$, 0.09 ± 0.03, ***p-value = 0.0005). **(d–f)** Fat body pAKT analysis on HSD. **(d,e)** Immunostaining of feeding L3 larval fat bodies with anti-pAKT antibody in **(d)** control, *Hml*$^{\Delta}$ >/+, and **(e)** *Hml*$^{\Delta}$ >*/UAS Pvr*^{Act} backgrounds shows no change. **(f)** Immunoblot analysis of pAkt/Akt ratio in fat bodies of feeding L3 larvae of control (*Hml*$^{\Delta}$ >/+) and *Hml*$^{\Delta}$ >*/UAS Pvr*^{Act} reveals a small increase (fold change ± SD mentioned in the blots). β-Tubulin was used as the internal loading control. **(g)** Fat body analysis of *tobi* m*RNA* levels on HSD. Fold change is represented and statistical analysis was done using $\mathbf{C_t}$values (*Hml*$^{\Delta}$ >/+ on HSD, $n = 80$, 11.83 ± 1.32 and *Hml*$^{\Delta}$ >*/UAS Pvr*^{Act} on HSD, $n = 80$, 12.11 ± 0.73).

REFERENCES

1. Churchill ER, Dytham C, Thom MDF. Differing effects of age and starvation on reproductive performance in *Drosophila melanogaster*. *Sci Rep.* (2019) 9:2167. doi: 10.1038/s41598-019-38843-w
2. Matzkin LM, Johnson S, Paight C, Markow TA. Preadult parental diet affects offspring development and metabolism in *Drosophila melanogaster*. *PLoS ONE.* (2013) 8:e59530. doi: 10.1371/journal.pone.0059530
3. Ramond E, Petrignani B, Dudzic JP, Boquete JP, Poidevin M, Kondo S, et al. The adipokine NimrodB5 regulates peripheral hematopoiesis in *Drosophila*. *FEBS J.* (2020) 286:225–426. doi: 10.1111/febs.15237
4. van der Most PJ, de Jong B, Parmentier HK, Verhulst S. Trade-off between growth and immune function: a meta-analysis of selection

experiments. *Ecol Immunol.* (2011) 25:74–80. doi: 10.1111/j.1365-2435.2010.01800.x
5. Kraaijeveld AR, Godfray HC. Trade-off between parasitoid resistance and larval competitive ability in *Drosophila melanogaster*. *Nature.* (1997) 389:278–80. doi: 10.1038/38483
6. Banerjee U, Girard JR, Goins LM, Spratford CM. *Drosophila* as a genetic model for hematopoiesis. *Genetics.* (2019) 211:367–417. doi: 10.1534/genetics.118.300223
7. Tennessen JM, Thummel CS. Coordinating growth and maturation - insights from *Drosophila*. *Curr Biol.* (2011) 21:R750–7. doi: 10.1016/j.cub.2011.06.033
8. Rizki MT, Rizki RM. Functional significance of the crystal cells in the larva of *Drosophila melanogaster*. *J Biophys Biochem Cytol.* (1959) 5:235–40. doi: 10.1083/jcb.5.2.235
9. Hanson MA, Dostálová A, Ceroni C, Poidevin M, Kondo S, Lemaitre B. Synergy and remarkable specificity of antimicrobial peptides *in vivo* using a systematic knockout approach. *Elife.* (2019) 8:e44341. doi: 10.7554/eLife.48778
10. Mukherjee T, Kim WS, Mandal L, Banerjee U. Interaction between Notch and Hif-alpha in development and survival of *Drosophila* blood cells. *Science.* (2011) 332:1210–3. doi: 10.1126/science.1199643
11. Rizki TM, Rizki RM. Lamellocyte differentiation in *Drosophila* larvae parasitized by Leptopilina. *Dev Comp Immunol.* (1992) 16:103–10. doi: 10.1016/0145-305X(92)90011-Z
12. Evans CJ, Hartenstein V, Banerjee U. Thicker than blood: conserved mechanisms in *Drosophila* and vertebrate hematopoiesis. *Dev Cell.* (2003) 5:673–90. doi: 10.1016/S1534-5807(03)00335-6
13. Holz A, Bossinger B, Strasser T, Janning W, Klapper R. The two origins of hemocytes in *Drosophila*. *Development.* (2003) 130:4955–62. doi: 10.1242/dev.00702
14. Tepass U, Fessler LI, Aziz A, Hartenstein V. Embryonic origin of hemocytes and their relationship to cell death in *Drosophila*. *Development.* (1994) 120:1829–37.
15. Leitão AB, Sucena É. *Drosophila* sessile hemocyte clusters are true hematopoietic tissues that regulate larval blood cell differentiation. *Elife.* (2015) 4:e06166. doi: 10.7554/eLife.06166
16. Shim J, Mukherjee T, Mondal BC, Liu T, Young GC, Wijewarnasuriya DP, et al. Olfactory control of blood progenitor maintenance. *Cell.* (2013) 155:1141–53. doi: 10.1016/j.cell.2013.10.032
17. Makhijani K, Alexander B, Rao D, Petraki S, Herboso L, Kukar K, et al. Regulation of *Drosophila* hematopoietic sites by Activin-β from active sensory neurons. *Nat Commun.* (2017) 8:15990. doi: 10.1038/ncomms15990
18. Shim J, Mukherjee T, Banerjee U. Direct sensing of systemic and nutritional signals by haematopoietic progenitors in *Drosophila*. *Nat Cell Biol.* (2012) 14:394–400. doi: 10.1038/ncb2453
19. Yu S, Luo F, Jin LH. The *Drosophila* lymph gland is an ideal model for studying hematopoiesis. *Dev Comp Immunol.* (2018) 83:60–9. doi: 10.1016/j.dci.2017.11.017
20. Woodcock KJ, Kierdorf K, Pouchelon CA, Vivancos V, Dionne MS, Geissmann F. Macrophage-derived upd3 cytokine causes impaired glucose homeostasis and reduced lifespan in *Drosophila* fed a lipid-rich diet. *Immunity.* (2015) 42:133–44. doi: 10.1016/j.immuni.2014.12.023
21. Boulan L, Milán M, Léopold P. The systemic control of growth. *Cold Spring Harb Perspect Biol.* (2015) 7:a019117. doi: 10.1101/cshperspect.a019117
22. Mirth CK, Riddiford LM. Size assessment and growth control: how adult size is determined in insects. *Bioessays.* (2007) 29:344–55. doi: 10.1002/bies.20552
23. Colombani J, Raisin S, Pantalacci S, Radimerski T, Montagne J, Léopold P. A nutrient sensor mechanism controls *Drosophila* growth. *Cell.* (2003) 114:739–49. doi: 10.1016/S0092-8674(03)00713-X
24. Géminard C, Rulifson EJ, Léopold P. Remote control of insulin secretion by fat cells in *Drosophila*. *Cell Metab.* (2009) 10:199–207. doi: 10.1016/j.cmet.2009.08.002
25. Cattenoz PB, Sakr R, Pavlidaki A, Delaporte C, Riba A, Molina N, et al. Temporal specificity and heterogeneity of *Drosophila* immune cells. *EMBO J.* (2020) 39:e104486. doi: 10.15252/embj.2020104486
26. DiAngelo JR, Bland ML, Bambina S, Cherry S, Birnbaum MJ. The immune response attenuates growth and nutrient storage in *Drosophila* by reducing insulin signaling. *Proc Natl Acad Sci USA.* (2009) 106:20853–8. doi: 10.1073/pnas.0906749106
27. Palanker Musselman L, Fink JL, Baranski TJ. CoA protects against the deleterious effects of caloric overload in *Drosophila*. *J Lipid Res.* (2016) 57:380–7. doi: 10.1194/jlr.M062976
28. Davoodi S, Galenza A, Panteluk A, Deshpande R, Ferguson M, Grewal S, et al. The immune deficiency pathway regulates metabolic homeostasis in *Drosophila*. *J Immunol.* (2019) 202:2747–59. doi: 10.4049/jimmunol.1801632
29. Roth SW, Bitterman MD, Birnbaum MJ, Bland ML. Innate immune signaling in *Drosophila* blocks insulin signaling by uncoupling pi(3,4,5)p3 production and Akt activation. *Cell Rep.* (2018) 22:2550–6. doi: 10.1016/j.celrep.2018.02.033
30. Bajgar A, Dolezal T. Extracellular adenosine modulates host-pathogen interactions through regulation of systemic metabolism during immune response in *Drosophila*. *PLoS Pathog.* (2018) 14:e1007022. doi: 10.1371/journal.ppat.1007022
31. Krejcova G, Danielova A, Nedbalova P, Kazek M, Strych L, Chawla G, et al. *Drosophila* macrophages switch to aerobic glycolysis to mount effective antibacterial defense. *Elife.* (2019) 8:e50414. doi: 10.7554/eLife.50414
32. Kraakman MJ, Murphy AJ, Jandeleit-Dahm K, Kammoun HL. Macrophage polarization in obesity and type 2 diabetes: weighing down our understanding of macrophage function? *Front Immunol.* (2014) 5:470. doi: 10.3389/fimmu.2014.00470
33. Charroux B, Royet J. Elimination of plasmatocytes by targeted apoptosis reveals their role in multiple aspects of the *Drosophila* immune response. *Proc Natl Acad Sci USA.* (2009) 106:9797–802. doi: 10.1073/pnas.0903971106
34. Evans CJ, Olson JM, Ngo KT, Kim E, Lee NE, Kuoy E, et al. G-TRACE: rapid Gal4-based cell lineage analysis in *Drosophila*. *Nat Methods.* (2009) 6:603–5. doi: 10.1038/nmeth.1356
35. Goto A, Kadowaki T, Kitagawa Y. *Drosophila* hemolectin gene is expressed in embryonic and larval hemocytes and its knock down causes bleeding defects. *Dev Biol.* (2003) 264:582–91. doi: 10.1016/j.ydbio.2003.06.001
36. Sinenko SA, Mathey-Prevot B. Increased expression of *Drosophila* tetraspanin, Tsp68C, suppresses the abnormal proliferation of ytr-deficient and Ras/Raf-activated hemocytes. *Oncogene.* (2004) 23:9120–8. doi: 10.1038/sj.onc.1208156
37. Nässel DR, Liu Y, Luo J. Insulin/IGF signaling and its regulation in *Drosophila*. *Gen Comp Endocrinol.* (2015) 221:255–66. doi: 10.1016/j.ygcen.2014.11.021
38. Britton JS, Lockwood WK, Li L, Cohen SM, Edgar BA. *Drosophila*'s insulin/PI3-kinase pathway coordinates cellular metabolism with nutritional conditions. *Dev Cell.* (2002) 2:239–49. doi: 10.1016/S1534-5807(02)00117-X
39. Pasco MY, Léopold P. High sugar-induced insulin resistance in *Drosophila* relies on the lipocalin Neural Lazarillo. *PLoS ONE.* (2012) 7:e36583. doi: 10.1371/journal.pone.0036583
40. Lee S, Dong HH. FoxO integration of insulin signaling with glucose and lipid metabolism. *J Endocrinol.* (2017) 233:R67–79. doi: 10.1530/JOE-17-0002
41. Hoehn KL, Hohnen-Behrens C, Cederberg A, Wu LE, Turner N, Yuasa T, et al. IRS1-independent defects define major nodes of insulin resistance. *Cell Metab.* (2008) 7:421–33. doi: 10.1016/j.cmet.2008.04.005
42. Böhni R, Riesgo-Escovar J, Oldham S, Brogiolo W, Stocker H, Andruss BF, et al. Autonomous control of cell and organ size by CHICO, a *Drosophila* homolog of vertebrate IRS1-4. *Cell.* (1999) 97:865–75. doi: 10.1016/S0092-8674(00)80799-0
43. Suzawa M, Muhammad NM, Joseph BS, Bland ML. The toll signaling pathway targets the insulin-like peptide dilp6 to inhibit growth in *Drosophila*. *Cell Rep.* (2019) 28:1439–46.e5. doi: 10.1016/j.celrep.2019.07.015
44. Yu S, Zhang G, Jin LH. A high-sugar diet affects cellular and humoral immune responses in *Drosophila*. *Exp Cell Res.* (2018) 368:215–24. doi: 10.1016/j.yexcr.2018.04.032
45. Musselman LP, Fink JL, Narzinski K, Ramachandran PV, Hathiramani SS, Cagan RL, et al. A high-sugar diet produces obesity and insulin resistance in wild-type *Drosophila*. *Dis Model Mech.* (2011) 4:842–9. doi: 10.1242/dmm.007948
46. Musselman LP, Fink JL, Grant AR, Gatto JA, Tuthill BF 2nd, Baranski TJ. A complex relationship between immunity and metabolism in *Drosophila* diet-induced insulin resistance. *Mol Cell Biol.* (2018) 38:e00259–17. doi: 10.1128/MCB.00259-17

47. Musselman LP, Fink JL, Baranski TJ. Similar effects of high-fructose and high-glucose feeding in a *Drosophila* model of obesity and diabetes. *PLoS ONE*. (2019) 14:e0217096. doi: 10.1371/journal.pone.0217096
48. Duchek P, Somogyi K, Jékely G, Beccari S, Rørth P. Guidance of cell migration by the *Drosophila* PDGF/VEGF receptor. *Cell*. (2001) 107:17–26. doi: 10.1016/S0092-8674(01)00502-5
49. Zettervall CJ, Anderl I, Williams MJ, Palmer R, Kurucz E, Ando I, et al. A directed screen for genes involved in *Drosophila* blood cell activation. *Proc Natl Acad Sci USA*. (2004) 101:14192–7. doi: 10.1073/pnas.0403789101
50. Dragojlovic-Munther M, Martinez-Agosto JA. Multifaceted roles of PTEN and TSC orchestrate growth and differentiation of *Drosophila* blood progenitors. *Development*. (2012) 139:3752–63. doi: 10.1242/dev.074203
51. Wilcox G. Insulin and insulin resistance. *Clin Biochem Rev*. (2005) 26:19–39.
52. Brennan CA, Delaney JR, Schneider DS, Anderson KV. Psidin is required in *Drosophila* blood cells for both phagocytic degradation and immune activation of the fat body. *Curr Biol*. (2007) 17:67–72. doi: 10.1016/j.cub.2006.11.026
53. Shin M, Cha N, Koranteng F, Cho B, Shim J. Subpopulation of macrophage-like plasmatocytes attenuates systemic growth via JAK/STAT in the *Drosophila* fat body. *Front Immunol*. (2020) 11:63. doi: 10.3389/fimmu.2020.00063
54. Osborn O, Olefsky JM. The cellular and signaling networks linking the immune system and metabolism in disease. *Nat Med*. (2012) 18:363–74. doi: 10.1038/nm.2627
55. Shia AK, Glittenberg M, Thompson G, Weber AN, Reichhart JM, Ligoxygakis P. Toll-dependent antimicrobial responses in *Drosophila* larval fat body require Spatzle secreted by haemocytes. *J Cell Sci*. (2009) 122:4505–15. doi: 10.1242/jcs.049155
56. Wang L, Kounatidis I, Ligoxygakis P. *Drosophila* as a model to study the role of blood cells in inflammation, innate immunity and cancer. *Front Cell Infect Microbiol*. (2014) 3:113. doi: 10.3389/fcimb.2013.00113
57. Chen MS, Obar RA, Schroeder CC, Austin TW, Poodry CA, Wadsworth SC, et al. Multiple forms of dynamin are encoded by shibire, a *Drosophila* gene involved in endocytosis. *Nature*. (1991) 351:583–6. doi: 10.1038/351583a0
58. Jaiswal JK, Rivera VM, Simon SM. Exocytosis of post-Golgi vesicles is regulated by components of the endocytic machinery. *Cell*. (2009) 137:1308–19. doi: 10.1016/j.cell.2009.04.064
59. Sieow JL, Gun SY, Wong SC. The sweet surrender: how myeloid cell metabolic plasticity shapes the tumor microenvironment. *Front Cell Dev Biol*. (2018) 6:168. doi: 10.3389/fcell.2018.00168
60. Shingleton AW, Das J, Vinicius L, Stern DL. The temporal requirements for insulin signaling during development in *Drosophila*. *PLoS Biol*. (2005) 3:e289. doi: 10.1371/journal.pbio.0030289
61. Garcia-Bellido A, Merriam JR. Parameters of the wing imaginal disc development of *Drosophila melanogaster*. *Dev Biol*. (1971) 24:61–87. doi: 10.1016/0012-1606(71)90047-9
62. Zmora N, Bashiardes S, Levy M, Elinav E. The role of the immune system in metabolic health and disease. *Cell Metab*. (2017) 25:506–21. doi: 10.1016/j.cmet.2017.02.006
63. Kitamoto T. Conditional modification of behavior in *Drosophila* by targeted expression of a temperature-sensitive shibire allele in defined neurons. *J Neurobiol*. (2001) 47:81–92. doi: 10.1002/neu.1018
64. Park SY, Ludwig MZ, Tamarina NA, He BZ, Carl SH, Dickerson DA, et al. Genetic complexity in a *Drosophila* model of diabetes-associated misfolded human proinsulin. *Genetics*. (2014) 196:539–55. doi: 10.1534/genetics.113.157602
65. Petraki S, Alexander B, Bruckner K. Assaying blood cell populations of the *Drosophila melanogaster* Larva. *J Vis Exp*. (2015) 2015:52733. doi: 10.3791/52733
66. Sharma S, Mathre S, Ramya V, Shinde D, Raghu P. Phosphatidylinositol 5 phosphate 4-Kinase regulates plasma-membrane PIP3 turnover and insulin signaling. *Cell Rep*. (2019) 27:1979–90.e7. doi: 10.1016/j.celrep.2019.04.084
67. Yamada T, Habara O, Yoshii Y, Matsushita R, Kubo H, Nojima Y, et al. The role of glycogen in development and adult fitness in *Drosophila*. *Development*. (2019) 146:dev176149. doi: 10.1242/dev.176149
68. Vishal K, Brooks DS, Bawa S, Gameros S, Stetsiv M, Geisbrecht ER. Adult muscle formation requires *Drosophila* moleskin for proliferation of wing disc-associated muscle precursors. *Genetics*. (2017) 206:199–213. doi: 10.1534/genetics.116.193813
69. Hummon AB, Lim SR, Difilippantonio MJ, Ried T. Isolation and solubilization of proteins after TRIzol extraction of RNA and DNA from patient material following prolonged storage. *Biotechniques*. (2007) 42:467–72. doi: 10.2144/000112401
70. Kubrak OI, Kučerová L, Theopold U, Nässel DR. The sleeping beauty: how reproductive diapause affects hormone signaling, metabolism, immune response and somatic maintenance in *Drosophila melanogaster*. *PLoS ONE*. (2014) 9:e113051. doi: 10.1371/journal.pone.0113051

Conflict of Interest: The authors declare that the research was conducted in the absence of any commercial or financial relationships that could be construed as a potential conflict of interest.

Advantages of publishing in Frontiers

OPEN ACCESS
Articles are free to read for greatest visibility and readership

FAST PUBLICATION
Around 90 days from submission to decision

HIGH QUALITY PEER-REVIEW
Rigorous, collaborative, and constructive peer-review

TRANSPARENT PEER-REVIEW
Editors and reviewers acknowledged by name on published articles

Frontiers
Avenue du Tribunal-Fédéral 34
1005 Lausanne | Switzerland

Visit us: www.frontiersin.org
Contact us: info@frontiersin.org | +41 21 510 17 00

REPRODUCIBILITY OF RESEARCH
Support open data and methods to enhance research reproducibility

DIGITAL PUBLISHING
Articles designed for optimal readership across devices

FOLLOW US
@frontiersin

IMPACT METRICS
Advanced article metrics track visibility across digital media

EXTENSIVE PROMOTION
Marketing and promotion of impactful research

LOOP RESEARCH NETWORK
Our network increases your article's readership